NIMS Monographs

Mitsuhiro Ebara
Yohei Kotsuchibashi
Ravin Narain
Naokazu Idota
Young-Jin Kim
John M. Hoffman
Koichiro Uto
Takao Aoyagi

# Smart Biomaterials

National Institute for Materials Science

Springer

# NIMS Monographs



For further volumes:
http://www.springer.com/series/11599

The NIMS Monographs are published by the National Institute for Materials Science (NIMS), a leading public research institute in materials science in Japan, in collaboration with Springer. The series present research results achieved by NIMS researchers through their studies on materials science as well as current scientific and technological trends in those research fields.

These monographs provide readers up-to-date and comprehensive knowledge about fundamental theories and principles of materials science as well as practical technological knowledge about materials synthesis and applications.

With their practical case studies the monographs in this series will be particularly useful to newcomers to the field of materials science and to scientists and engineers working in universities, industrial research laboratories, and public research institutes. These monographs will be also available for textbooks for graduate students.

National Institute for Materials Science
http://www.nims.go.jp/

Mitsuhiro Ebara · Yohei Kotsuchibashi
Ravin Narain · Naokazu Idota · Young-Jin Kim
John M. Hoffman · Koichiro Uto · Takao Aoyagi

# Smart Biomaterials

National Institute for Materials Science

Springer

Mitsuhiro Ebara
Yohei Kotsuchibashi
Koichiro Uto
Takao Aoyagi
National Institute for Materials Science
Tsukuba
Japan

Ravin Narain
University of Alberta
Edmonton, AB
Canada

Naokazu Idota
Waseda University
Tokyo
Japan

Young-Jin Kim
The University of Tokyo
Tokyo
Japan

John M. Hoffman
Stratos Genomics
Seattle,WA
USA

ISSN 2197-8891 ISSN 2197-9502 (electronic)
ISBN 978-4-431-54399-2 ISBN 978-4-431-54400-5 (eBook)
DOI 10.1007/978-4-431-54400-5
Springer Tokyo Heidelberg New York Dordrecht London

Library of Congress Control Number: 2014935978



Printed on acid-free paper

Springer is part of Springer Science+Business Media (www.springer.com)

# Preface

There is no doubt that the progress of medicine could not be achieved without biomaterials research. The elucidation of biological defense mechanisms by molecular biology and cell biology has enhanced biomaterials research. This, however, does not mean that numerous artificial organs have been realized; even though, by all rights, more products should be clinically available.

Human tissues or organs in the body have complicated functions and are not easy to replace with conventional artificial materials. We should design and synthesize materials with better performance than ever before.

Biofunctional polymers have been extensively studied for more than 40 years. Many interesting research results have been obtained, but their clinical applications are limited, even though the concepts are superlative. Investigations on a wide range of biofunctional polymers are driven by a number of researchers. Some of these polymers are defined as materials that respond to chemical stimuli, such as the concentration of certain chemicals and pH change, and physical stimuli, such as heat (temperature change), magnetic field, light, and electric field. They are also classified as intelligent or smart materials. Needless to say, human beings are dynamic organisms. Stimuli-responsive materials with intelligence and drive are also dynamic. To achieve more sophisticated drug treatment, or to substitute biological functions, the use of smart materials is inevitable.

The development of polymer chemistry with precise control of the molecular chain has contributed to the development of smart materials. Precise polymerization is a very important technology in designing actual materials with higher functions, because, by utilizing a low-molecular-weight distribution, it is possible to further improve the performance of smart materials. Moreover, integration with nanotechnology is also essential.

In this book, how to design smart materials and how to apply them to biomedical fields are described by experts in these fields. In Chap. 1, the significance of monomer design in preparing uniform functions is explained on the basis of simple polymer fundamentals. Chapter 2 provides descriptions on the preparation and application of stimuli-responsive smart hydrogels, aiming at biomedical applications. Materials showing dynamic movement in response to internal or external stimuli are used as actuators, and their combination with nanotechnology can realize new diagnostic devices. In Chap. 3, nanoassemblies and nanoparticles are described. They are key

materials in developing drug-targeting systems. Some passive drug-targeting systems based on enhanced permeation and retention effects are actually in clinical use. Smart nanoassemblies are promising for more efficient drug targeting. Chapter 4 deals with smart surfaces. It is one of the outstanding examples of a flat solid or particle surface modified to control the interaction of biomolecules for chromatographic separation. In Chap. 5, nanofibers with smart properties are described. Their biomedical applications are currently few, but they will surely be expanded through combination with other materials, such as nanoparticles, or surface modification. Chapter 6 presents smart bioconjugates. Precise polymerization techniques contribute to the preparation of the precursor, and the resulting bioconjugates are very useful in diagnosis. Some of them will be applied to the prevention of severe infections in developing countries. Finally, in Chap. 7, shape-memory materials are described. There is much research on the dynamic movement of polymeric shape-memory materials. This chapter also deals with surface shape-memory materials that will be of concern in mechanobiology.

This volume is sure to benefit materials researchers and developers, and we feel that it will serve as an invaluable textbook for anyone interested in smart biomaterials.

Takao Aoyagi

# Contents

# Chapter 1
# Introductory Guide to Smart Biomaterials

Looking back 50 years of the history in biomaterials research, at earlier stage, it was almost try and error. Based on vigorous and steady research, understanding the biological event at the interface between materials and human body has accelerated to develop bio-inert, bio-active polymeric materials or devices. The biomaterials research has shifted to next stage now. In order to develop highly-functional biomaterials, we should actively involve the molecular design based on materials science and nano-biotechnology. Nanostructured materials contribute to fabricate new diagnosis or medical devices and so on. That is, interdisciplinary research including biology, materials science and nanotechnology gives us new system or materials to open new generation. One of the examples is 'smart' biotechnologies using nanostructured stimuli-responsive polymers that respond to small changes in external stimuli with large discontinuous changes in their physical properties. These 'smart' biomaterials are designed to act as an "on-off" switch for drug delivery technologies, gene therapy, affinity separations, chromatography, diagnostics etc.

In this book, we would like to describe biomedical applications of smart materials. In terms of material type, the most commonly reported examples of stimuli-responsive materials are poly(*N*-isopropylacrylamide) (PNIPAAm) and its derivatives (Fig. 1.1). In terms of the characteristic phase transition behavior of hydrogels consisting of PNIPAAm, it was investigated in great detail by Prof. Tanaka from the Massachusetts Institute of Technology [1]. Stimuli-responsive materials respond to miniscule changes in their environment with drastic changes in their physical properties. Usually, when attempting to construct a particular response system, fundamental processes such as sensing, processing and actuating need to be combined. It is conceivable, however, that if stimuli-responsive materials are used, these processes can be realized by using a single material and that the system would become extremely simple. For this reason, in the nano-bio field, there is a strong focus on such materials for the purpose of constructing lab-on-chip and other types of microscopic systems. Such materials find application in a number of biomedical fields, for instance, as bioconjugates (developed

M. Ebara et al., *Smart Biomaterials*, NIMS Monographs,
DOI: 10.1007/978-4-431-54400-5_1,

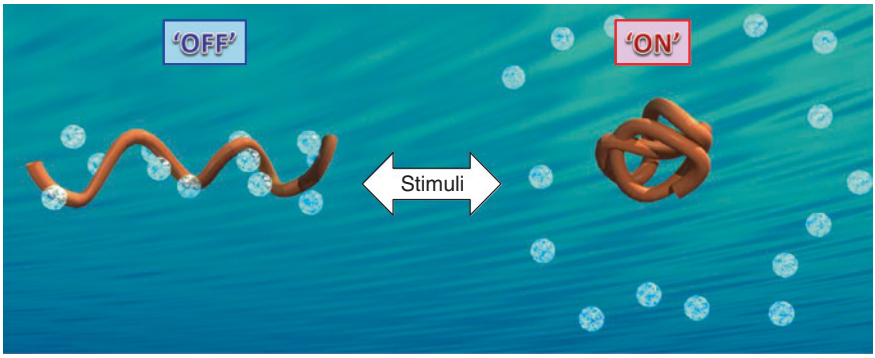


**Fig. 1.1** Schematic illustration of temperature-responsive phase transition behavior of poly(*N*-isopropylacrylamide) (PNIPAAm) in aqueous solution

by Hoffman et al.[2]) or in cell sheet engineering, which is actively advanced by Okano et al. [3]. The following chapters will present some typical biomedical applications. We hope that the contents would stimulate related research and hit on the nice idea of other than previous study.

Prior to the each research, the fundamentals and our concept on molecular design for NIPAAm-based functional polymer should be briefly described. Temperature-responsive polymers active in aqueous solution undergo reversible conformation changes (for example, coil-globule transformations) following the hydration and dehydration of the polymer chain in response to temperature changes. These transformations substantially change the solubility of the polymers in aqueous media. In terms of molecular structure, a single molecule combines amide, ether, amino and hydroxyl groups, which readily form hydrogen bonds, and alkyl groups, which have low affinity to water. Classical examples include alkylacrylamide, alkylmethacrylamide as well as poly (vinyl ether) with alkyl side chains and methylcellulose containing ethylene oxide side chains. These polymers are generally soluble in aqueous media at low temperature and suddenly become insoluble above a certain temperature threshold. This temperature threshold is called the lower critical solution temperature (abbreviated as LCST). Although materials which exhibit the opposite characteristics (upper critical solution temperature, abbreviated as UCST) are also known, examples are few.

In our laboratory, we polymerize monomers with new chemical structures based on NIPAAm and explore how polymers can be developed into functional materials. Considering chemical processes, for example, such as immobilization to fixed solid surfaces or nanoparticle and the preparation of conjugates of biomolecules such as peptide, protein, antibody and so on, NIPAAm itself is non-reactive, and therefore the problem of preparing functionalized polymers is extremely important. Many researchers solve this problem by copolymerization using ordinal functional monomer, acrylic acid (AAc) and other common monomers. However,

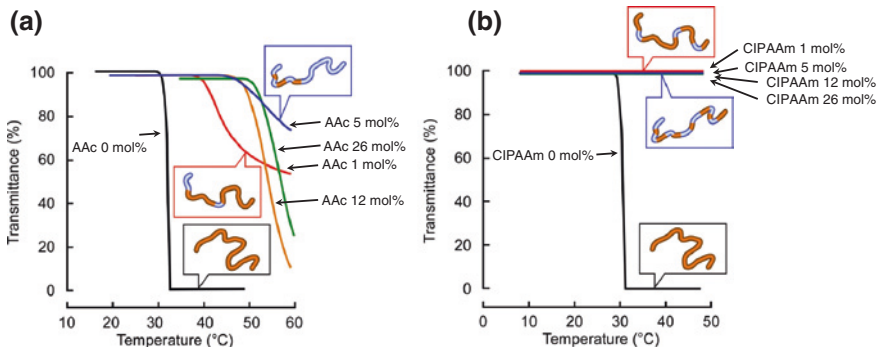


**Fig. 1.2** Temperature-dependent transmittance changes of aqueous solutions of NIPAAm copolymers at pH 12. **a** NIPAAm-co-AAc and **b** NIPAAm-co-CIPAAm

in performing copolymerization with functional monomers such as acrylic acid, there is a possibility of sensitivity loss due to failure to obtain a random arrangement of monomers due to the copolymerization reactivity ratio. One of the basic principles in polymer chemistry is that materials obtained by stopping the copolymerization at a rather early stage exhibit a highly random sequence; however, this is a problem from the perspective of yield. Low yields are detrimental to the progress of our research, which is conducted with the aim to develop polymers with practical application. Polymers that can be synthesized at low cost in high yield are expected to find practical applications with ease.

Figure 1.2a shows the temperature-responsive behavior of a NIPAAm copolymer prepared using AAc as a functional monomer. Naturally, the carboxyl group of AAc undergoes complete dissociation at a high pH well above the pKa of AAc (here, we chose pH 12 as an extreme example). The dissociated carboxyl group induces ionic hydration and electrostatic repulsion, as a result of which dehydration of the chain and subsequent aggregation become difficult. It is usually expected that a cloud point would not be observed; however, as can be seen in the figure, hazing is observed, contrary to expectation. This suggests that the monomer arrangement is not random. That is, if a hydrophilic monomer is inserted at probabilistically equal intervals, dehydration and aggregation of the chain would be difficult. However, if hydrophilic monomers are distributed disproportionately and the NIPAAm chain is continuous, the continuous part would be capable of undergoing dehydration and aggregation, similarly to that in homopolymers. The copolymerization reactivity ratios of the monomer for NIPAAm and AAc differ considerably, and rather than forming a randomly arranged copolymer, they would form segments similarly to block copolymers. This is considered to originate from the mixing of polymers similarly to the NIPAAm homopolymer. Indeed, it has been reported that the copolymerization reactivity ratios can differ by an order of 2 or more [4]. Therefore, to ensure that the copolymerization reactivity ratios were

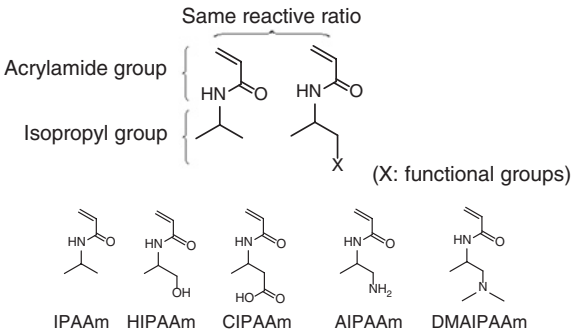


**Fig. 1.3** Chemical structures of newly designed *N*-isopropylacrylamide-based functional monomers

similar, we prepared the polymer, as shown in Fig. 1.3, from a NIPAAm derivative with a carboxyl group, 2-carboxyisopropylacrylamide (CIPAAm) [5]. The carboxyl group, which has strong effects on hydration and dehydration, was placed at the end of the isopropyl group, where the obstruction of the continuity of the isopropylamide group is minimal even after polymerization, and the polymerizable group is in the acrylamide form. As expected, the copolymer of NIPAAm and CIPAAm does not have a cloud point at pH 12 (Fig. 1.2b). Indeed, the copolymerization reactivity ratios were found to be similar, resulting in an ideal copolymerization reaction with a random distribution of comonomers [6]. Copolymers were also prepared from the monomers with amino groups and hydroxyl groups (as shown in Fig. 1.3), and it was found that they respond sensitively to temperature [7, 8].

As mentioned above, NIPAAm-based temperature-responsive polymers exhibit a cloud point in solution, which is governed by hydrophilicity and hydrophobicity. The concept of cloud point refers to a change in turbidity, which is of two types: phase transition from liquid to solid and liquid-liquid separation. LCST is generally used only as an index of temperature responsiveness, without distinguishing between these two types of change. Here, we introduce research aiming to clarify this point. In our research, we used the copolymer shown in Fig. 1.2b, which is based on NIPAAm and contains hydroxyl groups. We used this copolymer because it is non-ionic and is not affected by the pH of the surrounding environment, and also because it allows a margin for altering the monomer combinations owing to the low amount of hydration relative to that of ionic groups. We investigated the changes in cloud point of copolymers of NIPAAm monomers and NIPAAm-based monomers containing hydroxyl groups, whose cloud point shifts roughly linearly toward higher temperatures with increasing 2-hydroxylisopropylacrylamide (HIPAAm) content [8]. It is extremely interesting that a rather distinct cloud point is observed even when 50 % or more of the monomers contain hydroxyl groups. The results of differential scanning calorimetry (DSC) of NIPAAm-HIPAAm copolymers are also highly indicative of their temperature responsiveness. In the case of an HIPAAm content of

50 mol%, although there is a distinct cloud point, there is no peak in the DSC data. This means that the increase in turbidity is due to phase separation rather than phase transition with a high transition enthalpy change. Therefore, to estimate the expansion of the polymer chain in aqueous solutions and the hydration of the functional groups, we conducted $^{1}$H-NMR measurements to examine the behavior of NIPAAm-HIPAAm copolymers with high and low HIPAAm contents below and above the cloud point. In copolymers with a low content of hydroxyl groups, which exhibited a clear heat absorption peak in DSC, a notable peak reduction was observed at a higher content of HIPAAm. This indicates that dehydration occurs following the increase in temperature of the solution, and molecule mobility is drastically reduced. Conceivably, in this case, dehydration is insufficient and molecule movement is possible. That is, the observed cloud point possibly includes phase transition and phase separation, and this point can be elucidated by using a method such as $^{1}$H-NMR [9].

The changes in turbidity as a characteristic of polymers with hydration-dehydration temperature response include coil-globule phase transition induced by dehydration and liquid-liquid phase separation following the formation of coacervates with insufficient dehydration. Although polymers such as NIPAAm homopolymers typically undergo coil-globule transition, this shifts toward phase separation in the case of copolymerization with comonomers with high hydrophilicity. This is not limited to temperature-responsive polymers of the acrylamide type because partial hydrolysates of vinylacetamide and hydrophobic proteins such as the well-known biopolymer elastin form coacervates. Incidentally, and in contrast, the phase transition temperature can be effectively lowered by copolymerization with highly hydrophobic comonomers, which has been the subject of extensive research. The modulation of temperature threshold is critical to developing biomedical applications because the temperature of the human body changes within a few degrees. Moreover, the sharpness of the phase transition is sometimes important to realize the fabrication of sensitive biomedical systems. As stated above, we hope that the following chapters will stimulate further research and generate unexpected novel ideas.

In Chap 2, we focus on the synthesis, characterization, and applications of smart hydrogels. Because hydrogels contain a large fraction of aqueous solvent within their structure, smart hydrogels have been used especially for the ‘on-off’ control of drug release. In Chap. 3, we focus on smart nanoparticles including nanoassemblies. Because nanosized particles demonstrate unique properties, they can provide a particularly useful platform for wide-ranging therapeutic applications. In Chap. 4, we present rationally designed smart surfaces that exhibit switchable capture/release of biomolecules and cells. In Chap. 5, we describe recent advances of smart nanofibers fabricated by different methods. In Chap. 6, we focus on smart bioconjugates. The conjugation of a smart polymer to a single molecule can generate a nanoscale switch. In Chap. 7, we focus on shape-memory materials, especially shape-memory polymers. Recent reports on shape-memory surfaces are also included (Fig. 1.4).

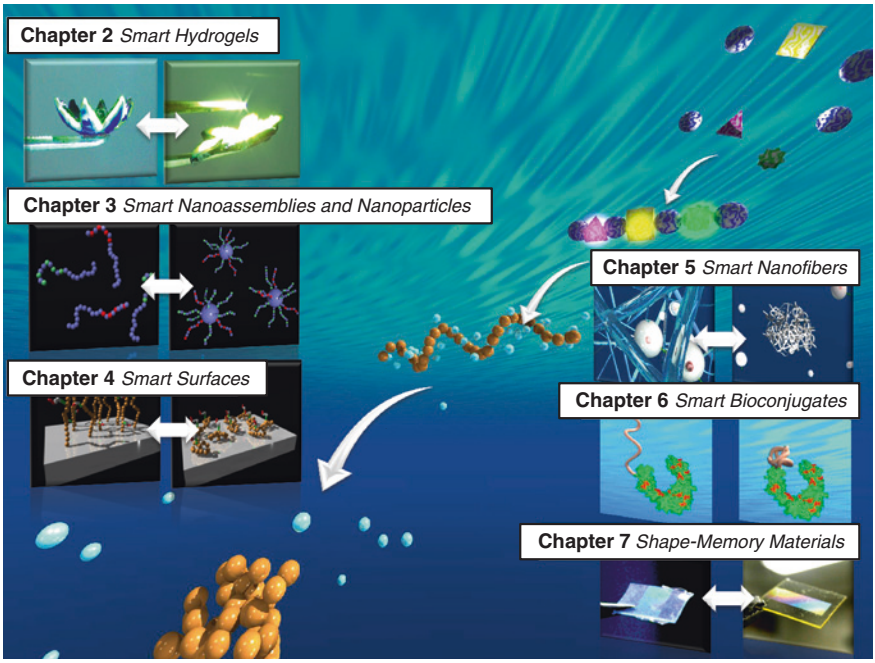


**Fig. 1.4** Unlike conventional biomaterials, 'smart' polymer-based biomaterials possess switchable and predictable capabilities, which make them particularly attractive for a variety of biomedical applications

## References

1. English AE, Tanaka T, Edelman ER (1997) Equilibrium and non-equilibrium phase transitions in copolymer polyelectrolyte hydrogels. J Chem Phys 107:1645–1654
2. Hoffman AS, Stayton PS, Bulmus V, Chen G, Chen J, Cheung C, Chilkoti A, Ding Z, Dong L, Fong R, Lackey CA, Long CJ, Miura M, Morris JE, Murthy N, Nabeshima Y, Park TG, Press OW, Shimoboji T, Shoemaker S, Yang HJ, Monji N, Nowinski RC, Cole CA, Priest JH, Harris JM, Nakamae K, Nishino T, Miyata T (2000) Really smart bioconjugates of smart polymers and receptor proteins. J Biomed Mater Res 52:577–586. doi:10.1002/1097-4636(20001215)52:4<577:aid-jbm1>3.0.co;2-5
3. Yamada N, Okano T, Sakai H, Karikusa F, Sawasaki Y, Sakurai Y (1990) Thermo-responsive polymeric surfaces; control of attachment and detachment of cultured cells. Die Makromol Chem, Rapid Commun 11:571–576. doi:10.1002/marc.1990.030111109
4. Xue W, Champ S, Huglin MB (2000) Observations on some copolymerisations involving *N*-isopropylacrylamide. Polymer 41:7575–7581. http://dx.doi.org/10.1016/S0032-3861(00)00171-3
5. Aoyagi T, Ebara M, Sakai K, Sakurai Y, Okano T (2000) Novel bifunctional polymer with reactivity and temperature sensitivity. J Biomater Sci Polym Ed 11:101–110. doi:10.1163/156856200743526
6. Kanda T, Yamamoto K, Aoyagi T (2005) *N*-Isopropylacrylamide-based temperature-responsive polymer with carboxyl groups for controlled drug release. J Photopolym Sci Technol 18:515–518

7. Yoshida T, Aoyagi T, Kokufuta E, Okano T (2003) Newly designed hydrogel with both sensitive thermo response and biodegradability. J Polym Sci, Part A: Polym Chem 41:779–787. doi:10.1002/pola.10595
8. Maeda T, Kanda T, Yonekura Y, Yamamoto K, Aoyagi T (2006) Hydroxylated poly(*N*-isopropylacrylamide) as functional thermoresponsive materials. Biomacromolecules 7:545–549. doi:10.1021/bm050829b
9. Maeda T, Yamamoto K, Aoyagi T (2006) Importance of bound water in hydration–dehydration behavior of hydroxylated poly(*N*-isopropylacrylamide). J Colloid Interface Sci 302:467–474. http://dx.doi.org/10.1016/j.jcis.2006.06.047

# Chapter 2
# Smart Hydrogels

## 2.1 Introduction

This chapter focuses on the synthesis, characterization, and applications of stimuli-responsive hydrogel-based materials. Hydrogels are three-dimensional (3D) materials with the ability to absorb large amounts of water while maintaining their dimensional stability. The 3D integrity of hydrogels in their swollen state is maintained by either physical or chemical crosslinking [1–3]. Chemically crosslinked networks have permanent junctions, while physical networks have transient junctions that arise from either polymer chain entanglements or physical interactions such as ionic interactions, hydrogen bonds, or hydrophobic interactions [4]. Indeed, there are many different macromolecular structures that are possible for physical and chemical hydrogels. They include the following: crosslinked or entangled networks of linear homopolymers, linear copolymers, and block or graft copolymers; polyion-multivalent ion, polyion–polyion or H-bonded complexes; hydrophilic networks stabilized by hydrophobic domains; and interpenetrating polymer networks (IPNs) or physical blends. Hydrogels may also have many different physical forms, including (a) solid molded forms (e.g., soft contact lenses), (b) pressed powder matrices (e.g., pills or capsules for oral ingestion), (c) microparticles (e.g., as bioadhesive carriers or wound treatments), (d) coatings (e.g., on implants or catheters; on pills or capsules, or coatings on the inside capillary wall in capillary electrophoresis), (e) membranes or sheets (e.g., as a reservoir in a transdermal drug delivery patch; or for 2D electrophoresis gels), (f) encapsulated solids (e.g., in osmotic pumps), and (g) liquids (e.g., that form gels upon heating or cooling) [5]. Hydrogels can also be separated into two groups on the basis of their natural or synthetic origins [6, 7]. Hydrogel-forming natural polymers include proteins such as collagen and gelatin, and polysaccharides such as alginate and agarose. These hydrogels have many advantageous features, including low toxicity and good biocompatibility, because their chemical structures are similar to those of the bioactive glycosaminoglycan (GAG) molecules (e.g., heparin sulfate, chondroitin sulfate, and hyaluronan) present in the native extracellular

M. Ebara et al., *Smart Biomaterials*, NIMS Monographs,
DOI: 10.1007/978-4-431-54400-5_2,

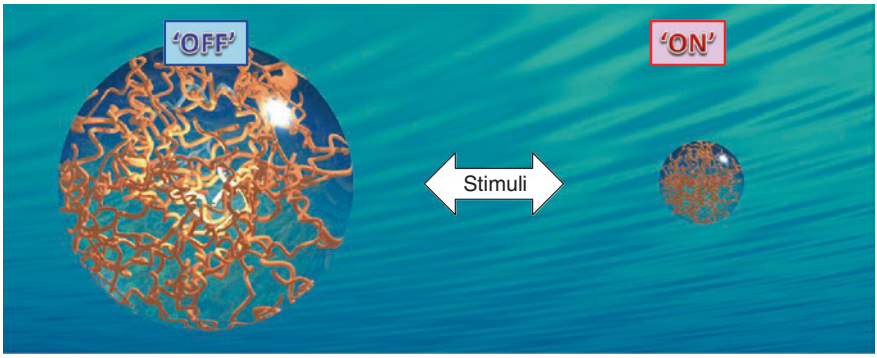


**Fig. 2.1** Schematic illustration of a smart hydrogel that can undergo reversible volume phase transitions upon minute changes in environmental condition

matrix (ECM). Synthetic polymers that form hydrogels are traditionally prepared using chemical polymerization methods. Approaches applying genetic engineering and biosynthetic methods to create unique hydrogel materials have recently been reported [8, 9].

Hydrogels have been of great interest to biomaterial scientists for many years since the pioneering work of Wichterle and Lim in [10] on crosslinked 2-hydroxyethyl methacrylate (HEMA) hydrogels. Lower interfacial tension, soft and tissue like physical properties, higher permeability to undersized molecules, and release of entrapped molecules in a controlled manner have made hydrogels a focus of exploration in different biomedical fields. Successful examples include wound dressings [11–13], superabsorbents [14], drug delivery systems [15–18], and tissue engineering [17, 19]. In particular, hydrogels have been used extensively in the development of drug delivery systems, because hydrogels can not only protect the drug from hostile environments but also control drug release by changing the gel structure in response to environmental stimuli. Hydrogels containing such 'sensor' properties can undergo reversible volume phase transitions or gel–sol phase transitions upon minute changes in the environmental condition. These types of stimuli-responsive hydrogels are also called 'smart' hydrogels (Fig. 2.1) [20, 21]. Many physical and chemical stimuli have been applied to induce various responses of the smart hydrogel systems. The physical stimuli include temperature, electric fields, solvent composition, light, pressure, sound and magnetic fields, whereas the chemical or biochemical stimuli include pH, ions and specific molecular recognition events. Smart hydrogels have been used in diverse applications, such as in making actuators [22–25] and valves [26–28], in the immobilization of enzymes and cells [20, 29–31], in sensors [16, 32, 33], and in concentrating dilute solutions in bioseparation [34, 35].

Despite significant advances in smart hydrogels, however, conventional hydrogels have limited utility in manipulating their swelling/shrinking kinetics for practical applications owing to their size dependence [36]. As both gel swelling and

shrinking kinetics are typically governed by diffusion-limited polymer network transport in water, the inverse of the rate is proportional to the square of the gel dimension [37]. Therefore, the molecular design of polymer architectures of smart hydrogels is particularly important to show the potentially powerful combination of thermodynamic and kinetic regulation of smart hydrogels. Fast-response hydrogels, for example, benefit from converting external stimuli into local alteration of mechanical or physical properties that then prompt drug release and smart actuators. To increase the response of gel dynamics, several strategies have been explored. Owing to the intrinsic diffusion dependence, reducing gel size is one technique known to achieve rapid kinetics. Other techniques include making the gel heterogeneous, such as producing a microporous gel structure to increase the contacting surface area between polymer and solvent [38]. Novel strategies focusing on different hydrogel architectures have also been proposed [39–41].

This chapter focuses on smart hydrogels from the viewpoints of their preparation methods, characterizations and applications. Sections 2.2 and 2.3 describe the classifications of smart hydrogels on the basis of the preparation methods and stimuli, respectively. Special attention has been paid to the effects of hydrogel architecture son 'on-off' switchable swelling/shrinking properties, because the characteristics and some potential applications of the gels are related to their preparation methods. The characterization methods are discussed in Sect. 2.4. In Sect. 2.5, certain applications of the smart hydrogels are discussed. The chapter ends with a look at some of the future trends in the applications in biotechnology and biomedicine.

## 2.2 Classification on the Basis of Preparation Methods

Hydrogels can be classified in several ways depending on the preparation methods. Among them, one of the important classifications is based on their crosslinking nature. The detailed classification is presented in Table 2.1. In chemically crosslinked gels, covalent bonds are present between different polymer chains. Therefore, they are stable and cannot be dissolved in any solvents unless the covalent crosslink points are cleaved. In physically crosslinked gels, dissolution is prevented by physical interactions, which exist between different polymer chains. They are advantageous for a great number of pharmaceutical and biomedical applications because the use of crosslinking agents is avoided.

### *2.2.1 Physically Crosslinked Hydrogels*

In recent years, there has been increasing interest in physically crosslinked gels. The main reason is that the use of crosslinking agents in the preparation of such hydrogels is avoided. To create physically crosslinked gels, different methods

**Table 2.1** Methods for synthesizing physically and chemically crosslinked hydrogels

| Physically crosslinked hydrogels |
|---|
| • Ionic interactions (alginate etc.) |
| • Hydrophobic interactions (PEO–PPO–PEO etc.) |
| • Hydrogen bonding interactions (PAAc etc.) |
| • Stereocomplexation (enantiomeric lactic acid etc.) |
| • Supramolecular chemistry (inclusion complex etc.) |
| **Chemically crosslinked hydrogels** |
| • Polymerization (acryloyl group etc.) |
| • Radiation (γ-ray etc.) |
| • Small-molecule crosslinking (glutaraldehyde etc.) |
| • Polymer–polymer crosslinking (condensation reaction etc.) |

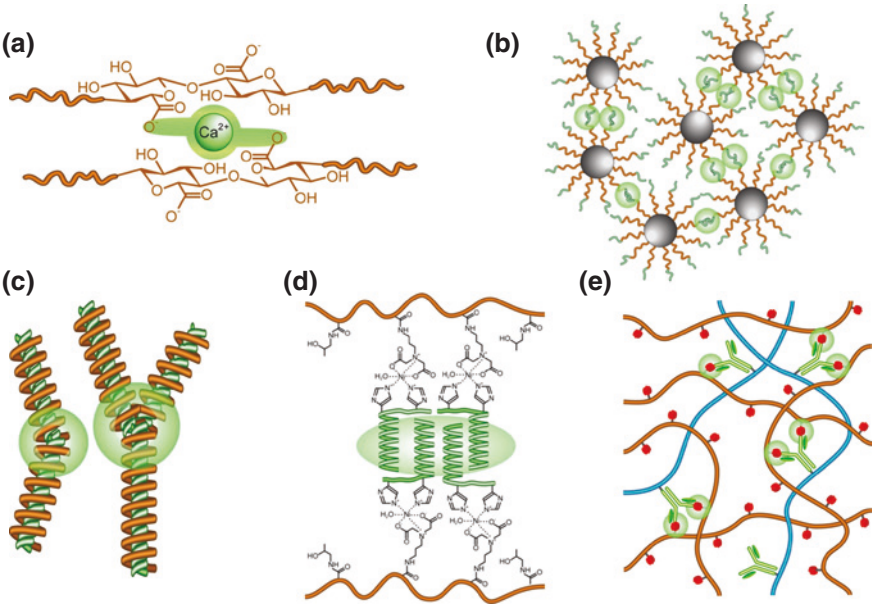


**Fig. 2.2** Schematic of methods for formation of physically crosslinked hydrogels via. **a** Ionic interactions, **b** hydrophobic interactions, **c** self-assembling of stereocomplex formation, **d** coiled-coil interactions, **e** specific molecular recognition

have been investigated. Alginate is a well-known example of a polymer that can be crosslinked by ionic interactions. It is a polysaccharide with mannuronic and glucuronic acid residues and can be crosslinked by calcium ions (Fig. 2.2a) [42]. Crosslinking can be carried out at room temperature and physiological pH. Therefore, alginate gels are frequently used as a matrix for the encapsulation of living cells [43] and for the release of proteins [44]. Interestingly, the gels can be destabilized by the extraction of Ca ions from the gel by a chelating agent. The

activity of incorporated proteins within the gel can be modulated by treating the particles with anionic polymers [45]. Iskakov et al. [46] have demonstrated time-programmed release of macromolecular drugs from calcium alginate gel beads modified with an anionic polymer, poly(carboxy-*n*-propylacrylamide-*co*-dimethylacrylamide) (P(CNPAAm-*co*-DMAAm), of varying coating thickness from 25 to 125 μm. The lag time for pulsatile release of dextran was regulated by adjusting the copolymer coating thickness. The hydrolytic degradation of gel microspheres based on calcium crosslinked phosphazene polyelectrolytes, poly [di(carboxylatophenoxy)phosphazene] (PCPP) and poly[(carboxylatophenoxy) (glycinato)phosphazene] (PCGPP) was also demonstrated by Andrianov et al. [47]. The degradation rates can be increased by the incorporation of hydrolysis-sensitive glycinato groups as the pendant structures in the polymer. Alginate gel is also formed by gelation with polycations such as polylysine [48]. Ionic interaction is also formed by mixing negatively and positively charged microspheres. Dextran microspheres coated with anionic and cationic polymers exhibit spontaneous gelation upon mixing owing to ionic complex formation between the oppositely charged microparticles [49].

Hydrophobic interactions have also been exploited to design physically crosslinked gels. Amphiphilic block and graft copolymers can self-assemble in water to form organized structures such as polymeric micelles and hydrogels, in which the hydrophobic segments of the polymers are aggregated (Fig. 2.2b). Physically crosslinked hydrogels are generally obtained from multiblock copolymers or graft copolymers. The latter can be composed of a water-soluble polymer backbone, for example, a polysaccharide, to which hydrophobic units are attached, or hydrophobic chains containing water-soluble grafts. The most commonly used thermogelling polymers are Pluronics®and Tetronics® [50]. Micelles are formed at low concentrations in water, and at higher concentrations, thermoreversible gels are formed. Some of them have been approved by the FDA and EPA for applications in food additives, pharmaceutical ingredients and agricultural products. To add a biodegradable capacity, the PPO segment of PEO–PPO–PEO block copolymers is often replaced by a biodegradable poly(L-lactic acid) (PLLA) [51] or poly(DL-lacticacid-*co*-glycolic acid) (PLGA) [52] segment. When low-molecular-weight PEG versus high-molecular-weight PLGA was used, the aqueous solution of PEG–PLGA–PEG triblock copolymer forms a solution at room temperature, where as at body temperature, it becomes a gel within a few seconds. The molecular architecture was not limited to the A-B-A-type block copolymer, but expanded into three-dimensional, hyper branched structures, such as a star-shaped structure [53]. Proper combinations of molecular weight and polymer architecture resulted in gels with different LCST values. Hydrophobic cholesterol-bearing pullulan also forms hydrogel nanoparticles upon self-aggregation in water [54, 55]. Chitosan solutions containing glycerol-2-phosphate (β-GP), which undergo temperature-controlled pH-dependent sol–gel transition at a temperature close to 37 °C, have recently been proposed [56, 57]. The combination of chitosan and PEG also forms a gel that releases bovine serum albumin (BSA) over 70 h [58]. Other chitosan hydrogels that respond to external changes have

been prepared by grafting with PNIPAAm [59]. This type of gel-forming polymer has recently become increasingly attractive as an injectable hydrogel for the development of therapeutic implants.

Hydrogen bonding interactions can also be used to form physically crosslinked gel-like structures. Mixtures of two or more natural polymers can display rheological synergism, meaning that the viscoelastic properties of the polymer blends are more gel-like than those of the constituent polymers measured individually [60–62]. Blends of, for example, gelatin–agar, starch–carboxymethyl cellulose, and hyaluronic acid–methylcellulose form physically crosslinked gel-like structures that are injectable. Poly(acrylic acid) (PAAc) and poly(methacrylic acid) (PMAAc) form complexes with PEG. These complexes are held together by hydrogen bonds between the oxygen of the PEG and the carboxylic group of PAAc or PMAAc, where hydrophobic interactions also play a role [63]. Hydrogen bonding has also been observed in poly(methacrylic acid-*g*-ethylene glycol) [P(MMc-*g*-EG)] [64]. The hydrogen bonds are only formed when the carboxylic acid groups are protonated. This implies that the swelling of these gels is strongly dependent on the pH. However, hydrogen-bonded networks can dilute and disperse over a few hours owing to the influx of water, restricting their use to relatively short-acting drug release systems [65].

Crystallization of polymers has also been used to form physically crosslinked gels. When aqueous solutions of poly(vinyl alcohol) (PVA) undergo a freeze–thawing process, a strong and highly elastic gel is formed. Gel formation is ascribed to the formation of PVA crystallites that act as physical crosslinking sites in the network [66]. Stenekes et al. [67] have reported the preparation of dextran hydrogels and microspheres based on crystallization. Although dextrans are known to be highly soluble in water, precipitation was observed in concentrated aqueous solutions of low-molecular-weight dextran. The precipitation process was accelerated by stirring and by the presence of salts. The precipitates were insoluble in water at room temperature, but readily dissolved in boiling water or dimethyl sulfoxide (DMSO).

A novel hydrogel concept based on the self-assembly of a stereocomplex formation has been reported (Fig. 2.2c). The ability of PLA to form stereocomplexes was first described by Tsuji et al. [68]. In general, stereocomplex formation occurs in, for example, PLLA and PDLA. To create hydrogels crosslinked by stereocomplex formation, enantiomeric lactic acid oligomers were coupled to dextran [69]. In recent years, hydrogels have been described for drug delivery systems based on stereocomplex formation. In blends of triblock copolymers of PLLA–PEG–PLLA and PDLA–PEG–PDLA, stereocomplex formation occurs. The release of bovine serum albumin (BSA) from microspheres based on these triblock copolymers has been studied by Lim and Park [70]. The major advantage of this system is that a hydrogel was easily formed upon dissolving each product in water and mixing the solution. One significant limitation of stereocomplexation is, however, the relatively restricted range of polymer compositions that can be used.

The ubiquitous noncovalent interactions in biological systems are also being used to generate hydrogels with unique, dynamic functions [71]. Biological systems are dominated by noncovalent interactions, which can be defined as intermolecular

interactions, in which there is no change in either chemical bonding or electron pairing [72]. These interactions provide an excellent mechanism for dynamically regulating the assembly and function of biological systems. Petka et al. [8] have created hydrogels based on the "leucine zipper" motif. The formation of coiled-coil aggregates of the terminal domains in near-neutral aqueous solutions triggers the formation of a three-dimensional polymer network, with the polyelectrolyte segment retaining solvent and preventing precipitation of the chain. Dissociation of the coiled-coil aggregates through the elevation of pH or temperature causes dissolution of the gel and a return to the viscous behavior that is characteristic of polymer solutions. Another distinctive quality of proteins has been used to design proteins that self-assemble into fibers. In a particularly well-characterized example, repeating strands of β-sheet-forming peptides are used to drive the stacking assembly of amyloid-like nanofibers [73]. In addition, heterodimeric proteins with subunits that interact with one another via specific hetero-subunit interactions [74, 75] have been designed to assemble into two-dimensional protein filaments of less than 100 nm in diameter. Cappello et al. [76, 77] prepared sequential block copolymers containing a repetition of silk-like and elastine-like blocks, in which the insoluble silk-like segments are associated in the form of aligned hydrogen-bonded beta strands or sheets. Stewart et al. [9, 78] investigated natural and engineered proteins that show coiled-coil interactions and used the mas crosslinkers for poly(*N*-(2-hydroxypropyl)methacrylamide) (PHPMA) (Fig. 2.2d). One end of the proteins was attached to the polymer backbone by metal complexes between histidine tags and metal-chelating ligands on the polymer. The hydrogel including the natural protein showed a temperature-induced collapse close to the melting temperature of the coiled-coil protein, which was attributed to the change from an elongated rod-like coiled-coil conformation to random coils. Thus, the large number of known protein–protein interactions and the now routine ability to synthesize new proteins or fusion proteins via recombinant DNA technology suggest that noncovalent assembly via protein-domain recognition could become an adaptable synthetic mechanism in bio-nanotechnology.

Gels can be formed by crosslinking interactions that occur upon antigen–antibody binding. Miyata et al. [79] prepared such a hydrogel by grafting the antigen and corresponding antibody to the polymer network, so that binding between the two introduces crosslinks in the network (Fig. 2.2e). Competitive binding of the free antigen triggers a change in gel volume owing to the breaking of these noncovalent crosslinks. Reversible swelling/shrinking was observed upon alternating exposure of the hydrogel to antigen-containing and antigen-free solutions. In addition, hydrogel membranes displaying on/off switching behavior with respect to protein permeation through the membranes were prepared, suggesting that this approach might permit drug delivery in response to a specific antigen. A highly specific interaction between glucose and Concanavalin A (Con A) has also been used to form crosslinks between glucose-containing polymer chains. Since Con A exists as a tetramer at physiological pH and each subunit has a glucose binding site, Con A can function as a crosslinking agent for glucose-containing polymer chains. Because of the noncovalent interaction between glucose and Con A, the formed crosslinks are reversible [80–82].

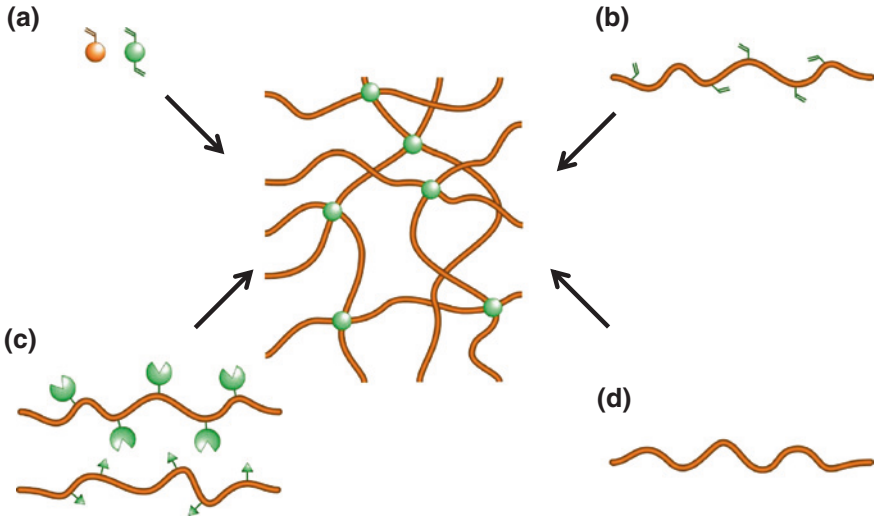


**Fig. 2.3** Schematic of methods for formation of chemically crosslinked hydrogels by radical polymerization of **a** vinyl monomers and **b** macromonomers **c** reaction of pendant functional groups, and **d** high-energy radiation

### *2.2.2 Chemically Crosslinked Hydrogels*

While physically crosslinked hydrogels have the general advantages of forming gels without the need for chemical modification or the addition of crosslinking entities, they also have limitations. It is difficult to decouple variables such as gelation time, network pore size, chemical functionalization, and degradation time; this restricts the design flexibility of a physically crosslinked hydrogel because its strength is directly related to the chemical properties of the constituent gelators. In contrast, chemical crosslinking results in a network with a relatively high mechanical strength and, depending on the nature of the chemical bonds in the building blocks and the crosslinks, relatively long degradation times. Chemically crosslinked gels are also mechanically stable owing to the covalent bond in these gels. Chemically crosslinked gels can be obtained by radical polymerization of low-molecular-weight monomers in the presence of a crosslinking agent (Fig. 2.3a). One of the most widely used methods for the preparation of NIPAAm-based hydrogels is a redox polymerization using ammonium persulphate (APS) as an initiator and *N, N, N′, N′*-tetramethylethylenediamine (TEMED) as a catalyst. TEMED accelerates the rate of formation of free radicals from persulfate, and these in turn catalyze polymerization. The persulfate free radicals convert monomers to free radicals that react with unactivated monomers to begin the polymerization chain reaction. The elongating polymer chains are randomly crosslinked by a crosslinker, resulting in a gel with a characteristic formulation that depends on such parameters as the polymerization conditions and monomer/

crosslinker concentrations. This is a very efficient system that results in the rapid formation of the gel even under mild conditions. Moreover, stimuli-responsive hydrogels can be easily obtained by copolymerization with, for example, NIPAAm or AAc. A great variety of smart hydrogels have been synthesized by this procedure [41, 79, 83–85]. However, unreacted peroxydisulfate and TEMED as well as their degradation products must be extracted from the gel before in vivo application. Moreover, this initiator system can also damage proteins once they are present during the preparation of the gels. In particular, methionine residues of the protein can be oxidized [86].

Aside from radical polymerization of mixtures of vinyl monomers, chemically crosslinked hydrogels can also be obtained by radical polymerization of polymers derivatized with polymerizable groups (macromonomer) (Fig. 2.3b). (Meth) acrylate groups can be introduced in water-soluble polymers using, for example (meth)acryloyl chloride, methacrylic anhydride, and bromoacetyl bromide. Moreover (meth)acrylic groups have been introduced in mono- and disaccharides, which can be used for the synthesis of hydrogels [87]. A hydrogel is formed after the addition of an APS/TEMED initiator system to an aqueous solution of the methacryl-dextran-containing *N, N′*-methylene-bis-acrylamide (MBAAm). Water-soluble polymers other than dextran, namely, albumin [88] (hydroxyethyl)starch [89], poly-aspartamide [90], poly(vinyl alcohol) [91] and hyaluronic acid [92], have also been derivatized with (meth)acrylic groups. In recent years, UV-induced polymerization has been frequently used to prepare hydrogels [93–96]. Moreover, with UV-induced polymerization, patterned structures can be prepared. It should be noted that when the UV polymerization is carried out in the presence of a drug, the network structure might be affected [97]. Moreover, the type of photo initiator as well as the solvent in which it is dissolved should be selected with care, since they may leak out from the formed hydrogel. Finally, once the polymerization is carried out in the presence of a protein, the potential damage of the radicals formed on the protein structure should be assessed [98].

If polymers have pendant functional groups (e.g., OH, COOH, and $NH_2$), covalent linkages between polymer chains can be established by the reaction of functional groups with complementary reactivity such as an amine-carboxylic acid or an isocyanate-OH/$NH_2$ reaction, or by Schiff base formation (Fig. 2.3c). For example, water-soluble polymers with hydroxyl groups can be crosslinked using glutaraldehyde [99, 100]. Amine-containing polymers can be crosslinked with the same reagent under mild conditions whereby so-called Schiff bases are formed. This has been investigated particularly for the preparation of crosslinked proteins [101, 102]. Because glutaraldehyde is a toxic compound that even at low concentration shows cell growth inhibition, alternatives have been developed. Crosslinking of gelatin using polyaldehydes obtained by partial oxidation of dextran has been reported [103]. Lee et al. [104] have reported crosslinking of poly(aldehyde guluronate) (PAG)with adipic acid dihydrazide. When an antineoplastic agent, daunomycin, was present during the hydrogel formation process, the drug was grafted onto the polymer matrix through a covalent linkage. Owing to the hydrolysis of this linkage, daunomycin was released in a time frame

of 2 days to 6 weeks [105]. Hyaluronic acid hydrogels were also obtained by the derivatization of hyaluronic acid with adipic dihydrazide followed by crosslinking with a macromolecular crosslinker. These gels are enzymatically degradable with hyaluronidase and therefore have the potential to act as a delivery matrix for sustained release of drugs at wound sites [106]. Water-soluble polymers can also be converted into hydrogels via addition reactions. For example, polysaccharides can be crosslinked with 1, 6-hexamethylenediisocyanate [107], divinyl sulfone [108], or 1, 6-hexane dibromide [109] and many other reagents. The network properties can be easily tailored by adjusting the concentration of the dissolved polymer and the amount of crosslinking agent. However, the crosslinking reactions are preferably carried out in organic solvents, because water can also react with the crosslinking agent. Furthermore, since the crosslinking agents are toxic, the gels must be extracted extensively to remove traces of unreacted agents.

Condensation reactions between hydroxyl groups or amines with carboxylic acids or derivatives are frequently applied to the synthesis of polymers to yield polyesters and polyamides, respectively. These reactions can also be used for the preparation of hydrogels. A very efficient reagent to crosslink water-soluble polymers with amide bonds is *N, N*-(3-dimethylaminopropyl)-*N*-ethyl carbodiimide (EDC). Kuijpers et al. [110] described the preparation of gelatin hydrogels using this reagent. During the reaction, *N*-hydroxysuccinimide (NHS) is added to suppress possible side reactions and to have better control over the crosslink density of the gels. Eiselt et al. [111] developed a method to covalently crosslink alginate and PEG-diamines using EDC in order to obtain alginate gels with better mechanical properties than the ionically crosslinked gels. The mechanical properties could be controlled by adjusting the amount of PEG-diamine in the gel and the molecular weight of PEG. de Nooy et al. [112, 113] have described the synthesis of polysaccharide hydrogels via the Passerini and Ugi condensation reactions. In the Passerini condensation, a carboxylic acid and an aldehyde or ketone are condensed with an isocyanide to yield an α-(acryloxy)amide. In the Ugi condensation, an amine is added to this reaction mixture, finally yielding an α-(acylamino) amide. The reaction canbe carried out in water at slightly acidic pH and at room temperature. Since the Passerini condensation yields hydrogels with ester bonds in their crosslinks, these gels degrade at ambient temperature and pH 9.5. Since gels prepared using the Ugi condensation contain amide bonds in their crosslinks, these gels were stable under these conditions. Yoshida et al. [114] have prepared temperature-responsive hydrogels using NIPAAm copolymers with poly(amino acid)s as a side-chain group and activated ester groups. The hydrogels easily crosslinked with the degradable poly(amino acid) chains upon merely mixing the copolymer aqueous solutions (Fig. 2.4).

A novel hydrogel concept based on enzymatic reaction has also been reported. A tetrahydroxy PEG was functionalized with glutaminyl groups (PEG-Qa). PEG networks were then formed by the addition of transglutaminase to aqueous solutions of PEG-Qa and poly(lysine-*co*-phenylalanine) [115]. This enzyme catalyzes the reaction between the γ-carboxamide group of the PEG-Qa and the ε-amine group of lysine to yield an amide linkage between the polymers. Poly(lysine-co-phenylalanine) was also replaced by lysine end-functionalized PEG, and

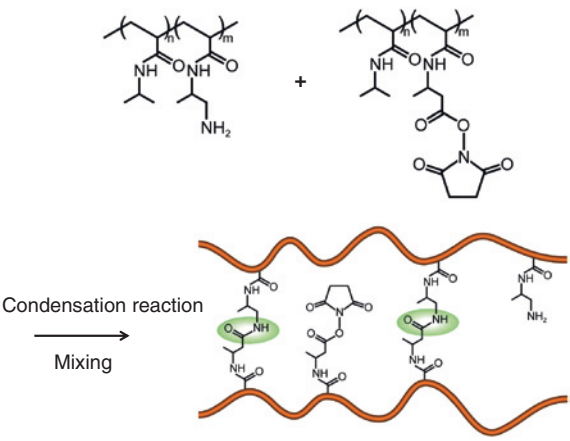


**Fig. 2.4** Preparation of a temperature-responsive hydrogel crosslinked with biodegradable poly(amino acid) chains via condensation reaction [114]

hydrogels were formed once transglutaminase was added to an aqueous solution of peptide-modified macromers [116].

High-energy radiation, such as gamma (γ) and electron beam radiation, can be used to polymerize unsaturated compounds (Fig. 2.3d). On exposure to γ or electron beam radiation, aqueous solutions of polymers form radicals on the polymer chains (e.g., by the hemolytic scission of C–H bonds). Also, the radiolysis of water molecules generates the formation of hydroxyl groups that can attack polymer chains, again resulting in the formation of microradicals. Recombination of these microradicals on different chains results in the formation of covalent bonds and finally in a crosslinked structure. PVA [117], PEG [118], and PAAc [119] are well-known examples of polymers that can be crosslinked with high-energy irradiation. The swelling and permeability characteristics of the gel depend on the extent of polymerization as a function of polymer and radiation dose (in general, crosslinking density increases with increasing radiation dose). Hirasa et al. [120, 121] have reported on fast-response, temperature-sensitive poly(viny1 methyl ether) (PVME) and PNIPAAm hydrogels prepared by γ-ray irradiation [122]. The structure of PVME hydrogels is dependent on the intensity of the γ-rays and the temperature during irradiation. When the radiation intensity is lower than 1.5 kGy $h^{-1}$, the temperature of the PVME solution does not change at room temperature during irradiation. Under this condition, PVME was crosslinked below LCST; therefore, a transparent gel with a homogeneous and dense structure was formed. On the other hand, the temperature of the PVME solution was increased by exposure to radiation of high intensity (9.8 kGy $h^{-1}$). At this position, an opaque gel with a heterogeneous and microporous structure was formed. This gel had a large surface area for its volume, and swelled and shrank very quickly upon changing the temperature. The author's group has designed photo-crosslinkable NIPAAm copolymers with a UV-reactive benzophenone (BP) conjugated comonomer [31, 123]. The photo-crosslinking was carried out by making use of the photo chemistry of the BP groups, the photochemically produced triplet state of which can abstract hydrogen atoms from almost any polymer, thus generating radicals (Fig. 2.5). In general, BP is excited indirectly to the lowest triplet state (π–π*) by direct absorption into the

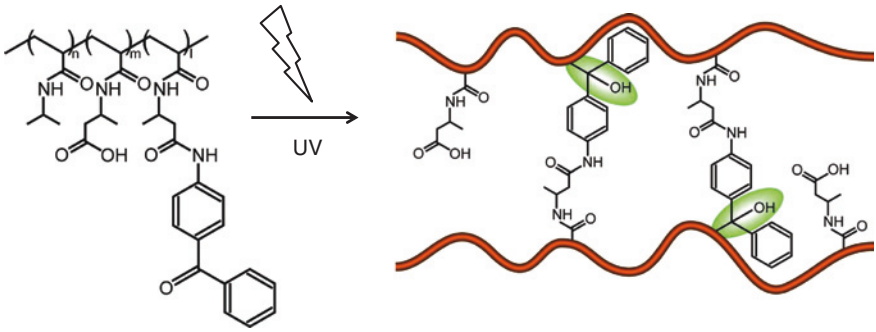


**Fig. 2.5** Photo-crosslinking of UV-reactive benzophenone conjugated temperature-responsive copolymer [31, 123]

singlet state ($\pi$–$\pi^*$) upon irradiation with UV light. The BP ketyl radical and an on-chain polymer radical readily recombine to generate a new C–C bond, thereby resulting in crosslinking within the polymer networks. The advantage of using this process for gel formation is that it can be carried out in water under mild conditions without the use of a crosslinking agent. However, there are some drawbacks to using this method; the bioactive material must be loaded after gel formation, as irradiation might damage the agent. Also, in some gels such as PEG and PVA, the crosslinks consist of C–C bonds, which are not biodegradable.

## 2.3 Classification on the Basis of Stimuli

Smart hydrogels could be further classified as either physical- or chemical-stimuli-responsive hydrogels. The physical stimuli, such as temperature, electric or magnetic fields, and mechanical stress, will affect the level of various energy sources and alter molecular interactions at critical onset points (Fig. 2.6). Chemical stimuli, such as pH, ionic factors and chemical agents, will change the interactions between polymer chains or between polymer chains and solvent at the molecular level. Recently, biochemical stimuli have been considered as another category that involves the responses to antigen, enzyme, ligand, and other biochemical agents. Some systems have been developed to combine two stimuli-responsive mechanisms into one polymer system, the so-called dual-responsive polymer systems.

### *2.3.1 Physical Stimuli*

Temperature-responsive hydrogels are probably the most commonly studied class of environmentally sensitive polymer systems. Temperature-responsive hydrogels can be classified as positive or negative temperature-responsive systems.

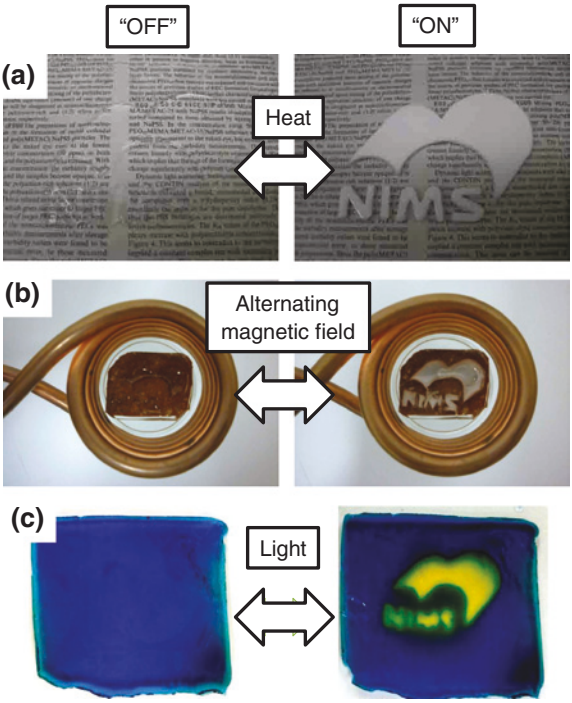


**Fig. 2.6** Photographs of **a** temperature- **b** alternating-magnetic-field-, and **c** photoresponsive hydrogels

Physically crosslinked thermosensitive hydrogels may undergo sol–gel phase transitions instead of volume change at a critical solution temperature. Positive temperature-responsive hydrogels show phase transition at a critical temperature called the upper critical solution temperature (UCST). Hydrogels made from polymers with UCST shrink when cooled below their UCST. Negative temperature-responsive hydrogels have a lower critical solution temperature (LCST). These hydrogels shrink upon heating at above their LCST (see Chap. 1). Chemically crosslinked thermosensitive hydrogels undergo volume change rather than sol–gel transitions. Certain molecular interactions, such as hydrophobic associations and hydrogen bonds, play a vital role in the abrupt volume change of these hydrogels at the critical solution temperature. In the swollen state, water molecules form hydrogen bonds with polar groups of polymer backbone within the hydrogels and organize around hydrophobic groups as iceberg water. At the critical solution temperature, hydrogen bonding between the polymer and water, compared with polymer–polymer and water–water interactions, becomes unfavorable. This forces the quick dehydration of the system and water is released out of the hydrogel with a large gain in entropy, resulting in shrinkage of the polymeric structure. Of the many temperature-responsive polymers, PNIPAAm is probably the most extensively used because its LCST is close to body temperature. Copolymers of NIPAAm can also be made using other monomers to alter the LCST.

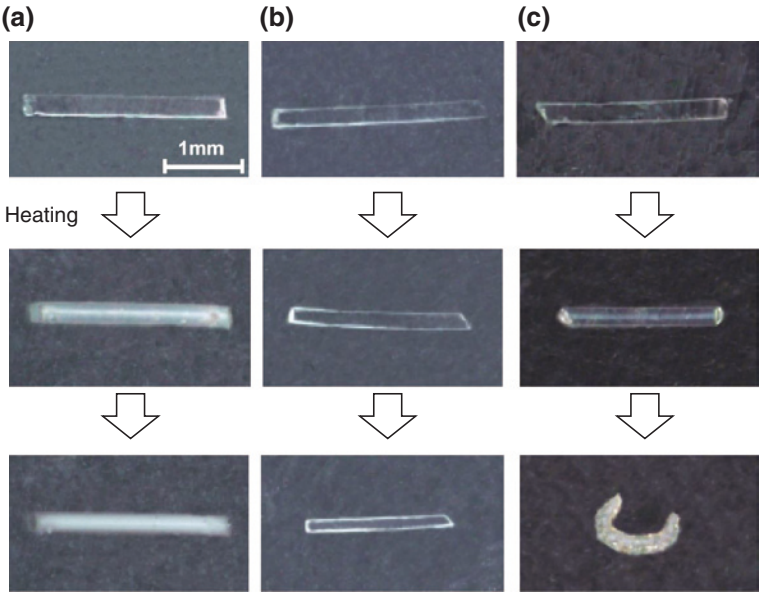


**Fig. 2.7** Photographs of shrinking behaviors of **a** PNIPAAm, **b** P(NIPAAm-*co*-AAc), and **c** P(NIPAAm-*co*-CIPAAm) hydrogels after temperature change from 10 to 40 °C [128]

In general, the sudden temperature changes from below to above the transition temperature lead to the formation of dense and less permeable surface skin layers on PNIPAAm gels [124]. The PNIPAAm gel changes from transparent to opaque after temperature change (Fig. 2.7a). To accelerate gel shrinkage, the introduction of hydrophilic molecules such as AAc into gels is one promising strategy (Fig. 2.7b). However, random introduction of a large amount of hydrophilic monomers into PNIPAAm hydrogels without compromising their intrinsic temperature sensitivity has proven difficult [125]. To overcome this, the authors have synthesized a new 2-carboxyisopropylacrylamide (CIPAAm) with structural similarity to NIPAAm side chains but also including a carboxylate group [126]. NIPAAm-CIPAAm hydrogels exhibited large and sensitive volume phase transitions in response to temperature changes even though carboxylate groups in CIPAAm exist in dissociated states at pH 7.4 [40, 127]. Initially transparent gels turned opaque upon heating from 10 to 40 °C owing to skin layer formation at the gel surface (Fig. 2.7c). However, gel shrinking was not stopped, regardless of the skin layer formation, owing to the sufficient hydrophilic carboxylate content allowing water movement [128]. Therefore, maintaining the isopropylamide side chain alignment within the copolymer chains may facilitate the introduction of large amounts of functional groups into NIPAAm copolymer gels without losing phase transition behavior. The new monomer, CIPAAm, should prove useful in introducing functional carboxyl groups into temperature-responsive PNIPAAm hydrogels while

maintaining their intrinsic temperature-sensitive behavior. Certain types of block copolymers made of poly(ethylene oxide)(PEO) and poly(propylene oxide) (PPO) also possess an inverse temperature-sensitive property. Because of their LCST at around body temperature, they have been used widely in the development of controlled drug delivery systems based on the sol–gel phase conversion at body temperature. A large number of PEO–PPO block copolymers are commercially available under the names of Pluronics® (or Poloxamers®) and Tetronics® [50]. Temperature-sensitive hydrogels can also be made using temperature-sensitive crosslinking agents. A hybrid hydrogel system was assembled from water-soluble synthetic polymers and a well-defined protein-folding motif, the coiled coil [9]. The hydrogel under went temperature-induced collapse owing to the cooperative conformational transition. Using temperature-sensitive crosslinking agents adds a new dimension in designing temperature-sensitive hydrogels.

Photoresponsive hydrogels have been used in a number of biotechnologyapplications, such as photocontrolled enzymatic bioprocessing [129], phototriggered targeted drug delivery systems [130], and photocontrolled separation/recovery systems in bioMEMs formats. Since the light stimulus can be imposed instantly and delivered in specific amounts with high accuracy, light-sensitive hydrogels may possess special advantages over others [131]. For example, the sensitivity of temperature-sensitive hydrogels is rate limited by thermal diffusion, while pH-sensitive hydrogels can be limited by hydrogen ion diffusion. The capacity for instantaneous delivery of the sol–gel stimulus makes the development of light-sensitive hydrogels important for various applications in both engineering and biochemical fields. Photoresponsive hydrogels can be separated into UV-sensitive and visible-light-sensitive hydrogels. Unlike UV light, visible light is readily available, inexpensive, safe, clean and easily manipulated. Typical photoreactive guests in polymersare azobenzene [132], triphenylmethane [133] and spiropyran [134] groups, which have been entrapped, crosslinked, and introduced as side chains or part of the main chain in polymermatrices. The UV-sensitive hydrogels were synthesized by introducing a leuco derivative molecule, bis(4-dimethylamino)phe nylmethylleucocyanide, into the polymer network [133]. Triphenylmethane leuco derivatives are normally neutral but dissociate into ion pairs under ultraviolet irradiation, producing triphenylmethyl cations. Because the leuco derivative molecule can be ionized upon ultraviolet irradiation, the UV-light-induced swelling was observed owing to an increase in osmotic pressure within the gel. Sumaru et al. [134] have prepared a photo responsive hydrogel by radical copolymerization of NIPAAm, a vinyl monomer having a spirobenzopyran residue, and a crosslinker. It was observed that the permeability for a 1 mM HCl aqueous solution increased twofold in response to the blue light irradiation, and this photo response of the permeability was confirmed to be repeatable. Takashima et al. [135] have designed a photo responsive supramolecular actuator by integrating host–guest interactions and photoswitching ability in a hydrogel. A photoresponsive supramolecular hydrogel with α-cyclodextrin as a host molecule and an azobenzene derivative as a photoresponsive guest molecule exhibits reversible macroscopic deformations

in both size and shape when irradiated by ultraviolet light at 365 nm or visible light at 430 nm. The deformation of the supramolecular hydrogel depends on the incident direction. The selectivity of the incident direction allows plate-shaped hydrogels to bend in water. Irradiating with visible light immediately restores the deformed hydrogel. A light-driven supramolecular actuator with α-cyclodextrin and azobenzene stems from the formation and dissociation of an inclusion complex by ultraviolet or visible light irradiation. Visible-light-sensitive hydrogels can also be prepared by introducing alight-sensitive chromophore (e.g., trisodium salt of copper chlorophyllin) to NIPAAm hydrogels [136]. When light (e.g., 488 nm) is applied to the hydrogel, it is absorbed by the chromophore, and then dissipated locally as heat by radiationless transitions, increasing the 'local' temperature of the hydrogel. The temperature increase alters the swelling behavior of NIPAAm hydrogels. The authors have integrated a photoinitiated proton-releasing reaction of *o*-nitrobenzaldehyde (NBA) into pH-responsive hydrogels [137]. NBA-integrated hydrogels demonstrated quick release of protons upon UV irradiation, allowing the pH inside the gel to decrease below the p$K_a$ of the polymer within one minute. Spatial control of gel shrinkage was also made possible by irradiating UV light to a limited region of the gel through a photomask.

Electric current can also be used as an environmental signal to induceresponses of hydrogels. Hydrogels sensitive to electric current are usually made of polyelectrolytes, as are pH-sensitive hydrogels. Electrosensitive hydrogels undergo shrinking or swelling in the presence of an applied electric field. Sometimes, the hydrogels show swelling on one side and shrinking on the other side, resulting in the bending of the hydrogels. Osadaand and Hasebe [138] reported an electrically activated artificial muscle system that is contracted by an electrical stimulus under isothermal conditions. They reported that the addition of NaCl increased the rate of water release, whereas the addition of organic solvents such as ethanol, acetone, or water reduced the rate of water release, and the contraction that resulted from the electrostatic interaction between charged macromolecules and the electrodes led to extensive dehydration of the gel. Tanaka et al. [139] studied the effect of electric current on the contraction behavior of partially hydrolyzed polyacrylamide gels in a mixture of 50 % acetone and water. They observed that the contraction was most significant and rapid in water, whereas with increasing acetone percentage, the rate of contraction decreased gradually.

The concept that hydrogels may undergo pressure-induced volume phase transition originates from thermodynamic calculations based on the uncharged hydrogel theory. According to the theory, hydrogels that are collapsed at low pressure would expand at higher pressure. Experiments with PNIPAAm hydrogels confirmed this prediction [140]. The effect of hydrostatic pressure on the swelling of temperature-sensitive gels has also been studied by measuring the volume change of the beads of PNIPAAm gel, poly(*N*-n-propylacrylamide) gel, and poly(*N, N*-diethylacrylamide) gel under pressure up to 120 atm [141]. The excess enthalpy and excess volume of the gel-water systems during the volume phasetransition of the gels were measured. The degree of swelling of hydrogels increased under hydrostatic pressure when the temperature was close to its LCST.

### 2.3.2 Chemical Stimuli

While physical stimuli are advantageous because they allow local and remote control, they result in a discontinuous response when the stimulus is turned 'off'. In other words, only the illuminated region is active, and continuous illumination is necessary. In the human body, however, the appearance of numerous bioactive molecules is tightly controlled to maintain a normal metabolic balance via the feedback system called homeostasis. For example, hormones or cytokines not only act locally (local signals), but also travel to other locations in the body via blood circulation (remote signals) [142]. These signals are sometimes amplified or transferred to another signal by sequentially interacting with many other different molecules. A representative process is blood coagulation, which is a complex sequence involving numerous clotting factors. The concentration gradients of protons (pH), ions, and oxidizing or reducing agents are also important characteristics observed in living systems. The human body exhibits variations in pH along the gastrointestinal tract, tumoral areas, inflamed or infected tissues, and the endosomal lumen.

pH-responsive hydrogels are made of polymeric backbones with ionic pendant groups that can accept or donate protons in response to an environmental pH change. As the environmental pH changes, the degree of ionization in a pH-responsive hydrogel is dramatically changed at a specific pH known as $pK_a$ or $pK_b$. This rapid change in the net charge of ionized pendant groups causes abrupt volume transition by generating electrostatic repulsive forces between ionized groups, which creates a large osmotic swelling force. There are two types of pH-responsive hydrogels: anionic and cationic hydrogels. Poly(acrylic acid) (PAAc) becomes ionized at high pH, where as poly(*N, N′*-diethylaminoethyl methacrylate) (PDEAEM) becomes ionized at low pH. pH-sensitive hydrogels have been most frequently used to develop controlled release formulations for oral administration. The pH inthe stomach (<3) is quite different from the neutral pH in the intestine, and such a difference is large enough to elicit pH-dependent behavior of polyelectrolyte hydrogels. Hydrogels made of PAAc or PMAAc can be used to develop formulations that release drugs in a neutral pH environment [143]. Hydrogels made of polyanions (e.g., PAA) were developed for colon-specific drug delivery. Swelling of such hydrogels in the stomach is minimal, and thus, the drug release is also minimal. The extent of swelling increases as the hydrogel passes down the intestinal tract owing to the increase in pH leading to the ionization of the carboxylic groups. However, only in the colon can the azoaromatic crosslinks of the hydrogels be degraded by azoreductase produced by the microbial flora of the colon [144]. On the other hand, when a drug is loaded into hydrogels made of copolymers of MMA and *N, N′*-dimethylaminoethyl methacrylate (DMAEM), it is released at zero order at pH 3–5, but not released at neutral pH [145]. The lower extracellular pH of solid tumors has also been exploited in many therapeutic strategies based on drug delivery [146]. These extra cellular microenvironments have an acidic pH primarily because of the accumulation of excess lactic acid, which

is produced because of the high rate of glycolysis in tumor microenvironments [147]. Some other pathologic tissues, such as ischemic or infected sites, are also more acidic than normal tissues. In addition, the pH values of endosomal and lysosomal vesicles inside cells are lower than that of the cytosol, and this difference has been utilized for intracellular delivery [148]. Garbern et al. [149] have reported the use of pH- and temperature-responsive injectable hydrogels, synthesized from copolymers of NIPAAm and propylacrylic acid (PAAc), for delivering drugs to regions of local acidosis. P(NIPAAm-co-PAA) exhibits a sharp transition near body temperature, as indicated by its LCST in the pH range of 5–6. This system undergoes reversible gelation at moderately acidic pH values (~pH 5–6), but remains soluble at normal physiological pH (7.4). In general, the incorporation of carboxylic acid-derived monomers, such as AAc or MAAc, results in low p$K_a$ values, which limit the use of these polymers for drug targeting to very low pH systems, such as the stomach. Because PAA polymers can also destabilize membranes in the endosome, this pH-responsive system has been shown to enhance the cytosolic delivery of nucleic acids [150], anticancer drugs [151], and an internalizing antibody [152].

Glucose-sensitive hydrogels have also been developed by many researchers because one of the most challenging problems in controlled drug delivery is the development of self-regulated (modulated) insulin delivery systems. The delivery of insulin is different from the delivery of other drugs, since insulin must be delivered in an exact amount at the exact time of need. Thus, self-regulated insulin delivery systems require glucose-sensing ability and an automatic shut-off mechanism. Many hydrogel systems have been developed for modulating insulin delivery, and all of them have a glucose sensor built into the system. Con A has been frequently used in modulated insulin delivery [82]. In this type of system, insulin molecules are attached to a support or carrier through specific interactions that can be interrupted by glucose itself. This generally requires the introduction of functional groups onto insulin molecules. In one approach, insulin was chemically modified to introduce glucose, which binds particularly to Con A [153]. Glucose-sensitive phase-reversible hydrogels can also be prepared without using Con A. Kataoka and coworkers have developed a self-regulated insulin delivery system using phenylboronic acid (PBA), a synthetic molecule capable of reversibly binding with 1, 2- or 1, 3-cis-diols including glucose [16, 154–156]. PBA and its derivatives are known to form covalent complexes with polyol compounds including glucose (Fig. 2.8). The glucose-dependent shift in the equilibrium of PBA between the uncharged and anionically charged forms, when coupled with a properly amphiphilic three-dimensional backbone (or gel), could induce a reversible change in the volume of the gel. The resultant rapid change in hydration under certain conditions could cause a localized dehydration of the gel surface, that is, the so-called skin layer, thus offering a method for instantly controlling the permeation of gel-loaded insulin.

For some biomedical applications, it is highly desirable and useful to develop a material or device that can respond to specific proteins such as antigens [157]. The concept is the same as that used in glucose-sensitive phase-reversible hydrogels. A

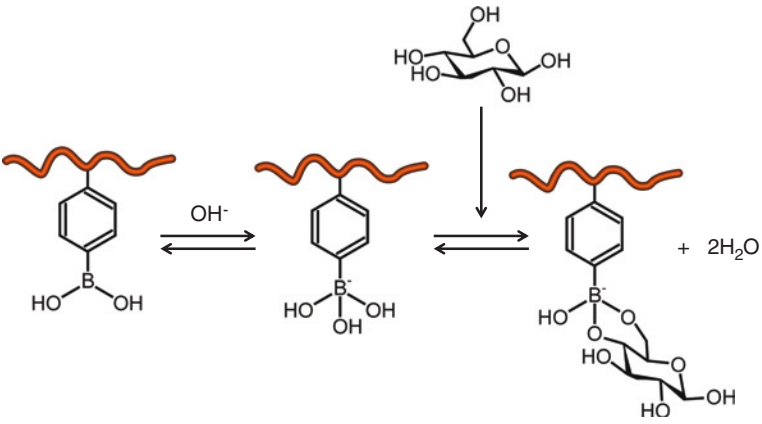


**Fig. 2.8** Glucose-dependent equilibria of phenylboronic acid [16, 154–156]

semi-interpenetrating network hydrogel was prepared by grafting an antigen and a corresponding antibody to different polymer networks [79]. The gel is formed by crosslinking interactions that occur upon antigen–antibody binding. Hydrogel swelling is triggered in the presence of free antigens that compete with the polymer-bound antigen, leading to a reduction in the crosslinking density. Suzuki et al. [158] reported thrombin-induced infection-responsive hydrogels for the controlled release of antibiotics at the site and time of infection. PVA hydrogels loaded with grafted gentamycin were prepared. Gentamycin was chemically attached to the polymer backbone through peptide linkers that can be enzymatically degraded by thrombin. Exudates from the dorsal pouch of rats infected by *Pseudomonas aeruginosa* showed significantly higher thrombin like enzymatic activity toward a certain peptide sequence than exudates from noninfected wounds. DNA-responsive hydrogels have also been reported to be capable of swelling and shrinking in response to specific DNAs [159, 160].

Yoshida and coworkers have demonstrated an autonomic swelling-shrinking oscillation by integrating the chemical oscillation of the Belousov–Zhabotinsky (BZ) reaction into the hydrogel [161–163]. The BZ reaction is often analogically compared with the TCA cycle, which is a key metabolic process taking place in the living body. The over all process of the BZ reaction is the oxidation of anorganic substrate, such as malonic acid (MA) or citric acid, by an oxidizing agent (bromateion) in the presence of a strong acid and a metal catalyst. A copolymer gel that consists of NIPAAm and ruthenium tris(2, 2′-bipyridine) ($Ru(bpy)_3^{2+}$) was prepared. The $Ru(bpy)_3^{2+}$, acting as a catalyst for the BZ reaction, was appended to the polymer chains of NIPAAm. The poly(NIPAAm-*co*- $Ru(bpy)_3^{2+}$) gels have a phase transition temperature owing to the thermosensitive constituent NIPAAm. They have further demonstrated a novel biomimetic ‘self-walking’ gel actuator that can walk spontaneously with a worm like motion without switching of external stimuli [23].

## 2.4 Characterization Methods

A variety of techniques for characterizing hydrogels have been reported in the literature. The physical behavior of hydrogels is dependent on their equilibrium and dynamic swelling behavior in water, since upon preparation, they must be brought into contact with water to yield the final, swollen network structure. The most important parameters that define the structure and properties of swollen hydrogels are the polymer volume fraction in the swollen state, the effective molecular weight of the polymer chain between crosslinking points, and the correlation distance between two adjacent crosslinks [164, 165]. Rubber-elasticity theory and equilibrium-swelling theory are extensively applied to describe these three dependent parameters. The theoretical basis for the understanding of polymer solutions was developed independently by Flory [166] and Huggins [167] 70 years ago. Hydrogels have a variety of properties, such as absorption capacity, swelling behavior, permeability, surface properties, optical properties and mechanical properties, which make them promising materials for a wide variety of applications. The characteristics of the polymer chains and the crosslinking structures in these aqueous solutions play an important role in the outcome of the properties of the hydrogel.

### *2.4.1 Water in Hydrogels*

When a dry hydrogel begins to absorb water, the first water molecules entering the matrix will hydrate the most polar, hydrophilic groups, leading to ‘primary bound water’. As the polar groups are hydrated, the network swells and exposes hydrophobic groups, which also interact with water molecules, leading to hydrophobically bound water or ‘secondary bound water’. Primary and secondary bound water are often combined and simply called ‘total bound water’. After the water has interacted with both hydrophilic and hydrophobic sites, the osmotic driving force of the network chains allows the network to absorb more water. Finally, the balance between the retraction force and the infinite dilution force establishes an equilibrium swelling level. The additional water absorbed beyond the total bound water is defined as ‘free water’ or ‘bulk water’ [21]. There are a number of methods for estimating the relative amounts of free and bound water, as fractions of the total water content. The use of small molecular probes, DSC, and NMR are the three major methods. When probe molecules are used, the labeled probe solution is equilibrated with the hydrogel, and the concentration of the probe molecule in the gel at equilibrium is measured. The use of DSC is based on the assumption that only the free water may be frozen, so it is assumed that the endotherm measured when warming the frozen gel represents the melting of the free water, and that value will yield the amount of free water in the hydrogel sample being tested.

### 2.4.2 Thermodynamics of Hydrogel Swelling

The physical behavior of hydrogels is dependent on their equilibrium and dynamic swelling behavior in water. The Flory-Huggins theory can be used to calculate the thermodynamic behavior of hydrogel swelling [166, 167]. Considering the isotropic crosslinked structure of hydrogel, the total Gibbs free energy change of the system, upon swelling, can be written as

$$\Delta G = \Delta G_{\text{mixture}} + \Delta G_{\text{elastic}}. \tag{2.1}$$

Here, $\Delta G_{\text{elastic}}$ is the contribution due to the elastic retractive forces and $\Delta G_{\text{mixture}}$ represents the thermodynamic compatibility of the polymer and the swelling agent (water).

In order to express the chemical potential change of water in terms of elastic and mixing contributions at any time of swelling, the differentiating Eq. (2.1) with respect to the water molecules in the system gives

$$\mu_1 - \mu_{1,0} = \Delta\mu_{\text{mixture}} + \Delta\mu_{\text{elastic}}. \tag{2.2}$$

Here, $\mu_1$ is the chemical potential of water within the gel and $\mu_{1,0}$ is the chemical potential of pure water.

At equilibrium, the chemical potentials of water inside and outside of the gel must be equal. Therefore, the elastic and mixing contributions to the chemical potential will balance one another at equilibrium. The change in chemical potential upon mixing can be determined from the heat of mixing and the entropy of mixing. Using the Flory–Huggins theory, the chemical potential of mixing can be expressed as

$$\Delta\mu_{\text{mixture}} = RT(\text{In}(1 - 2v_{2,s}) + v_{2,s} + \chi_1 v_{(2,s)}^2), \tag{2.3}$$

where $\chi_1$ is the polymer–water interaction parameter, $\upsilon_{2,\text{s}}$ is the polymer volume fraction of the gel, $T$ is the absolute temperature, and $R$ is the gas constant.

This thermodynamic swelling contribution is counter balanced by the retractive elastic contribution of the crosslinked structure. The latter is usually described by the rubber elasticity theory and its variations. Equilibrium is attained in a particular solvent at a particular temperature when the two forces become equal. The volume degree of swelling, Q (i.e., the ratio of the actual volume of a sample in the swollen state divided by its volume in the dry state), can then be determined from Eq. (2.4).

$$v_{2,\text{s}} = V_p/V_{gel} = 1/Q \tag{2.4}$$

### 2.4.3 Swelling Ratios

The swelling behavior of hydrogel systems is an important parameter governing their applications specifically in pharmaceutical, ophthalmology and tissue engineering. The polymer chains in a hydrogel interact with the solvent molecule and tend to expand to the fully solvated state, while the crosslinked structure applies

a retractive force to pull the chains inside. Equilibrium is achieved when these expanding and retracting forces counter balance each other. The equilibrium swelling ratio or water content, given by Eq. (2.5), is generally used to describe the swelling behavior of hydrogels.

$$Equilibrium\ swelling\ ratio = W_{swollen}/W_{dry} \tag{2.5}$$

Here, $W_{swollen}$ is the weight of the swollen gel, and $W_{dry}$ is the weight of the dry gel.

The swelling kinetics of hydrogels can also be determined from the swelling kinetic curves. First, the weight of the dry gel ($W_0$) is determined. The dried gel was then immersed in an excess amount of water until the swelling equilibrium was attained. The weight of the wet gel ($W_t$) was determined after the removal of the surface water. The swelling ratio was calculated with the following equation.

$$Swelling\ ratio = (W_t - W_0)/W_0 \tag{2.6}$$

Many groups have investigated the swelling/shrinking kinetics of PNIPAAm gels when the temperature is increased or decreased to above or below the LCST, respectively. For example, Yoshida and coworkers have compared the shrinking kinetics of PNIPAAm gels with different architectures. Comb-type PNIPAAm hydrogels collapsed from a fully swollen state in less than 20 min, whereas similar gels without grafted side chains took more than one month to undergo full shrinking [41, 168]. They also reported a comb-type grafted hydrogel composed of PEO graft chains in the crosslinked PNIPAAm network [125]. The swelling characteristics are crucial to the use of hydrogels in biomedical and pharmaceutical applications since the equilibrium swelling ratio affects the solute diffusion coefficient, surface wettability and mobility and optical and mechanical properties of the hydrogel. The swelling properties are determined by many factors, including the type and composition of monomers, crosslinking density and other environmental factors such as temperature, pH and ionic strength.

### *2.4.4 Mechanical Properties*

The mechanical properties of hydrogels depend on their composition and structure [169]. Generally speaking, the polymer gels are very weak, i.e., gels are soft and brittle, and the gel cannot with stand large deformation. This is mainly due to the fact that gels are far from fully connected polymer networks and contain various types of inhomogeneities, such as dangling chains and loops. Biopolymers, such as gelatin gels and polysaccharides, have been extensively investigated because of their variety of applications in products such as cosmetics and foods. The mechanical performance of conventional hydrogels can be expressed as elastic modulus. The elastic modulus can range from kPa to MPa, e.g., gelatin gel and agarose. The mechanical properties of these gels, however, have been mostly evaluated by shearing or compression, not by stretching, because of poor deformability.

Chemical gels, made via the copolymerization of a monomer in the presence of a crosslinker or by crosslinking of polymer chains, are also mechanically weak. The mechanical properties of the hydrogel are affected by the comonomer composition, crosslinking density, polymerization conditions and degree of swelling. The mechanical strength of the hydrogel is often derived entirely from the crosslinks in the system, particularly in the swollen state where physical entanglements are almost nonexistent. The dependence of mechanical properties on crosslink density has been studied intensively by many researchers. However, it should be noted that when the crosslinking density is altered, changes in properties other than strength also occur. Recently, new types of gels capable of large deformation have been developed. Okumura and Ito [170] developed a slide-ring (SR) gel (also called topological gel) by crosslinking polyrotaxane, which consists of PEG threaded through a ring molecule of cyclodextrin (CD). Because CDs are not covalently bonded to the axis polymer, the crosslinks can slide along the axial chain, and thus, the SR gels show unique mechanical and swelling properties. Gong et al. [171] have succeeded in creating double-network (DN) gels, which exhibit toughness and very large energy dissipation. For example, a DN composed of two mechanically weak hydrophilic networks, poly(2-acrylamido-2-methylpropanesulfonic acid) and polyacrylamide, provides a hydrogel with outstanding mechanical properties. Hydrogels containing about 90 % water possessed an elastic modulus of 0.3 MPa and fracture stress of ~10 MPa, demonstrating both hardness and toughness. This was explained by the effective relaxation of locally applied stress and the dissipation of crack energy through a combination of the different structures and densities of the two networks.

Many experimental methods were previously employed to characterize the mechanical properties, mainly Young's modulus of hydrogels. Common methods include simple tensile testing to determine the rubber elastic behavior or dynamic mechanical analysis under tension or shear to determine the viscoelastic properties. For most uniaxial tensile tests, the hydrogel samples are cut and prepared into a dumb bell shape and placed between two clamps [172]. Tests are run at constant extension rates with varying loads until the sample reaches ultimate failure. The stress–strain ($\sigma$–$\varepsilon$) behavior of the samples can be obtained from these tests and the slope of this data would provide Young's modulus of the hydrogels. In addition ($\sigma$) versus ($\varepsilon - 1/\varepsilon^2$) can also be plotted, and using the rubber elasticity equations, the shear modulus ($G$) can be obtained from the slope of the plot. Figure 2.9 shows the typical experimental stress–strain behavior of a crosslinked gel along with the results of theoretical statistical thermodynamic predictions. Compression testing is similar to tensile testing, except that instead of pulling the sample, it is compressed. The hydrogels are usually prepared as round samples, and compression tests are performed to plot the stress–strain curves. Young's modulus of the hydrogels is the slope of these curves. In theory, the values of Young's modulus obtained from tensile and compression tests for a particular hydrogel must be the same; however, it has been found that the values can differ. This could be attributed to the difference in the thickness of samples, which could lead to a difference in the diffusion of reactive species during polymerization.

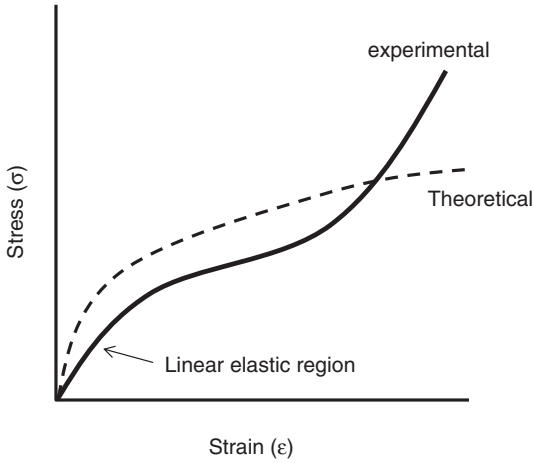


**Fig. 2.9** Theoretical and experimental stress-strain curves for hydrogels

Atomic force microscopy (AFM) can be used not only for imaging the topography of surfaces, but also for measuring forces on a molecular level. To investigate the mechanical properties of soft matrices or thin films, the sample is compressed by the indenting AFM tip. The loading force is calculated from the deflection and spring constant of the cantilever. To calculate Young's modulus of the material, force-indentation curves are recorded and fitted to the Hertz model, which describes the elastic deformation of two spherical surfaces under load [173].

### *2.4.5 Rheology*

The rheological properties are very much dependent on the types of structure (i.e., association, entanglement, and crosslinks) present in the system. Polymer solutions are essentially viscous at low frequencies and tend to fit the scaling laws: $G' \sim \omega^2$ and $G'' \sim \omega$. At high frequencies, elasticity dominates ($G' > G''$). This corresponds to Maxwell-type behavior with a single relaxation time, which may be determined from the crossover point, and this relaxation time increases with concentration. Crosslinked microgel dispersions exhibit $G'$ and $G''$ that are almost independent of oscillation frequency.

### *2.4.6 Surface Properties*

The surface of a hydrogel can be rough, smooth or stepped; it can be composed of different chemistries or could be highly crystalline, disordered and inhomogeneous. Studies have been performed on the importance of roughness, wettability,

surface mobility, chemical composition, crystallinity and heterogeneity; however, significant research has not yet been performed on determining which parameters are of utmost importance in understanding biological responses to surfaces. Some of the techniques used for determining the surface property include electron spectroscopy, secondary ion mass spectrometry, scanning electron microscopy (SEM), Fourier transform infrared spectroscopy (FTIR), scanning tunneling microscopy (STM) and atomic force microscopy (AFM). FTIR is a useful technique for identifying the chemical structure of a substance. This technique is widely used to investigate the structural arrangement in a hydrogel by comparison with the starting materials. SEM can be used to provide information about the sample surface topography, composition, and other properties such as electrical conductivity. This is a powerful technique widely used to visualize the characteristic 'network' structure in hydrogels. The information obtained through these methods can be used to monitor contamination, ensure surface reproducibility and explore the interaction of the hydrogels with living systems.

### *2.4.7 Other Techniques*

The main methods used to characterize and quantify the amount of free and bound water in hydrogels are differential scanning calorimetry (DSC) and nuclear magnetic resonance (NMR). Proton NMR gives information about the interchange of water molecules between the so-called free and bound states. The use of DSC is based on the assumption that only the free water may be frozen, so it is assumed that the endotherm measured when warming the frozen gel represents the melting of the free water, and that value will yield the amount of free water in the hydrogel sample being tested. The amount of bound water is then obtained from the difference between the measured total water content of the hydrogel test specimen and the calculated free water content. Thermogravimetric (TG) analysis and X-ray diffraction are also used to confirm the formation of crosslinked network gel structures of hydrogels. Neutron scattering based techniques have been used to study the relationship of the structure of polymer gels and mechanical properties [174, 175].

## 2.5 Applications of Smart Hydrogels

Hydrogels have received considerable attention in the last few decades owing to their exceptional promise in biomaterial applications. PHEMA was the first synthetic hydrogel to be synthesized in 1936 by DuPont scientists [176], and was established as an excellent candidate for contact lens applications by Wichterle and Lim [10]. Since then, hydrogels have been of great interest to biomaterial scientists. Some of the most successfully demonstrated applications are described in the following subsections.

### 2.5.1 'On–Off' Drug Delivery Systems

Well-designed drug delivery systems must control solute release over time. Various biomaterials have been investigated to control drug release; however, among them, hydrogels show two distinct advantages. (1) The rate of drug release can be controlled in many ways such as by changing the crosslinking density, preparing the hydrogel with monomers of controlled hydrophilicity, or controlling the ratio of hydrophilic to hydrophobic monomers. (2) Hydrogels may interact less strongly with drugs; consequently, a larger fraction of active molecules of a drug, especially proteins and peptides, can be released through hydrogel carriers. Better control over the delivery of drugs to specific sites in the body at specific times would reduce unwanted side effects and improve medical treatment dramatically (Fig. 2.10a). 'Smart' hydrogels are promising materials for controlling drug delivery, since they change their properties in response to specific stimuli. Temperature-responsive hydrogels have been studied most extensively to obtain an 'on–off' drug release profile in response to a stepwise temperature change. Okano et al. [177–179] have achieved complete and rapid 'on–off' regulation of drug permeation in response to stepwise temperature changes by using temperature-responsive hydrogels comprising PNIPAAm. A dense gel surface layer (skin layer) is established immediately after temperature increase above the hydrogel's collapse temperature. A possible explanation for this skin layer formation is that, at temperatures above its collapse point, the outermost gel layer interacts with its environment and then dehydrates quickly, forming a dense surface layer within seconds. The formed skin layer is dense enough to stop or retard the flux of water inside the gel to the outside of the gel. Gel surface skin layer formation can be controlled by changing the gel polymer chemistry, namely, the lengths of alkyl side chains on comonomers used during gel co-polymerization. Marked differences are observed in the initial shrinking process between three types of PNIPAAm-derived gels copolymerized with alkyl methacrylate comonomers, butyl methacrylate (BMA), hexyl methacrylate (HMA) and lauryl methacrylate (LMA) after temperature increase from 20 to 30 °C. P(IPAAm-*co*-HMA) and P(IPAAm-*co*-LMA) gels, both with longer alkyl side chains, shrank to only 20–30 % of their original volume observed at 20 °C, whereas P(IPAAm-*co*-BMA) gels shrank up to 80–90 % after equilibration. This result indicates that the rapid formation of a thin and dense skin layer can be regulated by selecting appropriate alkyl side chain lengths. With the longer alkyl side chains, denser skin layers were formed, preventing water efflux. The 'on–off' drug release in response to smaller temperature changes between 36 and 38 °C was also achieved, as demonstrated in Fig. 2.10b [180]. Both hydrophilic *N, N*-dimethylacrylamide (DMAAm) and hydrophobic BMA were incorporated into NIPAAm copolymer hydrogels, producing an LCST near 37 °C while maintaining high thermosensitivity. The rapid increase in release rate is attributed to a squeezing effect of drug molecules resulting from the shrinking of the gel surface region.

Another example of 'on–off' drug release control is achieved by using sugar-responsive gels for the possible treatment of diabetes mellitus. Pancreatic islets

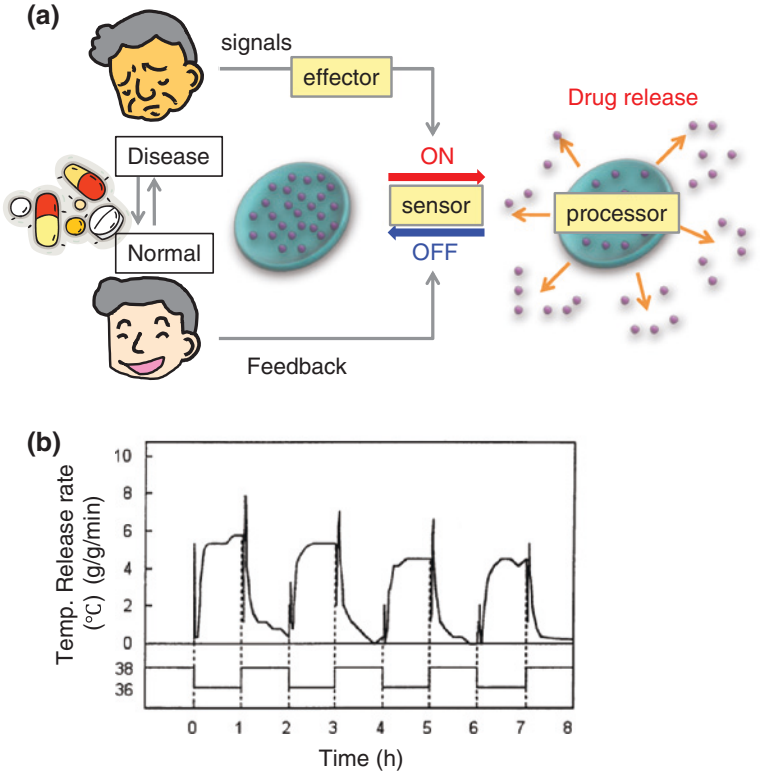


**Fig. 2.10** **a** Design concept for 'smart' drug delivery systems with sensor, processor, and effector functions, which can respond directly to a person's individual needs. **b** 'On-off' drug release from temperature-responsive hydrogels in response to stepwise temperature changes between 36 and 38 °C [180]

release insulin to lower the blood glucose level and regulate the glucose level within the range from 70 to 110 mg/dl by an autofeedback mechanism under healthy physiological conditions. It is necessary to externally administer exogenous insulin to diabetic patients (type I IDDM) who cannot control their blood glucose level. However, overdose may result in hypoglycemia and coma, which is a life-threatening state for these patients. Therefore, insulin must be carefully administered to avoid hypoglycemia in diabetic patients. Thus, in order to maintain a physiological glucose level, artificial systems sensing glucose and releasing appropriate amounts of insulin have been investigated. Kataoka et al. [154] have designed glucose-responsive gels composed of PNIPAAm derivatized with phenylboronic acid (PBA) groups as the glucose-sensing moiety. Significantly, PBA groups in aqueous solution are equilibrated between undissociated and dissociated forms, as shown in Fig. 2.8. Such equilibrium is shifted in the direction of increasing charged phenylboronates through complexation with glucose because only

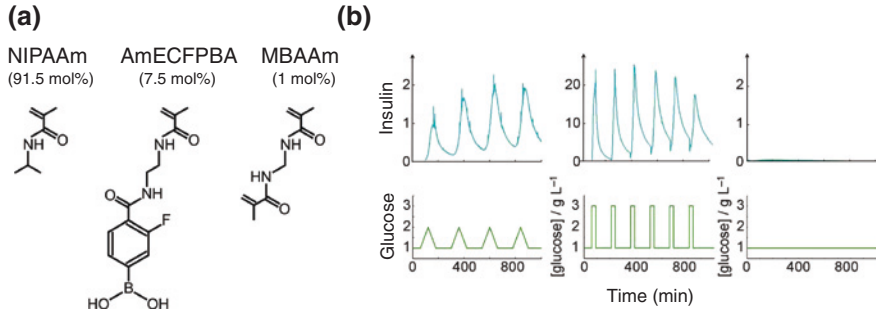


**Fig. 2.11** **a** Chemical structures of monomers contained in glucose-sensitive hydrogels and their optimized molar amounts in the feed to obtain glucose sensitivity under physiological pH and temperature [155, 198]. **b** (*Top*) Time course of changes in fluorescence intensity of FITC-labeled insulin released from glucose-sensitive gels under physiological conditions. (*Bottom*) Temporal patterns of fluctuation in glucose concentration [16]

charged boronates form stable complexes with cis-diols such as glucose under aqueous conditions. The PNIPAAm-PBA gels have volume transition temperatures that shift with glucose concentration. Interestingly, the gels are in collapsed states below 100 mg/dL glucose and in swollen states above 300 mg/dL glucose at 28 °C and pH 9. Such a glucose concentration range corresponds to the normal glucose levels in our body. Glucose-responsive insulin release was also performed using NB gels. Matsumoto and coworkers have further developed this glucose-responsive hydrogel system to operate under physiological conditions (pH 7.4, 37 °C), aiming for future use in a self-regulated insulin delivery system to treat diabetes mellitus. The approach involves the use of a newly synthesized phenylborate derivative, 4-(1,6-dioxo-2, 5-diaza-7-oxamyl) phenylboronic acid (DDOPBA), possessing an appreciably low p$K_a$ (~7.8) as a glucose-sensing moiety, as well as the adoption of PNIPMAAm as the main chain that exhibits critical solution behavior in the range close to physiological temperature (Fig. 2.11a) [155, 156]. Glucose- and pH-dependent changes in the critical solution behavior of the resultant copolymers were investigated at varying temperatures, revealing definite glucose sensitivities near the physiological conditions. The release of insulin from the gel has been continuously controlled by the skin layer with close correspondence to each addition pattern of glucose (Fig. 2.11b) [16].

Brazel and Peppas [181] reported pulsatile drug-releasing hydrogels to create both pH- and temperature-triggered devices for coronary-thrombosis-induced heart attack and stroke patients. Thrombolytic and antithrombotic agents represented by heparin and streptokinase have minute-order half-lives in circulation and are only required when blood clots form and specifically only at the site of the clot. To produce a therapeutic device with responsive hydrogels, they synthesized P(IPAAm-*co*-MAA) gels and investigated the release profiles of biologically active agents as a function of pulsatile pH and temperature. Streptokinase release was seen only when the gels were exposed to low temperature below the

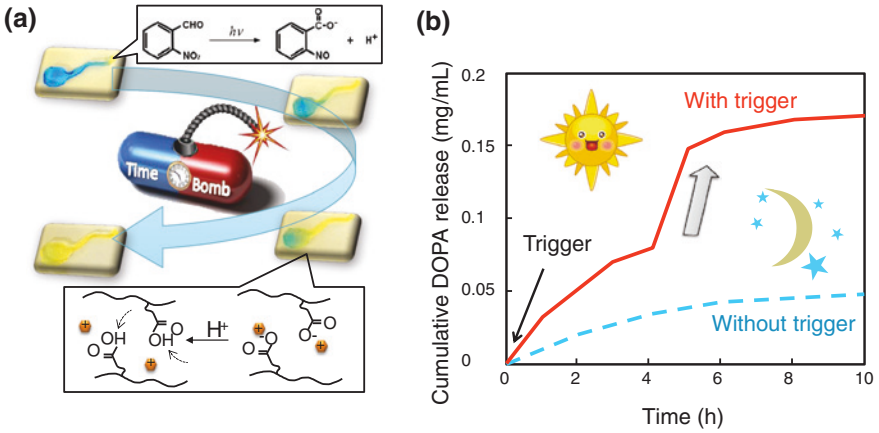


**Fig. 2.12** **a** Schematic of timed explosive drug release from pH-responsive hydrogels utilizing a phototriggered spatial pH-jump reaction [137]. **b** Drug release profiles of DOPA from gels with and without UV irradiation [130]

LCST and pH above p$K_a$. Drug release was observed to immediately decrease and completely stop after simultaneously decreasing the pH and increasing the temperature. After changes in both pH and temperature, the gel networks began to collapse. Their mesh sizes, representative of the space available for drug diffusion, dropped rapidly from approximately 12.5 to less than 10 nm, making it difficult for streptokinase of approximately 5.5 nm molecular diameter to diffuse through the collapsing pores. Heparin release from the gels, however, was not controlled because the mesh sizes of the gels were too large to control heparin diffusion (approximately 3 nm molecular diameter), even in the collapsed gel state.

Recently, the authors have developed an approach that could allow a more subtle control and timing of drug delivery. Although smart hydrogels are promising materials for controlling drug delivery, they usually require continuous stimulation to maintain these changes. We demonstrated the control of the acidity inside a pH-responsive hydrogel by loading it with a compound called NBA (Fig. 2.12a) [137]. This releases protons, which increase the acidity, when irradiated with UV light. When an NBA-loaded hydrogel was irradiated, the acidity increased inside; if only part of the gel was irradiated, the acidity throughout increased gradually as protons diffused. We loaded a hydrogel with NBA and L-DOPA, a precursor of the brain chemical dopamine that is used in the treatment of Parkinson's disease. The change in acidity of the gel upon UV irradiation caused L-DOPA to be released because the acidity disrupted the interaction of L-DOPA with the molecules in the gel [130]. Irradiation with UV not only enhanced the overall L-DOPA release from the hydrogel, but also caused an extra 'explosive' release five hours after irradiation (Fig. 2.12b). This allowed the drug release to be timed, as well as triggered, in a controlled manner. Being able to control the release of drugs from hydrogels by triggering a change in acidity could help indesigning programmable drug delivery techniques that offer improved targeting of treatment.

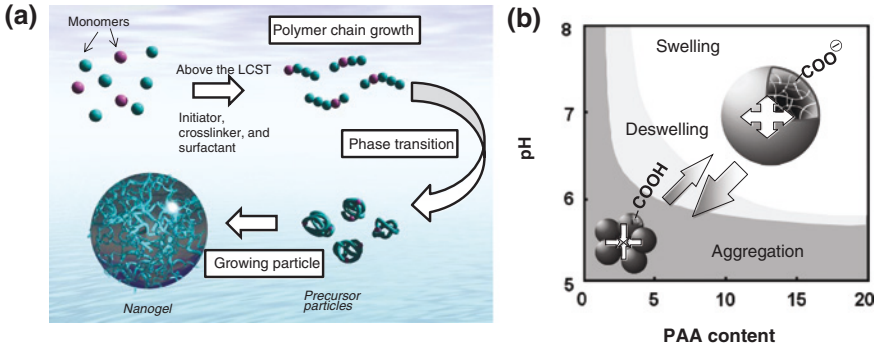


**Fig. 2.13** **a** Schematic illustration of precipitation polymerization method used for preparation of smart nanogels. **b** Swelling-deswelling-aggregation diagrams for P(NIPAAm-*co*-PAAc) nanogels [184]

Smart hydrogels in the form of microgels and nanogels have also been developed by many researchers, because they display many advantages when they are used in biological applications. PNIPAAm gel particles are typically prepared by precipitation polymerization or emulsion polymerization [182, 183]. In the precipitation polymerization approach, the polymerization of monomers and crosslinkers is initiated in water by a free-radical initiator at temperatures above the LCST. Once the growing polymer chains reach a critical length, they collapse and phase separate to form colloidal particles (Fig. 2.13a). This method offers numerous advantages, such as the production of highly uniform particles and the ability to control particle parameters, such as the size, charge, and crosslinking density. Omura et al. [184] developed a smart nanogel system that fully swells at normal physiological pH values but undergoes a sharp volume phase transition at moderately acidic pH values. The nanogels were prepared by precipitation polymerization of NIPAAm and PAAc in the presence of the crosslinker, MBAAm. At room temperature, the NIPAAm-PAAcnanogels were discrete, spherical structures with diameters ranging from 200 to 250 nm. The hydrodynamic diameter of the nanogels decreased to ca. 100–150 nm when the solution temperature was increased to 37 °C. At 37 °C, when the p$K_a$ was below that of the NIPAAm-PAAc, the gels collapsed and aggregated. However, at 37 °C and a physiological pH of 7.4, the nanogels did not fully collapse owing to the charge–charge repulsion derived from the ionized carboxyl groups of the PAAc (Fig. 2.13b). Thus, such nanogel particles could be useful for releasing drugs in regions of local acidosis, including sites of infection, tumors, ischemia, and intracellular endosomes.

### *2.5.2 Injectable Hydrogels*

One of the most obvious ways to provide sustained-release medication is to place the drug in a delivery system and inject or implant the system into the body tissue. Injection of an in situ gel-forming biopolymer is thus becoming increasingly

attractive for the development of therapeutic implants and vehicles [185, 186]. Copolymers of poly(ethylene oxide) (PEO) and poly(propylene oxide) (PPO) (knownas poloxamers) in aqueous solutions are well-known thermoset gel-forming materials in situ [187], but lack physiological degradability and induce unexpected increases in the level of plasma cholesterol or triglycerides in rats when injected intraperitoneally. To add a biodegradable capacity, the PPO segment of PEO–PPO–PEO block copolymers is often replaced by a biodegradable PLLA [51] or PLGA [52] segment. When low-molecular-weight PEG versus high-molecular-weight PLGA isused, the aqueous solution of PEG–PLGA–PEG triblock copolymer forms a solution at room temperature, whereas, at body temperature, it becomes a gel within a few seconds. The molecular architecture was not limited to the A-B-A-type block copolymer, but expanded into 3D, hyper branched structures, such as a star-shaped structure [53]. Chenite et al. [56] developed novel thermally sensitive combinations of chitosan/polyol salts, which turn into gel implants when injected in vivo. These formulations possess a physiological pH and can be kept as liquid below room temperature for encapsulating living cells and therapeutic proteins; they form monolithic gels at body temperature. When injected in vivo, the liquid formulations turn into gel implants in situ. This system was used successfully to deliver biologically active growth factors in vivo as well as an encapsulating matrix for living chondrocytes for tissue engineering applications.

Thermosensitive, specific-ion-sensitive or pH-sensitive hydrogels have been examined for their potential as vehicles for ocular drugs. The eye presents a challenge in the development of sustained or controlled release systems owing to its sensitivity and effective protection mechanisms, such as lacrimal secretion and blinking reflex, which cause rapid drainage of bioactive agents after topical administration. Therefore, in situ gels are preferred since they are conveniently dropped as a solution into the eye, where they undergo transition into a gel. Poloxamers, as thermogelling polymers, could be applicable for the development of effective ophthalmic drug delivery [188]. Ion-sensitive polymers belong to the group of in situ gelling materials mainly used for ocular drug delivery. The presence of alginate polymers significantly extended the duration of the pressure-reducing effect of pilocarpine to 10 h, allowing only once a day administration in the case of carteolol [189].

Recently, a number of researchers have investigated the use of pH as a stimulus for reversible gelation in polymeric systems [190–192]. The pH-sensitive system could facilitate drug delivery to regions of local acidosis, including sites of infection, neoplasia, or ischemia. The incorporation of carboxylic acid-derived monomers, such as AAc or MAAc, has been carried out to impart pH sensitivity in a variety of copolymers. With p$K_a$ values lower than the physiologic pH of 7.4 (p$K_a$ 4–5), these polymers can be designed to target acidic regions. However, under physiological conditions, the very low p$K_a$ values of PAAc and PMAAc generally limit the use of these polymers for drug targeting to very low pH systems such as the stomach. Hoffmanand colleagues have reported that the longer alkyl segments on PAAc raise the carboxylate p$K_a$ and facilitate sharp phase transitions at pH values greater than pH 6.0 [193, 194]. They have developed injectable NIPAAm-PAAc copolymers for the delivery of angiogenic growth factors [149]. NIPAAm-PAAc copolymers undergo sharp, reversible gelation at intermediate

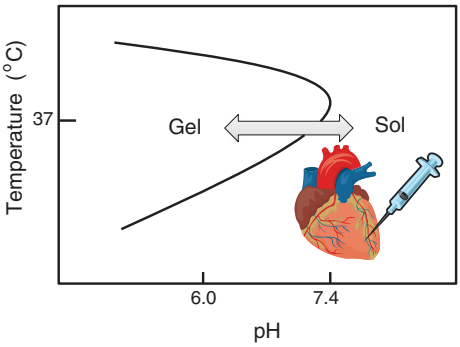


**Fig. 2.14** Typical phase diagram of pH- and temperature-responsive block copolymers in solution. These types of copolymer could be useful in providing sustained delivery of therapeutic molecules to regions of local acidosis such as ischemic tissue

acidic pH (~pH 5−6) but remain soluble at normal physiologic pH (7.4). This pH response could first promote gel formation in diseased tissue exhibiting local acidosis, and second, promote polymer dissolution and elimination once the tissue has returned to normal physiologic pH. Such a system could be useful in providing sustained delivery of therapeutic molecules to regions of ischemia, such as in therapeutic angiogenesis that has the potential to promote healing of ischemic tissue (Fig. 2.14).

The vagina, in addition to being an important organ of the reproductive tract, serves as a potential route for drug administration. It has been reported that 30–50 % of vaginitis episodes are due to *Candida* infection and that two-thirds of all women experience acute episodes of vaginal candidiasis at least once during their lifetime [195]. For vaginal delivery systems of antifungal agents to be more effective, they need to reside at the sites of infection for a prolonged period. Formulations based on a thermoplastic graft copolymer that undergoes in situ gelation have been developed to enable the prolonged release of active ingredients such as nonoxynol-9, progestins, estrogens, peptides and proteins [196]. This polymer offered prolonged antifungal activity over several days against *Candida albicans* vaginitis while reducing the toxicity of the drug on epithelial cells.

### *2.5.3 Tissue Engineering*

Tissue engineering has emerged as a promising technology for the design of an ideal, responsive, living substitute with properties similar to those of the native tissue [19]. Scaffolds play an important role in scaffold-guided in vitro tissue engineering. Scaffolds are basically 3D structural templates that support cell adhesion, migration, differentiation, and proliferation and provide guidance for neotissue formation. Hydrogels in particular have emerged as useful scaffolding biomaterials as they most closely resemble the natural tissues. Moreover, the aqueous environment provided by hydrogels mimics those of cells in the body. Both synthetic and natural hydrogels are used as scaffolds for tissue engineering in order

to repair cartilage, tendon, ligament, skin, blood vessels and heart valves [6]. The synthetic hydrogels focused on for use as scaffolds are polyurethanes (PU), PEO, PNIPAAm, PVA, PAAc and poly(propylene furmarate-*co*-ethylene glycol) [P(PF-co-EG)], whereas naturally derived hydrogels are agarose, alginate, chitosan, collagen, fibrin, gelatin, and hyaluronic acid (HA). Injectable hydrogels are also promising substrates for tissue engineering applications owing to their high tissue like water content, ability to homogeneously encapsulate cells, efficient mass transfer, easily manipulated physical properties and minimally invasive delivery [6, 197]. The hydrogel precursor loaded with growth factors or targeted cells can be injected into the wound site, where it undergoes a sol–gel transition in situ owing to physical or chemical stimuli.

Matsuda and coworkers have designed a thermoresponsive cell-adhesive matrix using PNIPAAm-grafted gelatin [198] and HAs [199]. The PNIPAAm-grafted HAs were water soluble at room temperature, where as they precipitated at temperatures above approximately 34 °C in water. Copolymers composed of HA and PNIPAAm have also been prepared by Ha et al. [200] to create temperature-sensitive injectable gels. Semi-telechelic PNIPAAm, with amino groups at the end of each main chain, was synthesized by radical polymerization using 2-aminoethanethiol hydrochloride (AESH) as the chain transfer agent, and was then grafted onto the carboxyl groups of HA using carbodiimide chemistry. The result of the thermooptical analysis revealed that the phase transition of the PNIPAAm-grafted HA solution occurred at approximately 30–33 °C. PNIPAAm-grafted HA exhibited an increase in viscosity above 35 °C, thus allowing the gels to maintain their shape for 24 h after in vivo administration. Stile et al. [201] have developed NIPAAm-based hydrogels that support tissue formation in vitro. Loosely crosslinked PNIPAAm and P(NIPAAm-*co*-AAc) hydrogels were synthesized with *N, N′*-methylenebis(acrylamide) crosslinker. At room temperature, the hydrogels were transparent and extremely pliable, where as at 37 °C, the matrices became opaque and were significantly more rigid. The P(NIPAAm-co-AAc) hydrogel demonstrated significantly less volume change between room temperature and 37 °C, contained significantly more water at 37 °C, and had an LCST that was significantly higher than that of the PNPAAm hydrogel. The hydrogels supported bovine articular chondrocyte viability for at least 28 days of in vitro culture, and cartilage-like tissue was formed in the matrices. These hydrogels can be injected through a small-diameter aperture and offer the benefit of in situ stabilization without the possible deleterious effects of in situ polymerization.

Smart hydrogels can also be applied to cell encapsulation. Cell technology provides a promising therapeutic modality for diabetes, hemophilia, cancer and renal failure [202–204]. The selection of a suitable biomaterial as a membrane for encapsulating cells is the major challenge to be overcome to enable successful cell encapsulation therapy. Biocompatibility, microporous structure, and minimal surface irritation within the surrounding tissues of hydrogel shave made them attractive for this application. They can be designed with the required porosity that resists any entrance of immune cells while allowing stimuli, oxygen, nutrients, and waste transfer through the pores. Genetically modified alginates and polyethylene

oxide-based hydrogels have been studied as cell encapsulation systems. Most problems of the in situ gelation system, however, lie with the reagents and the by-products of crosslinked hydrogels, which have the potential to be toxic to cells [205]. Increased cell death has been observed with a high concentration of exposed unreacted side chains after gelation [206]. Moreover, release of the encapsulated cells from vehicles is a difficult, potentially harmful process. The authors have recently developed temperature-responsive crosslinked nanofibers and demonstrated the ability to capture, encapsulate, and release cells by dynamically transforming the fibrous structure of the nanofibers into hydrogel-like structures by wrapping, swelling, and shrinking processes in response to alterations of external temperature [31]. By using external signals, cell capture, encapsulation, and release were successfully demonstrated. The released cells show excellent viability and proliferation behavior. This study extends the capture and release methods to a variety of bioactive compounds, the activity of which can be controlled by switching their accessibility to the environment. Further functionalization of the nanofibers could also be used for the immobilization of peptides or antibodies, which are highly promising for the separation, purification, preservation, and delivery of the target molecules and cells.

ECM-mimicking enzyme-responsive hydrogel scaffolds that permit cell migration have also been developed by Lutolfand et al. [207, 208]. They used oligopeptides as crosslinkers in PEG-based hydrogels. The peptide sequences are cleavable by matrix metalloproteinases (MMPs) to forma gel into which cells can infiltrate. MMPs are a family of enzymes that play many roles including the breakdown of ECM molecules during tissue remodeling and disease. Therefore, the integration of MMP-cleavable sites is a logical approach toward ECM mimics. The potential for bone tissue engineering was tested by loading the gel with bone morphogenetic protein-2 (BMP-2), which is known to be involved in bone formation. An assessment of the degradation behavior of MMPs and the cell invasion of provisional matrices revealed that the healing response in vivo depends on the enzymatic sensitivity of the matrix. Kim et al. [209] have also created an injectable hydrogel of NIPAAm-AActo mimic the ECM. These hydrogels are prepared by crosslinking an MMP-13/collagenase-3-degradable peptide sequence and NIPAm in the presence of Arg-Gly-Asp-modified PAAc. The proteolytic degradation and cell adhesion properties of this hydrogel were studied using rat calvarial osteoblasts. Collagenase was found to degrade the hydrogel at a rate dependent on the concentration of collagenase in relation to the PAAc chain. There is an increase in cell migration in MMP-degradable hydrogels compared with nondegradable gels, indicating the advantage of bioresponsive hydrogels.

### *2.5.4 Actuators*

Smart hydrogels have also been applied to biomimetic actuators or artificial muscles because polymers that undergo dimensional changes in response to various

environmental stimuli are capable of transducing chemical or physical energy directly into mechanical work. Conducting polymers, such as polypyrrole (PPy), polythiophene, and polyaniline, have attracted considerable attention because dimensional changes resulting from electrochemical doping and dedoping in an electrolyte solution or in a swollen state can be applied to produce electroactive polymer (EAP) actuators or artificial muscles [210, 211]. Osada et al. [24] reported electrically driven systems comprising polymer gels and electrodes that were actuated to bend and stretch repeatedly in response to alternating voltages, whereby the mechanical motion of these gels was in fact driven by the direction of the electric field. Okuzaki et al. [212, 213] have reported that electrochemically synthesized PPy films contracted in air under the application of an electric field. The motion of the film is driven by the reversible absorption of water vapor.

Temperature-responsive PNIPAAm-based actuators that bend in response to a temperature change have been reported as well. Hu et al. [214] described partially interpenetrated polymer networks composed of PNIPAAm and poly(acrylamide) (PAAm) hydrogels, so-called "bi-gels", which bend into circles in response to increasing temperature. These"bi-gels" grasp or release an object simply by adjusting the water temperature. Stoychev et al. [215] have reported the fabrication of 3D microobjects by the controlled folding/bending of a thin film, i.e., "microorigami". In this approach, two polymers were used. The first one is thermoresponsive PNIPAAm. In aqueous media, PNIPAAm reversibly changes its solubility at 33 °C. The second polymer is hydrophobic and water-insoluble poly(ε-caprolactone) (PCL). Both polymers were deposited ona substrate in the form of a crosslinked bilayer. Swelling and shrinking of PNIPAm resulted in reversible rolling of the bilayer and enabled the formation of tubes. Four- and six-arm self-folding capsules were fabricated and applied for reversible encapsulation of yeast cells (Fig. 2.15). Jeong et al. [216] have also constructed reversible color- and shape-tunable photonic actuators by transforming the programmed 2D structures to the 3D objects via the bending, twisting and folding mechanisms. A thermally curable hydrophobic poly(dimethylsiloxane) (PDMS) and a UV-curablehydrophilic PU/HEMA elastomeric blending precursor are selected as constituents because of their flexibility, optical transparency and dramatically different swelling responses to selected solvents. By changing the geometrical factor, selected materials and polarity of the solvents, the desired shape and color of the scrolled, helical, and cubic actuators can be achieved. When the folding, bending, and twisting technologies are combined with lithographic patterning technology in micrometer length scale, this unique technique may have great potential for applications in mechanical actuators and optoelectronic and biomimetic devices. He et al. demonstrated this concept on the example of a millimeter-size PMMA-PHEMA bilayer with an attached mucoadhesive drug layer. The nonswelling PHEMA layer serves as a diffusion barrier, minimizing any drug leakage in the intestine [217]. The resulting unidirectional release provides improved drug transport through the mucosal epithelium. The functionality of this device is successfully demonstrated in vitro using a porcine small intestine. Asoh et al. [22] reported a novel strategy for the preparation of thermoresponsive bending gradient

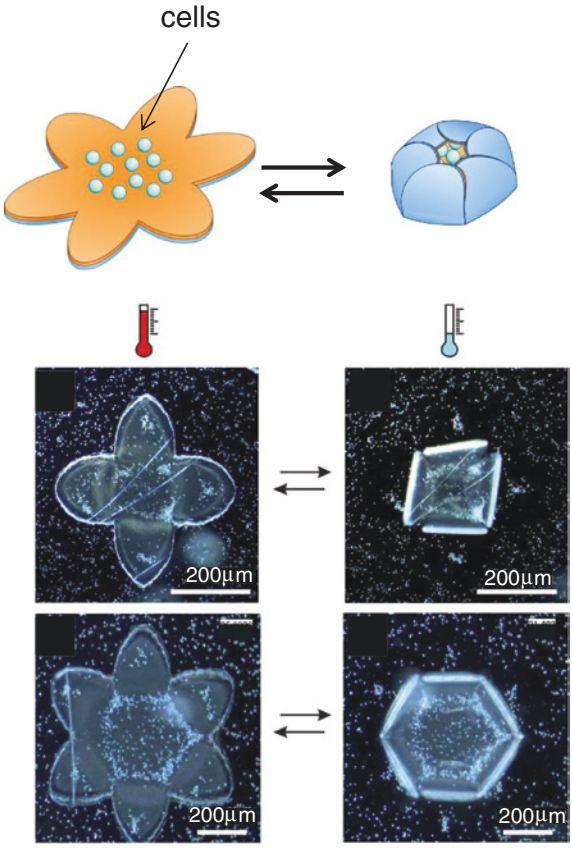


**Fig. 2.15** Encapsulation of yeast cells inside the self-folding star-shaped polymer bilayer. Yeast cells are adsorbed on the polymer bilayer at elevated temperature. Cooling leads to swelling of the thermoresponsive polymer and folding of the capsules. Further heating results in unfolding of the capsules and release of the cells [215]

gels. PNIPAAm gels with two types of nanostructured gradients, consisting of eithersilica nanoparticles or nanopores, showed uniquely different bending properties depending on their shrinkage characteristics. These gradient gels were simply fabricated through electrophoresis and subsequent photo-polymerization. Differences in the physical properties between the two sides of the gradient gels are the driving force behind the bending of the gels. Zhang et al. have reported near-IR optically responsive hydrogels using single-walled carbon nanotube (SWNT)-PNIPAAm composite hydrogels. They demonstrated a well-defined, ultra fast response of the SWNT-PNIPAAm hydrogel actuators to near-IR laser excitation, making this design viable for many optically triggered applications [218].

In addition to physical signal-responsive systems, there are also several examples of bilayer systems that fold in response to chemical stimuli. The use of polymers sensitive to chemical signals allows the design of biomimetic actuators folding in response to specific chemical signals. Among them, pH-responsive systems are particularly important because the human body presents variations in pH along the gastrointestinal tract, in specific tissues (and tumoral areas) and insubcellular compartments. pH-sensitive self-folding materials are commonly designed

using weak polyelectrolytes as active polymers. Their ionic groups are counter balanced with oppositely charged ions that gradually diffuse into/out of polymer networks to induce spontaneous changes in their characteristics with temporal activation, which is observed in living systems, such as muscle and ciliary movement, pulsatile secretion of hormone, and brain waves. Luchnikov and coworkers demonstrated that the polystyrene (PS)-poly(4-vinyl pyridine) (PVP) bilayer [219], as well as the PS-PVP-PDMS trilayer [220], can roll at low pH when PVP is protonated and swells in water. The use of layers with a two-dimensional gradient of thickness allowed a thorough investigation of the folding. Bassik et al. [221] fabricated millimeter-size PEG/P(NIPAAm-*co*-AAc) bilayers that can snap in response to the pH signal. In contrast to physical stimuli that can easily penetrate through materials (e.g., heat, light, magnetic field, etc.), however, changing the pH quickly and precisely at a particular location in the system has been a major challenge, particularly inside hydrogels. From these perspectives, the authors focused on the photoinitiated proton-releasing reaction of 'photoacid generators' (PAGs), the p$K_a$ of which, in an excited state, is significantly different from that in the ground state. We have successfully integrated the PAG into pH-responsive P(NIPAAm-*co*-CIPAAm) hydrogels to demonstrate rapid proton release upon UV irradiation, resulting in the decrease of intragel pH to below the p$K_a$ of P(NIPAAm-*co*-CIPAAm) [130, 137]. We have demonstrated photo induced reversible control of self-bending using PAG-integrated pH-responsive bilayer hydrogels consisting of a polyacid P(NIPAAm-*co*-CIPAAm) layer and a poly base P(NIPAAm-*co*-*N, N′*-dimethylaminopropylacylamide: DMAPAAm) layer [222]. The adhesion of these two layers was achieved by employing a semi-IPN using linear PAAc and branched poly(ethyleneimine) (PEI) chains, which form polyion complexes at the interface of the two gels via electrophoresis [25]. Reversible bending was successfully demonstrated in response to 'on–off' UV irradiation (Fig. 2.16). Additionally, self-bending of the non-UV-irradiated region of the gel was also achieved because the generated protons gradually diffused toward the nonirradiated region. The proposed system can be potentially applied in the fields of mechanical actuators, controlled encapsulation and drug release, robotics and microfluidic technologies because control over autonomous motion by both physical and chemical signals is essential as a programmable system for real biomedical and nanotechnological applications.

Smart hydrogels have also been incorporated into microfluidic devices to reduce the system complexity [223]. Microfluidics is the science and technology of designing and manufacturing devices that deal with the behavior, precise control and manipulation of small volumes of fluids [224]. Although recent progress in microfabrication techniques such as multilayer soft lithography enables us to design sophisticated microchips with hundreds of independent valves, most microfluidic materials themselves still lack stand-alone abilities. Therefore, it becomes increasingly apparent that on-demand switchable materials that can respond to external stimuli or their environment to produce dynamic and reversible change in critical properties have enabled progress in a growing number of diverse applications including bio/chemical analysis, chemical synthesis, cell

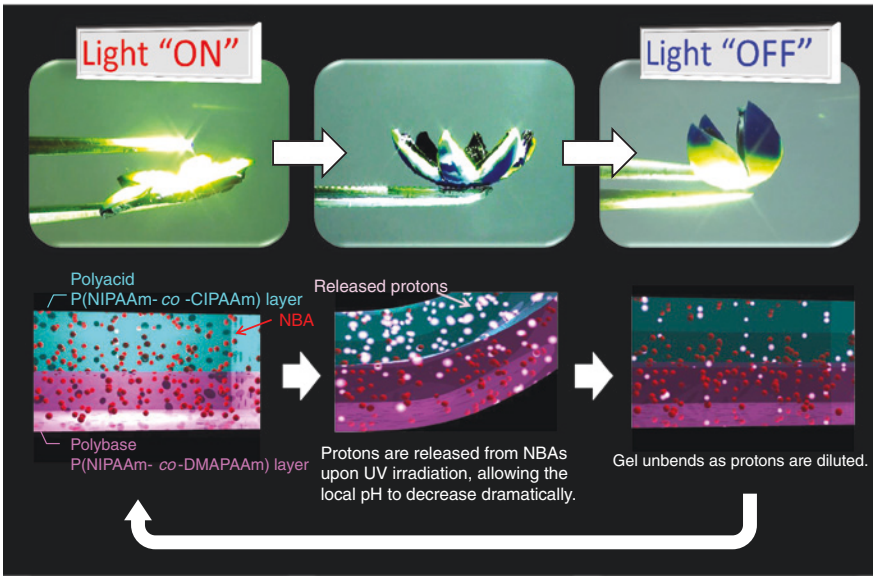


**Fig. 2.16** Photoinduced reversible self-bending/straightening of PAG-integrated pH-responsive bilayer hydrogels consisting of polyacid P(NIPAAm-*co*-CIPAAm) and polybase P(NIPAAm-*co*-DMAPAAm)layers. The bilayer gels bend upward to the polyacid side when the light is turned on ('on' stage) because protons are released from PAG, allowing the local pH to decrease dramatically. After the UV light is turned off ('off' stage), the gels straighten to the original shape as protons are diluted [25, 222]

manipulation, biomedical monitoring, and point-of-care clinical diagnostics. From these perspectives, 'smart' microfluidic systems have been extensively studied using stimuli-responsive materials because they can receive device-generated signals and act as switches by themselves. Beebe et al. [26], for example, used a pH-responsive hydrogel-based valve that opened or closed depending on the pH of the flowing solution (Fig. 2.17a). Bistrip valves and arrowhead-shape valves have also been reported to allow flow in only one direction [225, 226]. Autonomous micromixers and micropumps have also been developed using pH- and temperature-responsivehydrogels, electroplated nickel (Ni) impellers, and magnetic stirrers (Fig. 2.17b) [227]. The Ni impeller was coupled with an underlying rotating magnetic stirrer that was constantly on. When the local environment pH was decreased, the hydrogel ring shrank, allowing the Ni impeller to rotate freely; however, when the local pH was raised above its transition point, the hydrogel ring expanded into a mushroom cap shape that exerts both downward and lateral forces on the Ni impeller, thus stopping the rotation of the Ni impeller. The 'smart liquid microlens' concept with the temperature-sensitive NIPAAm hydrogel that expands at low temperatures and contracts at high temperatures has also been demonstrated (Fig. 2.17c). In this system, the meniscus between water and oil was used as an optical lens and its focal length was adjusted by changing the curvature of

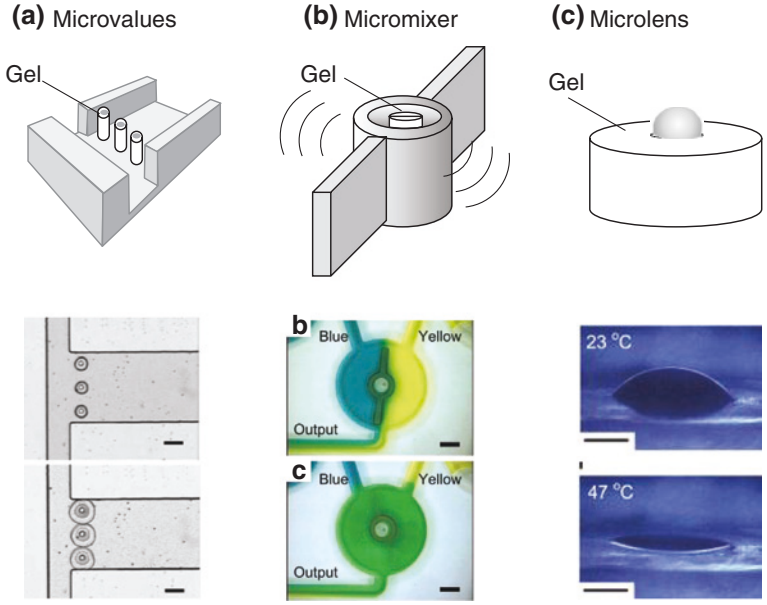


**Fig. 2.17** Autonomous microfluidics with smart hydrogels. **a** Autonomous flow control in microfluidic channels using pH-sensitive hydrogel valves [26]. **b** Autonomous microfluidic mixers using a pH-responsive hydrogel [227]. **c** Smart microlenses. The water–oil interface forms the liquid microlens. The microchannels allow the flow of fluids to the microlens structure [223]

this meniscus. The authors have recently described a facile approach to fabricate "smart" microfluidic channels that demonstrated a shape-memory-driven geometric switch and a new mechanism of flow control. We present on-demand switchable microchip materials that display potent rewritable and shape-memory properties, which are shown to contribute to fluidic control as pumps and valves [27]. This new class of smart microfluidic control techniques enables portable microfluidic-based diagnostic tools for biomedical applications and environmental monitoring with on-site analysis capability.

While stimuli-responsive polymers were designed to receive device-generated signals, which can act as switches, there has also been a dynamic growth in interest in self-actuating materials in recent years. Feinberg et al. [228] have demonstrated a self-walking bioactuator using biohybrid materials of engineered tissues and synthetic polymer thin films. They cultured cardiomyocytes on PDMS thin films micropatterned with ECM proteins to promote spatially ordered 2D myogenesis. The centimeter-scale constructs performed functions as diverse as gripping, pumping, walking, and swimming with fine spatial and temporal control and the generation of specific forces as high as 4 millinewtons per square millimeter. Yoshida and Okanohave [229] successfully shown a novel biomimetic gel actuator that can walk spontaneously with a worm like motion without switching of external stimuli. The self-oscillating motion is produced by dissipating chemical energy

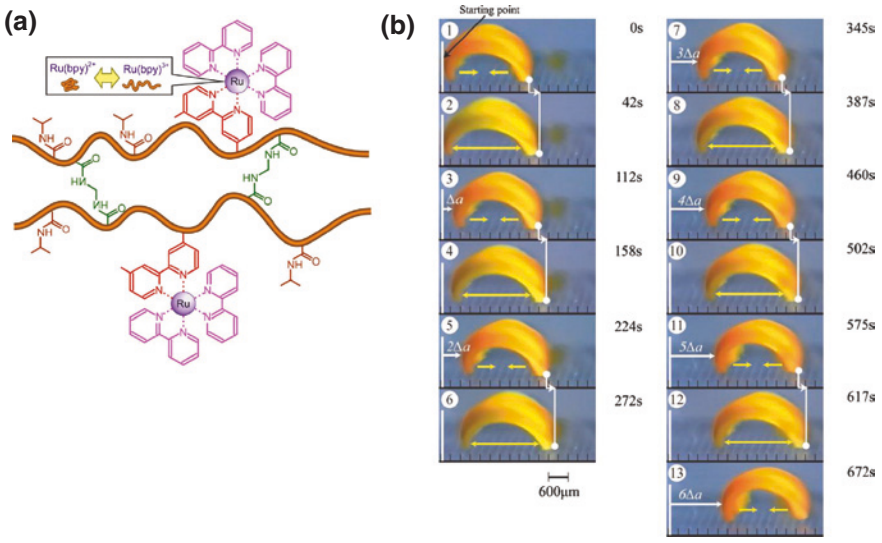


**Fig. 2.18** **a** Chemical structure of P(NIPAAm-*co*-Ru(bpy)$_3$) gel. **b** Time course of self-walking motion of gel actuator (odd number: bending process at reduced state; even number: stretching process with propagation of chemical wave) [23]

from an oscillating reaction, that is, the BZ reaction [230, 231] occurring inside the gel. They prepared a copolymer gel of NPAAm in which ruthenium(II) tris-(2, 2′-bipyridine) (Ru(bpy)$_3^{2+}$), a catalyst for the BZ reaction, is covalently bonded to the polymer chain (Fig. 2.18a). The P(NIPAAm-*co*-Ru(bpy)$_3$) gel swells and deswells at the oxidized and reduced states of Ru(bpy)$_3$, respectively. The BZ reaction in the gel generates periodic redox changes of Ru(bpy)$_3$, and the chemical oscillation induces mechanical oscillation of the polymer network [232]. Although the gel is completely composed of synthetic polymer, it shows autonomous motion as if it is alive. To cause an anisotropic contraction with curvature changes, a gel strip with a gradient structure was prepared. By coupling with a ratchet mechanism, the gel walks with repeated bending and stretching motions by itself like a looper at a speed of 170 μm/min (Fig. 2.18b) [23]. This "self-walking" gel actuator could serve as a new frame work for a biomimetic robot.

### *2.5.5 Sensors*

Biomolecule-sensitive hydrogels that undergo swelling changes in response to specific biomolecules can be modified to design smart hydrogels that could degrade in response to an increase in the concentration of specific biomolecules. For example, the widely researched glucose-sensitive hydrogels have the ability to sense the levels of blood glucose and release insulin in accordance with the

glucose levels [155, 156, 233, 234]. NIPAAm copolymer microgels have been shown tobe an excellent platform for designing label-free glucose-sensing materials. Sorrell and Serpe [235] reported that aminophenylboronic acid (APBA)-functionalized P(NIPAm-*co*-AAc) microgels in an etalon respond to 3 mg/mL glucose concentrations by red shifting their reflectance peaks by 110 upto 150 nm. Additionally, APBA-functionalized microgels have a depressed volume phase transition temperature of 18–20 °C, which shifts to 24–26 °C after glucose binding. These materials showed a marked visual color change, which is a first step towards developing direct-readout sensor devices. Wang et al. reported on the fabrication of multifunctional ratiometric probes for glucose and temperatures based on thermo responsive PNIPAAm microgels covalently incorporated with APBA, fluorescence resonance energy transfer (FRET) donor dyes, 4-(2-acryloyloxyethylamino)-7-nitro-2, 1, 3-benzoxadiazole (NBDAE), and rhodamine B-based FRET acceptors (RhBEA) [236]. The spatial proximity of FRET donors and acceptors within microgels can be tuned via thermo-induced microgel collapse or glucose-induced microgel swelling at appropriate pH and temperatures, leading to the facile modulation of FRET efficiencies. APBA moieties within P(NIPAM-APBA-NBDAE-RhBEA) microgels can bind with glucose at appropriate pH to form cyclic boronate moieties that can decrease the p$K_a$ of APBA residues and increase the volume phase transition temperature of microgels.

Miyata and coworkers have reported a specific antigen-sensing semi-interpenetrating (semi-IPN) hydrogel network [32, 79, 237]. The hydrogel was fabricated by first polymerizing the vinyl-conjugated form of goat anti-rabbit (GAR) IgG (i.e., GAR IgG coupled to *N*-succinimidylacrylate) and then copolymerizing GAR IgG with vinyl-modified rabbit IgG, in the presence of the crosslinker, MBAAm. Noncovalent crosslinking between grafted antigens and antibodies resulted in shrinking of the hydrogel network in the absence of free antigens in the system. However, when free antigens were present in the system, the hydrogel network swelled owing to the rupture of the antigen-antibody crosslinks. This was due to competitive binding (to the immobilized antibodies) exhibited by the immobilized and free antigens in the solution. They also reported tumor-marker-responsive gels that exhibited volume changes in response to a tumor-specific marker glycoprotein (α-fetoprotein, AFP) [157]. The glycoprotein-imprinted gel shrank in response to a target glycoprotein but a nonimprinted gel swelled slightly. The glycoprotein-responsive shrinking of the imprinted gel was caused by the formation of lectin-glycoprotein-antibody complexes that acted as reversible crosslinking points. As the shrinking behavior of biomolecularly imprinted gels in response to glycoproteins enables the accurate detection and recognition of tumor-specific marker glycoproteins, they have many potential applications as smart devices in sensing systems and for molecular diagnostics.

A hydrogel membrane sensitive to the metabolite nicotinamide adenine dinucleotide (NAD) and containing immobilized ligands and receptors was also investigated for the controlled diffusion of model proteins [238]. Both cibacron blue (ligand) and lysozyme (receptor) were covalently linked to dextran. NAD serves as a competing ligand and competes with cibacron blue in its interaction with

lysozyme. With the use of cytochrome C and hemoglobin as model proteins to examine the diffusion across the hydrogel membrane in response to differential concentrations of NAD, saturation kinetics was observed. This approach of sensing ambient levels of NAD can be generalized to diagnose the levels of different analytes by suitably selecting a competing ligand-receptor interaction, thereby affecting the permeability of the polymer membrane.

Molecular imprinting is a versatile method for creating macromolecular matrices (hosts) that display selective molecular recognition behavior. This is achieved by enabling the synthetic hosts to "memorize" the out fits of targeted guests. Oya et al. were pioneers in proposing the creation of stimuli-sensitive gels with the ability to recognize and capture target molecules using polymer networks consisting of at least two species of monomers, each playing a different role. One forms a complex with the template (i.e., the functional or absorbing monomers capable of interacting ionically with a target molecule), and the other allows the polymers to swell and shrink reversibly in response to environmental changes (i.e., a smart component such as NIPAAm). The gel is synthesized in the collapsed state and, after polymerization, is washed in a swelling medium. The imprinted cavities develop affinity for the template molecules when the functional monomers come into proximity, but when they are separated, the affinity diminishes. The proximity is controlled by the reversible phase transition that consequently controls the adsorption/release of the template (Fig. 2.19) [239]. The design of a precise macromolecular chemical architecture that can recognize target molecules from an ensemble of closely related molecules has a large number of potential applications. The main thrust of research in this field includes separation processes, immunoassays and biosensor recognition elements.

### *2.5.6 Self-Healing*

While stimuli-responsive polymers were designed to function as passive structures, there has also been a dynamic growth in interest in dynamically restructuring or self-healing polymers in recent years [240]. Such materials can undergo autonomic healing to repair damage and thus offer a new route towards safer, longer-lasting products and components. Among them, self-healing soft materials such as hydrogels are particularly promising for a variety of medical applications owing to their biocompatibility and mechanical similarity to natural tissues. Self-healing hydrogels, for example, have unique advantages as injectable biomaterials, which are increasingly being explored to minimize the risks and complications associated with surgical implantation [241]. The first reported approach for the design of self-healing materials was based on the microencapsulation of a reactive species that can polymerize or react with the matrix when released upon rupture of the encapsulating agents [242]. This reaction, at the damage site, was irreversible and the supply of healing agents was depleted locally. Therefore, the repair could not be repeated. Although some other approaches were adopted to attain multiple

**Fig. 2.19** Reversible molecular adsorption based on multiple-point interaction by shrinkable gels. Shrunken gels at 55 °C (*upper dish*) and swollen gels at 25 °C (*lower dish*) under illumination with UV. In the shrunken state, the gel adsorbed all of the pyranine molecules, but in the swollen state, the gel released them all, as shown by their fluorescence [239]

healing cycles of a single crack, repetitive healing was very rare in such systems. From these perspectives, intrinsic self-healing materials capable of repetitive repair are an increasingly active research area of particular scientific and commercial interest.

Intrinsic self-healing can be accomplished through thermally reversible reactions [243], hydrogen bonding [244], ionomeric coupling [245], a dispersed meltable thermoplastic phase [246], or polymer diffusion [247]. Among these strategies, the gelation techniques based on selective or specific interactions were found to be more promising. Host–guest interactions, for example, have been widely used in the construction of self-healing hydrogels (Fig. 2.20a). The combination of multiple noncovalent interactions, such as hydrogen bonding, π–π stacking, charge transfer, and hydrophobic interactions between two complementary compounds, not only gives them a good binding affinity but also allows them to form complexes with fixed host–guest geometry and directionality [248]. On the other hand, metal-ligand interactions were also found to be promising because they are not only thermodynamically stable but also kinetically labile. Moreover, their reversibility can be selectively tuned by using different metal ions. Beck and Rowan have demonstrated the construction of room-temperature healable gels via the self-assembly of ditopic ligands, consisting of a 2, 6-bis(1-methylbenzimidazolyl) pyridine (BIP) moiety attached to either end of a PEG core, in the presence

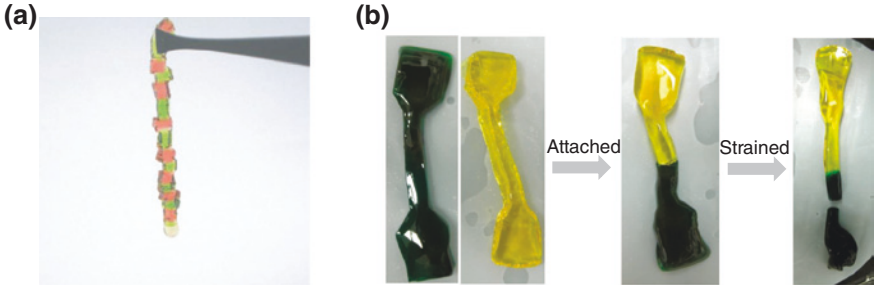


**Fig. 2.20** Photographs of self-healing hydrogels. The self-healing is accomplished through **a** host–guest interactions [248], and **b** metal–ligand complexation [251]

of transition metal/lanthanide ions [249]. Holten-Andersen et al. [250] have developed a simple method for controlling catechol–$Fe^{3+}$ interpolymer crosslinking, inspired by the pH jump experienced by proteins during the maturation of a mussel byssus secretion. The catechol–$Fe^{3+}$ bonds can spontaneously reform after breaking, and such a network displays high elastic moduli. The authors have also prepared rapid self-healable and biocompatible hydrogels by the selective formation of metal-ligand complexes between selected metal ions and phosphate end groups of PEG (Fig. 2.20b). The gels were rapidly formed with trivalent metal ions such as $Fe^{3+}$, $V^{3+}$, $Al^{3+}$, $Ti^{3+}$, and $Ga^{3+}$, which have small ion radii. We have also demonstrated a gel–sol/sol–gel transition by switching the redox states of $Fe^{3+}/Fe^{2+}$ ions [251]. Learning from biological systems, the proposed phosphate-metal-ion-based self-healable hydrogels could become attractive candidates for various biomedical and environmental applications.

## 2.6 Conclusions and Future Trends

Smart hydrogels have the remarkable ability to respond to stimuli in a variety of ways. Because some environmental variables, such as low pH and elevated temperatures, are found in the body, smart hydrogels have enormous potential in various biomedical applications. For example, different types of smart hydrogels have been investigated for a series of drugs in vitro or in vivo. As a result, new and interesting controlled and sustained delivery strategies have become available. The fascinating properties of the stimuli-sensitive polymers are promising for many future applications and offer possible use as the next generation of materials in biological, biomedical and pharmaceutical products. Fundamental studies also greatly contributed to our present understanding of this unique class of materials. Although the concepts of these smart hydrogels are sound, the practical applications require significant improvements in the hydrogel properties. The most significant weakness of all these hydrogels is that their response time is too slow.

Thus, fast-acting hydrogels are still necessary. The synthesis of new polymers and cross linkers with more biocompatibility and better biodegradability would also be essential for successful applications. It is also expected that principles from the expanding research area of supramolecular chemistry will be applied to design novel types of hydrogels with tailored properties, which can preferably be prepared in an aqueous environment. Also, protein engineering might contribute to the development of hydrogel systems with very precise control over their microstructure, and thus, their properties. Again, smart hydrogels are an interesting class of materials that can be prepared by a variety of methods. Concurrent developments in the design of new responsive polymers along with structure-property evaluations are vital for practical applications of smart hydrogels. Not only does this enable the application of smart hydrogels to existing scientific problems, but it also allows previously unimagined technological directions to be explored.

## References


1. Hennink WE, van Nostrum CF (2002) Novel crosslinking methods to design hydrogels. Adv Drug Del Rev 54:13–36. doi:http://dx.doi.org/10.1016/S0169-409X(01)00240-X
2. Kamath KR, Park K (1993) Biodegradable hydrogels in drug delivery. Adv Drug Del Rev 11:59–84. doi:http://dx.doi.org/10.1016/0169-409X(93)90027-2
3. Schacht EH (2004) Polymer chemistry and hydrogel systems. J Phys: Conf Ser 3:22
4. Jen AC, Wake MC, Mikos AG (1996) Review: hydrogels for cell immobilization. Biotechnol Bioeng 50:357–364. doi:10.1002/(sici)1097-0290(19960520)50:4<357:aid-bit2>3.0.co;2-k
5. Hoffman AS (2002) Hydrogels for biomedical applications. Adv Drug Del Rev 54:3–12. doi:http://dx.doi.org/10.1016/S0169-409X(01)00239-3
6. Lee KY, Mooney DJ (2001) Hydrogels for tissue engineering. Chem Rev 101:1869–1880. doi:10.1021/cr000108x
7. Narain R (2011) Engineered carbohydrate-based materials for biomedical applications: polymers, surfaces, dendrimers, nanoparticles, and hydrogels. Wiley
8. Petka WA, Harden JL, McGrath KP, Wirtz D, Tirrell DA (1998) Reversible hydrogels from self-assembling artificial proteins. Science 281:389–392. doi:10.1126/science.281.5375.389
9. Wang C, Stewart RJ, Kopeček J (1999) Hybrid hydrogels assembled from synthetic polymers and coiled-coil protein domains. Nature 397:417–420
10. Wichterle O, Lim D (1960) Hydrophilic gels for biological use. Nature 185:117–118. doi:10.1038/185117a0
11. Azad AK, Sermsintham N, Chandrkrachang S, Stevens WF (2004) Chitosan membrane as a wound-healing dressing: characterization and clinical application. J Biomed Mater Res B Appl Biomater 69B:216–222. doi:10.1002/jbm.b.30000
12. Kickhöfen B, Wokalek H, Scheel D, Ruh H (1986) Chemical and physical properties of a hydrogel wound dressing. Biomaterials 7:67–72. doi:http://dx.doi.org/10.1016/0142-9612(86)90092-X
13. Yoo H-J, Kim H-D (2008) Synthesis and properties of waterborne polyurethane hydrogels for wound healing dressings. J Biomed Mater Res B Appl Biomater 85B:326–333. doi:10.1002/jbm.b.30950
14. Chen J, Park H, Park K (1999) Synthesis of superporous hydrogels: hydrogels with fast swelling and superabsorbent properties. J Biomed Mater Res 44:53–62. doi:10.1002/(sici)1097-4636(199901)44:1<53:aid-jbm6>3.0.co;2-w
15. Jafari B, Rafie F, Davaran S (2011) Preparation and characterization of a novel smart polymeric hydrogel for drug delivery of insulin. BioImpacts 1:135–143. doi:10.5681/bi.2011.018

16. Matsumoto A, Ishii T, Nishida J, Matsumoto H, Kataoka K, Miyahara Y (2012) A synthetic approach toward a self-regulated insulin delivery system. Angew Chem Int Ed 51:2124–2128. doi:10.1002/anie.201106252
17. Silva AKA, Richard C, Bessodes M, Scherman D, Merten O-W (2008) Growth factor delivery approaches in hydrogels. Biomacromolecules 10:9–18. doi:10.1021/bm801103c
18. Tanigo T, Takaoka R, Tabata Y (2010) Sustained release of water-insoluble simvastatin from biodegradable hydrogel augments bone regeneration. J Controlled Release 143:201–206. doi:http://dx.doi.org/10.1016/j.jconrel.2009.12.027
19. Langer R, Vacanti J (1993) Tissue engineering. Science 260:920–926. doi:10.1126/science.8493529
20. Hoffman AS (1987) Applications of thermally reversible polymers and hydrogels in therapeutics and diagnostics. J Controlled Release 6:297–305. doi:http://dx.doi.org/10.1016/0168-3659(87)90083-6
21. Hoffman AS (2012) Hydrogels for biomedical applications. Adv Drug Del Rev 64, Suppl:18–23. doi:http://dx.doi.org/10.1016/j.addr.2012.09.010
22. T-A Asoh, Matsusaki M, Kaneko T, Akashi M (2008) Fabrication of temperature-responsive bending hydrogels with a nanostructured gradient. Adv Mater 20:2080–2083. doi:10.1002/adma.200702727
23. Maeda S, Hara Y, Sakai T, Yoshida R, Hashimoto S (2007) Self-walking gel. Adv Mater 19:3480–3484. doi:10.1002/adma.200700625
24. Osada Y, Okuzaki H, Hori H (1992) A polymer gel with electrically driven motility. Nature 355:242–244
25. Techawanitchai P, Ebara M, Idota N, Asoh T-A, Kikuchi A, Aoyagi T (2012) Photoswitchable control of pH-responsive actuators via pH jump reaction. Soft Matter 8:2844–2851
26. Beebe DJ, Moore JS, Bauer JM, Yu Q, Liu RH, Devadoss C, Jo B-H (2000) Functional hydrogel structures for autonomous flow control inside microfluidic channels. Nature 404:588–590
27. Ebara M, Uto K, Idota N, Hoffman JM, Aoyagi T (2013) Rewritable and shape-memory soft matter with dynamically tunable microchannel geometry in a biological temperature range. Soft Matter
28. Idota N, Kikuchi A, Kobayashi J, Sakai K, Okano T (2005) Microfluidic valves comprising nanolayered thermoresponsive polymer-grafted capillaries. Adv Mater 17:2723–2727. doi:10.1002/adma.200402068
29. Dong LC, Hoffman AS (1986) Thermally reversible hydrogels: III. Immobilization of enzymes for feedback reaction control. J Controlled Release 4:223–227. doi:http://dx.doi.org/10.1016/0168-3659(86)90006-4
30. Ebara M, Yamato M, Aoyagi T, Kikuchi A, Sakai K, Okano T (2008) A novel approach to observing synergy effects of PHSRN on integrin–RGD binding using intelligent surfaces. Adv Mater 20:3034–3038. doi:10.1002/adma.200702308
31. Kim Y-J, Ebara M, Aoyagi T (2012) A smart nanofiber web that captures and releases cells. Angew Chem Int Ed 51:10537–10541. doi:10.1002/anie.201204139
32. Miyata T, Uragami T, Nakamae K (2002) Biomolecule-sensitive hydrogels. Adv Drug Del Rev 54:79–98. doi:http://dx.doi.org/10.1016/S0169-409X(01)00241-1
33. Watanabe M, Akahoshi T, Tabata Y, Nakayama D (1998) Molecular specific swelling change of hydrogels in accordance with the concentration of guest molecules. J Am Chem Soc 120:5577–5578. doi:10.1021/ja973070n
34. Feil H, Bae YH, Feijen J, Kim SW (1991) Molecular separation by thermosensitive hydrogel membranes. J Membr Sci 64:283–294. doi:http://dx.doi.org/10.1016/0376-7388(91)80099-R
35. Freitas RFS, Cussler EL (1987) Temperature sensitive gels as extraction solvents. Chem Eng Sci 42:97–103. doi:http://dx.doi.org/10.1016/0009-2509(87)80213-0
36. Zhang X-Z (2005) Reflexive polymers and hydrogels. Macromol Chem Phys 206:1691–1691. doi:10.1002/macp.200500275
37. Matsuo ES, Tanaka T (1988) Kinetics of discontinuous volume-phase transition of gels. J Chem Phys 89:1695–1703

38. Wu XS, Hoffman AS, Yager P (1992) Synthesis and characterization of thermally reversible macroporous poly(N-isopropylacrylamide) hydrogels. J Polym Sci, Part A: Polym Chem 30:2121–2129. doi:10.1002/pola.1992.080301005
39. Chen G, Hoffman AS (1995) Graft copolymers that exhibit temperature-induced phase transitions over a wide range of pH. Nature 373:49–52
40. Ebara M, Aoyagi T, Sakai K, Okano T (2000) Introducing reactive carboxyl side chains retains phase transition temperature sensitivity in N-Isopropylacrylamide copolymer gels. Macromolecules 33:8312–8316. doi:10.1021/ma000121j
41. Yoshida R, Uchida K, Kaneko Y, Sakai K, Kikuchi A, Sakurai Y, Okano T (1995) Comb-type grafted hydrogels with rapid deswelling response to temperature changes. Nature 374:240–242
42. Gacesa P (1988) Alginates. Carbohydr Polym 8:161–182. doi:http://dx.doi.org/10.1016/0144-8617(88)90001-X
43. Goosen MFA, O'Shea GM, Gharapetian HM, Chou S, Sun AM (1985) Optimization of microencapsulation parameters: Semipermeable microcapsules as a bioartificial pancreas. Biotechnol Bioeng 27:146–150. doi:10.1002/bit.260270207
44. Gombotz WR, Wee S (1998) Protein release from alginate matrices. Adv Drug Del Rev 31:267–285. doi:http://dx.doi.org/10.1016/S0169-409X(97)00124-5
45. Mumper RJ, Huffman AS, Puolakkainen PA, Bouchard LS, Gombotz WR (1994) Calcium-alginate beads for the oral delivery of transforming growth factor-β1 (TGF-β1): stabilization of TGF-β1 by the addition of polyacrylic acid within acid-treated beads. J Controlled Release 30:241–251. doi:http://dx.doi.org/10.1016/0168-3659(94)90030-2
46. Iskakov RM, Kikuchi A, Okano T (2002) Time-programmed pulsatile release of dextran from calcium-alginate gel beads coated with carboxy-n-propylacrylamide copolymers. J Controlled Release 80:57–68. doi:http://dx.doi.org/10.1016/S0168-3659(01)00551-X
47. Andrianov AK, Payne LG, Visscher KB, Allcock HR, Langer R (1994) Hydrolytic degradation of ionically cross-linked polyphosphazene microspheres. J Appl Polym Sci 53:1573–1578. doi:10.1002/app.1994.070531203
48. Liu L-S, Liu S-Q, Ng SY, Froix M, Ohno T, Heller J (1997) Controlled release of interleukin-2 for tumour immunotherapy using alginate/chitosan porous microspheres. J Controlled Release 43:65–74. doi:http://dx.doi.org/10.1016/S0168-3659(96)01471-X
49. Van Tomme SR, van Steenbergen MJ, De Smedt SC, van Nostrum CF, Hennink WE (2005) Self-gelling hydrogels based on oppositely charged dextran microspheres. Biomaterials 26:2129–2135. doi:http://dx.doi.org/10.1016/j.biomaterials.2004.05.035
50. Bromberg LE, Ron ES (1998) Temperature-responsive gels and thermogelling polymer matrices for protein and peptide delivery. Adv Drug Del Rev 31:197–221. doi:http://dx.doi.org/10.1016/S0169-409X(97)00121-X
51. Jeong B, Bae YH, Lee DS, Kim SW (1997) Biodegradable block copolymers as injectable drug-delivery systems. Nature 388:860–862
52. Jeong B, Bae YH, Kim SW (2000) Drug release from biodegradable injectable thermosensitive hydrogel of PEG–PLGA–PEG triblock copolymers. J Controlled Release 63:155–163. doi:http://dx.doi.org/10.1016/S0168-3659(99)00194-7
53. Jeong B, Choi YK, Bae YH, Zentner G, Kim SW (1999) New biodegradable polymers for injectable drug delivery systems. J Controlled Release 62:109–114. doi:http://dx.doi.org/10.1016/S0168-3659(99)00061-9
54. Akiyoshi K, Kobayashi S, Shichibe S, Mix D, Baudys M, Wan Kim S, Sunamoto J (1998) Self-assembled hydrogel nanoparticle of cholesterol-bearing pullulan as a carrier of protein drugs: complexation and stabilization of insulin. J Controlled Release 54:313–320. doi:http://dx.doi.org/10.1016/S0168-3659(98)00017-0
55. Taniguchi I, Akiyoshi K, Sunamoto J (1999) Self-aggregate nanoparticles of cholesteryl and galactoside groups-substituted pullulan and their specific binding to galactose specific lectin, RCA120. Macromol Chem Phys 200:1554–1560. doi:10.1002/(sici)1521-3935(19990601)200:6<1554:aid-macp1554>3.0.co;2-v

56. Chenite A, Chaput C, Wang D, Combes C, Buschmann MD, Hoemann CD, Leroux JC, Atkinson BL, Binette F, Selmani A (2000) Novel injectable neutral solutions of chitosan form biodegradable gels in situ. Biomaterials 21:2155–2161. doi:http://dx.doi.org/10.1016/S0142-9612(00)00116-2
57. Molinaro G, Leroux J-C, Damas J, Adam A (2002) Biocompatibility of thermosensitive chitosan-based hydrogels: an in vivo experimental approach to injectable biomaterials. Biomaterials 23:2717–2722. doi:http://dx.doi.org/10.1016/S0142-9612(02)00004-2
58. Bhattarai N, Ramay HR, Gunn J, Matsen FA, Zhang M (2005) PEG-grafted chitosan as an injectable thermosensitive hydrogel for sustained protein release. J Controlled Release 103:609–624. doi:http://dx.doi.org/10.1016/j.jconrel.2004.12.019
59. Kim SY, Cho SM, Lee YM, Kim SJ (2000) Thermo- and pH-responsive behaviors of graft copolymer and blend based on chitosan and N-isopropylacrylamide. J Appl Polym Sci 78:1381–1391. doi:10.1002/1097-4628(20001114)78:7<1381:aid-app90>3.0.co;2-m
60. Bajpai AK, Shrivastava J (2005) In vitro enzymatic degradation kinetics of polymeric blends of crosslinked starch and carboxymethyl cellulose. Polym Int 54:1524–1536. doi:10.1002/pi.1878
61. Gupta D, Tator CH, Shoichet MS (2006) Fast-gelling injectable blend of hyaluronan and methylcellulose for intrathecal, localized delivery to the injured spinal cord. Biomaterials 27:2370–2379. doi:http://dx.doi.org/10.1016/j.biomaterials.2005.11.015
62. Liu J, Lin S, Li L, Liu E (2005) Release of theophylline from polymer blend hydrogels. Int J Pharm 298:117–125. doi:http://dx.doi.org/10.1016/j.ijpharm.2005.04.006
63. Eagland D, Crowther NJ, Butler CJ (1994) Complexation between polyoxyethylene and polymethacrylic acid—The importance of the molar mass of polyoxyethylene. Eur Polym J 30:767–773. doi:http://dx.doi.org/10.1016/0014-3057(94)90003-5
64. Bell CL, Peppas NA (1996) Modulation of drug permeation through interpolymer complexed hydrogels for drug delivery applications. J Controlled Release 39:201–207. doi:http://dx.doi.org/10.1016/0168-3659(95)00154-9
65. Haglund BO, Joshi R, Himmelstein KJ (1996) An in situ gelling system for parenteral delivery. J Controlled Release 41:229–235. doi:http://dx.doi.org/10.1016/0168-3659(96)01333-8
66. Yokoyama F, Masada I, Shimamura K, Ikawa T, Monobe K (1986) Morphology and structure of highly elastic poly(vinyl alcohol) hydrogel prepared by repeated freezing-and-melting. Colloid Polym Sci 264:595–601. doi:10.1007/bf01412597
67. Stenekes RJH, Talsma H, Hennink WE (2001) Formation of dextran hydrogels by crystallization. Biomaterials 22:1891–1898. doi:http://dx.doi.org/10.1016/S0142-9612(00)00375-6
68. Tsuji H, Horii F, Nakagawa M, Ikada Y, Odani H, Kitamaru R (1992) Stereocomplex formation between enantiomeric poly(lactic acid)s. 7. Phase structure of the stereocomplex crystallized from a dilute acetonitrile solution as studied by high-resolution solid-state carbon-13 NMR spectroscopy. Macromolecules 25:4114–4118. doi:10.1021/ma00042a011
69. de Jong SJ, De Smedt SC, Wahls MWC, Demeester J, Kettenes-van den Bosch JJ, Hennink WE (2000) Novel self-assembled hydrogels by stereocomplex formation in aqueous solution of enantiomeric lactic acid oligomers grafted to dextran. Macromolecules 33:3680–3686. doi:10.1021/ma992067g
70. Lim DW, Park TG (2000) Stereocomplex formation between enantiomeric PLA–PEG–PLA triblock copolymers: characterization and use as protein-delivery microparticulate carriers. J Appl Polym Sci 75:1615–1623. doi:10.1002/(sici)1097-4628(20000328)75:13<1615:aid-app7>3.0.co;2-l
71. Mohammed JS, Murphy WL (2009) Bioinspired design of dynamic materials. Adv Mater 21:2361–2374. doi:10.1002/adma.200803785
72. Kollman PA (1977) Noncovalent interactions. Acc Chem Res 10:365–371. doi:10.1021/ar50118a003
73. West MW, Wang W, Patterson J, Mancias JD, Beasley JR, Hecht MH (1999) De novo amyloid proteins from designed combinatorial libraries. Proc Natl Acad Sci 96:11211–11216. doi:10.1073/pnas.96.20.11211

74. Ogihara NL, Ghirlanda G, Bryson JW, Gingery M, DeGrado WF, Eisenberg D (2001) Design of three-dimensional domain-swapped dimers and fibrous oligomers. Proc Natl Acad Sci 98:1404–1409. doi:10.1073/pnas.98.4.1404
75. Ye B, Maret W, Vallee BL (2001) Zinc metallothionein imported into liver mitochondria modulates respiration. Proc Natl Acad Sci 98:2317–2322. doi:10.1073/pnas.041619198
76. Cappello J, Crissman J, Dorman M, Mikolajczak M, Textor G, Marquet M, Ferrari F (1990) Genetic engineering of structural protein polymers. Biotechnol Progr 6:198–202. doi:10.1021/bp00003a006
77. Cappello J, Crissman JW, Crissman M, Ferrari FA, Textor G, Wallis O, Whitledge JR, Zhou X, Burman D, Aukerman L, Stedronsky ER (1998) In situ self-assembling protein polymer gel systems for administration, delivery, and release of drugs. J Controlled Release 53:105–117. doi:http://dx.doi.org/10.1016/S0168-3659(97)00243-5
78. Chen L, Kopeček J, Stewart RJ (2000) Responsive hybrid hydrogels with volume transitions modulated by a titin immunoglobulin module. Bioconjugate Chem 11:734–740. doi:10.1021/bc000046h
79. Miyata T, Asami N, Uragami T (1999) A reversibly antigen-responsive hydrogel. Nature 399:766–769. doi:http://www.nature.com/nature/journal/v399/n6738/suppinfo/399766a0_S1.html
80. Lee SJ, Park K (1996) Synthesis and characterization of sol–gel phase-reversible hydrogels sensitive to glucose. J Mol Recognit 9:549–557. doi:10.1002/(sici)1099-1352(199634/12)9:5/6<549:aid-jmr299>3.0.co;2-c
81. Obaidat A, Park K (1996) Characterization of glucose dependent gel–sol phase transition of the polymeric glucose-concanavalin a hydrogel system. Pharm Res 13:989–995. doi:10.1023/a:1016090103979
82. Obaidat AA, Park K (1997) Characterization of protein release through glucose-sensitive hydrogel membranes. Biomaterials 18:801–806. doi:http://dx.doi.org/10.1016/S0142-9612(96)00198-6
83. Matsuo ES, Tanaka T (1992) Patterns in shrinking gels. Nature 358:482–485
84. Tanaka T (1978) Collapse of gels and the critical endpoint. Phys Rev Lett 40:820–823
85. Tanaka T, Sun S-T, Hirokawa Y, Katayama S, Kucera J, Hirose Y, Amiya T (1987) Mechanical instability of gels at the phase transition. Nature 325:796–798
86. Cadée JA, van Steenbergen MJ, Versluis C, Heck AJR, Underberg WJM, den Otter W, Jiskoot W, Hennink WE (2001) Oxidation of recombinant human interleukin-2 by potassium peroxodisulfate. Pharm Res 18:1461–1467. doi:10.1023/a:1012213108319
87. Edman P, Ekman B, Sjöholm I (1980) Immobilization of proteins in microspheres of biodegradable polyacryldextran. J Pharm Sci 69:838–842. doi:10.1002/jps.2600690725
88. Park K (1988) Enzyme-digestible swelling hydrogels as platforms for long-term oral drug delivery: synthesis and characterization. Biomaterials 9:435–441. doi:http://dx.doi.org/10.1016/0142-9612(88)90009-9
89. Heller J, Pangburn SH, Roskos KV (1990) Development of enzymatically degradable protective coatings for use in triggered drug delivery systems: derivatized starch hydrogels. Biomaterials 11:345–350. doi:http://dx.doi.org/10.1016/0142-9612(90)90112-4
90. Giammona G, Pitarresi G, Cavallaro G, Buscemi S, Saiano F (1999) New biodegradable hydrogels based on a photocrosslinkable modified polyaspartamide: synthesis and characterization. Biochimica et Biophysica Acta (BBA)—Gen Subj 1428:29–38. doi:http://dx.doi.org/10.1016/S0304-4165(99)00051-3
91. Martens P, Anseth KS (2000) Characterization of hydrogels formed from acrylate modified poly(vinyl alcohol) macromers. Polymer 41:7715–7722. doi:http://dx.doi.org/10.1016/S0032-3861(00)00123-3
92. Jin Y, Yamanaka J, Sato S, Miyata I, Yomota C, Yonese M (2001) Recyclable characteristics of hyaluronate–polyhydroxyethyl acrylate blend hydrogel for controlled releases. J Controlled Release 73:173–181. doi:http://dx.doi.org/10.1016/S0168-3659(01)00234-6
93. Doycheva M, Petrova E, Stamenova R, Tsvetanov C, Riess G (2004) UV-induced crosslinking of poly(ethylene oxide) in aqueous solution. Macromol Mater Eng 289:676–680. doi:10.1002/mame.200400073

94. Fedorovich NE, Oudshoorn MH, van Geemen D, Hennink WE, Alblas J, Dhert WJA (2009) The effect of photopolymerization on stem cells embedded in hydrogels. Biomaterials 30:344–353. doi:http://dx.doi.org/10.1016/j.biomaterials.2008.09.037
95. Lee HJ, Matsuda T (1999) Surface photograft polymerization on segmented polyurethane using the iniferter technique. J Biomed Mater Res 47:564–567. doi:10.1002/(sici)1097-4636(19991215)47:4<564:aid-jbm13>3.0.co;2-3
96. Rodrigues MR, Gasetta D (2007) Hydrogels produced by photocrosslinking of dextran chain: characterization and properties. J Carbohydr Chem 26:439–453. doi:10.1080/07328300701737912
97. Ward JH, Peppas NA (2001) Preparation of controlled release systems by free-radical UV polymerizations in the presence of a drug. J Controlled Release 71:183–192. doi:http://dx.doi.org/10.1016/S0168-3659(01)00213-9
98. Mironi-Harpaz I, Wang DY, Venkatraman S, Seliktar D (2012) Photopolymerization of cell-encapsulating hydrogels: Crosslinking efficiency versus cytotoxicity. Acta Biomater 8:1838–1848. doi:http://dx.doi.org/10.1016/j.actbio.2011.12.034
99. Dai WS, Barbari TA (1999) Hydrogel membranes with mesh size asymmetry based on the gradient crosslinking of poly(vinyl alcohol). J Membr Sci 156:67–79. doi:http://dx.doi.org/10.1016/S0376-7388(98)00330-5
100. Peppas NA, Berner Jr RE (1980) Proposed method of intracopdal injection and gelation of poly (vinyl alcohol) solution in vocal cords: polymer considerations. Biomaterials 1:158–162. doi:http://dx.doi.org/10.1016/0142-9612(80)90039-3
101. Jameela SR, Jayakrishnan A (1995) Glutaraldehyde cross-linked chitosan microspheres as a long acting biodegradable drug delivery vehicle: studies on the in vitro release of mitoxantrone and in vivo degradation of microspheres in rat muscle. Biomaterials 16:769–775. doi:http://dx.doi.org/10.1016/0142-9612(95)99639-4
102. Tabata Y, Ikada Y (1989) Synthesis of gelatin microspheres containing interferon. Pharm Res 6:422–427. doi:10.1023/a:1015991617704
103. Draye J-P, Delaey B, Van de Voorde A, Van Den Bulcke A, Bogdanov B, Schacht E (1998) In vitro release characteristics of bioactive molecules from dextran dialdehyde cross-linked gelatin hydrogel films. Biomaterials 19:99–107. doi:http://dx.doi.org/10.1016/S0142-9612(97)00164-6
104. Lee KY, Bouhadir KH, Mooney DJ (1999) Degradation behavior of covalently cross-linked poly(aldehyde guluronate) hydrogels. Macromolecules 33:97–101. doi:10.1021/ma991286z
105. Bouhadir KH, Kruger GM, Lee KY, Mooney DJ (2000) Sustained and controlled release of daunomycin from cross-linked poly(aldehyde guluronate) hydrogels. J Pharm Sci 89:910–919. doi:10.1002/1520-6017(200007)89:7<910:aid-jps8>3.0.co;2-#
106. Luo Y, Kirker KR, Prestwich GD (2000) Cross-linked hyaluronic acid hydrogel films: new biomaterials for drug delivery. J Controlled Release 69:169–184. doi:http://dx.doi.org/10.1016/S0168-3659(00)00300-X
107. Hovgaard L, Brøndsted H (1995) Dextran hydrogels for colon-specific drug delivery. J Controlled Release 36:159–166. doi:http://dx.doi.org/10.1016/0168-3659(95)00049-E
108. Gehrke SH, Uhden LH, McBride JF (1998) Enhanced loading and activity retention of bioactive proteins in hydrogel delivery systems. J Controlled Release 55:21–33. doi:http://dx.doi.org/10.1016/S0168-3659(98)00019-4
109. Coviello T, Grassi M, Rambone G, Santucci E, Carafa M, Murtas E, Riccieri FM, Alhaique F (1999) Novel hydrogel system from scleroglucan: synthesis and characterization. J Controlled Release 60:367–378. doi:http://dx.doi.org/10.1016/S0168-3659(99)00091-7
110. Kuijpers AJ, van Wachem PB, van Luyn MJA, Engbers GHM, Krijgsveld J, Zaat SAJ, Dankert J, Feijen J (2000) In vivo and in vitro release of lysozyme from cross-linked gelatin hydrogels: a model system for the delivery of antibacterial proteins from prosthetic heart valves. J Controlled Release 67:323–336. doi:http://dx.doi.org/10.1016/S0168-3659(00)00221-2
111. Eiselt P, Lee KY, Mooney DJ (1999) Rigidity of two-component hydrogels prepared from alginate and poly(ethylene glycol)-diamines. Macromolecules 32:5561–5566. doi:10.1021/ma990514m

112. de Nooy AEJ, Capitani D, Masci G, Crescenzi V (2000) Ionic polysaccharide hydrogels via the Passerini and Ugi multicomponent condensations: synthesis, behavior and solid-state NMR characterization. Biomacromolecules 1:259–267. doi:10.1021/bm005517h
113. de Nooy AEJ, Masci G, Crescenzi V (1999) Versatile synthesis of polysaccharide hydrogels using the Passerini and Ugi multicomponent condensations. Macromolecules 32:1318–1320. doi:10.1021/ma9815455
114. Yoshida T, Aoyagi T, Kokufuta E, Okano T (2003) Newly designed hydrogel with both sensitive thermoresponse and biodegradability. J Polym Sci, Part A: Polym Chem 41:779–787. doi:10.1002/pola.10595
115. Sperinde JJ, Griffith LG (1997) Synthesis and characterization of enzymatically-cross-linked poly(ethylene glycol) hydrogels. Macromolecules 30:5255–5264. doi:10.1021/ma970345a
116. Sperinde JJ, Griffith LG (2000) Control and prediction of gelation kinetics in enzymatically cross-linked poly(ethylene glycol) hydrogels. Macromolecules 33:5476–5480. doi:10.1021/ma000459d
117. Peppas NA, Merrill EW (1977) Crosslinked poly(vinyl alcohol) hydrogels as swollen elastic networks. J Appl Polym Sci 21:1763–1770. doi:10.1002/app.1977.070210704
118. Kofinas P, Athanassiou V, Merrill EW (1996) Hydrogels prepared by electron irradiation of poly(ethylene oxide) in water solution: unexpected dependence of cross-link density and protein diffusion coefficients on initial PEO molecular weight. Biomaterials 17:1547–1550. doi:http://dx.doi.org/10.1016/0142-9612(96)89781-X
119. Jabbari E, Nozari S (2000) Swelling behavior of acrylic acid hydrogels prepared by γ-radiation crosslinking of polyacrylic acid in aqueous solution. Eur Polym J 36:2685–2692. doi:http://dx.doi.org/10.1016/S0014-3057(00)00044-6
120. Kishi R, Ichijo H, Hirasa O (1993) Thermo-responsive devices using poly(vinyl methyl ether) hydrogels. J Intell Mater Syst Struct 4:533–537. doi:10.1177/1045389x9300400413
121. Suzuki M, Hirasa O (1993) An approach to artificial muscle using polymer gels formed by micro-phase separation. In: Dušek K (ed) responsive gels: volume transitions II, vol 110. Advances in polymer science. Springer, Berlin, pp 241–261. doi:10.1007/BFb0021135
122. Kishi R, Hirasa O, Ichijo H (1997) Fast responsive poly(N-sopropylacrylamide) hydrogels prepared by γ-ray irradiation. Polym Gels Networks 5:145–151. doi:http://dx.doi.org/10.1016/S0966-7822(96)00037-8
123. Matsukuma D, Yamamoto K, Aoyagi T (2006) Stimuli-responsive properties of n-isopropylacrylamide-based ultrathin hydrogel films prepared by photo-cross-linking. Langmuir 22:5911–5915. doi:10.1021/la060438y
124. Bae Y, Okano T, Kim S (1991) "On–Off" thermocontrol of solute transport. I. Temperature dependence of swelling of N-isopropylacrylamide networks modified with hydrophobic components in water. Pharm Res 8:531–537. doi:10.1023/a:1015871732706
125. Kaneko Y, Nakamura S, Sakai K, Aoyagi T, Kikuchi A, Sakurai Y, Okano T (1998) Rapid deswelling response of poly(N-isopropylacrylamide) hydrogels by the formation of water release channels using poly(ethylene oxide) graft chains. Macromolecules 31:6099–6105. doi:10.1021/ma971899g
126. Aoyagi T, Ebara M, Sakai K, Sakurai Y, Okano T (2000) Novel bifunctional polymer with reactivity and temperature sensitivity. J Biomater Sci Polym Ed 11:101–110. doi:10.1163/156856200743526
127. Ebara M, Yamato M, Hirose M, Aoyagi T, Kikuchi A, Sakai K, Okano T (2003) Copolymerization of 2-carboxyisopropylacrylamide with N-isopropylacrylamide accelerates cell detachment from grafted surfaces by reducing temperature. Biomacromolecules 4:344–349. doi:10.1021/bm025692t
128. Ebara M, Aoyagi T, Sakai K, Okano T (2001) The incorporation of carboxylate groups into temperature-responsive poly(N-isopropylacrylamide)-based hydrogels promotes rapid gel shrinking. J Polym Sci, Part A: Polym Chem 39:335–342. doi:10.1002/1099-0518(20010201)39:3<335:aid-pola1000>3.0.co;2-h

129. Shimoboji T, Larenas E, Fowler T, Kulkarni S, Hoffman AS, Stayton PS (2002) Photoresponsive polymer–enzyme switches. Proc Natl Acad Sci 99:16592–16596. doi:10.1073/pnas.262427799
130. Techawanitchai P, Idota N, Uto K, Ebara M, Aoyagi T (2012) A smart hydrogel-based time bomb triggers drug release mediated by pH-jump reaction. Sci Technol Adv Mat 13:064202
131. Tomatsu I, Peng K, Kros A (2011) Photoresponsive hydrogels for biomedical applications. Adv Drug Del Rev 63:1257–1266. doi:http://dx.doi.org/10.1016/j.addr.2011.06.009
132. Shinkai S, Kinda H, Manabe O (1982) Photoresponsive complexation of metal cations with an azobenzene-crown-azobenzene bridge immobilized in polymer supports. J Am Chem Soc 104:2933–2934. doi:10.1021/ja00374a045
133. Mamada A, Tanaka T, Kungwatchakun D, Irie M (1990) Photoinduced phase transition of gels. Macromolecules 23:1517–1519. doi:10.1021/ma00207a046
134. Sumaru K, Ohi K, Takagi T, Kanamori T, Shinbo T (2006) Photoresponsive properties of poly(N-isopropylacrylamide) hydrogel partly modified with spirobenzopyran. Langmuir 22:4353–4356. doi:10.1021/la052899+
135. Takashima Y, Hatanaka S, Otsubo M, Nakahata M, Kakuta T, Hashidzume A, Yamaguchi H, Harada A (2012) Expansion–contraction of photoresponsive artificial muscle regulated by host–guest interactions. Nat Commun 3:1270. doi:http://www.nature.com/ncomms/journal/v3/n12/suppinfo/ncomms2280_S1.html
136. Suzuki A, Tanaka T (1990) Phase transition in polymer gels induced by visible light. Nature 346:345–347
137. Techawanitchai P, Ebara M, Idota N, Aoyagi T (2012) Light-induced spatial control of pH-jump reaction at smart gel interface. Colloids Surf B Biointerfaces 99:53–59. doi:http://dx.doi.org/10.1016/j.colsurfb.2011.09.039
138. Osada Y, Hasebe M (1985) Electrically activated mecnanochemical devices using polyelectrolyte gels. Chem Lett 14:1285–1288
139. Tanaka T, Nishio I, Sun S-T, Ueno-Nishio S (1982) Collapse of gels in an electric field. Science 218:467–469. doi:10.1126/science.218.4571.467
140. Lee KK, Cussler EL, Marchetti M, McHugh MA (1990) Pressure-dependent phase transitions in hydrogels. Chem Eng Sci 45:766–767. doi:10.1016/0009-2509(90)87019-o
141. Zhong X, Wang Y-X, Wang S-C (1996) Pressure dependence of the volume phase-transition of temperature-sensitive gels. Chem Eng Sci 51:3235–3239. doi:http://dx.doi.org/10.1016/0009-2509(95)00344-4
142. Nichols TC, Fischer TH, Deliargyris EN, Baldwin AS (2001) Role of nuclear factor-kappa B (NF-κB) in inflammation, periodontitis, and atherogenesis. Ann Periodontol 6:20–29. doi:10.1902/annals.2001.6.1.20
143. Brannon-Peppas L, Peppas NA (1990) Dynamic and equilibrium swelling behaviour of pH-sensitive hydrogels containing 2-hydroxyethyl methacrylate. Biomaterials 11:635–644. doi:http://dx.doi.org/10.1016/0142-9612(90)90021-H
144. Ghandehari H, Kopečková P, Kopecek J (1997) In vitro degradation of pH-sensitive hydrogels containing aromatic azo bonds. Biomaterials 18:861–872. doi:http://dx.doi.org/10.1016/S0142-9612(97)00007-0
145. Siegel RA, Falamarzian M, Firestone BA, Moxley BC (1988) pH-Controlled release from hydrophobic/polyelectrolyte copolymer hydrogels. J Controlled Release 8:179–182. doi:http://dx.doi.org/10.1016/0168-3659(88)90044-2
146. Lee ES, Gao Z, Bae YH (2008) Recent progress in tumor pH targeting nanotechnology. J Controlled Release 132:164–170. doi:http://dx.doi.org/10.1016/j.jconrel.2008.05.003
147. Gatenby RA, Gillies RJ (2004) Why do cancers have high aerobic glycolysis? Nat Rev Cancer 4:891–899
148. Duncan R (1999) Polymer conjugates for tumour targeting and intracytoplasmic delivery. The EPR effect as a common gateway? Pharm Sci Technol Today 2:441–449. doi:http://dx.doi.org/10.1016/S1461-5347(99)00211-4
149. Garbern JC, Hoffman AS, Stayton PS (2010) Injectable pH- and temperature-responsive poly(N-isopropylacrylamide-co-propylacrylic acid) copolymers for delivery of angiogenic growth factors. Biomacromolecules 11:1833–1839. doi:10.1021/bm100318z

150. Convertine AJ, Diab C, Prieve M, Paschal A, Hoffman AS, Johnson PH, Stayton PS (2010) pH-responsive polymeric micelle carriers for siRNA drugs. Biomacromolecules 11:2904–2911. doi:10.1021/bm100652w
151. Ta T, Convertine AJ, Reyes CR, Stayton PS, Porter TM (2010) Thermosensitive liposomes modified with poly(N-isopropylacrylamide-co-propylacrylic acid) copolymers for triggered release of doxorubicin. Biomacromolecules 11:1915–1920. doi:10.1021/bm1004993
152. Berguig GY, Convertine AJ, Shi J, Palanca-Wessels MC, Duvall CL, Pun SH, Press OW, Stayton PS (2012) Intracellular delivery and trafficking dynamics of a lymphoma-targeting antibody-polymer conjugate. Mol Pharm 9:3506–3514. doi:10.1021/mp300338s
153. Brownlee M, Cerami A (1979) A glucose-controlled insulin-delivery system: semisynthetic insulin bound to lectin. Science 206:1190–1191. doi:10.1126/science.505005
154. Kataoka K, Miyazaki H, Bunya M, Okano T, Sakurai Y (1998) Totally synthetic polymer gels responding to external glucose concentration: their preparation and application to on–off regulation of insulin release. J Am Chem Soc 120:12694–12695. doi:10.1021/ja982975d
155. Matsumoto A, Ikeda S, Harada A, Kataoka K (2003) Glucose-responsive polymer bearing a novel phenylborate derivative as a glucose-sensing moiety operating at physiological pH conditions. Biomacromolecules 4:1410–1416. doi:10.1021/bm034139o
156. Matsumoto A, Yoshida R, Kataoka K (2004) Glucose-responsive polymer gel bearing phenylborate derivative as a glucose-sensing moiety operating at the physiological pH. Biomacromolecules 5:1038–1045. doi:10.1021/bm0345413
157. Miyata T, Jige M, Nakaminami T, Uragami T (2006) Tumor marker-responsive behavior of gels prepared by biomolecular imprinting. P Natl Acad Sci USA 103:1190–1193. doi:10.1073/pnas.0506786103
158. Suzuki Y, Tanihara M, Nishimura Y, Suzuki K, Kakimaru Y, Shimizu Y (1998) A new drug delivery system with controlled release of antibiotic only in the presence of infection. J Biomed Mater Res 42:112–116. doi:10.1002/(sici)1097-4636(199810)42:1<112:aid-jbm14>3.0.co;2-n
159. Murakami Y, Maeda M (2005) DNA-responsive hydrogels that can shrink or swell. Biomacromolecules 6:2927–2929. doi:10.1021/bm0504330
160. Nagahara S, Matsuda T (1996) Hydrogel formation via hybridization of oligonucleotides derivatized in water-soluble vinyl polymers. Polym Gels Netw 4:111–127. doi:http://dx.doi.org/10.1016/0966-7822(96)00001-9
161. Suzuki D, Sakai T, Yoshida R (2008) Self-flocculating/self-dispersing oscillation of microgels. Angew Chem Int Ed 47:917–920. doi:10.1002/anie.200703953
162. Yoshida R, Takahashi T, Yamaguchi T, Ichijo H (1996) Self-oscillating gel. J Am Chem Soc 118:5134–5135. doi:10.1021/ja9602511
163. Yoshida R, Takahashi T, Yamaguchi T, Ichijo H (1997) Self-oscillating gels. Adv Mater 9:175–178. doi:10.1002/adma.19970090219
164. Lin C-C, Metters AT (2006) Hydrogels in controlled release formulations: network design and mathematical modeling. Adv Drug Del Rev 58:1379–1408. doi:http://dx.doi.org/10.1016/j.addr.2006.09.004
165. Peppas NA, Hilt JZ, Khademhosseini A, Langer R (2006) Hydrogels in biology and medicine: from molecular principles to bionanotechnology. Adv Mater 18:1345–1360. doi:10.1002/adma.200501612
166. Flory PJ (1942) Thermodynamics of high polymer solutions. J Chem Phys 10:51–61
167. Huggins ML (1942) Some properties of solutions of long-chain compounds. J Phys Chem 46:151–158. doi:10.1021/j150415a018
168. Kaneko Y, Yoshida R, Sakai K, Sakurai Y, Okano T (1995) Temperature-responsive shrinking kinetics of poly (N-isopropylacrylamide) copolymer gels with hydrophilic and hydrophobic comonomers. J Membr Sci 101:13–22. doi:http://dx.doi.org/10.1016/0376-7388(94)00268-4
169. Shibayama M (2012) Structure-mechanical property relationship of tough hydrogels. Soft Matter 8:8030–8038
170. Okumura Y, Ito K (2001) The polyrotaxane gel: a topological gel by figure-of-eight cross-links. Adv Mater 13:485–487. doi:10.1002/1521-4095(200104)13:7<485:aid-adma485>3.0.co;2-t
171. Gong JP, Katsuyama Y, Kurokawa T, Osada Y (2003) Double-network hydrogels with extremely high mechanical strength. Adv Mater 15:1155–1158. doi:10.1002/adma.200304907

172. Anseth KS, Bowman CN, Brannon-Peppas L (1996) Mechanical properties of hydrogels and their experimental determination. Biomaterials 17:1647–1657. doi:http://dx.doi.org/10.1016/0142-9612(96)87644-7
173. Brandl F, Sommer F, Goepferich A (2007) Rational design of hydrogels for tissue engineering: impact of physical factors on cell behavior. Biomaterials 28:134–146. doi:http://dx.doi.org/10.1016/j.biomaterials.2006.09.017
174. Shibayama M (2011) Small-angle neutron scattering on polymer gels: phase behavior, inhomogeneities and deformation mechanisms. Polym J 43:18–34
175. Shibayama M, Tanaka T, Han CC (1992) Small angle neutron scattering study on poly(N-isopropyl acrylamide) gels near their volume-phase transition temperature. J Chem Phys 97:6829–6841. doi:doi:http://dx.doi.org/10.1063/1.463636
176. Strain DE, Kennelly RG, Dittmar HR (1939) Methacrylate resins. Ind Eng Chem 31:382–387. doi:10.1021/ie50352a003
177. Okano T, Bae YH, Jacobs H, Kim SW (1990) Thermally on-off switching polymers for drug permeation and release. J Controlled Release 11:255–265. doi:http://dx.doi.org/10.1016/0168-3659(90)90138-J
178. Yoshida R, Sakai K, Okano T, Sakurai Y (1992) Surface-modulated skin layers of thermal responsive hydrogels as on-off switches: II. Drug permeation. J Biomater Sci Polym Ed 3:243–252. doi:10.1163/156856292x00150
179. Yoshida R, Sakai K, Okano T, Sakurai Y, You Han B, Sung Wan K (1992) Surface-modulated skin layers of thermal responsive hydrogels as on-off switches: I. Drug release. J Biomater Sci Polym Ed 3:155–162. doi:10.1163/156856291x00250
180. Yoshida R, Sakai K, Okano T, Sakurai Y (1995) Modulating the phase transition temperature and thermosensitivity in N-isopropylacrylamide copolymer gels. J Biomater Sci Polym Ed 6:585–598. doi:10.1163/156856294x00536
181. Brazel CS, Peppas NA (1996) Pulsatile local delivery of thrombolytic and antithrombotic agents using poly(N-isopropylacrylamide-co-methacrylic acid) hydrogels. J Controlled Release 39:57–64. doi:http://dx.doi.org/10.1016/0168-3659(95)00134-4
182. Pelton R (2000) Temperature-sensitive aqueous microgels. Adv Colloid Interface Sci 85:1–33. doi:http://dx.doi.org/10.1016/S0001-8686(99)00023-8
183. Pelton RH, Chibante P (1986) Preparation of aqueous latices with N-isopropylacrylamide. Colloids Surf 20:247–256. doi:http://dx.doi.org/10.1016/0166-6622(86)80274-8
184. Omura T, Ebara M, Lai JJ, Yin X, Hoffman AS, Stayton PS (2014) Design of smart nanogels that respond to physiologically relevant pH values and temperature. J Nanosci Nanotechnol 14:2557–2562. doi:10.1166/jnn.2014.855/
185. Nguyen MK, Lee DS (2010) Injectable biodegradable hydrogels. Macromol Biosci 10:563–579. doi:10.1002/mabi.200900402
186. Winternitz C, Jackson J, Oktaba A, Burt H (1996) Development of a polymeric surgical paste formulation for taxol. Pharm Res 13:368–375. doi:10.1023/a:1016032207246
187. Malmsten M, Lindman B (1992) Self-assembly in aqueous block copolymer solutions. Macromolecules 25:5440–5445. doi:10.1021/ma00046a049
188. Wei G, Xu H, Ding PT, Li SM, Zheng JM (2002) Thermosetting gels with modulated gelation temperature for ophthalmic use: the rheological and gamma scintigraphic studies. J Controlled Release 83:65–74. doi:http://dx.doi.org/10.1016/S0168-3659(02)00175-X
189. Cohen S, Lobel E, Trevgoda A, Peled Y (1997) A novel in situ-forming ophthalmic drug delivery system from alginates undergoing gelation in the eye. J Controlled Release 44:201–208. doi:http://dx.doi.org/10.1016/S0168-3659(96)01523-4
190. Bossard F, Aubry T, Gotzamanis G, Tsitsilianis C (2006) pH-Tunable rheological properties of a telechelic cationic polyelectrolyte reversible hydrogel. Soft Matter 2:510–516
191. Shim WS, Kim SW, Lee DS (2006) Sulfonamide-based pH- and temperature-sensitive biodegradable block copolymer hydrogels. Biomacromolecules 7:1935–1941. doi:10.1021/bm0600567
192. Shim WS, Yoo JS, Bae YH, Lee DS (2005) Novel injectable pH and temperature sensitive block copolymer hydrogel. Biomacromolecules 6:2930–2934. doi:10.1021/bm050521k

193. Murthy N, Campbell J, Fausto N, Hoffman AS, Stayton PS (2003) Design and synthesis of pH-responsive polymeric carriers that target uptake and enhance the intracellular delivery of oligonucleotides. J Controlled Release 89:365–374. doi:http://dx.doi.org/10.1016/S0168-3659(03)00099-3
194. Yin X, Hoffman AS, Stayton PS (2006) Poly(N-isopropylacrylamide-co-propylacrylic acid) copolymers that respond sharply to temperature and pH. Biomacromolecules 7:1381–1385. doi:10.1021/bm0507812
195. Ross RA, Lee M-LT, Onderdonk A (1995) Effect of Candida albicans infection and clotrimazole treatment on vaginal microflora in vitro. Obstet Gynecol 86:925–930. doi:http://dx.doi.org/10.1016/0029-7844(95)00318-L
196. Chang JY, Oh Y-K, Kong HS, Kim EJ, Jang DD, Nam KT, Kim C-K (2002) Prolonged antifungal effects of clotrimazole-containing mucoadhesive thermosensitive gels on vaginitis. J Controlled Release 82:39–50. doi:http://dx.doi.org/10.1016/S0168-3659(02)00086-X
197. Drury JL, Mooney DJ (2003) Hydrogels for tissue engineering: scaffold design variables and applications. Biomaterials 24:4337–4351. doi:http://dx.doi.org/10.1016/S0142-9612(03)00340-5
198. Matsuda T (2004) Poly(N-isopropylacrylamide)-grafted gelatin as a thermoresponsive cell-adhesive, mold-releasable material for shape-engineered tissues. J Biomater Sci Polym Ed 15:947–955. doi:10.1163/1568562041271101
199. Ohya S, Nakayama Y, Matsuda T (2001) Thermoresponsive artificial extracellular matrix for tissue engineering: hyaluronic acid bioconjugated with poly(N-isopropylacrylamide) grafts. Biomacromolecules 2:856–863. doi:10.1021/bm010040a
200. Ha DI, Lee SB, Chong MS, Lee YM, Kim SY, Park YH (2006) Preparation of thermoresponsive and injectable hydrogels based on hyaluronic acid and poly(N-isopropylacrylamide) and their drug release behaviors. Macromol Res 14:87–93. doi:10.1007/bf03219073
201. Stile RA, Burghardt WR, Healy KE (1999) Synthesis and characterization of injectable poly(N-isopropylacrylamide)-based hydrogels that support tissue formation in vitro. Macromolecules 32:7370–7379. doi:10.1021/ma990130w
202. Lee DY, Nam JH, Byun Y (2007) Functional and histological evaluation of transplanted pancreatic islets immunoprotected by PEGylation and cyclosporine for 1 year. Biomaterials 28:1957–1966. doi:http://dx.doi.org/10.1016/j.biomaterials.2006.12.015
203. Miura S, Teramura Y, Iwata H (2006) Encapsulation of islets with ultra-thin polyion complex membrane through poly(ethylene glycol)-phospholipids anchored to cell membrane. Biomaterials 27:5828–5835. doi:http://dx.doi.org/10.1016/j.biomaterials.2006.07.039
204. Teramura Y, Kaneda Y, Iwata H (2007) Islet-encapsulation in ultra-thin layer-by-layer membranes of poly(vinyl alcohol) anchored to poly(ethylene glycol)–lipids in the cell membrane. Biomaterials 28:4818–4825. doi:http://dx.doi.org/10.1016/j.biomaterials.2007.07.050
205. Williams CG, Malik AN, Kim TK, Manson PN, Elisseeff JH (2005) Variable cytocompatibility of six cell lines with photoinitiators used for polymerizing hydrogels and cell encapsulation. Biomaterials 26:1211–1218. doi:http://dx.doi.org/10.1016/j.biomaterials.2004.04.024
206. Salinas CN, Cole BB, Kasko AM, Anseth KS (2007) Chondrogenic differentiation potential of human mesenchymal stem cells photoencapsulated within poly(ethylene glycol)-arginine-glycine-aspartic acid-serine thiol-methacrylate mixed-mode networks. Tissue Eng 13:1025–1034. doi:10.1089/ten.2006.0126
207. Lutolf MP, Hubbell JA (2005) Synthetic biomaterials as instructive extracellular microenvironments for morphogenesis in tissue engineering. Nat Biotech 23:47–55
208. Lutolf MP, Lauer-Fields JL, Schmoekel HG, Metters AT, Weber FE, Fields GB, Hubbell JA (2003) Synthetic matrix metalloproteinase-sensitive hydrogels for the conduction of tissue regeneration: engineering cell-invasion characteristics. Proc Natl Acad Sci 100:5413–5418. doi:10.1073/pnas.0737381100
209. Kim S, Chung EH, Gilbert M, Healy KE (2005) Synthetic MMP-13 degradable ECMs based on poly(N-isopropylacrylamide-co-acrylic acid) semi-interpenetrating polymer networks. I. Degradation and cell migration. J Biomed Mater Res, Part A 75A:73–88. doi:10.1002/jbm.a.30375

210. Kwon GH, Park JY, Kim JY, Frisk ML, Beebe DJ, Lee S-H (2008) Biomimetic soft multifunctional miniature aquabots. Small 4:2148–2153. doi:10.1002/smll.200800315
211. Smela E, Inganäs O, Lundström I (1995) Controlled folding of micrometer-size structures. Science 268:1735–1738. doi:10.1126/science.268.5218.1735
212. Okuzaki H, Hosaka K, Suzuki H, Ito T (2010) Effect of temperature on humido-sensitive conducting polymer actuators. Sens Actuators A: Phys 157:96–99. doi:http://dx.doi.org/10.1016/j.sna.2009.10.022
213. Okuzaki H, Kunugi T (1998) Electrically induced contraction of polypyrrole film in ambient air. J Polym Sci, Part B: Polym Phys 36:1591–1594. doi:10.1002/(sici)1099-0488(19980715)36:9<1591:aid-polb16>3.0.co;2-0
214. Hu Z, Zhang X, Li Y (1995) Synthesis and application of modulated polymer gels. Science 269:525–527. doi:10.1126/science.269.5223.525
215. Stoychev G, Puretskiy N, Ionov L (2011) Self-folding all-polymer thermoresponsive microcapsules. Soft Matter 7:3277–3279
216. Jeong K-U, Jang J-H, Kim D-Y, Nah C, Lee JH, Lee M-H, Sun H-J, Wang C-L, Cheng SZD, Thomas EL (2011) Three-dimensional actuators transformed from the programmed two-dimensional structures via bending, twisting and folding mechanisms. J Mater Chem 21:6824–6830
217. He H, Guan J, Lee JL (2006) An oral delivery device based on self-folding hydrogels. J Controlled Release 110:339–346. doi:http://dx.doi.org/10.1016/j.jconrel.2005.10.017
218. Zhang X, Pint CL, Lee MH, Schubert BE, Jamshidi A, Takei K, Ko H, Gillies A, Bardhan R, Urban JJ, Wu M, Fearing R, Javey A (2011) Optically- and thermally-responsive programmable materials based on carbon nanotube-hydrogel polymer composites. Nano Lett 11:3239–3244. doi:10.1021/nl201503e
219. Luchnikov V, Sydorenko O, Stamm M (2005) Self-rolled polymer and composite polymer/metal micro- and nanotubes with patterned inner walls. Adv Mater 17:1177–1182. doi:10.1002/adma.200401836
220. Kumar K, Nandan B, Luchnikov V, Simon F, Vyalikh A, Scheler U, Stamm M (2009) A novel approach for the fabrication of silica and silica/metal hybrid microtubes. Chem Mater 21:4282–4287. doi:10.1021/cm901472x
221. Bassik N, Abebe BT, Laflin KE, Gracias DH (2010) Photolithographically patterned smart hydrogel based bilayer actuators. Polymer 51:6093–6098. doi:http://dx.doi.org/10.1016/j.polymer.2010.10.035
222. Asoh T-A, Kikuchi A (2010) Electrophoretic adhesion of stimuli-responsive hydrogels. Chem Commun 46:7793–7795
223. Dong L, Jiang H (2007) Autonomous microfluidics with stimuli-responsive hydrogels. Soft Matter 3:1223–1230
224. Whitesides GM (2006) The origins and the future of microfluidics. Nature 442:368–373
225. Beebe DJ, Moore JS, Yu Q, Liu RH, Kraft ML, Jo B-H, Devadoss C (2000) Microfluidic tectonics: a comprehensive construction platform for microfluidic systems. Proc Natl Acad Sci 97:13488–13493. doi:10.1073/pnas.250273097
226. Yu Q, Bauer JM, Moore JS, Beebe DJ (2001) Responsive biomimetic hydrogel valve for microfluidics. Appl Phys Lett 78:2589–2591
227. Agarwal AK, Sridharamurthy SS, Beebe DJ, Hongrui J (2005) Programmable autonomous micromixers and micropumps. J Microelectromech Syst 14:1409–1421. doi:10.1109/jmems.2005.859101
228. Feinberg AW, Feigel A, Shevkoplyas SS, Sheehy S, Whitesides GM, Parker KK (2007) Muscular thin films for building actuators and powering devices. Science 317:1366–1370. doi:10.1126/science.1146885
229. Yoshida R, Okano T (2010) Stimuli-responsive hydrogels and their application to functional materials. In: Ottenbrite RM, Park K, Okano T (eds) Biomedical applications of hydrogels handbook. Springer, New York, pp 19–43. doi:10.1007/978-1-4419-5919-5_2
230. Vanag VK, Yang L, Dolnik M, Zhabotinsky AM, Epstein IR (2000) Oscillatory cluster patterns in a homogeneous chemical system with global feedback. Nature 406:389–391
231. Zaikin AN, Zhabotinsky AM (1970) Concentration wave propagation in two-dimensional liquid-phase self-oscillating system. Nature 225:535–537

232. Yoshida R (2010) Self-oscillating gels driven by the belousov-zhabotinsky reaction as novel smart materials. Adv Mater 22:3463–3483. doi:10.1002/adma.200904075
233. Zhang Y, Guan Y, Zhou S (2006) Synthesis and volume phase transitions of glucose-sensitive microgels. Biomacromolecules 7:3196–3201. doi:10.1021/bm060557s
234. Zhang Y, Guan Y, Zhou S (2007) Permeability control of glucose-sensitive nanoshells. Biomacromolecules 8:3842–3847. doi:10.1021/bm700802p
235. Sorrell C, Serpe M (2012) Glucose sensitive poly (N-isopropylacrylamide) microgel based etalons. Anal Bioanal Chem 402:2385–2393. doi:10.1007/s00216-012-5736-x
236. Wang D, Liu T, Yin J, Liu S (2011) Stimuli-responsive fluorescent poly(N-isopropylacrylamide) microgels labeled with phenylboronic acid moieties as multifunctional ratiometric probes for glucose and temperatures. Macromolecules 44:2282–2290. doi:10.1021/ma200053a
237. Miyata T, Asami N, Uragami T (1999) Preparation of an antigen-sensitive hydrogel using antigen−antibody bindings. Macromolecules 32:2082–2084. doi:10.1021/ma981659g
238. Tang M, Zhang R, Bowyer A, Eisenthal R, Hubble J (2004) NAD-sensitive hydrogel for the release of macromolecules. Biotechnol Bioeng 87:791–796. doi:10.1002/bit.20210
239. Oya T, Enoki T, Grosberg AY, Masamune S, Sakiyama T, Takeoka Y, Tanaka K, Wang G, Yilmaz Y, Feld MS, Dasari R, Tanaka T (1999) Reversible molecular adsorption based on multiple-point interaction by shrinkable gels. Science 286:1543–1545. doi:10.1126/science.286.5444.1543
240. Syrett JA, Becer CR, Haddleton DM (2010) Self-healing and self-mendable polymers. Polym Chem UK 1:978–987
241. Pawar GM, Koenigs M, Fahimi Z, Cox M, Voets IK, Wyss HM, Sijbesma RP (2012) Injectable hydrogels from segmented PEG-bisurea copolymers. Biomacromolecules 13:3966–3976. doi:10.1021/bm301242v
242. White SR, Sottos NR, Geubelle PH, Moore JS, Kessler MR, Sriram SR, Brown EN, Viswanathan S (2001) Autonomic healing of polymer composites. Nature 409:794–797
243. Yoshie N, Watanabe M, Araki H, Ishida K (2010) Thermo-responsive mending of polymers crosslinked by thermally reversible covalent bond: polymers from bisfuranic terminated poly(ethylene adipate) and tris-maleimide. Polym Degrad Stab 95:826–829. doi:http://dx.doi.org/10.1016/j.polymdegradstab.2010.01.032
244. Cui J, Ad Campo (2012) Multivalent H-bonds for self-healing hydrogels. Chem Commun 48:9302–9304
245. Hunt JN, Feldman KE, Lynd NA, Deek J, Campos LM, Spruell JM, Hernandez BM, Kramer EJ, Hawker CJ (2011) Tunable, high modulus hydrogels driven by ionic coacervation. Adv Mater 23:2327–2331. doi:10.1002/adma.201004230
246. Yoshie N, Saito S, Oya N (2011) A thermally-stable self-mending polymer networked by Diels–Alder cycloaddition. Polymer 52:6074–6079. doi:http://dx.doi.org/10.1016/j.polymer.2011.11.007
247. Prager S, Tirrell M (1981) The healing process at polymer–polymer interfaces. J Chem Phys 75:5194–5198
248. Harada A, Kobayashi R, Takashima Y, Hashidzume A, Yamaguchi H (2011) Macroscopic self-assembly through molecular recognition. Nat Chem 3:34–37. doi:http://www.nature.com/nchem/journal/v3/n1/abs/nchem.893.html#supplementary-information
249. Beck JB, Rowan SJ (2003) Multistimuli, multiresponsive metallo-supramolecular polymers. J Am Chem Soc 125:13922–13923. doi:10.1021/ja038521k
250. Holten-Andersen N, Harrington MJ, Birkedal H, Lee BP, Messersmith PB, Lee KYC, Waite JH (2011) pH-induced metal-ligand cross-links inspired by mussel yield self-healing polymer networks with near-covalent elastic moduli. Proc Natl Acad Sci. doi:10.1073/pnas.1015862108
251. Sato T, Ebara M, Tanaka S, Asoh T-A, Kikuchi A, Aoyagi T (2013) Rapid self-healable poly(ethylene glycol) hydrogels formed by selective metal-phosphate interactions. PCCP 15:10628–10635. doi:10.1039/c3cp50165e

# Chapter 3
# Smart Nanoassemblies and Nanoparticles

## 3.1 Introduction

This chapter provides an introduction to smart nanoassemblies and nanoparticles as well as recent applications in biosensing, drug delivery, and bioimaging. Nanoparticles provide a particularly useful platform, demonstrating unique properties with potentially wide-ranging therapeutic applications. The wide variety of core materials makes nanoparticles an excellent platform for a broad range of biological and biomedical applications. Particular attention is also paid to nanoassemblies, because organization proceeds with low energy consumption by the use of various interactions in the self-assembly processes. Indeed, self-assembly can occur spontaneously in nature, for example, in cells such as the self-assembly of the lipid bilayer membrane. Self-assembly has been repeated since the appearance of water on Earth. Life on this planet is also repeating a similar cycle. Living things sustain their outward appearance by self-organization of innumerable cells by using energy supplied from other life forms and the system of self-assembly of molecules. Then, what is the 'trigger' for the self-assembly of molecules in the living body? The answer is a combination of several kinds of interaction such as hydrophobic-hydrophobic, electrostatic, coordinate bond, hydrogen bond, and ligand-receptor. By using these 'triggers', we can design 'smart' block copolymers that gain and lose their amphiphilic property in response to external stimuli, resulting in stimuli-responsive micelle formation/deformation (Fig. 3.1) [1].

The self-assembly by macromolecules/polymers has also been applied to combine metal and inorganic particles as organic-inorganic hybrid materials. Well-defined assembly designs may seem impossible, like stones scattered in water forming a small shrine automatically. In the development of biomaterials, however, the exact control of self-assembly is one of the great challenges. The biocompatibility of materials is also an important factor for biomaterials, as well as their controlled structures. The origin of controlled drug delivery using biomaterials dates back to the 1960s, and the material sizes have been continuously decreasing (macrosize in the 1970s, microsize in the 1980s, and nanosize

M. Ebara et al., *Smart Biomaterials*, NIMS Monographs,
DOI: 10.1007/978-4-431-54400-5_3,

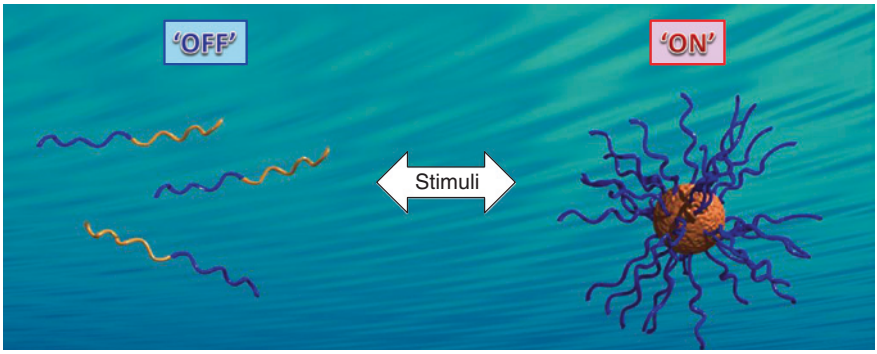


**Fig. 3.1** Schematic illustration of a smart self-assembly system. When block copolymers are designed with a stimuli-responsive polymer as the inner core and hydrophilic polymers as the outer shell, the copolymer gains and loses its amphiphilic property in response to external stimuli, resulting in stimuli-responsive micelle formation/deformation [Ref. 1]

in the 1990s~) with the development of technologies [2, 3]. On the basis of the Ringsdorf model for polymer drugs [4], various types of nanomaterial have been developed. As the representative materials for nanostructure formation in water by self-assembly, amphiphilic block copolymers have been used [5]. The amphiphilic block copolymers are composed of hydrophilic and hydrophobic blocks, and form nanostructures such as micelles and vesicles for their thermodynamic stability. As the hydrophilic block, poly(ethylene glycol) (PEG) has been most studied. PEG is a material approved by the Food and Drug Administration (FDA), and is applied in a wide range of fields owing to its biocompatibilities that originate from the neutral charge and high excluded volume effect. For example, PEGylated enzymes and proteins have been increased their stability and circulation time [6]. To obtain interesting properties, PEGylated materials for drug carriers have been prepared actively in laboratories, and some drug-loaded carriers are already available on the market.

The ideal method of polymer-conjugated drug carriers has been discussed on the basis of three concepts, which are (1) PEGylation, (2) enhanced permeability and retention (EPR) effect, and (3) active targeting [2, 3]. The EPR effect was found by Maeda et al. [7], which is a phenomenon whereby nanoparticles tend to accumulate in tumor tissue for the gap of the blood vessel around the tumor caused by the rapid growth of cancer cells, and their underdeveloped lymph vessel. Moreover, these drug carriers must also be designed with appropriate sizes to overcome living barriers, for instance, the reticuloendothelial system (RES) and so on. The system of nanocarriers accumulated in a tumor by the EPR effect is known as passive targeting. On the other hand, for more effective accumulation, nanocarriers with an affinity site on the surface have been reported to interact with target cells; this system is called active targeting. Cancer cells usually express superabundant receptors such as low-molecular-weight compounds and antibodies, as compared with normal cells. In active targeting, the receptors are used

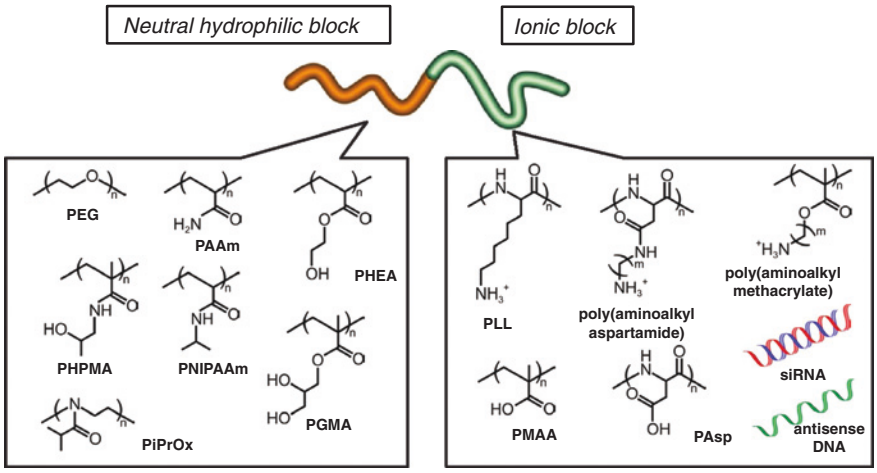


**Fig. 3.2** Block copolymers consisting of neutral hydrophilic lock and ionic block for drug delivery systems [Ref. 13]

as targeting sites for the injected nanocarriers. However, these cancer cells are usually located outside of blood vessels. Therefore, nanocarriers for active targeting firstly experience the EPR effect, and the diameter plays an important factor in this targeting. Kataoka and coworkers have prepared various types of self-assembled micelle consisting of biocompatible block copolymers. For example, a block copolymer of PEG-*b*-poly(α,β-aspartic acid) was prepared, and the α,β-aspartic acid units were combined with the anticancer drug doxorubicin (DOX) by covalent bonds. The amphiphilic block copolymers formed micelles consisting of the combined DOX at the core in aqueous media. Moreover, the combined DOX in a polymer structure could interact with free DOX by their π–π interaction, which led to the efficient drug loading into the core part [8, 9]. The poly(α,β-aspartic acid) blocks can also interact with polymers with a positive charge by electrostatic interaction. Harada et al. prepared unique micelles called polyion complex (PIC) micelles by mixing the block copolymers of PEG-*b*-poly(α,β-aspartic acid) and PEG-*b*-poly(L-lysine). The properties including diameter were controlled by adjusting the mixture ratios of block copolymers [10]. Charged enzymes and nucleic acids are also incorporated into the micelle structure by the electrostatic interactions. In fact, the nucleic acids interacted with PEG-*b*-poly(L-lysine), which successfully formed a well-defined nanoassembly [11]. Moreover, micelles formed by disulfide bonds were collapsed to locate in an endocytotic reducing environment for an effective drug delivery system [12]. It is important to deliver these drug materials to target cells and organelles without their disintegration in the living body. Drug delivery system (DDS) using these biocompatible micelles will be paid increasing attention (Fig. 3.2) [13]. Triblock copolymers of poly(ethylene oxide) (PEO)/poly(propylene oxide) (PPO) known as Pluronics® have been conjugated with various materials for DDS [14]. Moreover, PEGylated liposome-DOX

has already been used for medical treatment as Doxil®, which was approved by the FDA in 1995. In the future, many kinds of PEGylated carrier will appear on the market following clinical tests.

These self-assemblies of block copolymers triggered by their different solubility on each block are also observed in organic solvents as well as in aqueous solution. Semsarilar et al. polymerized block copolymers with poly(benzylmethacrylate) (PBzMA) block in methanol or ethanol solution. During the polymerization, the block copolymers changed their structures, such as sphere, worm, and vesicle, depending on the polymer length of the PBzMA block [15]. From the point of view of structural design, it is of great interest that the assembled nanostructures are controlled by the designed block copolymers although the polymers are composed of the same raw materials. Recently, stimuli-responsive block copolymers have been focused on for their controlled properties by changing the external environment such as temperature, pH, light, and molecules. For example, hydrophilic-hydrophilic block copolymers turn the properties to amphiphilic or hydrophobic-hydrophobic one by the external environment. The unique 'on-off' switching system has been applied in a wide range of fields including biomaterials. The preparation of well-defined functional nanomaterials is closely related to the improvement and simplicity of the polymerization technique. Nowadays, controlled living radical polymerizations (CLRPs) such as nitroxide-mediated radical polymerization (NMP), atom transfer radical polymerization (ATRP), and reversible addition fragmentation chain transfer (RAFT) polymerization lead to the preparation of well-defined polymers to laboratories [16–20]. Moreover, the click chemistry proposed by Sharpless and coworkers has also been a powerful tool for polymer design [21]. These preparation techniques have been applied to not only polymer design but also organic-inorganic hybrid materials. Regarding metal nanoparticles including quantum dots (QDs), for example, their dispersion ability in solution is usually poor with decreasing diameter because of strong aggregation due to the large surface area. However, these inorganic nanoparticles modified by hydrophilic polymers can be prevented from aggregating with each other, and show high dispersibility. Methods that involve grafting-to, grafting-from, and layer-by-layer (LbL) processes are usually used for the modifications. Moreover, the polymerization conditions are shifted to bioinert conditions such as low-temperature, metal-free, and organic-solvent-free conditions, which accelerate the application of these prepared materials to biomaterials. Therefore, polymers are directly polymerized from biomolecules such as enzymes, nucleic acids, and proteins for additional properties and functions of polymers [22].

In this chapter, we focus on smart nanoassemblies and nanoparticles as biomaterials. The synthesis and characterization methods are discussed in Sects. 3.2 and 3.3, respectively. In Sect. 3.4, special attention is paid to the recent advances in stimuli-responsive nanoassemblies and nanoparticles. In Sect. 3.5, certain applications are discussed. The chapter ends with an overview of some of the future trends in applications in biotechnology and biomedicine.

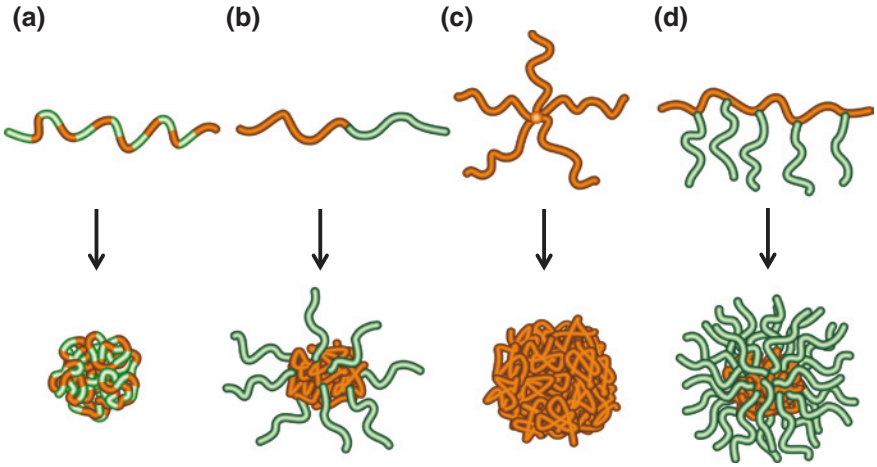


**Fig. 3.3** Various types of polymeric architectures. **a** Random, **b** block, **c** star, and **d** graft copolymers

**Table 3.1** Advantages and disadvantages of CLRPs

| | NMP | ATRP | RAFT |
|---|---|---|---|
| Advantages | Without transition metals<br>Low coloration<br>Low odor | Versatile | Without transition metals<br>Versatile |
| Disadvantages | Low versatile | With transition metals | Coloration<br>Potential for odor |

## 3.2 Synthetic Methods

### *3.2.1 Controlled Living Radical Polymerizations*

The design of polymers based on their hydrophilic-hydrophobic balance is of great importance to form stable self-assembled structures. The polymer design, such as compositions, structures, and properties, has been achieved using Controlled Living Radical Polymerizations (CLRP) methods. CLRPs are radical polymerizations to polymerize polymers with controlled molecular weight and narrow molecular weight distribution by utilizing the equilibrium between active and dormant species [16–20]. Moreover, polymers obtained by these CLRPs can restart their polymerizations from the end of the chain, which leads to the preparation of block copolymers. Therefore, these CLRPs have led to the generation of several types of polymer structure such as block copolymers, star copolymers, graft copolymers, surface modifications, and gels owing to their easy methods and the wide range of polymerizable monomers (Fig. 3.3).

There are mainly three types of CLRPs such as nitroxide-mediated radical polymerization (NMP), atom transfer radical polymerization (ATRP), and Reversible addition-fragmentation chain transfer (RAFT) polymerization. The advantages and disadvantages of these CLRPs are summarized in Table 3.1. NMP uses reversible relationships of active and dormant species via temperature control without adding an external radical and metal catalysis [16]. ATRP uses an oxidation–reduction reaction of transition metals, which start their polymerization to generate a radical by pulling out the halogen group at ATRP initiators owing to interaction with a complex consisting of a metal catalyst and a ligand [17, 18]. The reversible extraction of the halogen groups for generating radicals and their inclining equilibrium to dormant species lead to the formation of well-defined polymer structures. As transition metals, copper and ruthenium are mainly used for the ATRP, and, as other metals, iron, titanium, cobalt, and nickel have been reported [23–26]. There are many advantages of the ATRP method, such as utility for various monomers and enabling the polymerization in solution under bioinert conditions. For the large-scale production of well-defined polymers by ATRP, experiments in cooperation with companies have also been carried out. From the point of view of application as biomaterials, however, it is necessary to completely remove the toxic transition metals. At the laboratory scale, the transition metals can be removed using a simple alumina column. Therefore, ATRP achieved with a small amount of transition metals is a great challenge for the large-scale production of polymers for use not only in the living body but also in the environment. Recently, various types of ATRP have been developed under this concept. For example, the reverse-ATRP and SR and NI-ATRP use Cu(II) with a higher stability during oxidation than Cu(I), which are used to reduce Cu(II) to Cu(I) by radical initiators such as azobisisobutyronitrile (AIBN) [27]. However, there are some side reactions due to AIBN and the large amount of metal catalyst is required, as well as the normal ATRP. The effects of metal catalysis and ligands in polymerizations have also been reported, and highly active ligands such as tris[2-(dimethylamino) ethyl]amine ($Me_6$TREN) lead to well-controlled polymerization with a small amount of a metal catalyst. Initiators for continuous activator regeneration (ICAR) can control the concentration of the Cu(I)-ligand complex by the use of a radical initiator to decrease the Cu(II) amount used by 100 ppm or less. The amount of catalyst in the polymerization is very small compared with that in normal ATRP, which requires 1,000–10,000 ppm. However, the ICAR polymerization also requires the use of radical initiators such as AIBN and 4,4′-azobis-4-cyanovaleric acid (ACVA) [28]. On the other hand, for activator generated by electron transfer (AGET)-ATRP, it is not necessary to use these radical initiators because the Cu(II) is reduced to Cu(I) by a reducing agent such as ascorbic acid, which achieves the controlled polymerization with a low catalyst concentration and no side reactions [29]. For CLRPs, oxygen is usually an inhibitor their interaction with radicals and has to be removed through degasification or replacement ($N_2$ or Ar gas) before the polymerizations. Recently, oxygen (inhibitor of polymerization) dissolved in polymerization solution has been used for oxidation to control the polymerization, known as activators regenerated by electron transfer (ARGET)-ATRP. This

polymerization can start by adding a suitable reducing agent without exactly removing oxygen [30]. Moreover, a combination between the oxidation-reduction reaction and an electric current has been reported to achieve the CLRP. In this case, the polymerization only proceeds when the power is on [31].

RAFT polymerization occurs later than ATRP [19, 20]. The polymerizations are controlled to propagate radicals by only adding a compound having a thiocarbonylthio group called RAFT agents in a typical radical polymerization system. The universalities for applicable monomers and solvents, and polymerization under bioinert and metal-free conditions are great advantages for application to biomaterials. However, there are some problems of the smell and coloration that originate from RAFT agents. The problems can be overcome by removing the structure of the RAFT agent at the terminal polymer chain by appropriate treatment. Recently, end groups of polymers derived by RAFT agents have been actively transformed to reactive groups for adding functionality to polymers, as shown later. The structures of RAFT agents have to be selected for the electronic properties of polymerized monomers. Dithio ester and trithio carbonate in the RAFT agents are generally suitable to polymerize a conjugated monomer. On the other hand, nonconjugated monomers are polymerized using a RAFT agent with xanthate and dithio carbamate. In other words, it is difficult to prepare a block polymer shown as poly(conjugated monomer)-*b*-poly(non-conjugated monomer) using one type of RAFT agent. A series of switchable RAFT agents with electronic structures have been reported for the preparation of poly(conjugated monomer)-*b*-poly(nonconjugated monomer) block copolymers [32]. The RAFT agents named universal (switchable) RAFT agents can polymerize both conjugated/nonconjugated monomers by controlling the pH of the polymerization solution. Pun and coworkers [33] have recently reported a neuron-targeted, reduction-responsive cationic block copolymer by a combination of RAFT polymerization of oligo(ethylene glycol) monoethyl ether methacrylate (OEGMA) and ATRP of glycidyl methacrylate (GMA), followed by postpolymerization decoration of reactive epoxy groups in the GMA block by tetraethylenepentamine (TEPA) (Fig. 3.4).

Recently, synthesis methods for conjugation between polymers and biomolecules (enzyme, protein, and nucleic acid) have been investigated using these CLRPs under bioinert condition, i.e., body temperature, buffer solution, and nontoxicity. Actually, several polymers have been polymerized in water solution by ATRP and RAFT, and these polymerizations have been directly used to combine with biomolecules [22]. Averick et al. prepared bovine serum albumin (BSA) protein combined with ATRP initiator, and poly(oligo(ethylene oxide) methacrylate) (POEOMA) was polymerized from the modified BSA in aqueous (or PBS) at 30 °C. This polymerization was under a bio-inert condition, which caused no damage to the proteins [34]. Narain et al. prepared poly(*N*-isopropylacryamide) (PNIPAAm) and biotinylated-PNIPAAm by RAFT polymerization. These polymers were coated on iron oxide nanoparticles (diameter, 10 nm), and conjugated with streptavidin with fluorescein biotins. The conjugate behaviors were measured as fluorescence intensity (Fig. 3.5) [35]. RAFT polymerizations have usually required polymerization temperature of 60–70 °C because radical initiators such as

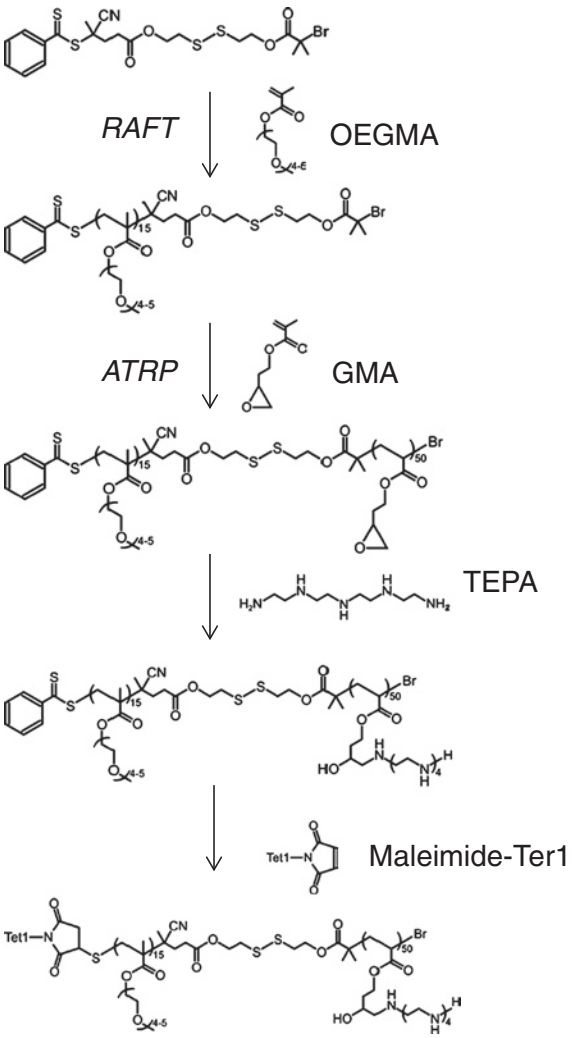


**Fig. 3.4** Synthesis of neuron-targeted copolymers using a reducible, RAFT-ATRP double-head agent [Ref. 33]

AIBN and ACVA require this temperature range for the generation of free radicals. These high temperatures will trigger the production of denatured proteins. Some radical initiators such as 2,2′-azobis(4-methoxy-2,4-dimethylvaleronitrile) (V-70) and 4,4′-Azobis[2-(imidazolin-2-yl)propane] dihydrochloride (VA-044), however, can generate radicals at lower temperature close to body temperature, which leads to a possibility of the RAFT polymerization under bio-inert condition [36, 37]. Li et al. [38] prepared a PNIPAAm-*b*-poly(*N*,*N*-dimethylacrylamide) (DMAAm) block copolymer from BSA protein by RAFT polymerization. The thiol groups on the BSA were modified with RAFT agents having maleimide by Michael addition reaction in PBS (pH 7.2, 5 %-DMF) at 25 °C. The PNIPAAm chain was continuously polymerized from the BSA with RAFT groups using VA-044 as the radical

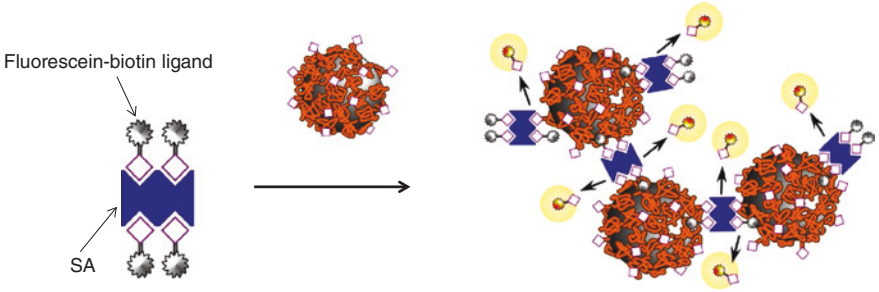


**Fig. 3.5** Conjugated temperature-responsive material of iron oxide nanoparticles coated by biotinylated-PNIPAAm and streptavidin [Ref. 35]

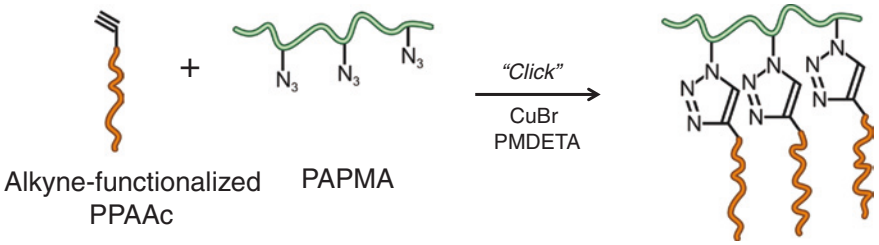


**Fig. 3.6** Synthetic pathway for the preparation of PPAAc graft copolymers from a PAPMA polymer backbone. PPAAc and PAPMA are assembled via a copper-catalyzed Huisgen 1,3-dipolar cycloaddition [Ref. 39]

initiator in PBS at 25 °C. Moreover, BSA-PNIPAAm was used as a macro-RAFT agent for the preparation of BSA-PNIPAAm-*b*-PDMAAm. The conjugated materials are given the temperature-responsive properties by the modified polymers and show association/aggregation with increasing solution temperature.

### *3.2.2 Click Chemistry*

Click chemistry has also been applied to the modification/control of the structure of polymers since it was proposed by Sharpless and coworkers [21]. The end groups at polymers polymerized by ATPR and RAFT can typically be transformed from halogen/thioester to azido/thiol for click reaction by simple treatment, which leads to the combination between CLRPs and click chemistry for the preparation of biomaterials. Crownover et al. [39] have synthesized poly(propylacrylic acid) (PPAAc) containing a single telechelic alkyne functionality via RAFT polymerization with an alkyne-functional chain transfer agent (CTA) and coupled to RAFT-polymerized poly(azidopropyl methacrylate) (PAPMA) through azide-alkyne [3 + 2] Huisgen cycloaddition (Fig. 3.6). Alkyne-azido click chemistry is one of

the most applied reactions for the modification of polymers. However, this click reaction requires toxic copper ion as a catalyst, which has to be removed before application to biomaterials. The copper ion can be used as a copper-ligand complex for ATRP as mentioned above. By using the copper ion, therefore, polymerization and modification of the polymers are achieved by a one-pot reaction as a combination between ATRP and click chemistry [40]. On the other hand, the click reaction between cyclic alkyne and azido dose not require adding a metal catalyst for their special structures [41]. Thiol-ene click chemistry has also been focused on as a click reaction in the absence of a metal catalyst [42, 43]. A polymer synthesized by RAFT polymerization is suitable for the thiol-ene click chemistry because the thiocarbonylthio groups at the polymer chain end are converted easily to thiol groups by a simple reduction treatment. These thiol-ene click chemistries require a radical source such as an initiator and UV light. The thiol groups in polymers are also used for interaction with a gold surface and reaction with maleinide groups, which promote the use of the thiol-ene click chemistry for the preparation of biomaterials. These combinations between CLRPs and click chemistry are expected to be important tools for the design of polymers with unique properties and structures.

### *3.2.3 Self-Assembly*

Block copolymers prepared with stimuli-responsive properties can undergo self-assembly by recognizing their external environment such as solution, temperature, pH, light, and salt concentration. The interactions for forming self-assemblies are triggered by hydrophobic interaction, electrostatic interaction, coordinate bonds, and hydrogen bonds, and they have structures with thermodynamic stability. The most studied assembly formation on biomaterials is sphere type, such as micelles and vesicles. The self-assembly triggered by hydrophobic interaction is mainly carried out with amphiphilic block copolymers. As preparation methods for the self-assemblies, there are typically two methods as follows: (1) Block copolymers dissolved in a small amount of water-insoluble organic solution (e.g., chloroform and dichloromethane) are poured in water with vigorous stirring. (2) Block copolymers dissolved in a small amount of water-soluble organic solvent (e.g., *N*,*N*-dimethylformamide (DMF) and ethanol) are poured into a large amount of water for dialysis. In both methods, the self-assembly formation starts by removing the organic solvent from large amount of water. Moreover, it is possible to load a hydrophobic drug into the assembly core by dissolving the drug with block copolymers in organic solvent. In this way, these formations by self-assemblies have to foresee their interactions with each other, the molecules dissolved in solution, and their environment. The switchable property of stimuli-responsive polymers can be used as a basic concept to manufacture an attractive polymer system that gains and loses its amphiphilic property in response to external stimuli, resulting in stimuli-responsive micelle formation/deformation. PNIPAAm is one of the most studied temperature responsive polymers that show reversible hydration and dehydration in aqueous

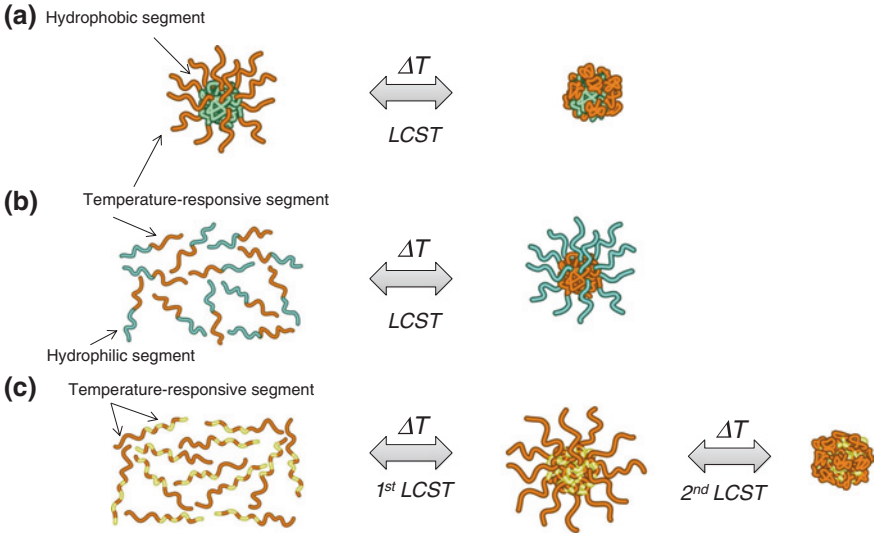


**Fig. 3.7** Temperature-responsive micellization behavior of PNIPAAm based block copolymers with **a** PNIPAAm as the outer shell, **b** PNIPAAm as the inner core, **c** and double LCSTs in aqueous solution. The assembly/aggregation are controlled due to the solution temperature

solution over the lower critical solution temperature (LCST) around 32 °C. When block copolymers are designed with PNIPAAm as the outer shell and hydrophobic polymers as the inner core, they form micelles with the drug below the LCST, whereas the drug release occurs above the LCST of PNIPAAm (Fig. 3.7a) [44, 45]. When block copolymers are designed with PNIPAAm as the inner core and hydrophilic polymers as the outer shell, they form micelles in aqueous solution and permit hydrophobic drug loading above the LCST (Fig. 3.7b) [46–48]. Increased complexity has also been demonstrated with double-responsive polymers with two stimuli-responsive blocks. Dual temperature-responsive block copolymers with tunable LCSTs, for example, allow the construction of reversible nanoassembly-forming species. The block copolymer can be transformed from a double-hydrophilic to an amphiphilic and finally to a double-hydrophobic block copolymer under bio-inert conditions. Therefore, nanoassembly and drug encapsulation occurred through simple mixing of polymer solutions with the drug below the LCSTs of both blocks, and upon heating at temperatures greater then the second LCST, the nanoassembly aggregated and the drug was released from the micelles (Fig. 3.7c) [49–51].

### *3.2.4 Precipitation Polymerization*

Hydrogels in the form of microgels and nanogels have been investigated because they display many advantages when they are used in biological applications as a result of their high water content and biocompatibility. They can absorb large

amounts of water or biological fluids because the polymer networks have a high affinity for water. However, they do not dissolve because they consist of a crosslinked network. PNIPAAm gel particles are typically prepared by precipitation polymerization or emulsion polymerization [52, 53]. In the precipitation polymerization approach, the polymerization of monomers and crosslinkers is initiated in water by a free-radical initiator at temperatures above the LCST. Once the growing polymer chains reach a critical length, they collapse and phase separate to form colloidal particles. This method offers numerous advantages, such as the production of remarkably uniform particles and the ability to control particle parameters, such as size, charge, and crosslinking density.

### *3.2.5 Coacervation*

Coacervation is a phase-separation phenomenon induces micro/nanoscale droplets, that is, "coacervate droplets", consisting of a concentrated colloid (or polymer) phase. The particulate coacervate droplets can be formed by external environment such as solution, temperature, pH, light, and salt concentration. It has been reported that a temperature-responsive type coacervation is also demonstrated in aqueous solutions. When such a temperature-responsive polymer is heated above the LCST in an aqueous medium, the polymer chains enter into a "partially" dehydrated state and then associate with each other via a hydrophobic interaction and hydrogen bonding, resulting in the formation of the coacervate droplets. Cooling the solution below the LCST leads to rehydration of the polymer chains, and the coacervate droplets disappear. Therefore, by crosslinking the polymer chains during the formation of the coacervate droplets above the LCST, it is expected to obtain the micro/nanoparticles. On the basis of this concept, a few research groups successfully synthesized these temperature-responsive hydrogel microspheres by utilizing the temperature-responsive type coacervation. However, it is still difficult to prepare a fine micro/nanoparticles with multi-stimuli responsive properties. To overcome this point, coacervate droplets were formed in the two-component nonionic poly(*N*-isopropylacrylamide-*co*-2-hydroxyisopropylacrylamide) (poly(NIPAAm-co-HIPAAm)) and ionic poly(NIPAAm-*co*-2-carboxyisopropylacrylamide) (poly(NIPAAm-*co*-CIPAAm)) aqueous system by heating the solution above their responsive temperature. The resulting coacervate droplets included both types of polymer chain. Divinyl sulfone, which crosslinks the hydroxyl groups of the poly(NIPAAm-*co*-HIPAAm), was added to the coacervate droplets. In this way, the stimulus-responsive semi-interpenetrating polymer network (IPN) hydrogel microsphere consisting of the poly(NIPAAm-*co*-HIPAAm) gel matrix and the linear poly(NIPAAm-*co*-CIPAAm) chains could be prepared, and their sizes were relatively homogeneous. That is, by utilizing the temperature-responsive coacervate droplets induced in the binary system, we could successfully prepare the fine stimuli-responsive semi-IPN hydrogel, and it was prepared by a simple and easy method [54–59].

### 3.2.6 Incorporation of Inorganic Nanomaterials

Besides the polymeric self-assemblies, there are other nanoparticles consisting of inorganic materials such as metal, quantum dot, and silica. Metal and quantum dot nanoparticles are usually combined with biocompatible polymers owing to their original high aggregation and toxic properties. Their structures as nanomaterials are relatively simple such as sphere, rod, and cube. However, inorganic silica particles that have high biocompatibility and stability can be controlled on the diameters between nano- and micro-orders, and their structures are also easily controlled, not only as a sphere but also other complex structures, which lead to their extensive application to for biomaterials. As preparation methods of silica particles, the 'reverse microemulsion method' and 'Stöber method' have been widely used [60, 61]. In the reverse microemulsion method, the diameters of the silica particles are controlled in nano-order by changing the amounts of water, oil, and surfactant at a desirable reaction temperature. On the other hand, in the 'Stöber method', the diameters are dependent on the reaction temperature and concentration of starting materials such as tetraethyl orthosilicate (TEOS), ethanol, water, and ammonia solution, which are controlled from nano- to micro-order under an appropriate reactive condition. Toxicity is also very important for the materials used as biomaterials. Therefore, silica particles have been extensively studied in terms of their toxicity since the development of the preparation methods. Generally, toxicity increases with decreasing diameter because of the extremely high surface area of silica particles, especially nanoparticles. Moreover, the accumulation of silica materials to organ in vivo is dependent on the diameters. These phenomena with regard to diameter are not only related to silica particles but also other metal particles of similar sizes. In other words, the properties of the particles, namely, their toxicity and accumulation to organs, are strongly affected by the size, shape, and surface area, which will be mentioned in Sect. 3.5 in detail. Moreover, the preservation of silica particles has also been investigated for their easy handling and transportation. For example, silica nanoparticles (SiNPs) collected by freeze drying as powder can be conveniently transported. However, upon redispersion, it is difficult to obtain a clear redispersion with decreasing diameter, because of their strong aggregation caused by a high surface area. Lin et al. reported that mesoporous silica nanoparticles (MSiNPs) modified by dual organosilane (hydrophilic and hydrophobic silane) showed a high redispersion in water after being collected as powder by freeze drying. The dried MSiNPs of 60 nm diameter were dispersed in a biological solution, and their high dispersibility was maintained over 15 days [62]. Like the MSiNPs with a pore structure and a high surface area, several types of silica structure such as hemispherical, discoidal, cylindrical, dual mesoporous, hollow, ellipsoidal, raspberry-like, chrysanthemum-like, and janus have been developed for adding functionalities [63–69]. Decuzzi et al. prepared silica materials with different formations (spherical, hemispherical, discoidal, and cylindrical) to investigate the accumulation in organs, which is dependent on their structures by injection via the tail vein [63].

Silica materials have many silanol groups on their surface, and the groups are used as reactive groups with amine, carboxylic acid, and so on. Moreover, a compound having a triethoxysilane group (e.g., 3-Aminopropyltriethoxysilane (APTEOS)) can directly react with silanol groups on the silica materials by covalent bonds. These simple surface modifications of silica particles are applied in combination with low/high-molecular-weight molecules, enzymes, nucleic acids, proteins, and metals, and are also used as reactive groups for ATRP, RAFT, and click chemistry. In this way, nanoassemblies and nanoparticles are easily designed with complicated functionalities by the combination of preparation methods as mentioned above. These new preparation methods for nanomaterials will be reported continuously, and it is expected for mass-production of biomaterials.

## 3.3 Characterization Methods

Physicochemical properties of nanoassemblies and nanoparticles have been measured for objects as follows: (1) parameters in solvent such as diameter, numbers of block copolymers consisting of assemblies, and surface charge; (2) determination of assembly behaviors; and (3) visualization of the nanostructures as images using microscopes such as the scanning electron microscope (SEM), transmission electron microscope (TEM), and atomic force microscope (AFM).

### *3.3.1 Determination of Particle Sizes and Zeta Potential*

Size and surface property of nanomaterials are significantly important characteristics toward the biomedical applications. For example, the positively charged particle would be more effective as a gene transfection carrier because cell membrane carries a negative charge. The size or shape is also important parameters for a nanomaterial's utilization of specific endocytosis trafficking. Dynamic light scattering (DLS) is a typical measurement method for diameters of nanoassemblies and nanoparticles. When light is irradiated to the dispersion of nanomaterials with Brownian motion, the scattered light shows Doppler shift depending on the motion of nanomaterials. The dynamics of nanomaterials are estimated by analyzing the scattered light data. From autocorrelation function, the relationship between attenuation constant ($\Gamma$) and translational diffusion coefficient ($D$) is shown as the following numerical formula.

$$D = \Gamma / q^2 \tag{3.1}$$

($q = (4\pi n_0/\lambda_0)\sin(\theta/2)$, $n_0$: refraction index of the solvent, $\lambda_0$: wavelength)

The hydrodynamic radius ($R_h$) is calculated using the Einstein-Stokes relation as below.

$$R_h = kT/6\pi\eta D \tag{3.2}$$

($k$ Boltzmann's constant, $T$ absolute temperature, $\eta$ solvent viscosity).

The analytical range of the diameter is from the nano- to micro-order, and the diameters can be measured not only in aqueous solutions but also in organic solvents. Moreover, by adding an electric field to the dispersion, surface charges of the nanomaterials are estimated, which is known as the zeta potential. It is used for calculating the migration velocity of nanomaterials in an electric field, which is proportional to the surface charges. The zeta potential ($\xi$) is shown in Smoluchowski's equation.

$$\xi = 4p\pi\eta U/\varepsilon \tag{3.3}$$

($U = V/E$, $U$ electrical mobility, $V$ migration velocity, $E$ electric field, $\eta$ solvent viscosity, $\varepsilon$ dielectric constant of the solvent).

Static light scattering (SLS) that uses the intensity of scattered light as a function of scattering angles can be used to calculate the absolute molecular weight ($M$) and second virial coefficient ($A_2$) as follows.

$$KC/R_\theta = 1/M\left(1 + 1/3\left\langle R_g^2\right\rangle q^2\right) + 2A_2C \tag{3.4}$$

($R_\theta$ Rayleigh ratio, $K$ optical constant, $R_g$ radius of gyration, $C$ concentration).

These $M$, $A_2$, and root-mean square radius of gyration $\langle R_g^2\rangle^{1/2}$ are obtained using the Zimm plot that is shown using the calculated Rayleigh ratio from the dispersion samples at different concentrations. From these values, the numbers of polymer in one assembly can be calculated.

### *3.3.2 Microscopic Observations*

Microscopes such as SEM, TEM, and AFM are powerful tools for the direct observation of nanomaterial formation (Fig. 3.8). Samples for these microscopes are prepared by the simple dropping of a dispersion of nanomaterials on substrates. Dip-coating and spin-coating are also typical methods to prepare the samples for microscopy. Figure 3.8a shows a SEM image of polymeric nanoparticles. The nanoparticles of samples for SEM are usually coated with a thin layer (~10 nm) such as carbon, gold, and platinum to obtain a high resolution. Therefore, the nanoparticles in the SEM image include those thin layers in the diameters. Moreover, dried polymeric samples for SEM measurement lead to smaller diameters than the swelled hydrodynamic diameters determined by DLS. Hierarchical structures can also be obserbed by SEM (Fig. 3.8b). Figure 3.8c, d shows TEM images of SiNPs. As one of the advantages, the samples for TEM do not need to be coated by metallic thin layers. TEM grids are usually covered with a transparent thin membrane on which samples are trapped, and the dispersion solvent of the samples has to be selected with the nondestruction of the thin membrane. Figure 3.8e shows an AFM image of SiNPs, which can be used to measure not only the diameter but also the structural roughness. In this way, nanostructures are directly measured using these types of microscope.

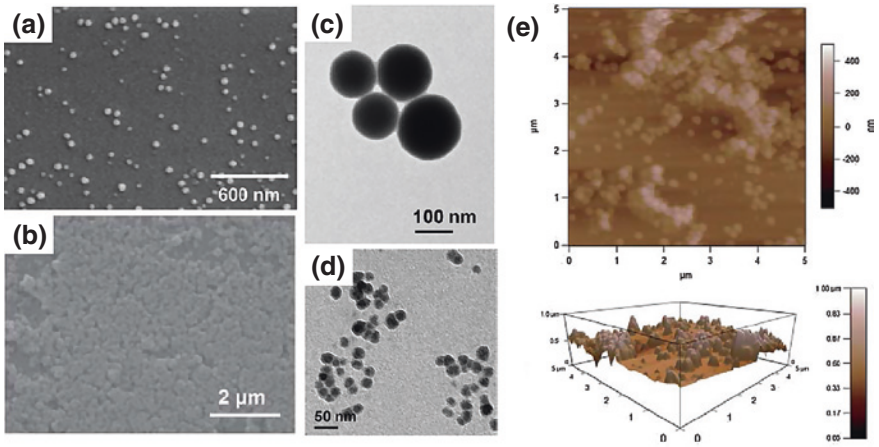


**Fig. 3.8** Microscopy images: SEM images of **a** polymeric assemblies, **b** silica nanoparticles, **c**, **d** TEM images of silica nanoparticles, and **e** AFM images of silica nanoparticles

### *3.3.3 Dynamic Observations of Conformational Changes*

Self-assembly behaviors are affected by many factors such as polymer lengths, hydrophilic/hydrophobic balances, compositions, electric charges, and crystallization. $^{1}$H NMR has been used for the estimation of the self-assembly behavior of polymers by calculating their composition. The assembly core usually shows no proton peak owing to their solid property and hydrophilic shell part. In our group, double temperature-responsive block polymers of PNIPAAm-*b*-P(NIPAAm-*co*-HMAAm) were dissolved in $D_2O$ at different solution temperatures to estimate their changing compositions owing to self-assembly. Below the lower critical solution temperature (LCST) of the PNIPAAm block, the HMAAm content was around 9 mol %, which was close to the HMAAm content in PNIPAAm-*b*-P(NIPAAm-*co*-HMAAm). On the other hand, the HMAAm content was increased by about 22 mol % when the temperature reached 37.5–50 °C (over LCST of PNIPAAm block). The 22 mol % was similar to the HMAAm content in the P(NIPAAm-*co*-HMAAm) block (Fig. 3.9) [51]. In this way, the peaks from $^{1}$H NMR data lead to the detection of the self-assembly behavior as their polymer compositions change. However, the sample is usually required to have a comparatively high concentration of 5–10 mg/mL.

The critical micelle concentration (CMC) is widely used to determine the self-assembly behavior of polymers. Micelles consisting of polymers have high thermodynamic stability, and the CMC ($10^{-6}$–$10^{-7}$ M) is more than 1,000 times lower than that of typical surfactants ($10^{-3}$–$10^{-4}$ M). Moreover, the stability of assemblies increases by crosslinking the core or shell part. As the measurement method for the CMC, fluorescent molecules are often used. The fluorescent molecules sensitively recognize the changes in the environment as changes in fluorescence intensity and/

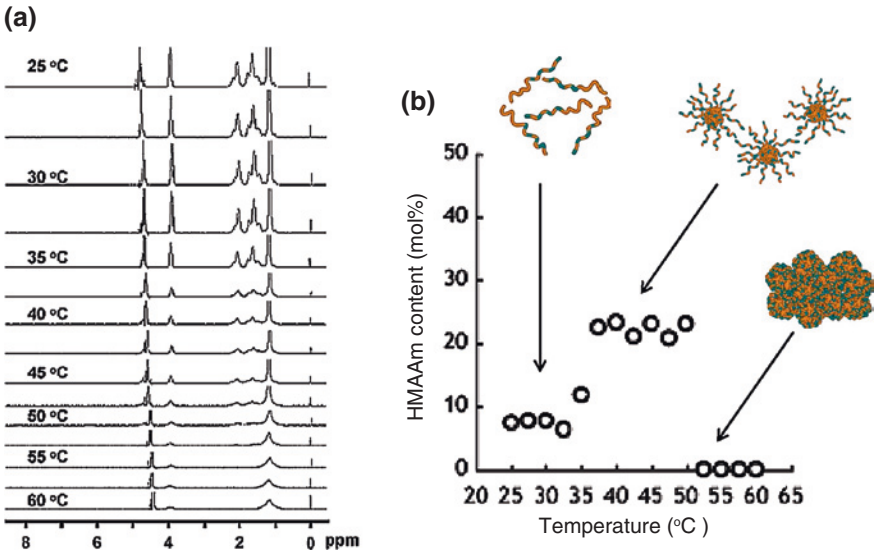


**Fig. 3.9** **a** Temperature-dependent $^1$H NMR spectra of PNIPAAm-*b*-P(NIPAAm-*co*-HMAAm) copolymer in $D_2O$. **b** HMAAm contents in the PNIPAAm-*b*-P(NIPAAm-*co*-HMAAm) copolymer are calculated from $^1$H NMR spectra [Ref. 51]

or peak shifts; this property is very useful for investigating the polymeric assembly behaviors at low concentrations. In the case of pyrene, in hydrophobic environment, the fluorescence intensity is increased and the ratio of two vibronic bands ($I_1/I_3$) is decreased [70, 71]. Eight-anilino-1-naphthalenesulfonic acid ammonium salt hydrate (ANS) is a fluorescent molecule with a higher water solubility than that of pyrene, which can be used to detect assembly behaviors of polymers as a blue shift of the emission maximum [72]. The authors prepared double temperature-responsive block copolymers of PNIPAAm-*b*-poly(NIPAAm-*co*-*N*-(isobutoxymethyl) acrylamide (BMAAm)), and investigated the assembly behaviors using fluorescent molecules of pyrene and ANS (Fig. 3.10a) [50]. The block copolymer was designed to assemble at 27.5 °C in water. As a result, the CMC was calculated as 10 mg/L using the $I_1/I_3$ of pyrene at 27.5 °C (Fig. 3.10b). Moreover, the maximum wavelength of ANS showed a reversible shift between 515 and 460 nm at 17.5 and 27.5 °C, respectively, which suggested that the block copolymers assembled reversibly with changes in. In fact, the nanoassemblies were observed to be 88 ± 20 nm in diameter by DLS measurement (Fig. 3.10c).

Winnik and coworkers prepared temperature-responsive polymers with fluorescent molecules modified at polymer chains by a covalent bond, and directly investigated the assembly behaviors as fluorescence intensity dependent on solution temperature. Interestingly, the compositions (the location of fluorescent molecules), polymer lengths, and solvents affected the intensities [73–75]. Recently, polymers having complex structures including fluorescent molecules have been

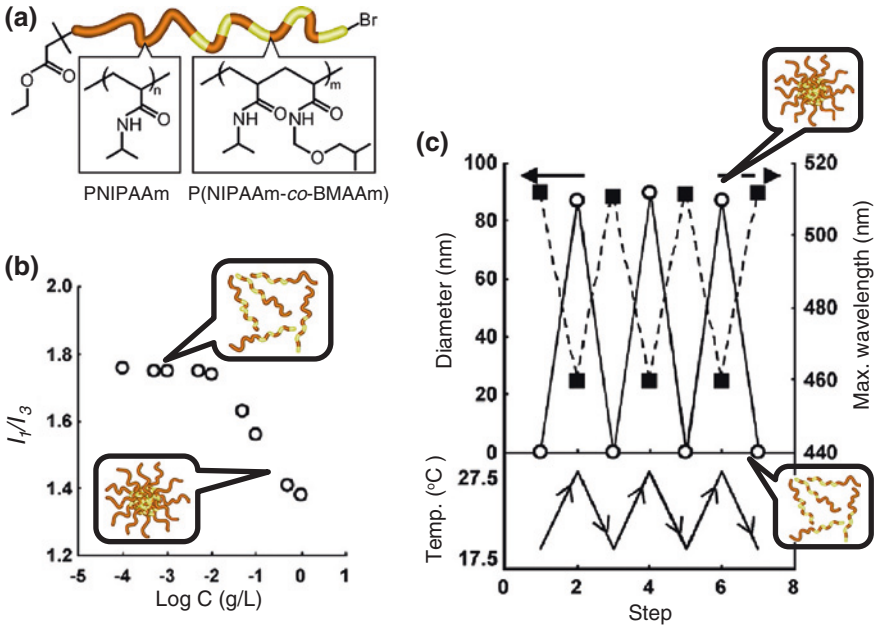


**Fig. 3.10** **a** Chemical structure of dual temperature-responsive PNIPAAm-*b*-P(NIPAAm-*co*-BMAAm) copolymer. **b** Change in fluorescence intensity ratio of $I_1/I_3$ of pyrene as a function of copolymer concentration. **c** Reversible self-assembly formation of the copolymer in response to temperature cycle between 17.5 and 27.5 °C, followed by DLC and maximum wavelength of fluorescent ANS [Ref. 50]

easily prepared by the combination of CLRPs and click chemistry (see Sect. 3.2), and their solution behaviors have been estimated. Duan et al. synthesized a fluorescent initiator of 1-pyreneyl 2-chloropropionate for ATRP, and polymerized PNIPAAm with 2–6 kDa molecular weights using the initiator [76]. Yip et al. synthesized α,ω-diisobutylsulfanylthiocarbonylsulfanyl-PNIPAAm by RAFT polymerization. Sequentially, both ends of the chain were converted to thiol groups, and were reacted with 4-(1-pyrenyl)butyl iodide in DMF to prepare PNIPAAm (6–45 kDa) with the pyrene groups at both ends [77]. Moreover, Scales and coworkers treated the chain end of PNIPAAm to convert the end groups to a thiol group using the reducing agent $NaBH_4$, and the thiol groups were combined with pyrene molecules [78]. In this way, the fluorescent molecules can be located at any place in the polymer chain by simple preparation methods, which have led to much knowledge on the assembly behaviors. A temperature-responsive polymer having fluorescent units was applied as a monitor of local temperature in living cells by the difference in fluorescence intensity depending on the organelles (Fig. 3.11) [79]. The polymers were composed of a temperature-responsive part, a fluorescent part, and an anionic hydrophilic part to prevent the precipitation, and the temperature of the cell organelles using the difference in lifetime of the fluorescent units was successfully measured.

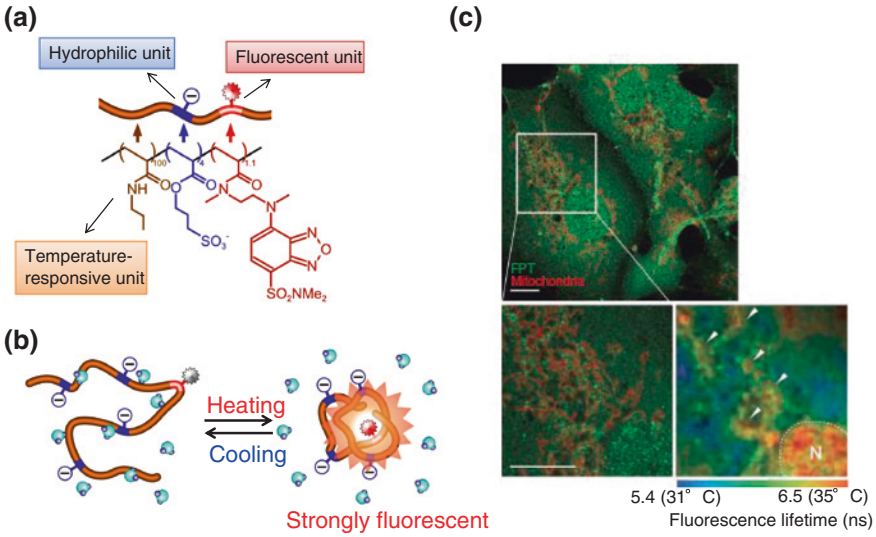


**Fig. 3.11** Intracellular temperature mapping with a fluorescent polymeric thermometer. **a** Chemical structure of the fluorescent polymeric thermometer. **b** Functional diagram in an aqueous medium. **c** Confocal fluorescence images of FPT (*green*) and Mito Tracker Deep Red FM (*Red upper* and *left lower*) and fluorescence lifetime image of FPT (*right lower*). *Arrowheads* point to local heat production. *N* indicates the nucleus [Ref. 79]

Recently, fluorescence resonance energy transfer (FRET) has been focused on owing the unique properties. The phenomenon occurs as the transfer of the fluorescence of a fluorescent molecule (donor) to another fluorescent molecule (acceptor) as excitation energy [80]. As requirements for the FRET, 'overlap of spectra between donor and acceptor molecules', 'approach of donor and acceptor molecules in a range of 1–10 nm', and 'dipolar orientation' are required. Owing to its high sensitivity, simplicity, and wide range of wavelengths, FRET is applied to the analysis of the biological interaction of biomolecules such as nucleic acids and proteins. Moreover, FRET systems have also been applied to the study of self-assembly behaviors of polymers [81]. Monitoring of the self-assembly behaviors using these fluorescent molecules is expected to open a new stage of material design.

## 3.4 Multi-stimuli-Responsive 'Smart' Nanoassemblies and Nanoparticles

### *3.4.1 Double-Temperature-Responsive Systems*

Block copolymers having double-temperature-responsive properties possess abilities for both drug loading and drug release by only changing the temperature. In other words, the block copolymers are required to change their properties

on each block successively from hydrophilic-hydrophilic to amphiphilic, and hydrophobic-hydrophobic properties. There were few reports of block copolymers having double-temperature responsiveness [82–85]. However, the LCST on blocks was completely fixed by their monomer structures, and there was no report on the controlled LCSTs on both blocks, i.e., controlled double-temperature responsibilities. We have focused on this point, and prepared block copolymers consisting of PNIPAAm and P(NIPAAm-*co*-*N*-hydroxymethyl acrylamide (HMAAm)) by one-pot ATRP [86]. For the control of the LCSTs in a copolymer block of P(NIPAAm-*co*-HMAAm), first, the HMAAm was copolymerized at different contents of 10–50 mol %. PNIPAAm copolymerized with the HMAAm is expected to increase the LCSTs owing to hydrophilic property of HMAAm as compared with NIPAAm. In fact, the LCSTs measured by transmittance change were increased at 40, 47, 56, and 70 °C by increasing the copolymerized HMAAm contents that were 10, 20, 30, and 42 mol %, respectively. Moreover, P(NIPAAm-*co*-HMAAm) with 50 mol % HMAAm showed no LCST. These results suggested that the LCST of PNIPAAm was controlled by copolymerization with desirable contents of hydrophilic HMAAm monomer. Reaction ratios of copolymerized monomers are also important to design the functionality. In the case of the existence of a remarkable difference in the reaction ratios, generally, the copolymers cannot have a uniform random structure in the polymer chain. As a result, the copolymers show nonsensitive responsiveness to external stimuli. On the other hand, copolymers consisting of monomers with similar reaction ratios have a fine random structure, which leads to sensitive responsive properties. HMAAm is an acrylamide-type monomer, which is expected to have a random structure with NIPAAm for their closed monomer structures with NIPAAm. Block copolymers of PNIPAAm-*b*-P(NIPAAm-*co*-HMAAm) polymerized by ATRP were observed to show double temperature-responsive behavior in aqueous solution by transmittance change, $^{1}$H NMR, and DLS measurements. The HMAAm contents in the P(NIPAAm-*co*-HMAAm) block were controlled as 10, 22, 34, and 52 mol %, respectively. In transmittance change functionalized as temperature, all the block copolymers showed transmittance change decreased at 34 °C owing to the dehydration of a common PNIPAAm block, and the LCSTs of the P(NIPAAm-*co*-HMAAm) block increased with increasing HMAAm contents, as well as those of the copolymers. Moreover, the LCST of the P(NIPAAm-*co*-HMAAm) block of 52 mol % was not observed. From the $^{1}$H NMR data, the HMAAm contents in the block copolymers changed at LCSTs of both responsive blocks. These results suggested that the block copolymers sequentially had hydrophilic-hydrophilic, amphiphilic, and hydrophobic-hydrophobic properties with increasing temperature. When the solution temperature is between the LCSTs, the amphiphilic block copolymers are expected to form an assembled structure. In fact, these block copolymers formed assemblies of 150 nm in diameter above the LCST of the PNIPAAm block, and showed aggregation/precipitation above the LCST of the P(NIPAAm-*co*-HMAAm) block located at the assembly shell part. The assembly phenomena were completely reversible depending on the solution

temperature. These results suggest that the assembly behaviors could be controlled to design the LCSTs of each block in the block copolymers.

However, these assemblies have to be used above LCST of the PNIPAAm block to keep the assembled structures. In other words, drug-loaded assemblies prepared by increasing solution temperature, it has to be stored at over 32 °C to keep their structures. This is not practical for drug carriers. Therefore, in the assemblies, LCSTs of the core part as well as the shell part should be controlled. The hydrophobic *N*-(isobutoxymethyl)acrylamide (BMAAm) monomer as compared with NIPAAm was copolymerized for the preparation of P(NIPAAm-*co*-BMAAm) copolymers. The BMAAm monomer is also a nonionic/inexpensive acrylamide-type monomer, and P(NIPAAm-*co*-BMAAm) is expected to show lower the LCST. The P(NIPAAm-*co*-BMAAm)s were polymerized to estimate their LCSTs by ATRP at different BMAAm contents of 4.8, 10, and 17 mol %, respectively [50]. The LCSTs were measured on the basis of transmittance change functionalized as temperature, and were decreased by increasing the BMAAm contents, which were 27, 23, and 17 °C. On the basis of the result, P(NIPAAm-*co*-BMAAm)-*b*-PNIPAAm was prepared. The BMAAm contents in P(NIPAAm-*co*-BMAAm) blocks were controlled at 5, 10, and 15 mol %, respectively. Double temperature-responsive properties were also observed in these block copolymers as transmittance change, and the LCSTs in the P(NIPAAm-*co*-BMAAm) block were decreased by increasing the BMAAm contents. The diameter change functionalized as temperature in the block copolymer (BMAAm content in P(NIPAAm-*co*-BMAAm) block = 10 mol %) was investigated. The block copolymer was completely dissolved in aqueous solution at 17.5 °C. At 27.5 °C above the LCST of the P(NIPAAm-*co*-BMAAm) block, the block copolymer formed assemblies of 80 nm diameter, which were observed to have a structure consisting of a P(NIPAAm-*co*-BMAAm) core and a PNIPAAm shell by $^{1}$H NMR. The Tyndall effect, which is a phenomenon for nanoparticles, was also observed as a light blue solution. Moreover, the assemblies aggregated with each other and precipitated at 32.5 °C for the dehydration of the PNIPAAm shell. The behavior was completely reversible depending on the solution temperature. These results suggested that the LCST of core parts were also controlled by simple copolymerization, and the block copolymer formed assemblies at room temperature. These double temperature-responsive block copolymers are expected to achieve both drug loading and release only by changing the temperature in the absence of a toxic organic solvent (Fig. 3.12).

Some of the polymers consisting of monomers with ethylene glycol at the side chain show temperature-responsive properties for their balance of hydrophilicity and hydrophobicity. Aoshima and coworkers polymerized alkoxyethyl vinyl ether monomers by cationic polymerization in the presence of salts [82–84]. The polymerized polymers showed temperature-responsive properties depending on the monomer structures. For example, poly(2-methoxy-ethyl vinyl ether) (PMOVE) showed the LCST at 70 °C measured by transmittance change. On the

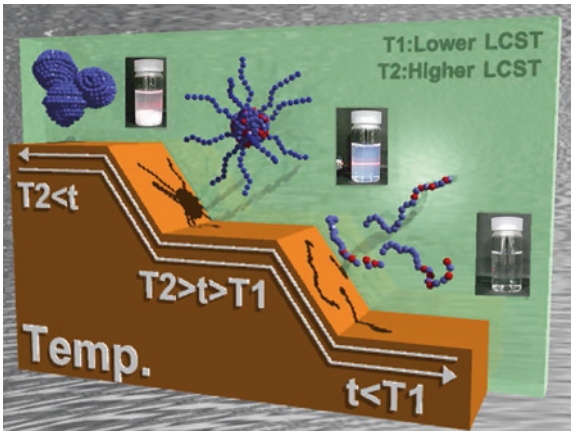


**Fig. 3.12** Schematic illustration of a double temperature-responsive block copolymer system [Ref. 50]

other hand, poly(2-ethoxy-ethyl vinyl ether) (PEOVE), which is a hydrophobic structure as compared with PMOVE, showed a transmittance decrease at 20 °C. A block copolymer of poly(2-(2-etoxy)ethoxyethyl vinyl ether) (PEOEOVE)-*b*-PMOVE was observed to show double temperature-responsive properties at 40 and 60–70 °C by transmittance and endothermic changes, and the solution viscosity was increased owing to gelation at between 40 and 60 °C. The gelation was needed for uniform diameters of nanoassemblies (i.e., block copolymers with low PDI). In fact, the block copolymer having large PDI showed no gel structures. Lutz et al. designed the LCST of polymers using 2-(2-methoxyethoxy)ethyl methacrylate ($MEO_2MA$) and oligo(ethylene glycol) methacrylate (OEGMA) [87, 88]. The LCSTs of $PMEO_2MA$ and POEGMA were 28 and 90 °C, respectively. Therefore, their copolymers were expected to have LCSTs between 28 and 90 °C with different monomer contents. The LCSTs were increased to 32, 37, 39, 44, 49, and 59 °C by increasing the OEGMA contents, which were 6, 8, 10, 16, 20, and 33 mol %, respectively. According to the LCST data, the relationship between the LCSTs and contents of OEGMA can be expressed using a numerical formula, $\text{LCST} = 28 + 1.04 \times DP_{\text{OEGMA}}$ ($R^2 = 0.996$). Notwithstanding that LCSTs are dependent on polymer chain length, terminal group, salt concentration, and so on, these mathematical expressions are very important for understanding the responses. Moreover, polymers of P($MEO_2MA$-*co*-OEGMA) and PNIPAAm having similar LCSTs were prepared to compare their LCSTs depending on the chain lengths, concentrations, and salt concentrations. These PEG-derived monomers are expected to apply as biomaterials owing to their biocompatibilities, temperature-responsive properties, and prevention of nonspecific adsorption (Fig. 3.13). In addition to this, PEG-derived materials have been reported as shown in Sects. 3.5.1 and 3.5.2. PH-responsive properties have also been applied to polymer structures. Manganiello et al. prepared poly(poly(*N*,*N*-dimethylaminoethyl methacrylate))-*b*-poly(diethylaminoethyl methacrylate-*co*-butyl methacrylate) (P(DMAEMA-*b*-P(DEAEMA-*co*-BMA)) for gene delivery [89].

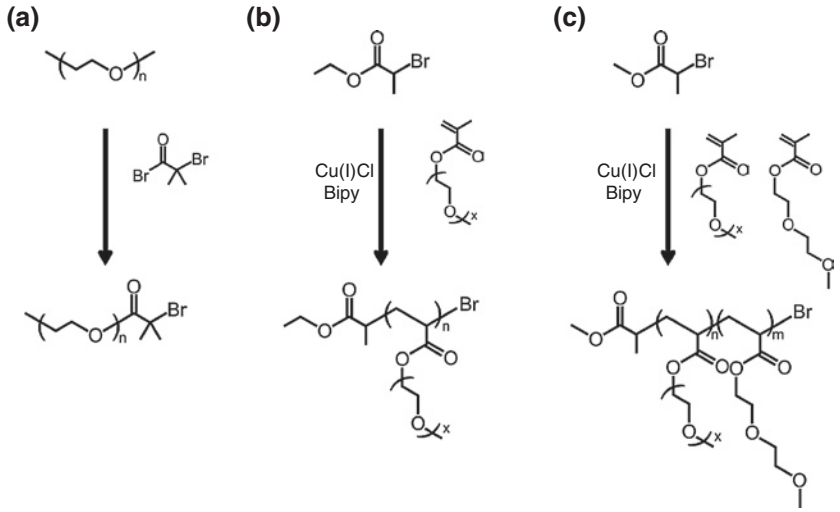


**Fig. 3.13** Various synthetic strategies for PEG-based copolymers used in ATRP [Ref. 87]. **a** Macroinitiator approach. **b** OEGMA macromolecular brushes. **c** Copolymer approach

## *3.4.2 Multi-stimuli-Responsive Systems*

### 3.4.2.1 Linear and Branched Polymers

Recently, a combination of these stimulus-responsive properties has been focused on for adding complex functionalities in assemblies/particles. For example, drug carriers consisting of both temperature- and pH-responsive properties can change their properties by changing the temperature and pH of the external environment. These doubly temperature- and pH-responsive assemblies are applied to drug release triggered by hyperthermia and acidic environment in endosomes. The preparation method for multi-stimuli-responsive assemblies has been actively reported. For example, assemblies that are composed of ABC-type block copolymers form core, corona, and shell structures with multi stimuli responsiveness. Zhang et al. prepared the ABC-type block copolymer of PEG-*b*-poly(4-vinylpyridine)-*b*-PNIPAAm with both temperature- and pH-responsive properties [90]. The block copolymers formed a nanoassembly surrounded by a hydrophilic PEG chain, and the core and corona parts were exchanged by temperature and pH. The assemblies were composed of a PNIPAAm block as a core at 50 °C, pH 2. On the other hand, a poly(4-vinylpyridine) block was located as a core part at 25 °C, pH 6.5. Concerning stimulus-responsive polymers located at the corona or shell part in the assemblies; however, their physiochemical properties are different from those of free polymers in solution because of the local high concentration with high density. The polymer density of the shell part is also an important factor for the design

of drug carriers. Xu et al. [91] prepared a double temperature-responsive polymer of PNIPAAm-*b*-(poly(2-(dimethylamino)ethyl methacrylate) (PDMA)) from the surface groups of a hyperbranched polyester, and estimated the diameter change functionalized as temperature. The hyperbranched particles showed two steps of decrease in diameter with increasing solution temperature. Interestingly, the decrease in diameter by dehydration of the PNIPAAm block started from 20 °C. This responsive temperature was lower than that of the free PNIPAAm (32 °C). The different temperature-responsive properties are assumed for the pseudo-high concentration of the polymer chain located in the particle shell.

Branched (or miktoarm) polymers that are Y- and H-type polymers have also been used for the preparation of multi-stimuli-responsive nanoassemblies. Liu et al. [92] synthesized Y-type miktoarm PEG(-*b*-poly(methacrylic acid) (PMAAc))-*b*-poly(2-(diethylamino)ethyl methacrylate) (PDEA) by the combination of ATRP and click chemistry. However, these preparation methods for multi-functional nanoassemblies are difficult to prepare with increasing the number of functionalities. In the case of Y-type polymers consisting of hydrophobic A and hydrophilic B and C blocks; however, the content ratios of hydrophilic B and C blocks in the assembly shell are fixed as 50 %, and it is difficult to change the ratio for their structure. In this way, the increase in the number of functionalities in assembly means that there are complex structures and many types of raw material are needed. Therefore, it is a great challenge to prepare multi-functional nanoassemblies having a controlled polymer contents in the shell.

#### 3.4.2.2 Assemblies Consisting of Mixed Block Copolymers

Recently, methods using mixed block copolymers with a common hydrophobic block have been focused on for the preparation of multi-functional nanoassemblies. Ye et al. [93] prepared two types of block copolymer, namely, polystyrene (PS)-*b*-PEO and PS-*b*-PNIPAAm. These block copolymers were composed of the common hydrophobic PS block. Therefore, a mixture solution of the block copolymers formed a nanoassembly with PEO and the PNIPAAm blocks in their shell triggered by the self-assembly of the PS block. First, these block copolymers were dissolved in 0.4 mL of tetrahydrofuran (THF), and the mixture solution was dropped in 40 mL of water at 20 °C with stirring. The block copolymers formed nanoassemblies with the evaporation of the organic solvent. The content ratios of PEO and the PNIPAAm block were easily controlled to change the mixture ratios of the block copolymers. As other methods for the preparation of multi-functional nanoassemblies, Kim et al. [94] used stereocomplex interaction between poly(D-lactic acid) (PDLA) and poly(L-lactic acid) (PLLA). The mixture solution including two block copolymers of PDLA-*b*-PEO and PLLA-*b*-PNIPAAm was also formed by nanoassembly with PEO and the PNIPAAm block in the shell. In this case, the nanoassemblies were prepared to dissolve in water without an organic solvent because of their relatively low molecular weights (2 Kg/mol). Santis et al. [95] reported a multi-functional nanoassembly using electrostatic interaction. The

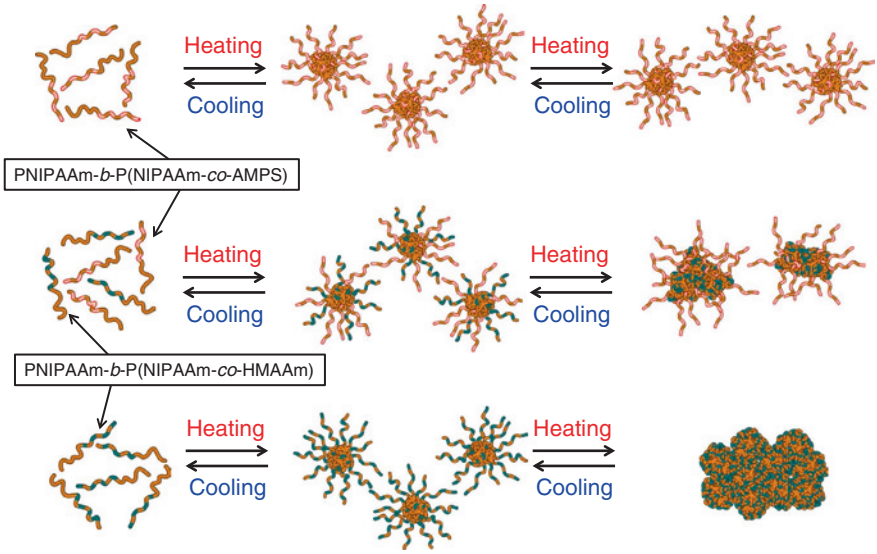


**Fig. 3.14** Schematic representation of the tunable characteristics of nanoassemblies by mixing of PNIPAAm-*b*-P(NIPAAm-*co*-HMAAm) and PNIPAAm-*b*-P(NIPAAm-*co*-AMPS) for controlling the surface properties [Ref. 49]

prepared poly((3-acrylamidopropyl)trimethylammonium chloride) (PAMPTMA)-*b*-PEO and poly(sodium 2-acrylamido-2-methylpropanesulfonic acid) (PAMPS)-*b*-PNIPAAm were separately dissolved in 0.001 M $NaCl_{aq.}$. Sequentially, these solutions were mixed to form a nanoassembly called a polyion complex (PIC) micelle in the absence of an organic solvent owing to their hydrophilic properties. However, it is difficult to collapse these micelle structures with a strongly electrostatic interaction. In this way, assemblies sometimes require toxic organic solvents to form their structure, and the salts are required for the collapse of the structures. Therefore, it is a great challenge to control the assembly and collapse of nanoassemblies in the absence of organic solvents and salt addition. To address this problem, we prepared multi-functional nanoassemblies using temperature-responsive block copolymers (Fig. 3.14). The block copolymers were PNIPAAm-*b*-P(NIPAAm-*co*-HMAAm) and PNIPAAm-*b*-P(NIPAAm-*co*-AMPS), which were composed of a common PNIPAAm block [49]. The block copolymers were dissolved in water as a mixture solution. Self-assembly started by increasing the solution temperature above the LCST of the PNIPAAm block, and the temperature-responsive P(NIPAAm-*co*-HMAAm) block and negatively charged P(NIPAAm-*co*-AMPS) block were located at the shell in the nanoassembly. The individual diameters of PNIPAAm-*b*-P(NIPAAm-*co*-HMAAm) and PNIPAAm-*b*-P(NIPAAm-*co*-AMPS) at 40 °C were 148 ± 36 and 240 ± 59 nm, respectively. From the results of computer simulation, Palyulin et al. [96] suggested that mixed AB and AC block copolymers (A: common hydrophobic block, B

and C: hydrophilic blocks) formed a nanoassembly, and the content ratios of B and C at the shell were random. In our case, in fact, the diameter of the mixed assemblies consisting of PNIPAAm-*b*-P(NIPAAm-*co*-HMAAm) and PNIPAAm-*b*-P(NIPAAm-*co*-AMPS) [mixture ratio: 1:1 (wt)] was 178 ± 53 nm, and the diameters were controlled by adjusting the mixture ratios. Moreover, assemblies aggregated with each other by increasing the solution temperature above the LCST of the P(NIPAAm-*co*-HMAAm) block. However, the aggregation showed high stability similarly to nanoparticles with a narrow size distribution. These results suggest that a hydrophilic P(NIPAAm-*co*-AMPS) block with a negative charge was located in the shell part at random, and their electrostatic repulsion prevented unnecessary aggregation. This preparation system, that is, using a common temperature-responsive block, can achieve to form nanoassemblies without organic solvents. Their assembly and collapse behaviors can be controlled easily by changing the solution temperature. Moreover, as an advantage, the functionalities and content ratios of the shell are also adjusted by the mixture ratios of the block copolymers. On the basis of this concept, we successfully prepared a nanoassembly with three types of block in the shell part at room temperature (Fig. 3.15) [1].

The three block copolymers were polymerized by RAFT polymerization, and were composed of a P(NIPAAm-*co*-BMAAm) block with LCST at 17 °C as a common temperature-responsive block. As another block in the block copolymers, a temperature-responsive P(NIPAAm-*co*-HMAAm) block (LCST: 35 °C), a biocompatible PEG block, and a P(NIPAAm-*co*-HMAAm) (LCST: 70 °C)-*b*-poly(2-lactobionamidoethyl methacrylate) (LAMA) block were selected. The P(NIPAAm-*co*-HMAAm) block (LCST: 35 °C) and LAMA block were designed in such a way that the controlled drug release was triggered by temperature and targeting ability, respectively. LAMA is a sugar monomer having a galactose group developed by Narain and Armes [97], which can be directly synthesized without the protection of the galactose groups. HepG2 cells are known to express the galactose receptors on their surface. Ahmed et al. prepared several types of polymer having galactose and glucose groups such as homopolymers, copolymers, hyperbranched polymers, and nanogels. These materials were conjugated with DNA to investigate cell toxicity and transfection effect for a gene delivery system [98]. The three types of block copolymer formed nanoassemblies by dehydration of the P(NIPAAm-*co*-BMAAm) block, and the individual diameters were 93 ± 19 nm (P(NIPAAm-*co*-BMAAm)-*b*-P(NIPAAm-*co*-HMAAm)), 99 ± 39 nm (P(NIPAAm-*co*-BMAAm)-*b*-PEG), and 104 ± 22 nm (P(NIPAAm-*co*-BMAAm)-*b*-P(NIPAAm-*co*-HMAAm)-*b*-PLAMA) at 25 °C. On the other hand, an assembly consisting of the three types of block copolymer showed a diameter of 122 ± 28 nm at 25 °C. Interestingly, the mixture solution of the three types of block copolymer showed only one LCST as transmittance change caused by a common P(NIPAAm-*co*-BMAAm) block. The transmittance decrease of P(NIPAAm-*co*-HMAAm) blocks (LCST: 35 and 70 °C) was not observed despite the fact that the individual solutions of P(NIPAAm-*co*-BMAAm)-*b*-P(NIPAAm-*co*-HMAAm) and P(NIPAAm-*co*-BMAAm)-*b*-P(NIPAAm-*co*-HMAAm)-*b*-PLAMA showed two steps of transmittance change functionalized as temperature. In these phenomena,

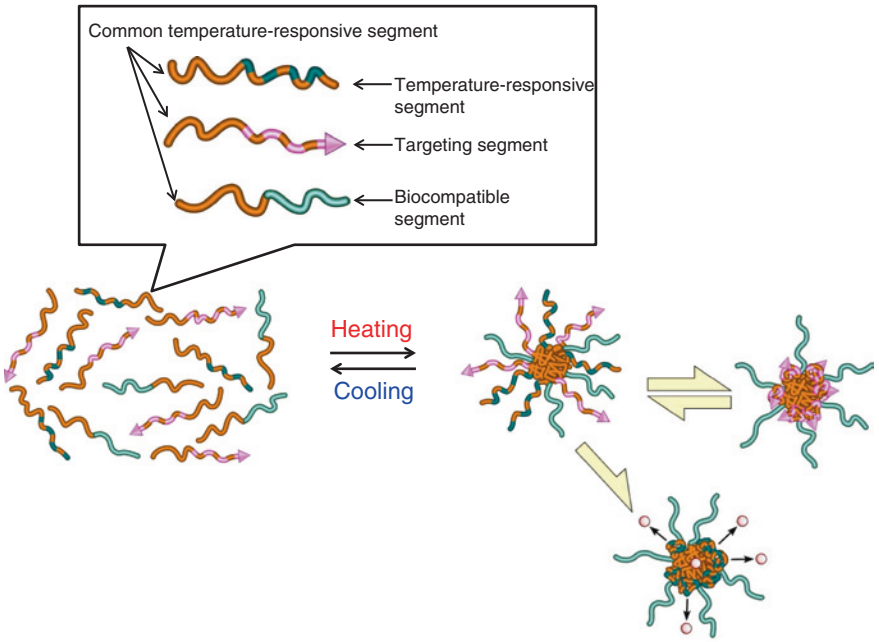


**Fig. 3.15** Schematic representation of the multi-stimuli-responsive nanoassembly by mixing of selected block copolymers with common temperature-responsive block [Ref. 1]

it was assumed that hydrophilic PEG and LAMA blocks at the shell increased the stability of the assemblies and the hydrophilic properties prevented the aggregation of assemblies caused by dehydration of the P(NIPAAm-*co*-HMAAm) blocks. In other words, P(NIPAAm-*co*-HMAAm) blocks were thought to show their LCSTs in the assemblies. According to $^{1}$H NMR, in fact, P(NIPAAm-*co*-HMAAm) blocks in the assemblies showed their temperature-responsive properties. Therefore, nanoassemblies consisting of the mixed block copolymers are expected to release the loaded drug in the core by changing the temperature. The dithioester group of P(NIPAAm-*co*-BMAAm)-*b*-P(NIPAAm-*co*-HMAAm) was converted to the thiol group by simple reduction treatment, and the thiol groups were used as the reactive site with fluorescein isothiocyanate (FITC) for the in vitro test. The fluorescent nanoassemblies with or without the LAMA block were incubated with HepG2 cells to investigate the interaction behavior. As a result, the nanoassembly having the LAMA block showed higher fluorescence intensity than that with the non-LAMA block. These results suggested that mixed block copolymers with a common temperature-responsive block formed a multi-functional nanoassembly by increasing the temperature. Moreover, the functionalities could be easily controlled using the mixed block copolymers. These multi-functional nanoassemblies possessing biocompatibilities, drug release, and targeting ability are expected to apply in a wide range of fields. However, the structures are

usually complex with increasing numbers of functionalities and many types of raw material are needed. This fact becomes an obstacle for bringing nanomaterials to the market from laboratory. Concerning the material design, in the future, it will be challenge to prepare multi-functional nanoassemblies consisting of a few types of raw material by a simple method.

## 3.5 Applications of Smart Nanoassemblies and Nanoparticles

### *3.5.1 Targeted Drug Delivery*

The accumulation of nanocarriers in a tumor owing to the EPR effect is known as passive targeting. On the other hand, the targeting system of carriers having affinity with specific cancer cells has been called active targeting. The nanocarriers of active targeting are equipped with some factors for recognizing the cancer cells such as low-molecular-weight molecules, peptides, antibodies, and so on. The receptor of folic acid ($M_w = 441.40$) is expressed on various types of cell surface that are malignancies of the ovary, brain, kidney, breast, myeloid cell, and normal lung cell. Therefore, folic acid molecules are combined with drug carriers such as copolymers, micelles, and liposomes for active targeting [99, 100]. Bae et al. [101] prepared folate-PEG-(poly(aspartate hydrazone adriamycin) (P(Asp-Hyd-ADR))) as a unique drug carrier for a targeting system. The block copolymers were composed of a hydrophilic PEG block and a hydrophobic P(Asp-Hyd-ADR), and the folate unit was placed at the end of the polymer chain. The P(Asp-Hyd-ADR) blocks were combined with ADR of anticancer drugs, and became the core part of the self-assembly surrounded by PEG shells in aqueous solution. In other words, the folate unit was placed on the micelles and showed high accumulation ability in cancer cells owing to the strong interaction between folate units and their receptors (Fig. 3.16). After being taken into the cell, the acidic endocytic environment triggered the dissolution of the hydrazone part that connects between ADR and the main chain, and ADR was released from the micelles with the collapse of assemblies.

Carbohydrates are abundant materials in nature and are inexpensive biomolecules. In the living body, however, carbohydrates play important roles in cellular recognition processes, for instance, cell growth regulation, differentiation, adhesion, cancer cell metastasis, cellular trafficking, inflammation by bacteria and viruses, and immune response [102–107]. Moreover, cancer cells usually express sites that recognize carbohydrates, which are used in combination with drug carriers for the active targeting system [102, 103]. These carbohydrates also interact with proteins. Generally, the interaction force between carbohydrates and protein is weak. By preparing the local high-concentration areas of the carbohydrates on

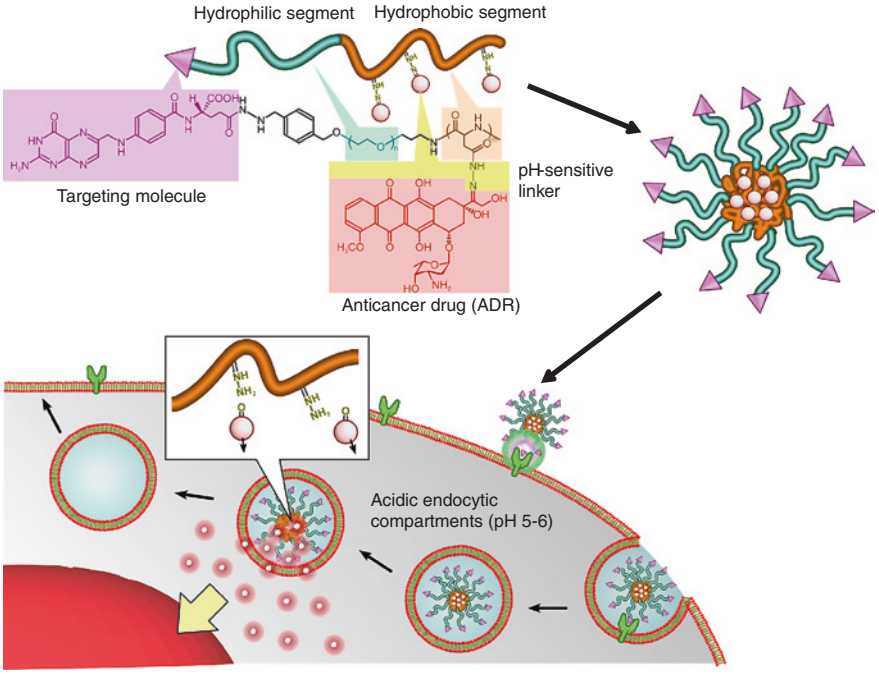


**Fig. 3.16** Preparation of multi-functional polymeric micelles with tumor selectivity for active drug targeting and pH sensitivity for intracellular site-specific drug transport [Ref. 101]

materials, however, the interaction force is markedly increased, which is known as the glycol-cluster effect [108]. We have to consider these unique phenomena during drug carrier design.

Peptides and proteins are composed of 20 types of amino acid. The peptides are used as not only peptide medicines but also drug carriers for their easy structural control. Mao et al. [109] focused on the cationic human immunodeficiency virus (HIV)-1 Tat peptide that is composed of 6 arginine units and 2 lysine units in the sequence. The HIV-1 Tat peptide is known to show high permeability to the cell membrane, which has been combined with several materials such as polymers, metal particles, proteins, peptides, and nucleic acids for effective delivery into the cytoplasm [110, 111]. They prepared fluorescein isothiocyanate (FITC)-SiNPs-Tat peptide of 200 nm in diameter, and estimated their ability for permeability and targeting to the nucleus. The Tat peptide, that is, H-Try-Gly-Arg-Lys-Lys-Arg-Arg-Gln-Arg-Arg-Arg-OH, was combined with FITC-SiNPs having an aldehyde group via a covalent bond at differential modified amounts (2 and 3.5 μg/mg). These FITC-SiNPs-Tat peptides were incubated with HepG2 cells in DMEM/10 % FBS at 37 °C. The uptake to HepG2 cells was observed as fluorescence intensities that were increased with increasing amounts of Tat peptides. After incubation for

8 h, the fluorescence intensities of the FITC-SiNPs-Tat peptide were 3 times (2 μg of Tat peptide) and 4.5 times (3.5 μg of Tat peptide) higher than that of FITC-SiNPs-$NH_2$. Moreover, the FITC-SiNPs-Tat peptides were observed to transfer into the nucleus after 24 h by confocal laser scanning microscopy (CLSM).

The objective parts for targeting systems are not only cancer cells. Drug delivery to the brain is generally difficult owing to the blood brain barrier (BBB) for which it is a great challenge to develop a passable system [112]. Ku et al. [113] reported effective drug delivery to the brain using PEGylated dendrimers for their increased circulation time. PEGylated PAMAM dendrimers were conjugated with fluorescein-doped magnetic SiNPs (PEGylated PFMSiNPs, diameter 80–90 nm, $\zeta$-potential +1.49 mV), and their physiochemical properties and accumulated amount in the brain through the BBB were determined. The PEGylated PFMSiNPs were observed to locate in brain tissues and neurons by their diffusion from the blood vessel despite the fact that non-PEGylated PFMSiNPs could not pass through the BBB.

Boronic acid and its ester compounds are applied to catalysis for stereo-controlled synthesis and diagnosis/therapy for HIV, obesity, diabetes, and cancers [114–116]. Their reversible boronic-diol interactions have been particularly used as a system consisting of copolymers, micelles, and gels for insulin release triggered by glucose concentrations [117–122]. For their high p*K*a as compared with the biological environment, however, there is problem that boronic groups cannot effectively interact with diol groups at pH 7.4. The control of p*K*a closed to biological pH for a strong interaction between boronic groups and diol has been reported by controlled polymer structures and compositions. Bérubé et al. [123] controlled p*K*a and the interaction with diol to design the boronic structures. Shiino et al. reported the effective interaction between boronic acid and diol at pH 7.4 by copolymerization with monomers having amino groups. The adjoining amino groups showed electronic interaction with boronic acid, which led to decreasing p*K*a [124]. Recently, the benzoxaborole group has been reported to show strong interaction with saccharides at pH 7.4 as compared with boronic acid, as reported by Hall [125]. Moreover, as in other research studies, the benzoxaborole groups were used for the neutralization of HIV by their interaction with the mannose group of gp 120 expressed on the virus, which were applied to the targeting system for HIV (Fig. 3.17) [126].

The mitochondria located in a cell are known as an energy source for the cell, and are considered to have some relationship with the apoptosis of cancer cells. Therefore, the targeting system for mitochondria may open a new stage in medical fields. Mo et al. [127] successfully delivered a drug to the mitochondria in cancer cells using zwitterionic oligopeptide liposomes that converted the properties from negative charge (during blood circulation) to positive one (in cancer cells). In this way, effective drug delivery by active targeting has been achieved by designing the structures of carriers. It is very important for these targeting systems to prevent nonspecific interaction with enzymes, proteins, and normal cells in the living body. Moreover, their excretion processes from the living body also have to be included in the targeting systems. Novel targeting systems will be reported sequentially to solve these problems in the future.

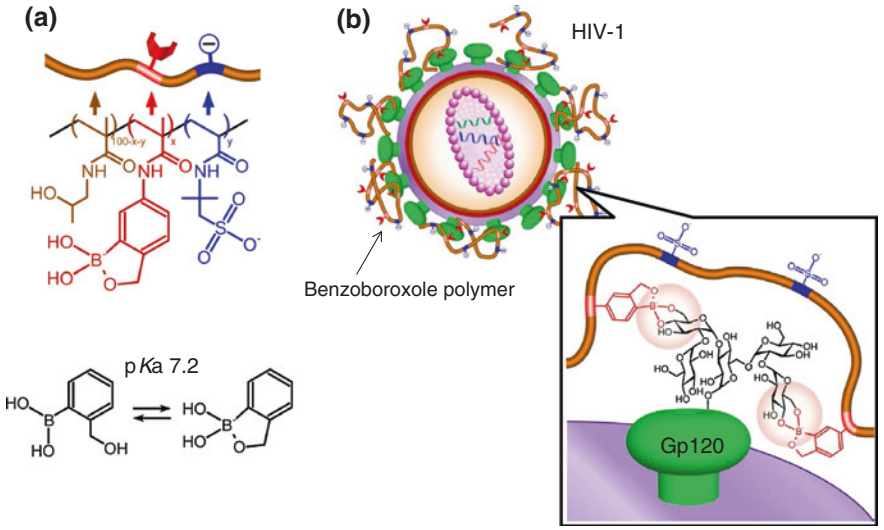


**Fig. 3.17** Graphical depiction of the multivalent benzoboroxole-functionalized polymer interacting with the gp120 complex of HIV-1. **a** Chemical structure of benzoboroxole and the linear water-soluble polymers containing benzoboroxole and 2-acrylamido-2-methyl-1-propanesulfonic acid synthesized using HPMA polymer backbone. **b** Schematic illustration of the binding between the polymers and gp120 through interactions between benzoboroxole groups and the glycosylated regions [Ref. 126]

### *3.5.2 Biosensing and Bioimaging*

Early detection is important for medical treatment. To realize this, several types of nanomaterial such as fluorescent organic molecules, quantum dots (QDs), metal particles, and inorganic particles have been developed. There are also various types of equipment in medical fields such as for optical imaging, magnetic resonance imaging (MRI), computed tomography (CT), ultrasound (US), positron emission tomography (PET), and single-photon emission computed tomography (SPEC) for the microscopic detection of abnormalities in the body [128, 129]. FITC and rhodamine are used as typical fluorescent molecules with low-molecular weight for experiment in vitro and in vivo. However, the fluorescent wavelength of FITC has low permeability in vivo, and rhodamine shows higher toxicity than FITC. As other problems, moreover, these low-molecular weight of fluorescent molecules are usually deactivated in the living body by aggregation/decomposition and interactions with solvents, oxygen, ions, enzymes, and proteins [130].

QDs possessing a nanoscale structure and high quantum yield are composed of II–VI or III–V elements or semiconductors, and the fluorescent wavelengths are widely controlled by their compositions and diameters. Because of their high aggregation and toxicity, however, it is necessary to add biocompatible functionalities for their application as biomaterials [131, 132]. Moreover, metal

nanoparticles such as gold, silver, platinum, and magnetic particles also have the tendency to show high aggregation and toxicity with decreasing diameter [133–135]. Therefore, from the structural point of view, it is very important to achieve high fluorescence intensity, high dispersibility, and low toxicity of fluorescent materials. For solving these problems, biocompatible polymers and silica materials are used as conjugated materials to protect these fluorescent materials from body environments. Silica materials are suitable to coat for fluorescent materials for their biocompatibility, high dispersibility, and easy modification. Preparations of the silica particles by the reverse microemulsion method and Stöber method are described in Sect. 3.2.6. Structures of silica materials, not only a simple sphere but also various structures such as mesoporous, rod, and hollow structures have been reported. At first, the relationship between diameter and toxicity of spherical silica particles was investigated. Small silica nanoparticles (SiNPs < 100 nm) are more toxic then large ones owing to their high surface area. Napierska et al. investigated the cell toxicity (endothelium cell (EAHY 926 cell line)) of SiNPs of different sizes (14–335 nm) by MTT and lactate dehydrogenase (LDH) assays [136]. In fact, the large SiNPs (104 and 335 nm) showed lower toxicity ($TC_{50}$ > 1,000 μg/cm$^2$ on MTT and LDH assay) than the small SiNPs (14–16 nm, $TC_{50}$ < 50 μg/cm$^2$). Hydroxyl groups on silica materials can be used as reactive groups, which are easily modified by functional groups such as amine, carboxylic acid, and thiol. Therefore, these functional groups lead to easy coating of polymers on the silica surfaces. Nanoparticles coated with poly(ethylene glycol) (PEG) usually avoid the reticuloendothelial system (RES) in the body to achieve a long circulation time [137]. Cauda et al. prepared organic-inorganic materials that were mesoporous silica nanoparticles (MSiNPs: diameter = 47 nm, pore size = 4 nm) combined with PEG-silane ($M_w$ = 550 and 5,000 g/mol, and the mixture (75 % of 550, 25 % of 5,000) [138]. The stabilities of these PEG-coated MSiNPs were measured for 1 month in simulated body fluid (SBF) at 37 °C. Results showed that the PEG-coated MSiNPs maintained their structures after 1 month despite the fact that the MSiNPs without PEG chains were decomposed into needlelike crystal structures. There are many reports on imaging materials coated with silica particles. Bardi et al. prepared amine-functionalized-CdSe/ZnS QD-doped SiNPs (QD-SiNPs) with different diameters from 25 to 50 nm, and their potential as imaging materials and gene carriers was estimated using MIH-3T3 and human neuroblastoma SH-SY5Y cells [139]. The prepared QD-SiNPs showed low toxicity and the number of viable cells in culture did not decrease over 24 h at different concentrations from 0.1 to 10 μg/mL. Moreover, high transfection effects were also observed on the QD-SiNPs. Ow et al. compared the fluorescence intensities of three materials, namely, free tetramethylrhodamine isothiocyanate (TRITC, 1.0 nm), aggregated TRITC (2.2 nm), and TRITC-loaded SiNPs (15 nm). The TRITC-loaded SiNPs showed the highest fluorescence intensity and stability for protection by the silica domain. Interestingly, the free TRITC showed higher fluorescence intensity than the aggregated TRITC, which are expected for quenching by aggregating with each other [140]. However, these fluorescent molecules may leak from coating materials. The authors prepared FITC-loaded SiNPs (FITC-SiNPs) using TEOS

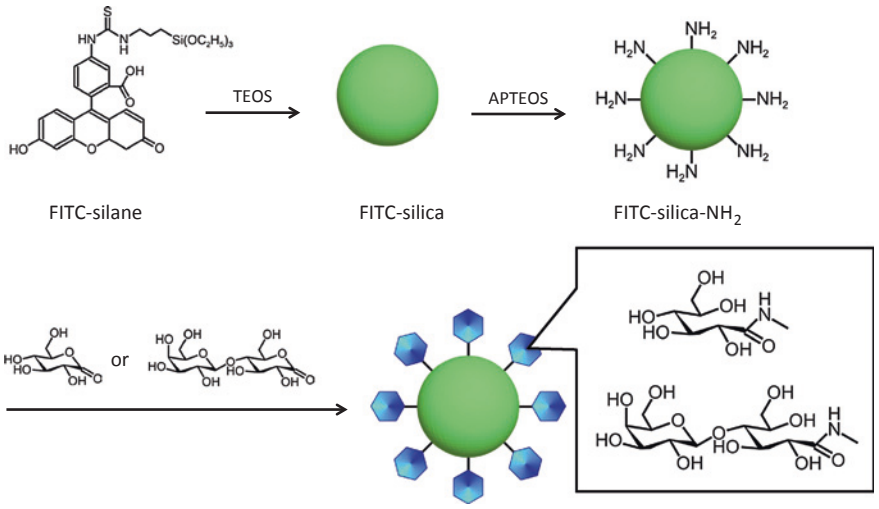


**Fig. 3.18** Preparation of FITC-doped silica nanoparticles with gluconolactone or lactobionolactone on the surface [Ref. 141]

and FITC-silane by the Stöber method. The FITC was combined with SiNPs via a covalent bond to possess the high stability. Moreover, hydroxyl groups on the FITC-SiNPs were reacted with APTEOS (FITC-Silica-$NH_2$) that was used for modification with sugar compounds of gluconolactone (FITC-Silica-G) and lactobionolactone (FITC-Silica-L) [141]. The diameters of FITC-Silica-G and FITC-Silica-L were 149 ± 11 and 147 ± 12 nm, respectively, and they showed high fluorescence intensities in PBS buffer. These sugar-coated SiNPs possessed high stability and low toxicity for the biocompatibilities. The FITC-Silica-L was especially expected as a targeting material to HepG2 cells that express the asialoglycoprotein receptors (ASGPRs) on the surface. According to the MTT assay results, all the FITC-Silica-$NH_2$, FITC-Silica-G, and FITC-Silica-L were observed to have low toxicities to HepG2 cells in a wide range of concentrations (0.0007–1.7 mg/mL). Moreover, the FITC-Silica-L strongly interacted with HepG2 and lectin of $RCA_{120}$. In this way, silica particles can easily incorporate fluorescent materials into the core for the protection of the fluorescence intensity from biological environments, and are modified on their surface by simple treatments, which are great advantages for material design (Fig. 3.18). The authors also synthesized SiNPs (127 ± 11 nm) with alkene groups on the surface using a 3-(trimethoxysilyl)propyl methacrylate (MPS). The alkene groups were used to obtain polymer-modified SiNPs by ene-thiol click chemistry. For this purpose, pH-responsive poly(2-(diethylamino)ethyl methacrylate) (PDEAEMA ($M_n$ = 5200 g/mol, $M_w/M_n$ = 1.22)) and temperature-responsive PNIPAAm ($M_n$ = 6300 g/mol, $M_w/M_n$ = 1.15) were polymerized by RAFT polymerization. Sequentially, the dithio ester groups at the end chain were converted to thiol groups by a simple reduction treatment. The modified SiNPs and polymers were combined by ene-thiol

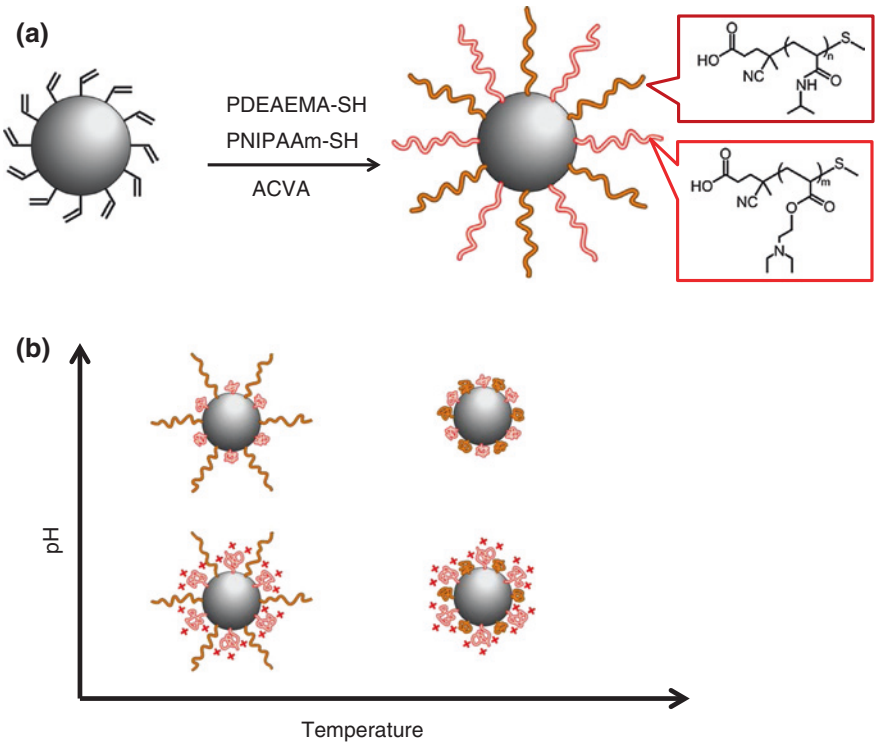


**Fig. 3.19** **a** Preparation of pH and temperature-responsive silica nanoparticles by one-pot thiol-ene click chemistry. **b** The functionalized silica nanoparticles show both pH- and temperature-responsive behavior depending on the ratio of the two polymers on the surface [Ref. 142]

click chemistry at differential polymer compositions (PDEAEMA:PNIPAAm (wt) = 100:0, 75:25, 50:50, 25:75, 0:100) [142] (Fig. 3.19). The polymer on SiNPs showed doubly pH- and temperature-responsive properties, and the diameters were controlled for the polymer compositions and external environments.

Metal nanoparticles such as gold and iron are known to radiate heat by the irradiation of infrared rays and magnetic fields. Infrared therapy has been applied as a medical treatment because of its high permeability to a living body as compared with other types of light with low wavelength. The tuned magnetic fields can also be used to irradiate the living body. In our group, magnetic iron nanoparticles were successfully coated with temperature-responsive polymers by several preparation methods, and the properties of the conjugated particles were sensitive to increasing temperature and magnetic field irradiation [143, 144]. Thomas et al. focused on zinc-doped iron oxide nanocrystals (Zn-$Fe_3O_4$) with a 3-fold hyperthermic effect and a 10-fold MRI contrast as compared with undoped iron crystals, and prepared Zn-$Fe_3O_4$-doped MSiNPs having a supermolecule compound of *N*-(6-*N*-Aminohexyl)aminomethyltriethoxysilane and cucurbit [6] uril on the surface [145]. The modified MSiNPs achieved controlled drug release as a remote

control owing to the exothermic property of Zn-$Fe_3O_4$ by irradiation of magnetic fields, and showed effective cell toxicity on breast cancer cells (MDA-MB-231). These exothermic nanoparticles coated with silica particles are expected to show local heating only on the silica surface, which can create a separate column system, for instance, steroid drugs, proteins, and cells without any thermal damage to these separated materials. In this way, the combination of imaging materials and biocompatible polymer/silica particles is expected to improve their capability as diagnostic materials. These particles also usually played the role of a drug carrier. Therefore, particles with abilities of both diagnosis and therapy are applied as 'smart' materials in the biomedical field.

### *3.5.3 Others*

Generally, fluorine materials show oil repellency owing to their low surface free energy, and water drop touching on a flat fluorine surface is calculated with a contact angle (CA) of about 120°. The fluorine substrates having roughness with nano- and microscale structures, however, show CAs over 150° and a low sliding angle called super-hydrophobicity. These structures showing super-hydrophobic properties are often observed in the natural world. For example, the lotus leaf shows a super-hydrophobic property owing to its waxy surface and nano/microroughness structure, which is known as the lotus effect. Surface properties are determined by their surface energy and surface roughness, which are explained using the Wenzel and Cassie/Baxter theories [146, 147]. In the Wenzel theory, a water droplet is completely in contact with the surface of the substrate. On the other hand, there is air between the water droplet and the substrate owing to ditches as described in the Cassie/Baxter theory. Recently, bioinspired materials, which are materials with structures mimicking living things, have been developed, and their hydrophobic properties have been investigated. Miyauchi et al. [148] prepared a polystyrene (PS) material having a structure mimicked a leaf-surface of a silver chrysanthemum by electrospinning, and the CA was over 150°. Zhang et al. [149] reported a unique substrate showing anisotropic CA to transcribe the wing of a grasshopper to poly(dimethylsiloxane) (PDMS) film. In this way, it is very important to control the surface roughness (structure) as part of the material design. As a typical method for the preparation of roughness, the photoresist has been extensively used in the top–down method. In the top–down method for large-scale production, however, there are some problems such as a multistep preparation process and the removal of vice-generative productions. Recently, the method for creation of effective roughness on substrates using self-assemble materials has been focused on as a bottom-up method. Karunakaran et al. [150] prepared effectively a rough surface on substrates using silica nanoparticles (SiNPs) with different sizes. The SiNPs were 20 and 100 nm in diameter, and were alternately coated on substrates as a monolayer. In other words, there are bilayers of SiNPs on the substrates.

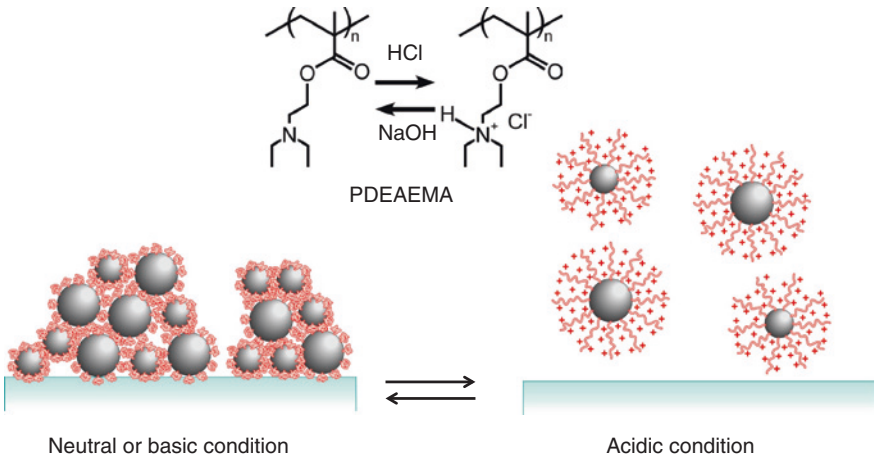


**Fig. 3.20** Schematic representation of the roughness structured by silica nanoparticles of different sizes with pH responsive PDEAEMA [Ref. 151]

Subsequently, the SiNP-coated substrates were treated with perfluorosilane, and their surface properties were estimated. Interestingly, the substrates coated with size different SiNPs showed super-hydrophobic properties despite the fact that the CAs of the substrate coated by SiNPs with a monolayer (10, 50, and 100 nm) were below 150°. These results suggest that rough structures are effectively constructed using size different SiNPs by the bottom–up method. In this case, however, it is difficult to remove the coated SiNPs from the substrate because of their strong perfluorosilane treatment. The authors synthesized pH-responsive poly(2-(diethylamino)ethyl methacrylate) (PDEAEMA) from SiNPs of 20 and 128 nm diameter by surface-initiated ATRP [151]. The substrates modified by a mixture of size different SiNPs showed high CA (124 ± 6°) as compared with that of individual SiNPs of 20 or 128 nm diameter (Fig. 3.20). Stratakis et al. [152] prepared PDEAEMA from the substrate with a high roughness by surface-initiated ATRP as a pH-switchable surface. Our CA data was close to the CA of the PDEAMEA-modified substrate under alkali condition. These results suggest that the mixture of SiNPs can result in high roughness on the substrates. According to the root-mean-square (RMS) value for estimation of the roughness parameters by AFM, mixed SiNPs in fact showed a higher RMS than individual SiNPs. Moreover, fluorescein isothiocyanate (FITC)-loaded SiNPs (132 nm) with PDEAEMA were also prepared by surface-initiated ATRP for the measurement of their adsorption/desorption behavior on the substrates depending on the pH. Results showed that PDEAEMA-modified SiNPs were adsorbed on the substrates under neutral and alkali conditions and were desorbed from the substrates under acid condition for the pH-responsive PDEAEMA, which were observed using SEM and a plate reader. This simple method is expected to open a new stage for the universal modification method to any substrates.

The preparation of self-assemblies in situ has also been reported. A dendrimer is a material with branched structures that are perfectly arranged, which is applied in a wide range of fields for their loading ability of materials and simple modification of functionalities. Haba et al. for example, successfully prepared a temperature-responsive poly(aminoamine) (PAMAM) dendrimer on which the *N*-isopropylamide (NIPAM) was modified via covalent bonds. The surfaces of dendrimer materials have similar structures to temperature-responsive PNIPAAm polymers. Moreover, the LCSTs were controlled with adjusting the chain length between the PAMAM dendrimer and NIPAM. These results suggest that clusters of NIPAM groups are important to show temperature-responsive properties [153]. Our group prepared conjugated materials of PAMAM and di- or tri-block copolymers. The block copolymers of PNIPAAm-*b*-poly(methacrylic acid) (PMAAc) and PMAAc-*b*-PNIPAAm-*b*-PMAAc were combined with PAMAM by covalent bonds. Interestingly, the aggregation behavior triggered by changing the pH and temperature was found to be different for the structures of modified di- or tri-block copolymers [154]. Akin et al. developed a material with a unique structure that was a quantum dot (QD, 5.6 nm) coated by PAMAM dendrimers. The QD with dendrimers showed high stability in aqueous solution, and the diameters were different in terms of the numbers of modified PAMAM dendrimers (numbers of PAMAM dendrimers/diameter = 14/33 nm and 28/59 nm). The QD-PAMAM dendrimers modified using the HER2 antibody on the surface showed targeting ability to MCF-7 cells expressing antibody receptors [155]. Recently, hyperbranched materials have been focused on for their simple polymerization. The well-defined structures of hyperbranched materials are inferior compared with those of dendrimers, but their loading abilities and controlled diameter range are suitable for application as biomaterials. The preparation methods for hyperbranched materials are almost the same as typical controlled living radical polymerizations (CLRPs). The formation of the hyperbranches is achieved by only adding a chemical compound with divinyl groups as a crosslinker into the CLRP system. The diameters are easily controlled via changing the concentration of the starting materials. Ahmed et al. [105] prepared hyperbranched materials using *N*,*N*′-methylenebisacrylamide as the crosslinker by RAFT polymerization. The hyperbranch materials were composed of copolymers that were sugar polymers of poly(3-gluconamidopropyl methacrylamide (PGAPMA)) or poly(2-lactobionamidoethyl methacrylamide (LAEMA)) and poly(2-aminoethyl methacrylamide (AEMA)) with cationic charge. The cationic AEMA units were used to interact with anionic nucleic acids by electrostatic interactions, and the conjugated materials having nanoorder scale achieved low toxicity, high dispersion ability, and high transfection ability. However, these hyperbranched materials usually possess wide size distributions. Considering their applications as biomaterials, narrow size distributions are strongly required in their structures. For solving the problem, Min et al. polymerized two types of monomer having methacryl and 2-bromoisobutyrate groups in emulsions by ATRP. According to their concept, the emulsions are individual, and the generated radicals in an emulsion cannot transfer to other emulsions, which lead to a narrow size distribution in their hyperbranched materials. In fact, the polymerized hyperbranched materials showed narrow size distributions (PDI < 1.3)

as compared with polymerized materials without emulsions [156]. Moreover, the preparation of a core-shell nanogel in situ by a similar polymerization method with hyperbranched materials has been reported. In this case, a macroinitiator (ATRP) or macro-CTA (RAFT) is needed in the polymerization system as the shell part. These gels have also been applied as carriers for their excellent loading abilities such as molecules, enzymes, proteins, nucleic acids, and inorganic materials [157]. In this way, unique preparation methods/systems enable the achievement of not only material design but also effective large-scale production (low cost, quick reaction, and little amount of chemical waste).

## 3.6 Conclusions and Future Trends

This chapter focused on nanoassemblies and nanoparticles as biomaterials, and introduced by categories: synthesis, polymerizations, characterizations, and applications using current reports. Multi-functional nanomaterials with various structures have been synthesized by simple preparation methods, which are combinations of living radical polymerizations and click chemistry. The form, diameters, and surface properties of nanomaterials are observed using powerful tools such as microscopes (SEM, TEM, AFM, etc.), DLS, SLS, and zeta potential. Moreover, the self-assembly behaviors are also estimated using fluorescent molecules. Recently, several types of nanoassembly/nanoparticle have been developed using these preparation and analysis techniques as unique drug carriers for biomedical fields. These drug carriers possess unique properties, namely, biocompatibilities, long circulation time, active targeting, controlled drug release, and biodegradation for a desirable carrier system. On the basis of these results, what kind of material design do we need for the development of nanoassemblies/nanoparticles in the future? We have focused on self-assemblies (formation of particles) using the metastable state of materials. The control of the metastable state is difficult because their property tends to shift to the stable state. If a nanomaterial that can switch from stable to metastable states as triggered by the external environment can be developed, this nanomaterial may be applied as an energy pump of living cells for triggering apoptosis, which may be a drug-free treatment strategy. The development of multi-functional nanomaterials using structural designs, controlled self-assemblies, and a few types of raw material is one of our challenges. Seemingly, there may be a contradiction in the material design. However, we are convinced that these revolutionary material designs open a new stage in the nanofield.

## References

1. Kotsuchibashi Y, Ebara M, Idota N, Narain R, Aoyagi T (2012) A ‘smart’ approach towards the formation of multifunctional nano-assemblies by simple mixing of block copolymers having a common temperature sensitive segment. Polym Chem-Uk 3:1150–1157

2. Hoffman AS (2008) The origins and evolution of "controlled" drug delivery systems. J Controlled Release 132:153–163. doi:http://dx.doi.org/10.1016/j.jconrel.2008.08.012
3. Nishiyama N, Kataoka K (2006) Nanostructured devices based on block copolymer assemblies for drug delivery: designing structures for enhanced drug function. In: Satchi-Fainaro R, Duncan R (eds) Polymer therapeutics II. Advances in polymer science, vol 193. Springer, Heidelberg, pp 67–101. doi:10.1007/12_025
4. Ringsdorf H (1975) Structure and properties of pharmacologically active polymers. J Polym Sci: Polym Symp 51:135–153. doi:10.1002/polc.5070510111
5. Zhang L, Eisenberg A (1995) Multiple morphologies of "crew-cut" aggregates of polystyrene-b-poly(acrylic acid) block copolymers. Science 268:1728–1731. doi:10.1126/science.268.5218.1728
6. Davis FF (2002) The origin of pegnology. Adv Drug Del Rev 54:457–458. doi:http://dx.doi.org/10.1016/S0169-409X(02)00021-2
7. Maeda H, Wu J, Sawa T, Matsumura Y, Hori K (2000) Tumor vascular permeability and the EPR effect in macromolecular therapeutics: a review. J Controlled Release 65:271–284. doi:http://dx.doi.org/10.1016/S0168-3659(99)00248-5
8. Yokoyama M, Okano T, Sakurai Y, Kataoka K (1994) Improved synthesis of adriamycin-conjugated poly (ethylene oxide)-poly (aspartic acid) block copolymer and formation of unimodal micellar structure with controlled amount of physically entrapped adriamycin. J Controlled Release 32:269–277. doi:http://dx.doi.org/10.1016/0168-3659(94)90237-2
9. Yokoyama M, Fukushima S, Uehara R, Okamoto K, Kataoka K, Sakurai Y, Okano T (1998) Characterization of physical entrapment and chemical conjugation of adriamycin in polymeric micelles and their design for in vivo delivery to a solid tumor. J Controlled Release 50:79–92. doi:http://dx.doi.org/10.1016/S0168-3659(97)00115-6
10. Harada A, Kataoka K (1995) Formation of polyion complex micelles in an aqueous milieu from a pair of oppositely-charged block copolymers with poly(ethylene glycol) segments. Macromolecules 28:5294–5299. doi:10.1021/ma00119a019
11. Katayose S, Kataoka K (1997) Water-soluble polyion complex associates of DNA and poly(ethylene glycol)-poly(L-lysine) block copolymer. Bioconjugate Chem 8:702–707. doi:10.1021/bc9701306
12. Takae S, Miyata K, Oba M, Ishii T, Nishiyama N, Itaka K, Yamasaki Y, Koyama H, Kataoka K (2008) PEG-detachable polyplex micelles based on disulfide-linked block catiomers as bioresponsive nonviral gene vectors. J Am Chem Soc 130:6001–6009. doi:10.1021/ja800336v
13. Lee Y, Kataoka K (2009) Biosignal-sensitive polyion complex micelles for the delivery of biopharmaceuticals. Soft Matter 5:3810–3817
14. Kabanov AV, Chekhonin VP, Alakhov VY, Batrakova EV, Lebedev AS, Melik-Nubarov NS, Arzhakov SA, Levashov AV, Morozov GV, Severin ES, Kabanov VA (1989) The neuroleptic activity of haloperidol increases after its solubilization in surfactant micelles: micelles as microcontainers for drug targeting. FEBS Lett 258:343–345. doi:http://dx.doi.org/10.1016/0014-5793(89)81689-8
15. Semsarilar M, Jones ER, Blanazs A, Armes SP (2012) Efficient synthesis of sterically-stabilized nano-objects via RAFT dispersion polymerization of benzyl methacrylate in alcoholic media. Adv Mater 24:3378–3382. doi:10.1002/adma.201200925
16. Georges MK, Veregin RPN, Kazmaier PM, Hamer GK (1993) Narrow molecular weight resins by a free-radical polymerization process. Macromolecules 26:2987–2988. doi:10.1021/ma00063a054
17. Kato M, Kamigaito M, Sawamoto M, Higashimura T (1995) Polymerization of methyl methacrylate with the carbon tetrachloride/dichlorotris-(triphenylphosphine)ruthenium(II)/methylaluminum bis(2,6-di-tert-butylphenoxide) initiating system: possibility of living radical polymerization. Macromolecules 28:1721–1723. doi:10.1021/ma00109a056
18. Wang J-S, Matyjaszewski K (1995) "Living"/controlled radical polymerization. Transition-metal-catalyzed atom transfer radical polymerization in the presence of a conventional radical initiator. Macromolecules 28:7572–7573. doi:10.1021/ma00126a041

19. Chiefari J, Chong YK, Ercole F, Krstina J, Jeffery J, Le TPT, Mayadunne RTA, Meijs GF, Moad CL, Moad G, Rizzardo E, Thang SH (1998) Living free-radical polymerization by reversible addition–fragmentation chain transfer: the RAFT process. Macromolecules 31:5559–5562. doi:10.1021/ma9804951
20. Chong YK, Le TPT, Moad G, Rizzardo E, Thang SH (1999) A more versatile route to block copolymers and other polymers of complex architecture by living radical polymerization: the RAFT process. Macromolecules 32:2071–2074. doi:10.1021/ma981472p
21. Kolb HC, Finn MG, Sharpless KB (2001) Click chemistry: diverse chemical function from a few good reactions. Angew Chem Int Ed 40:2004–2021. doi:10.1002/1521-3773(20010601)40:11<2004:aid-anie2004>3.0.co;2-5
22. Sumerlin BS (2012) Proteins as initiators of controlled radical polymerization: grafting-from via ATRP and RAFT. ACS Macro Lett 1:141–145. doi:10.1021/mz200176g
23. Kabachii YA, Kochev SY, Bronstein LM, Blagodatskikh IB, Valetsky PM (2003) Atom transfer radical polymerization with Ti(III) halides and alkoxides. Polym Bull 50:271–278. doi:10.1007/s00289-003-0157-9
24. Onishi I, Baek K-Y, Kotani Y, Kamigaito M, Sawamoto M (2002) Iron-catalyzed living radical polymerization of acrylates: iodide-based initiating systems and block and random copolymerizations. J Polym Sci, Part A: Polym Chem 40:2033–2043. doi:10.1002/pola.10299
25. Wang B, Zhuang Y, Luo X, Xu S, Zhou X (2003) Controlled/"living" radical polymerization of MMA catalyzed by cobaltocene. Macromolecules 36:9684–9686. doi:10.1021/ma035334y
26. Granel C, Dubois P, Jérôme R, Teyssié P (1996) Controlled radical polymerization of methacrylic monomers in the presence of a bis(ortho-chelated) arylnickel(II) complex and different activated alkyl halides. Macromolecules 29:8576–8582. doi:10.1021/ma9608380
27. Qiu J, Gaynor SG, Matyjaszewski K (1999) Emulsion polymerization of n-butyl methacrylate by reverse atom transfer radical polymerization. Macromolecules 32:2872–2875. doi:10.1021/ma981695f
28. Konkolewicz D, Magenau AJD, Averick SE, Simakova A, He H, Matyjaszewski K (2012) ICAR ATRP with ppm Cu catalyst in water. Macromolecules 45:4461–4468. doi:10.1021/ma300887r
29. Jakubowski W, Matyjaszewski K (2005) Activator generated by electron transfer for atom transfer radical polymerization. Macromolecules 38:4139–4146. doi:10.1021/ma047389l
30. Matyjaszewski K, Dong H, Jakubowski W, Pietrasik J, Kusumo A (2007) Grafting from surfaces for "everyone": ARGET ATRP in the presence of air. Langmuir 23:4528–4531. doi:10.1021/la063402e
31. Magenau AJD, Strandwitz NC, Gennaro A, Matyjaszewski K (2011) Electrochemically mediated atom transfer radical polymerization. Science 332:81–84. doi:10.1126/science.1202357
32. Benaglia M, Chiefari J, Chong YK, Moad G, Rizzardo E, Thang SH (2009) Universal (switchable) RAFT agents. J Am Chem Soc 131:6914–6915. doi:10.1021/ja901955n
33. Wei H, Schellinger JG, Chu DSH, Pun SH (2012) Neuron-targeted copolymers with sheddable shielding blocks synthesized using a reducible, RAFT-ATRP double-head agent. J Am Chem Soc 134:16554–16557. doi:10.1021/ja3085803
34. Averick S, Simakova A, Park S, Konkolewicz D, Magenau AJD, Mehl RA, Matyjaszewski K (2012) ATRP under biologically relevant conditions: grafting from a protein. ACS Macro Lett 1:6–10. doi:10.1021/mz200020c
35. Narain R, Gonzales M, Hoffman AS, Stayton PS, Krishnan KM (2007) Synthesis of monodisperse biotinylated p(NIPAAm)-coated iron oxide magnetic nanoparticles and their bioconjugation to streptavidin. Langmuir 23:6299–6304. doi:10.1021/la700268g
36. Convertine AJ, Ayres N, Scales CW, Lowe AB, McCormick CL (2004) Facile, controlled, room-temperature RAFT polymerization of N-isopropylacrylamide. Biomacromolecules 5:1177–1180. doi:10.1021/bm049825h
37. Convertine AJ, Lokitz BS, Vasileva Y, Myrick LJ, Scales CW, Lowe AB, McCormick CL (2006) Direct synthesis of thermally responsive DMA/NIPAM diblock and

DMA/NIPAM/DMA triblock copolymers via aqueous, room temperature RAFT polymerization. Macromolecules 39:1724–1730. doi:10.1021/ma0523419
38. Li M, Li H, De P, Sumerlin BS (2011) Thermoresponsive block copolymer-protein conjugates prepared by grafting-from via RAFT polymerization. Macromol Rapid Commun 32:354–359. doi:10.1002/marc.201000619
39. Crownover E, Duvall CL, Convertine A, Hoffman AS, Stayton PS (2011) RAFT-synthesized graft copolymers that enhance pH-dependent membrane destabilization and protein circulation times. J Controlled Release 155:167–174. doi:http://dx.doi.org/10.1016/j.jconrel.2011.06.013
40. Mespouille L, Vachaudez M, Suriano F, Gerbaux P, Coulembier O, Degée P, Flammang R, Dubois P (2007) One-pot synthesis of well-defined amphiphilic and adaptative block copolymers via versatile combination of "click" chemistry and ATRP. Macromol Rapid Commun 28:2151–2158. doi:10.1002/marc.200700400
41. Chakrabarty R, Stang PJ (2012) Post-assembly functionalization of organoplatinum(II) metallacycles via copper-free click chemistry. J Am Chem Soc 134:14738–14741. doi:10.1021/ja3070073
42. Hoyle CE, Bowman CN (2010) Thiol-ene click chemistry. Angew Chem Int Ed 49:1540–1573. doi:10.1002/anie.200903924
43. Kade MJ, Burke DJ, Hawker CJ (2010) The power of thiol-ene chemistry. J Polym Sci, Part A: Polym Chem 48:743–750. doi:10.1002/pola.23824
44. Nakayama M, Okano T, Miyazaki T, Kohori F, Sakai K, Yokoyama M (2006) Molecular design of biodegradable polymeric micelles for temperature-responsive drug release. J Controlled Release 115:46–56. doi:http://dx.doi.org/10.1016/j.jconrel.2006.07.007
45. Chung JE, Yokoyama M, Yamato M, Aoyagi T, Sakurai Y, Okano T (1999) Thermoresponsive drug delivery from polymeric micelles constructed using block copolymers of poly(N-isopropylacrylamide) and poly(butylmethacrylate). J Controlled Release 62:115–127. doi:http://dx.doi.org/10.1016/S0168-3659(99)00029-2
46. Virtanen J, Holappa S, Lemmetyinen H, Tenhu H (2002) Aggregation in aqueous poly(N-isopropylacrylamide)-block-poly(ethylene oxide) solutions studied by fluorescence spectroscopy and light scattering. Macromolecules 35:4763–4769. doi:10.1021/ma012239l
47. Motokawa R, Morishita K, Koizumi S, Nakahira T, Annaka M (2005) Thermosensitive diblock copolymer of poly(N-isopropylacrylamide) and poly(ethylene glycol) in water: polymer preparation and solution behavior. Macromolecules 38:5748–5760. doi:10.1021/ma047393x
48. Zhang W, Shi L, Wu K, An Y (2005) Thermoresponsive micellization of poly(ethylene glycol)-b-poly(N-isopropylacrylamide) in water. Macromolecules 38:5743–5747. doi:10.1021/ma0509199
49. Kotsuchibashi Y, Ebara M, Yamamoto K, Aoyagi T (2011) Tunable stimuli-responsive self-assembly system that forms and stabilizes nanoparticles by simple mixing and heating/cooling of selected block copolymers. Polym Chem-Uk 2:1362–1367
50. Kotsuchibashi Y, Ebara M, Yamamoto K, Aoyagi T (2010) "On–off" switching of dynamically controllable self-assembly formation of double-responsive block copolymers with tunable LCSTs. J Polym Sci, Part A: Polym Chem 48:4393–4399. doi:10.1002/pola.24226
51. Kotsuchibashi Y, Kuboshima Y, Yamamoto K, Aoyagi T (2008) Synthesis and characterization of double thermo-responsive block copolymer consisting N-isopropylacrylamide by atom transfer radical polymerization. J Polym Sci, Part A: Polym Chem 46:6142–6150. doi:10.1002/pola.22925
52. Pelton R (2000) Temperature-sensitive aqueous microgels. Adv Colloid Interface Sci 85:1–33. doi:10.1016/s0001-8686(99)00023-8
53. Parasuraman D, Sarker AK, Serpe MJ (2012) Poly(N-isopropylacrylamide)-based microgels and their assemblies for organic-molecule removal from water. Chem Phys Chem 13:2507–2515. doi:10.1002/cphc.201200025
54. Aoyagi T, Ebara M, Sakai K, Sakurai Y, Okano T (2000) Novel bifunctional polymer with reactivity and temperature sensitivity. J Biomater Sci Polym Ed 11:101–110. doi:10.1163/156856200743526

55. Ebara M, Aoyagi T, Sakai K, Okano T (2001) The incorporation of carboxylate groups into temperature-responsive poly(N-isopropylacrylamide)-based hydrogels promotes rapid gel shrinking. J Polym Sci, Part A: Polym Chem 39:335–342. doi:10.1002/1099-0518(20010201)39:3<335:aid-pola1000>3.0.co;2-h
56. Maeda T, Kanda T, Yonekura Y, Yamamoto K, Aoyagi T (2006) Hydroxylated poly(N-isopropylacrylamide) as functional thermoresponsive materials. Biomacromolecules 7:545–549. doi:10.1021/bm050829b
57. Maeda T, Takenouchi M, Yamamoto K, Aoyagi T (2006) Analysis of the formation mechanism for thermoresponsive-type coacervate with functional copolymers consisting of N-isopropylacrylamide and 2-Hydroxyisopropylacrylamide. Biomacromolecules 7:2230–2236. doi:10.1021/bm060261m
58. Maeda T, Takenouchi M, Yamamoto K, Aoyagi T (2009) Coil-globule transition and/or coacervation of temperature and pH dual-responsive carboxylated poly(N-isopropylacrylamide). Polym J 41:181–188
59. Maeda T, Akasaki Y, Yamamoto K, Aoyagi T (2009) Stimuli-responsive coacervate induced in binary functionalized poly(N-isopropylacrylamide) aqueous system and novel method for preparing semi-IPN microgel using the coacervate. Langmuir 25:9510–9517. doi:10.1021/la9007735
60. Arriagada FJ, Osseo-Asare K (1999) Synthesis of nanosize silica in a nonionic water-in-oil microemulsion: effects of the water/surfactant molar ratio and ammonia concentration. J Colloid Interface Sci 211:210–220. doi:http://dx.doi.org/10.1006/jcis.1998.5985
61. Stöber W, Fink A, Bohn E (1968) Controlled growth of monodisperse silica spheres in the micron size range. J Colloid Interface Sci 26:62–69. doi:http://dx.doi.org/10.1016/0021-9797(68)90272-5
62. Lin Y-S, Abadeer N, Hurley KR, Haynes CL (2011) Ultrastable, redispersible, small, and highly organomodified mesoporous silica nanotherapeutics. J Am Chem Soc 133:20444–20457. doi:10.1021/ja208567v
63. Decuzzi P, Godin B, Tanaka T, Lee SY, Chiappini C, Liu X, Ferrari M (2010) Size and shape effects in the biodistribution of intravascularly injected particles. J Controlled Release 141:320–327. doi:http://dx.doi.org/10.1016/j.jconrel.2009.10.014
64. Niu D, Ma Z, Li Y, Shi J (2010) Synthesis of core-shell structured dual-mesoporous silica spheres with tunable pore size and controllable shell thickness. J Am Chem Soc 132:15144–15147. doi:10.1021/ja1070653
65. Chen Y, Chen H, Guo L, He Q, Chen F, Zhou J, Feng J, Shi J (2009) Hollow/rattle-type mesoporous nanostructures by a structural difference-based selective etching strategy. ACS Nano 4:529–539. doi:10.1021/nn901398j
66. Chen Y, Chen H, Zeng D, Tian Y, Chen F, Feng J, Shi J (2010) Core/shell structured hollow mesoporous nanocapsules: a potential platform for simultaneous cell imaging and anticancer drug delivery. ACS Nano 4:6001–6013. doi:10.1021/nn1015117
67. Ishii H, Sato K, Nagao D, Konno M (2012) Anionic liposome template synthesis of raspberry-like hollow silica particle under ambient conditions with basic catalyst. Colloids Surf B Biointerfaces 92:372–376. doi:http://dx.doi.org/10.1016/j.colsurfb.2011.11.005
68. Zhang H, Li Z, Xu P, Wu R, Jiao Z (2010) A facile two-step synthesis of novel chrysanthemum-like mesoporous silica nanoparticles for controlled pyrene release. Chem Commun 46:6783–6785
69. Teo BM, Suh SK, Hatton TA, Ashokkumar M, Grieser F (2011) Sonochemical synthesis of magnetic janus nanoparticles. Langmuir 27:30–33. doi:10.1021/la104284v
70. Astafieva I, Zhong XF, Eisenberg A (1993) Critical micellization phenomena in block polyelectrolyte solutions. Macromolecules 26:7339–7352. doi:10.1021/ma00078a034
71. Masci G, Diociaiuti M, Crescenzi V (2008) ATRP synthesis and association properties of thermoresponsive anionic block copolymers. J Polym Sci, Part A: Polym Chem 46:4830–4842. doi:10.1002/pola.22816
72. S-i Yusa, Shimada Y, Mitsukami Y, Yamamoto T, Morishima Y (2004) Heat-induced association and dissociation behavior of amphiphilic diblock copolymers synthesized via revers-

ible addition-fragmentation chain transfer radical polymerization. Macromolecules 37: 7507–7513. doi:10.1021/ma0492519
73. Yip J, Duhamel J, Qiu XP, FoM Winnik (2011) Long-range polymer chain dynamics of pyrene-labeled poly(N-isopropylacrylamide)s studied by fluorescence. Macromolecules 44:5363–5372. doi:10.1021/ma2007865
74. Winnik FM (1990) Fluorescence studies of aqueous solutions of poly(N-isopropylacrylamide) below and above their LCST. Macromolecules 23:233–242. doi:10.1021/ma00203a040
75. Ringsdorf H, Venzmer J, Winnik FM (1991) Fluorescence studies of hydrophobically modified poly(N-isopropylacrylamides). Macromolecules 24:1678–1686. doi:10.1021/ma00007a034
76. Duan Q, Miura Y, Narumi A, Shen X, Sato S-I, Satoh T, Kakuchi T (2006) Synthesis and thermoresponsive property of end-functionalized poly(N-isopropylacrylamide) with pyrenyl group. J Polym Sci, Part A: Polym Chem 44:1117–1124. doi:10.1002/pola.21208
77. Yip J, Duhamel J, Qiu XP, Winnik FM (2011) Fluorescence studies of a series of monodisperse telechelic α,ω-dipyrenyl poly(N-isopropylacrylamide)s in ethanol and in water. Can J Chem 89:163–172. doi:10.1139/v10-117
78. Scales CW, Convertine AJ, McCormick CL (2006) Fluorescent labeling of RAFT-generated poly(N-isopropylacrylamide) via a facile maleimide-thiol coupling reaction. Biomacromolecules 7:1389–1392. doi:10.1021/bm060192b
79. Okabe K, Inada N, Gota C, Harada Y, Funatsu T, Uchiyama S (2012) Intracellular temperature mapping with a fluorescent polymeric thermometer and fluorescence lifetime imaging microscopy. Nat Commun 3:705. doi:http://www.nature.com/ncomms/journal/v3/n2/suppinfo/ncomms1714_S1.html
80. Sapsford KE, Berti L, Medintz IL (2006) Materials for fluorescence resonance energy transfer analysis: beyond traditional donor-acceptor combinations. Angew Chem Int Ed 45:4562–4589. doi:10.1002/anie.200503873
81. Li C, Liu S (2012) Polymeric assemblies and nanoparticles with stimuli-responsive fluorescence emission characteristics. Chem Commun 48:3262–3278
82. Aoshima S, Oda H, Kobayashi E (1992) Synthesis of thermally-induced phase separating polymer with well-defined polymer structure by living cationic polymerization. I. Synthesis of poly(vinyl ether)s with oxyethylene units in the pendant and its phase separation behavior in aqueous solution. J Polym Sci, Part A: Polym Chem 30:2407–2413. doi:10.1002/pola.1992.080301115
83. Aoshima S, Sugihara S (2000) Syntheses of stimuli-responsive block copolymers of vinyl ethers with side oxyethylene groups by living cationic polymerization and their thermosensitive physical gelation. J Polym Sci, Part A: Polym Chem 38:3962–3965. doi:10.1002/1099-0518(20001101)38:21<3962:aid-pola130>3.0.co;2-9
84. Seno K-I, Kanaoka S, Aoshima S (2008) Thermosensitive diblock copolymers with designed molecular weight distribution: synthesis by continuous living cationic polymerization and micellization behavior. J Polym Sci, Part A: Polym Chem 46:2212–2221. doi:10.1002/pola.22556
85. Skrabania K, Kristen J, Laschewsky A, Akdemir Ö, Hoth A, Lutz J-F (2006) Design, synthesis, and aqueous aggregation behavior of nonionic single and multiple thermoresponsive polymers. Langmuir 23:84–93. doi:10.1021/la061509w
86. Kotsuchibashi Y, Yamamoto K, Aoyagi T (2009) Assembly behavior of double thermoresponsive block copolymers with controlled response temperature in aqueous solution. J Colloid Interface Sci 336:67–72. doi:http://dx.doi.org/10.1016/j.jcis.2009.03.093
87. Lutz J-F, Hoth A (2006) Preparation of ideal PEG analogues with a tunable thermosensitivity by controlled radical copolymerization of 2-(2-Methoxyethoxy)ethyl methacrylate and oligo(ethylene glycol) methacrylate. Macromolecules 39:893–896. doi:10.1021/ma0517042
88. Lutz J-F, Akdemir Ö, Hoth A (2006) Point by point comparison of two thermosensitive polymers exhibiting a similar LCST: is the age of poly(NIPAM) over? J Am Chem Soc 128:13046–13047. doi:10.1021/ja065324n

89. Manganiello MJ, Cheng C, Convertine AJ, Bryers JD, Stayton PS (2012) Diblock copolymers with tunable pH transitions for gene delivery. Biomaterials 33:2301–2309. doi:http://dx.doi.org/10.1016/j.biomaterials.2011.11.019
90. Zhang W, Shi L, Ma R, An Y, Xu Y, Wu K (2005) Micellization of thermo- and pH-responsive triblock copolymer of Poly(ethylene glycol)-b-poly(4-vinylpyridine)-b-poly(N-isopropylacrylamide). Macromolecules 38:8850–8852. doi:10.1021/ma050998o
91. Xu J, Luo S, Shi W, Liu S (2005) Two-stage collapse of unimolecular micelles with double thermoresponsive coronas. Langmuir 22:989–997. doi:10.1021/la0522707
92. Liu H, Li C, Liu H, Liu S (2009) pH-responsive supramolecular self-assembly of well-defined zwitterionic ABC miktoarm star terpolymers. Langmuir 25:4724–4734. doi:10.1021/la803813r
93. Ye X, Fei J, Xu K, Bai R (2010) Effect of polystyrene-b-poly(ethylene oxide) on self-assembly of polystyrene-b-poly(N-isopropylacrylamide) in aqueous solution. J Polym Sci, Part B: Polym Phys 48:1168–1174. doi:10.1002/polb.22006
94. Kim SH, Tan JPK, Nederberg F, Fukushima K, Yang YY, Waymouth RM, Hedrick JL (2009) Mixed micelle formation through stereocomplexation between enantiomeric poly(lactide) block copolymers. Macromolecules 42:25–29. doi:10.1021/ma801739x
95. Santis SD, Ladogana RD, Diociaiuti M, Masci G (2010) Pegylated and thermosensitive polyion complex micelles by self-assembly of two oppositely and permanently charged diblock copolymers. Macromolecules 43:1992–2001. doi:10.1021/ma9026542
96. Palyulin VV, Potemkin II (2008) Mixed versus ordinary micelles in the dilute solution of AB and BC diblock copolymers. Macromolecules 41:4459–4463. doi:10.1021/ma8003949
97. Narain R, Armes SP (2003) Direct synthesis and aqueous solution properties of well-defined cyclic sugar methacrylate polymers. Macromolecules 36:4675–4678. doi:10.1021/ma034321h
98. Ahmed M, Narain R (2013) Progress of RAFT based polymers in gene delivery. Prog Polym Sci. doi:http://dx.doi.org/10.1016/j.progpolymsci.2012.09.008
99. Oerlemans C, Bult W, Bos M, Storm G, Nijsen JF, Hennink W (2010) Polymeric micelles in anticancer therapy: targeting, imaging and triggered release. Pharm Res 27:2569–2589. doi:10.1007/s11095-010-0233-4
100. Bae Y, Kataoka K (2009) Intelligent polymeric micelles from functional poly(ethylene glycol)-poly(amino acid) block copolymers. Adv Drug Del Rev 61:768–784. doi:http://dx.doi.org/10.1016/j.addr.2009.04.016
101. Bae Y, Jang W-D, Nishiyama N, Fukushima S, Kataoka K (2005) Multifunctional polymeric micelles with folate-mediated cancer cell targeting and pH-triggered drug releasing properties for active intracellular drug delivery. Mol Bio Syst 1:242–250
102. Ahmed M, Narain R (2011) Cationic glycopolymers: engineered carbohydrate-based materials for biomedical applications. Wiley, New York, pp 143–165. doi:10.1002/9780470944349.ch3
103. Ahmed M, Narain R (2011) Glycopolymer bioconjugates: engineered carbohydrate-based materials for biomedical applications. Wiley, New York, pp 167–188. doi:10.1002/9780470944349.ch4
104. Ahmed M, Narain R (2011) The effect of polymer architecture, composition, and molecular weight on the properties of glycopolymer-based non-viral gene delivery systems. Biomaterials 32:5279–5290. doi:http://dx.doi.org/10.1016/j.biomaterials.2011.03.082
105. Ahmed M, Narain R (2012) The effect of molecular weight, compositions and lectin type on the properties of hyperbranched glycopolymers as non-viral gene delivery systems. Biomaterials 33:3990–4001. doi:http://dx.doi.org/10.1016/j.biomaterials.2012.02.015
106. Maruyama A, Ishihara T, Kim J-S, Kim SW, Akaike T (1997) Nanoparticle DNA carrier with poly(L-lysine) grafted polysaccharide copolymer and poly(d,l-lactic acid). Bioconjugate Chem 8:735–742. doi:10.1021/bc9701048
107. Hasegawa U, Nomura S-iM, Kaul SC, Hirano T, Akiyoshi K (2005) Nanogel-quantum dot hybrid nanoparticles for live cell imaging. Biochem Biophys Res Commun 331:917–921. doi:http://dx.doi.org/10.1016/j.bbrc.2005.03.228

108. Lee YC, Lee RT (1995) Carbohydrate-protein interactions: basis of glycobiology. Acc Chem Res 28:321–327. doi:10.1021/ar00056a001
109. Mao Z, Wan L, Hu L, Ma L, Gao C (2010) Tat peptide mediated cellular uptake of $SiO_2$ submicron particles. Colloids Surf B Biointerfaces 75:432–440. doi:http://dx.doi.org/10.1016/j.colsurfb.2009.09.017
110. Tkachenko AG, Xie H, Coleman D, Glomm W, Ryan J, Anderson MF, Franzen S, Feldheim DL (2003) Multifunctional gold nanoparticle-peptide complexes for nuclear targeting. J Am Chem Soc 125:4700–4701. doi:10.1021/ja0296935
111. Sethuraman VA, Bae YH (2007) TAT peptide-based micelle system for potential active targeting of anti-cancer agents to acidic solid tumors. J Controlled Release 118:216–224. doi:http://dx.doi.org/10.1016/j.jconrel.2006.12.008
112. Chavanpatil MD, Khdair A, Panyam J (2006) Nanoparticles for cellular drug delivery: mechanisms and factors influencing delivery. J Nanosci Nanotechnol 6:2651–2663. doi:10.1166/jnn.2006.443
113. Ku S, Yan F, Wang Y, Sun Y, Yang N, Ye L (2010) The blood–brain barrier penetration and distribution of PEGylated fluorescein-doped magnetic silica nanoparticles in rat brain. Biochem Biophys Res Commun 394:871–876. doi:http://dx.doi.org/10.1016/j.bbrc.2010.03.006
114. Lee JCH, McDonald R, Hall DG (2011) Enantioselective preparation and chemoselective cross-coupling of 1,1-diboron compounds. Nat Chem 3:894–899. doi:http://www.nature.com/nchem/journal/v3/n11/abs/nchem.1150.html#supplementary-information
115. Rauniyar V, Zhai H, Hall DG (2008) Catalytic enantioselective allyl- and crotylboration of aldehydes using chiral diol•$SnCl_4$ complexes. Optimization, substrate scope and mechanistic investigations. J Am Chem Soc 130:8481–8490. doi:10.1021/ja8016076
116. Cambre JN, Sumerlin BS (2011) Biomedical applications of boronic acid polymers. Polymer 52:4631–4643. doi:http://dx.doi.org/10.1016/j.polymer.2011.07.057
117. Böeseken J (1949) The use of boric acid for the determination of the configuration of carbohydrates. In: Pigm WW, Wolfro ML (eds) Advances in carbohydrate chemistry, vol 4. Academic Press, New York, pp 189–210. doi:http://dx.doi.org/10.1016/S0096-5332(08)60049-1
118. Matsumoto A, Yamamoto K, Yoshida R, Kataoka K, Aoyagi T, Miyahara Y (2010) A totally synthetic glucose responsive gel operating in physiological aqueous conditions. Chem Commun 46:2203–2205
119. Kataoka K, Miyazaki H, Bunya M, Okano T, Sakurai Y (1998) Totally synthetic polymer gels responding to external glucose concentration: their preparation and application to on-off regulation of insulin release. J Am Chem Soc 120:12694–12695. doi:10.1021/ja982975d
120. Matsumoto A, Ikeda S, Harada A, Kataoka K (2003) Glucose-responsive polymer bearing a novel phenylborate derivative as a glucose-sensing moiety operating at physiological pH conditions. Biomacromolecules 4:1410–1416. doi:10.1021/bm034139o
121. Qin Y, Cheng G, Sundararaman A, Jäkle F (2002) Well-defined boron-containing polymeric lewis acids. J Am Chem Soc 124:12672–12673. doi:10.1021/ja020773i
122. Roy D, Cambre JN, Sumerlin BS (2009) Triply-responsive boronic acid block copolymers: solution self-assembly induced by changes in temperature, pH, or sugar concentration. Chem Commun 0:2106–2108
123. Bérubé M, Dowlut M, Hall DG (2008) Benzoboroxoles as efficient glycopyranoside-binding agents in physiological conditions: structure and selectivity of complex formation. J Org Chem 73:6471–6479. doi:10.1021/jo800788s
124. Shiino D, Murata Y, Kubo A, Kim YJ, Kataoka K, Koyama Y, Kikuchi A, Yokoyama M, Sakurai Y, Okano T (1995) Amine containing phenylboronic acid gel for glucose-responsive insulin release under physiological pH. J Controlled Release 37:269–276. doi:http://dx.doi.org/10.1016/0168-3659(95)00084-4
125. Hall DG (2011) Boronic acids-preparation, applications in organic synthesis, medicine, and materials, 2nd edn. Wiley-VCH, Weinheim, p 701. ISBN 9783527325986

126. Mahalingam A, Geonnotti AR, Balzarini J, Kiser PF (2011) Activity and safety of synthetic lectins based on benzoboroxole-functionalized polymers for inhibition of HIV entry. Mol Pharm 8:2465–2475. doi:10.1021/mp2002957
127. Mo R, Sun Q, Xue J, Li N, Li W, Zhang C, Ping Q (2012) Multistage pH-responsive liposomes for mitochondrial-targeted anticancer drug delivery. Adv Mater 24:3659–3665. doi:10.1002/adma.201201498
128. Willmann JK, van Bruggen N, Dinkelborg LM, Gambhir SS (2008) Molecular imaging in drug development. Nat Rev Drug Discov 7:591–607. doi:http://www.nature.com/nrd/journal/v7/n7/suppinfo/nrd2290_S1.html
129. Lee D-E, Koo H, Sun I-C, Ryu JH, Kim K, Kwon IC (2012) Multifunctional nanoparticles for multimodal imaging and theragnosis. Chem Soc Rev 41:2656–2672
130. Feng W, Wee Beng T, Yong Z, Xianping F, Minquan W (2006) Luminescent nanomaterials for biological labelling. Nanotechnology 17:R1
131. Medintz IL, Uyeda HT, Goldman ER, Mattoussi H (2005) Quantum dot bioconjugates for imaging, labelling and sensing. Nat Mater 4:435–446
132. Hoshino A, Fujioka K, Oku T, Suga M, Sasaki YF, Ohta T, Yasuhara M, Suzuki K, Yamamoto K (2004) Physicochemical properties and cellular toxicity of nanocrystal quantum dots depend on their surface modification. Nano Lett 4:2163–2169. doi:10.1021/nl048715d
133. Jain PK, El-Sayed IH, El-Sayed MA (2007) Au nanoparticles target cancer. Nano Today 2:18–29. doi:http://dx.doi.org/10.1016/S1748-0132(07)70016-6
134. Pinho SLC, Pereira GA, Voisin P, Kassem J, Bouchaud V, Etienne L, Peters JA, Carlos L, Mornet S, Geraldes CFGC, Rocha J, Delville M-H (2010) Fine tuning of the relaxometry of $\gamma$-$Fe_2O_3$@$SiO_2$ nanoparticles by tweaking the silica coating thickness. ACS Nano 4:5339–5349. doi:10.1021/nn101129r
135. Giovanetti LJ, Ramallo-López JM, Foxe M, Jones LC, Koebel MM, Somorjai GA, Craievich AF, Salmeron MB, Requejo FG (2012) Shape changes of Pt nanoparticles induced by deposition on mesoporous silica. Small 8:468–473. doi:10.1002/smll.201101293
136. Napierska D, Thomassen LCJ, Rabolli V, Lison D, Gonzalez L, Kirsch-Volders M, Martens JA, Hoet PH (2009) Size-dependent cytotoxicity of monodisperse silica nanoparticles in human endothelial cells. Small 5:846–853. doi:10.1002/smll.200800461
137. Owens III DE, Peppas NA (2006) Opsonization, biodistribution, and pharmacokinetics of polymeric nanoparticles. Int J Pharm 307:93–102. doi:http://dx.doi.org/10.1016/j.ijpharm.2005.10.010
138. Cauda V, Argyo C, Bein T (2010) Impact of different PEGylation patterns on the long-term bio-stability of colloidal mesoporous silica nanoparticles. J Mater Chem 20:8693–8699
139. Bardi G, Malvindi MA, Gherardini L, Costa M, Pompa PP, Cingolani R, Pizzorusso T (2010) The biocompatibility of amino functionalized CdSe/ZnS quantum-dot-doped $SiO_2$ nanoparticles with primary neural cells and their gene carrying performance. Biomaterials 31:6555–6566. doi:http://dx.doi.org/10.1016/j.biomaterials.2010.04.063
140. Ow H, Larson DR, Srivastava M, Baird BA, Webb WW, Wiesner U (2004) Bright and stable core-shell fluorescent silica nanoparticles. Nano Lett 5:113–117. doi:10.1021/nl0482478
141. Kotsuchibashi Y, Zhang Y, Ahmed M, Ebara M, Aoyagi T, Narain R (2013) Fabrication of FITC-doped silica nanoparticles and study of their cellular uptake in the presence of lectins. J Biomed Mater Res Part A. doi:10.1002/jbm.a.34498
142. Kotsuchibashi Y, Ebara M, Aoyagi T, Narain R (2012) Fabrication of doubly responsive polymer functionalized silica nanoparticles via a simple thiol-ene click chemistry. Polym Chem-Uk 3:2545–2550
143. Wakamatsu H, Yamamoto K, Nakao A, Aoyagi T (2006) Preparation and characterization of temperature-responsive magnetite nanoparticles conjugated with N-isopropylacrylamide-based functional copolymer. J Magn Magn Mater 302:327–333. doi:http://dx.doi.org/10.1016/j.jmmm.2005.09.032
144. Yamamoto K, Matsukuma D, Nanasetani K, Aoyagi T (2008) Effective surface modification by stimuli-responsive polymers onto the magnetite nanoparticles by layer-by-layer method. Appl Surf Sci 255:384–387. doi:10.1016/j.apsusc.2008.06.065

145. Thomas CR, Ferris DP, Lee J-H, Choi E, Cho MH, Kim ES, Stoddart JF, Shin J-S, Cheon J, Zink JI (2010) Noninvasive remote-controlled release of drug molecules in vitro using magnetic actuation of mechanized nanoparticles. J Am Chem Soc 132:10623–10625. doi:10.1021/ja1022267
146. Wenzel RN (1936) Resistance of solid surfaces to wetting by water. Ind Eng Chem 28:988–994. doi:10.1021/ie50320a024
147. Cassie ABD, Baxter S (1944) Wettability of porous surfaces. Trans Faraday Soc 40:546–551
148. Miyauchi Y, Ding B, Shiratori S (2006) Fabrication of a silver-ragwort-leaf-like superhydrophobic micro/nanoporous fibrous mat surface by electrospinning. Nanotechnology 17:5151
149. Zhang T, Li M, Su B, Ye C, Li K, Shen W, Chen L, Xue Z, Wang S, Jiang L (2011) Bioinspired anisotropic micro/nano-surface from a natural stamp: grasshopper wings. Soft Matter 7:7973–7975
150. Karunakaran RG, Lu C-H, Zhang Z, Yang S (2011) Highly transparent superhydrophobic surfaces from the coassembly of nanoparticles ($\leq$100 nm). Langmuir 27:4594–4602. doi:10.1021/la104067c
151. Kotsuchibashi Y, Faghihnejad A, Zeng H, Narain R (2013) Construction of 'smart' surfaces with polymer functionalized silica nanoparticles. Polym Chem-Uk 4:1038–1047
152. Stratakis E, Mateescu A, Barberoglou M, Vamvakaki M, Fotakis C, Anastasiadis SH (2010) From superhydrophobicity and water repellency to superhydrophilicity: smart polymer-functionalized surfaces. Chem Commun 46:4136–4138
153. Haba Y, Kojima C, Harada A, Kono K (2007) Comparison of thermosensitive properties of poly(amidoamine) dendrimers with peripheral N-isopropylamide groups and linear polymers with the same groups. Angew Chem Int Ed 46:234–237. doi:10.1002/anie.200603346
154. Kuboshima Y, Yamamoto K, Aoyagi T (2008) Preparation and characterization of nanosized complexes consisting of stimuli-responsive block copolymers and PAMAM dendrimers. Trans Mater Res Soc Jpn 33:149–152
155. Akin M, Bongartz R, Walter JG, Demirkol DO, Stahl F, Timur S, Scheper T (2012) PAMAM-functionalized water soluble quantum dots for cancer cell targeting. J Mater Chem 22:11529–11536
156. Min K, Gao H (2012) New method to access hyperbranched polymers with uniform structure via one-pot polymerization of inimer in microemulsion. J Am Chem Soc 134:15680–15683. doi:10.1021/ja307174h
157. Kotsuchibashi Y, Agustin RVC, Lu J-Y, Hall DG, Narain R (2013) Temperature, pH, and glucose responsive gels via simple mixing of boroxole- and glyco-based polymers. ACS Macro Lett 2:260–264. doi:10.1021/mz400076p

# Chapter 4
# Smart Surfaces

## 4.1 Introduction

Biomaterials have been roughly divided into either endogenous materials in living organisms, materials designed to cure humans, or materials applicable for contact with biomolecules. Such "biocompatibility" is the most essential feature of biomaterials. Thus, it is reasonable to claim that the development of novel biomaterials led to control of the biocompatibility of materials in the early stage of their applications in the biomedical field. In this context, bulk biocompatible materials were developed from a wide range of artificial metals, ceramics, or polymers, and biological materials [1]. Commercial-grade biomaterials generally have good bulk properties such as mechanical and optical properties, but they often exhibit relatively poor biocompatibility.

If this is the case, can non-biocompatible materials be used as biomaterials even if they have other excellent functions? A key technology used to overcome the limited biocompatibility of bulk materials is surface modification. Because every biomolecular interaction of a biomaterial occurs at a material surface, surface modification is an attractive technique for obtaining biocompatible materials. The critical factors determining surface biocompatibility are wettability, chemical composition, charge, and structure. In particular, synthetic polymers are highly promising materials that can be easily modified to prepare functional polymers on the basis of molecular design by selecting suitable monomers and polymerization conditions. Since the late 1960s, polyurethane (PU), polytetrafluoroethylene (PTFE), polyethylene, poly(methyl methacrylate) (PMMA), poly(ethylene oxide) (PEO), poly(2-hydroxyethyl methacrylate) (PHEMA), and poly(ethylene terephthalate) (PET) have been extensively studied with the aim of developing antithrombogenic materials [2]. By performing studies on the biocompatibility of synthetic polymer surfaces, it has been found that surface wettability plays a critical role in biomolecular adsorption and deformation on a substrate surface via a hydrophobic interaction. Hydrophilic PEO coatings are particularly attractive for regulating the nonfouling property of biomaterial surfaces [3]. Coated PEO

M. Ebara et al., *Smart Biomaterials*, NIMS Monographs,
DOI: 10.1007/978-4-431-54400-5_4,

chains strongly interact with water molecules and retain the expanded volume of the random coil, which prevents protein adsorption on the material surface. PEO-based block copolymers have been prepared to improve the biocompatibility and stability of physical coatings such as those containing segmented PU [4], poly(propylene oxide) (PPO) [5], and heparin [6]. A number of research groups have demonstrated the decreased adsorption of plasma and other proteins on PEO surfaces.

In 1979, Ratner et al. [7] found that a particular ratio of hydrophilic to hydrophobic sites on a surface may be important for obtaining optimum biocompatibility, and amphiphilic block copolymers have been focused on to determine the microscopic phase separation structure of hydrophilic and hydrophobic domains. Okano et al. [8] have demonstrated that a HEMA-styrene block copolymer has good antithrombogenicity and suppresses the adhesion and deformation of platelets. In the 1980s, the biocompatibility of a variety of block copolymers comprising HEMA-EO [9], HEMA-dimethylsiloxane (DMS) [9], and styrene-amine [10] was studied and the biocompatibility was greatest when the surface of the block copolymer exhibited a lamellar structure with a pitch of 30–50 nm [11]. Thus, the inhibition of biomolecular adsorption suggests that an important factor determining biocompatibility is not only the magnitude of the total solid surface free energy but also the ratio of the polar to dispersion force contributions. In the 1990s, a biomimicking approach to improving biocompatibility using polymer grafting was reported by Ishihara et al. [12]. They were inspired by the excellent biocompatibility of phospholipids in biomembranes and synthesized a functional monomer having a phosphorylcholine residue, 2-methacryloyloxyethyl phosphorylcholine (MPC). The grafting of this phospholipid polymer significantly reduces the amount of plasma protein adsorption compared with that of conventional biocompatible polymers [12]. This is because the high free water fraction in the phosphorylcholine groups induces the reversible adsorption of proteins without significant conformational changes [13], various types of zwitterionic polymer such as phosphobetaine, sulfobetaine, and carboxybetaine have recently been developed as part of a broad range of biomedical and engineering materials [14].

Whereas considerable effort has been made to improve static biocompatibility by polymer grafting, some researchers have focused on the dynamic regulation of biomolecular adsorption/desorption on a polymer-grafted surface. The hydration of grafted polymer chains is a key factor in protein adsorption; thus, changes in surface wettability triggered by applying a signal are desirable for dynamically controlling the adhesion of cells and proteins on a material surface. Poly(*N*-isopropylacrylamide) (PNIPAAm), which has controllable wettability, has been focused on as a means of realizing this strategy. The properties of this polymer were first reported in 1968 by Heskins and Guillet [15]. Temperature-responsive PNIPAAm exhibits a reversible temperature-responsive soluble/insoluble change in an aqueous medium at 32 °C known as the lower critical solution temperature (LCST). This change is useful because it occurs at a similar temperature to that of the human body. In the 1990s, Okano et al. [16] succeeded in developing enzyme-free cultured cell recovery systems using the dramatic thermoresponsive

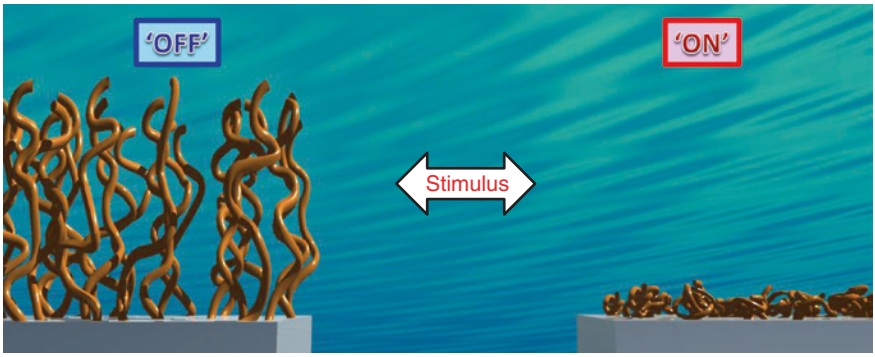


**Fig. 4.1** Schematic illustration of phase transition behavior for a smart polymer-grafted surface

hydrophilic/hydrophobic property changes on PNIPAAm-modified surfaces. The PNIPAAm chain also changes between coil and globule structures in water depending on the temperature, and the thermally induced control of solute permeation through a porous membrane [17] and elution behavior in size exclusion chromatography (SEC) [18] using the conformational change in PNIPAAm chains grafted onto pore surfaces has been reported. The availability and uniqueness of PNIPAAm-grafted surfaces have been demonstrated, and various stimuli-responsive polymers have been used as smart polymers to prepare smart biomaterial surfaces. The development of smart surfaces has expanded the range of strategies available for biomedical and engineering applications compared with the defense of molecular adsorption in the conventional concept of polymer grafting. Since the 2000s, advances in controlled living radical polymerization (CLRP) [19] and the synthesis of self-assembled monolayers (SAMs) [20] have enabled precise control of the graft architecture of smart polymers on a surface. Moreover, lithographic fabrication techniques [21] have enabled the realization of patterned polymer grafting and the application of smart surfaces in microfluidic systems. Nowadays, a large number of research strategies have been embodied as possible applications in the biomaterials field by modulation of the surface properties and conformational structures using grafted smart polymer (Fig. 4.1).

This chapter focuses on the synthesis, characterization, and applications of smart polymer-grafted surfaces. In the following sections of this chapter, we review a variety of smart polymer-grafted surfaces used to develop biomaterial applications. Section 4.2 describes the classifications of smart surfaces based on the graft architecture and materials/substrates used for surface modification. Grafting procedures used for realizing the surface design of grafted smart polymers are described in Sect. 4.3, which are categorized as 'grafting to' or 'grafting from' methods. The surface characterization and analysis of the phase transition behavior on smart surfaces are discussed in Sect. 4.4. In Sect. 4.5, typical and recent biomedical applications using smart polymer-grafted surfaces are introduced, such as adsorption control, cell culture, biomimetics, chromatography, and microfluidics.

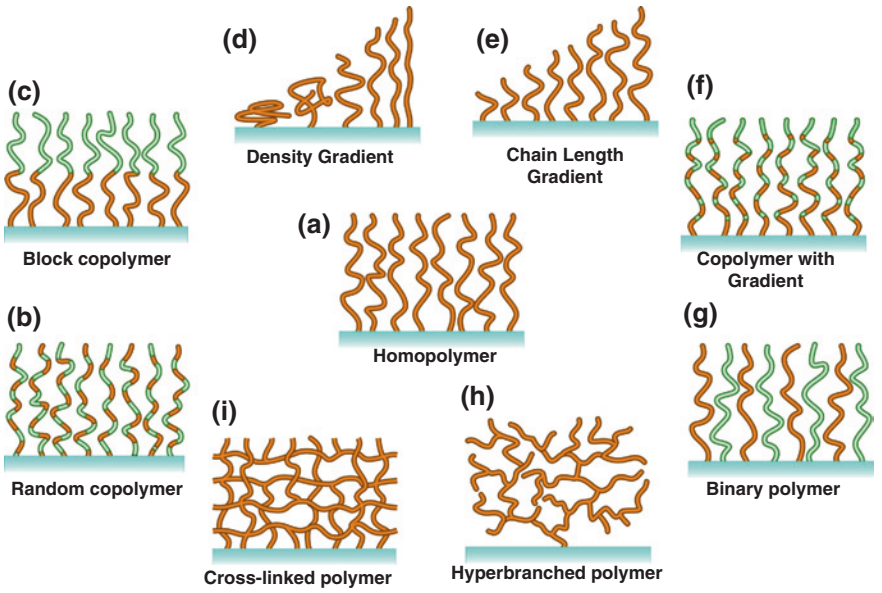


**Fig. 4.2** Types of graft architectures used for surface modification of polymer chains. **a** Homopolymers, **b** random copolymers, **c** block copolymers, **d** grafted polymers with gradient density, **e** grafted polymers with chain length gradient, **f** grafted copolymers with composition gradient, **g** binary copolymers, **h** hyperbranched polymers, and **i** cross-linked polymers

## 4.2 Classification Based on Surface Modifications

Since grafted polymers are anchored onto the surfaces of solid substrates, the graft architectures of smart polymer chains on the surfaces affect their conformational changes induced by external stimuli, allowing control of their wettability, adhesive, adsorptive, mechanical, and optical properties. In addition, suitable choices of substrates and materials depending on the target application are important in surface modification strategies. In this section, important factors in surface modification for biomedical applications are classified in terms of graft architectures and substrates/materials.

### *4.2.1 Graft Architectures*

Surface-initiated polymerization (a 'grafting from' method) is basically applied to terminal-end graft architectures (Fig. 4.2a–i), and the application of CLRP to this method enables the control of the architecture of grafted polymers. In recent research, binary and branched polymer architectures have been prepared, and copolymerization has been applied to block and random copolymers as well as

various types of gradient. Furthermore, the use of cross-linking agents has induced the grafting of polymers with three-dimensional networks. In the 'grafting to' method, the modulation of functional groups in polymer chains to induce surface binding enables the control of various graft architectures the 'grafting from' method. These different architectures are discussed in this section.

Grafted homopolymer chains (Fig. 4.2a) can be prepared by simple polymerization from initiator-immobilized surfaces or to modify polymer chains having terminal functional groups onto surfaces mediated by reactive silanes via self-assembly. Terminally attached linear homopolymers are a fundamental architecture of grafted polymer chains, and their conformation depends on the graft density on the surfaces. These conformations were described as pancake, mushroom, and brush by De Gennes [22]. When the distance between neighboring grafted chains is small and the chains have a high density, steric repulsion leads to chain stretching and the brush conformation of the grafted polymers. The grafted polymer chains adopt mushroom and pancake conformations when the distance is much greater than the radius of gyration of chains with a lower graft density.

As the basis of homopolymer chains, grafted random copolymers (Fig. 4.2b) can be prepared by polymerization of a mixture of two or more monomers. Such random copolymers have mainly been prepared to tune surface properties such as hydrophilicity/hydrophobicity, electrostaticity, and responsiveness as well as to add functionality. Although the copolymer composition fundamentally depends on the monomer ratio in the feed, caution is advised when combining different types of monomer because of differences in monomer reactivity. In particular, sometimes properties of the functional groups of comonomers, such as electric charge and spatial structure, affect the polymerization process [23]. In addition, the incorporation of comonomers into smart polymers tends to change the phase transition point and weaken the responsiveness external stimuli. For example, the incorporation of acrylic acid (AAc) into PNIPAAm reduces the cooperative hydrophobic aggregation of the polymer chains at the phase transition [24]. Continuous pendant isopropylamide groups in the polymers contribute to a distinct phase transition because the main mechanism of thermally induced phase separation involves the cooperative thermal release of water clustered around aligned hydrophobic isopropyl groups. On the other hand, for grafted block copolymers (Fig. 4.2c) prepared by the sequential polymerization of all comonomers, the stimuli-responsive block segments independently undergo phase separation as well as the homopolymer [25]. Since the grafted block copolymers are tethered on solid substrates, the selection of suitable polymer blocks for the exposed and anchored sides is important to regulate the molecular interaction and phase transition behavior. Recent advances in CLRP have enabled the routine synthesis of grafted block copolymers to control the nanostructures of phase-separated thin layers [19]. Because CLRP generally includes a step that induces the temporal deactivation of free radicals, the reinitiation of the sequential polymerization of other comonomers can be achieved from the surface pregrafted with polymer chains. Using these methods, it is possible to easily modify multi-block copolymers on surfaces and change the graft density of block copolymers.

CLRP can also be used to prepare grafted (co)polymers with a gradient, wherein one or more physicochemical properties vary continuously along the substrate. Grafted polymers with a gradient prepared via CLRP are mainly categorized into three groups: those with graft density (Fig. 4.2d), molecular weight (Fig. 4.2e), and copolymer composition (Fig. 4.2f) gradients. The preparation of grafted (co)polymers with a gradient requires a particular apparatus and inventive strategies, and numerous procedures have been proposed. Grafted polymers with molecular weight and copolymer composition gradients can be obtained by the gradual addition of a reaction mixture [26], the use of microchannels filled with a solution having a gradient [27], by applying a capillary force through dipping the substrate into solution [28], and by gradual chemical etching [29]. Grafted polymers with a graft density gradient are prepared by applying an initiator with a concentration gradient along the substrate together with inactive molecules in the same manner as the preparations of grafter polymers with molecular weight and copolymer composition gradients. These methodologies also enable the simultaneous control of other graft architectures, and the effects of various polymer compositions on surface properties can be investigated using a substrate. Heterogeneous binary grafted polymers are composed of two or more distinct polymer chains grafted on the same substrate (Fig. 4.2g). They are commonly generated by randomly grafting multiple incompatible polymers one after the other on the surface. Thus, polymer chains with different functional groups are cografted on surfaces for surface modification in both 'grafting to' [30] and 'grafting from' methods [31]. As another approach, Y-shaped difunctional silanes can be used to subsequently graft polymers on surfaces [32]. The covalent grafting of polymer chains on a surface maintains the nanoscopic domains scaled with molecular dimensions and prevents the occurrence of a large phase separation in the mixed polymer. Because such nanosize phase separations often induce biocompatible properties, binary grafted polymers can potentially be used to tune interactions in protein adsorption and cell adhesion. It is possible for smart polymers to switch the surface properties between the characteristics of two incompatible polymers by applying an external stimuli [33].

Hyperbranched polymers are synthetic treelike macromolecules that belong to the class of dendritic polymers [34], which have densely branched structures and a large number of end groups (Fig. 4.2h). The hyperbranched polymers have incompletely branched structures, whereas dendrimers have completely branched topologies. Using 'grafting from' methods, hyperbranched grafted polymers can be prepared from initiator-immobilized surfaces by ring-opening polymerization [35] and the self-condensing vinyl polymerization (SCVP) of inimers (initiator monomers) [36], which consist of both polymerizable vinyl and initiating groups. On the other hand, the procedure for preparing hyperbranched grafted polymers using 'grafting to' methods employs graft-on-a-graft chemistry involving the condensation of a carboxylic acid derivative with an amine or hydroxyl nucleophile [37]. Hyperbranched grafting not only provides a large number of functional groups at the terminal polymers but also compensates for inefficiencies in coverage of grafted polymers on the surface, owing to increases in the number

of grafting points and polymer density with the progression of reactions. These advantages of hyperbranched grafted polymers make them useful in the effective conjugation of biological molecules onto surfaces [38]. Cross-linked grafted polymers have a three-dimensional network enabling the formation of a gel on surfaces (Fig. 4.2i). These polymers are mainly prepared via two pathways: the surface-initiated polymerization of bifunctional monomers and postmodification by adding cross-linking agents to the grafted polymers. *N*,*N*′-methylene-bisacrylamide (MBAAm) and ethylene glycol dimethacrylate (EGDMA) derivatives are extensively used as bifunctional monomers. For postmodification, versatile cross-linking reactions have been demonstrated such as the condensation of glycidyl derivatives with amine groups [39] and noncovalent reversible coordination with metal ions [40]. Although the cross-linking of a grafted polymer is basically induced by the addition of cross-linking agents, side reactions during graft polymerization often induce cross-linking and the detachment of polymer layers from the surface [41]. The graft architecture of cross-linked polymers allows polymer layers to completely cover substrates, similarly to that of hyperbranched polymers. However, small biomolecules easily diffuse and are retained in the cross-linked network of polymer layers on surfaces, and the control of adsorption on surfaces by switching stimuli is difficult for smart polymers [42].

### *4.2.2 Substrates/Materials*

The surface modification of smart polymers can modulate the surface properties of solid substrates through the polymer characteristics and external stimuli. Thus, the selection of appropriate methods and functional groups for immobilization onto surfaces is important for grafting polymers suitable for the type of substrate and their material properties (Fig. 4.3a). The substrate shape can be varied depending on the target biomedical application, and substrates may be flat plates, porous membranes, particles, and microchannels. In addition, there are also numerous types of material used in the modification of substrates, including silicon oxides, silicons, mica, metals, cellulose, and synthetic polymers. Since the appropriate functional groups for polymer grafting depend on the surface modification method, described in later sections, the focus of this section is to discuss strategies on the basis of the intended use and fundamental surface functionalization of each substrate and material.

A flat plate is one of the most commonly used substrates modified with polymer chains, and their surface properties can be easily characterized by performing various measurements. Since a large number of measurement apparatus have been designed for target planar substrates, many researchers have routinely used flat plates for the examination of polymer grafting. Flat plates can also be easily handled and are frequently used as substrates for cell cultures and the control of protein adsorption in biomedical applications (Sects. 4.5.1 and 4.5.2). However, the precise composition of grafted polymers, including their molecular weight and distribution,

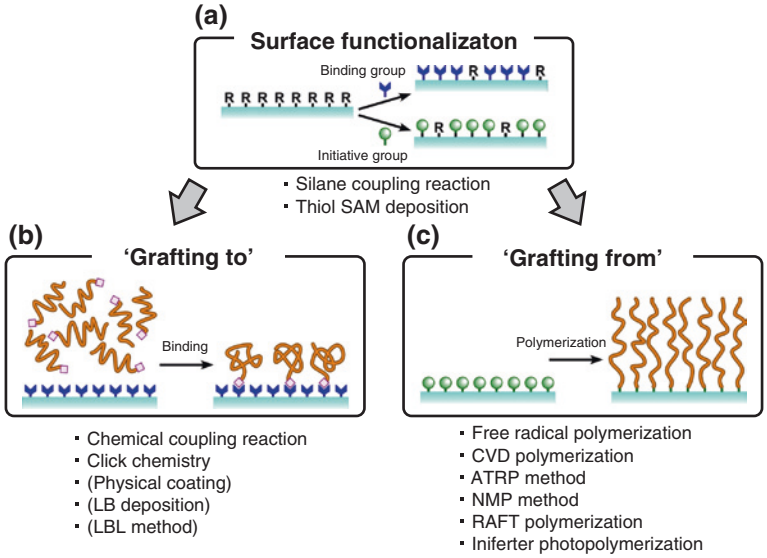


**Fig. 4.3** Synthetic methods for polymer-grafted surfaces. **a** Immobilization of functional groups for polymer grafting, **b** 'grafting to' approach via physical adsorption or chemical bonding, and **c** 'grafting from' approach via surface-initiated polymerization

is difficult to determine using planar substrates with small surface areas because of their ultrathin layers of the grafted polymers. On the other hand, polymer-grafted particles, particularly those having porous structures, are used to measure the molecular weight and distribution by cleaving the polymers from the surfaces (details are described in Sect. 4.4.1). The dispersion and aggregation behavior of particles can be easily observed in solution, in contrast to planar substrates. Micro-order porous particles have large specific surface areas, and can be used as chromatographic materials for biomolecular separation (Sect. 4.5.4) and as drug carriers in drug delivery systems (DDSs) to enhance the interaction between polymer-grafted surfaces and biomolecules. Porous membranes have the advantages of both easy handling and a large surface area of particles. They have been conventionally used as biomaterials to filter and dialyze bioactive compounds, and have also been used as biosensors, cell culture substrates, and drug delivery devices [43]. The grafting of smart polymers onto the surface enables the selectivity of mass transfer and the interfacial properties to be controlled using external stimuli. In the human body, the quantities of various bioactive molecules are tightly controlled to maintain a metabolic balance via biological signals, and stimuli-responsive porous membranes grafted with a smart polymer have been used to mimic the homeostasis induced by changing the stimuli (Sect. 4.5.3). Over the past two decades, microfluidic technology has been an attractive area of research owing to the unique physicochemical properties that can be realized by the geometry of microchannels. These properties include short diffusion times, large specific surface areas, and small volumes

[44]. The employment of microfluidic materials in capillary and chip devices has enabled the use of conventional biomaterials in high-efficiency and rapid assay systems. However, complicated microfabrications are often required to manipulate the microfluids and solutes in microchannels because of difficulty in handling due to their micron-size dimensions. Modification of the surfaces of microchannels with smart polymers enables easy manipulation of fluids by external control of the surface properties via stimuli switching, because of the strong effect of surface properties in microfluidics (Sect. 4.5.5).

The aforementioned substrates are made of various materials, and a wide range of protocols for the immobilization of functional groups onto surfaces via grafting with polymer chains employing both the 'grafting from' and 'grafting to' methods have been proposed. Silicon oxides including glass and quartz have been among the basic materials used to modify substrates such as flat plates, particles, and capillaries. To allow the use of ordinary protocols for surface functionalization, thin layers comprising silicon oxide have often been deposited onto metal substrates. To realize the surface immobilization of functional groups, organosilane coupling reagents are commonly used, which have functional groups that react with both inorganic and organic molecules [45]. There are many organic functional groups in commercially available silane reagents that react with organic materials, such as amino, thiol, epoxy, and vinyl groups. The part that reacts with inorganic materials comprises alkoxy or chlorosilyl groups, which react with silanol groups on silicon oxide substrates via a condensation reaction called 'silanization'. For effective silanization, the substrates are cleaned to remove organic admolecules, and silanol groups are activated using piranha solution ($H_2SO_4/H_2O_2$) and $O_2$ plasma treatment. The condensation reaction between silanol groups during silanization proceeds through hydrolysis, and it is very sensitive to various experimental factors such as humidity, concentration, temperature, and pH. To prepare stable monolayered silanes, vapor phase reactions under atmospheric or vacuum conditions are often used instead of common liquid phase reactions to avoid the deposition of aggregated silanes [46]. After silanization, the stability of binding of silane molecules with multiple silyl groups onto silicon oxide surfaces is increased by post-baking to enhance the dehydration of unreacted silyl groups. Polymer chains are grafted onto the silanized surfaces or appropriate initiators and linkers are further introduced into the functional groups of immobilized silanes.

Silicon substrates can also be silanized by the deposition of thin oxide films as well as silicon oxides. In addition, a robust silicon surface can be constructed through Si–H bonding via the UV-induced coupling of chloromethyl styrene [47]. The Si–H bonds are dissociated by UV exposure to generate radicals, which subsequently react with an alkene. Although phyllosilicate mica is modified with polymer chains via adsorption and Langmuir–Blodgett (LB) deposition because of its chemically inert surface, the mica can be covalently immobilized with various silane molecules by exposing it to water vapor plasma [48]. Because silicon and mica substrates have extremely smooth surfaces at the atomic level, they have been used to precisely determine the properties of polymer-grafted surfaces since the effects of surface roughness can be ignored.

Transition metals including Au, Ag, Cu, Pt, Hg, and Fe have high affinity to sulfur and selenium compounds, enabling the adsorption of robust chemicals on surfaces. In particular, alkanethiols and alkanedisulfides are well known to immobilize onto metal surfaces as SAMs. Such high-affinity binding has mainly been reported for thin metal layers on the above-mentioned flat substrates by metal vapor deposition. Thiol SAMs exhibit dense immobilization with a specific angle depending on the transition metal and its crystal planes, for example, an angle of ca. 30º is obtained for the all-trans structure on Au(111) [20]. The presence of functional groups on the opposite side to thiol groups enables the grafting of polymers onto metal substrates. Thiol SAMs are extremely easily formed by simply immersing a metal substrate into a reaction mixture under mild conditions. Therefore, the SAM technique has been extensively used in various applications, surface property measurements, and patterning methods. Functional silane molecules can also be introduced onto transition metal surfaces using organosilane molecules by the deposition of oxide layers as well as silicon.

Cellulose and chitosan, which are among the most abundant natural polymers, are composed of repeating units of glucose bound together by inter- and intramolecular hydrogen bonds. The hydroxyl groups of the repeated glucose units in cellulose can act as chemical nodes that react with nucleophilic or electrophilic groups to modify functional molecules on surfaces. In addition, polymers can also be grafted onto cellulose to directly polymerize hydroxyl groups on the surfaces by ring-opening polymerization [49]. In this method, the hydroxyl group is generally used to initiate the ring-opening polymerization of cyclic monomers such as ε-caprolactone and lactide (Please refer to Chap. 7). In contrast, synthetic inert polymers such as PTFE, polystyrene (PS), poly(dimethylsiloxane) (PDMS), and PET usually require either a surface-activation process for the introduction of functional groups or direct graft polymerization. Plasma treatment and UV exposure are both powerful tools for surface-activation processes to modify inert polymer substrates with hydroxyl or carboxyl groups. Polymer chains can be grafted onto the activated surfaces, and a variety of grafting methods can be used to further modify polymer chains with initiators and linkers. Inert polymer substrates can also be activated by chemical treatment using $KMnO_4$ [50]. In direct graft polymerization via UV irradiation, the addition of benzophenone is effective for abstracting a hydrogen atom from neighboring aliphatic C–H groups to form a C–C bond [51]. Electron beam (EB) irradiation also enables the direct polymerization and modification of polymer substrates coated with monomer solutions [52].

## 4.3 Synthetic Methods

In the previous sections, pretreatments involving modification with polymer chains to activate and introduce functional groups onto surfaces according to the type of material and graft architecture were discussed. The next step is the selection of the method of modification with polymer chains. A variety of grafting techniques

have been developed to simplify the modification process and precisely control the composition and architecture of grafted polymers. In addition, micro- and nanopatterning techniques for polymer grafting have been also been proposed for mimicking the in vivo cellular microenvironment and have been applied to biological assays and regenerative medicines dealing with cell functions. These techniques of synthesizing grafted polymers have various advantages and disadvantages, and should be selected according to the target application. In this section, basic methodologies of polymer grafting and patterning are described, and their features and advantages for the fabrication of smart biomaterial surfaces are discussed. The following fundamental methods for polymer grafting and the fabrication of patterns can be applied to not only smart polymers but also various synthetic polymers.

## *4.3.1 Polymer Grafting Methods*

There are two well-known types of method of surface modification with polymer chains, categorized as 'grafting to' and 'grafting from' methods. Each technique has some inherent advantages and disadvantages related to the preparation process, the control of grafted polymer structures, and surface properties. A great deal of effort over a long time has been put into the development and improvement of these methods. Conventional and advanced techniques based on the 'grafting to' and 'grafting from' methods are described in the following sections.

### 4.3.1.1 'Grafting to' Approach

In the 'grafting to' approach, polymer grafting requires the synthesis of polymers with functional groups beforehand to enable a reaction with the activated surfaces of substrates, as mentioned in Sect. 4.2.2. This is followed by the attachment of polymers onto the surfaces through either physical adsorption or chemical bonding (Fig. 4.3b). The physical adsorption of polymer chains on a surface is a simple method of surface modification, and the adsorption phenomenon depends on the selective uptake through interactions such as hydrogen bonding, hydrophobic interactions, electrostatic interactions, and van der Waals force.

A typical grafting method via physical adsorption is LB deposition, which employs a SAM of an amphiphilic polymer with a hydrophilic head and a hydrophobic tail [53]. The amphiphilic polymer acts as a surfactant in water, and is vertically oriented to form a monolayer at the air–water interface when its concentration is less than the critical micelle concentration (CMC). The density of the oriented monolayer increases with increasing surface pressure at the air–water interface, and the monolayer ultimately becomes a closely packed two-dimensional solid. The dense amphiphilic polymer monolayer can be transferred onto the surface of a solid substrate by immersion into or emersion from the water. Such a monolayer is known as an LB film. The grafting direction of the amphiphilic polymer on the

surface depends on the hydrophilic or hydrophobic property of the substrate; the contact angle increases and decreases in the case of modification by immersion and emersion, respectively. A multilayered LB film can be obtained by repeated immersions and emersions of the modified substrate because amphiphilic segments with opposite wettability are alternatively exposed on the surface.

Whereas strict control of the physical conditions is needed for LB deposition, the layer-by-layer (LbL) method is a simple modification process based on physical adsorption. The LbL method is based on the alternating adsorption of layers with different chemical features such as electrostatic interaction, stereocomplexity, metal coordination, and hydrogen-bonding between the polymer layers [54]. In general, in the LbL method, synthetic polymers having charged and electronegative functional groups in the side chains are initially attached onto the substrate surface. This is followed by the build-up of alternate polymer layers simply by the addition of polymer chains with inverse functional groups. This simple method is independent of the geometrical features of the modified substrate and can be used with various types of polymer including proteins, nucleic acids, and glycopolymers. Thus, grafting with smart polymers by the LbL method has been widely reported as a means of controlling the surface properties by stimuli switching [55]. Although LbL deposition has several useful features, the poor mechanical properties and long-term stability of the polymer layers, particularly in the case of stimuli-responsive smart polymers, is one of the serious drawbacks of this method because surface modification occurs through reversible physical adsorption.

On the other hand, the 'grafting to' approach based on chemical bonding enables the more stable modification of polymer chains owing to irreversible covalent bonding such as with amide and esters. In this approach, functional groups, which provide binding sites for polymer grafting, are incorporated into side chains and ends of polymer chains, which can be tethered to substrate surfaces with reactive groups by a coupling reaction, by radical addition, via a thiol SAM, or by a condensation reaction. A variety of functional groups have been used for the chemical bonding reactions in polymer grafting such as carboxyl, amine, hydroxyl, halogen, mercapto, and organosilane groups. Since the polymers are synthesized beforehand, their molecular weights, side chain densities, and nanoarchitectures can be readily transferred onto surfaces. Thus, this method is advantageous for fabricating complicated graft architectures. For example, grafting with a gradient can be prepared on the surfaces of substrates by imposing a temperature gradient [56], and the use of polymers with functional groups incorporated in both side chains and terminals leads to a comb-type architecture [57]. Recently, click chemistry has attracted attention as a more effective and rapid grafting method, which was first described by Sharpless et al. [58]. Click chemistry is based on mimicking nature in organic synthesis to induce highly reactive and selective carbon–heteroatom bonding between relatively simple functional groups. A typical click reaction is the formation of a 1,2,3-triazole ring by a cycloaddition reaction between an alkyne and an azido, where the reaction rate and regioselectivity are significantly increased by the addition of Cu(I) ions. As other examples of click chemistry, the Diels–Alder reaction, thiol-ene reaction, and (4+1) cycloaddition have been used not only to graft polymer chains onto substrates but

also in the fields of drug discovery, nanotechnology, and bioconjugation. However, the chemical bonding in the 'grafting to' approach is typically insufficient for the high-density grafting of polymer chains, particularly in the case of single-point grafting. The excluded volume effect of polymer chains grafted onto substrate surfaces prevents the diffusion of the unreacted polymer chains in solution, resulting in a significant decrease in the probability of reaction with functional groups on the surfaces with increasing graft density.

#### 4.3.1.2 'Grafting from' Approach

The 'grafting from' technique commonly utilizes direct polymerization from substrate surfaces by immobilization with initiating functional groups (Fig. 4.3c). In contrast to 'grafting to' methods, small monomers can easily penetrate through the already grafted polymer layer; thus, grafted polymers with a high density can be prepared even in the case of surface modification with long polymer chains.

This method often uses free-radical polymerization [59]. In this chemical process, free radicals are generated from immobilized initiators, such as azo-, peroxide, and photoinitiators, by heating, UV exposure, or adding polymerization accelerators. The subsequent polymerization from the surface is similar to conventional methods in bulk solution, although it is difficult to regulate the chain length and density of grafted polymers under these reaction conditions. The molecular weight of polymer chains prepared by free-radical polymerization generally cannot be controlled because of the occurrence of irreversible chain transfer and termination reactions, leading to large molecular weight distributions. In addition, the initiation efficiency of conventional initiators for free-radical polymerization is low (e.g., the half-life temperature of 10 h for azobisisobutyronitrile (AIBN) is ca. 65 °C), meaning that part of the immobilized initiators does not participate in the polymerization from the surface. Although conventional free radical polymerization proceeds in the liquid phase, chemical vapor deposition (CVD) polymerization allows the synthesis of grafted polymers by delivering monomers to a substrate surface through the vapor phase [60]. In this system, a monomer vapor is generated under vacuum conditions at a modest temperature for the selective formation of free radicals from an initiator without the cracking of monomers, and the adsorption and polymerization proceed on the cooled substrate. The initiation of the polymerization is induced by heating, UV exposure, voltage application, or plasma irradiation. The advantages of CVD polymerization are that grafted polymer layers can be formed in a single processing step, and polymers with limited solubility can be deposited onto surfaces, such as fluoropolymers and electrically conducting polymers. Since CVD polymerization is based on conventional free-radical polymerization, this method has limited capability to precisely regulate the graft architecture.

To overcome this problem, grafted polymers prepared by a 'grafting from' method using CLRP techniques have been proposed in the last two decades [19]. Although CLRP includes termination reactions as well as conventional

free-radical polymerization, it has a reversible activation/deactivation process. It is important to control the activation and deactivation of free radicals in the CLRP process to make the dormant species predominant at equilibrium. The control of activation/deactivation minimizes the contribution of termination reactions. Consequently, well-defined polymers with narrow molecular weight distributions can be obtained under appropriate CLRP conditions. Applying CLRP techniques for surface-initiated polymerization allows the simultaneous solution of the problems associated with conventional 'grafting to' and 'grafting from' methods. The CLRP techniques are classified according to the type of activation/deactivation control, and each surface-initiated CLRP method is discussed in the following.

Atom transfer radical polymerization (ATRP) has rapidly achieved widespread use in the field of polymer chemistry since it was first reported in 1995 [61], and it is now the most actively and extensively used technique among the CLRP methods based on surface initiation. ATRP relies on the reversible redox process of a dormant halide-terminated polymer chain end catalyzed by a transition-metal complex. The ATRP initiators include alkyl halides, and the oxidized transition-metal complex is used to select the terminal halogen atom of the initiator, leading to the generation of active species with a rate constant of activation ($k_{act}$). For surface-initiated ATRP, the initiator molecules are immobilized onto the substrate surface, similarly to conventional free-radical polymerization. Free radicals are simultaneously deactivated at the growing polymer ends by rebinding with halogen atoms with a rate constant of deactivation ($k_{deact}$). This occurs through the reversible deoxidization of the transition-metal complex. When $k_{deact}$ is sufficiently larger than $k_{act}$, the dormant species of the radicals in the polymer chain is predominant, minimizing the contribution of termination reactions [23]. The minimization of termination reactions allows the living propagation of free radicals for chain growth, leading to narrow molecular weight distributions. A significant characteristic of the ATRP process is the effective initiation of ATRP initiators. In ATRP, the number of growing polymer chains is dependent on the initiator concentration in the feed because of the fast initiation reactions and negligible termination reactions. Namely, almost all the initiators immobilized onto the substrate can be used to induce polymerization from the surface under ideal ATRP conditions, and a high density of grafted polymer chains can be achieved to form brush-like structures. In ATRP, the complexation of the transition metals with the ligand is important for controlling the chain growth of polymers; thus, protection is often needed, which is provided by a monomer having functional groups with ligating properties (e.g., −COOH). Successful ATRP requires the selection of the appropriate transition metal, ligand, initiator, solvent, and polymerization conditions depending on the type of monomer. Because ATRP has several advantages for polymer grafting, novel ATRP techniques have been proposed and are being developed. For instance, surface-initiated reverse ATRP enables the use of a conventional radical initiator in a controlled manner [62], and activators (re)generated by electron transfer (A(R)GET) ATRP can reduce the amount of copper to a few ppm by using a reducing agent such as ascorbic acid or Sn 2-ethyhexanoate [63]. Since copper compounds are toxic to the human body, this method is suitable for

biomedical use. In particular, ARGET ATRP also has improved tolerance toward oxygen and radical traps during polymerization, enabling the preparation of well-defined polymer grafts.

Nitroxide-mediated radical polymerization (NMP) is based on the reversible capping of radicals in growing polymer ends by a nitroxide as well as by ATRP kinetics [64]. A typical NMP initiator is 2,2,6,6-tetramethylpiperodinyloxy (TEMPO), which is a functional alkoxyamine that acts as a generator of both reactive free radicals and stable nitroxide radicals. When TEMPO is immobilized onto a substrate, these radicals can be simultaneously cleaved off the surface by heating the substrates [65]. The generated free radicals propagate, causing the polymer chains to grow with the control of reversible activation/deactivation through the nitroxide radicals, which do not react with monomers. A special feature of the NMP technique is that only a heating process is required to initiate living polymerization; no external radical source or metal complex is necessary. This advantage obviates the need for further purification steps and reduces the risk of contamination, making the NMP technique useful for biomedical applications. On the other hand, surface-initiated NMP is unsuitable for thermally sensitive monomers and substrates because the activation of the NMP initiators usually requires a high temperature.

Reversible addition fragmentation chain transfer (RAFT) polymerization is based on reversible chain transfer via a degenerative exchange process with dormant species, in contrast to ATRP and NMP [66]. The key factor in the polymerization is the RAFT agent, which is typically a dithiocarbonyl compound, described as S=C(Z)S−R. The reversible chain transfer process during polymer chain growth involves the equilibrium between the addition of a polymeric radical to S=C and the fragmentation of the RAFT adduct radical (S–R) in the RAFT agent. When the addition state of two polymer chains to both sulfur atoms in the RAFT agent is predominant, living chain growth can be achieved, reducing the effect of termination reactions. The substituent Z group contributes to the addition and fragmentation rates and the R group should have a good radical leaving property for the initiating species [67]. In the RAFT process, the initiation of chain growth is the same as that in free-radical polymerization, and adding only the appropriate RAFT agent in the conventional system is needed to induce living chain growth. Thus, a wide range of monomers can be used in RAFT polymerization, which is more tolerant of functional groups and simple polymerization conditions than other CLRP methods. There are two strategies for pretreating the functional surfaces of substrates in surface-initiated RAFT polymerization: immobilization with a free-radical initiator and the immobilization of a RAFT agent onto the surfaces. Care should be taken when using a surface immobilized with a RAFT agent. In the introduction of a RAFT agent onto a surface via the Z group, the polymerization process from the surface is similar to that in the ‘grafting to’ approach because the growing polymer chains are reversibly added to and cleaved from the functional surface [68]. Namely, it is difficult for polymer chains to approach RAFT agent on the surface, similarly to in the aforementioned ‘grafting to’ methods.

Another method of CLRP using a reversible chain transfer process is the iniferter photopolymerization method, which was proposed earlier than RAFT [69]. The word of iniferter is derived from the functional molecules used to control the chain growth. These molecules can simultaneously act as initiators, chain transfer agents (CTAs), and terminators. Iniferter photopolymerization is based on photolysis chemistry using dithiocarbamate compounds, which can generate alkyl and dithiocarbamyl radicals. Although the alkyl radical readily reacts with the monomer, resulting in the growth of chains, the dithiocarbamyl radical reversibly recombines with the alkyl radical of a CTA or terminator, which is similar to the role of TEMPO in NMP. Because of the radical generation from dithiocarbamate compounds by photolysis, the polymerization proceeds only during photoirradiation and can be repeatedly reinitiated by photoirradiation. The presence of a dithiocarbamyl radical at the growing polymer end is important for maintaining the CLRP process, and the addition of *N*,*N*,*N*′,*N*′, -tetraethylthiuram disulfide is effective in this method to increase the concentration of dithiocarbamyl radicals upon photolysis [70]. Surface-initiated iniferter photopolymerization can be achieved by the immobilization of dithiocarbamate compounds onto substrate surfaces. The concentration of radicals in this method is directly related to the intensity of photoirradiation; thus, it will be difficult to fabricate uniform grafted polymer layers on the surface of three-dimensional substrates such as microchips and capillaries.

### *4.3.2 Micro- and Nanopatterning Processes*

Micro- and nanopatterning processes have been conventionally developed as standard methods in the semiconductor industry. Nowadays, numerous studies are carried out in the biological and biomedical fields with the aim of developing technologies to precisely control the topological and surface properties of polymer-grafted substrates at the cellular and molecular levels. The main approaches in the preparation of the surface patterning to enable the grafting of polymers include photolithography, laser ablation, EB lithography, dip-pen lithography, and contact printing.

In various patterning technologies, photolithography is one of the most basic methods used for microscale patterning [21], as shown in Fig. 4.4a. In photolithographic methods, patterns are fabricated by selectively exposing a surface spin-coated with a photoresist to UV through a photomask. The most commonly used photoresists are thermosetting polymer resins with a photosensitive property enabling the decomposition or formation of cross-linking by UV irradiation; such photoresists are called positive and negative resists, respectively. After the UV exposure, the decomposed or cross-linked patterns of the photoresist on the surface are developed through dissolution in an appropriate solvent, resulting in the fabrication of a patterned photoresist on the surface. Consequently, polymer chains can only be grafted to (or from) the patterned area on the photoresist-coated surface, and the pattern of the grafted polymer is obtained by removing all

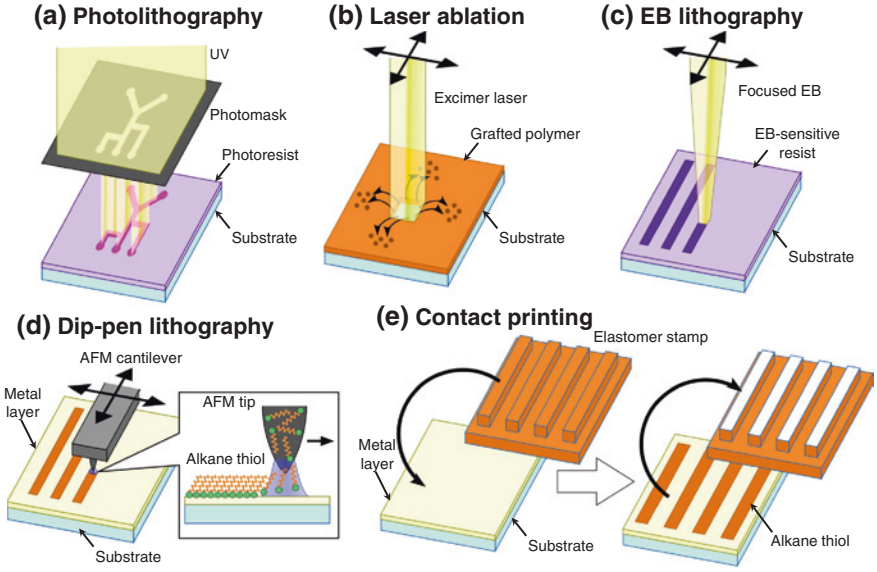


**Fig. 4.4** General micro- and nanopatterning methods used to obtain polymer-grafted surfaces. **a** Photolithography, **b** laser ablation, **c** EB lithography, **d** dip-pen lithography, and **e** contact printing for thiol SAM patterning

the residual photoresist from the surface. A pattern comprising a binary grafted polymer can also be prepared by sequential polymer grafting after removing the rest of the photoresist from the surface. Polymer grafts can be directly patterned by polymerization from substrate surfaces through site-specific exposure by using photoinitiators, high-energy beams (e.g., EB, plasma), and iniferter photopolymerization [71]. Such polymer grafting via a partial mask on the surface is one of the fundamental approaches for the modification of patterned surfaces not only in photolithography but also in other patterning methods. Photolithography is a cost-effective, high-throughput technique suitable for large-area surface patterning, because patterns formed on a photomask can be simultaneously transferred to photoresist-coated substrates by exposure to UV irradiation. Although the resolution of the patterns produced by photolithography is usually of micrometer order, higher resolution patterns of sub-100-nm resolution can be fabricated; however, this requires special apparatus and techniques such as nonconventional masks, a light source with a short wavelength, and advanced lithographic optical techniques and setups [72].

Another approach for the fabrication of patterns is direct writing, which eliminates the need for a mask. The method of laser ablation allows both approaches of exposure through a photomask and direct writing depending on the purpose (Fig. 4.4b) [73]. In this method, a pulsed ArF or KrF excimer laser (wavelengths, 193 and 248 nm, respectively) is used as a light source, and part of the substrate grafted with polymer chains is exposed to the laser beam to ablate

the polymer chains from the surface. Only areas irradiated by the excimer laser allow the ablation of grafted polymers, resulting in a patterned polymer-grafted surface. Patterns of grafted polymers can be prepared using a photomask as well as by a photolithographic technique. In the direct writing approach, the excimer laser beam is focused onto the grafted surfaces, and then either the laser beam or the substrate is moved in the *x*- and *y*-directions to generate the desired patterns. Although this method has the advantage that photoresist is not required for fabrication of the patterns, it has the same limitation on the patterning resolution as photolithography. In addition, it is possible to damage the basal substrate, particularly if it is made of a synthetic polymer, by applying a laser beam with high intensity [74].

An alternative approach to the direct writing technique is EB lithography (Fig. 4.4c) [75]. This technique requires a surface to first be coated with an electron-sensitive resist, which reacts with a beam of high-energy electrons. The coated substrate is placed in the vacuum chamber of an EB lithography system, and focused through electronic lenses is used to draw a pattern on the substrate using a computer-controlled EB scanner. The patterned electron-sensitive resist is fabricated by a development process after the exposure; subsequently, the grafted polymers can be patterned using a resist-coated substrate as well as a photolithographic method. A major advantage of EB lithography is the nm-order resolution of the patterns. The EB lithographic process can be optimized by considering many factors, including electron scattering in the resist and backscattering from the substrate, resulting in high-resolution patterning with a resolution of several nm. In addition, nanopatterned polymers can also be fabricated on surfaces in a single step by simultaneous local polymerization and direct surface grafting from monomers through the EB lithographic process because the irradiation of high-energy electrons allows graft polymerization [76]. Considering the applications of patterning in the biomedical field, the sensitive resist remaining on the surface may change the surface properties of the grafted polymers, making them toxic to cultured cells and human bodies. Therefore, a resist-free patterning process should be used for biomaterials. On the other hand, EB lithography requires expensive equipment, and considerable time is required to fabricate a large-area pattern with high resolution.

Dip-pen lithography, which is a direct writing method using a scanning probe, is a nanoscale patterning technique that does not require a high-energy light source (Fig. 4.4d) [77]. This technique is based on delivering reagents as chemical inks directly to nanoscopic regions of a substrate surface using the tip of an atomic force microscope (AFM) cantilever as a nanoscale pen, the details of which are described in Sect. 4.4.1. The chemical ink molecules are physically adsorbed onto the surface of the AFM cantilever tip. Moving the ink-coated tip toward a target surface under ambient conditions induces the generation of a water meniscus (adsorbed water) between the tip and the surface. The ink molecules adsorbed onto the AFM cantilever tip can be transported to the surface via capillary forces by scanning the tip with the water meniscus. When alkanethiols are used as delivered reagents for polymer grafting, patterned functional SAMs can be created on transition-metal surfaces using this method. Thus, nanopatterns of grafted polymers

can be realized using either a 'grafting from' or 'grafting to' method. Although this patterning process is slow because only an AFM probe tip is used, by increasing the number of tips and using a parallel probe, the throughput of pattern drawing can be increased, as has been demonstrated [78]. Dip-pen lithography has a good cost performance in terms of the pattern resolution compared with EB lithography; however, the patterning range on the substrate is limited for this method because of the small scanning area of conventional AFM apparatus, which is usually ca. 100 $\mu m^2$.

Many of the above lithographic techniques require specific and expensive instruments to prepare micro- and nanopatterns, and limited patterning performances in terms of resolution and throughput. Contact printing is an efficient technique for patterning of large areas on substrate surfaces with relatively high resolution down to the sub-micrometer range [79], as shown in Fig. 4.4e. In the contact printing method, functional molecules for polymer grafting are first adsorbed onto the surface of an elastomer stamp with patterned structures, which is typically made of PDMS. The patterned functional molecules on the stamp are used as chemical inks to be printed onto the entire surface of a substrate, which is followed by grafting with polymer chains. Although the basic concept of transferring chemical inks for contact printing is similar to that in dip-pen lithography, it is possible to obtain a high throughput and a large patterning area using this technique. As an alternative approach to contact printing, the functional molecules are spin-coated on a substrate, and their pattern is formed by the removal of nonpatterned functional molecules via stamping the patterned elastomer. The patterned structures on elastomer stamps can be effectively fabricated using SU-8 resin as a mold, which is a negative photoresist containing eight epoxy groups [80]. In contrast, these structures can be prepared by conventional photolithography and EB lithography with an etching process. This photoresist provides a three-dimensional cross-linked structure with thicknesses ranging from less than 100 nm to several 100 $\mu m$ realized through exposure to UV light, and this structure exhibits high mechanical, thermal, and chemical stabilities. This method is convenient and widely used for patterning biological molecules in cell biological applications. Since the contact printing process involves various manual operations instead of using automatic and expensive instruments, it requires a great deal of skill to fabricate a precise pattern comprising functional molecule layers on a substrate surface.

## 4.4 Characterization Methods

As described above, various graft architectures and two-dimensional patterns of polymer layers can be prepared on substrates using appropriate polymer-grafting and lithographic methods. To apply the features of polymer-grafted substrates in the biomedical field, their compositions and structures must be confirmed by suitable characterization methods. In addition, a wide variety of stimuli-responsive characteristics of grafted smart polymers such as chain mobility, hydration, and molecular interaction

reflect their surface properties induced by stimuli switching. In this section, methods of characterizing the compositions and structures of grafted polymers and of analyzing surface properties upon a change in the stimuli are introduced, and the structures and properties of grafted smart polymers depended on analytical methods is discussed.

### *4.4.1 Structural Characterization*

Structural characterization is important for judging the success of polymer grafting and modifying the surface for biomaterial applications. However, grafted polymer layers on substrate surfaces are usually ultrathin with nanometer thickness, and many analytical techniques in polymer science are suitable for characterizing the bulk and solution-based polymers. Considering the sample handling and detection limit of measurement tools, it is a challenging task to directly confirm the compositions and structures of grafted polymer chains. Thus, we should select appropriate tools depending on the structural factors to characterize grafted polymers using a limited range of analytical techniques. Typical factors that can be measured for the characterization of grafted polymer structure surfaces include surface morphology, chemical composition, molecular weight, layer thickness, graft density, and surface potential.

To observe the surface morphology, microscopic techniques capable of atomic-level observation are necessary such as AFM and scanning electron microscope (SEM). AFM is a high-resolution scanning probe method. An AFM probe consists of a microscale cantilever having a sharp tip with a nanoscale radius of curvature. In AFM observation, there are basically two operation modes: contact and noncontact processes. In the contact mode, there is an attractive force between the AFM cantilever tip and the substrate surface when the probe is made to approach close to a sample substrate. This force induces contact with the sample and deflects the cantilever in accordance with Hooke's law [81]. Scanning the AFM probe on the surface leads to changes in cantilever deflection, which can be detected by reflecting a laser on the cantilever. The sample surface morphology can be observed by $x$–$y$ mapping of the cantilever deflection. In the noncontact mode, the cantilever is continuously oscillated with a frequency near its resonant frequency and the oscillation amplitude of a few nm to avoid contact with the substrate. The force between the AFM cantilever tip and substrate leads to a shift in the resonant frequency of the cantilever. Consequently, information of the sample surface in the $z$-direction can be obtained by monitoring this shift. Because the tip-substrate distance is maintained through automatic $z$-axial changes in the AFM scanner position by a feedback loop system, the tip of the cantilever does not come in contact with the substrate under appropriate conditions. Noncontact mode AFM observation is more suitable for polymer-grafted surfaces than contact-mode observation to avoid the deformation of the polymer layers due to the contact with the AFM cantilever tip [82]. Furthermore, hydrated polymer layers can be measured in an aqueous solution using an AFM by changing the external stimuli; thus, other

surface properties of grafted polymers can also be analyzed (see Sect. 4.4.2). However, AFM has limited use for spherical substrates, hollow capillaries, and high-aspect-ratio structures as well as for regions of micrometer size.

In contrast, SEM can be used with various types of substrate structure and allows the observation of surfaces by scanning with exposure to a focused EB similar to that in an EB lithographic system. The exposure of a substrate surface to an EB induces the generation of secondary electrons from the region subjected to irradiation. In SEM observation, the generated secondary electrons are detected, and the number of detected electrons is converted into a brightness signal, which also depends on the surface roughness, resulting in an image of the surface morphology. Since an EB has an extremely short wavelength, the resolution of SEM observation is on the nanometer scale, similar to that of an AFM. On the other hand, by exposing a specimen to a focused EB in a chamber under a high vacuum of below $10^{-3}$ Pa, SEM can be used for imaging a completely dry sample. A conductive thin layer such as carbon or metal is usually coated onto the surface of nonconductive polymers and substrates to prevent the electrification of the sample. However, coating with carbon or metal may conceal the structural features of ultrathin grafted polymers. In this case, environmental SEM is a useful tool for the observation of noncoated samples at a low pressure of a few kPa [83].

Although it is difficult to directly determine whether or not polymers have been grafted onto substrates by morphological evaluation, measurement of the chemical composition of grafted polymers is important for such a determination. X-ray photoelectron spectroscopy (XPS), which is also known as electron spectroscopy for chemical analysis (ESCA), is a practical method of quantitatively determining the elemental compositions and electronic states of organic compounds on a surface. XPS spectra can be obtained by irradiating a substrate with an X-ray beam and detecting the kinetic energy ($E_k$) and the number of electrons emitted from the irradiated surface. Because the energy of an X-ray with a particular wavelength ($\nu$) is known, the electron binding energy ($E_b$) of the emitted electrons can be determined using the following equation:

$$E_k = h\nu - E_b - \phi, \tag{4.1}$$

where $h$ is Planck's constant and $\phi$ is the work function of the spectrometer. Although $E_b$ denotes the inherent value for an element, its value slightly changes depending on the degree of electron bond polarization between neighboring atoms, which is called the chemical shift. Thus, quantitative information on the chemical composition of grafted polymers can be obtained by a peak-fitting process of the XPS spectra. The depth resolution in XPS is commonly 1–10 nm, and this method is suitable for characterizing the nanoscale polymer layers on surfaces. In XPS measurement, depth profiling and mapping of the grafted polymer composition can also be performed by changing the incident angle of the X-ray beam and scanning the specimen stage, respectively [84]. Note that in this analysis, sample electrification is caused by the irradiation of an X-ray beam, similarly to in SEM, leading to a large energy shift in the XPS spectra.

An alternative practical approach is attenuated total reflection Fourier transform infrared spectroscopy (ATR-FTIR). FTIR can determine the chemical compositions present in a sample by from the IR absorbance, which depends on the interatomic motion of the chemical bonds through changes in the dipole moment. Since it is difficult to detect ultrathin grafted polymers by the transmission method of FTIR analysis, the ATR mode in FTIR can be used to characterize their composition. In the ATR mode, the incident IR beam passes through a high-refractive-index (RI) prism, usually made of ZnSe, Ge, or diamond crystal that is attached to a sample substrate under a total-internal-reflection condition, and an evanescent wave generated at the reflected interface is used to expose the sample to IR. This wave is a near-field standing wave. The evanescent wave irradiates the sample substrate at a distance of 100 nm order from the reflected interface, and only the IR absorbance near the grafted polymer layers can be detected. In addition, the ATR-FTIR absorbance of grafted polymer layers can also be used for quantitative analysis by applying the Lambert–Beer law. Although ATR-FTIR has the advantage of a short analysis time under ambient conditions, the sampling depth is relatively larger than that in XPS, resulting in a low detection limit. Other analysis methods that can be used to characterize the composition of grafted polymers are time-of-flight secondary ion mass spectroscopy (TOF-SIMS) [85], Auger electron spectroscopy (AES) [86], and near-edge X-ray absorption fine structure (NEXAFS) spectroscopy [87].

In polymer chemistry, the molecular weight of synthetic polymers and its distribution are generally measured by gel permeation chromatography (GPC), which is a separation technique based on differences in molecular size. In the case of polymer-grafted surfaces, GPC allows the measurement of grafted polymer chains after cleavage from the substrate by immersion in a strong acid or alkali, such as hydrochloric acid, hydrofluoric acid, or sodium hydroxide solution. This method requires grafted substrates with a large surface area, such as nanoparticles and porous materials, to obtain a sufficient amount of polymer to measure. In the case of using this approach, the polymers cleaved from the surfaces of porous silica particles exhibit a relatively large molecular weight distribution because of the geometric effect of porous structures [88], even though the polymer-grafted particles are prepared by surface-initiated ATRP. In addition, the stereoregularity of grafted polymers harvested from silica nanoparticle chains can also be characterized by nuclear magnetic resonance (NMR) spectroscopy [89]. For other substrates with a small surface area, an alternative method can be used for the analysis of grafted polymers prepared by surface-initiated CLRP in which a sacrificial initiator is added to the polymerization reaction to synthesize free polymers. It has been reported that the number-average molecular weight and the polydispersity index of polymers generated in solution from a sacrificial initiator are in good agreement with those of the polymer chains [90]. On the other hand, Kim et al. [91] investigated the differences in the rate-limiting steps and kinetics between surface-initiated and heterogeneous bulk CLRPs.

Characterization of the thickness of grafted polymers is an important factor to indicate the degree of chain growth in ‘grafting from’ methods. Ellipsometry

is a useful tool to determine the layer thickness of modified surfaces in each grafting process. In this method, linearly polarized incident light is directed onto a flat sample through a compensator, and the reflection is detected via an analyzer while changing the incident angle, which results in an elliptical change in polarization. The change in polarization correlates with the thickness and refractive index (RI) of layers on the sample; thus, the thickness of grafted polymers can be estimated by fitting the experimental data with an optical layer model. Although ellipsometric analysis has a high resolution of up to ca. 1 nm, the exact RIs of the grafted layers are required. In fact, the RI of grafted polymer layers is dependent on their composition, graft density, and molecular weight [92]; thus, accurate determination of the thickness of an ultrathin layer is difficult without any other measurement. Because ellipsometry is tolerant of the measuring conditions, the thickness of hydrated grafted polymers can also be obtained by changing the stimuli [93]. Recently, an instrument for thickness measurement using reflectometric interference spectroscopy (RIfS), which is similar to ellipsometry, has become commercially available [94]. As described below in greater detail, surface plasmon resonance (SPR) and X-ray reflectometry (XR) can also be used to estimate polymer layer thickness; however, they require a fitting process that involves the determination of other parameters in addition to those required in ellipsometry. As another approach, AFM is practical for directly measuring the thickness of a patterned grafted polymer after mechanically removing part of the polymer-grafted surface. These characterization methods are basically applicable to flat surfaces, whereas dynamic light scattering (DLS) is suitable for the thickness measurement of polymer-grafted particles (please refer to Chap. 3).

The graft density ($\sigma$) of polymer chains on substrate surfaces can be calculated using their number-average molecular weight ($M_n$) and dry polymer thickness ($h$), determined by the above methods, using the following equation [95]:

$$\sigma = h\rho N_a / M_n, \tag{4.2}$$

where $\rho$ is the density of the grafted polymer and $N_a$ is Avogadro's number. On the other hand, knowing the amount of grafted polymer is useful for calculating graft density, which can be measured by thermogravimetric analysis (TGA). In TGA, the physical weight loss of a polymer-grafted substrate is monitored as a function of temperature while temperature is increased at a constant heating rate, and the amount of the grafted polymer can be determined by increasing the temperature until the polymer is vaporized (> ca. 500 °C). Since the limit of detection for TGA is a few μg, the weight loss of an ultrathin grafted polymer can be measured. Polymeric particles are not suitable for measuring the amount of grafted polymer by TGA because the substrates disappear. The density of grafted polymer is calculated using the amount of grafted polymer ($m_p$) with the following equation [96]:

$$\sigma = m_p N_a / M_n, \tag{4.3}$$

The amount of grafted polymer can also be obtained by ATR-FTIR [97] and elemental analysis [88].

Analysis of changes in the surface potential, which is also called the zeta potential, is essential for confirming the successful surface modification of pH-responsive, polymer-grafted, and anionic/cationic functional surfaces. The zeta potential of polymer-grafted surfaces can be indirectly measured using electrokinetic phenomena such as electrophoresis and electroosmotic flow. Electrophoresis is the forward motion of particles having electrically charged surfaces toward an electrode with the opposite charge to the particles when the particles are dispersed in an electrolyte solution under an electric field. The electrophoretic mobility of particles depends on the degree of surface charges, and the measurement of the mobility allows the zeta potential of a particle sample to be measured; details of this method are given in Chap. 3. Electroosmotic flow is commonly used to estimate the zeta potential on flat substrates, capillaries, and microchannels. In a channel comprising sample surfaces, ions in an electrolyte solution that are oppositely charged to those of the sample accumulate on the surfaces to form an electrical double layer. Under an electric field, the accumulated ions in the electrical double layer are induced to move toward an electrode by the Coulomb force, resulting in electroosmotic flow. By dispersing neutral particles in the electrolyte solution, the zeta potential of the sample surface can be estimated to measure the mobility of particle samples. The profile of particle mobility at the center of a channel is approximately given with the following equation for the case where $k > 5$ [98]:

$$U_a(z) = AU_0(z/b)^2 + \Delta U_0(z/b) - (1 - A)U_0 + U_p \tag{4.4}$$

$$A = 1/((2/3 - (0.420166/k)), \tag{4.5}$$

where $z$ is the channel depth, $U_a(z)$ is the apparent electrophoretic mobility of a particle at position $z$, $U_p$ is the true electrophoretic mobility of the particles, $z/b$ is the thickness of the channel, $U_0$ is the average mobility of the osmotic flow at the upper and lower channel walls, $\Delta U_0$ is the difference between the velocities of osmotic flow at the upper and lower channel walls, and $k$ is the ratio between the two side lengths of the rectangular cross section. Measuring the streaming current of the accumulated ions under an electric field also allows the zeta potential on flat substrates to be determined.

### *4.4.2 Phase Transition Analysis*

Surfaces onto which smart polymers have been grafted exhibit changes in their conformational structures and surface properties in response to external stimuli switching. Furthermore, the architectures and primary structures of grafted polymer chains tend to significantly affect the stimuli-dependent properties of biomolecular interactions. Thus, characterization of the changes in the responses of surfaces can provide important information not only for confirming the success of surface modification but also for the subsequent development of biomaterials. Here, techniques

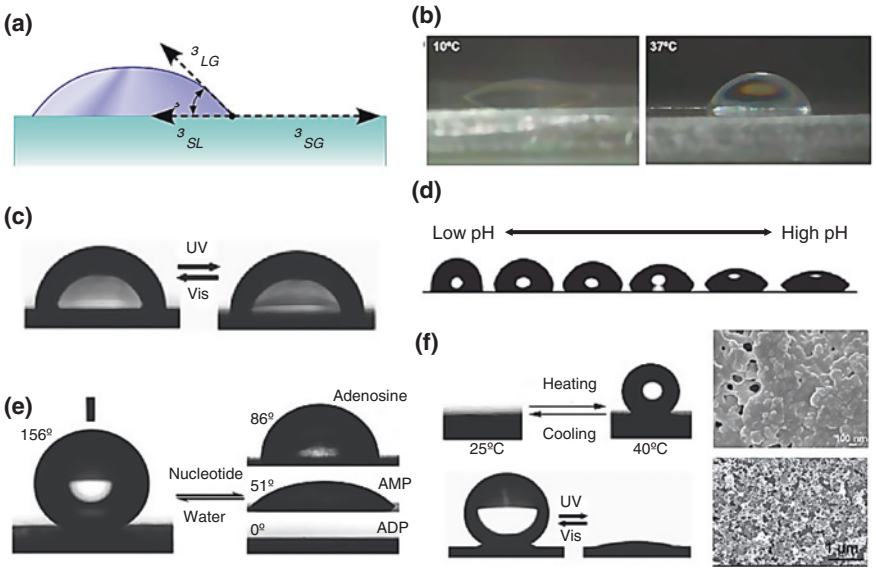


**Fig. 4.5** Changes in surface wettability for smart polymer-grafted surfaces. **a** Contact angle (θ) of a liquid on a substrate at the gas–liquid interface, and changes in contact angle for **b** thermoresponsive [100], **c** photoresponsive [105], **d** pH-responsive [106], **e** biomolecule-responsive surfaces [107], and **f** roughness-enhanced changes in wettability for thermoresponsive and photoresponsive surfaces (microscopic images: surface roughness) [105, 110]

for analyzing the phase transition behavior of smart polymer-grafted surfaces are described. These techniques can be used to investigate the effects of the conformation on the surface properties.

The measurement of contact angles on smart polymer-grafted surfaces is the most typical characterization carried out to determine changes in their aqueous wettability (hydration) upon applying a stimulus. Biomolecules are always surrounded by water in the human body, and their interaction with substrate surfaces is mediated through water molecules; thus, the aqueous wettability of substrates is an important factor in the design of biomaterial surfaces. The contact angle ($\theta$) is the angle of a liquid on a substrate at the gas–liquid interface (Fig. 4.5a), and the wettability (cos $\theta$) is obtained from Young's equation:

$$\gamma_{SG} = \gamma_{SL} + \gamma_{LG} \cos\theta, \tag{4.6}$$

where $\gamma_{SG}$, $\gamma_{SL}$, and $\gamma_{LG}$ are the interfacial energies between solid–gas, solid–liquid, and liquid–gas interfaces, respectively. There are various techniques for measuring contact angles such as the static/dynamic sessile drop method and the Wilhelmy method [99]. Among these techniques, the static sessile drop method is extensively used to determine surface wettability, which is measured from the shape of a static water droplet on a substrate. Thermoresponsive PNIPAAm is well known to exhibit changes in wettability in response to changes in temperature [100], as

shown in Fig. 4.5b. The values and transition temperatures of the contact angle are significantly dependent on the primary structure of grafted PNIPAAm chains, such as the polymer thickness [101], graft density [102], tacticity [89], incorporation of comonomers [103], and graft architecture [57]. The aqueous wettability of PNIPAAm-grafted surfaces is usually observed to change gradually in a temperature range of ca. 10 °C across their LCST, although the aqueous solution undergoes a distinct phase transition at the LCST. This is due to the restriction of the conformational change by tethering the PNIPAAm chains to the surface (see below for further details). As an alternative thermoresponsive smart polymer, a copolymer comprising 2-(2-methoxyethoxy)ethyl methacrylate ($MEO_2MA$) and oligo(ethylene glycol)methacrylate (OEGMA) has recently been used for surface modifications [104]. The transition temperature of the contact angle for P($MEO_2MA$-*co*-OEGMA)-grafted surfaces is finely tunable by adjusting the OEGMA content in the copolymer. Since it is physically difficult to instantaneously change the temperature, other stimuli such as photoirradiation [105], changes in pH [106], and the addition of biomolecules [107] have also been investigated as triggers for changing surface wettability (Fig. 4.5c–e). In addition, the graft copolymerization of different types of smart polymer can be used to obtain dual-responsive surfaces with switchable wettability, such as temperature-/pH-responsive P(NIPAAm-*co*-AAc) [108] and temperature-/photoresponsive P(*N*,*N*-dimethylacrylamide (DMAAm)-*co*-4-phenylazopheny acrylate) [109]. The grafting of polymer chains onto substrates can also affect aqueous wettability, particularly through changes in the surface roughness. Substrates with micro- or nanogrooves may have enhanced stimuli-responsive wettability [105, 110], resulting in reversible switching between superhydrophilicity and superhydrophobicity (Fig. 4.5f). This roughness-enhanced aqueous wettabiliy is induced by the lotus effect, which refers to the surface structures similar to the superhydrophobic leaves of lotus flowers [111].

Surface wettability is a macroscopic characteristic of smart polymer-grafted surfaces, which is induced by their hydration and conformational changes in response to external stimuli. To characterize the microscopic features, many analysis techniques have been demonstrated. A quartz crystal microbalance (QCM) has been used to investigate the hydration state of surface-grafted PNIPAAm chains in real time temperature [112]. Using a QCM, the adsorption of molecules on a quartz crystal probe surface can be sensitively detected as a change in mass by measuring the shifts in the resonance frequency of the probe. The relationship between the resonance frequency shift ($\Delta f$) and the change in mass ($\Delta m$) on the probe surface follows the Sauerbrey equation:

$$\Delta f = -2f_0^2 \Delta m / \left(A\sqrt{\rho\mu}\right), \tag{4.7}$$

where $f_0$ is the resonance frequency, $A$ is the probe area, $\rho$ is the density of the crystal, and $\mu$ is the shear modulus of the quartz. A QCM can be used for measurement in a liquid environment, and its sensitivity of a few ng allows the changes in hydration of a smart polymer-grafted surface to be evaluated. In addition, the dissipation mode (QCM-D), which is defined as the relative energy loss during one oscillation

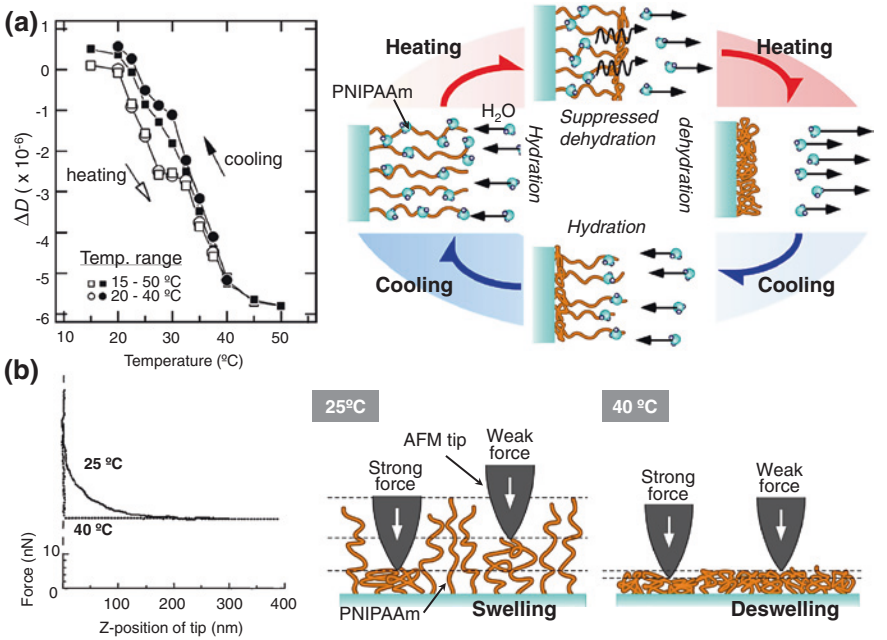


**Fig. 4.6** Phase transition analysis of smart polymer chains grafted on substrate surfaces. **a** QCM-D measurement of PNIPAAm-grafted surface used to investigate thermally induced real-time changes in hydration [112]. **b** Temperature dependence of force-distance curve between PNIPAAm-grafted surface and AFM tip [82]

cycle, can provide information on the viscoelasticity of grafted polymers [113]. This technique allows the change in $\Delta m$ due to the gain/loss of water molecules to be derived from the thermally induced changes in hydration/dehydration for grafted PNIPAAm. In the dissipation mode, the plateau of the $\Delta D$ shift was observed at 30 °C during heating, as shown in Fig. 4.6a. This implies that the free outer PNIPAAm layers first collapse with increasing temperature, and the subsequent dehydration of the inside layer is suppressed by the limited polymer mobility and the permeation of water through the rigid outer layer. The conformational changes of grafted smart polymers are suppressed through their anchoring to the surface.

The conformational changes in smart polymers on a substrate surface can also be estimated from the layer thickness, which reflects the stimuli-induced swelling/shrinking. The aforementioned ellipsometry is an appropriate tool for sensitively detecting in situ changes in layer thickness at the nanometer scale for PNIPAAm [93], poly[2-(dimethylamino)ethyl methacrylate](PDMAEMA) [114], and so forth. The results of ellipsometry for the transition of PNIPAAm-grafted layers indicate the existence of two layers below the LCST; a diluted layer with a small RI on the side of the grafted PNIPAAm exposed to water and a dense layer with a large RI near the surface. Increasing the temperature on the surface results in the formation of a single layer with a homogeneous density; consequently, there

is a flexible outer layer of grafted PNIPAAm chains, which provides a model for investigation by QCM. SPR spectroscopy is a widely used technique for the surface-sensitive in situ analysis of molecular adsorption on a substrate. Surface plasmon polaritons excited by an incident *p*-polarized light under a total-reflected condition propagate along the metal/dielectric interface of a metal-coated substrate. SPR occurs when the wavenumber of the incident beam corresponds to that of the surface plasmon polaritions, where the incident angle is called as the plasmon-coupling angle. These oscillations are very sensitive to changes in this boundary, resulting in a shift of the plasmon-coupling angle upon the adsorption of molecules on the metal surface. The numerical fitting of experimental data based on Fresnel's equation enables the modeling of the layer structure on the surface, in which the RI of each layer is important, similarly to in ellipsometric modeling. Although this technology is extensively used to measure molecular adsorption kinetics, studies have been carried out to investigate phase transition analysis of stimuli-responsive layers [115]. The incorporation of noble metal nanoparticles into grafted polymer chains leads to a significant increase in SPR sensitivity [116].

The use of an elastically deformable cantilever can provide information on the mechanical and viscoelastic properties of surface-grafted smart polymers using various modes of an AFM. Kidoaki et al. [82] reported the direct characterization of thermoresponsive structural changes on PNIPAAm-grafted surfaces in water by obtaining the force-distance curve using an AFM in contact mode, as shown in Fig. 4.6b. The approach trace of the force-distance curve indicated long-range steric repulsion and swollen layers that were a few times thicker than the compressed PNIPAAm layers at 25 °C. On the other hand, the range of repulsion significantly decreased at 40 °C, and the layer thickness remained constant upon compression by the AFM cantilever tip, which indicates the existence of mechanically tight PNIPAAm layers without long-range diffusion through layers above the LCST. A silicon cantilever allows the modification of smart polymers on the top of surfaces, and the in-plane compressive stress generated by the phase transition of the polymer layers leads to the deflection of the substrate. This deformation as a function of the amount of swelling of the smart polymers has been used to characterize the phase transition behavior [117]. There is a specific instrument for measuring the force-distance relationship, whose principle relies on the concept of the AFM approach. This instrument is known as the surface force apparatus (SFA). In the SFA technique, the mechanical force between two sample substrates is sensitively detected using a cantilevered spring with precise control of the distance through piezoelectric positioning elements [118]. Consequently, the SFA is ideally suited to measuring distance-dependent surface interactions and much longer range forces more accurately. Changes in the structure and function of polymeric materials in response to external physicochemical stimuli have also been elucidated in detail by the measurement of surface forces. Kurihara et al. [119] have examined the ionization and structural changes in poly(methacrylic acid) (PMAAc) amphiphilic brush layers as a function of pH and added salt concentration. When more carboxyl groups of PMAAc were ionized at a higher pH,

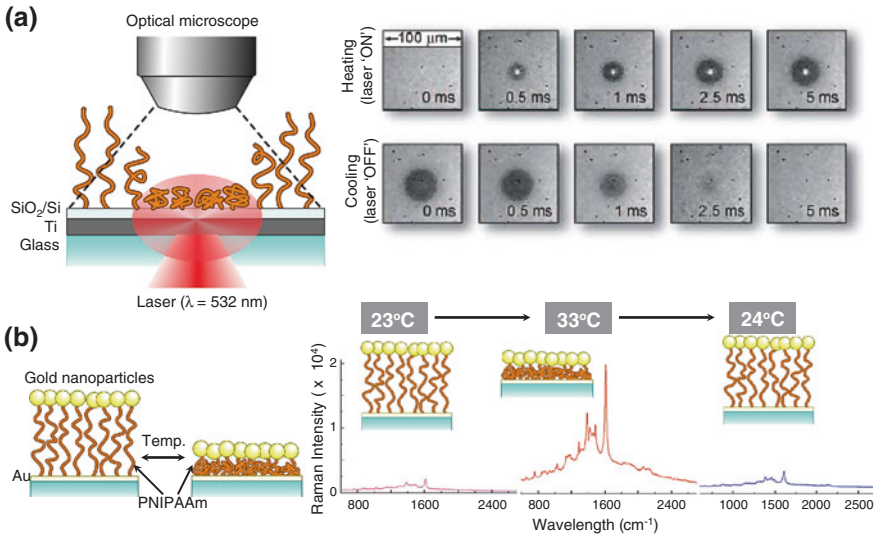


**Fig. 4.7** Novel approaches to phase transition analysis of smart polymer chains grafted on substrate surfaces. **a** Optical microscopic real-time observation of temperature-dependent swelling/deswelling for PNIPAAm brushes by stroboscopic photothermal laser manipulation [119], and **b** enhanced SERS for detecting phase transition behavior of surface-grafted PNIPAAm by electromagnetic coupling [120]

longer ranges of repulsion were observed owing to the extension of polyelectrolyte chains. The addition of a monovalent salt enhanced the ionization of PMAAc chains and restrained the repulsion at a longer separation distance, as expected from the shielding effect of counter ions.

As mentioned above, conventional surface analysis techniques have been effectively used to investigate the phase transition behavior of surface-grafted smart polymers. Even now, effective analysis methods are being proposed through inventive characterization approaches using existing apparatus. For instance, Amiri Naini et al. [120] used an optical microscope to observe the temperature-dependent switching kinetics of PNIPAAm brushes at the water/substrate interface in real time by a stroboscopic photothermal laser manipulation technique. The photothermal effect enables the generation of thermal energy through the photoexcitation of materials by laser irradiation and is useful for rapidly increasing the temperature at the water/substrate interface. In this analysis, surface-oxidized Si/Ti-coated glass plates were used as a grafting substrate to provide the basis for noninvasive, label-free monitoring of the phase transition behavior using an ordinary reflective optical microscope. The optical microscopy observation enabled the real-time monitoring of the reversible deswelling/swelling process of grafted PNIPAAm brushes with a collapsed thickness of 65 nm (Fig. 4.7a). This approach has the advantage of allowing real-time visible monitoring of the intrinsic switching kinetics of grafted smart polymers with excellent temporal resolution. On the

other hand, Gehan et al. [121] effectively analyzed the phase transition behavior of the PNIPAAm-grafted surface of a gold-coated substrate using surface-enhanced Raman scattering (SERS). Raman scattering is the inelastic scattering of a photon, which depends on the molecular constituents and structures, and SERS is a surface-sensitive technique that enhances Raman scattering through the adsorption of molecules on rough metal nanoparticle surfaces. Large enhancements of the electric field can be obtained in SERS by decreasing the gap between two metal surfaces. Gehan et al. immobilized gold nanoparticles on the free end of grafted PNIPAAm on a gold-coated substrate, and the shrinkage of the polymer chains upon an increase in the external temperature reversibly induced a significant enhancement of SERS, enabling phase transition analysis (Fig. 4.7b). SERS has the potential to enable single-molecular detection under ideal conditions; thus, this approach can provide an effective platform for analyzing the phase transition kinetics of grafted smart polymers at the molecular level. We have recently demonstrated the hydration state of PNIPAAm chains grafted onto the surface of porous silica particles by observing the mobility of water molecules using NMR [96]. NMR is a physical phenomenon in which magnetic nuclei in a static magnetic field absorb and re-emit electromagnetic radiation at a specific resonance frequency that depends on the chemical composition and structure of a sample. Although NMR has been extensively used for structural characterization, the magnetic relaxation time provides information on the molecular mobility of the sample, which is the process by which excited and coherent nuclei return to the thermodynamic state ($T_1$: spin-lattice relaxation time) and the random magnetization vector ($T_2$: lattice-lattice relaxation time) in the magnetic field. In particular, low-field pulsed NMR is useful for analyzing low molecular mobility such as that of absorbed water and confined molecules. This approach enables the evaluation of the molecular mobility of water around grafted PNIPAAm chains on a surface of porous particles. The values of $T_1$ and $T_2$ for water in pores of silica beads with PNIPAAm brushes were changed discontinuously between 25 and 30 °C, which are within the range of LCSTs. Although an increase in $T_1$ was observed for 10–30 nm porous silica particles grafted with PNIPAAm with increasing temperature, $T_1$ for particles with a 5 nm pore size decrease upon heating, indicating that the mobility of water molecules in smaller pores was restricted by the dehydration of PNIPAAm brushes. This method enables the in situ characterization of the phase transitions in confined nano- and microspaces of smart polymers grafted on surfaces.

## 4.5 Applications of Smart Surfaces

The phase transition behavior and conformational switching of smart polymer-grafted surfaces in response to external stimuli play an important role in changes in biomolecular interactions as well as in determining the permeability, mechanical, and optical properties of surfaces. Stimuli-responsive features are attractive for the

remote and timely control of surface functions depending on circumstances. Thus, many researchers have routinely proposed novel techniques and methodologies for smart polymer-grafted surfaces to realize more effective and controllable biomaterials. Through the strategic design of the monomer structure, graft architecture, substrate, and stimulus type for smart polymer-grafted surfaces, a wide range of biomedical applications have been demonstrated. This section focuses on typical and recent applications using smart biomaterial surfaces such as adhesion control, cell cultures, biomimetics, separation, and microfluidic substrates.

### *4.5.1 Adsorption Control*

In various biomaterial applications, the adsorption of biomolecules onto surfaces is the most important means of modulating the biocompatibility, nonfouling, antibacterial property, cell adhesion, and biological cascade properties of the surfaces. When proteins and peptides in aqueous solution come in contact with a solid substrate, they are rapidly adsorbed on the surface of the material via various interactions including hydrophobic and electrostatic interactions and hydrogen bonding. The conformational changes in the biomolecules accompanying the interaction induce irreversible and stable adsorption on the substrate surfaces. Numerous adhesive cells and bacteria require adsorbed basal protein layers to attach onto a solid substrate. Hence, the surface properties of substrates in terms of aqueous wettability and electrostatic behavior are essential for controlling biomolecular adhesion. In fact, hydrophilic PEO and poly (2-methacryloyloxyethyl phosphorylcholine) (PMPC) have been extensively used as grafted polymers to prevent protein adsorption, resulting in a fine biocompatible biomaterial surface [122]. To further improve the control of adsorption, stimuli-responsive smart polymers have been grafted onto substrate surfaces to allow the reversible adhesion of bioactive compounds. The understanding of biomolecular adsorption on smart polymer-grafted surfaces is one of the most fundamental factors to develop novel biomedical applications, such as cell recovery systems, biomimetic materials, separation analysis, and diagnostic devices. Controlling the adhesion of bioactive compounds using smart polymer-grafted surfaces is discussed here, and adhesive cultured cells are described in Sect. 4.5.2.

Protein adsorption processes are affected by complicated factors and depend on the correlation between the physicochemical properties of the material, protein, and solution [123]. Among these properties, surface hydrophobicity is expected to play a major role in protein adsorption. Proteins generally maintain their higher-order structure through the intricate balance of intramolecular hydrophobic interactions, and are folded into a single, discrete conformation in aqueous solution. The contact of proteins with a substrate induces their adhesion onto the surface through a hydrophobic interaction, resulting in the simultaneous deformation of the hydrophobic domains of the proteins and the release of bound water from the interfaces. Although protein desorption occurs in processes such as dynamic exchange,

the conformational change tends to result in the accumulation of proteins on the surfaces as a stable multilayer. Consequently, the proteins remain irreversibly adsorbed on the interface. The control of the initial adsorption on a substrate is important for biomaterial surfaces, not only to acquire biocompatibility but also to maintain the biological activity of a protein, which is determined by its higher-order structures. From this perspective, the design of the hydrophilic/hydrophobic property changes on a smart polymer-grafted surface has been studied with the aim of controlling the initial adsorption of proteins to enable their harvest while maintaining their bioactivity. Although various types of stimuli-responsive surface have been proposed for controlling protein adsorption, characterization of the performance of smart biomaterial surfaces is mainly carried out by SPR spectroscopy [124] and QCM measurement [125] as described in Sect. 4.4. These methods enable the real-time monitoring of protein adsorption kinetics on sample surfaces with high molecular-level sensitivity. Alternatively, fluorescence analysis and enzymatic immunoassay are also used to determine the binding constant in the equilibrium state according to the switching of the surface properties of smart biomaterials. Many smart biomaterial surfaces have been developed on the basis of the protein adsorption behavior in real time and/or at equilibrium binding.

The main class of smart polymers used for adsorption control is based on PNIPAAm, whose grafted surface exhibits hydrophilic/hydrophobic changes in response to changes in the external temperature. Decreasing the temperature on the surface to below the LCST causes PNIPAAm to become hydrophilic, enabling the switchable removal of adsorbed proteins. Similarly to wettability control on the surfaces, the primary structures of grafted PNIPAAm chains contribute to the efficiency of protein adsorption/desorption caused by changes in temperature. Yu et al. [126] have investigated static protein adsorption on end-tethered PNIPAAm brushes with various thicknesses of the grafted layer prepared via surface-initiated ATRP. Although even the thinner PNIPAAm brush surfaces (<15 nm) strongly inhibited the adsorption of human serum albumin (HSA) compared with the unmodified surface at 23 and 37 °C, the difference in protein adsorption at temperatures above and below the LCST was notable for a grafted surface with 38.1 nm thickness. Xue et al. [127] varied the grafting density of PNIPAAm-modified surfaces to examine the effect of grafting density on temperature-dependent protein adsorption. Their experimental data also revealed subtle differences in the low bovine serum albumin (BSA) adsorption on brushes; however, proteins adsorb on less dense brushes (0.08 chains/nm$^2$), which allow them to penetrate the layer and interact more extensively with the grafted chains. Considering that the grafted surface is hydrophobic at temperatures below the LCST, the protein-repelling property may be due to the hydrophilicity of PNIPAAm chains. Since intermolecular hydrogen bonds are formed with water molecules at the amide groups in PNIPAAm [110], the abundant free water molecules around the grafted polymer chains should play a critical role in resisting the initial adsorption of proteins. Regarding other surface-grafted thermoresponsive polymers, oligo(ethylene glycol) (OEG) derivatives have been studied for the control of protein adsorption, such as P(MEO$_2$MA-*co*-OEGMA)

[104] and poly(2-(2-methoxyethoxy)ethyl methacrylate) (PMDMA) [128]. Although the basically hydrophilic OEG exhibits low protein adsorption, Zareie et al. [129] controlled the affinity binding of a protein through conformational changes in OEG SAMs on a substrate. They prepared mixed SAMs comprising disulfide-linked OEG and biotinylated thiol molecules on a gold-coated surface, and the affinity interaction between streptavidin (SA) and biotinylated molecules was regulated by the swelling/shrinking behavior of the grafted OEG in response to changes in temperature. The capture and release of proteins using conformational changes were also demonstrated by grafting with a thermoresponsive elastin-like polypeptide (Val-Pro-Gly-*X*-Gly, *X* is any amino acid except Pro) [130]. Not only the surface wettability but also the conformation in grafted smart polymers is a useful approach to control protein adsorption by temperature switching. Other stimuli-induced protein adsorption on grafted surfaces, which has been extensively reported, includes changes in the electrochemical stimuli using low-density ionizable alkanethiolate SAMs [131], and the control of bioactivity by photochemical signals based on the *trans–cis* isomerization of azobenzene-incorporated polymers [132].

On the other hand, bacterial adsorption is also a critical issue in biomedical applications in terms of protection against bacterial infection from contaminated materials [133]. Smart polymer grafting is increasingly required for self-cleaning and the biological assay of collected bacteria. There are two major approaches to control bacterial adsorption on a polymer-grafted surface. The active approach is to kill bacteria using antimicrobial materials. Since the isoelectric point of most bacterial strains is usually in the pH range of 1.5–4.5 [134], cationic materials, such as quaternary ammonium salt derivatives, are powerful agents against bacteria [135]. The alternative approach is to repel bacteria using nonfouling coatings similarly to the case of protein adsorption. As a smart polymer exhibiting these antibacterial features, pH-responsive zwitterionic polymers have great potential for controlling the attack and release of bacteria on a grafted surface. Lee et al. [136] grafted chitosans with quaternary ammonium salts onto an epoxide-derivatized surface as a pH-responsive antibacterial material. This surface displayed a high positive charge between pH 2.97 and 8.2 and exhibited reversible and tunable swelling/shrinking behavior upon varying the pH of the solution, resulting in a significant reduction of *S. aureus* colonization at pH 7.3. Mi et al. [137] reported a tunable mixed-charge copolymer surface containing positively charged (2-(acryloyloxy)ethyl)trimethyl ammonium chloride (TMA) and negatively charged 2-carboxyethyl acrylate (CAA) that exhibited nonfouling properties that depended on the environmental pH. The surface of P(TMA-*co*-CAA) brushes has no charge under neutral and basic conditions, but is positively charged under acidic conditions. Changing the solution pH from 4.5 to 10.0 led to a six fold decrease in the number of *S. epidermidis* cells on the grafted surfaces. Cao et al. [138] developed an innovative system that repeatedly switched between attacking and repelling against bacteria using a novel smart polymer. In this polymer, the substituent in the side-chain alternates between two equilibrium states: cationic *N*,*N*-dimethyl-2-morpholinone(CB-ring) and zwitterionic

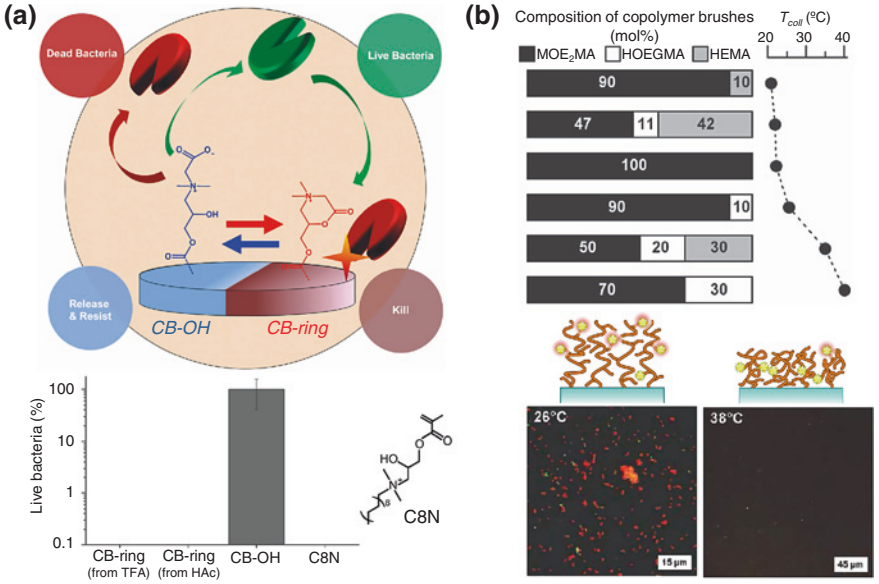


**Fig. 4.8** Smart antibacterial surfaces. **a** Reversible switching between attacking and defending against bacteria using zwitterionic-polymer-grafted surfaces [137], and **b** control of bacterial adhesion on P(MEO2MA-co-HOEGMA-co-HEMA)-grafted surfaces bearing magainin-I by temperature switching [138]

carboxyl betaine (CB–OH), as shown in Fig. 4.8a. Under dry conditions, CB-ring, obtained from CB–OH by adding either trifluoroacetic acid (TFA) or acetic acid (HAc), can kill over 99.9 % of *E. coli* K12 cells attached on the grafted surfaces. The immersion of the substrate into a neutral or basic aqueous medium allows the CB-ring to immediately hydrolyze to CB–OH in the grafted polymer, and the CB–OH state simultaneously releases dead bacteria from its surface and exhibits a bacteria-repellent property. CB–OH can be converted back to the CB-ring under acidic conditions, thereby regenerating the bacteria-killing function. Such a repeatable function based on a simple operation is a successful model for various smart biomaterial surfaces. Alternatively, the incorporation of an antibacterial molecule into conventional smart polymer chains is also useful for controlling bacterial adhesion. Laloyaux et al. [139] fabricated surface-grafted P($MEO_2$MA-*co*-OEGMA-*co*-HEMA), into which magainin-I was introduced as an antimicrobial peptide to resist bacterial adhesion through temperature switching. A large fraction of dead adhered bacterial cells were observed on the surface incubated at 26 °C, which is below the LCST, and the grafted polymer brushes acted as cell-repellent surfaces against *L. ivanovii* cells at 38 °C, above the LCST (Fig. 4.8b). Importantly, the phase transition temperature can be easily modulated by adjusting the composition of the monomer mixture. An adjustable signal for changing the surface property is also important in the development of practical biomaterials using smart polymer-grafted surfaces.

### 4.5.2 Cell Culture

In the last several decades, cell culture for biomedical and clinical applications has been one of the most active areas of research in the field of smart biomaterial surfaces. Protein adsorption and subsequent cell adhesion are frequently disadvantageous for the realization of biomaterials in vitro and in vivo, and many researchers have attempted to control the interactions between material interfaces, proteins, and cells to acquire material biocompatibility. There are two steps in the process by which cells attach onto material surfaces: 'passive adhesion' and 'active adhesion' [100]. Passive adhesion involves physicochemical interactions between the material surface, adsorbed proteins and adhering cells, and active adhesion involves the activation of spontaneous receptor-mediated interactions and is followed by passive adhesion. The cell-material interaction in passive adhesion occurs reversibly and without metabolic signaling in a cell; thus, the key factors enabling the inhibition of passive adhesion by material surfaces involve the static control of various physicochemical characteristics, such as wettability, phase separation, charge, mechanical properties, surface roughness, and so forth. The control of these static properties of material surfaces has led to the development of implantable artificial organs, biosensor devices, and nonthrombogenic surgical instruments. On the other hand, active adhesion involves cellular metabolic processes using ATP to change the cellular morphologies so that they spread on surfaces and initiate the signaling process depending on their phenotypes. The cells spread on material surfaces rarely detach spontaneously from the surfaces without the reversal of adhesion from active to passive, even if the static surface properties are controlled. Thus, the enzymatic proteolysis of extracellular matrix (ECM) proteins and the chelation of divalent cations such as $Ca^{2+}$ ions to deactivate cell integrin receptors are conventionally used to control actively adhered cells. However, these processes cause significant damage to the cells, resulting in the hydrolysis of various membrane-associated proteins such as ion channels and growth factor receptors. Noninvasive modulation from active cell adhesion to detachment requires dynamic changes in the surface properties of cell culture materials without any enzymes and chelators.

In the 1990s, Okano and co-workers proposed a novel detachment technique for actively adhered cells using PNIPAAm-grafted tissue culture polystyrene (TCPS) dishes simply by lowering the temperature [16, 140], as shown in Fig. 4.9a. Various types of cell adhered onto PNIPAAm-grafted surfaces at 37 °C, with morphologies ranging from being round to flat; these morphologies correspond to the consumption of ATP by metabolically active adhesion. The number of cultured cells on the PNIPAAm-grafted surfaces increased with incubation time and these cells proliferated and became confluent after 7 days in the case of endothelial cells. Their growth curves and adhesion morphologies on PNIPAAm-grafted dishes were almost the same as those on commercially available TCPS. Figure 4.9b shows changes in the number of endothelial cells

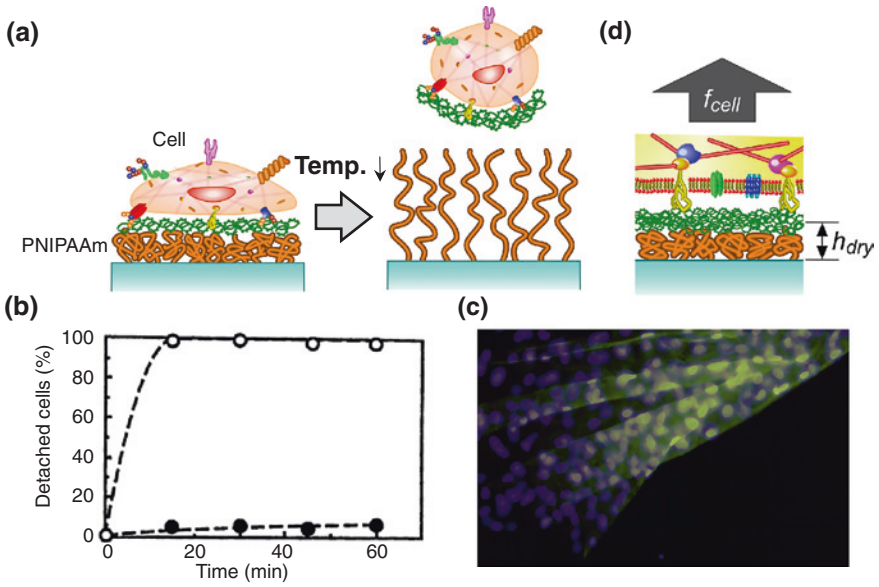


**Fig. 4.9** Smart cell culture surfaces. **a** Noninvasive harvest of cells cultured on PNIPAAm-grafted surfaces by lowering the temperature, **b** time dependence of endothelial cell detachment from PNIPAAm-grafted TCPS after 2 days of culture followed by decreasing the temperature to 10 °C [139], and **c** endothelial cell sheets detaching from temperature-responsive culture surfaces after low-temperature treatment (double-staining with anti-fibronectin (*FN*) antibody and a fluorescent dye for nuclei) [141]

that detached from PNIPAAm-grafted surfaces with time when the temperature is reduced to 10 °C after endothelial cells were cultured at 37 °C for 2 days. All the attached cells detached from the PNIPAAm-grafted dishes after 15 min, whereas the number of cells that detached from ungrafted dishes was negligible. Decreasing the culture temperature to a value below the LCST induces a change in surface wettability from hydrophobic to hydrophilic, leading to the release of the adhered cells. The detachment of cells from surfaces requires the adherent cells to change their membrane shape, consuming internal metabolic energy, and the hydration of grafted PNIPAAm layers on surfaces by lowering the temperature induces the suppression of cellular metabolism [141]. This system allows the preservation of intact membranes and adhesive proteins, because only interactions between adhesive proteins on the basal side of the cultured cells and the grafted PNIPAAm on the surfaces are disrupted, as shown in Fig. 4.9c. Thus, confluent cultured cells were harvested as a contiguous cell sheet from the thermoresponsive surfaces while maintaining cell–cell junctions and basal ECMs [142]. Since adhesive proteins derived from cells are also harvested at the same time, the cell sheets can readily adhere to various surfaces including culture dishes, other cell sheets and host tissues. Using this recovery system, various tissue reconstructions have been demonstrated such as ocular

surfaces [143], periodontal ligaments [144], cardiac patches [145], and bladder augmentation [146].

Thermally induced dynamic changes in the surface properties of PNIPAAm-grafted surfaces are a key factor in the regulation of cellular interactions with surfaces used for cell adhesion/detachment. Thus, the conformation of PNIPAAm grafted on surfaces has a significant effect on cell adhesion/detachment behavior. Akiyama et al. [74] investigated factors affecting the thermal control of cell adhesion/detachment on PNIPAAm-grafted TCPS prepared by EB irradiation. The adhesion control of bovine carotid artery endothelial cells (BAECs) was achieved on surfaces grafted with PNIPAAm in the density range of 1.5–2.0 $\mu g/cm^2$, whereas no cell adhesion at 37 °C and no cell detachment by lowering the temperature to 20 °C were observed above and below this range, respectively. This threshold density of grafted PNIPAAm for the effective control of cell adhesion/detachment corresponds to a polymer layer thickness of ca. 20–30 nm on the surface. Such ultrathin PNIPAAm layers on TCPS are relatively hydrophobic owing to the restriction of polymer chain mobility by the hydrophobic interaction with TCPS interfaces. On the other hand, the outer PNIPAAm layers have high molecular mobility, leading to greater hydrophilicity with increasing graft polymer thickness on the surface. In fact, the appropriate density of grafted PNIPAAm on glass substrates more hydrophilic than TCPS is ca. 2.0 $\mu g/cm^2$ for cell adhesion/detachment because of the weaker hydrophobic interaction at the interfaces [147]. Takahashi et al. [97] controlled the graft density and chain length of PNIPAAm on glass surfaces through surface-initiated RAFT polymerization to investigate the relationship between the graft composition and the adhesion property of BAECs. At a certain graft density, grafted PNIPAAm with molecular weights of $M_n = 23{,}000$ and 49,000 showed a good adhesion property, although fewer than 20 % of cells adhered to surfaces grafted with polymers with $M_n = 58{,}000$. By contrast, the detachment of BAECs from surfaces upon lowering the temperature to 20 °C was faster for PNIPAAm-grafted surfaces with a higher graft density and longer chain length. Cell sheets were successfully harvested from surfaces grafted with PNIPAAm with a graft density of 0.03 chains/$nm^2$ with $M_n = 49{,}000$, or at higher graft density (0.04 chains/$nm^2$). Therefore, a suitable balance between the smart polymer composition, the amount of grafting, the chain density, and the molecular weight is important for the control of cell adhesion/detachment by changing the temperature.

Such a correlation between the control of cell adhesion and the polymer composition on the surface has been discussed not only in the above experimental studies but also on the basis of theoretical approaches. Halperin et al. [148] theoretically considered cell detachment by calculating the change in coupling upon hydration in integrin-mediated environmental sensing for a cell culture on grafted PNIPAAm in a serum-containing medium. Their discussion focused on two processes of cell adhesion to a solid substrate: serum-bearing ECMs adsorb on the surface and cells subsequently become attached to the adsorbed ECMs, which provide ligands to integrin receptors anchored at the cell ventral membrane. In the case of a cell culture on PNIPAAm-grafted surfaces, cell adhesion

can confine the grafted polymer through a disjoining force ($f_{cell}$) derived from the osmotic pressure of swollen polymer layers as shown in Fig. 4.9d, because the cell membrane cannot penetrate into the chains. When the grafted PNIPAAm collapses at 37 °C, this disjoining force prevents cell adhesion at a dry polymer thickness $h_{dry}$ exceeding 25 nm, which is the length of the extracellular integrin tail and the thickness of the adsorbed ECM layer [149]. Lowering the temperature to a value below the LCST induces polymer swelling, increasing the value of $f_{cell}$, and placing the integrin-ECM bonds under tension, thus shortening their lifetime according to Bell's law [150]. Increasing $f_{cell}$ may also accelerate the desorption of ECM proteins bound to cells. Both effects contribute to the kinetics of cell detachment. On the basis of this consideration, the effects of the degree of polymerization, graft density, and temperature on $f_{cell}$ were investigated by theoretical analysis [151–153]. $f_{cell}$ is almost zero at 37 °C when $h_{dry} \geq 25$ nm and increases with decreasing temperature below the LCST. An increase in the degree of polymerization of grafted PNIPAAm chains induces a rapid increase in $f_{cell}$, and high grafting densities suppress the adsorption of ECM proteins thus in turn suppressing cell adhesion. By comparison with the measured cell-pulling strength ($1 \text{ pN} < f_{cell} < 1.5 \times 10^6$ pN) [154], this analysis allows rationalization of the experimental observations associated with cell adhesion and detachment. Another factor affecting cell detachment from PNIPAAm-grafted surfaces is the elastic deformation of the grafted layers. Galaev et al. [155] have reported that the elastic deformation of NIPAAm-based hydrogels results in the release of multiple bound particles, whereas no release of single-bound proteins occurs upon elastic deformation. The adhesion of cells through their membrane receptors is employed in polyvalent interactions, and such multiple bonds can be easily disrupted by the elastic deformation of hydrated PNIPAAm layers. In addition, cells can detach from the surface when they lose the intracellular tension exerted by the cytoskeleton [141]. Since multiple factors are involved in the detachment of cells from smart polymer-grafted surfaces, determination of the most critical mechanism is currently an active area of research.

The shape of the substrate used for surface modification with PNIPAAm can provide useful assistance in the control of cell adhesion and tissue reconstruction. For example, a porous cell culture membrane was employed as a grafting substrate to accelerate cell detachment [156]. The porous structure facilitates the access of water to allow the swelling of PNIPAAm when the temperature is lowered to a value below the LCST, whereas the hydration of grafted PNIPAAm is suppressed owing to the limited water supply on a flat substrate. Matsuda fabricated a three-dimensional tubular structure consisting of cultured cells using PNIPAAm-grafted gelatin and a glass capillary [157]. By infusing a culture medium into the PNIPAAm-grafted capillary at 20 °C after cell culture on the inner wall, a vascular-like cell tube composed of ECs could be harvested with deposited ECM on the basal side of the tissue. Tamura et al. [158] have recently cultivated Chinese hamster ovary (CHO-K1) cells on PNIPAAm-grafted surfaces of microspheres in a stirred suspension for application to cell therapy. This suspension culture system can realize both effective cell proliferation and subsequent thermally induced

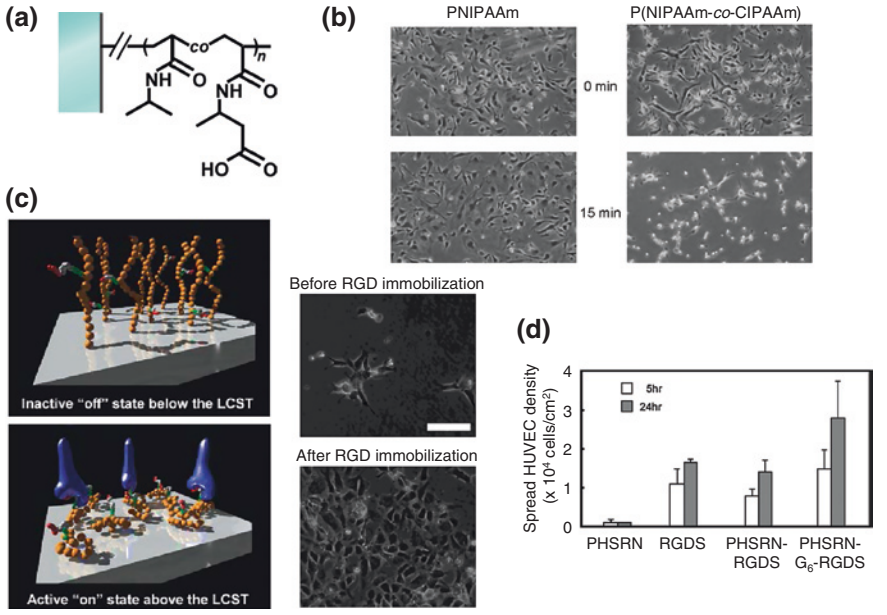


**Fig. 4.10** Functional thermoresponsive cell culture surfaces using CIPAAm. **a** Chemical structure of P(NIPAAm-co-CIPAAm)-grafted surfaces, **b** accelerated rate of BAEC detachment on P(NIPAAm-co-CIPAAm)-grafted surfaces compared with that on PNIPAAm-grafted surfaces [164], **c** control of specific interactions between immobilized RGDS peptides in P(NIPAAm-co-CIPAAm)-grafted surfaces and cell integrin receptors for serum-free culture (photographs: HUVEC adhesion without serum at 37 °C, scale: 100 μm) [160], and **d** enhanced specific interaction between RGDS peptides and cell integrin receptors by synergistic effect of PHSRN on P(NIPAAm-co-CIPAAm)-grafted surfaces [163]

cell detachment depending on the amount of grafted PNIPAAm and the diameter of the microspheres. They also reported the incorporation of positively charged 3-acrylamidopropyl trimethylammoniumchloride (APTAC) into PNIPAAm grafted on the microspheres to facilitate their dispersibility, resulting in enhanced cell proliferation [159]. Strategies based on the substrate shape have potential use for improved smart cell culture systems and mold-releasable materials in biomedical applications.

From the perspective of molecular design, the introduction of functional groups or biomolecules into grafted PNIPAAm chains is effective for enabling cell adhesion control on surfaces, although it is necessary to prevent the deterioration of the thermoresponsive property resulting from the use of another comonomer. Aoyagi et al. [160] have developed 2-carboxyisopropylacrylamide (CIPAAm) as a novel NIPAAm-based functional monomer, whose polymer has continuous parallel isopropylamide groups (Fig. 4.10a), enabling a steep phase transition to be maintained as well as the formation of an NIPAAm homopolymer. Ebara and co-workers found that cell adhesion/detachment can be achieved on P(NIPAAm-*co*-CIPAAm)-grafted surfaces as well as on PNIPAAm surfaces by changing the

temperature [161–165]. Furthermore, the grafted surface allows the rate of cell detachment from P(NIPAAm-*co*-CIPAAm)-grafted surfaces to be accelerated compared with that from a conventional homopolymer surface [165], as shown in Fig. 4.10b. This is due to the accelerated hydration of polymers grafted on the surfaces by the incorporation of ionized carboxyl groups, inducing the rapid swelling and subsequent lifting of cells from them. They also immobilized a cell-adhesive Arg-Gly-Asp-Ser (RGDS) peptide on grafted P(NIPAAm-*co*-CIPAAm) via a condensation reaction between an amino terminal in RGDS and a carboxyl group in the copolymer chain [161–164]. Under a serum-free cell culture condition, significant differences in the spreading of human umbilical vein endothelial cells (HUVECs) on the copolymer-grafted surfaces were observed before and after RGDS immobilization at 37 °C (Fig. 4.10c). This enhanced cell adhesion property of the grafted P(NIPAAm-*co*-CIPAAm)-bearing peptides is caused by a specific interaction between the cellular integrin and the RGDS residue. On the other hand, HUVECs can be detached from the surfaces by reducing the temperature to a value below the polymer LCST, where the detachment behavior depends on the immobilized RGDS content. This mechanism is considered to be based on a decrease in the cell tension of spreading HUVECs resulting from surface swelling through the hydration of grafted copolymers, which induces a decrease in the specific integrin-RGDS association. To control the affinity of binding on smart copolymer-grafted surfaces, Ebara et al. [163] controlled the access of integrin to RGDS by tethering a poly(ethylene glycol) (PEG) chain as a spacer, and the synergistic effects on cell adhesion of a Pro-His-Ser-Arg-Asn (PHSRN) sequence, derived from RGDS using a hexamer glycine ($G_6$) linker were investigated by changing the distance between the peptide and the grafted polymer [164]. The peptide-bearing copolymer distance significantly affects the release time of cells from the surfaces when the temperature is lowered. In particular, the initial cell adhesion was enhanced on PHSRN-$G_6$-RGDS-immobilized surfaces (Fig. 4.10d) because the synergistic PHSRN was located ca. 3.5 nm away from the RGD loop in a natural fibronectin, which corresponds to the chain length of the $G_6$ linker. In addition, the further immobilization of insulin into the smart copolymer as a cell growth factor promotes not only cell adhesion but also cell proliferation on the surface [166]. The incorporation of peptides into grafted polymers enables the growth of a serum-free cell culture for safe clinical applications and underlines the importance of molecular design for grafted smart polymers to control cell adhesion on surfaces. Recently, we have prepared smart copolymer brushes comprising NIPAAm and 2-lactobionamidoethyl methacrylate (LAMA), which has a galactose residue to specifically bind to asialoglycoprotein receptors of hepatocytes, to regulate hepatocyte-selective adhesion through temperature alterations [25]. The polymer brushes containing LAMA promoted HepG2 cell adhesion at 37 °C through a specific interaction with sugar moieties, although NIH-3T3 fibroblasts did not adhere on the surfaces under serum-free conditions. The adhered HepG2 successfully detached from the PNIPAAm-*b*-PLAMA brush surfaces when the temperature was reduced to 25 °C, while almost all cells remained on the P(NIPAAm-*co*-LAMA) brush surfaces. These results were due to the difference in the phase transition temperatures

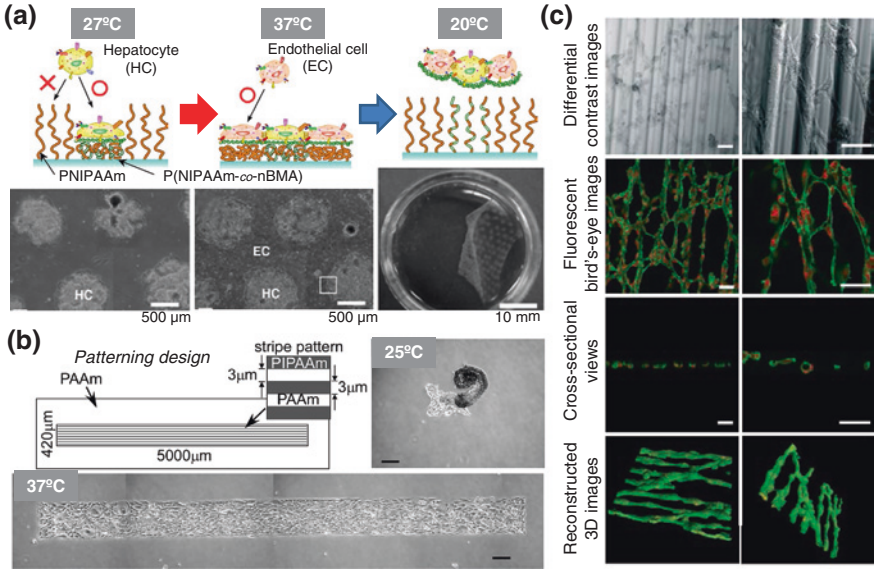


**Fig. 4.11** Smart patterned surfaces for reconstruction of cell structures. **a** Hepatocyte and BAEC coculture and harvesting of cocultured cell sheets using a dual patterned surface comprising PNIPAAm and P(NIPAAm-co-BMA) [166], **b** aligned adhesion of fibroblasts at 37 °C and folding detachment of the cell sheet by reducing the temperature on PNIPAAm and PAAm patterned surfaces (scale: 200 μm) [76], and **c** capillary network structures of BAECs cultured on PNIPAAm-grafted microtexture surfaces (photographs: stained with Alexa 488-conjugated phalloidin to label F-actin (*green*) and ethidium homodimer-1 to label the nuclei (*red*), scale: 50 μm) [168]

from NIPAAm homopolymer for surface wettability changes, depending on the sequences of hydrophilic LAMA in the polymer brushes. Therefore, the graft architecture of smart polymers is also important in the modulation of surface properties for the harvest of stimuli-induced cells.

Cell patterning on PNIPAAm-grafted surfaces provides a potential tool for the construction and recovery of functional tissue-mimicking cell sheet materials for clinical applications. A patterning strategy for polymer grafting and substrate surfaces is required to fabricate the in vivo-like cell structures. Tsuda and co-workers prepared patterned thermoresponsive surfaces of PNIPAAm and P(NIPAAm-*co*-*n*-butyl methacrylate (BMA)) to demonstrate a stepwise phase transition induced by temperature modulation [103, 167]. In this approach, hepatocytes are selectively cultured only on relatively hydrophobic P(NIPAAm-*co*-BMA) domains at 27 °C because of the decrease in LCST caused by the incorporation of hydrophobic BMA into the PNIPAAm chain, whereas PNIPAAm domains show hydrophilic and cell repellent properties at this temperature (Fig. 4.11a). BAECs subsequently seed after a 4-day culture of the primary cells and can adhere onto hydrophobized PNIPAAm domains at 37 °C, resulting in a patterned coculture of hepatocytes and BAECs. Consequently, the cocultured cell monolayers can be recovered simply

by reducing the temperature to 20 °C, which is below the LCSTs of both grafted domains. The physiological functions of hepatocytes, such as albumin secretion and ammonium metabolism in the patterned coculture, are enhanced with increasing number of heterotypic cell-cell interactions. Thus, this method can provide a functional cell sheet through heterotypic cell communication such as that in the liver and pancreas. As another example of using a patterning technique, the use of line-space micropatterning, such as in the case of producing PNIPAAm patterns on cell-repellent poly(acrylamide) (PAAm)-modified surfaces and microtextured substrates grafted with PNIPAAm, leads to aligned and elongated cells adhesion on the surface along the major axis of the patterns [76, 168]. The aligned confluent cells can be harvested as a cell sheet by changing the temperature, and the cell sheets strongly contract in the stripe pattern direction, resulting in shrinkage and folding along the patterns (Fig. 4.11b). This technique could be useful for the construction of muscle cell sheets with efficient shrinkage/relaxation in a specific direction. Stripe microgrooves of a PNIPAAm-grafted substrate can also induce the capillary network formation of BAECs with 5–20 μm inner diameters by cultivation on the surface [169], as shown in Fig. 4.11c. The construction of BAEC networks using PNIPAAm-grafted patterns with multilayered cultures by combining micropatterned endothelial cells with fibroblast monolayer sheets has been reported [170]. These several strategic methods of designing the patternins on PNIPAAm-grafted surfaces could lead to a breakthrough in the next generation of tissue engineering.

A variety of smart polymer-grafted surfaces have been developed to be alternately used with PNIPAAm for the control of cell adhesion. For instance, P($MEO_2$MA-*co*-OEGMA) exhibits LCSTs between 26 and 90 °C, which can be precisely adjusted by varying the composition, and the grafted surface enables the control of cell adhesion [171]. This smart substrate combines the advantageous features of thermoresponsive PNIPAAm surfaces and biocompatible PEG surfaces. Applying the same concept, Pluronic F68 and F127 as poloxamers [172], xyloglucan as a major hemicellulose [173], and elastin-like polypeptides [174] are used as low-toxicity thermoresponsive cell culture substrates. The use of light as a trigger to detach cells from a substrate has also been extensively studied using photoresponsive polymer grafting, particularly for dynamic cell patterning. Two approaches are mainly used in photoinduced cell detachment: the incorporation of photocleavable or photochromic residues into the grafted polymers. In the case of photocleavable smart polymers, it is necessary that the protective group allows cell adhesion, and the grafted surface exhibits a cell-repellent property after cleaving through UV exposure. Byambaa et al. [175] prepared a surface-grafted smart polymer comprising a photocleavable monomer and MPC to control cell adhesion/detachment by UV irradiation, as shown in Fig. 4.12a. The smart surface was negatively charged and relatively hydrophobic, enabling cell adhesion, and photoirradiation changed the surface property to neutral and hydrophilic, derived from the cell-repellent MPC units. Photodegradable polymer-grafted surfaces comprising repeated ketal or acetal units allow in situ cell detachment through UV exposure,

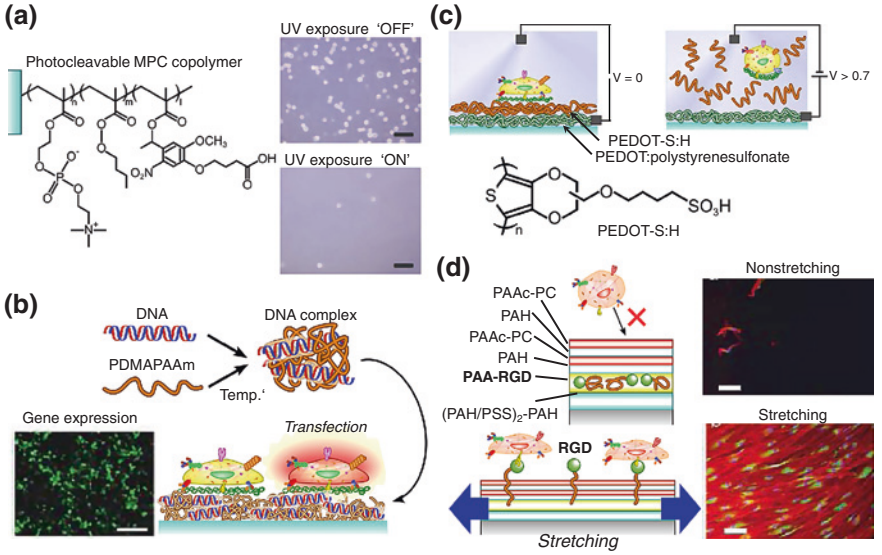


**Fig. 4.12** Control of cell adhesion on smart surfaces triggered by the switching of various stimuli. **a** Photocleavable MPC-copolymer-grafted surfaces (scale: 100 μm) [174]. **b** PDMAPAAm-grafted surfaces combined with DNA for surface-mediated transfection (scale: 200 μm) [180], **c** electrodegradable PEDOT-S:H-grafted surfaces [182], and **d** cyto-mechanoresponsive PAAc-PC/PAH/PAAc-RGD multilayer surfaces (scale: 100 μm) [183]

similarly to photocleavable polymers [176]. In photochromic smart polymers with azobenzene or spiropyran residues, the cell adhesion property can be regulated by reversible photoinduced isomerization of the functional groups in the grafted polymers [177, 178]. Liu et al. [178] prepared a PEG-based SAM with an embedded azobenzene group containing RGD peptide. The background of grafted PEG prevents nonspecific adhesion, and the azobenzene moiety can be reversibly converted between the E and Z configurations to either present or mask the RGD ligand and hence modulate biospecific cell adhesion via the irradiation of visible (450–490 nm) or UV (340–380 nm) light. Although photochemical cell detachment is useful as a time-space control technique, the use of ultraviolet UV light may damage both SAMs and adherent cells. Among the smart cell culture systems, the use of a pH-responsive polymer is one of the simplest and most versatile techniques for cell adhesion control by changing the pH and ion strength in the culture medium [179]. In addition, a pH-responsive polymer that includes various charged species such as DNA and growth factors can be simultaneously grafted onto a substrate [180]. Iwai et al. [181] used grafted poly(*N*,*N*-dimethylaminopropyl acrylamide) (PDMAPAAm) combined with DNA to carry out surface-mediated transfection during cell culture, as shown in Fig. 4.12b. These grafted surfaces showed high cell viability and transgene expression upon using small amounts of PDMAEMA. Because this polymer also has a thermoresponsive property, the grafted surface allows cell detachment

through changes in temperature. Electrochemical stimulation has also been used as a trigger for cell detachment to control the reductive desorption of a thiol SAM [182] or the disintegration of a polymer from an electrode surface by applying potential. For example, Persson et al. [183] reported the use of conductive poly(3,4-ethylenedioxythiophene) (PEDOT-S:H) as shown in Fig. 4.12c. As another novel approach, Davila et al. [184] developed a cyto-mechanoresponsive surface that allows cell adhesion in response to mechanical stretching. This grafted surface comprises PAAc-bearing RGD peptides under a cell-repellent PAAc-phosphorylcholine (PC)/poly(allylamine hydrochloride) (PAH) multilayer on a silicone substrate, and the cell-adhesive RGD can be exposed by stretching the film (Fig. 4.12d). The amount of exposed ligands from the multilayer can be regulated by adjusting the stretching ratio of the substrate, and the density of adhesive ligands can be gradually changed during cell culture simply by stretching. Therefore, attempts to realize molecular design of smart polymer-grafted surfaces will be continued in the future to achieve more effective and simpler control of the cell adhesion property.

### *4.5.3 Biomimetics*

Biomimetics involves the mimesis of structures and functions inspired by nature and biological systems for the design and engineering of materials. In the human body, mechanical and physical functions are induced by external stimuli to maintain a normal metabolism via a feedback system that includes sudoriferous pores, papillae, muscles, and ion channels. The conversion of the response to a stimuli into mechanical actuation and permeability has been focused on as a means of developing smart artificial devices such as stimuli-sensitive actuators, gating nanochannels, and self-healing devices [185]. In addition, the commercialization of light- and heat-sensitive materials that use the energy from ambient changes should result in a substantial reduction in energy consumption. Surface modification with smart polymers has also been used as a biomimetic process to control the transformation and pore size of original substrate structures through conformational changes by stimuli switching. Although biomimetics is a concept of biomaterials themselves in the wide sense, in this section, we focus on the control of mass transfer and actuation in response to stimuli using smart polymer-grafted surfaces.

The biomimetic control of mass transfer through the stimuli-responsive features of grafted smart polymers has been routinely demonstrated using porous materials, particularly polymeric membranes [43]. The conformation of smart polymers can be made to change in response to the local environment, leading to reversible changes in the permeability and selectivity of membranes. When smart polymers are modified on the pore surfaces of membranes, stimuli-induced changes in the degree of their swelling and shrinkage commonly lead to the opening and closing of the pores (Fig. 4.13a), hence triggering changes in the membrane

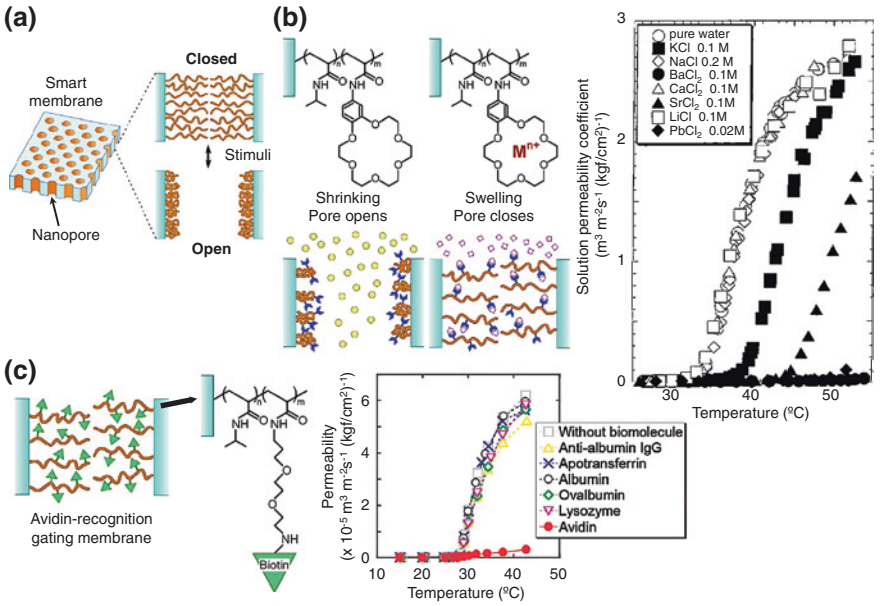


**Fig. 4.13** Stimuli-induced control of mass transfer through smart polymer-grafted pore surfaces of porous membranes. **a** Concept of permeation control through smart porous membranes via their conformational changes, **b** ion-selective gating membrane grafted with NIPAAm and BCAM copolymers [199], and **c** avidin-recognition gating membrane grafted with biotinylated PNIPAAm [201]

permeability and selectivity. Thermoresponsive PNIPAAm compounds have been conventionally used as a grafted smart polymer to control the water flux and molecular permeability in porous membranes [186]. Allen et al. [187] prepared a smart mesoporous glass frit grafted with PNIPAAm containing silica nanoparticles through covalent LbL assembly with polyethylenimine to realize responsive permeability. The introduction of silica nanoparticles into the PNIPAAm layers increases the surface roughness, thus enhancing thermoresponsive changes in wettability, resulting in a greater than 1,000-fold difference in permeability to water compared with permeability to aqueous solutions of sodium sulfate. Such conformational responsiveness of grafted PNIPAAm is significantly influenced by the chain length and graft density. Li et al. [188] controlled the chain length and graft density of grafted PNIPAAm in the pores of anodic aluminum oxide (AAO) porous membranes by surface-initiated ATRP. The diffusional permeability of vitamin B12 through membranes at a temperature by the conformational changes of grafted PNIPAAm on the pores depended on both the chain length and graft density, and the effect of the chain length was greater than that of the graft density. Kuroki et al. [189] optimized the chain length at a low density (ca. 0.01 chains/$nm^2$) in PNIPAAm-grafted polycarbonate membranes for effective pore gating. They isolated grafted PNIPAAm from the substrate to estimate the filling ratio of

dry polymer layers in the pores. The permeability of the shrunk PNIPAAm was nearly unchanged for a filling ratio from 0 to 20 %, and dramatically decreased upon the swelling of grafted PNIPAAm with a filling ratio of up to 10 %, resulting in a sufficiently high filling ratio of 10–20 % to induce a marked change in the water permeability. As alternative temperature-sensitive smart polymers to PNIPAAm, poly(*N*-vinylcaprolactam) [190], thermoresponsive PU [191], and poly(*N*,*N*-diethylacrylamide) (PDEAAm) [192] have been grafted onto porous membranes for the control of permeability.

pH-responsive smart polymers involving derivatives of PAAc and PDMAEMA have also been widely used to fabricate porous membranes with variable barrier properties [193]. These grafted membranes enable the control of the pore size in response to changes in pH and ionic strength. In pH-responsive porous membranes, a lower graft density results in better permeability of buffer solutions, similarly to PNIPAAm-grafted surfaces [194]. The conformational changes of smart polymers may be more flexible at a lower graft density because of the weaker interactions between neighboring grafted polymers. Kaetsu et al. [195] used pH-responsive membranes for drug permeation and the release of methylene blue as a model drug by coating PAAc on a porous polymeric film. The smart porous membranes allowed the permeation of the model drug under acidic conditions alkaline conditions. In addition, they immobilized glucose oxidase onto grafted polymer layers, and programmed drug release through the membranes was achieved in response to the addition of glucose via the generation of gluconic acids in an enzymatic reaction. Zhang et al. [196] investigated the controlled release of various proteins and peptides using a porous membrane coated with dual-responsive P(NIPAAm-*co*-MAAc)-grafted nanoparticles. The pore sizes of the dual-responsive membranes were controlled by changing the temperature and pH at the boundary of the LCST as well as the value of $pK_a$, and the molecular permeability was found to depend on the molecular radius of the proteins and peptides. These studies demonstrate that smart porous membranes can be applied as a carrier to control drug release by stimuli switching.

Other signals for switching the permeability of smart porous membranes include the UV exposure and the addition of specific chemical reagents. In the case of photoresponsive porous membranes, UV irradiation usually induces the isomerization of photochromic residues in grafted smart polymers, including derivatives of azobenzene [197] and spiropyran [198], to leading to structurale changes that enable the control of the pore size. To realize smart porous membranes that respond to a specific molecule, strategies are required to prepare smart polymers conjugated with molecular recognition sites. Yamaguchi et al. [199] designed ion-specific temperature-responsive gating membranes grafted with a copolymer of NIPAAm and benzo-18-crown-6-acrylamide (BCAm). The benzo-18-crown-6 residues in the grafted copolymers can recognize specific ions (e.g., $Pb^{2+}$, $Ba^{2+}$, $Sr^{2+}$, and $K^{+}$), and the binding with ions induces a change in the phase transition temperature [200], as shown in Fig. 4.13b. By inducing a shift in LCST, the swelling/shrinking behavior of grafted P(NIPAAm-*co*-BCAm) was controlled at a certain temperature by adding a specific ion, resulting in temperature-responsive permeability. Using a

similar concept, $\beta$-cyclodextrin residues were incorporated into grafted PNIPAAm on porous membranes to modulate the phase transition temperature by the specific binding of naphthalene derivatives [201]. Kuroki et al. [202] developed a biomolecular recognition gating system based on thermoresponsive phase transitions assisted by the binding of avidin to biotinylated NIPAAm copolymer grafted onto porous membranes. In this system, linear P(NIPAAm-*co*-biotin-PEG2-acrylamide) modified on the surfaces of porous membranes can specifically bind biotin residues with avidin molecules to induce the cross-linking of grafted copolymers in the pores at a temperature lower than the LCST. Since nonspecifically bound molecules in a membrane pore do not produce cross-linking, permeability with biomolecular recognition can be achieved by shrinking the grafted copolymers by increasing the temperature to above the LCST, as shown in Fig. 4.13c. In fact, the avidin-bound smart porous membranes exhibited a dramatic decrease in permeability above 30 °C, although the permeability coefficients with nonspecific biomolecules were almost the same as that without biomolecules in the temperature range of 15–45 °C. These smart membranes with bioaffinity are highly attractive for use in controlled release systems, chemical separation systems, sensors and actuators, and so forth.

Compared with smart gating membranes, stimuli-responsive actuators comprising smart polymer-grafted surfaces have been less reported because of the small mechanical forces generated by the swelling/shrinking behavior of the ultrathin polymer layers. Bulk hydrogels and shape-memory polymers (SMPs) have been mainly studied as smart actuating materials (see Chaps. 2 and 7). Recently, nanoscale deformation in response to external stimuli has been demonstrated using smart-polymer grafting techniques [203]. Aizenberg and co-workers have developed hydrogen-actuated integrated response system (HAIRS), in which soft and hard elements are combined to enable the reversible actuation of rigid surface nano- and microstructures by polymer layers [204, 205]. For example, they covalently modified PAAm hydrogel layers on a silicon substrate with an array of high-aspect-ratio nanocolumns mediated with poly(glycidyl methacrylate) (PGMA) grafting [205], as shown in Fig. 4.14a. The nanocolumns were put in motion by the "muscle" of the ultrathin hydrogel layers, which swell or contract depending on the humidity. The actuation in response to changes in humidity can be controlled to produce a variety of reversible elaborate micropatterns. By further controlling the stress field in the substrate and with the assistance of a catalytic reaction, Aizenberg and co-workers demonstrated a self-regulating, self-powered, homeostatic material capable of precisely tailored chemo-mechanochemical feedback loops at the nano- or microscale [204]. Although smart bending has only provided microscopic actuation so far, Zou et al. [206] investigated the macroscopic stimuli-responsive bending and stretching of soft plasticized poly(vinyl chloride) (pPVC) by grafting PDMAAm at a high graft density onto its surface by surface-initiated ATRP. In this protocol, PDMAAm was grafted onto one or both sides of the pPVC surfaces to control bending and stretching, respectively, and the degree of deformation depended on the polymerization time owing to the increase in the graft density of the polymer chains (Fig. 4.14b). The PDMAAm-grafted substrates exhibited reversible deformation during the drying-wetting process, and provided

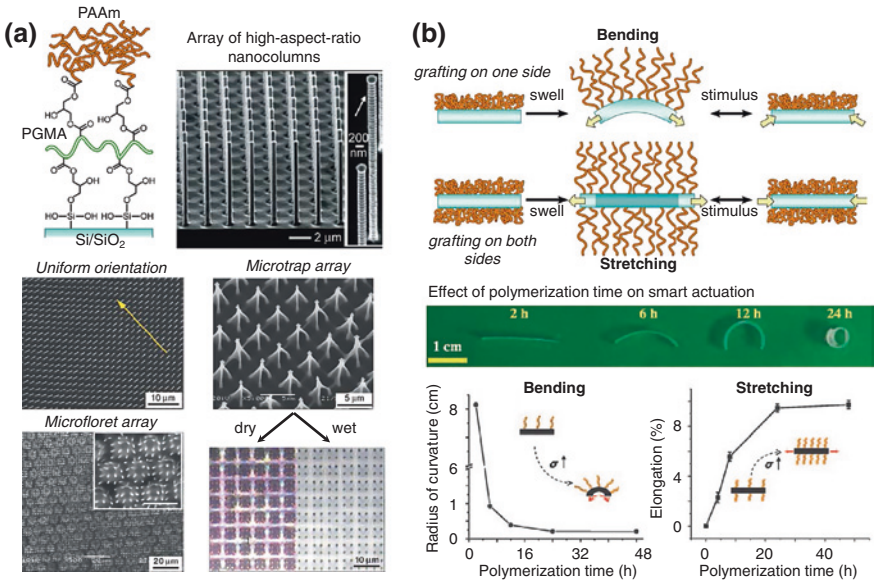


**Fig. 4.14** Stimuli-responsive mechanical actuation by conformational changes in smart polymer grafted on substrates. **a** Reversible actuation of nanocolumn arrays grafted with PAAm/PGMA layers depending on humidity level [204], and **b** bending and stretching actuation of PDMAAm-grafted pPVC substrate by drying–wetting process [205]

even higher actuator strain than that of some electro-active polymers (EAPs) upon the application of a moderate force per unit length. In addition, they attempted to prepare temperature- and pH-responsive actuators using NIPAAm and aminopropyl methacrylate (APMA), resulting in successful deformation and reversibility in the copolymer with PDMAAm upon temperature and pH switching. Although these stimuli-responsive actuators using smart polymer-grafted surfaces still have lower mechanical performance than bulk materials, these technologies have the potential to be used in artificial muscles and for microscopic manipulation in biomedical science and nanotechnology.

### *4.5.4 Chromatography*

High-performance liquid chromatography (HPLC) has been routinely used to separate and purify mixed molecules in the field of analytical chemistry. Commonly, the purpose of HPLC separation has been to control the partitioning of analytes between mobile and stationary phases. The types of HPLC separation are classified in terms of the molecular interactions between analytes and stationary phases, which depend on their polarity, hydrophobic property, electrostatic property, chirality, molecular size, and biospecificity. In particular, reverse-phase liquid

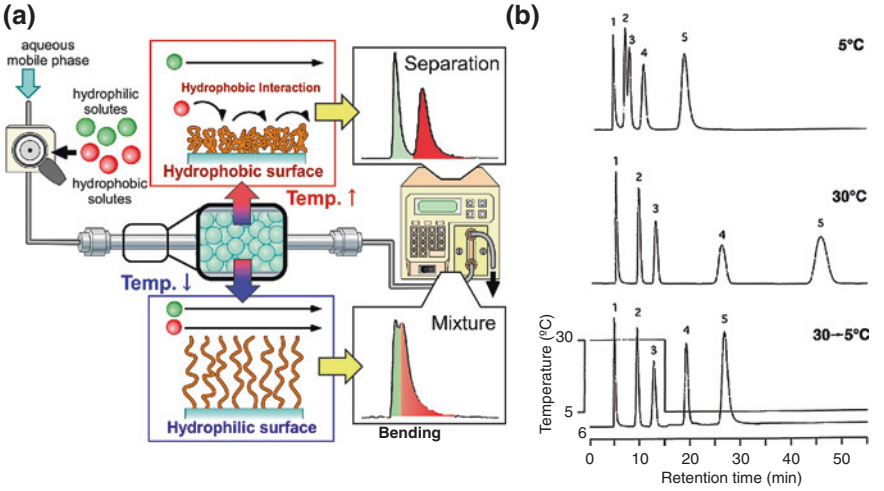


**Fig. 4.15** Smart chromatography. **a** Aqueous temperature-responsive chromatography system using PNIPAAm-grafted porous silica particles, and **b** chromatograms of a mixture of four steroids and benzene with step gradient obtained by changing column temperature (peaks: *1* benzene, *2* cortisone, *3* prednisolone, *4* hydrocortisone acetate; and *5* testosterone) [207]

chromatography (RPLC) based on the control of hydrophobic interactions is one of the most commonly used HPLC tools because of its fast separation and simple operation via only changes in the elution process. However, organic solvents are needed to control the retention and selectivity of the analytes in conventional RPLC. This leads to the denaturation and loss of bioactive molecules and generates a large amount of organic waste fluids, which are harmful to the environment. Therefore, the simple modulation of the surface properties of stationary phases under aqueous conditions has been desired to avoid the use of organic solvents for inducing changes in mobile phase properties in pharmaceutical and biological separation and purification. Kanazawa et al. [207] developed a novel chromatography system with a constant aqueous mobile phase using PNIPAAm-grafted silica beads as a stationary phase. Changes in the structure and properties of the grafted PNIPAAm chains can induce the "on/off" switching of hydrophobic interactions between the PNIPAAm-grafted stationary phase and biomolecules via changes in the hydrophilic/hydrophobic property in response to changes in the external temperature (Fig. 4.15a). In this system, the separation of mixed solutes can be achieved simply by regulating the external temperature under isocratic aqueous mobile phases, making this method suitable for the separation of bioactive compounds such as peptides and proteins. In the early stages of such aqueous thermoresponsive chromatography, free ends of PNIPAAm chains were grafted onto aminopropyl silica surfaces via an activated ester-amine coupling reaction. On the thermoresponsive column, an increase in the retention times of various steroids was observed with increasing temperature, particularly between 25 and 35 °C; this

temperature range includes the LCST of PNIPAAm. In an ordinary RPLC column, the retention times of steroids decrease at a high temperature by the decreasing adsorption of solute molecules on the stationary phases owing to the enhanced molecular mobility. In the smart chromatography system, the elution behavior of mixed steroids can be dynamically modulated using a column packed with silica beads grafted with the NIPAAm copolymerized with hydrophobic BMA by applying a step temperature gradient [208], as shown Fig. 4.15b. These steroids were not resolved on the thermoresponsive column at the lower partition at a temperature of 5 °C, while a relatively long analysis time was required for sufficient separation of the steroids at 30 °C. When the column temperature was decreased to 5 °C after the separation of the solutes with lower hydrophobicity at 30 °C, the retention times of the steroids with higher hydrophobicity were decreased, resulting in the steroids being separated earlier than in the case of applying a high temperature. This was due to the effective changes in the thermodynamic property of PNIPAAm-grafted surfaces. Thus, smart thermoresponsive HPLC systems are advantageous for controlling the retention times of analytes by simply modulating the external temperature without the addition of organic solvents to the mobile phases, and the separation of various biomolecules using this system has been demonstrated such as peptides [208] and proteins [209], in addition to the metabolism of drugs [210].

In thermoresponsive smart chromatography, the graft conformation of PNIPAAm on the surface is essential for separation efficiency because the chain mobility is strongly affected by the modulation of the surface properties by changes in temperature. Kikuchi and Okano [42] reported the effect of the graft architecture of PNIPAAm on column matrix surfaces on the elution behavior of steroids. Although surfaces grafted with the free ends of PNIPAAm exhibited sharp retention peaks, their retention times were relatively short because of the low graft density resulting from the ‘grafting to’ method. Longer retention and effective modulation of the elution appeared in the case of grafting the free PNIPAAm onto PNIPAAm looped chain grafted surfaces than the surfaces with grafted PNIPAAm loops, owing to the increased number of PNIPAAm layers on the surfaces after modification with the free ends of PNIPAAm chains. As surfaces with PNIPAAm hydrogel layers have a three-dimensional cross-linked structure, the peaks of steroids in chromatograms are significantly broadened by the penetration of analyte molecules into the cross-linked structure and the restriction of the mobility of PNIPAAm chains. Nagase et al. [88] investigated the effects of graft density and chain length on the separation efficiency of steroids by the ‘grafting from’ surface-initiated ATRP method. Shorter PNIPAA brushes with a low graft density exhibited longer retention times for steroids than brushes with a high density owing to the interaction with the exposed hydrophobic silinized surface of silica particles. On the other hand, the retention on less dense PNIPAAm brush surfaces with longer chains increased above the LCST of PNIPAAm, because at a lower temperature the hydrated PNIPAAm chains prevent the hydrophobic interactions with the basal silinized surface. In denser and longer PNIPAAm brush columns, the restricted mobility of the grafted PNIPAAm chains leads to

partial dehydration over a broad temperature range, resulting in small changes in the retention of steroids. Thus, the elution behavior of analyte molecules is significantly affected not only by the architecture of grafted PNIPAAm chains on the surface but also by the properties of the packed basal silica beads [211].

Another design parameter of smart stationary phases is the packing state of the silica beads in the column. The packing state affects the diffusion pathway and flow resistance, which are fundamental factors of chromatographic separation efficiency. Over the past decade, monolithic columns comprising silica and a polymer have attracted attention as new chromatographic matrices that can be used as alternatives to packed silica beads [212]. Monolithic silica columns have a three-dimensional interconnected skeleton structure that provides high porosity, low resistance to hydraulic flow, and fast mass transfer. Temperature- and pH-responsive smart polymers have been directly grafted onto monolithic columns, and their effectiveness in separating steroids [213] and proteins [214, 215] has been investigated. For biomolecular separation in aqueous mobile phases, the type of substance used with the chromatographic matrices is also an important factor because acidic and/or alkaline conditions may hinder the surface modification of smart polymers, particularly in the case of silica-based materials. Nagase et al. [216] examined the stability in neutral- to high-pH mobile phases to determine the reproducibility of separating steroids using various graft configurations of PNIPAAm on silica beads. Dense brush structures of PNIPAAm exhibited high separation reproducibility under an alkaline condition because the polymer brushes prevented the access of water to basal silica surfaces, thus inhibiting the hydrolysis of silica and the cleavage of grafted polymers. The incorporation of hydrophobic *tert*-butylacrylamide (tBAAm) into PNIPAAm brushes leads to the reproducible separation of steroids with greater resistance to alkaline conditions. As another approach to improving the separation stability, polymer-based materials have been used for chromatographic matrices. Mizutani et al. [217] reported the ATRP of NIPAAm from polymer-based porous beads chloromethylated by the Friedel-Crafts reaction using $ZnCl_2$, and the effective separation of angiotensin subtypes and insulin [218]. In pH-responsive chromatography, polymer matrices have been often used to change the pH of aqueous mobile phases within a wide range [214, 219].

On the basis of the concept of thermoresponsive separation using PNIPAAm-grafted surfaces, various types of smart chromatography have been proposed. Generally, thermoresponsive ionic copolymers exhibit an apparent shift in p$K_a$ depending on temperature changes [220], and polymer-grafted surfaces can control the simultaneous hydrophobic and electrostatic interactions via changes in the charge density under thermal stimuli. Kobayashi et al. [221, 222] exploited smart ion-exchange chromatography to obtain a dual response to pH and temperature using cross-linked P(NIPAAm-*co*-AAc-*co*-tBAAm)-grafted silica bead surfaces. The retention times of catecholamines and angiotensin subtype derivatives for the copolymer-grafted column were reduced above the LCST as a result of the decrease in anionic charge density at a neutral pH by the aggregation of copolymers. On the other hand, more of the analytes were retained in the stationary

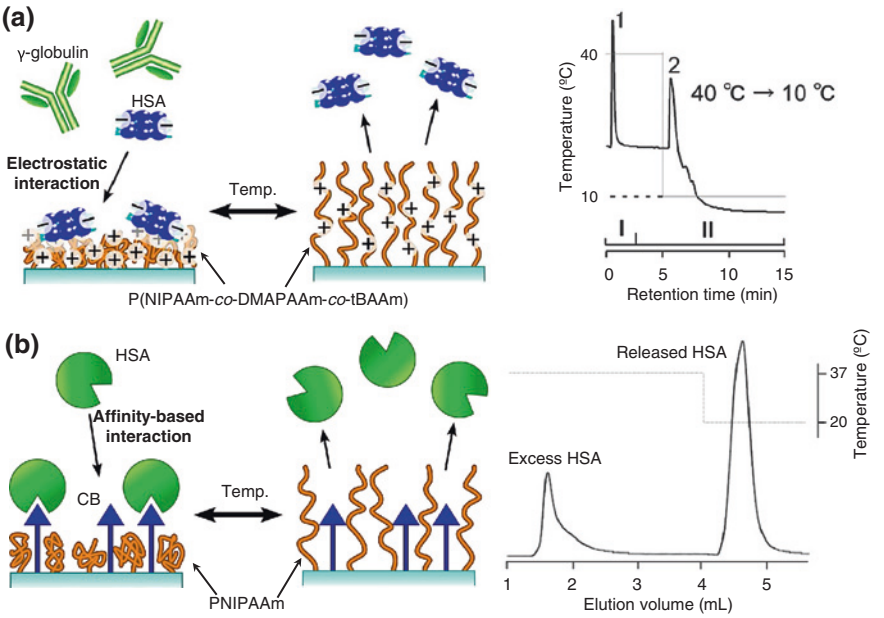


**Fig. 4.16** Protein purification in ion-exchange and affinity smart chromatography using step temperature gradient. **a** Electrostatic-interaction-driven HAS separation using P(NIPAAm-co-DMAPPAm-co-tBAAm)-grafted silica particles (chromatogram peaks: *1* γ-globulin, *2* HAS) [223], and **b** affinity regulation based on effects of forced release induced by conformational changes in PNIPAAm chains grafted on silica particles [226]

phases via a hydrophobic interaction with increasing temperature below the LCST at pH = 7.0 and between 10 and 50 °C under an acidic condition below the p$K_a$ of the copolymers. Employing a similar mechanism to that of the apparent shift in p$K_a$, the incorporation of cationic DMAPPAm into PNIPAAm grafted onto silica beads was used for the separation of oligonucleotides [223] and plasma proteins [224] through thermoresponsive changes in cationic charge densities (Fig. 4.16a).

Smart polymer-grafted surfaces exhibit not only hydrophilic/hydrophobic property changes but also coil/globule transitions of the polymer chains in response to external stimuli. Using the conformational changes in grafted PNIPAAm chains on surfaces, smart SEC has been investigated as a means of controlling the pore sizes of materials packed in columns by changing the temperature. Gewehr et al. [18] prepared free-end PNIPAAm-grafted porous silica beads through a coupling reaction between amino and carboxyl groups for the size-dependent separation of dextrans with changes in temperature. In the conventional SEC mode, substances with smaller molecular weights are retained longer owing to their permeation through the column matrices. In the case of PNIPAAm-grafted surfaces, the molecular-weight-dependent retention times of dextran samples were observed, similarly to normal SEC, and the elution was discontinuously extended by increasing the temperature because of the larger pores resulting from the aggregation of

PNIPAAm chains above the LCST. The successful size-dependent separation of various compounds has been demonstrated using this smart SEC [225]; however, the retention times for some proteins were longer at high temperatures, probably owing to the interaction of the hydrophobic segments of the proteins with the hydrophobized PNIPAAm-grafted surfaces [226]. Thus, the control of the pore size and the nature of the polymer-grafted surfaces is important to precisely modulate the elution behavior in smart SEC systems.

The conformational changes of grafted PNIPAAm chains were also utilized for smart affinity chromatography through their excluded volume effects. Yoshizako et al. [227] controlled the affinity binding of serum albumin to Cibacron Blue F3G-A (CB) by changing the expansion/aggregation of grafted PNIPAAm chains in a chromatographic column. In this system, the lengths of free-end PNIPAAm chains and spacer molecules between CB and silica bead surfaces were precisely controlled to regulate the access of serum albumin to CB by changing the PNIPAAm conformation (Fig. 4.16b). At temperatures above the LCST of PNIPAAm, serum albumin can conjugate to CB because the length of the aggregated PNIPAAm chains was smaller than that of the CB bound with the spacers. When lowering the temperature to below the LCST, the expansion of grafted PNIPAAm reduced the binding capacity between serum albumin and CB by their excluded volume effects, leading to the release of the proteins from the surfaces. Such thermally modulated affinity binding/release of target molecules can also be achieved by the incorporation of ligands with affinity into PNIPAAm chains grafted on silica beads, for example, using lactose/galactose-specific lectin [228] and phenylboronic acid (PBA) [229] as ligands for glycoprotein and *cis*-diol compounds as target molecules, respectively.

As described above, thermoresponsive PNIPAAm has been mainly used for the surface modification of chromatographic matrices; thus, their performance is adversely affected by changes in temperature in the entire column or in aqueous mobile phases. We have developed a self-heating system using magnetite nanoparticles as the stationary phase for thermoresponsive chromatography (Fig. 4.17a), which generate heat through magnetic hysteresis following the application of an alternating magnetic field (AMF) [230]. CIPAAm was copolymerized with NIPAAm to modify aminopropylsilane on a magnetite–silica composite via a coupling reaction, and smart polymer-grafted magnetic nanoparticles (MNPs) were packed into a chromatography column and used for the separation of steroids [231]. The retention times of all steroids using the P(NIPAAm-*co*-CIPAAm)-grafted column increased because the surface became hydrophobic owing to AMF-mediated heat generation, whereas these changes were not observed without the application of an AMF. Compared with the retention times of steroids determined by the above-mentioned thermoresponsive chromatographic methods, the temperature around the packed MNPs was estimated to be 48 °C in spite of the constant room temperature of the entire column and eluent. Therefore, this smart chromatography system could be useful for the separation of bioactive compounds by locally controlling the temperature of the grafted surface simply by the ‘on–off’ switching of an AMF. Yagi et al. [232] also modulated the elution behavior

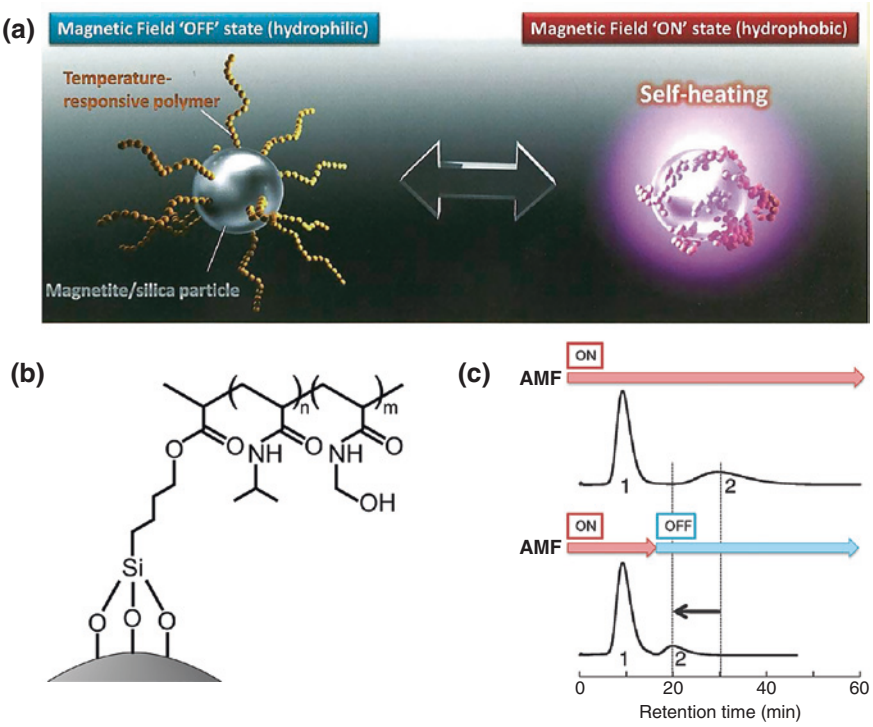


**Fig. 4.17** Self-heating smart polymer-grafted particles for thermoresponsive chromatography by applying AMF [232]. **a** Schematic illustration of self-heating system to induce phase transition of thermoreponsive polymer grafted on magnetite nanoparticles, **b** chemical structure of P(NIPAAm-HMAAm)-grafted magnetite nanoparticles, **c** modulation of steroid elution on self-heating smart column by 'on–off' switching of AMF (chromatogram peaks: *1* hydrocortisone; *2* testosterone)

of steroids via the graft architecture of polymers on magnetic surfaces by changing the contents of carboxyl groups in the polymers, which were bound at various points to the aminated surfaces. Techawanitchai et al. [233] investigated the effect of thermal dynamics under an AMF on the retention times of steroids using free-end P(NIPAAm-*co*-hydroxymethylacrylamide (HMAAm))-grafted magnetite/silica nanoparticles (Fig. 4.17b). The temperature of MNPs subjected to an AMF rapidly increased to 60 °C within 15 min, and the retention times of steroids were also significantly increased after 10–15 min of AMF irradiation following the self-heating generation of magnetic nanoparticles. On the basis of the elution kinetics under an AMF, the elution process for steroids can be modulated to shorten the total analysis time by turning off the AMF during the elution process, as shown in Fig. 4.17c. In this system, the relationship between the LCST of the grafted polymers and the dynamics of the self-heating generation from the MNPs is important for regulating the elution behavior, and its optimization will enable the more accurate, prompt, and simpler control of biomolecular separation.

### 4.5.5 Microfluidics

Since Terry et al. [234] initially proposed the assembly of silicon micromechanical devices for miniaturized gas chromatography in the 1970s, there have been many studies on exploiting the potential benefits of microsize apparatus compared with systems of a conventional size. These miniaturized microfluidic devices have been rapidly advanced by the elucidation of microscopic features on a microchannel surface and the development of microfabrication technologies as described in Sect. 4.3.2. From the physical characteristics in the microchannel, microfluidic systems with various advantages can be obtained, including the reduced consumption of reagents, a short analysis time, sensitivity, portability allowing in situ and real-time analysis, and disposability [235]. The predominant physical factors in a microspace, which are different from those at the laboratory scale, should be understood for the development of microfluidic devices. The predominant factors in microfluidics include laminar flow, molecular diffusion, specific surface area, and surface tension [44]. Laminar flow is stable in a fluid stream that is independent of time and is determined by the Reynolds number (*Re*) as follows:

$$Re = \rho v D_h / \mu, \tag{4.8}$$

where $\rho$ is the fluid density, $v$ is the linear velocity of the fluid, $\mu$ is the fluid viscosity, and $D_h$ is the hydraulic diameter; these factors depend on the cross-sectional geometry of the channel. The fluid generally exhibits a laminar flow at a small *Re* (<2,300). Since *Re* depends on the flow rate and channel dimensions, the laminar flow in a microchannel can always be observed under ordinary flow conditions. The laminar flow allows two or more continuous streams of heterogeneous fluids in contact with each other. The diffusion process involves the dispersion of a solvent with a high concentration throughout a volume over time, where the rate of diffusion is estimated by Fick's one-dimensional law,

$$\partial C / \partial t = -D \partial^2 C / \partial x^2, \tag{4.9}$$

where $C$ is the solute concentration at the distance $x$ and time $t$, and $D$ is the diffusion coefficient of the solute. Decreasing the channel dimensions results in a shorter diffusion time, leading to quicker mixing through molecular diffusion in the microchannel. Specific surface area is one of the most important factors in surface chemistry in a microchannel, which is inversely proportional to the distance. The increase in the specific surface area when using a microchannel is considerable, which can provide not only enhanced molecular interaction at the interfaces but also a small heat capacity. Such a large specific surface area induces a large effect of surface tension rather than gravitational force. The pressure derived from the surface tension ($\gamma$) at an interface between the liquid and gas phases is described by the Young–Laplace equation,

$$\Delta P = 2\gamma \cos\theta / d, \tag{4.10}$$

where $\theta$ is the contact angle of the surface and $d$ is the channel radius; thus, the surface wettability of microchannel walls is a key factor in controlling the

microfluid. Regarding these distinctive features of microchannels, the surface properties are critical in microfluidic systems, and a variety of possible applications in the biomedical and analytical fields have been demonstrated using the smart polymer grafting approach.

Manipulating the flow in microchannels using valves is essential for many microfluidic applications to control chemical and biological processes under a continuous flow. A number of miniaturized mechanical valves fabricated by micromachining technologies have been developed; however, these valves require the construction of complicated movable vents and parts for external control of the channels. Alternatively, stimuli-induced valves of miniaturized hydrogels comprising smart polymers can be prepared in microchannels by photopolymerization through a photomask. Beebe et al. [236] developed the first valve made of pH-sensitive P(AAc-*co*-HEMA) micro-hydrogel in a microchannel, and the flow was controlled by changing the volume, which depended on the pH of the fluid. This concept of hydrogel valves has been widely applied using various smart polymers to control microfluids using the temperature, UV, or an electromagnetic field as a trigger [237]. As a further advance in smart microvalves, there have been reports of thermoresponsive microfluidic valves comprising PNIPAAm-grafted surfaces [238]. A nanolayered PNIPAAm-grafted capillary (polymer thickness: ~200 nm) showed a high flow resistance at 10 °C and an identical pressure drop to that of a bare capillary of 50 μm diameter above 30 °C. Interestingly, the back pressure observed for larger-diameter PNIPAAm-grafted capillaries does not change with temperature. Therefore, the microviscosity of the aqueous solution only affects the pressure-driven flow at a hydrated polymer layer interface in smaller capillaries and at temperatures below the LCST. Using a PNIPAAm-grafted capillary, the oscillatory on/off control of a microfluid can be observed by inducing dynamic cycles of stepwise temperature switching between 30 and 35 °C. The relative contributions of the interactions between the surface and bulk phases become significant, and the surface wettability can dominate the fluid dynamics within microchannels. Thus, microchannel surface modification is frequently employed to regulate microfluidics. For instance, laminar flow switching in microchannels can be dynamically modulated through electrowetting [239], and the stop valves for microfluidics can be fabricated by the superhydrophobic patterning of microchannel surfaces [240]. Such microfluidic valves are expected to be the focus of increased attention in the near future because numerous studies will be required to achieve the regulation of surface properties using smart polymers.

Realizing practical applications of biomicrofluidic systems for total analysis on a chip will require the miniaturization components used to purify target analytes within a microchannel. Microfluidic technologies are suitable for addressing the enormous and diverse challenges in the development of effective separation systems. Capillary electrophoresis is an electrokinetic manipulation technique used to separate biomolecules according to their electrostatic properties and is typically used in microfluidics [241]. In pressure-driven microfluidic separation based on conventional HPLC, the surface area is increased using fabrication techniques to enhance the molecular interaction with stationary phases [242]. The applicability of these

approaches has been investigated in many studies; however, there are disadvantages associated with the use of high voltages and organic solvents even now. Utilizing smart polymer-grafted surfaces as a stationary phase in microchannels allows the elution control of bioactive compounds in a single aqueous mobile phase, similarly to in conventional thermoresponsive HPLC. In addition, the small heat capacity of smart polymer-grafted microchannels, which is one of their microfluidic features, is effective for rapidly controlling their surface properties. We have demonstrated microfluidic elution control using PNIPAAm-grafted capillaries [101]. The baseline separation of steroids in PNIPAAm-grafted capillaries was successfully achieved within 10 min simply by increasing the temperature, and the hydrophobic interaction was enhanced by the graft copolymerization of NIPAAm and hydrophobic BMA [102]. Huber et al. [243] developed thermoresponsive microfluidic devices that were programmed to dynamically adsorb and release proteins upon changes in temperature. The adsorption of myoglobin on a microfluidic device containing a PNIPAAm film took less than 1 s after heating to a value above the LCST, and the desorption process was completed within 2 s with decreasing temperature. This result indicates that the specific characteristics of the heating and cooling cycles in microchannels lead to dynamic and rapid switching of the surface properties. Chen and Li [244] used a PNIPAAm-grafted surface to extract a specific genomic DNA sequence from human blood using a microfluidic system. In this system, target DNA molecules were captured by grafted PNIPAAm layers at 25 °C through hydrogen bonding, and released from the layers as a result of their shrinkage upon heating to 60 °C.

While these examples of separation are driven by nonspecific interactions, Stayton and co-workers have investigated a novel affinity-based purification technique based on the biotin-SA system using nanoparticles modified with PNIPAAm chains [245–249]. They first comodified PINPAAm and biotinylated PEG on nanoparticle surfaces to simultaneously control the reversible adsorption on microfluidic channel walls and the capture/release of target biotinylated biomolecules through the use of SA molecules to bridge the nanoparticles via temperature changes (Fig. 4.18a) [249]. The eluted samples after temperature switching contain only target anti-digoxin IgG, which competes with digoxigenin when using this protocol. This platform is completely general in that any biomolecule that can be biotinylated and bound to the surface of nanoparticles can be immobilized in a microfluidic channel. Advances in smart purification techniques using microfluidic systems have allowed PNIPAAm to be grafted onto microchannel walls to provide complementary surface traps (Fig. 4.18b) [245], enabling MNPs to be easily manipulated [247] as well as the incorporation of a circular reactor and transverse flow in a microchip to enhance the efficiency of capture/release [246]. Recently, Lai et al. [248] have explored bioseparation and target isolation under a continuous flow process using MNPs grafted with pH-responsive polymers. In this process, biotinylated P(*tert*-butyl methacrylate (tBMA)-*co*-NIPAAm)-grafted MNPs are conjugated with SA, and are aggregated to capture target molecules in the lower-pH (=7.4) stream of two laminar flows, where the other stream has a pH of 8.3 (Fig. 4.18c). The conjugated MNPs move into the higher-pH stream upon the application of a magnetic field, and consequently, only bound target analytes can

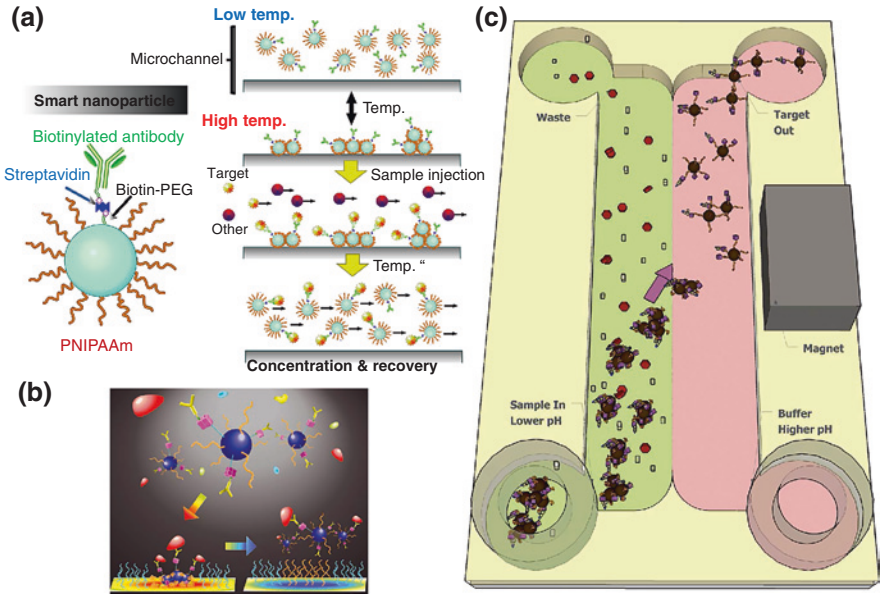


**Fig. 4.18** Smart microfluidic immunoassay. **a** Diagrammatic representation of the smart bead immunoassay system, **b** switchable surface traps of smart nano-particles using PNIPAAm-grafted microchannels [244], **c** target analyte separation in a microfluidic channel facilitated by pH-responsive MNPs under isothermal conditions. The left stream (*green*) is a sample that has been preincubated with MNPs. MNP aggregation is induced by adding a lower-pH buffer in the sample flowstream. The pH of the right stream (*pink*) is chosen to reverse MNP aggregation. A rare-earth magnet provides a sufficient magnetic field to attract the aggregates laterally into the higher-pH flowstream. The conjugate aggregates move out of the sample flowstream and into the higher-pH stream, where they return to a dispersed state, carrying the bound target analyte with them [247]

be recovered from the outlet. This stimuli-responsive purification system has been shown to transfer 81 % of a model protein target from an input flow stream to a second flowstream in a continuous-flow H-filter device. Such affinity-based conjugation using smart polymer-grafted surfaces in microchannels is promising for the purification of diagnostic targets and immunoassay on a point-of-care microchip.

Microfluidic-based cell research has made significant advances over the past decade for biological assay, cell sorting, and tissue engineering [250]. This is because microchannels enable the duplication of complicated geometries and allow the mimicking of networks in vivo and can be fabricated with microscale sizes similar to those of living cells. The control of cell adhesion using smart polymer-grafted surfaces for microfluidic biological studies and biomedical applications has recently been reported. Ernst et al. [251] reported the effect of shear stress on cell detachment from P[NIPAAm-*co*-poly(ethyleneglycol)methacrylate (PEGMA)]-grafted surfaces in a microchannel. The number of fibroblasts that detached from the surface at 25 °C increased with increasing flow velocity up to 300 μm/s, whereas hardly any cells detached at 37 °C at flow velocities of above

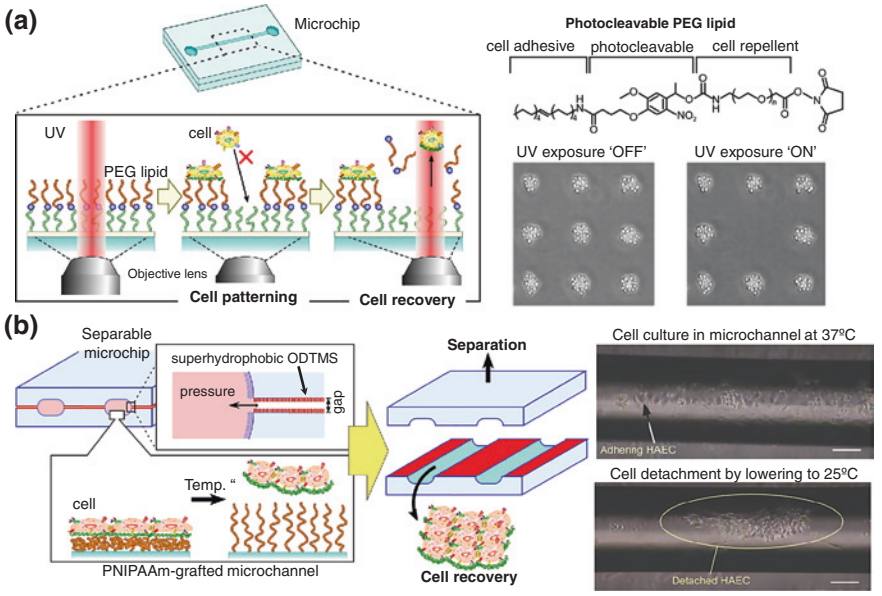


**Fig. 4.19** Control of cell adhesion in microchannels grafted with smart polymers. **a** Dynamic cell patterning in microchannel using photocleavable smart PEG lipid-grafted surfaces [254], and **b** smart separable microchip with PNIPAAm and ODTMS patterned surfaces for harvesting of cultured cells in microchannels via temperature changes (scale: 100 μm) [256]

800 μm/s when shear stress was applied. Tang et al. [252] fabricated a microchip for systematic analysis to investigate the effect of shear stress by applying hydrodynamic resistance. Finding the effect of shear stress will be helpful for microfluidic cell research on controlling cell adhesion on smart polymer-grafted surfaces under various flow conditions. For cell screening and sorting in microfluidic systems, adhesion-controllable smart polymers containing PNIPAAm [253] and photocleavable biocompatible polymers [254] have been grafted with patterned structures onto microchannel surfaces. Yamaguchi et al. [255] used a PEG lipid consisting of an oleyl groupand an *o*-nitrobenzyl photocleavable linker as a grafted polymer to realize light-induced cell patterning in a microchannel. In this study, areas of the PEG chains were exposed to irradiation with UV to repel cell attachment with pinpoint accuracy, although the oleyl groups in the PEG lipid allowed cell adhesion on nonirradiated areas (Fig. 4.19a). Since the light-induced inhibition of cell adhesion enables in situ patterning with high resolution, this approach is suitable for developing techniques for heterogeneous cell assay and sorting in a microchannel. Although complicated tissue structures such as microvascular structures can be constructed by microfluidic cell culture [256], it has been difficult to harvest cells from a hermetic microchannel. If a reversible separable microchip is used to recover the cultured cells, the leakage from the microchannels during cell culture will induce contamination, damaging the cells. Yamashita et al. [257]

developed a smart separable microchip using pattern grafting with PNIPAAm and octadecyltrimethoxysilane (ODTMS). The superhydrophobic ODTMS patterns on the substrate surfaces except on the microchannels controlled the interfacial pressure at the liquid/vapor phase between two grafted substrates to suppress leakage from the slight gap, and the PNIPAAm patterns on the microchannel surfaces enabled the detachment of cultured cells upon decreasing the temperature (Fig. 4.19b). Using the microchip, HAECs proliferated in the microchannel under continuous flow conditions, and were harvested as a cell sheet by reducing the culture temperature from 37 to 22 °C. This strategy can potentially be used as a fundamental technique of cell recovery for vascular tissue engineering.

## 4.6 Conclusions and Future Trends

This chapter focused on the strategic design of smart polymer-grafted surfaces for biomaterial use. The smart surfaces in this chapter were categorized according to their graft architecture and substrate type, and synthesis and characterization methods were introduced to realize possible biomedical applications including adhesion control, cell culture, biomimetics, chromatography, and microfluidics. The preparation approaches of grafted surfaces mainly involve a 'grafting to' method or a 'grafting from' method, which enables the primary structure of the grafted polymers to be modulated using CLRP techniques. To characterize the chemical and structural features of ultrathin polymer layers, surface-specialized tools are required such as AFM, XPS, ellipsometry, and SPR. Some of these analytical tools can also be used to evaluate the phase transition behavior of grafted smart polymers in response to changes in a stimulus. The biomaterials allowing the grafting of smart polymers usually have the capability of either adhesion control or conformational changes on the surfaces. The control of biomolecular and cellular adhesion can be applied in practical biomedical applications including the harvest of cell sheets for tissue engineering and aqueous chromatographic separation. Stimuli-induced conformational changes allow the regulation of mass transport through nanopores and the mechanical actuation of modified substrates in a biomimetic manner. Recently, these concepts of smart surface application have been integrated into microfluidic devices to facilitate analytical and engineering processes using the physical characteristics in microchannels. These versatile applications through various types of stimuli switching have been achieved by the precise molecular and grafting design of smart polymers.

Surface properties are an essential factor of all biomaterials; thus, the grafting of stimuli-responsive polymers leads to a variety of biomaterial applications. Although there are numerous practical biomaterials using smart polymer-grafted surfaces, improving the reversibility, stability, and durability of the changes in stimuli-responsive surface properties is desired for implantable and industrial uses of smart surfaces as well as for conventional biocompatible surfaces. On the other hand, there are as many strategies as there are researchers in the design of

smart polymer-grafted surfaces. By the integration of these technologies, smart computing surfaces, such as DNA and protein computers [258, 259], could be fabricated by using multi-stimuli responsive properties, in addition to the realization of multicomponent grafting, signal transfer systems, high-speed nanoscopic detection, and so forth. Such an approach may not only have a scientific impact but also improve the conventional technologies used in smart polymer-grafted surfaces, enabling advances in biomaterial applications.

## References


1. Ratner BD, Hoffman AS, Schoen FJ, Lemons JE (2013) Biomaterials science: an introduction to materials in medicine, 3rd edn. Academic, New York
2. Castner DG, Ratner BD (2002) Biomedical surface science: foundations to frontiers. Surf Sci 500:28–60. doi:10.1016/s0039-6028(01)01587-4
3. Lee J, Lee H, Andrade J (1995) Blood compatibility of polyethylene oxide surfaces. Prog Polym Sci 20:1043–1079. doi:10.1016/0079-6700(95)00011-4
4. Lyman DJ, Loo BH (1967) New synthetic membranes for dialysis. IV. a copolyether-urethane membrane system. J Biomed Mater Res 1:17–26. doi:10.1002/jbm.820010105
5. Bots JGF, van der Does L, Bantjes A (1986) Small diameter blood vessel prostheses from blends of polyethylene oxide and polypropylene oxide. Biomaterials 7:393–399. doi:10.1016/0142-9612(86)90011-6
6. Park KD, Okano T, Nojiri C, Kim SW (1988) Heparin immobilization onto segmented polyurethaneurea surfaces—effect of hydrophilic spacers. J Biomed Mater Res 22:977–992. doi:10.1002/jbm.820221103
7. Ratner BD, Hoffman AS, Hanson SR, Harker LA, Whiffen JD (1979) Blood-compatibility-water-content relationships for radiation-grafted hydrogels. J Polym Sci Polymer Symposia 66:363–375
8. Okano T, Nishiyama S, Shinohara I, Akaike T, Sakurai Y, Kataoka K, Tsuruta T (1981) Effect of hydrophilic and hydrophobic microdomains on mode of interaction between block polymer and blood platelets. J Biomed Mater Res 15:393–402. doi:10.1002/jbm.820150310
9. Okano T, Aoyagi T, Kataoka K, Abe K, Sakurai Y, Shimada M, Shinohara I (1986) Hydrophilic-hydrophobic microdomain surfaces having an ability to suppress platelet aggregation and their in vitro antithrombogenicity. J Biomed Mater Res 20:919–927. doi:10.1002/jbm.820200707
10. Kataoka K, Okano T, Sakurai Y, Nishimura T, Maeda M, Inoue S, Tsuruta T (1982) Effect of microphase separated structure of polystyrene/polyamine graft copolymer on adhering rat platelets in vitro. Biomaterials 3:237–240. doi:10.1016/0142-9612(82)90026-6
11. Shimada M, Unoki M, Inaba N, Tahara H, Shinohara I, Okano T, Sakurai Y, Kataoka K (1983) Effect of adsorbed protein on the adhesion behaviour of platelet to the microdomain surface of 2-hydroxyethyl methacrylate-styrene block copolymer. Eur Polymer J 19:929–933. doi:10.1016/0014-3057(83)90051-4
12. Ishihara K, Aragaki R, Ueda T, Watenabe A, Nakabayashi N (1990) Reduced thrombogenicity of polymers having phospholipid polar groups. J Biomed Mater Res 24:1069–1077. doi:10.1002/jbm.820240809
13. Ishihara K, Nomura H, Mihara T, Kurita K, Iwasaki Y, Nakabayashi N (1998) Why do phospholipid polymers reduce protein adsorption? J Biomed Mater Res 39:323–330. doi:10.1002/(sici)1097-4636(199802)39:2<323:aid-jbm21>3.0.co;2-c
14. Jiang S, Cao Z (2010) Ultralow-fouling, functionalizable, and hydrolyzable zwitterionic materials and their derivatives for biological applications. Adv Mater 22:920–932. doi:10.1002/adma.200901407

15. Heskins M, Guillet JE (1968) Solution properties of poly(N-isopropylacrylamide). J Macromol Sci Part A Chem 2:1441–1455. doi:10.1080/10601326808051910
16. Okano T, Yamada N, Sakai H, Sakurai Y (1993) A novel recovery system for cultured cells using plasma-treated polystyrene dishes grafted with poly(N-isopropylacrylamide). J Biomed Mater Res 27:1243–1251. doi:10.1002/jbm.820271005
17. Nonaka T, Ogata T, Kurihara S (1994) Preparation of poly(vinyl alcohol)-graft-N-isopropylacrylamide copolymer membranes and permeation of solutes through the membranes. J Appl Polym Sci 52:951–957. doi:10.1002/app.1994.070520713
18. Gewehr M, Nakamura K, Ise N, Kitano H (1992) Gel permeation chromatography using porous glass beads modified with temperature-responsive polymers. Die Makromol Chemie 193:249–256. doi:10.1002/macp.1992.021930123
19. Barbey R, Lavanant L, Paripovic D, Schüwer N, Sugnaux C, Tugulu S, Klok H-A (2009) Polymer brushes via surface-initiated controlled radical polymerization: synthesis, characterization, properties, and applications. Chem Rev 109:5437–5527. doi:10.1021/cr900045a
20. Love JC, Estroff LA, Kriebel JK, Nuzzo RG, Whitesides GM (2005) Self-assembled monolayers of thiolates on metals as a form of nanotechnology. Chem Rev 105:1103–1170. doi:10.1021/cr0300789
21. Pease RF, Chou SY (2008) Lithography and other patterning techniques for future electronics. Proc IEEE 96:248–270. doi:10.1109/jproc.2007.911853
22. Fleer GJ, Stuart MAC, Scheutjens MHM, Cosgrove T, Vincent B (1993) Polymers at interfaces. Chapman & Hall, London
23. Matyjaszewski K, Xia J (2001) Atom transfer radical polymerization. Chem Rev 101:2921–2990. doi:10.1021/cr940534g
24. Feil H, Bae YH, Feijen J, Kim SW (1993) Effect of comonomer hydrophilicity and ionization on the lower critical solution temperature of N-isopropylacrylamide copolymers. Macromolecules 26:2496–2500. doi:10.1021/ma00062a016
25. Idota N, Ebara M, Kotsuchibashi Y, Narain R, Aoyagi T (2012) Novel temperature-responsive polymer brushes with carbohydrate residues facilitate selective adhesion and collection of hepatocytes. Sci Technol Adv Mat 13:064206
26. Xu C, Wu T, Mei Y, Drain CM, Batteas JD, Beers KL (2005) Synthesis and characterization of tapered copolymer brushes via surface-initiated atom transfer radical copolymerization. Langmuir 21:11136–11140. doi:10.1021/la051853d
27. Xu C, Barnes SE, Wu T, Fischer DA, DeLongchamp DM, Batteas JD, Beers KL (2006) Solution and surface composition gradients via microfluidic confinement: fabrication of a statistical-copolymer-brush composition gradient. Adv Mater 18:1427–1430. doi:10.1002/adma.200502341
28. Tomlinson MR, Genzer J (2008) Formation and properties of multivariant assemblies of surface-tethered diblock and triblock copolymers. Polymer 49:4837–4845. doi:10.1016/j.polymer.2008.08.048
29. Wang XJ, Bohn PW (2007) Spatiotemporally controlled formation of two-component counter propagating lateral graft density gradients of mixed polymer brushes on planar Au surfaces. Adv Mater 19:515–520. doi:10.1002/adma.200601516
30. Zhao B (2003) Synthesis of binary mixed homopolymer brushes by combining atom transfer radical polymerization and nitroxide-mediated radical polymerization. Polymer 44:4079–4083. doi:10.1016/s0032-3861(03)00322-7
31. Minko S, Patil S, Datsyuk V, Simon F, Eichhorn K-J, Motornov M, Usov D, Tokarev I, Stamm M (2002) Synthesis of adaptive polymer brushes via “grafting to” approach from melt. Langmuir 18:289–296. doi:10.1021/la015637q
32. Zhao B, He T (2003) Synthesis of well-defined mixed poly(methyl methacrylate)/polystyrene brushes from an asymmetric difunctional initiator-terminated self-assembled monolayer. Macromolecules 36:8599–8602. doi:10.1021/ma035285p
33. Luzinov I, Minko S, Tsukruk VV (2004) Adaptive and responsive surfaces through controlled reorganization of interfacial polymer layers. Prog Polym Sci 29:635–698. doi:10.1016/j.progpolymsci.2004.03.001

34. Gao C, Yan D (2004) Hyperbranched polymers: from synthesis to applications. Prog Polym Sci 29:183–275. doi:10.1016/j.progpolymsci.2003.12.002
35. Bergbreiter DE, Kippenberger AM (2006) Hyperbranched surface graft polymerizations. Adv Polym Sci 198:1–49. doi:10.1007/12_059
36. Mori H, Müller AHE (2003) Hyperbranched (meth)acrylates in solution, melt, and grafted from surfaces. Top Curr Chem 228:1–37. doi:10.1007/b11004
37. Kleinfeld ER, Ferguson GS (1996) Healing of defects in the stepwise formation of polymer/silicate multilayer films. Chem Mater 8:1575–1578. doi:10.1021/cm960073a
38. Lee PH, Sawan SP, Modrusan Z, Arnold LJ, Reynolds MA (2002) An efficient binding chemistry for glass polynucleotide microarrays. Bioconjug Chem 13:97–103. doi:10.1021/bc015523q
39. Yu WH, Kang ET, Neoh KG (2004) Controlled grafting of well-defined epoxide polymers on hydrogen-terminated silicon substrates by surface-initiated ATRP at ambient temperature. Langmuir 20:8294–8300. doi:10.1021/la036089e
40. Loveless DM, Abu-Lail NI, Kaholek M, Zauscher S, Craig SL (2006) Reversibly cross-linked surface-grafted polymer brushes. Angew Chem Int Ed 45:7812–7814. doi:10.1002/anie.200602508
41. Tugulu S, Klok H-A (2008) Stability and nonfouling properties of poly(poly(ethylene glycol) methacrylate) brushes under cell culture conditions. Biomacromolecules 9:906–912. doi:10.1021/bm701293g
42. Kikuchi A, Okano T (2002) Intelligent thermoresponsive polymeric stationary phases for aqueous chromatography of biological compounds. Prog Polym Sci 27:1165–1193. doi:10.1016/s0079-6700(02)00013-8
43. Wandera D, Wickramasinghe SR, Husson SM (2010) Stimuli-responsive membranes. J Membr Sci 357:6–35. doi:10.1016/j.memsci.2010.03.046
44. Beebe DJ, Mensing GA, Walker GM (2002) Physics andapplications of microfluidics in biology. Annu Rev Biomed Eng 4:261–286. doi:10.1146/annurev.bioeng.4.112601.125916
45. Sagiv J (1980) Organized monolayers by adsorption. 1. Formation and structure of oleophobic mixed monolayers on solid surfaces. J Am Chem Soc 102:92–98. doi:10.1021/ja00521a016
46. Hozumi A, Ushiyama K, Sugimura H, Takai O (1999) Fluoroalkylsilane monolayers formed by chemical vapor surface modification on hydroxylated oxide surfaces. Langmuir 15:7600–7604. doi:10.1021/la9809067
47. Xu FJ, Yuan ZL, Kang ET, Neoh KG (2004) Branched fluoropolymer-Si hybrids via surface-initiated ATRP of pentafluorostyrene on hydrogen-terminated Si(100) surfaces. Langmuir 20:8200–8208. doi:10.1021/la048706k
48. Okusa H, Kurihara K, Kunitake T (1994) Chemical modification of molecularly smooth mica surface and protein attachment. Langmuir 10:3577–3581. doi:10.1021/la00022a034
49. Schreiber F (2000) Structure and growth of self-assembling monolayers. Prog Surf Sci 65:151–257. doi:10.1016/s0079-6816(00)00024-1
50. Carlmark A, Larsson E, Malmström E (2012) Grafting of cellulose by ring-opening polymerisation—A review. Eur Polymer J 48:1646–1659. doi:10.1016/j.eurpolymj.2012.06.013
51. Coiai S, Passaglia E, Ciardelli F (2006) Gradient density grafted polymers on ground tire rubber particles by atom transfer radical polymerization. Macromol Chem Phys 207:2289–2298. doi:10.1002/macp.200600376
52. Matsukuma D, Yamamoto K, Aoyagi T (2006) Stimuli-responsive properties of N-isopropylacrylamide-based ultrathin hydrogel films prepared by photo-cross-linking. Langmuir 22:5911–5915. doi:10.1021/la060438y
53. Zasadzinski J, Viswanathan R, Madsen L, Garnaes J, Schwartz D (1994) Langmuir-blodgett films. Science 263:1726–1733. doi:10.1126/science.8134836
54. Ariga K, Hill JP, Ji Q (2007) Layer-by-layer assembly as a versatile bottom-up nanofabrication technique for exploratory research and realistic application. Phys Chem Chem Phys 9:2319. doi:10.1039/b700410a

55. Yamamoto K, Matsukuma D, Nanasetani K, Aoyagi T (2008) Effective surface modification by stimuli-responsive polymers onto the magnetite nanoparticles by layer-by-layer method. Appl Surf Sci 255:384–387. doi:10.1016/j.apsusc.2008.06.065
56. Ionov L, Zdyrko B, Sidorenko A, Minko S, Klep V, Luzinov I, Stamm M (2004) Gradient polymer layers by "grafting to" approach. Macromol Rapid Commun 25:360–365. doi:10.1002/marc.200300216
57. Yakushiji T, Sakai K, Kikuchi A, Aoyagi T, Sakurai Y, Okano T (1998) Graft architectural effects on thermoresponsive wettability changes of poly(N-isopropylacrylamide)-modified surfaces. Langmuir 14:4657–4662. doi:10.1021/la980090+
58. Kolb HC, Finn MG, Sharpless KB (2001) Click chemistry: diverse chemical function from a few good reactions. Angew Chem Int Ed 40:2004–2021. doi:10.1002/1521-3773(20010601)40:11<2004:aid-anie2004>3.0.co;2-5
59. Rühe J, Knoll W (2002) Functional polymer brushes. J Macromol Sci Part C Polym Rev 42:91–138. doi:10.1081/mc-120003096
60. Asatekin A, Barr MC, Baxamusa SH, Lau KKS, Tenhaeff W, Xu J, Gleason KK (2010) Designing polymer surfaces via vapor deposition. Mater Today 13:26–33. doi:10.1016/s1369-7021(10)70081-x
61. Wang J-S, Matyjaszewski K (1995) Controlled/"living" radical polymerization. Atom transfer radical polymerization in the presence of transition-metal complexes. J Am Chem Soc 117:5614–5615. doi:10.1021/ja00125a035
62. Sedjo RA, Mirous BK, Brittain WJ (2000) Synthesis of polystyrene-block-poly(methyl methacrylate) brushes by reverse atom transfer radical polymerization. Macromolecules 33:1492–1493. doi:10.1021/ma991549p
63. Matyjaszewski K, Dong H, Jakubowski W, Pietrasik J, Kusumo A (2007) Grafting from surfaces for "everyone": ARGET ATRP in the presence of air. Langmuir 23:4528–4531. doi:10.1021/la063402e
64. Hawker CJ, Bosman AW, Harth E (2001) New polymer synthesis by nitroxide mediated living radical polymerizations. Chem Rev 101:3661–3688. doi:10.1021/cr990119u
65. Husseman M, Malmström EE, McNamara M, Mate M, Mecerreyes D, Benoit DG, Hedrick JL, Mansky P, Huang E, Russell TP, Hawker CJ (1999) Controlled synthesis of polymer brushes by "living" free radical polymerization techniques. Macromolecules 32:1424–1431. doi:10.1021/ma981290v
66. Chiefari J, Chong YK, Ercole F, Krstina J, Jeffery J, Le TPT, Mayadunne RTA, Meijs GF, Moad CL, Moad G, Rizzardo E, Thang SH (1998) Living free-Radical polymerization by reversible addition−fragmentation chain transfer: the RAFT process. Macromolecules 31:5559–5562. doi:10.1021/ma9804951
67. Coote ML (2004) Ab initio study of the addition-fragmentation equilibrium in RAFT polymerization: when is polymerization retarded? Macromolecules 37:5023–5031. doi:10.1021/ma049444w
68. Zhao PS (2006) Synthesis of well-defined homopolymer and diblock copolymer grafted onto silica particles by Z-supported RAFT polymerization. Macromolecules 39:8603–8608. doi:10.1021/ma061586y
69. Otsu T, Yoshida M (1982) Role of initiator-transfer agent-terminator (iniferter) in radical polymerizations: polymer design by organic disulfides as iniferters. Die Makromolekulare Chemie Rapid Commun 3:127–132. doi:10.1002/marc.1982.030030208
70. Otsu T, Matsumoto A (1998) Controlled synthesis of polymers using the iniferter technique: developments in living radical polymerization. Adv Polym Sci 136:75–137. doi:10.1007/3-540-69682-2_3
71. Nakayama Y, Matsuda T (1996) Surface macromolecular architectural designs using photograft copolymerization based on photochemistry of benzyl N, N-diethyldithiocarbamate. Macromolecules 29:8622–8630. doi:10.1021/ma9606014
72. Bloomstein TM, Marchant MF, Deneault S, Hardy DE, Rothschild M (2006) 22-nm immersion interference lithography. Opt Express 14:6434. doi:10.1364/oe.14.006434

73. Srinivasan R, Braren B (1989) Ultraviolet laser ablation of organic polymers. Chem Rev 89:1303–1316. doi:10.1021/cr00096a003
74. Akiyama Y, Kikuchi A, Yamato M, Okano T (2004) Ultrathin poly(N-isopropylacrylamide) grafted layer on polystyrene surfaces for cell adhesion/detachment control. Langmuir 20:5506–5511. doi:10.1021/la036139f
75. Altissimo M (2010) E-beam lithography for micro-/nanofabrication. Biomicrofluidics 4:026503. doi:10.1063/1.3437589
76. Idota N, Tsukahara T, Sato K, Okano T, Kitamori T (2009) The use of electron beam lithographic graft-polymerization on thermoresponsive polymers for regulating the directionality of cell attachment and detachment. Biomaterials 30:2095–2101. doi:10.1016/j.biomaterials.2008.12.058
77. Ginger DS, Zhang H, Mirkin CA (2004) The evolution of dip-pen nanolithography. Angew Chem Int Ed 43:30–45. doi:10.1002/anie.200300608
78. Bullen D, Chung S-W, Wang X, Zou J, Mirkin CA, Liu C (2004) Parallel dip-pen nanolithography with arrays of individually addressable cantilevers. Appl Phys Lett 84:789. doi:10.1063/1.1644317
79. Xia Y, Whitesides GM (1997) Extending microcontact printing as a microlithographic technique. Langmuir 13:2059–2067. doi:10.1021/la960936e
80. Liu J, Cai B, Zhu J, Ding G, Zhao X, Yang C, Chen D (2004) Process research of high aspect ratio microstructure using SU-8 resist. Microsyst Technol 10:265–268. doi:10.1007/s00542-002-0242-2
81. Cappella B, Dietler G (1999) Force-distance curves by atomic force microscopy. Surf Sci Rep 34:1–104. doi:10.1016/s0167-5729(99)00003-5
82. Kidoaki S, Ohya S, Nakayama Y, Matsuda T (2001) Thermoresponsive structural change of a poly(N-isopropylacrylamide) graft layer measured with an atomic force microscope. Langmuir 17:2402–2407. doi:10.1021/la001522v
83. Danilatos GD (1988) Foundations of environmental scanning electron microscopy. Adv Electron Electron Phys 71:109–250. doi:10.1016/s0065-2539(08)60902-6
84. Seah MP (1980) The quantitative analysis of surfaces by XPS: a review. Surf Interface Anal 2:222–239. doi:10.1002/sia.740020607
85. Belu AM, Graham DJ, Castner DG (2003) Time-of-flight secondary ion mass spectrometry: techniques and applications for the characterization of biomaterial surfaces. Biomaterials 24:3635–3653. doi:10.1016/s0142-9612(03)00159-5
86. Felton MJ (2003) Product review: on the surface with auger electron spectroscopy. Anal Chem 75(269):271-A. doi:10.1021/ac031343t
87. Watts B, Ade H (2012) NEXAFS imaging of synthetic organic materials. Mater Today 15:148–157. doi:10.1016/s1369-7021(12)70068-8
88. Nagase K, Kobayashi J, Kikuchi A, Akiyama Y, Kanazawa H, Okano T (2008) Effects of graft densities and chain lengths on separation of bioactive compounds by nanolayered thermoresponsive polymer brush surfaces. Langmuir 24:511–517. doi:10.1021/la701839s
89. Idota N, Nagase K, Tanaka K, Okano T, Annaka M (2010) Stereoregulation of thermoresponsive polymer brushes by surface-initiated living radical polymerization and the effect of tacticity on surface wettability. Langmuir 26:17781–17784. doi:10.1021/la1024229
90. Tsujii Y, Ohno K, Yamamoto S, Goto A, Fukuda T (2006) Structure and properties of high-density polymer brushes prepared by surface-initiated living radical polymerization. Adv Polym Sci 197:1–45. doi:10.1007/12_063
91. Kim J-B, Huang W, Miller MD, Baker GL, Bruening ML (2003) Kinetics of surface-initiated atom transfer radical polymerization. J Polym Sci Part A Polym Chem 41:386–394. doi:10.1002/pola.10568
92. Burkert S, Bittrich E, Kuntzsch M, Müller M, Eichhorn K-J, Bellmann C, Uhlmann P, Stamm M (2010) Protein resistance of PNIPAAm brushes: application to switchable protein adsorption. Langmuir 26:1786–1795. doi:10.1021/la902505q

93. Kooij ES, Sui X, Hempenius MA, Zandvliet HJW, Vancso GJ (2012) Probing the thermal collapse of poly(N-isopropylacrylamide) grafts by quantitative in situ ellipsometry. J Phys Chem B 116:9261–9268. doi:10.1021/jp304364m
94. Proll G, Markovic G, Steinle L, Gauglitz G (2009) Reflectometric interference spectroscopy. Methods Mol Biol 503:167–178. doi:10.1007/978-1-60327-567-5_8
95. Biesalski M, Rühe J (2002) Scaling laws for the swelling of neutral and charged polymer brushes in good solvents. Macromolecules 35:499–507. doi:10.1021/ma001776n
96. Idota N, Tsukahara T, Ebara M, Aoyagi T in preparation
97. Takahashi H, Nakayama M, Yamato M, Okano T (2010) Controlled chain length and graft density of thermoresponsive polymer brushes for optimizing cell sheet harvest. Biomacromolecules 11:1991–1999. doi:10.1021/bm100342e
98. Mori S, Okamoto H (1980) A unified theory of determining the electrophoretic velocity of mineral particles in the rectangular micro-electrophoresis cell. Fusen 27:117–126
99. Good RJ (1992) Contact angle, wetting, and adhesion: a critical review. J Adhes Sci Technol 6:1269–1302. doi:10.1163/156856192x00629
100. Kikuchi A, Okano T (2005) Nanostructured designs of biomedical materials: applications of cell sheet engineering to functional regenerative tissues and organs. J Controlled Release 101:69–84. doi:10.1016/j.jconrel.2004.08.026
101. Idota N, Kikuchi A, Kobayashi J, Akiyama Y, Sakai K, Okano T (2006) Thermal modulated interaction of aqueous steroids using polymer-grafted capillaries. Langmuir 22:425–430. doi:10.1021/la051968h
102. Idota N, Kikuchi A, Kobayashi J, Sakai K, Okano T (2012) Modulation of graft architectures for enhancing hydrophobic interaction of biomolecules with thermoresponsive polymer-grafted surfaces. Colloids Surf B 99:95–101. doi:10.1016/j.colsurfb.2011.10.033
103. Tsuda Y, Kikuchi A, Yamato M, Sakurai Y, Umezu M, Okano T (2004) Control of cell adhesion and detachment using temperature and thermoresponsive copolymer grafted culture surfaces. J Biomed Mater Res 69A:70–78. doi:10.1002/jbm.a.20114
104. Lutz J-F (2011) Thermo-switchable materials prepared using the OEGMA-platform. Adv Mater 23:2237–2243. doi:10.1002/adma.201100597
105. Lim HS, Lee WH, Lee SG, Lee D, Jeon S, Cho K (2010) Effect of nanostructure on the surface dipole moment of photoreversibly tunable superhydrophobic surfaces. Chem Commun 46:4336. doi:10.1039/c0cc00323a
106. Tauk L, Schröder AP, Decher G, Giuseppone N (2009) Hierarchical functional gradients of pH-responsive self-assembled monolayers using dynamic covalent chemistry on surfaces. Nat Chem 1:649–656. doi:10.1038/nchem.400
107. Qing G, Wang X, Fuchs H, Sun T (2009) Nucleotide-responsive wettability on a smart polymer surface. J Am Chem Soc 131:8370–8371. doi:10.1021/ja9028632
108. Xia F, Feng L, Wang S, Sun T, Song W, Jiang W, Jiang L (2006) Dual-responsive surfaces that switch between superhydrophilicity and superhydrophobicity. Adv Mater 18:432–436. doi:10.1002/adma.200501772
109. Yuan W, Jiang G, Wang J, Wang G, Song Y, Jiang L (2006) Temperature/light dual-responsive surface with tunable wettability created by modification with an azobenzene-containing copolymer. Macromolecules 39:1300–1303. doi:10.1021/ma051989i
110. Sun T, Wang G, Feng L, Liu B, Ma Y, Jiang L, Zhu D (2004) Reversible switching between superhydrophilicity and superhydrophobicity. Angew Chem Int Ed 43:357–360. doi:10.1002/anie.200352565
111. Barthlott W, Neinhuis C (1997) Purity of the sacred lotus, or escape from contamination in biological surfaces. Planta 202:1–8. doi:10.1007/s004250050096
112. Annaka M, Yahiro C, Nagase K, Kikuchi A, Okano T (2007) Real-time observation of coil-to-globule transition in thermosensitive poly(N-isopropylacrylamide) brushes by quartz crystal microbalance. Polymer 48:5713–5720. doi:10.1016/j.polymer.2007.06.067
113. Rodahl M, Kasemo B (1996) A simple setup to simultaneously measure the resonant frequency and the absolute dissipation factor of a quartz crystal microbalance. Rev Sci Instrum 67:3238–3241. doi:http://dx.doi.org/10.1063/1.1147494

114. Sanjuan S, Perrin P, Pantoustier N, Tran Y (2007) Synthesis and swelling behavior of pH-responsive polybase brushes. Langmuir 23:5769–5778. doi:10.1021/la063450z
115. Plunkett KN, Zhu X, Moore JS, Leckband DE (2006) PNIPAM chain collapse depends on the molecular weight and grafting density. Langmuir 22:4259–4266. doi:10.1021/la0531502
116. Tokareva I, Minko S, Fendler JH, Hutter E (2004) Nanosensors based on responsive polymer brushes and gold nanoparticle enhanced transmission surface plasmon resonance spectroscopy. J Am Chem Soc 126:15950–15951. doi:10.1021/ja044575y
117. Zhou F, Shu W, Welland ME, Huck WTS (2006) Highly reversible and multi-stage cantilever actuation driven by polyelectrolyte brushes. J Am Chem Soc 128:5326–5327. doi:10.1021/ja060649p
118. Leckband D (1995) The surface force apparatus—a tool for probing molecular protein interactions. Nature 376:617–618. doi:10.1038/376617a0
119. Kurihara K, Kunitake T, Higashi N, Niwa M (1992) Surface forces between monolayers of anchored poly(methacrylic acid). Langmuir 8:2087–2089. doi:10.1021/la00045a003
120. Amiri Naini C, Franzka S, Frost S, Ulbricht M, Hartmann N (2011) Probing the intrinsic switching kinetics of ultrathin thermoresponsive polymer brushes. Angew Chem Int Ed 50:4513–4516. doi:10.1002/anie.201100140
121. Hln Gehan, Fillaud L, Chehimi MM, Aubard J, Hohenau A, Felidj N, Mangeney C (2010) Thermo-induced electromagnetic coupling in gold/polymer hybrid plasmonic structures probed by surface-enhanced Raman scattering. ACS Nano 4:6491–6500. doi:10.1021/nn101451q
122. Chen H, Yuan L, Song W, Wu Z, Li D (2008) Biocompatible polymer materials: role of protein–surface interactions. Prog Polym Sci 33:1059–1087. doi:10.1016/j.progpolymsci.2008.07.006
123. Norde W, Haynes CA (1995) Reversibility and the mechanism of protein adsorption. In: Proteins at interfaces II: fundamentals and applications. ACS symposium series. American Chemical Society, Washington, DC
124. Homola J (2008) Surface plasmon resonance sensors for detection of chemical and biological species. Chem Rev 108:462–493. doi:10.1021/cr068107d
125. Cooper MA, Singleton VT (2007) A survey of the 2001 to 2005 quartz crystal microbalance biosensor literature: applications of acoustic physics to the analysis of biomolecular interactions. J Mol Recognit 20:154–184. doi:10.1002/jmr.826
126. Yu Q, Zhang Y, Chen H, Wu Z, Huang H, Cheng C (2010) Protein adsorption on poly(N-isopropylacrylamide)-modified silicon surfaces: effects of grafted layer thickness and protein size. Colloids Surf B 76:468–474. doi:10.1016/j.colsurfb.2009.12.006
127. Xue C, Yonet-Tanyeri N, Brouette N, Sferrazza M, Braun PV, Leckband DE (2011) Protein adsorption on poly(N-isopropylacrylamide) brushes: dependence on grafting density and chain collapse. Langmuir 27:8810–8818. doi:10.1021/la2001909
128. Kitano H, Kondo T, Suzuki H, Ohno K (2010) Temperature-responsive polymer-brush constructed on a glass substrate by atom transfer radical polymerization. J Colloid Interface Sci 345:325–331. doi:10.1016/j.jcis.2009.10.004
129. Zareie HM, Boyer C, Bulmus V, Nateghi E, Davis TP (2008) Temperature-responsive self-assembled monolayers of oligo(ethylene glycol): control of biomolecular recognition. ACS Nano 2:757–765. doi:10.1021/nn800076h
130. Hyun J, Lee W-K, Nath N, Chilkoti A, Zauscher S (2004) Capture and release of proteins on the nanoscale by stimuli-responsive elastin-like polypeptide "switches". J Am Chem Soc 126:7330–7335. doi:10.1021/ja049721e
131. Liu Y, Mu L, Liu B, Zhang S, Yang P, Kong J (2004) Controlled protein assembly on a switchable surface. Chem Commun 1194. doi:10.1039/b400776j
132. Pearson D, Downard AJ, Muscroft-Taylor A, Abell AD (2007) Reversible photoregulation of binding of α-chymotrypsin to a gold surface. J Am Chem Soc 129:14862–14863. doi:10.1021/ja0766674
133. Glinel K, Thebault P, Humblot V, Pradier CM, Jouenne T (2012) Antibacterial surfaces developed from bio-inspired approaches. Acta Biomater 8:1670–1684. doi:10.1016/j.actbio.2012.01.011

134. Harden VP, Harris JO (1953) The isoelectric point of bacterial cells. J Bacteriol 65:198–202
135. Tiller JC, Liao CJ, Lewis K, Klibanov AM (2001) Designing surfaces that kill bacteria on contact. Proc Natl Acad Sci 98:5981–5985. doi:10.1073/pnas.111143098
136. Lee H-S, Eckmann DM, Lee D, Hickok NJ, Composto RJ (2011) Symmetric pH-dependent swelling and antibacterial properties of chitosan brushes. Langmuir 27:12458–12465. doi:10.1021/la202616u
137. Mi L, Bernards MT, Cheng G, Yu Q, Jiang S (2010) pH responsive properties of non-fouling mixed-charge polymer brushes based on quaternary amine and carboxylic acid monomers. Biomaterials 31:2919–2925. doi:10.1016/j.biomaterials.2009.12.038
138. Cao Z, Mi L, Mendiola J, Ella-Menye J-R, Zhang L, Xue H, Jiang S (2012) Reversibly switching the function of a surface between attacking and defending against bacteria. Angew Chem Int Ed 51:2602–2605. doi:10.1002/anie.201106466
139. Laloyaux X, Fautré E, Blin T, Purohit V, Leprince J, Jouenne T, Jonas AM, Glinel K (2010) Temperature-responsive polymer brushes switching from bactericidal to cell-repellent. Adv Mater 22:5024–5028. doi:10.1002/adma.201002538
140. Okano T, Yamada N, Okuhara M, Sakai H, Sakurai Y (1995) Mechanism of cell detachment from temperature-modulated, hydrophilic-hydrophobic polymer surfaces. Biomaterials 16:297–303. doi:http://dx.doi.org/10.1016/0142-9612(95)93257-E
141. Yamato M, Okuhara M, Karikusa F, Kikuchi A, Sakurai Y, Okano T (1999) Signal transduction and cytoskeletal reorganization are required for cell detachment from cell culture surfaces grafted with a temperature-responsive polymer. J Biomed Mater Res 44:44–52. doi:10.1002/(sici)1097-4636(199901)44:1<44:aid-jbm5>3.0.co;2-x
142. Kushida A, Yamato M, Konno C, Kikuchi A, Sakurai Y, Okano T (1999) Decrease in culture temperature releases monolayer endothelial cell sheets together with deposited fibronectin matrix from temperature-responsive culture surfaces. J Biomed Mater Res 45:355–362. doi:10.1002/(sici)1097-4636(19990615)45:4<355:aid-jbm10>3.0.co;2-7
143. Nishida K, Yamato M, Hayashida Y, Watanabe K, Yamamoto K, Adachi E, Nagai S, Kikuchi A, Maeda N, Watanabe H, Okano T, Tano Y (2004) Corneal reconstruction with tissue-engineered cell sheets composed of autologous oral mucosal epithelium. N Engl J Med 351:1187–1196. doi:10.1056/NEJMoa040455
144. Hasegawa M, Yamato M, Kikuchi A, Okano T, Ishikawa I (2005) Human periodontal ligament cell sheets can regenerate periodontal ligament tissue in an athymic rat model. Tissue Eng 11:469–478. doi:10.1089/ten.2005.11.469
145. Shimizu T, Yamato M, Isoi Y, Akutsu T, Setomaru T, Abe K, Kikuchi A, Umezu M, Okano T (2002) Fabrication of pulsatile cardiac tissue grafts using a novel 3-dimensional cell sheet manipulation technique and temperature-responsive cell culture surfaces. Circ Res 90:40–48. doi:10.1161/hh0302.105722
146. Shiroyanagi Y, Yamato M, Yamazaki Y, Toma H, Okano T (2004) Urothelium regeneration using viable cultured urothelial cell sheets grafted on demucosalized gastric flaps. BJU Int 93:1069–1075. doi:10.1111/j.1464-410X.2004.04783.x
147. Fukumori K, Akiyama Y, Yamato M, Kobayashi J, Sakai K, Okano T (2009) Temperature-responsive glass coverslips with an ultrathin poly(N-isopropylacrylamide) layer. Acta Biomater 5:470–476. doi:10.1016/j.actbio.2008.06.018
148. Halperin A, Kröger M (2012) Theoretical considerations on mechanisms of harvesting cells cultured on thermoresponsive polymer brushes. Biomaterials 33:4975–4987. doi:10.1016/j.biomaterials.2012.03.060
149. Iwanaga Y, Braun D, Fromherz P (2001) No correlation of focal contacts and close adhesion by comparing GFP-vinculin and fluorescence interference of DiI. Eur Biophys J 30:17–26. doi:10.1007/s002490000119
150. Bell G (1978) Models for the specific adhesion of cells to cells. Science 200:618–627. doi:10.1126/science.347575
151. Afroze F, Nies E, Berghmans H (2000) Phase transitions in the system poly(N-isopropylacrylamide)/water and swelling behaviour of the corresponding networks. J Mol Struct 554:55–68. doi:10.1016/s0022-2860(00)00559-7

152. Halperin A, Kröger M (2011) Collapse of thermoresponsive brushes and the tuning of protein adsorption. Macromolecules 44:6986–7005. doi:10.1021/ma201006h
153. Zhulina EB, Borisov OV, Priamitsyn VA (1990) Theory of steric stabilization of colloid dispersions by grafted polymers. J Colloid Interface Sci 137:495–511. doi:10.1016/0021-9797(90)90423-l
154. Moore SW, Roca-Cusachs P, Sheetz MP (2010) Stretchy proteins on stretchy substrates: the important elements of integrin-mediated rigidity sensing. Dev Cell 19:194–206. doi:10.1016/j.devcel.2010.07.018
155. Galaev IY, Dainiak MB, Plieva F, Mattiasson B (2007) Effect of matrix elasticity on affinity binding and release of bioparticles. Elution of bound cells by temperature-induced shrinkage of the smart macroporous hydrogel. Langmuir 23:35–40. doi:10.1021/la061462e
156. Kwon OH, Kikuchi A, Yamato M, Sakurai Y, Okano T (2000) Rapid cell sheet detachment from poly(N-isopropylacrylamide)-grafted porous cell culture membranes. J Biomed Mater Res 50:82–89. doi:10.1002/(sici)1097-4636(200004)50:1<82:aid-jbm12>3.0.co;2-7
157. Matsuda T (2004) Poly(N-isopropylacrylamide)-grafted gelatin as a thermoresponsive cell-adhesive, mold-releasable material for shape-engineered tissues. J Biomater Sci Polym Ed 15:947–955. doi:10.1163/1568562041271101
158. Tamura A, Kobayashi J, Yamato M, Okano T (2012) Temperature-responsive poly(N-isopropylacrylamide)-grafted microcarriers for large-scale non-invasive harvest of anchorage-dependent cells. Biomaterials 33:3803–3812. doi:10.1016/j.biomaterials.2012.01.060
159. Tamura A, Nishi M, Kobayashi J, Nagase K, Yajima H, Yamato M, Okano T (2012) Simultaneous enhancement of cell proliferation and thermally induced harvest efficiency based on temperature-responsive cationic copolymer-grafted microcarriers. Biomacromolecules 13:1765–1773. doi:10.1021/bm300256e
160. Aoyagi T, Ebara M, Sakai K, Sakurai Y, Okano T (2000) Novel bifunctional polymer with reactivity and temperature sensitivity. J Biomater Sci Polym Ed 11:101–110. doi:10.1163/156856200743526
161. Ebara M, Yamato M, Aoyagi T, Kikuchi A, Sakai K, Okano T (2004) Temperature-responsive cell culture surfaces enable "on−off" affinity control between cell integrins and RGDS ligands. Biomacromolecules 5:505–510. doi:10.1021/bm0343601
162. Ebara M, Yamato M, Aoyagi T, Kikuchi A, Sakai K, Okano T (2004) Immobilization of cell-adhesive peptides to temperature-responsive surfaces facilitates both serum-free cell adhesion and noninvasive cell harvest. Tissue Eng 10:1125–1135. doi:10.1089/ten.2004.10.1125
163. Ebara M, Yamato M, Aoyagi T, Kikuchi A, Sakai K, Okano T (2008) The effect of extensible PEG tethers on shielding between grafted thermo-responsive polymer chains and integrin—RGD binding. Biomaterials 29:3650–3655. doi:10.1016/j.biomaterials.2008.05.030
164. Ebara M, Yamato M, Aoyagi T, Kikuchi A, Sakai K, Okano T (2008) A novel approach to observing synergy effects of PHSRN on integrin—RGD binding using intelligent surfaces. Adv Mater 20:3034–3038. doi:10.1002/adma.200702308
165. Ebara M, Yamato M, Hirose M, Aoyagi T, Kikuchi A, Sakai K, Okano T (2003) Copolymerization of 2-Carboxyisopropylacrylamide with N-Isopropylacrylamide accelerates cell detachment from grafted surfaces by reducing temperature. Biomacromolecules 4:344–349. doi:10.1021/bm025692t
166. Hatakeyama H, Kikuchi A, Yamato M, Okano T (2006) Bio-functionalized thermoresponsive interfaces facilitating cell adhesion and proliferation. Biomaterials 27:5069–5078. doi:10.1016/j.biomaterials.2006.05.019
167. Tsuda Y, Kikuchi A, Yamato M, Nakao A, Sakurai Y, Umezu M, Okano T (2005) The use of patterned dual thermoresponsive surfaces for the collective recovery as co-cultured cell sheets. Biomaterials 26:1885–1893. doi:10.1016/j.biomaterials.2004.06.005
168. Lin JB, Isenberg BC, Shen Y, Schorsch K, Sazonova OV, Wong JY (2012) Thermo-responsive poly(N-isopropylacrylamide) grafted onto microtextured poly(dimethylsiloxane) for aligned cell sheet engineering. Colloids Surf B 99:108–115. doi:10.1016/j.colsurfb.2011.10.040

169. Tsuda Y, Yamato M, Kikuchi A, Watanabe M, Chen G, Takahashi Y, Okano T (2007) Thermoresponsive microtextured culture surfaces facilitate fabrication of capillary networks. Adv Mater 19:3633–3636. doi:10.1002/adma.200700988
170. Tsuda Y, Shimizu T, Yamato M, Kikuchi A, Sasagawa T, Sekiya S, Kobayashi J, Chen G, Okano T (2007) Cellular control of tissue architectures using a three-dimensional tissue fabrication technique. Biomaterials 28:4939–4946. doi:10.1016/j.biomaterials.2007.08.002
171. Wischerhoff E, Uhlig K, Lankenau A, Börner HG, Laschewsky A, Duschl C, Lutz J-F (2008) Controlled cell adhesion on PEG-based switchable surfaces. Angew Chem Int Ed 47:5666–5668. doi:10.1002/anie.200801202
172. Higuchi A, Aoki N, Yamamoto T, Miyazaki T, Fukushima H, Tak TM, Jyujyoji S, Egashira S, Matsuoka Y, Natori SH (2006) Temperature-induced cell detachment on immobilized pluronic surface. J Biomed Mater Res Part A 79A:380–392. doi:10.1002/jbm.a.30773
173. Seo S-J, Park I-K, Yoo M-K, Shirakawa M, Akaike T, Cho C-S (2004) Xyloglucan as a synthetic extracellular matrix for hepatocyte attachment. J Biomater Sci Polym Ed 15:1375–1387. doi:10.1163/1568562042368059
174. Mie M, Mizushima Y, Kobatake E (2008) Novel extracellular matrix for cell sheet recovery using genetically engineered elastin-like protein. J Biomed Mater Res B Appl Biomater 86B:283–290. doi:10.1002/jbm.b.31019
175. Byambaa B, Konno T, Ishihara K (2012) Cell adhesion control on photoreactive phospholipid polymer surfaces. Colloids Surf, B 99:1–6. doi:10.1016/j.colsurfb.2011.08.029
176. Pasparakis G, Manouras T, Selimis A, Vamvakaki M, Argitis P (2011) Laser-induced cell detachment and patterning with photodegradable polymer substrates. Angew Chem Int Ed 50:4142–4145. doi:10.1002/anie.201007310
177. Edahiro J, Sumaru K, Tada Y, Ohi K, Takagi T, Kameda M, Shinbo T, Kanamori T, Yoshimi Y (2005) In situ control of cell adhesion using photoresponsive culture surface. Biomacromolecules 6:970–974. doi:10.1021/bm0493382
178. Liu D, Xie Y, Shao H, Jiang X (2009) Using azobenzene-embedded self-assembled monolayers to photochemically control cell adhesion reversibly. Angew Chem Int Ed 48:4406–4408. doi:10.1002/anie.200901130
179. Cole MA, Voelcker NH, Thissen H, Griesser HJ (2009) Stimuli-responsive interfaces and systems for the control of protein–surface and cell–surface interactions. Biomaterials 30:1827–1850. doi:10.1016/j.biomaterials.2008.12.026
180. Tang Z, Wang Y, Podsiadlo P, Kotov NA (2006) Biomedical applications of layer-by-layer assembly: From biomimetics to tissue engineering. Adv Mater 18:3203–3224. doi:10.1002/adma.200600113
181. Iwai R, Kusakabe S, Nemoto Y, Nakayama Y (2012) Deposition gene transfection using bioconjugates of DNA and thermoresponsive cationic homopolymer. Bioconjug Chem 23:751–757. doi:10.1021/bc2005768
182. Shah S, Lee JY, Verkhoturov S, Tuleuova N, Schweikert EA, Ramanculov E, Revzin A (2008) Exercising spatiotemporal control of cell attachment with optically transparent microelectrodes. Langmuir 24:6837–6844. doi:10.1021/la800231e
183. Persson KM, Karlsson R, Svennersten K, Löffler S, Jager EWH, Richter-Dahlfors A, Konradsson P, Berggren M (2011) Electronic control of cell detachment using a self-doped conducting polymer. Adv Mater 23:4403–4408. doi:10.1002/adma.201101724
184. Davila J, Chassepot A, Longo J, Boulmedais F, Reisch A, Frisch B, Meyer F, Voegel J-C, Mésini PJ, Senger B, Metz-Boutigue M-H, Hemmerlé J, Lavalle P, Schaaf P, Jierry L (2012) Cyto-mechanoresponsive polyelectrolyte multilayer films. J Am Chem Soc 134:83–86. doi:10.1021/ja208970b
185. Pasparakis G, Vamvakaki M (2011) Multiresponsive polymers: nano-sized assemblies, stimuli-sensitive gels and smart surfaces. Polym Chem 2:1234. doi:10.1039/c0py00424c
186. Schild HG (1992) Poly(N-isopropylacrylamide): experiment, theory and application. Prog Polym Sci 17:163–249. doi:10.1016/0079-6700(92)90023-r

187. Allen AL, Tan KJ, Fu H, Batteas JD, Bergbreiter DE (2012) Solute- and temperature-responsive "smart" grafts and supported membranes formed by covalent layer-by-layer assembly. Langmuir 28:5237–5242. doi:10.1021/la204626e
188. Li P-F, Xie R, Jiang J-C, Meng T, Yang M, Ju X-J, Yang L, Chu L-Y (2009) Thermo-responsive gating membranes with controllable length and density of poly(N-isopropylacrylamide) chains grafted by ATRP method. J Membr Sci 337:310–317. doi:10.1016/j.memsci.2009.04.010
189. Kuroki H, Ohashi H, Ito T, Tamaki T, Yamaguchi T (2010) Isolation and analysis of a grafted polymer onto a straight cylindrical pore in a thermal-responsive gating membrane and elucidation of its permeation behavior. J Membr Sci 352:22–31. doi:10.1016/j.memsci.2010.01.052
190. Lequieu W, Shtanko N, Duprez F (2005) Track etched membranes with thermo-adjustable porosity and separation properties by surface immobilization of poly(N-vinylcaprolactam). J Membr Sci. doi:10.1016/j.memsci.2005.02.007
191. Zhou H, Chen Y, Fan H, Shi H, Luo Z, Shi B (2008) The polyurethane/$SiO_2$ nano-hybrid membrane with temperature sensitivity for water vapor permeation. J Membr Sci 318:71–78. doi:10.1016/j.memsci.2008.02.024
192. Wu G, Li Y, Han M, Liu X (2006) Novel thermo-sensitive membranes prepared by rapid bulk photo-grafting polymerization of N, N-diethylacrylamide onto the microfiltration membranes Nylon. J Membr Sci 283:13–20. doi:10.1016/j.memsci.2006.05.017
193. Zhao C, Nie S, Tang M, Sun S (2011) Polymeric pH-sensitive membranes—a review. Prog Polym Sci 36:1499–1520. doi:10.1016/j.progpolymsci.2011.05.004
194. Tomicki F, Krix D, Nienhaus H, Ulbricht M (2011) Stimuli-responsive track-etched membranes via surface-initiated controlled radical polymerization: influence of grafting density and pore size. J Membr Sci 377:124–133. doi:10.1016/j.memsci.2011.04.028
195. Kaetsu I, Nakayama H, Uchida K, Sutani K (2001) Radiation curing of intelligent coating on biofunctional membranes. Radiat Phys Chem 60:513–520. doi:10.1016/s0969-806x(00)00409-6
196. Zhang K, Wu XY (2004) Temperature and pH-responsive polymeric composite membranes for controlled delivery of proteins and peptides. Biomaterials 25:5281–5291. doi:10.1016/j.biomaterials.2003.12.032
197. Weh K, Noack M, Ruhmann R, Hoffmann K, Toussaint P, Caro J (1998) Modification of the transport properties of a polymethacrylate-azobenzene membrane by photochemical switching. Chem Eng Technol 21:408. doi:10.1002/(sici)1521-4125(199805)21:5<408:aid-ceat408>3.0.co;2-1
198. Chung D-J, Ito Y, Imanishi Y (1994) Preparation of porous membranes grafted with poly(spiropyran-containing methacrylate) and photocontrol of permeability. J Appl Polym Sci 51:2027–2033. doi:10.1002/app.1994.070511207
199. Yamaguchi T, Ito T, Sato T, Shinbo T, Nakao S-i (1999) Development of a fast response molecular recognition Ion gating membrane. J Am Chem Soc 121:4078–4079. doi:10.1021/ja984170b
200. Ito T, Hioki T, Yamaguchi T, Shinbo T, Nakao S-i, Kimura S (2002) Development of a molecular recognition ion gating membrane and estimation of its pore size control. J Am Chem Soc 124:7840–7846. doi:10.1021/ja012648x
201. Yang M, Xie R, Wang J-Y, Ju X-J, Yang L, Chu L-Y (2010) Gating characteristics of thermo-responsive and molecular-recognizable membranes based on poly(N-isopropylacrylamide) and β-cyclodextrin. J Membr Sci 355:142–150. doi:10.1016/j.memsci.2010.03.015
202. Kuroki H, Ito T, Ohashi H, Tamaki T, Yamaguchi T (2011) Biomolecule-recognition gating membrane using biomolecular cross-linking and polymer phase transition. Anal Chem 83:9226–9229. doi:10.1021/ac202629h
203. Huck WTS, Vamvakaki M (2008) Responsive polymers for nanoscale actuation. Mater Today 11:24–32. doi:10.1016/s1369-7021(08)70146-9
204. He X, Aizenberg M, Kuksenok O, Zarzar LD, Shastri A, Balazs AC, Aizenberg J (2012) Synthetic homeostatic materials with chemo-mechano-chemical self-regulation. Nature 487:214–218. doi:10.1038/nature11223

205. Sidorenko A, Krupenkin T, Taylor A, Fratzl P, Aizenberg J (2007) Reversible switching of hydrogel-actuated nanostructures into complex micropatterns. Science 315:487–490. doi:10.1126/science.1135516
206. Zou Y, Lam A, Brooks DE, Srikantha Phani A, Kizhakkedathu JN (2011) Bending and stretching actuation of soft materials through surface-initiated polymerization. Angew Chem Int Ed 50:5116–5119. doi:10.1002/anie.201008252
207. Kanazawa H, Yamamoto K, Matsushima Y, Takai N, Kikuchi A, Sakurai Y, Okano T (1996) Temperature-responsive chromatography using poly(N-isopropylacrylamide)-modified silica. Anal Chem 68:100–105. doi:10.1021/ac950359j
208. Kanazawa H, Matsushima Y, Okano T (1998) Temperature-responsive chromatography. TrAC Trends Anal Chem 17:435–440. doi:10.1016/s0165-9936(98)00044-2
209. Kanazawa H, Yamamoto K, Kashiwase Y, Matsushima Y, Takai N, Kikuchi A, Sakurai Y, Okano T (1997) Analysis of peptides and proteins by temperature-responsive chromatographic system using N-isopropylacrylamide polymer-modified columns. J Pharm Biomed Anal 15:1545–1550. doi:10.1016/s0731-7085(96)02004-3
210. Kanazawa H (2007) Thermally responsive chromatographic materials using functional polymers. J Sep Sci 30:1646–1656. doi:10.1002/jssc.200700093
211. Nagase K, Kobayashi J, Kikuchi A, Akiyama Y, Annaka M, Kanazawa H, Okano T (2008) Influence of graft Interface polarity on hydration/dehydration of grafted thermoresponsive polymer brushes and steroid separation using all-aqueous chromatography. Langmuir 24:10981–10987. doi:10.1021/la801949w
212. Tanaka N, Kobayashi H, Nakanishi K, Minakuchi H, Ishizuka N (2001) Peer reviewed: monolithic LC columns. Anal Chem 73:420 A–429 A. doi:10.1021/ac012495w
213. Nagase K, Kobayashi J, Kikuchi A, Akiyama Y, Kanazawa H, Okano T (2011) Thermoresponsive polymer brush on monolithic-silica-rod for the high-speed separation of bioactive compounds. Langmuir 27:10830–10839. doi:10.1021/la201360p
214. Wei X, Qi L, Yang G, Wang F (2009) Preparation and characterization of monolithic column by grafting pH-responsive polymer. Talanta 79:739–745. doi:10.1016/j.talanta.2009.04.062
215. Zhang R, Yang G, Xin P, Qi L, Chen Y (2009) Preparation of poly(N-isopropylacrylamide)-grafted polymer monolith for hydrophobic interaction chromatography of proteins. J Chromatogr A 1216:2404–2411. doi:10.1016/j.chroma.2009.01.023
216. Nagase K, Kobayashi J, Kikuchi A, Akiyama Y, Kanazawa H, Okano T (2012) High stability of thermoresponsive polymer-brush-grafted silica beads as chromatography matrices. ACS Appl Mater Interfaces 4:1998–2008. doi:10.1021/am201832b
217. Mizutani A, Nagase K, Kikuchi A, Kanazawa H, Akiyama Y, Kobayashi J, Annaka M, Okano T (2010) Effective separation of peptides using highly dense thermo-responsive polymer brush-grafted porous polystyrene beads. J Chromatogr B 878:2191–2198. doi:10.1016/j.jchromb.2010.06.026
218. Mizutani A, Nagase K, Kikuchi A, Kanazawa H, Akiyama Y, Kobayashi J, Annaka M, Okano T (2010) Thermo-responsive polymer brush-grafted porous polystyrene beads for all-aqueous chromatography. J Chromatogr A 1217:522–529. doi:10.1016/j.chroma.2009.11.073
219. Shen Y, Qi L, Wei X, Zhang R, Mao L (2011) Preparation of well-defined environmentally responsive polymer brushes on monolithic surface by two-step atom transfer radical polymerization method for HPLC. Polymer 52:3725–3731. doi:10.1016/j.polymer.2011.06.041
220. Feil H, Bae YH, Feijen J, Kim SW (1992) Mutual influence of pH and temperature on the swelling of ionizable and thermosensitive hydrogels. Macromolecules 25:5528–5530. doi:10.1021/ma00046a063
221. Kobayashi J, Kikuchi A, Sakai K, Okano T (2002) Aqueous chromatography utilizing hydrophobicity-modified anionic temperature-responsive hydrogel for stationary phases. J Chromatogr A 958:109–119. doi:10.1016/s0021-9673(02)00388-6
222. Kobayashi J, Kikuchi A, Sakai K, Okano T (2003) Cross-linked thermoresponsive anionic polymer-grafted surfaces to separate bioactive basic peptides. Anal Chem 75:3244–3249. doi:10.1021/ac026364m

223. Ayano E, Sakamoto C, Kanazawa H, Kikuchi A, Okano T (2006) Separation of nucleotides with an aqueous mobile phase using pH- and temperature-responsive polymer modified packing materials. Anal Sci 22:539–543. doi:10.2116/analsci.22.539
224. Nagase K, Kobayashi J, Kikuchi A, Akiyama Y, Kanazawa H, Okano T (2011) Thermally-modulated on/off-adsorption materials for pharmaceutical protein purification. Biomaterials 32:619–627. doi:10.1016/j.biomaterials.2010.09.012
225. Hosoya K, Kimata K, Araki T, Tanaka N, Frechet JMJ (1995) Temperature-controlled high-performance liquid chromatography using a uniformly sized temperature-responsive polymer-based packing material. Anal Chem 67:1907–1911. doi:10.1021/ac00107a024
226. Lakhiari H, Okano T, Nurdin N, Luthi C, Descouts P, Muller D, Jozefonvicz J (1998) Temperature-responsive size-exclusion chromatography using poly(N-isopropylacrylamide) grafted silica. Biochimica et Biophysica Acta (BBA)—General Subjects 1379:303–313. doi:10.1016/s0304-4165(97)00110-4
227. Yoshizako K, Akiyama Y, Yamanaka H, Shinohara Y, Hasegawa Y, Carredano E, Kikuchi A, Okano T (2002) Regulation of protein binding toward a ligand on chromatographic matrixes by masking and forced-releasing effects using thermoresponsive polymer. Anal Chem 74:4160–4166. doi:10.1021/ac025523z
228. Yamanaka H, Yoshizako K, Akiyama Y, Sota H, Hasegawa Y, Shinohara Y, Kikuchi A, Okano T (2003) Affinity chromatography with collapsibly tethered ligands. Anal Chem 75:1658–1663. doi:10.1021/ac0263768
229. Liu Z, Ullah K, Su L, Lv F, Deng Y, Dai R, Li Y, Zhang Y (2012) Switchable boronate affinity materials for thermally modulated capture, separation and enrichment of cis-diol biomolecules. J Mater Chem 22:18753. doi:10.1039/c2jm33578f
230. Wang X, Gu H, Yang Z (2005) The heating effect of magnetic fluids in an alternating magnetic field. J Magn Magn Mater 293:334–340. doi:10.1016/j.jmmm.2005.02.028
231. Yagi H, Yamamoto K, Aoyagi T (2008) New liquid chromatography method combining thermo-responsive material and inductive heating via alternating magnetic field. J Chromatogr B 876:97–102. doi:10.1016/j.jchromb.2008.10.028
232. Yagi H, Ebara M, Yamamoto K, Aoyagi T (2011) Effect of grafted smart polymer architectures on interaction with hydrophobic molecules in newly developed induction heating chromatography system. Mater Sci Eng C 31:1681–1687. doi:10.1016/j.msec.2011.07.018
233. Techawanitchai P, Yamamoto K, Ebara M, Aoyagi T (2011) Surface design with self-heating smart polymers for on–off switchable traps. Sci Technol Adv Mater 12:044609. doi:10.1088/1468-6996/12/4/044609
234. Terry SC, Jerman JH, Angell JB (1979) A gas chromatographic air analyzer fabricated on a silicon wafer. IEEE Trans Electron Devices 26:1880–1886. doi:10.1109/t-ed.1979.19791
235. Manz A, Fettinger JC, Verpoorte E, Lüdi H, Widmer HM, Harrison DJ (1991) Micromachining of monocrystalline silicon and glass for chemical analysis systems A look into next century's technology or just a fashionable craze? TrAC, Trends Anal Chem 10:144–149. doi:10.1016/0165-9936(91)85116-9
236. Beebe DJ, Moore JS, Bauer JM, Yu Q, Liu RH, Devadoss C, Jo B-H (2000) Functional hydrogel structures for autonomous flow control inside microfluidic channels. Nature 404:588–590
237. Oh KW, Ahn CH (2006) A review of microvalves. J Micromech Microeng 16:R13–R39. doi:10.1088/0960-1317/16/5/r01
238. Idota N, Kikuchi A, Kobayashi J, Sakai K, Okano T (2005) Microfluidic valves comprising nanolayered thermoresponsive polymer-grafted capillaries. Adv Mater 17:2723–2727. doi:10.1002/adma.200402068
239. Huh D, Tkaczyk AH, Bahng JH, Chang Y, Wei H-H, Grotberg JB, Kim C-J, Kurabayashi K, Takayama S (2003) Reversible switching of high-speed air−liquid two-phase flows using electrowetting-assisted flow-pattern change. J Am Chem Soc 125:14678–14679. doi:10.1021/ja037350g
240. Takei G, Nonogi M, Hibara A, Kitamori T, Kim H-B (2007) Tuning microchannel wettability and fabrication of multiple-step Laplace valves. Lab Chip 7:596. doi:10.1039/b618851f

241. Pumera M, Escarpa A (2009) Nanomaterials as electrochemical detectors in microfluidics and CE: fundamentals, designs, and applications. Electrophoresis 30:3315–3323. doi:10.1002/elps.200900008
242. Reichmuth DS, Shepodd TJ, Kirby BJ (2005) Microchip HPLC of peptides and proteins. Anal Chem 77:2997–3000. doi:10.1021/ac048358r
243. Huber DL, Manginell RP, Samara MA, Kim BI, Bunker BC (2003) Programmed adsorption and release of proteins in a microfluidic device. Science 301:352–354. doi:10.1126/science.1080759
244. Chen J-K, Li J-Y (2010) Detection of specific DNA using a microfluidic device featuring tethered poly(N-isopropylacrylamide) on a silicon substrate. Appl Phys Lett 97:063701. doi:10.1063/1.3476356
245. Ebara M, Hoffman JM, Hoffman AS, Stayton PS (2006) Switchable surface traps for injectable bead-based chromatography in PDMS microfluidic channels. Lab Chip 6:843–848
246. Hoffman JM, Ebara M, Lai JJ, Hoffman AS, Folch A, Stayton PS (2010) A helical flow, circular microreactor for separating and enriching "smart" polymer–antibody capture reagents. Lab Chip 10:3130. doi:10.1039/c004978f
247. Lai JJ, Hoffman JM, Ebara M, Hoffman AS, Estournès C, Wattiaux A, Stayton PS (2007) Dual magnetic-/temperature-responsive nanoparticles for microfluidic separations and assays. Langmuir 23:7385–7391. doi:10.1021/la062527g
248. Lai JJ, Nelson KE, Nash MA, Hoffman AS, Yager P, Stayton PS (2009) Dynamic bioprocessing and microfluidic transport control with smart magnetic nanoparticles in laminar-flow devices. Lab Chip 9:1997–2002
249. Malmstadt N, Hoffman AS, Stayton PS (2004) "Smart" mobile affinity matrix for microfluidic immunoassays. Lab Chip 4:412–415
250. El-Ali J, Sorger PK, Jensen KF (2006) Cells on chips. Nature 442:403–411. doi:10.1038/nature05063
251. Ernst O, Lieske A, Jäger M, Lankenau A, Duschl C (2007) Control of cell detachment in a microfluidic device using a thermo-responsive copolymer on a gold substrate. Lab Chip 7:1322. doi:10.1039/b708619a
252. Tang Z, Akiyama Y, Itoga K, Kobayashi J, Yamato M, Okano T (2012) Shear stress-dependent cell detachment from temperature-responsive cell culture surfaces in a microfluidic device. Biomaterials 33:7405–7411. doi:10.1016/j.biomaterials.2012.06.077
253. Ma D, Chen H, Li Z, He Q (2010) Thermomodulated cell culture/harvest in polydimethylsiloxane microchannels with poly(N-isopropylacrylamide)-grafted surface. Biomicrofluidics 4:044107. doi:10.1063/1.3516038
254. Jang K, Xu Y, Tanaka Y, Sato K, Mawatari K, Konno T, Ishihara K, Kitamori T (2010) Single-cell attachment and culture method using a photochemical reaction in a closed microfluidic system. Biomicrofluidics 4:032208. doi:10.1063/1.3494287
255. Yamaguchi S, Yamahira S, Kikuchi K, Sumaru K, Kanamori T, Nagamune T (2012) Photocontrollable dynamic micropatterning of non-adherent mammalian cells using a photocleavable poly(ethylene glycol) lipid. Angew Chem Int Ed 51:128–131. doi:10.1002/anie.201106106
256. Borenstein JT, Terai H, King KR, Weinberg EJ, Kaazempur-Mofrad MR, Vacanti JP (2002) Microfabrication technology for vascularized tissue engineering. Biomed Microdevices 4:167–175. doi:10.1023/a:1016040212127
257. Yamashita T, Tanaka Y, Idota N, Sato K, Mawatari K, Kitamori T (2011) Cultivation and recovery of vascular endothelial cells in microchannels of a separable micro-chemical chip. Biomaterials 32:2459–2465. doi:10.1016/j.biomaterials.2010.12.012
258. Benenson Y, Gil B, Ben-Dor U, Adar R, Shapiro E (2004) An autonomous molecular computer for logical control of gene expression. Nature 429:423–429. doi:10.1038/nature02551
259. Wasserman WW, Vanunu O, Magger O, Ruppin E, Shlomi T, Sharan R (2010) Associating genes and protein complexes with disease via network propagation. PLoS Comput Biol 6:e1000641. doi:10.1371/journal.pcbi.1000641

# Chapter 5
# Smart Nanofibers

## 5.1 Introduction

'… biology is largely the study of fibers …,' wrote Joseph Needham in *Order and Life* in 1936 [1]. In our body, cells, tissues and organs rely on the fibrous structures as scaffolds, because almost all of the tissues and organs in the human body, such as the bone, skin, tendon and cartilage, are synthesized and hierarchically organized into fibrous structures with nano-/microsized fibers [2]. Therefore, fibrous materials have a major role to play in the rapidly expanding fields of biomedicine including biomaterials, tissue engineering and regenerative medicine. In particular, a well-defined nanofibrous structure is very similar to the extracellular matrix (ECM), which is a biomimetic [3]. From this regard, biomimetic fibrous structures have already been studied extensively as scaffolds and cell manipulation matrices. Among many materials for scaffold matrices, collagen is the most widely used material because it is the main component of ECM. Collagen and its blends are easily transformed into nanofibrous structures and have excellent biocompatibility and biodegradability [4]. The possibility of using fibrous collagen for the skin, [5] bone [6] and cartilage [7] has been confirmed. Recently, not only natural polymer fibers such as collagen, fibrinogen, and elastin fibers, which are the principal components of ECM, but also synthetic polymer fibers have been the focus of much interest in the field of biomaterials. For example, Hwang et al. [8] prepared poly(lactic-*co*-glycolic acid) (PLGA) microfibers for the investigation of the effects of the diameter of microfibers on the orientation of adherent cells. Poly(L-lactide) (PLLA), polydioxanone (PDS), and poly(glycolide-*co*-ε-caprolactone) (PGACL) fibers were studied by Zilberman et al. [9] for the development of stents. With increasing technological advances for the fabrication of fibers and synthesis of new polymers or copolymers, their versatile applications in the field of biomaterials have been extensively researched, for example, their use in scaffolds, [10] drug delivery systems (DDSs), [11] tissue engineering, [12] regenerative medicine [13] and wound dressing [14].

Over the past two decades, smart or intelligent materials have emerged as a new class of biomaterials [15, 16]. Smart materials possess unique self-alterable

M. Ebara et al., *Smart Biomaterials*, NIMS Monographs,
DOI: 10.1007/978-4-431-54400-5_5,

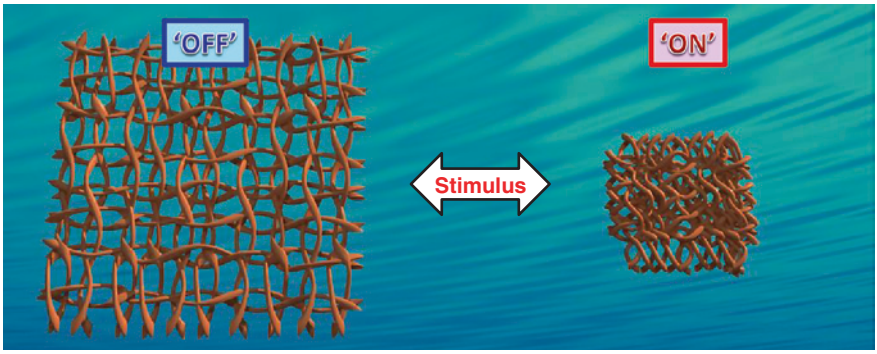


**Fig. 5.1** Schematic illustration of smart fiber with 'on–off' switchable property in response to small external stimuli

characteristics in response to the applied stimuli from their environment such as pH, [17] temperature, [18] electric/magnetic field [19, 20] and photo/UV irradiation [21]. These smart characteristics offer an opportunity for developing remote-controllable biomaterial systems on demand. As is well known, the human body has broad pH ranges in different cells, tissues or organs and maintains homeostasis. Therefore, the most interesting aspects about smart polymers in fields of biomedical or biomaterials science are their self-alterable characteristics in response to pH or temperature [17, 22]. Although many studies of smart materials such as hydrogels, films, surfaces or micelles and their results have been published, there are hardly any publications on smart fibers fabricated using stimulus-responsive polymers because of their instability in an aqueous solution [23]. Smart fibers with well-designed molecules and downsized to nanodimensions can show rapid and sharp responses compared with other types of material; in particular, nanosized fibers show a very high response rate [24]. This high response rate offers a possibility for manipulation of smart fibers for advanced applications. Furthermore, reversibly alterable properties can be used as 'on–off' systems that are triggered by applied stimuli on-demand remotely. The 'on–off' controllable smart fibers are a good candidate as not only biomaterials but also for other applications. In this chapter, we focus on biomaterial applications fabricated using smart fibers (Fig. 5.1).

In this regard, in this chapter, the unique features of fibers and smart fibers will be introduced. In the following sections of this chapter, we review different types of smart fiber with different applications in the fields of biomaterials and medicine. Firstly, the classification of fibers on the basis of fabrication methods will be introduced in Sect. 5.2. Secondly, methods of characterization of fibers will be described in Sect. 5.3. Thirdly, in Sects. 5.4 and 5.5, many smart fibers with different stimuli and their applications as biomaterials will be demonstrated, respectively. Finally, this chapter will be closed with a discussion of future trends and conclusions.

## 5.2 Classification of Fibers by Fabrication Methods

Recently, as fiber demand has been increasing continuously, diverse techniques have been developed to produce fibers of macromolecules or polymers. Various types of fiber can be fabricated using different techniques, including single fiber, nonwoven sheet fibers, core-shell or hollow fibers, small-fragment fibers and hydrogel-like fibers, and these techniques are also versatile. These techniques have both unique merits and demerits. Several representative techniques for the production of fibers are introduced in this section.

### *5.2.1 Self-assembly*

Self-assembly by a bottom–up method for the preparation of nanofibers from polymers, peptides and macromolecules is a versatile and powerful technique to construct well-defined nanostructures. This is accomplished by spontaneous and automatic organization of molecules into desired structures through various types of intermolecular interaction [25]. These interactions leading to the formation of fibrous structures include chiral dipole–dipole interactions, π–π stacking, hydrogen bonding, van der Waals interactions, interactions through hydrophobic forces, electrostatic interactions and interactions through repulsive steric forces, which bring smaller units together and form the shape of smaller units of molecules, which determine the overall shape of macromolecular nanofibers. In the tutorial review written by Gazit [26] the nanostructures of self-assembled peptides for various shapes of nanostructures are described. A small molecule is arranged concentrically such that interactions can occur among the concentrically arranged molecules. Boden's group has several publications about the self-assembly of peptides in which the effect of concentration on the formation of β-sheets are described. Monomers can be firstly formed into the tape phase by the increasing peptide monomer concentration. Then, the monomers grow to the fiber phase from the tape phase bypassing through two more phase stages, namely, the ribbon and fibril phases (bottom–up) [27]. This technique, that is, the self-assembly of peptides, is promising for the fabrication of a three-dimensional (3-D) scaffold with applications in biomaterials science, which have been introduced by Zhang et al. [28]. Self-assembled fiber formation using the common amphiphile peptide (PA) that relied on pH changes was also studied by Hartgerink et al. [29]. Tambralli et al. [30] prepared hybrid scaffolds with a combination of PCL nanofibers fabricated by electrospinning (see Sect. 5.2.2) and self-assembly.

Zang et al. [31] successfully demonstrated specific self-assembly techniques using the planar shape of π-conjugated molecules (Fig 5.2a) and π–π stacking interactions. Here, five techniques for the simple preparation of nanostructured fibers will be introduced: (1) rapid solution dispersion, (2) phase transfer, (3) vapor diffusion, (4) seeded growth, and (5) sol–gel process (Fig. 5.2).

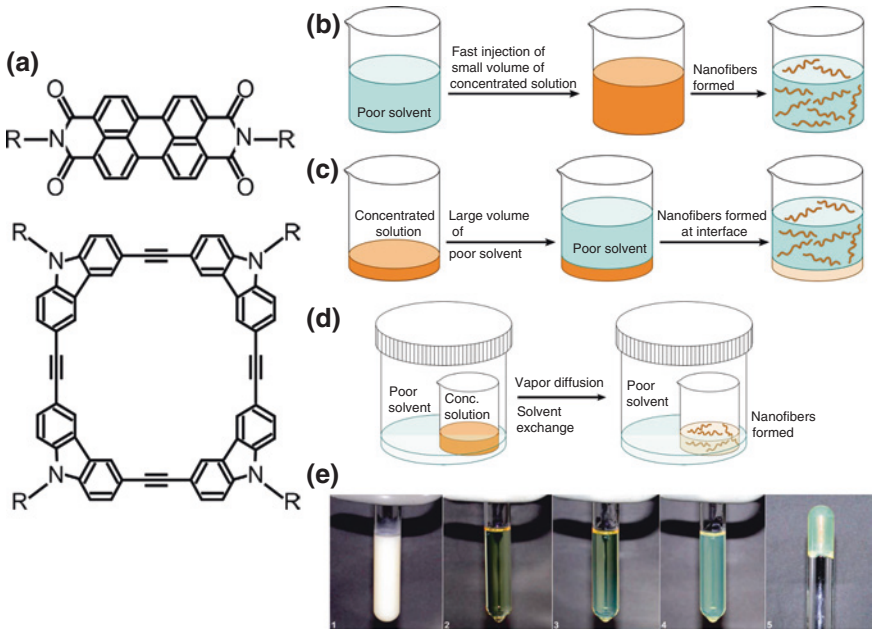


**Fig. 5.2** 1-D planar π-conjugated molecules for self-assembly: **a** perylene tetracarboxylic diimide (PTCDI, n-type) and arylene ethynylene macrocycle (AEM, p-type). Self-assembly methods: **b** rapid dispersion, **c** bisolvent phase transfer, **d** vapor diffusion, and **e** sol–gel process [31]

1. *Rapid solution dispersion*

   Nanofibers can simply be obtained by adding molecules at a critical minimum concentration into a poor solvent. Because molecules with predominant π–π stacking enable expedient self-assembly of the 1-D materials by rapid dispersion of the molecules from a 'good' solvent into a 'poor' solvent in which the molecules have low solubility, self-assembly of the molecules is expected to occur instantaneously (Fig. 5.2b).
2. *Phase transfer*
   This method is a very good option for slow-crystallization molecules because the slow crystallization occurs at the interface between 'good' and 'poor' solvents. For example, by selecting different solvents, the polarity of the mixed phase at the bisolvent interface can be adjusted over a wide range, providing variability for adjusting the solubility of target molecules and thus allowing for optimization of the self-assembly process (Fig. 5.2c).
3. *Vapor diffusion*
   This method is a more controlled process than the phase transfer for slowly crystallized molecules. The slow exchange between two solvents via vapor diffusion enables gradual, highly controlled adjustment of the solubility of the molecules (Fig. 5.2d).

4. *Seeded growth*
   This method is used to fabricate long nanofibers from an asymmetric molecule. Taking advantage of the miscibility of two solvents (water and alcohol), the solubility (or self-assembly) of the molecule can feasibly be controlled by adjusting the volume ratio of water to alcohol. By increasing the concentration of the water component, solvent polarity is increased, which will force the solvophobic association between the alkyl side chains, in a manner similar to the self-assembly of surfactants and other amphiphilic molecules.
5. *Sol–gel process*

   The cooling of a homogeneous solution of molecules in cyclohexane from a high temperature to room temperature leads to gelation of the solution. During the gelation, the molecules become highly organized, with optimal π–π stacking in conjunction with the side-chain association (Fig. 5.2e).

Yoshio et al. [32] introduced self-assembly under an electric field to control the alignment of self-assembled fibers. Using rod-type amide-containing mesogenic compounds in dodecylbenzene solution, fiber bridges were generated between gold electrodes by applying an AC electric field. The fibers grew from the negative charge to the positive charge direction following the application of an AC electric field and the fibers were formed in seconds. Moreover, the direction of fiber growth was markedly influenced by the magnitude of applied AC voltage and frequency.

### *5.2.2 Electrospinning*

Electrospinning has gained popularity over the last decade, and an electrical force is used to induce the formation of nonwoven polymer fibers from a polymer solution with the fiber diameters on the nanometer to micrometer scale or greater [33, 34]. In electrospinning, the 'Taylor cone' of a polymer solution droplet forms at the end of a capillary tip when electrical forces are applied [34]. When the electric field reaches a critical level at which the repulsive electric force overcomes the surface tension force, a charged jet of the solution is ejected from the tip of the 'Taylor cone'. As the jet diameter decreases when the jet flies to the collector, the radial forces from charged ions exceed the cohesive forces of the jet solution, causing it to split into many fibers. Furthermore, these divided fibers repel each other, leading to chaotic trajectories and bending instability. At the same time, the solvent evaporates and the polymer solidifies on the collector. Thus, continuous fibers are laid to form a nonwoven sheet. The representative features of electrospinning are as follows:

1. *Various polymers can be used*

   Natural polymers, synthesized polymers and proteins can be used for electrospinning and obtaining fine nanofibers.

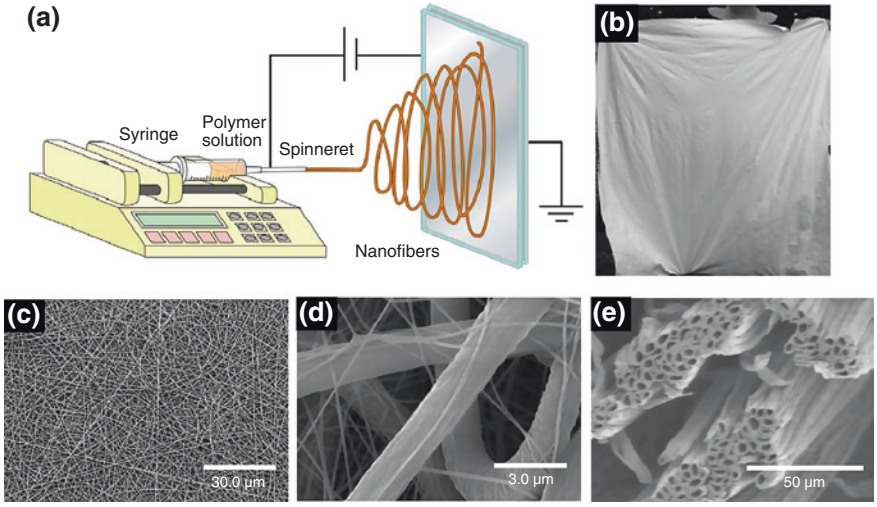


**Fig. 5.3** **a** Schematic diagram of horizontal set up of electrospinning apparatus [33]. **b** Nonwoven sheet-type electrospun fibers of bulk size. SEM images of **c** electrospun nanofibers, **d** hybrid electrospun nano/microfibersand, **e** hollow fibers [35]

2. *Time- and cost-effective method with simple experimental setup*
   A typical electrospinning setup consists of three main parts, a syringe pump, a collector, and a high-voltage source for generating a difference in electric potential between the syringe needle and the collector. Moreover, electrospinning can be carried out by applying a high voltage and pumping. To obtain a thin nanofiber sheet, only a few seconds is required (Fig. 5.3a).
3. *Bulk matter of fiber sheets can be prepared with nanoscale structure*
   Depending on the size of the collector and processing time, electrospun nanofiber sheets can be obtained as a bulk matter that can be as big as a human body (Fig. 5.3b) [35].
4. *Many types of fibrous scaffold can be obtained*
   The morphology of electrospun nanofibers can be controlled by changing the collector type, thereby obtaining, for example, randomly distributed, aligned or patterned types of nanofibers, hybrid fibers, and hollow or core-shell fibers. Other shapes of fibers can be obtained using modified electrospinning equipment (Fig. 5.3c–e) [35].
5. *Many parameters for electrospinning can be used*

   Fiber diameter or morphology can easily be controlled by changing the electrospinning parameters. The following affect the electrospinning process: solution, processing and ambient parameters (Table 5.1) [36].

**Table 5.1** Summary of effects of electrospinning parameters on fiber diameter and morphologies [36]

| Parameters | | Effects on fiber diameter and morphology |
|---|---|---|
| Solution | Concentration | Fiber diameter increased with increasing concentration |
| | Viscosity | Beads or particles can be generated by increasing viscosity. They disappear at a low viscosity |
| | Molecular weight and polydispersity index (PDI) | At a high molecular weight, the morphology is very uniform |
| | | At a low PDI, a very narrow diameter distribution can be obtained |
| | Surface tension | No conclusive link with fiber morphology; high surface tension results in instability of jets |
| | | Spinning is successful in solvents with a high dielectric constant |
| | Conductivity | Decrease in fiber diameter with increase in conductivity |
| Processing | Voltage | Decrease in fiber diameter with increase in voltage |
| | Flow rate | Lower flow rates yielded fibers with smaller diameters |
| | | High flow rates produced fibers with larger diameters or fibers that are not dry upon reaching the collector |
| | Type of collector | By changing collectors (plate, drum, area, etc.), aligned fibers, yarns, or braided or random fibers can be obtained |
| | Tip | Hollow or blended fibers can be obtained |
| | Distance between tip and collector | Generation of beads with too small and too large distances between the tip and collector |
| | | The minimum distance required for uniform fibers |
| Ambient | Temperature | Increase in temperature results in decrease in fiber diameter |
| | Humidity | High humidity results in formation of circular pores on the fibers |

### 5.2.3 Drawing

Drawing, a direct writing technique, is an optimized method for the fabrication of single fibers using a viscous polymer solution with volatile organic solvents. A continuous long linear fiber can be obtained by the drawing method, and the fiber diameter relies on the size of the needle (micropipette), polymer solution flow rate and temperature, which affect the viscosity of the polymer and the evaporation rate of the solvent.

Nain et al. [37, 38] proposed a custom point-to-point technique, which is a micropipette-based suspended polymer fiber drawing method for a single fiber (Fig. 5.4a). This technique has five steps as follows:

1. Raise the substrate until it comes into contact with the polymer droplet.
2. Move the micropipette vertically at a constant speed and stop at a constant height.
3. Move the stage along a predetermined trajectory at a constant speed while forming the solid polymer fiber by the evaporation of the solvent.
4. Allow the substrate to come into contact with the pipette to suspend the fiber.
5. Break the fiber or continue to draw subsequent ones.

Using this approach to prepare fibers, fibrous scaffolds are built sequentially with the desired geometrical spacing between consecutive fibers. Multiple layers are deposited similarly by repeating the above five steps in any desired angular orientation with respect to the predeposited layers. It is possible to increase the throughput of this technique and deposit multiple layers in a single step by using an array of individually controlled probes.

Furthermore, Berry et al. [39, 40] also reported on 3-D writing for biodegradable polymeric branched fibers by a method similar to the point-to-point technique. Such fibers are fabricated as follows (Fig. 5.4b):

1. The suspended fiber is drawn across a substrate frame.
2. The solution filament is drawn over the top of the fiber and briefly lowered to attach the two structures.
3. The syringe needle is lifted and moved to the final attachment point to complete the fabrication. This process is carried out quickly such that the top filament still contains some solvent when it contacts the bottom fiber, promoting adhesion between the two.

On the other hand, Harfenist et al. [41] developed a suspended-fiber fabrication method by which a previously deposited polymer solution droplet is contacted with a sharp probe tip such as an atomic force microscope (AFM) nanoprobe. The suspension is then connected to another previously deposited polymer solution droplet, thus forming a suspended fiber. This is a one-step method and very fast, within a few seconds, compared with other methods producing suspended fibers or structures.

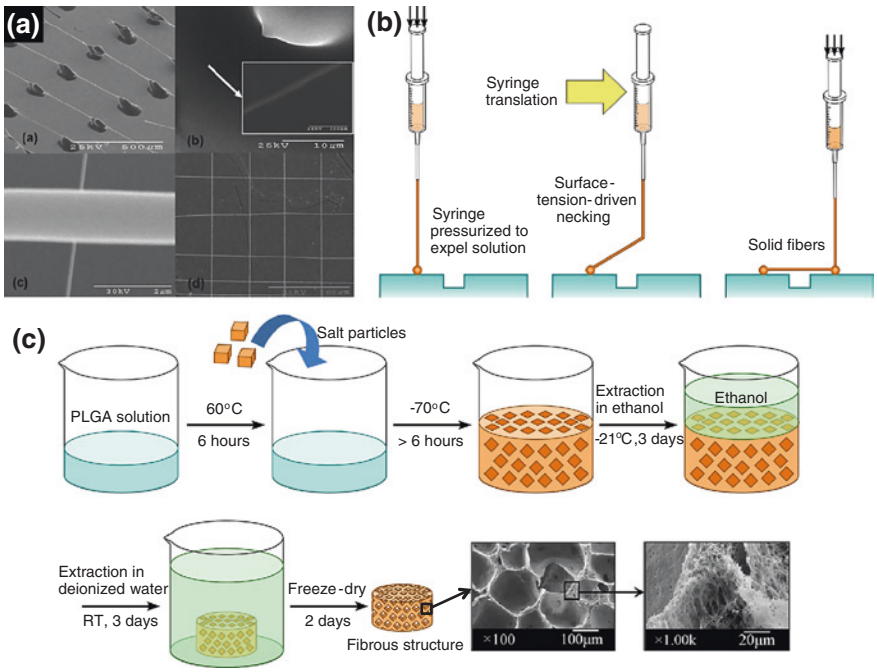


**Fig. 5.4** **a** SEM images of drawn suspended fibers [37] and **b** fiber fabrication process using direct drawing technique [40]. **c** Schematic illustration of preparation of fibers using phase-separation technique [43]

### *5.2.4 Phase Separation*

Phase separation is a method that has long been used to fabricate porous polymer fibrous membranes or sponges by inducing the separation of a polymer solution into two different phases, namely, the polymer-poor phase (low polymer concentration) and polymer-rich phase (high polymer concentration). This enables the preparation of a 3-D nanofibrous structure with interconnected pores. The main mechanism underlying the phase separation is physical incompatibility.

Yang et al. [42] and Mao et al. [43] developed a phase separation method for the preparation of 3-D scaffolds with the following steps (Fig. 5.4c):

1. Dissolution of polymers in solvent (good solvent).
2. Liquid–liquid phase separation (rapidly cooling).
3. Polymer gelation (gel point determined as afunction of temperature at which the gel flows).
4. Solvent leaching from polymer gel (solvent is exchanged with water).
5. Freezing and lyophilization under vacuum.

Liu and Ma [44] Chen and Ma [45] and Li et al. [46] introduced a thermally induced phase separation (TIPS) technique to prepare nanofibrous matrices. This technique is based on changes in thermal energy to induce the demixing of a homogeneous polymer solution into a multiphase system domain by quenching. In this process, the temperature of a polymer solution is decreased to induce separation into two phases, namely, the polymer-rich phase and polymer-poor phase either by solid–liquid demixing or liquid–liquid phase separation. The solvent occupying the polymer-poor phase is later removed by extraction or evaporation. After removing the solvent, different morphologies and characteristics of materials can be obtained depending on the system and phase separation conditions. One of the most attractive characteristics of TIPS over other techniques is the formation of not only an intrinsically interconnected polymer network but also an interconnected porous space in one simple process that is scalable, fast and controllable. TIPS is thus a very convenient methodology for fabricating porous materials as scaffold architectures that can be obtained by the manipulation of processing parameters and system properties.

### *5.2.5 Microfluidic Devices*

Recently, microfluidic devices have been developed for the fabrication of continuous single or hollow fibers. The microfluidic devices for fiber fabrication are also very simple and cost-effective, and complement the limitation of electrospinning in the manufacture of fibers in thick 3-D structures. Furthermore, methods using these devices are compatible with many biological materials and can be used to generate uniform fibers of micrometer diameter in a reproducible and scalable manner.

Lee's group introduced a method of fabricating microfibers by an 'on the fly' phase inversion (liquid to solid) process using a microfluidic device and developed a method of fabricating fibers or hollow fibers with high directionality [47, 48]. The microfluidic device consisted of a preperforated poly (dimethylsiloxane) (PDMS) structure, two pulled pipettes and one normal glass pipette. Along the perforated holes in the PDMS structure, the intermediate, inner, and outer pipettes were sequentially inserted, self-aligned, and fixed.

Recently, Kiriya et al. [49] have demonstrated the control of the internal morphology of macroscopic fibers consisting of assembled nanofibers that were prepared using a coaxial microfluidic channel with expansion and elongation of nanofibers. The internal morphology of the assembled nanofibers was controlled by regulating the flow rates of the core and sheath in a coaxial microfluidic device. The coaxial microfluidic device was constructed using two glass pipettes. A pulled round glass pipette was inserted into a square glass pipette, which acted as an outlet.

## 5.3 Characterization of Fibers

Understanding of characterization methodologies is very important for the optimization of fabrication conditions, accurate measurement, and further applications of fibers, because optimized conditions for characterization strongly depend on the nature of raw materials (stiffness, weakness, or toughness) or structure (1-, 2- or 3-D). Generally, the most important characteristics of fibers are those of their surfaces, which are observable using an optical microscope (OM), a fluorescence microscope, SEM, TEM, and AFM. These types of microscope can easily access the fiber surface and enable the observation of morphologies in a very wide range from the nanometer to millimeter scale. However, there are no significant characterization methods for smart fibers that have 'on–off' switch able properties in response to the environment. In this section, therefore, characterization methods for fibers and smart fibers are introduced.

### *5.3.1 Morphologies*

The morphologies of fibers or nanofibers are easily observed using OM, a fluorescence microscope, SEM, TEM, and AFM as mentioned above. Among them, SEM is most commonly used to confirm the morphologies or observe fracture surfaces (cross section). There are two observation modes, namely, the secondary electron (SE) image mode and backscattered electron (BSE) mode [50]. Usually, the SE image mode offers the highest resolution and the most convenient operation procedures. From SE images of fibers, their diameter, diameter distribution and pore size can be calculated. However, it is too difficult to confirm the morphology of the inside of fibers when composite fibers with nanoparticles or nanorods (any other additives) are embedded in the fiber. The BSE mode, however, enables the observation of additives in the fibers even when they are completely embedded in the fibers, [51] because electrons reflected from the sample by elastic scattering are more easily detected in the BSE mode than electrons emitted from deeper regions of the sample in the SE mode. Likewise, TEM is very useful and commonly used for the confirmation of embedded additives at a very high magnification compared with SEM in the BSE mode. Wang et al. [51] observed fibers and magnetic-field-responsive fibers using SEM (SE and BSE modes), a fluorescence microscope, and TEM (Fig. 5.5).

Nygaard et al. [52] examined the internal morphology of electrospun nanofibers using state-of-the-art synchrotron-radiation-based X-ray tomographic microscopy (XTM) (Fig. 5.6a, b). The response of a material to an applied stimulus is inherently 3-D. In reality, however, morphological property measurements conventionally rely on 2-D analytical techniques, such as SEM and TEM to explain 3-D responses. In addition, XTM is a unique technique that provides information on the internal structure of single fibers and beads. Analytical tools that have a spatial

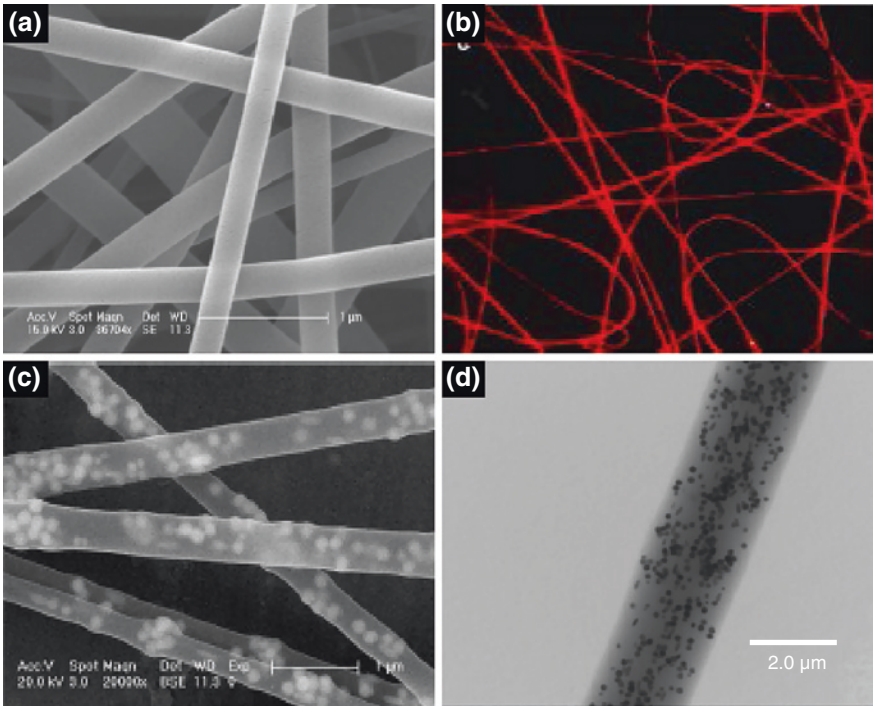


**Fig. 5.5** **a** SEM (SE mode) and **b** fluorescence microscopy images of electrospun nanofibers. **c** SEM (BSE mode) and **d** TEM images of magnetic-field-responsive-particle-embedded electrospun nanofibers [51]

resolution on the nanometer scale are indispensable in life and physical sciences. It is desirable that these tools also permit elemental and chemical identification on a scale of 10 nm or less, with large penetration depths. From these features, therefore, 3-D morphology images, cross-sectional images and density variation can be obtained by XTM.

On the other hand, AFM provides topological information on fiber surfaces. Among the many studies of fiber scanning using AFM, the most interesting one is that of real-time scanning using AFM reported by Okuzaki et al. [53] in 2009 (Fig. 5.6c). The fiber models were prepared by electospinning of a temperature-responsive polymer. By this real-time measurement with temperature change during scanning, the height, width, volume change, and shape of swollen and shrunk nanofibers were successfully obtained. This demonstrates that not only the swelling–deswelling but also the dissociation–association of nanofibers is crucial for the macroscopic volume changes of nanofibers. Furthermore, the authors have successfully demonstrated for the first time the shrinking of a single nanofiber by a temperature-modulated AFM technique in which a solution cell is heated from 25 to 40 °C when scanning starts. In addition, the time dependence of deswelling was also evaluated on the basis of a scanning frequency.

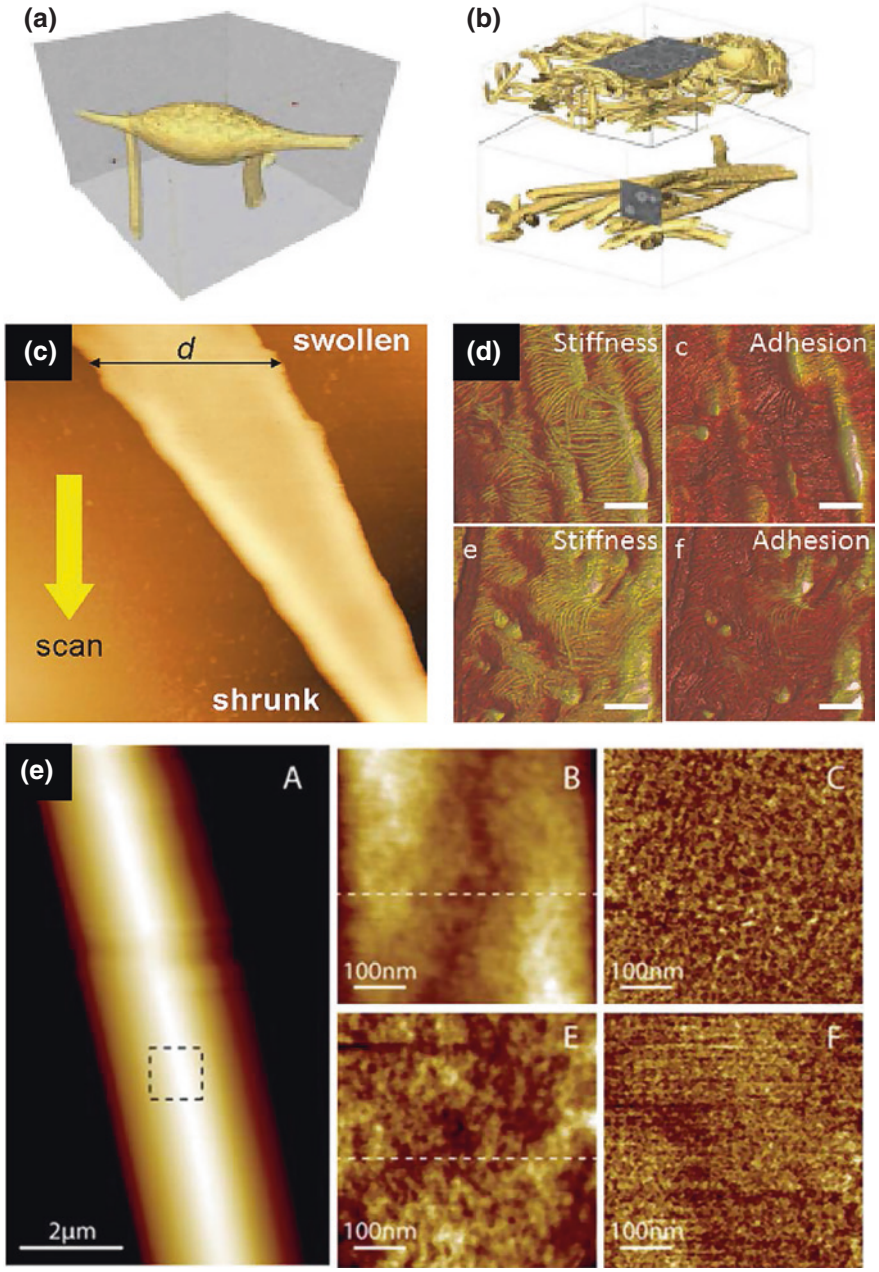


**Fig. 5.6** Images in **a** and **b** show XTM reconstructions of electrospun nanofibers [52]. **c** AFM image of temperature-modulated single electrospun nanofibers measured in tapping mode [53]. **d** In situ AFM images of temperature-controlled fibers (*upper*, 20 °C; *bottom*, 37 °C) [54]. **e** AFM quantitative nanomechanical mapping of the UV-responsive fibers before and after UV irradiation. (*A*): Overview of fibers; the inset square indicates the position where AFM nanomechanical maps are recorded (*B* and *E*): topography images before and after UV exposure, and (*C* and *F*): corresponding tip-sample adhesion maps of (*B* and *E*), respectively [55]

### 5.3.2 Mechanical Properties

By combining the tapping mode and torsion mode in AFM, the elastic modulus was derived from waveforms using the mathematical procedure reported by Chen et al. [54]. The interactions between the cantilever tip and the sample were determined from the long-range electrostatic and van der Waals forces and short-range mechanical restoration forces (Fig. 5.6d). In another report from the same group, they showed AFM based quantitative nanomechanical mapping (QNM), which is a novel AFM derived technique allowing for simultaneous recording of topographical and mechanical properties, thereby determining the nanoscale mechanical stiffness of the nanofibers and cantilever tip-sample interactions (Fig. 5.6e) [55]. The authors successfully observed morphological changes with/without UV irradiation using photoresponsive nanofibers. Furthermore, the maps of cantilever tip-sample interaction forces before and after in situ UV exposure were also successfully recorded. The capillarity between the cantilever tip and the sample appears each time when the tip interacts with the sample surface, which is reflected in the recorded adhesion forces between the tip and the sample during the force mapping. After UV exposure of nanofibers, the tip-sample interaction force decreased from $10.66 \pm 0.63$ to $5.91 \pm 0.42$ nN.

Kim et al. [23] demonstrated reversible changes in the tensile strength of temperature-responsive nanofibers with continuous temperature alternation (see Sect. 5.4.1). The basic concept is based on a creep test, which is one of the performance methods using a universal testing machine (UTM). The term creep refers to the total time-dependent deformation of a material under constant stress. Furthermore, relatively small loads applied over a long period of time can lead to a significant deformation of specimens. In the test, temperature-responsive nanofibers are set on the grips with constant stress, and then the nanofibers are sprayed with hot water [above lower critical solution temperature (LCST)]. The UTM chamber is set at a temperature lower than LCST. The creep curve is closely monitored in real time. Moreover, reversible changes in tensile strength can be observed by repeating water spraying at constant intervals.

### 5.3.3 Pore Size, Porosity and Surface Area

The most interesting characteristic of nanofibers is their having many pores of sub-nanometer to micrometer sizes or their high porosity. Although SEM and TEM are useful for the investigation of pores and their size, we were able to obtain only surface values. The typical methods for evaluation of the size, density and distribution of whole pores are (1) mercury intrusion porosimetry (MIP), (2) liquid extrusion porosimetry (LEP), and (3) capillary flow porosimetry (CFP). Regarding the measurement of the surface area of porous fibers, (4) the Brunauer, Emmett, and Teller (BET) gas adsorption model would be introduced.

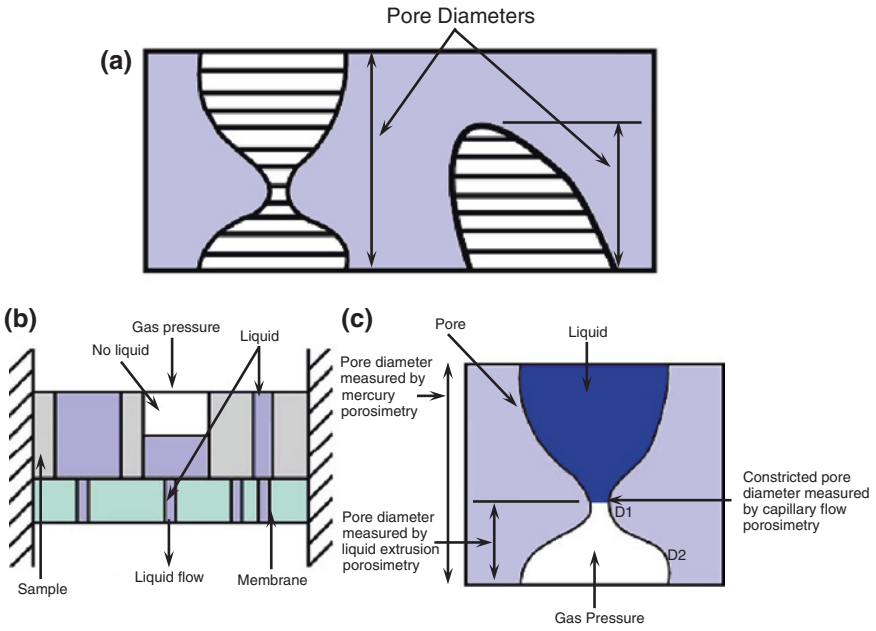


**Fig. 5.7** **a** All diameters and volumes of through and blind pores measurable by mercury intrusion porosimetry [56]. **b** Principle of liquid extrusion porosimetry (pore volume) [57]. **c** Diameter of through pore measurable by liquid extrusion porosimetry [58]

1. *MIP*

   MIP is the most frequently used porosimetric method. The principle of this method is based on the penetration of liquids into small cylindrical pores. In this method, a nonwetting liquid mercury is used, which does not swell or dissolve the fiber matrix and enters the pores spontaneously. The diameter of the pores is calculated from the pressure of liquid mercury, taking into account the surface tension and the wetting angle of the liquid mercury (Fig. 5.7a) [56].

$$\mathrm{D} = -2\gamma\cos\theta/p, \tag{5.1}$$

   where D is the pore diameter, $\gamma$ is the surface tension of mercury, $\theta$ is the contact angle of mercury and $p$ is the pressure of mercury upon intrusion into a pore.

   MIP provides data about pore size and distribution, bulk density and apparent density of the sample.

2. *LEP*

   Flow-through porosimetry avoids the use of a high applied pressure and is therefore well suited for characterizing relatively soft fibers. In LEP, the pores are spontaneously filled with a wetting liquid and the liquid is extruded from

pores by a nonreacting gas. It can be shown that the differential pressure is related to the size of pores [57].

$$\mathrm{D} = 4\gamma\cos\theta/p, \tag{5.2}$$

where D is the pore diameter, $\gamma$ is the surface tension of the liquid used, $\theta$ is the contact angle of the wetting liquid and $p$ is the differential pressure.
The volume of the liquid displaced, $V$, can be related to the change in interfacial area at the liquid and fiber interface.

$$p\mathrm{d}V = \gamma\cos\theta\mathrm{d}S, \tag{5.3}$$

where the surface area $S$ is obtained by integration of the function.
In LEP, the volume of extruded liquid is measured under the differential gas pressure applied over the liquid column. A membrane is placed under the fiber such that the largest pore of the membrane is smaller than the smallest pore of interest in a fiber (Fig. 5.7b). The pores of the fiber and the membrane are filled with a liquid, and the gas pressure is gradually increased to displace the liquid from the pores of the fiber. The liquid filling the pores of the membrane allows the extruded liquid from the pores of the fiber to flow out while preventing the gas from escaping. The measured volume of the liquid flowing out of the membrane gives the through-pore volume. Differential pressure yields the through-pore diameter, and the variation of volume with pressure yields the through-pore surface area. The flow rate of excess liquid maintained on the sample yields the liquid permeability. In this technique, only the through-pore volume and diameter are measured (Fig. 5.7c) [58].

3. *CFP*
   CFP is similar to LEP. The pores of a sample are filled with a wetting liquid that is extruded by a pressurized gas, permitting gas to flow through the empty pores. The differential pressure required to empty a pore of diameter D is given by Eq. 5.2 [59]. By liquid extrusion, the liquid column occupying through-channels is displaced by the gas. The gas displaces the liquid and the flow rate of the gas as a function of differential pressure is recorded. The largest pores are opened by the smallest pressure, called the 'bubble point'. On further pressure increase, the gas flow rate increases because an increasing number of small pores are opened.
4. *BET*

   BET measurement relying on gas adsorption involves several key assumptions [60]:

   (a) Gas interaction with the polymer occurs with a constant heat of adsorption and exclusively due to van der Waals interactions between the gas and the nanofiber surface.
   (b) Adsorbed molecules on the surface do not interact with each other.
   (c) Additional layers of gas molecules can be deposited on the surface of a complete or incomplete monolayer with the heat of adsorption being equal to the heat of liquefaction of the gas.

The specific surface area of a fiber is determined by physical adsorption of a gas on the surface of the fiber and by calculating the amount of the adsorbed gas corresponding to a monomolecular layer on the surface. Physical adsorption results from the van der Waals forces between the adsorbate gas molecules and the adsorbent surface area of the fiber. The determination is usually carried out at the temperature of liquid nitrogen. The amount of gas adsorbed can be measured by a volumetric or continuous flow procedure. The data are treated according to the BET adsorption isotherm equation (Eq. 5.4):

$$\frac{1}{W\left(\left(\frac{P0}{P}\right)-1\right)} = \frac{1}{WmC} + \frac{C-1}{WmC}\left(\frac{P}{P0}\right), \tag{5.4}$$

where $W$ is the weight of gas absorbed, $P/P0$ is the relative pressure ($P0$ is the saturation pressure of the gas), $Wm$ is the weight of the adsorbate as the monolayer, and $C$ is the BET constant.

## 5.4 Smart Fibers

In this section, representative smart fibers will be introduced, which are composed of polymers responsive to stimuli, including temperature, light/UV, pH or electric/magnetic field, which enable'on–off' switching and reversible property changes of nanofibers.

### *5.4.1 Temperature-Responsive Fibers*

The most widely used temperature-responsive polymers are poly(*N*-isopropylacrylamide) (PNIPAAm) and its derivations. A PNIPAAm solution, which undergoes a sharp and reversible phase transition from monophasic below a specific temperature to biphasic above it, generally exhibits the so-called lower critical solution temperature (LCST). The PNIPAAm has an LCST of 32 °C in aqueous solution. Below this temperature, the polymer is soluble owing to the predominance of hydrophilic interactions due to hydrogen bonding with water, whereas phase separation occurs above the LCST owing to the predominance of hydrophobic interactions. PNIPAAm has been extensively studied over the past few decades and it is generally used as a gel or grafting material. Rockwood et al. [59] and Okuzaki et al. [60] reported the preparation of PNIPAAm nanofibers by electrospinning under optimized conditions using different solvents. However, owing to the solubility of the NIPAAm homopolymer in an aqueous solution prepared below the LCST, the resulting nanofibers rapidly dissolve in water, whereas the nanofibers prepared above the LCST disperse and aggregate in water because of the lack of interpolymer and interfiber crosslinks that keep the nanofibers in

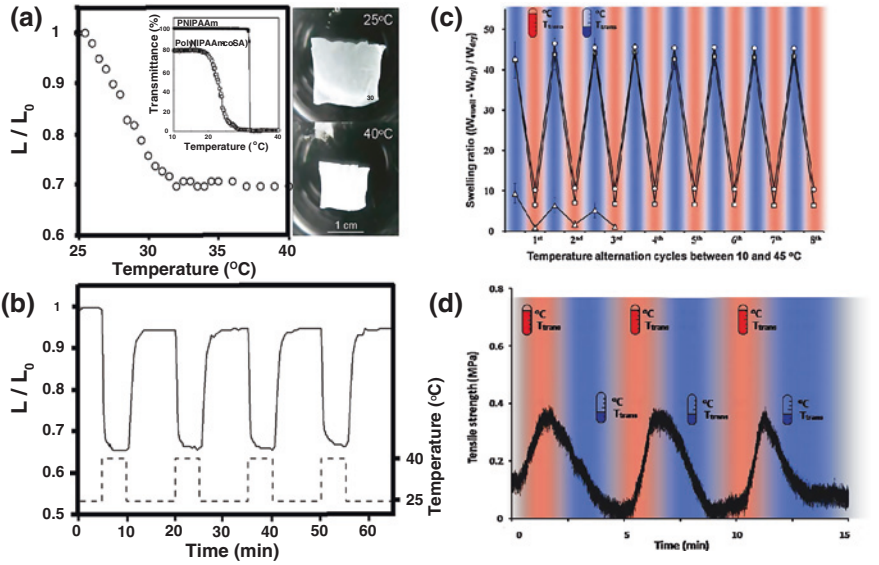


**Fig. 5.8** **a** Temperature-dependent relative length change of poly(NIPAAm-*co*-SA) nanofiber mat in pure water at 25 and 40 °C measured from optical images. The inset shows the temperature dependence of transmittance for PNIPAAm and poly(NIPAAm-*co*-SA) aqueous solutions ($L_0$: initial length of sample, $L$: length after the sample). **b** Reversibility and reproducibility of time-dependent deswelling and swelling of poly(NIPAAm-*co*-SA) nanofiber mat in pure water between 25 and 40 °C [53]. **c** Temperature-dependent variations of swelling ratio for the crosslinked poly(NIPAAm-*co*-HMAAm) nanofibers in response to cycles of temperature alternations between 10 and 45 °C [61]. **d** Temperature-dependent changes in tensile strength of a poly(NIPAAm-*co*-CIPAAm) nanofiber in response to temperature alternations between 10 and 37 °C [23]

the swollen state. Therefore, it can be considered that the incorporation of long sidechains into PNIPAAm to aggregate nanofibers in water via hydrophobic interactions can lead to the formation of interpolymer and interfiber physical crosslinks. From these perspectives, Okuzaki et al. [53] reported on a successful one-step fabrication of highly thermoresponsive PNIPAAm-based nanofibers cross-linked via hydrophobic interactions of stearyl side chains by electrospinning and also demonstrated for the first time the kinetics of volume changes of a single nanofiber (Fig. 5.8a, b). They synthesized poly(NIPAAm-*co*-stearyl acrylate (SA)) by free-radical polymerization with about 4 mol% SA and successfully prepared water-stable electrospun poly(NIPAAm-*co*-SA) nanofibers with an average diameter of 207 nm. The nanofiber exhibits shrinkage by 34 % of its initial length at 40 °C and swelling up to 95 % of the initial length at 25 °C, and reversible swelling and deswelling was repeated at least four times. In the case of bulk poly(NIPAAm-*co*-SA) gels soaked in aqueous solution, their swelling rate is much lower than that of poly(NIPAAm-*co*-SA) nanofibers because of the formation of a dense surface layer, which strongly hinders water diffusion. Furthermore,

the single-fiber height gradually decreased with increasing temperature, whereas the width significantly decreased, indicating the swelling of the nanofiber into a cylindrical shape.

In a similar study, Kim et al. [61] also studied the reversible change in swelling ratio in response to temperature (Fig. 5.8c). They successfully prepared temperature-responsive electrospun nanofibers by thermal curing (crosslinking). As a member of the NIPAAm family, *N*-hydroxymethylacrylamide (HMAAm) was copolymerized with NIPAAm by free-radical copolymerization because temperature-responsive HMAAm can be crosslinked by self-condensation at high temperatures (above 110 °C) (PNH). As a result of crosslinking, very stable nanofibers in aqueous solution were obtained and manipulated as a bulk material. The crosslinked nanofibers were incubated at various temperatures (above and below LCST) for 5 min, during which they shrank completely within 60 s, and this process was repeated for eight cycles. In the presence of higher than 5 mol% HMAAm in the copolymer, crosslinked nanofibers demonstrated temperature-responsive swelling and shrinking for at least eight cycles without weight loss. From these two examples, in general, the application of bulk materials such as hydrogels is limited by their slow response, and several techniques have been proposed to increase the response rate, such as reducing gel size and constructing an interconnected pore structure within the gel. Because of the high specific surface area, interconnected pores and high porosity of nanofibers, the nanofibers are more sensitive to external stimuli than their corresponding bulk materials. By extension of the above-mentioned examples, the same authors successfully prepared electrospun nanofiber mats that showed reversible tensile strength and size in aqueous solution in response to cycles of temperature alternation (Fig. 5.8d) [23]. The temperature-responsive nanofiber mats were prepared using the copolymers NIPAAm and 2-carboxyisopropylacrylamide (CIPAAm) conjugated to 4-aminobenzophenone (BP). CIPAAm also has an inherent LCST, which is much higher than that of NIPAAm, because it has the hydrophilic carboxyl group and BP is a photoinitiator. The crosslinked temperature-responsive nanofibers were obtained by UV irradiation for 30 min. When a crosslinked nanofiber mat was soaked in PBS and heated to 37 °C, the mat markedly shrank because of a conformational change of the copolymer. The temperature was then alternately decreased to lower than and increased to higher than the LCST and, correspondingly, the mat first swelled, and then shrank. In addition, the tensile strength of the crosslinked nanofiber mat was also measured using a tensile tester housed within a temperature-controlled chamber. The temperature within the chamber was alternated between 10 and 37 °C, and the changes in tensile strength were measured continuously while keeping the sample size constant. The tensile strength was found to change reversibly in response to temperature. Of particular interest is that the changes in tensile strength during each cycle were almost constant (approximately 400 kPa).

Fu et al. [62] prepared the temperature-sensitive nanofiber surface by a combination of reversible addition–fragmentation chain-transfer (RAFT) polymerization, atom transfer radical polymerization (ATRP), electrospinning, and “click chemistry” technology. The authors prepared block copolymers consisting of 4-vinylbenzyl

chloride (VBC) and glycidylmethacrylate (GMA) (PVBC-*b*-PGMA) by RAFT polymerization. The obtained block copolymers were transformed to electrospun nanofibers with diameters of 0.4–1.5 μm. Exposure to a sodium azide ($NaN_3$) solution not only affords nanofibers with azido groups on the surface but also leads to the crosslinking of nanofibers. One more step of click chemistry between the PVBC-*b*-PGMA nanofibers with azido groups on the surface (PVBC-*b*-PGMA-$N_3$) and alkyne-terminated polymers of NIPAAm ($PNIPAAm_{AT}$), which were prepared by ATRP, enables the preparation of a PVBC-*b*-PGMA nanofiber with temperature-sensitive PNIPAAm brushes on the surface (PVBC-*b*-PGMA-*g*-PNIPAAm). The PVBC-*b*-PGMA-*g*-PNIPAAm nanofiber surface was environmental-temperature-responsive, with a hydrophobic surface at 45 °C with a water contact angle of 140° and with a hydrophilic surface at 20 °C with a water contact angle of 30°.

The other type of temperature-responsive nanofiber was studied by Loh et al. [63] who prepared physical hydrogel nanofibers by electrospinning using the well-known biodegradable poly(ester urethane) comprising poly(ethylene glycol) (PEG), poly(propylene glycol) (PPG) and poly(ε-caprolactone) (PCL). In their study, the electrospun nanofibers transformed to hydrogel-like fibers upon swelling in aqueous solution caused by physical interactions between the hydrophobic segments. At 25 °C, the percentage of swollen nanofibers in the scaffold in water was 38 %; when the temperature was raised to 37 °C, the percentage in the scaffold was reduced to 19 %. The temperature change caused the volume of water trapped in the nanofiber mat to be reduced by about one-half. This is due to the PPG segment in the copolymer becoming more hydrophobic at higher temperatures. In this state, water is expelled from the nanofibers and the swelling decreases. This swelling–deswelling behavior of nanofibers offers the possibility of rapid and transient drug release, and drug delivery at an appropriate time and dosage. Webster et al. [64] prepared nanofibers using poly(*N*-vinylcaprolactam) (PVCL), which is more stable than PNIPAAm in terms of biotechnological applications. These fibers also reacted to temperature changes in terms of surface contact angle. Chen et al. [65] successfully fabricated nanofibers using blends of single-spinneret electrospun PNIPAAm and PCL; these nanofibers showed a self-assembled core-sheath structure and stimulus-responsive wettability of the PNIPAAm/PCL fibrous surfaces.

### *5.4.2 Photoresponsive Fibers*

As a trigger, the use of visible light and UV light is particularly attractive because its characteristics can be remotely and accurately controlled, quickly switched and easily focused into specific areas. Many studies of visible light- and UV-responsive fibers have focused on the characteristic features of these fibers formed into complex biological systems that are capable of exploiting light as an external source of energy and information. The representative photoresponsive phenomenon is photochromism, which is the reversible transformation of a chemical species between two isomeric forms by absorption of visible light or UV light.

In addition to color changes, these transformations are accompanied by changes in the physical and chemical properties of the species involved, such as alterations in the dipole moment, refractive index and geometrical structure. Importantly, these dynamic transformations can generate coincident changes in the optical, chemical, electrical and bulk properties of systems that incorporate them. Photochromic molecules, therefore, play a pivotal role in photoresponsive systems, which are capable of capturing optical signals and then converting them, through their isomerization, to useful properties. Benedetto et al. [66] studied photochromism using spiropyran (SP)-embedded electrospun nanofibers. The photochromism reaction of SP proceeds with electrocyclic ring opening followed by a molecular rotation; consequently, SP (off-state) changes to its open form, merocyanine (MC, on-state). The three images of nanofibers in their off-state SP form, emitting light upon excitement with UV light and in their on-state MC form after photoconversion, are shown in Fig. 5.9a and b.

Recently, β-cyclodextrin (CD) has attracted interest regarding its use in a guest–host system because βCD has a rigid and well-defined structure with a hydrophobic cavity. Various organic and inorganic guest molecules have been inserted into this cavity, resulting in the formation of inclusion complexes. In this regard, a $\beta CD_{sp}$ complex system was developed by De Sousa et al. [67] who synthesized a novel $\beta CD_{sp}$ complex conjugated to the poly(methacrylic acid) (PMAA) side chain. After electrospinning PMMA-$\beta CD_{sp}$, the photoresponsive property of the resulting PMMA-$\beta CD_{sp}$ nanofibers prepared on the basis of SP-MC isomerization was demonstrated. Upon exposure to visible light, the nanofibers exhibited a light red color associated with the MC form and the masked portion irradiated with visible light exhibited a white color associated with the SP form. When the nanofibers were exposed to UV light, the difference between these isomers was intensified owing to the fluorescence property of the MC form. In addition to the above-mentioned study, βCD was used in another study as the host part of a complex with 4-aminoazobenzene (AAB) as the guest molecule, which has a unique UV-responsive *trans-cis* isomerization property. Chen et al. [55] prepared hydroxypropyl-βCD (HPβCD)-AAB-inclusion complex (IC) fibers, and *trans-cis* isomerization of AAB triggered by UV light caused a significant change in the AAB molecular geometry and subsequently the dissociation of AAB from the ICs. Following UV irradiation after electrospinning, the uneven surface became smoother and the adhesion force between the cantilever tip and the sample was found to increase in a topological study by AFM quantitative nanomechanical mapping. The changeable light-driven wettability of electrospun fibers was reported by the same group [68]. The fibers consisting of azobenzene-modified PCL (PCL-azo) were synthesized by crosslinking PCL-azo with benzophenone-4-isothiocyanate (BPITC), which is a well-known heterobifunctional, photoreactive crosslinker (BP-azo/PCL). The *trans* isomer of PCL-azo changes to a *cis*-isomerized state corresponding to the $\pi$–$\pi^*$ transition band transformed to the n–$\pi^*$ transition band upon UV irradiation, whereby approximately 30 % of the population is transferred from the *trans* state to the *cis* state. Alterations of the chemical structures of the surface of fibers by UV irradiation can be used to

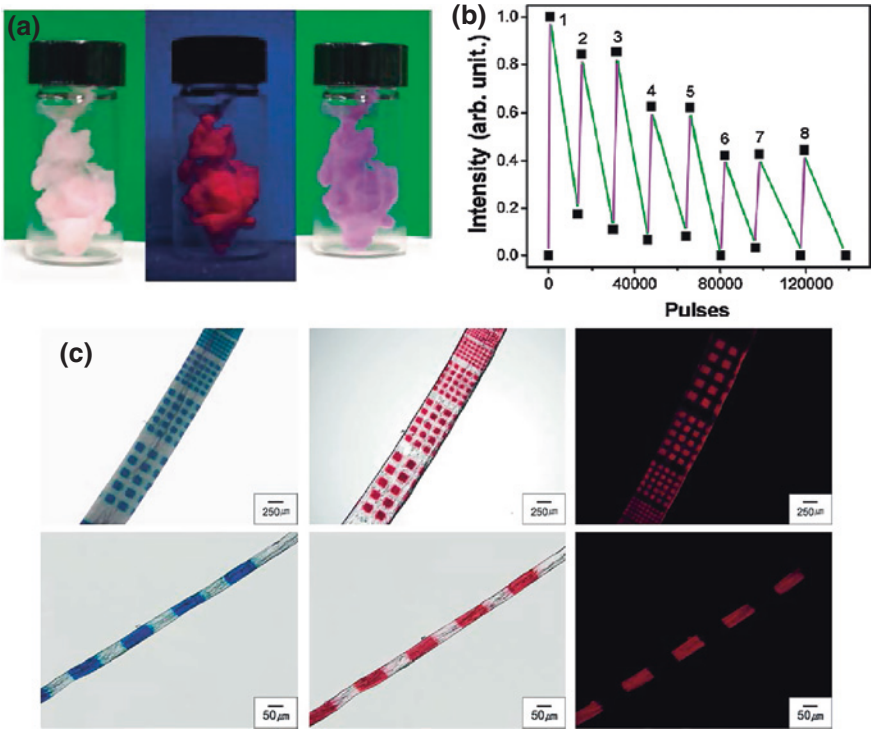


**Fig. 5.9** **a** Photographs of photoswitchable nanofibers in the off form (*left*), excited form (*center*), and on form (*right*). **b** Cyclic photoisomerization of nanofibers through integrated absorption. Absorption spectra collected upon alternatively irradiating the nanofibers with UV and green pulsed laser light [66]. **c** Images of a single patterned PCDA-embedded PMMA fiber with 30 wt% (*upper panels*) and 20 wt% (*bottom panels*) PMMA. Optical images (*left*) obtained after UV irradiation of the electrospun fiber. Optical (*middle*) and fluorescence (*right*) microscopy images obtained after heat treatment of the blue-patterned fiber [69]

trigger and manipulate various interfacial phenomena and properties, including the surface wettability of nanofibers. To determine whether the photoresponsiveness of azobenzene is retained in electrospun fibers, static and dynamic contact angle measurements were performed under UV irradiation. According to different molar ratios of BP-azo to PCL, the static contact angle increased from 121.3 to 132.2 with increasing BP-azo molar ratio. However, following UV irradiation, the static contact angle significantly decreased and then the wettability switched back to the previous one after exposure to visible light. This reversibility of wettability during photoswitching was observed for three to five cycles. The changes observed upon UV irradiation were due to the reversible *trans*-to-*cis* isomerization of the azobenzene groups. This *trans*-to-*cis* isomerization caused an increase in the dipole moment of azobenzene molecules, which cause the decrease in surface free energy, thus resulting in a more hydrophilic surface. An increased concentration

of azobenzene on the surface induced a larger decrease in the surface free energy upon *trans*-to-*cis* isomerization and consequently a smaller water contact angle.

Another method of preparing photoresponsive fibers by photochromism was introduced by Chae et al. [69] who developed a method using polydiacetylene (PDA) supramolecules embedded in PMMA electrospun fibers. PDA was synthesized by the photopolymerization of diacetylene (DA). Owing to their interesting stimulus–induced chromic transition and nonlinear optical properties, PDAs have been extensively investigated as potential chemosensors and photonic materials. They prepared DA-embedded fibers by electrospinning of a solution of a polymer and DA in an organic solvent. Self-assembly of DA occurs in the inner part of the fiber during electrospinning and evaporation of the solvent, because the attraction between the DA molecules is stronger than that between DA and the polymer. The patterned photochromism reaction can be induced by UV irradiation with a photomask on a single fiber that induced polymerization with a certain pattern. Following UV irradiation with a pattern, the fiber color changed to blue, which indicated that PDA was successfully produced from the DA monomer. Upon heating up to 110 °C, the blue color changed to red because PDA has a bichromic property, that is, it can undergo not only photochromism but also thermochromism (Fig. 5.9c).

### *5.4.3 pH-Responsive Fibers*

Regarding the biomaterial or biomedical applications of nanofibers, pH is the most important factor because our bodies are composed of various organs and tissues that have a wide range of pHs [17], such as the stomach (pHs 1–3), intestines (pHs 5–8), blood (pHs 7.3–7.5), tumors (pHs 6.5–7) and as well as intracellular organelle such as lysosomes (pHs 4.5–5). Therefore, pH-responsive polymers, that is, polymers that show dynamic responses to environmental pH, have attracted much attention. The pH-responsive polymers are polyelectrolytes that bear in their structure weak acidic or basic groups that either accept or release protons in response to changes in environmental pH. The pH-responsive polymers can be generated by conjugation of acidic or basic groups to the polymer backbone of polyelectrolytes that undergo ionization similarly to acidic or basic groups of monoacids or monobases. Following the exchange of the charge along the polymer backbone, the resulting electrostatic repulsion causes a reversible alteration in polymer properties such as size or volume, which strongly depend on pH, ionic strength and type of counterion. The transition from the collapsed state to the expanded state has been explained by changes in the osmotic pressure exerted by mobile counterions neutralizing the network charges. The pH range in which reversible phase transition occurs can be generally modulated by two strategies [70]:

1. Selection of the ionizable moiety with a pKa matching the desired pH range. Therefore, the proper selection between a polyacid or a polybase should be considered for the desired application.

2. Incorporation of hydrophobic moieties into the polymer backbone and control of their nature, amount and distribution. When ionizable groups become neutral and nonionized, and the electrostatic repulsion force disappears within the polymer network, hydrophobic interactions dominate. The introduction of a more hydrophobic moiety can offer a more compact conformation in the uncharged state and a more acute phase transition.

Here, examples of pH-responsive fibers with controlled swelling or volume are presented. Gestos et al. [71] prepared pH-responsive electrospun nanofibers using poly(acrylic acid) (PAA), which has the merits of biocompatibility and crosslink ability without the need for additional crosslinkers. The carboxylic groups not only play a role in pH responsiveness but also function as crosslinkers under UV irradiation. Therefore, the UV treatment time strongly affects the extent of swelling induced by pH switching. The 5-min UV-treated PAA nanofibers swelled at both pHs 3 and 8, and their swelling ratios decreased with increasing UV treatment time to 25 min. The 25-min UV-treated fiber attained swelling ratios of 0.91 at pH 3 and 2.0 at pH 8. The observed decrease in swelling ratio with increasing UV radiation dose is likely due to an increase in crosslink density. An increase in crosslink density introduces more constrained junctions into the network and a reduction in swelling. Somewhat unexpectedly, the 25-min UV-treated PAA nanofiber showed an initial shrinkage when first immersed in solution (pH 3). It is likely that leaching of low-molecular-weight soluble fragments and non-crosslinked PAA may counteract the swelling and produce a small reduction in dimensions. The subsequent pH switching reproducibly induced the expected swelling and shrinkage. Additionally, the mechanical resilience of fibers changed according to the pH and wet state. The 5-min UV-treated PAA fibers at pH 3 showed a stiffness of 0.10 $Nm^{-1}$, much lower than that of the 25-min UV-treated sample at 0.19 $Nm^{-1}$. As the cantilever stiffness (0.2 $Nm^{-1}$) is similar to that measured for the 25-min UV-treated sample, only the minimum stiffness can be inferred. Thus, in qualitative terms, PAA exposed to UV radiation for 25 min is at least twice as stiff as that exposed to UV radiation for only 5 min. This change in stiffness is consistent with the increase in crosslink density. Jin and Hsieh [24] carried out a similar study of electrospun nanofibers prepared from PAA and poly(vinyl alcohol) mixture solution. According to crosslink temperature and pH, the equilibrium swelling in planar dimensions, i.e., thickness and mass, was clearly demonstrated. With increasing crosslinking network density, the equilibrium swelling in planar dimensions, i.e., thickness and mass, decreased at the same pH. Furthermore, the equilibrium swelling of nanofibers increased with increasing pH.

Wang et al. [72] prepared pH-responsive fibers using a polybase material: a monodisperse triblock copolymer consisting of poly(methyl methacrylate)-*block*-poly(2-(diethylamino) ethyl methacrylate)-*block*-poly(methyl methacrylate) (PMMA-*b*-PDEA-*b*-PMMA). The fibers expanded at pH 7.3 and contracted at pH 3.5, because the triblock copolymer exhibited contrasting pH-responsive behaviors:

the polybase charge is neutral above pH 5 (collapsed) and positive below pH 5 (expanded). The fibers showed greater responsiveness than the control film because the surface area of the fibers significantly increased. This increased the rate of diffusion of the solvated hydrogen ions throughout the polymer matrix; thus, the responsiveness consequently increased.

### *5.4.4 Electric-Field-Responsive Fibers*

As mentioned in Sect. 5.2.2 on electrospinning, the electric field greatly affects fiber formation, morphology and diameter during electrospinning. Not only the electrospinning process, but also the electric field can affect the properties of fibers as an external stimulus.

Filipcsei et al. [73] reported on PDMS hydrogel fibers containing randomly distributed $TiO_2$ particles with electrically driven motility. The hydrogel fibers showed significant and rapid bending towards the cathode, when an external electric field was applied. This behavior was reversible with alternating positive and negative electrode application. The displacement of the free bottom end of the gel depends on the strength of the electric field. These experimental results are evidence that in the external electric field, the gel accumulates positive charges. A large deflection due to the interaction of the applied external electric field with the charged gel was observed. Furthermore, when one of the electrodes was replaced by a metal ball and the other electrode was a copper plate, deformation of a PDMS hydrogel fiber was also observed under anonuniform electric field. These results might be explained by electron migration. Under an applied electric field, $TiO_2$ particles emit electrons. As the electrons migrate to the anode, the particles incorporated in the hydrogel fiber obtain a positive charge. The Coulomb interactions of these charged particles with the external electric field are responsible for the gel deformation. Note that the bending was rapid and the final shape at equilibrium was reached within 5 s.

Li and Hsieh [74] prepared electrospun hydrogel fibers using a mixture of PAA and PVA at different ratios and investigated the swelling of the hydrogel fibers immersed in aqueous solution. Because of PAA, pronounced swelling of the electrospun hydrogel fibers was observed in response to pH (particularly between 4 and 7). The hydrogel fibers were induced to swell further by applying an electric field (10 V $cm^{-1}$). When the hydrogel fibers were exposed to an electric field, the swelling ratio significantly increased with increasing PAA content in the hydrogel fibers and the strength of the electric fields, and the swelling was reversible by the application and removal of the electric field. This increased swelling ratio was also accompanied by increased width and thickness of the hydrogel fibers. These data show that the pH-dependent swelling of the electrospun hydrogel fibers can be further augmented by the application of an electric field.

### 5.4.5 Magnetic-Field-Responsive Fibers

As most well-known magnetic-field-responsive materials, magnetite ($Fe_3O_4$) and maghemite ($\gamma$-$Fe_2O_3$) nanoparticles are easily found in nature and are components of obtained ferromagnetic phases [75]. The fibers that respond to the magnetic fields can be obtained by combining these magnetic nanoparticles (MNPs); such fibers have shape, size or swelling distortion owing to their unique self-heating property that occurs reversibly and instantaneously in the presence of an alternating magnetic field (AMF). There are two basic ways of preparing magnetic-field-responsive fibers, namely, incorporation and immobilization of MNPs in fibers or on the fiber surface. Firstly, Lin et al. [76] reported on two methods of preparing magnetic-field-responsive fibers with MNPs that were immobilized on the fiber surface. First, the magnetic-field-responsive fibers were fabricated by the adsorption of magnetic particles onto the electrospun chitosan fibers in MNP solution ($Fe_3O_4$). The crosslinked fibers were immersed in MNP solution for 1 h with continuous mechanical stirring. Then, the magnetic-field-responsive fibers were obtained after washing and freeze drying. Second, other magnetic-field-responsive chitosan fibers were prepared by immersing the crosslinked chitosan fibers in MNP solution ($Fe^{2+}$ and $Fe^{3+}$ mixture) for 1 h for the adsorption of Fe ions. Then, deoxygenated $NH_4OH$ solution was added dropwise to the mixture with vigorous stirring for 1 h, resulting in the formation of the magnetic-field-responsive fibers. Eventually, the magnetic-field-responsive fibers were obtained by washing and lyophilization. These two types of fiber clearly showed MNPs on the fiber surface, exhibiting typical superparamagnetic behavior at room temperature without a hysteresis loop (Fig. 5.10a). In further study of the time-dependent heating property of the chitosan-MNP fibers, the increase in temperature to 45 °C was observed in response to AMF. Secondly, Huang et al. [77] prepared MNP-incorporated polystyrene (PS) fibers by electrospinning. The MNPs were well encapsulated inside the fibers and no leakage of any particles was observed morphologically. From the heating capacity of PS-MNP fibers under an applied AMF, the temperature of 282 mg of PS-MNP fibers in 1 mL of water can increase from 23 to 83 °C in 180 s in response to AMF at 232 kHz. These results reveal a powerful heating capacity of the fibers. In addition, Wang et al. [78] also described a similar study, that is, the formation of superparamagnetic fibers containing stably dispersed MNPs by electrospinning (Fig. 5.10b). The MNPs were synthesized by an aqueous coprecipitation technique in the presence of a polymer that attaches to the particle surfaces and confers steric stabilization to the nanoparticles dispersed in the polymer solution. As the main polymer, PVA was used and all of the MNPs were well embedded in PVA fibers after electrospinning. As shown by a test using a superconducting quantum interference device (SQUID), the PVA-MNP fibers were easily magnetized by an external magnetic field, and the dipole moments of the nanoparticles were readily polarized in the direction of the external

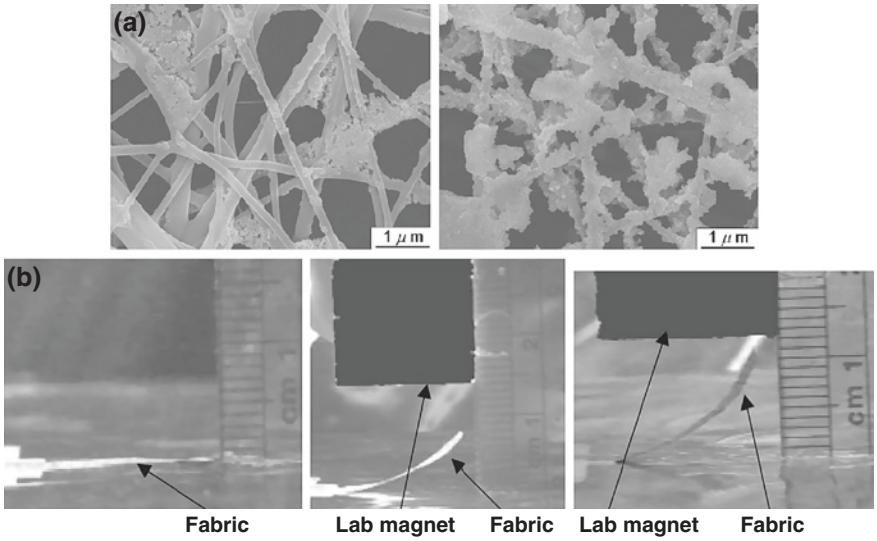


**Fig. 5.10** **a** SEM images of magnetic nanofiber composites with magnetic particles: (*left*) $Fe_3O_4$ (*right*) $Fe^{2+}/Fe^{3+}$ [76]. **b** Magnetic-field responsive behavior of PVA/magnetite fabric: (*left*) without magnetic field (*middle*) within low gradient of magnetic field, and (*right*) within high gradient of magnetic field [78]

magnetic field. It is well known that the magnetic dipole experiences a torque in a uniform magnetic field and a translational force in a magnetic field gradient. For the PVA-MNP fibers in an external magnetic field gradient, the fibers showed deformation by the translational force experienced by the embedded MNPs.

On the other hand, Kriha et al. [79] studied the controlled movement of short electrospun copolymers of methylmethacrylate (MMA) and 9-vinylanthracene (Anth) microfibers containing a superparamagnetic material, namely, fcc cobalt (Co)-based nanoparticles of 9 nm diameter. The prepared fibers were manipulated using a ferromagnet placed below the microscope slide. As a result, several fibers were moved simultaneously in the same direction with the ferromagnet, which can be advantageous for multifold simultaneous bridging of the target object. Two effects are exploited to manipulate the location and orientation of the superparamagnetic fibers using the external magnet.

1. A paramagnetic object tends to move in the direction of increasing magnetic field strength. Thus, by shifting the position of the magnet below the plane on which the fiber is dispersed in a water layer, one is able to induce translational motions of the fiber.
2. Anisotropic paramagnetic objects tend to align their principal axis of magnetization relative to the direction of the magnetic field lines. By rotating the magnet, one is thus able to induce rotational motions of the fibers.

### *5.4.6 Biomolecule-Responsive Fibers*

Because the stimulus-responsive fibers are becoming increasingly important in biomedical and biomaterial applications, recently, there has been increasing interest in fibers with functionality that induces responses upon exposure to biological small molecules or biomacromolecules. In particular, polymers that respond to glucose have received considerable attention because of their potential application in sensing proteins. Heo et al. [80, 81] successfully evaluated in vivo glucose-sensitive fibers. They designed and synthesized a unique fluorescent monomer based on diboronic acid that enables reversible responsiveness to glucose without any reagents or enzymes. This glucose-responsive fluorescent monomer (GF-monomer) was modified from a glucose-responsive fluorescent dye (GF dye). The principle underlying the glucose responsiveness of the GF dye is briefly explained as follows: the GF dye comprises a diboronic acid moiety and an anthracene moiety that act as the specific glucose-recognition site and the fluorogenic site, respectively (Fig. 5.11).

For the control of fiber degradation or fragmentation, the proteins are employed in protein-responsive fibers. Wang et al. [82] employed glutathione as an electrospun nanofiber degradation trigger. The protein-responsive nanofibers are composed of poly(2-hydroxypropyl methacrylate) (PHPMA), which is subsequently crosslinked with protein-cleavable disulfide-based dimethacrylate (DSDMA) branches that provide water-insoluble nanofibers. The swollen nanofibers in an aqueous solution allow the rapid diffusion of the glutathione throughout the fibers and hence ensure facile cleavage of the disulfide bonds. These branch sites can be considered to be the keystone for the reductive degradation of the copolymer fibers, because aqueous dissolution should occur once the copolymer has been converted into its low-molecular-weight primary chains. This means that protein degradation leads to the complete dissolution of the water-insoluble nanofibers. On the other hand, Law et al. [83] designed enzyme-responsive nanofibers that are composed of self-assembled hydrophobic β-sheet peptides incorporating protease-sensitive domains, fluorescent reporters, and hydrophilic PEG units. By incubating nanofibers with a urokinase plasminogen activator (uPA) as a fiber fragmentation inducer, assembled nanofibers were cleaved in response to uPA and FITC-conjugated fragments were released. Furthermore, this fragmentation shows uPA concentration dependence (in the absence of uPA, the fluorescence intensity baseline remained constant with time, suggesting that the formulations were stable). The length of these single self-assembled nanofibers can be controlled by adding uPA. These novel materials, which are protein-responsive fibers, could have important applications in in vivo protein imaging or as enzyme-responsive biopolymers for systemic drug delivery.

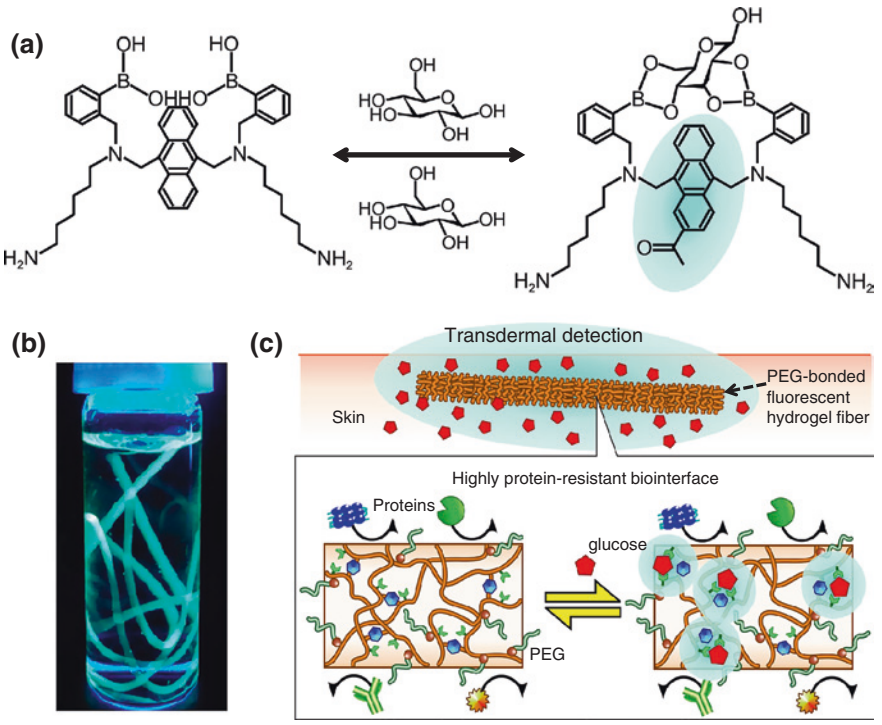


**Fig. 5.11** **a** Fluorescence intensity changes depending on the existence of a glucose molecule. **b** Fluorescent glucose-responsive monomer immobilized in hydrogel fibers in a glass vial with a 50 % glucose solution. **c** Conceptual illustration of the PEG-bonded fluorescent-hydrogel fiber for glucose monitoring. The fluorescent signal in response to blood glucose concentration is transmitted across the skin, enabling the detection of blood glucose concentration in a minimally invasive manner. The fiber shape is retained in the implantation site for a long period, and PEG-bonded PAM has an interface highly biocompatible with tissues; the PEG-bonded PAM hydrogel is highly resistant to protein adsorption, thereby reducing inflammation. As a result, the PEG-bonded fluorescent hydrogel fibers can be applied to long-term in vivo glucose monitoring [80, 81]

## 5.5 Applications of Smart Fibers

Although smart fibers are under development for a wide range of applications such as sensors, filters, biomaterials or textiles, biomaterials for smart fibers are most widely studied. Therefore, in this section, smart fibers for biomaterial applications will be discussed with some examples.

### 5.5.1 Sensors

The role of sensors is to transform physical or chemical responses into signals on the basis of the targeted application. In particular, polymeric electrospun nanofibers have been investigated as sensors of gases, chemicals, optical material and biomaterials. It is considered that highly sensitive sensors can be assembled using nanofibers that possess high surface area and porosity. Here, polymeric fibers for fabricating sensors will be discussed in detail.

Qi et al. [84] synthesized pure and KCl-doped $TiO_2$ nanofibers by electrospinning and calcination techniques for fabricating humidity sensors. The humidity sensing properties of the prepared nanofibers were investigated with a ZL5 intelligent LCR (L: inductance, C: capacitance, and R: resistance) test meter. All nanofibers were exposed to dry/wet/dry air cycles in order to test the different sensitivities to different relative humidities (RHs). As a result, the KCl-doped $TiO_2$ nanofibers showed improved humidity sensing properties with their resistances varying by more than four orders of magnitude, whereas the resistance changed only about two orders of magnitude for pure $TiO_2$ nanofibers. Furthermore, by increasing the RH from 11 to 95 %, the response time is only 3 s and the recovery time is 4 s for KCl-doped $TiO_2$ nanofibers. On the other hand, Li et al. [85] also fabricated a humidity sensor using electrospun $TiO_2$ nanofibers modified with LiCl. The as-prepared humidity sensor exhibits excellent sensing characteristics, including an ultrafast response (3 s) and recovery time (7 s) for measuring a wide RH range of 11–95 % in air at room temperature (25 °C) with the impedance changing from $10^7$ to $10^4$ Ω. In the pure $TiO_2$ nanofibers at a high RH, hydration of $H_3O^+$ is energetically favored in liquid water, which makes the resistance of these nanofibers decrease rapidly. For the KCl (LiCl)-doped $TiO_2$ nanofibers, besides the $H_3O^+$, KCl can dissolve in the adsorbed water, and the $K^+$ (or $Li^+$) and $Cl^-$ ions dissociated from these nanofibers can function as conduction carriers. Thus, the resistance continuously decreases by more than four orders of magnitude compared with the initial resistance.

Recently, Wang et al. [86, 87] have reported the fabrication of 'spider-web-like nanonets' as a humidity sensor (Fig. 5.12a, b). These spider-web-like nanonets were fabricated by electrospinning onto a quartz crystal microbalance (QCM). The QCM-based fibrous sensors presented the most obvious decrease infrequency shift in the RH range of 2–95 %, and the response time of the sensors to RH gradually decreased with increasing RH in the chamber. For a flat film sensor, the response decreased with increasing RH ranging from 2 to 80 %; however, it decreased to an unmeasurable value once the RH exceeded 80 %, which could be attributed to the mass loading of moisture. For fiber-coated sensors, however, the response showed an initial linear decrease in frequency corresponding to an increase in RH up to 50 %, and shifted to the opposite direction at a higher RH (>50 % RH), indicating that the moisture starts to be released from fibers at a higher RH.

On the other hand, Yang et al. [88] reported the fabrication of $SnO_2$ fibers for $H_2$ and $NO_2$ gas sensing. They prepared a sensor that consisted of palladium

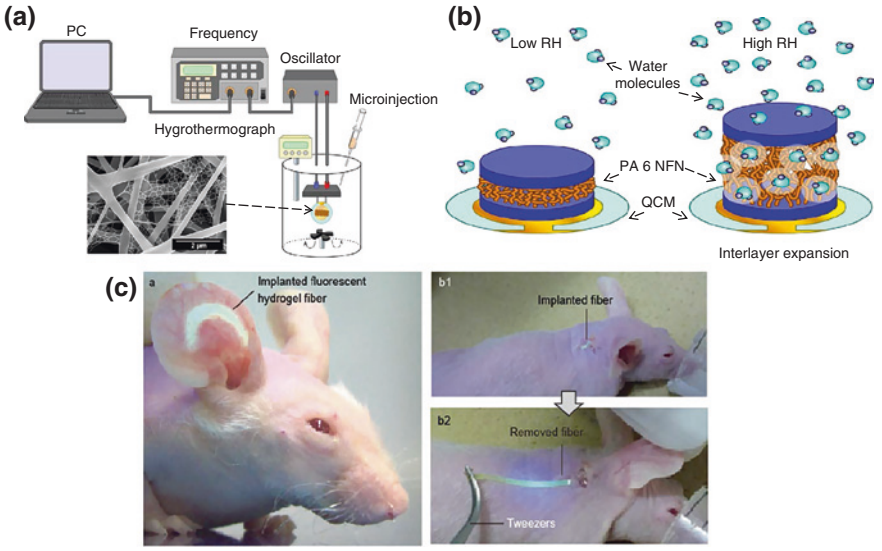


**Fig. 5.12** **a** Schematic diagram of relative humidity sensing system [86]. **b** Schematic illustration of humidity-sensing mechanism of a QCM-based PEI-PA 6 NFN sensor [87]. **c** (*left*) The fluorescence of the fibrous glucose sensor can be detected through the skin. The *fiber-shaped* sensor was implanted under the skin of the ear of a mouse. (*right*, *upper panel*) The fiber implanted in a mouse model (*right*, *bottom panel*) could be easily removed after use [90]

(Pd)-loaded $SnO_2$ fibers. This sensor showed a much higher sensitivity to $H_2$ than the sensor with non-Pd-loaded fibers, but very interestingly, this trend was reversed upon exposure to $NO_2$. The observation that the sensitivity to $NO_2$ was higher in the sensor with non-Pd-loaded $SnO_2$ fibers than in the sensor with Pd-loaded $SnO_2$ fibers suggests that the sensitization to $H_2$ by Pd loading is largely due to the catalytic effect of Pd loading as a means of increasing the sensitivity of $SnO_2$ sensors to reducing gases such as $H_2$, CO, $CH_4$, and other hydrocarbon gases, which is well known. The same group of researchers fabricated exhaled-breath-sensing $SnO_2$ fibers that have unique morphological features that can make multiple sensing layers within a single fiber rapidly and effectively accessible to large acetone molecules [89]. The thin wall of assembled $SnO_2$ fibers with wrinkled layers was successfully synthesized by electrospinning with controlled phase separation between precursor-rich phases and polymer-rich phases. In particular, elongated open pores are extensively formed on the surface of the wrinkled $SnO_2$ thin walls, and hollow voids are found between wrinkled $SnO_2$ walls. The densely packed $SnO_2$ fibers were also synthesized. Using the $SnO_2$ fibers assembled into a wrinkled wall, a superior detection capacity with an appreciably fast response was achieved at a low acetone concentration in a highly humid atmosphere (RH 80 %), which satisfies the minimum requirement for a real-time exhaled-breath sensing in the diagnosis of diabetes.

Among biosensors, glucose sensors have been extensively studied using many different materials. In particular, Heo et al. [80, 81, 90] developed a hydrogel fibrous glucose sensor that has the following significant advantages:

1. The fibers can remain at the implantation site for an extended period, whereas microbeads disperse from the implantation site.
2. The fibers can be implanted at a readily controllable fluorescence intensity by cutting them to a specified length, thereby enabling stable and repeatable sensing.
3. The fibers can be easily and nonsurgically removed from the body.

An in vivo glucose fiber sensor implanted under the ear skin of mice remained at the implantation site for an extended period because the increased contact area with the subcutaneous tissue decreased the mobility of the subcutaneous implants (Fig. 5.12c). Immediately after the implantation, the fiber sensor was visible through the ear skin of over 100 μm thickness. For glucose sensing, Heo and coworkers injected glucose to temporarily increase the glucose concentration to 300 mg $dL^{-1}$ and insulin to decrease the glucose concentration to below 140 mg $dL^{-1}$. As a result, the fluorescence intensity of hydrogel fibers constantly tracked the fluctuations in blood glucose concentration for two up-and-down cycles. For long-term monitoring, after about 4 months from implantation, the fluorescence intensity of hydrogel fibers responded to blood glucose concentration fluctuations in oneup-and-down cycle. These results indicate that the hydrogel fibers maintained their sensor functionality in vivo for a long period without inducing inflammatory reactions.

### *5.5.2 Controlled Drug Delivery Systems*

DDSs are quite interesting applications that have evolved over the years, long before sustained DDSs were developed. Recently, many researchers have focused on controlled DDSs because these have become possible with the use of smart materials with remotely controllable properties. Therefore, drugs can be released to targeted regions on demand.

Zhang and Yarin [91] introduced two types of smart nanofiber for the study of the release of a dye rhodamine 610 chloride as a drug model. The electrospun nanofibers were fabricated from poly(NIPAAm-*co*-MMA) and poly(NIPAAm-*co*-MMA-*co*-AAc) copolymers, which are temperature-responsive and pH/temperature dual-responsive copolymers, respectively. In the case of a dye release study using poly(NIPAAm-*co*-MMA) nanofibers, a relatively low cumulative release rate (on the order of 1 %) was observed below LCST, which resembled that of pure PMMA nanofibers. By the time the temperature crossed the LCST, however, the corresponding cumulative release rate had rapidly reached about 10 % and saturated at about 12 %. Moreover, the release rate demonstrated the largest thermal response. It is emphasized that poly(NIPAAm-*co*-MMA) nanofibers exhibited

a positive thermoresponsive release profile, that is, a higher release rate when the nanofibers shrink above LCST than when the nanofibers swell below LCST. On the other hand, the release patterns of many other PNIPAAm-based hydrogels known today are negatively thermosensitive. Further study was performed using poly(NIPAAm-*co*-MMA-*co*-AAc) nanofibers to examine the effect of pH on the dye release profile at body temperature. The release profile demonstrated that marked changes in the cumulative release level and release rate occur between pHs 6 and 7.

Cui et al. [92] fabricated pH-responsive nanofibers for a local drug delivery system by introducing acid-labile acetal groups into a biodegradable backbone. The drug (paracetamol)-incorporated nanofibers were prepared by electrospinning. The profile of drug release from the electrospun nanofibers prepared from an acid-labile polymer was evaluated in buffer solutions of different pHs (4.0, 5.5 and 7.0). In the absence of an acid group in the polymer, there were no significant differences in the profile among the buffer solutions of different pHs. Following the introduction of an acid group, significantly different drug release profiles were observed. The total amounts of the drug released were about 67 and 78 % after incubation in pH 5.5 and pH 4.0 buffer solutions, respectively, and only 26 % after incubation in pH 7.4. Moreover, the amount of the drug burst-released depended on the contents of acid-labile segments and the polymer nanofibers incubated in pH 4.0 medium. Additionally, when the pHs of buffer solutions were 5.5 and 4.0, the amount of drug released from pH-sensitive nanofibers increased owing to the pH-induced structural changes of the polymeric nanofibers and the degradation of the matrix polymer.

Here, we introduce a study of electroresponsive nanofibers by Yun et al. [93] for transdermal drug (ketoprofen) release. In this study, an effective transdermal delivery system (TDS) was developed by improving the electrosensitivity of nanofibers with the uniform distribution of an electroconducting material. Multi-walled carbon nanotubes (MWCNTs) were embedded in these nanofibers as the electroconducting material because they could improve both the electrical conductivity and mechanical strength of the nanofibers. To improve the dispersion of MWCNTs, the surface of MWCNTs was modified by oxyfluorination to introduce functional groups onto the surface of hydrophobic MWCNTs, which improved conductivity resulting in the increased electrosensitivity of hydrogels. As polymer matrices, a PVA and PAA mixture was used. The PVA/PAA/MWCNT nanofibers swelled in an aqueous solution. The swelling ratio of nanofibers decreased with increasing MWCNT content owing to the inhibition of swelling in the presence of MWCNTs. However, a totally different trend occurred for nanofibers in the presence of an electric field. The swelling ratio of nanofibers increased under an electric field with increasing MWCNT content. MWCNTs could form an efficient pathway of electric field owing to their own electrical conductivity. This electrical conductivity of MWCNTs contributed largely to the enhanced swelling of nanofibers by accelerating the ionization of functional groups in the hydrophilic polymers. The ionization of functional groups caused the electrostatic repulsion and hydrophilicity of the polymer chains to increase significantly (Fig. 5.13a). Furthermore, the swelling of nanofibers

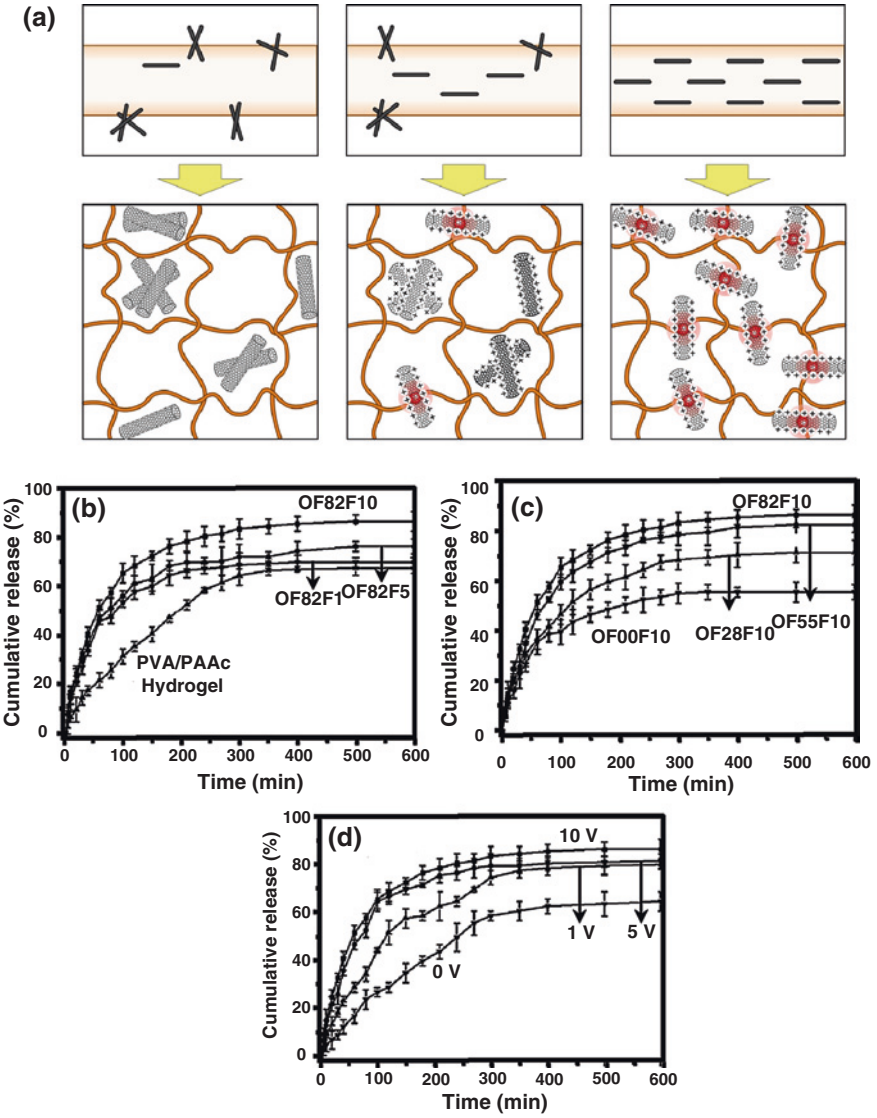


**Fig. 5.13** **a** Schematic representation of electrospinning process and role of functional groups on MWCNTs in maintainingdispersion stability: (*left*) high concentration of MWCNTs with high hydrophobicity (*middle*) low concentration of MWCNTs with high hydrophilicity, and (*right*) high concentration of MWCNTs with high hydrophilicity. Drug permeability of nanofibers depending on **b** content of oxyfluorinated MWCNTs under 10 V, **c** oxyfluorination conditions (hydrophilicity of MWCNTs) under 10 V, and **d** electric voltage [93]

was enhanced with increasing electric voltage. The higher the electric voltage applied to the nanofibers, the greater the ionization of functional groups. The ionized groups in the polymer matrices caused the faster and enhanced swelling of

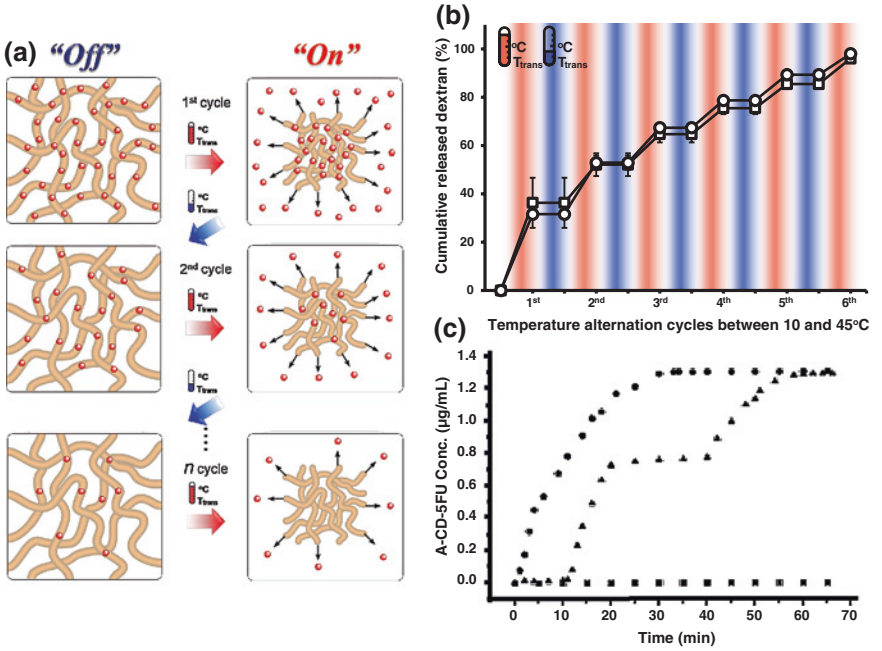


**Fig. 5.14** **a** Schematic of 'on–off' controlled release of dextran (*red*) from temperature-responsive nanofibers. Dextran-nanofibers offer the stepwise release of a certain amount of dextran within a short time in response to cycles of temperature alternations. **b** Release profiles of dextran from crosslinked PNH 5 (*squares*) and PNH 10 (*circles*) in response to cycles of temperature alternations between 10 and 45 °C [61]. **c** Profile of R-CD-5FU prodrug release from fiber surface with time. Prodrug release profile in the dark (*squares*). Prodrug release profile under continuous exposure to UV (*circles*). Prodrug release profile under intermittent exposure to UV at intervals of 10–20 and 40–70 min (*triangles*) [94]

nanofibers. A ketoprofen release test was performed on the skin of a hairless mouse model. The drug release behavior of nanofibers showed a similar trend to swelling behavior. The amount of released drug increased with increasing content of MWCNTs (Fig. 5.13b). The amount of released drug increased also with increasing hydrophilicity of MWCNTs (Fig. 5.13c) and in the presence of a high electric voltage (Fig. 5.13d). The swelling was the main factor in the drug release behavior of nanofibers. Therefore, the MWCNTs played an important role in the electrosensitive release of the drug from nanofibers.

Kim et al.[61] fabricated novel temperature-responsive nanofibers for 'on–off' drug release systems (Fig. 5.14a). They synthesized the nanofibers using the temperature-responsive polymer poly(NIPAAm-*co*-HMAAm), and FITC-dextran was directly embedded into these nanofibers as the drug model. The prepared nanofibers showed 'on–off' switchable swelling–shrinking behavior in response to temperature alternation cycles upon crossing the LCST; correspondingly, the dextran release profile showed the 'on–off' switchable behavior. After the first heating, approximately

30 % of the loaded dextran was released from the nanofibers. The release stopped after cooling below LCST but the release restarted upon the second heating. In this system, the dextran is released by it being squeezed out of the collapsed interconnected crosslinked polymer network. The release of dextran stops upon cooling because of the suppressed diffusion of the dextran molecules, which have a high molecular weight. Almost all of the dextran was released from the nanofibers after six temperature cycles (Fig. 5.14b). This kind of 'on–off' drug release system can release a certain amount of a drug within a short time after an off period that can be programmed according to the circadian rhythm of the disease being treated.

On the other hand, Fu et al. [94] studied the development of a novel photoresponsive 'on–off' release system for a prodrug based on host–guest interaction on the photoresponsive and crosslinked nanofiber surface. The nanofibers with stimulus-responsive surfaces were electrospun from the block copolymer prepared by controlled radical polymerization, and then the surfaces were modified with photosensitive 4-propargyloxyazobenzene (PAB) by 'click chemistry'. Following UV irradiation at a wavelength of 365 nm, the prodrug was released quickly from nanofiber surfaces, as the photosensitive group transformed from the *trans* form to the *cis* form configuration. In the dark, however, there was almost no release of the prodrug from the nanofiber surfaces, or between the host and the guest, that is, between the prodrug and the surfaces. Furthermore, this system showed a quick response and controllable release of the prodrug, as revealed by the multistep 'on–off' release profile under UV irradiation. The concentration of the prodrug in solution increases gradually in the next 10 min upon UV exposure. The concentration of the prodrug ceases to increase upon removal of the UV irradiation at $t = 20$ min. The concentration of the prodrug remains almost constant in the next 20 min, in the absence of UV irradiation. When UV irradiation is resumed at $t = 40$ min, the concentration of the prodrug in solution increases again (Fig. 5.14c).

### *5.5.3 Cell Manipulations*

In the biomaterial and biomedical fields, cell manipulations are good candidate applications of smart fibers including the cell culture substrate, cell capture and release membrane, control of cell functions, and so forth. There is an interesting report by Kriha et al. [79] on the controlled movement of short electrospun microfibers containing superparamagnetic cobalt (Co) nanoparticles. As a challenging example, controlled movement was demonstrated by the interconnection of hippocampal neurons. The cobalt nanoparticles were dispersed in the fluorescent polymeric microfibers by electrospinning and then the microfibers were cut into pieces of 50–100 mm length. The fibers dispersed in water were translationally moved by moving an external magnet horizontally or rotated by rotating the external magnet. The high control over fiber movement even allowed the researchers to position fibers so that a single fiber connected two primary hippocampal neurons within less than 30 s (Fig. 5.15a).

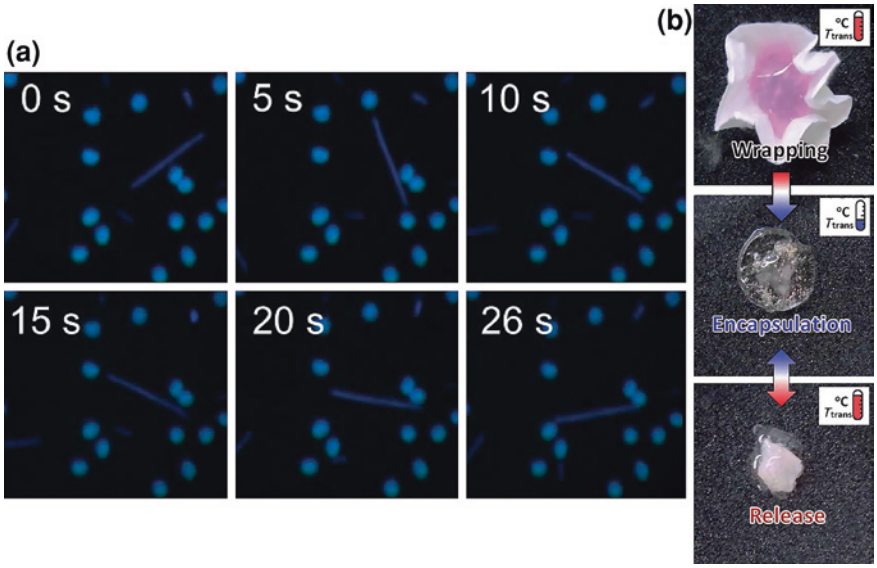


**Fig. 5.15** **a** Movement of co-embedded fibers dispersed in water droplet containing hippocampal cells (*blue spots*). The fibers were manipulated manually with a ferromagnet [79]. **b** Wrapping (*upper*), encapsulation (*middle*), and release (*bottom*) of cells by the fiber. The droplet containing cells is wrapped up at 37 °C (*upper*) and stably encapsulated inside the fiber, which transforms into a hydrogel-like morphology at 4 °C (*middle*). Upon heating the fiber again at 37 °C, it shrinks rapidly and releases the entrapped cells (*bottom*) [23]

Kim et al. [23] prepared a temperature-responsive fibrous hydrogel that was used as the cell capture and release membrane. The fibrous hydrogel captured and released cells by self-wrapping, encapsulation, and shrinking in response to temperature changes (Fig. 5.15b). In the cell culture medium at 37 °C, a droplet of cells was dropped on a fiber web, and immediately the web started to fold up and wrap around the droplet. The folding of the fiber web was very fast and was completed after 30 s. After 10 min at 37 °C, the fiber web was transferred to a refrigerator at 4 °C and allowed to swell for another 10 min. The fiber web became transparent with a hydrogel-like morphology, and the fibrous structure was maintained. When the web was heated again to 37 °C, the hydrogel-like fibrous web shrank and became opaque. After three cycles of temperature alternations, almost all of the cells (>95 %) seeded on the web were released, whereas only a few cells were released upon swelling during the cooling from 37 to 4 °C. Live/dead assay of the cells released from the web showed that almost all of the cells were alive, and the condition and proliferation of the cells were determined.

The most interesting application of magnetic-field-responsive fibers is in the hyperthermic treatment of cancer cells. Lin et al. [76] demonstrated Caco-2 (human colon adenocarcinoma) cell therapy using chitosan-MNP fibers that cause the temperature to rise to 44–45 °C, which is maintained owing to the heat generated in an alternating magnetic field (AMF). Owing to the hyperthermic effect

during Caco-2 cell culture, the cell viability in the presence of chitosan-MNPs was greatly reduced to below 70 % of control (without MNPs) when the magnetic field was turned on. A similar study was reported by Huang et al. [77]: PS-MNP nanofibers showed the hyperthermic effect on cultured SKOV-3 cells. When the PS-MNP nanofibers were exposed to the AMF for 10 min or longer, all the cancer cells were destroyed, and the association of the cancer cells with the nanofibers was also demonstrated. Here, improved hyperthermic smart fibers are introduced. Kim et al. [95] showed temperature-and magnetic-field-responsive electrospun nanofibers containing an antitumor drug (doxorubicin, DOX) and MNPs (Fig. 5.16a). Upon AMF application, the temperature-responsive nanofibers shrank in response to the increased temperature triggered by MNPs. The incorporated DOX was released from nanofibers owing to the hyperthermic effect. These nanofibers demonstrated the synergic effect of hyperthermia and chemotherapy for cancer cell therapy with the hyperthermic treatment time being less than 5 min, which can reduce the side effects on normal tissues or cells (Fig. 5.16b).

Yoshida et al. [96] developed reduction-responsive nonwoven fibers as a cell culture scaffold. They prepared water-soluble poly(γ-glutamic acid) (γ-PGA), which is secreted by a *Bacillus subtilis* strain. The reduction-responsive nanofibers were fabricated by crosslinking with cystamine-containing disulfide bonds (γ-PGA-SS). Cleaving the crosslinking networks is controllable under physiological conditions by altering the concentration of nontoxic reductants such as glutathione or cysteine. Such reductants cleave the disulfide bond into free thiol groups (–SH HS–), and thiol groups do not decrease the local pH. The obtained γ-PGA-SS nanofibers showed swelling in water and selective decomposition depending on the concentration of the L-cysteine solution. A high concentration of L-cysteine solution accelerated the decomposition of γ-PGA-SS nanofibers. This means that γ-PGA-SS nanofibers can be degraded in vivo depending on the concentration of biocompatible reductants. Another mouse L929 fibroblast culture study showed that cells adhered well and proliferated on the γ-PGA-SS nanofibers, and interactions between the cell pseudopodia and the γ-PGA-SS nanofibers were clearly observed. Furthermore, after the decomposition of γ-PGA-SS nanofibers by L-cysteine, living cells contained in the decomposed solution also well proliferated. These results suggest that fibrous networks are useful as cell culture scaffolds.

### *5.5.4 Filters*

Owing to the high specific surface area and high porosity of nanofibers, they have been developed as filter media, which are very useful for the separation or purification of not only waste water but also biomolecules. Furthermore, filtration has been improved and new types of nanofiber have been developed, such as hollow fibers. pH-responsive hollow fibers for protein antifouling were developed by Zou et al. [97]. The hollow fibers were prepared by a dry–wet spinning technique based on a liquid–liquid phase separation technique. Poly(MMA-*co*-AA-*co*-vinylpyrrolidone (VP)) terpolymer was synthesized to modify polyestersulfone (PES) hollow fiber

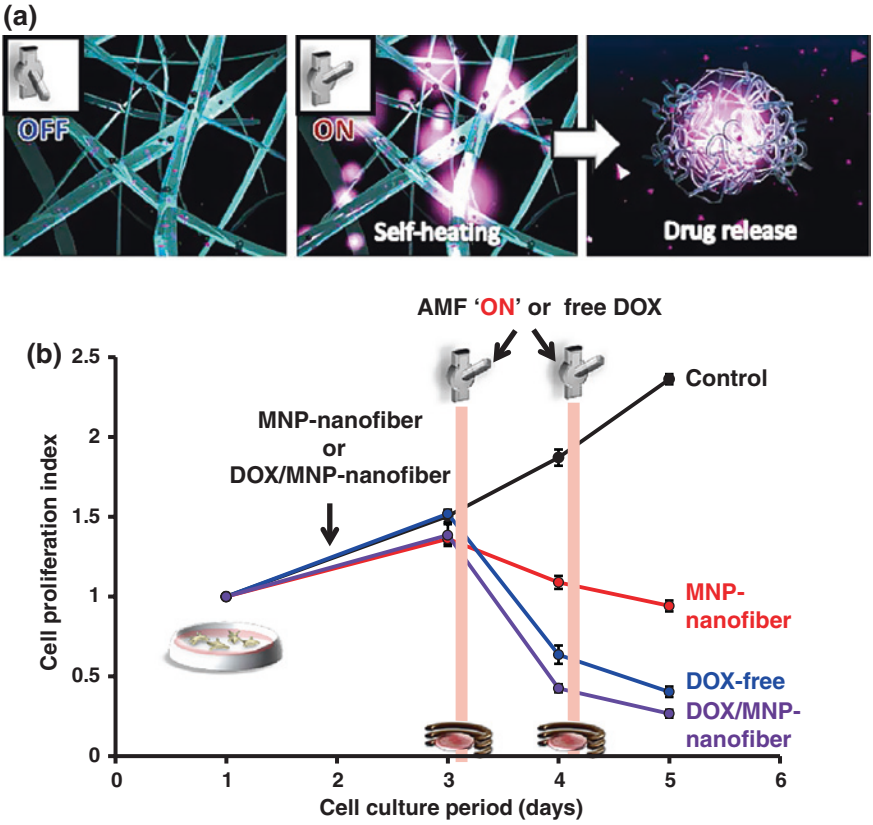


**Fig. 5.16** **a** Design concept for the hyperthermia nanofiber system with 'on–off' function utilizing MNPs dispersed in temperature-responsive polymers. An anticancer drug, DOX, is also incorporated into the nanofibers. **b** MTT assay result of in vitro anticancer tests using DOX/MNP-nanofibers and human melanoma cells. The cells were cultured at 37 °C for 2 days. MNP-nanofiber (*red line*) or DOX/MNP-nanofiber (*purple line*) was then added to the medium and co incubated with cells at 37 °C for another 24 h. AMF was then turned 'on' for 5 min to increase the medium temperature to 45 °C on days 3 and 4. Cells were also incubated in the absence of nanofibers with (*blue line*) and without (*black line*) DOX addition on days 3 and 4 [95]

membranes. When the pH changed from 2.0 to 11.0 in pH-responsive filtration, the fluxes increased under acid conditions owing to the increased hydrophilicity and showed pH dependence, that is, fluxes decreased with increasing pH. These results indicated that the flux variation increased with the increase in the amount of the terpolymer, and the pH sensitivity was caused by the dissociation of AA in the terpolymers. In a further study by the same group, they used another type of terpolymer (poly(St-*co*-AA-*co*-VP)), and two mechanisms underlying the functions of the pH-sensitive flat-sheet membranes (FSMs) and hollow fiber membranes (HFMs) were clarified, namely, the pore size change theory and electroviscous effect (Fig. 5.17a) [98]. Firstly, regarding the pore size change theory, the swelling-shrinking effect of

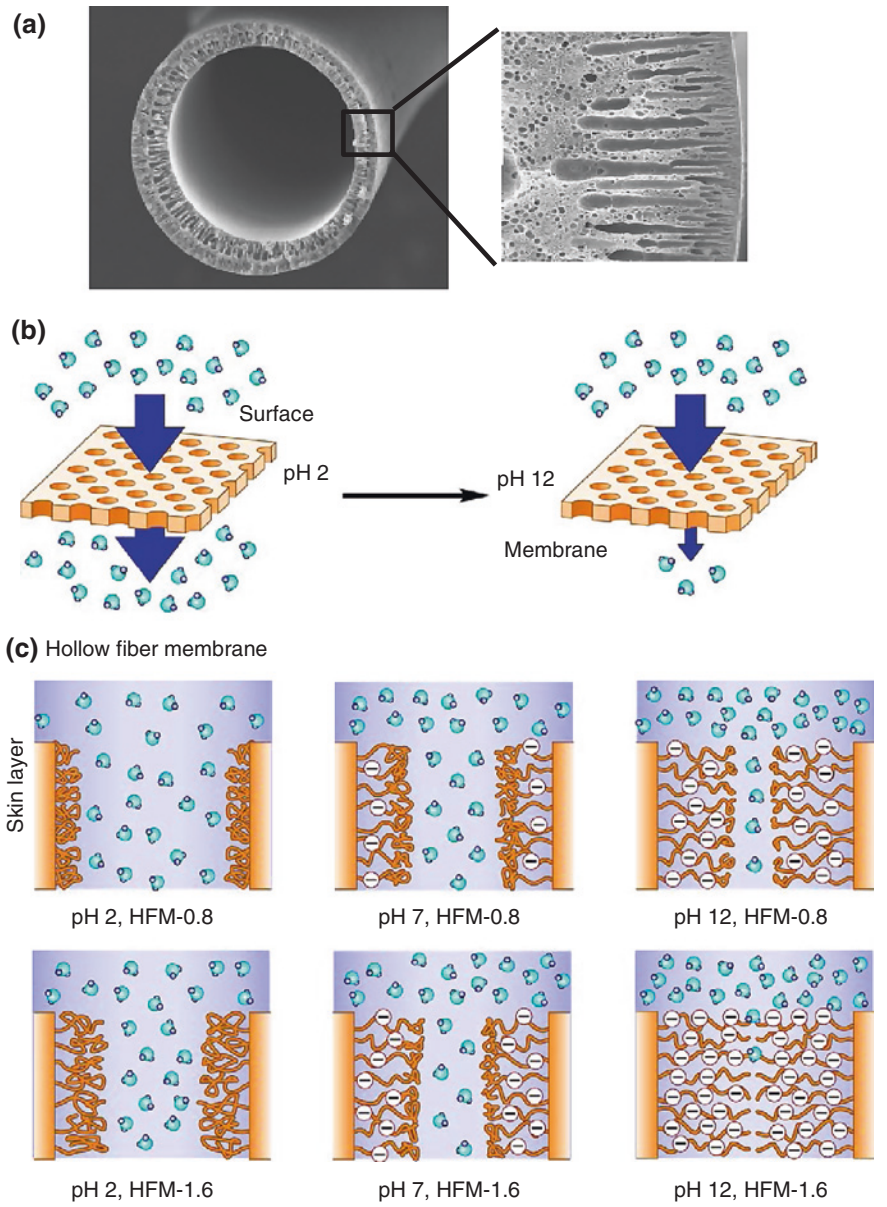


**Fig. 5.17** **a** Cross-sectional SEM images of pH-sensitive HFM. Tentative illustration of mechanism of pH-sensitive HFMs [97]. **b** Dead-end filtration using pH-sensitive flat-sheet membrane; **c** cross-flow filtration for pH-sensitive HFM. For better observation of the flux change, the water molecule was magnified, and decreasing the amount of water molecule did not provide the accurate scaledown of the water flux [98]

the ionized–deionized AA chain was deemed to be the main reason for the water flux change and solute rejection of the pore-filled pH-sensitive FSM (Fig. 5.17b). Secondly, regarding the electroviscous effect, the carboxylic acids of AA could dissociate to carboxylate ions at pH 12.0 to provide a high charge density in the copolymer, resulting in terpolymer swelling (Fig. 5.17c). Furthermore, the solution flowing through the pores in the membranes was affected by the electroviscous effect during the filtration. The electroviscous effect is a physical phenomenon that occurs when an electrolyte solution passes through a narrow capillary or pore with charged surfaces.

## 5.6 Conclusions and Future Trends

Fibers of various types at various production stages have already been explored for a wide range of applications in a variety of fields, including nanotechnology, textiles, industry, fuel cells, tissue engineering, regenerative medicine and biomaterials. These fibers, being particularly well-defined nanofibers, have astounding features as compared with other types of material, namely, high specific surface area, very high porosity and biomimetic properties, providing excellent potential applications. Therefore, fibers have been explored as cell culture scaffolds, DDSs and other biomaterial applications. Among these types of fiber, those that well combine with stimulus-responsive media, called smart fibers, can be turned on and off remotely (‘on–off’controllable) by applying external stimuli with the fiber features maintained. The applications of smart fibers are not limited in vitro or in vivo. Therefore, the smart fibers have received much attention from researchers because remotely controllable ‘on–off’ fiber systems could be good candidates for the treatment of cancer, damaged tissues or chronic diseases because they can be used to match the circadian rhythm of a disease. Unfortunately, the most serious limitation of fibers or smart fibers is their not being injectable into the body. Therefore, they are normally used in the form of mats, sheets or webs of bulk size. Nevertheless, mat- or sheet-type smart fibers offer an opportunity to develop useful applications, for example, dressings or anti-adhesion membranes for wounds. Further functionalization of smart fibers could also be used for the separation, purification and preservation of biomolecules or cells. Taking together all these merits of smart fibers (or fibers) and their potential applications, they can be utilized as key tools in a wide range of applications as well as cell or tissue therapy systems, DDSs and other biomaterial applications switchable by external remote control.

## References

1. Joseph HWB (1938) Order and life. In: Needham J, Sir Reader WD (eds) Philosophy 13:93–98. doi:10.1017/S0031819100014509 (Cambridge University Press, London, 1936 pp x + 178)
2. Zheng W, Zhang W, Jiang X (2010) Biomimetic collagen nanofibrous materials for bone tissue engineering. Adv Eng Mater 12:B451–B466. doi:10.1002/adem.200980087

3. Di Lullo GA, Sweeney SM, Körkkö J, Ala-Kokko L, San Antonio JD (2002) Mapping the ligand-binding sites and disease-associated mutations on the most abundant protein in the human, type I collagen. J Biol Chem 277:4223–4231. doi:10.1074/jbc.M110709200
4. He W, Yong T, Teo WE, Ma Z, Ramakrishna S (2005) Fabrication and endothelialization of collagen-blended biodegradable polymer nanofibers: potential vascular graft for blood vessel tissue engineering. Tissue Eng 11:1574–1588. doi:10.1089/ten.2005.11.1574
5. Ma L, Gao C, Mao Z, Zhou J, Shen J, Hu X, Han C (2003) Collagen/chitosan porous scaffolds with improved biostability for skin tissue engineering. Biomaterials 24:4833–4841. doi:http://dx.doi.org/10.1016/S0142-9612(03)00374-0
6. Pohunková H, Stehí J, Váchal J, čech O, Adam M (1996) Morphological features of bone healing under the effect of collagen-graft—glycosaminoglycan copolymer supplemented with the tripeptide Gly-His-Lys. Biomaterials 17:1567–1574. doi:http://dx.doi.org/10.1016/0142-9612(95)00310-X
7. Nehrer S, Breinan HA, Ramappa A, Hsu HP, Minas T, Shortkroff S, Sledge CB, Yannas IV, Spector M (1998) Chondrocyte-seeded collagen matrices implanted in a chondral defect in a canine model. Biomaterials 19:2313–2328. doi:http://dx.doi.org/10.1016/S0142-9612(98)00143-4
8. Hwang CM, Park Y, Park JY, Lee K, Sun K, Khademhosseini A, Lee SH (2009) Controlled cellular orientation on PLGA microfibers with defined diameters. Biomed Microdevices 11:739–746. doi:10.1007/s10544-009-9287-7
9. Zilberman M, Nelson KD, Eberhart RC (2005) Mechanical properties and in vitro degradation of bioresorbable fibers and expandable fiber-based stents. J Biomed Mater Res B Appl Biomater 74B:792–799. doi:10.1002/jbm.b.30319
10. Han D, Cheung KC (2011) Biodegradable cell-seeded nanofiber scaffolds for neural repair. Polymers 3:1684–1733. doi:10.3390/polym3041684
11. Chew SY, Park TG (2009) Nanofibers in regenerative medicine and drug delivery. Adv Drug Del Rev 61:987. doi:http://dx.doi.org/10.1016/j.addr.2009.07.004
12. Sell SA, McClure MJ, Garg K, Wolfe PS, Bowlin GL (2009) Electrospinning of collagen/biopolymers for regenerative medicine and cardiovascular tissue engineering. Adv Drug Del Rev 61:1007–1019. doi:http://dx.doi.org/10.1016/j.addr.2009.07.012
13. Lee KY, Jeong L, Kang YO, Lee SJ, Park WH (2009) Electrospinning of polysaccharides for regenerative medicine. Adv Drug Del Rev 61:1020–1032. doi:http://dx.doi.org/10.1016/j.addr.2009.07.006
14. Rho KS, Jeong L, Lee G, Seo BM, Park YJ, Hong SD, Roh S, Cho JJ, Park WH, Min BM (2006) Electrospinning of collagen nanofibers: effects on the behavior of normal human keratinocytes and early-stage wound healing. Biomaterials 27:1452–1461. doi:http://dx.doi.org/10.1016/j.biomaterials.2005.08.004
15. Holtz JH, Asher SA (1997) Polymerized colloidal crystal hydrogel films as intelligent chemical sensing materials. Nature 389:829–832
16. Kikuchi A, Okano T (2002) Intelligent thermoresponsive polymeric stationary phases for aqueous chromatography of biological compounds. Prog Polym Sci 27:1165–1193. doi:http://dx.doi.org/10.1016/S0079-6700(02)00013-8
17. Gupta P, Vermani K, Garg S (2002) Hydrogels: from controlled release to pH-responsive drug delivery. Drug Discovery Today 7:569–579. doi:http://dx.doi.org/10.1016/S1359-6446(02)02255-9
18. Stayton PS, Shimoboji T, Long C, Chilkoti A, Ghen G, Harris JM, Hoffman AS (1995) Control of protein-ligand recognition using a stimuli-responsive polymer. Nature 378:472–474. doi:10.1038/378472a0
19. Kwon IC, Bae YH, Kim SW (1991) Electrically credible polymer gel for controlled release of drugs. Nature 354:291–293. doi:10.1038/354291a0
20. Lai JJ, Hoffman JM, Ebara M, Hoffman AS, Estournès C, Wattiaux A, Stayton PS (2007) Dual magnetic-/temperature-responsive nanoparticles for microfluidic separations and assays. Langmuir 23:7385–7391. doi:10.1021/la062527g

21. Suzuki A, Tanaka T (1990) Phase transition in polymer gels induced by visible light. Nature 346:345–347. doi:10.1038/346345a0
22. Lage R, Diéguez C, Vidal-Puig A, López M (2008) AMPK: a metabolic gauge regulating whole-body energy homeostasis. Trends Mol Med 14:539–549. doi:http://dx.doi.org/10.1016/j.molmed.2008.09.007
23. Kim Y-J, Ebara M, Aoyagi T (2012) A smart nanofiber web that captures and releases cells. Angew Chem Int Ed 51:10537–10541. doi:10.1002/anie.201204139
24. Jin X, Hsieh YL (2005) pH-responsive swelling behavior of poly(vinyl alcohol)/poly(acrylic acid) bi-component fibrous hydrogel membranes. Polymer 46:5149–5160. doi:http://dx.doi.org/10.1016/j.polymer.2005.04.066
25. Kato T (2002) Self-assembly of phase-segregated liquid crystal structures. Science 295:2414–2418. doi:10.1126/science.1070967-a
26. Gazit E (2007) Self-assembled peptide nanostructures: the design of molecular building blocks and their technological utilization. Chem Soc Rev 36:1263–1269
27. Aggeli A, Bell M, Carrick LM, Fishwick CWG, Harding R, Mawer PJ, Radford SE, Strong AE, Boden N (2003) pH as a trigger of peptide β-sheet self-assembly and reversible switching between nematic and isotropic phases. J Am Chem Soc 125:9619–9628. doi:10.1021/ja021047i
28. Zhang S, Gelain F, Zhao X (2005) Designer self-assembling peptide nanofiber scaffolds for 3D tissue cell cultures. Semin Cancer Biol 15:413–420. doi:http://dx.doi.org/10.1016/j.semcancer.2005.05.007
29. Hartgerink JD, Beniash E, Stupp SI (2002) Peptide-amphiphile nanofibers: a versatile scaffold for the preparation of self-assembling materials. Proc Natl Acad Sci 99:5133–5138. doi:10.1073/pnas.072699999
30. Tambralli A, Blakeney B, Anderson J, Kushwaha M, Andukuri A, Dean D, Jun H-W (2009) A hybrid biomimetic scaffold composed of electrospun polycaprolactone nanofibers and self-assembled peptide amphiphile nanofibers. Biofabrication 1:025001. doi:10.1088/1758-5082/1/2/025001
31. Zang L, Che Y, Moore JS (2008) One-Dimensional Self-Assembly of Planar π-Conjugated Molecules: Adaptable Building Blocks for Organic Nanodevices. Acc Chem Res 41:1596–1608. doi:10.1021/ar800030w
32. Yoshio M, Shoji Y, Tochigi Y, Nishikawa Y, Kato T (2009) Electric field-assisted alignment of self-assembled fibers composed of hydrogen-bonded molecules having laterally fluorinated mesogens. J Am Chem Soc 131:6763–6767. doi:10.1021/ja8093718
33. Bhardwaj N, Kundu SC (2010) Electrospinning: a fascinating fiber fabrication technique. Biotechnol Adv 28:325–347. doi:http://dx.doi.org/10.1016/j.biotechadv.2010.01.004
34. Dahlin RL, Kasper FK, Mikos AG (2011) Polymeric nanofibers in tissue engineering. Tissue Eng Part B Rev 17:349–364. doi:10.1089/ten.teb.2011.0238
35. Agarwal S, Greiner A, Wendorff JH (2009) Electrospinning of manmade and biopolymer nanofibers—progress in techniques, materials, and applications. Adv Funct Mater 19:2863–2879. doi:10.1002/adfm.200900591
36. Huang ZM, Zhang YZ, Kotaki M, Ramakrishna S (2003) A review on polymer nanofibers by electrospinning and their applications in nanocomposites. Compos Sci Technol 63:2223–2253. doi:http://dx.doi.org/10.1016/S0266-3538(03)00178-7
37. Nain AS, Wong JC, Amon C, Sitti M (2006) Drawing suspended polymer micro-/nanofibers using glass micropipettes. Appl Phys Lett 89:183103–183105. doi:10.1063/1.2372694
38. Nain AS, Phillippi JA, Sitti M, MacKrell J, Campbell PG, Amon C (2008) Control of cell behavior by aligned micro/nanofibrous biomaterial scaffolds fabricated by spinneret-based tunable engineered parameters (STEP) technique. Small 4:1153–1159. doi:10.1002/smll.200800101
39. Berry SM, Harfenist SA, Cohn RW, Keynton RS (2006) Characterization of micromanipulator-controlled dry spinning of micro- and sub-microscale polymer fibers. J Micromech Microeng 16:1825. doi:10.1088/0960-1317/16/9/010

40. Berry SM, Warren SP, Hilgart DA, Schworer AT, Pabba S, Gobin AS, Cohn RW, Keynton RS (2011) Endothelial cell scaffolds generated by 3D direct writing of biodegradable polymer microfibers. Biomaterials 32:1872–1879. doi:http://dx.doi.org/10.1016/j.biomaterials.2010.11.023
41. Harfenist SA, Cambron SD, Nelson EW, Berry SM, Isham AW, Crain MM, Walsh KM, Keynton RS, Cohn RW (2004) Direct drawing of suspended filamentary micro- and nanostructures from liquid polymers. Nano Lett 4:1931–1937. doi:10.1021/nl048919u
42. Yang F, Murugan R, Ramakrishna S, Wang X, Ma YX, Wang S (2004) Fabrication of nano-structured porous PLLA scaffold intended for nerve tissue engineering. Biomaterials 25:1891–1900. doi:http://dx.doi.org/10.1016/j.biomaterials.2003.08.062
43. Mao J, Duan S, Song A, Cai Q, Deng X, Yang X (2012) Macroporous and nanofibrous poly(lactide-co-glycolide)(50/50) scaffolds via phase separation combined with particle-leaching. Mater Sci Eng C 32:1407–1414. doi:http://dx.doi.org/10.1016/j.msec.2012.04.018
44. Liu X, Ma PX (2009) Phase separation, pore structure, and properties of nanofibrous gelatin scaffolds. Biomaterials 30:4094–4103. doi:http://dx.doi.org/10.1016/j.biomaterials.2009.04.024
45. Chen VJ, Ma PX (2004) Nano-fibrous poly(L-lactic acid) scaffolds with interconnected spherical macropores. Biomaterials 25:2065–2073. doi:http://dx.doi.org/10.1016/j.biomaterials.2003.08.058
46. Li D, Krantz WB, Greenberg AR, Sani RL (2006) Membrane formation via thermally induced phase separation (TIPS): model development and validation. J Membr Sci 279:50–60. doi:http://dx.doi.org/10.1016/j.memsci.2005.11.036
47. Hwang CM, Khademhosseini A, Park Y, Sun K, Lee S-H (2008) Microfluidic chip-based fabrication of plga microfiber scaffolds for tissue engineering. Langmuir 24:6845–6851. doi:10.1021/la800253b
48. Lee KH, Shin SJ, Park Y, Lee SH (2009) Synthesis of cell-laden alginate hollow fibers using microfluidic chips and microvascularized tissue-engineering applications. Small 5:1264–1268. doi:10.1002/smll.200801667
49. Kiriya D, Kawano R, Onoe H, Takeuchi S (2012) Microfluidic control of the internal morphology in nanofiber-based macroscopic cables. Angew Chem Int Ed 51:7942–7947. doi:10.1002/anie.201202078
50. Danilatos GD (1991) Review and outline of environmental SEM at present. J Microsc Oxford 162:391–402. doi:10.1111/j.1365-2818.1991.tb03149.x
51. Wang H, Li Y, Sun L, Li Y, Wang W, Wang S, Xu S, Yang Q (2010) Electrospun novel bifunctional magnetic–photoluminescent nanofibers based on $Fe_2O_3$ nanoparticles and europium complex. J Colloid Interface Sci 350:396–401. doi:http://dx.doi.org/10.1016/j.jcis.2010.06.068
52. Nygaard JV, Uyar T, Chen M, Cloetens P, Kingshott P, Besenbacher F (2011) Characterisation of internal morphologies in electrospun fibers by X-ray tomographic microscopy. Nanoscale 3:3594–3597. doi:10.1039/c1nr10304k
53. Okuzaki H, Kobayashi K, Yan H (2009) Thermo-responsive nanofiber mats. Macromolecules 42:5916–5918. doi:10.1021/ma9014356
54. Chen M, Gao S, Dong M, Song J, Yang C, Howard KA, Kjems J, Besenbacher F (2012) Chitosan/siRNA nanoparticles encapsulated in PLGA nanofibers for siRNA delivery. ACS Nano 6:4835–4844. doi:10.1021/nn300106t
55. Chen M, Nielsen SR, Uyar T, Zhang S, Zafar A, Dong M, Besenbacher F (2013) Electrospun UV-responsive supramolecular nanofibers from a cyclodextrin-azobenzene inclusion complex. J Mater Chem C 1:850–855. doi:10.1039/c2tc00180b
56. Jena A, Gupta K (2002) Characterization of pore structure of filtration media. Fluid Part Separ J 14:227–241
57. Jena A, Gupta K (2002) A novel technique for pore structure characterization without the use of any toxic material. Nondestructive characterization of materials XI. Springer, Heidelberg
58. Jena A, Gupta K (2003) Liquid extrusion techniques for pore structure evaluation of nonwovens. Int Nonwovens J Fall 12:45–53

59. Rockwood DN, Chase DB, Akins Jr RE, Rabolt JF (2008) Characterization of electrospun poly(N-isopropyl acrylamide) fibers. Polymer 49:4025–4032. doi:http://dx.doi.org/10.1016/j.polymer.2008.06.018
60. Okuzaki H, Kobayashi K, Yan H (2009) Non-woven fabric of poly(N-isopropylacrylamide) nanofibers fabricated by electrospinning. Synth Met 159:2273–2276. doi:http://dx.doi.org/10.1016/j.synthmet.2009.07.046
61. Kim Y-J, Ebara M, Aoyagi T (2012) Temperature-responsive electrospun nanofibers for 'on–off' switchable release of dextran. Sci Technol Adv Mat 13:064203. doi:10.1088/1468-6996/13/6/064203
62. Fu GD, Xu LQ, Yao F, Zhang K, Wang XF, Zhu MF, Nie SZ (2009) Smart nanofibers from combined living radical polymerization, "click chemistry", and electrospinning. Acs Appl Mater Inter 1:239–243. doi:10.1021/am800143u
63. Loh XJ, Peh P, Liao S, Sng C, Li J (2010) Controlled drug release from biodegradable thermoresponsive physical hydrogel nanofibers. J Controlled Release 143:175–182. doi:http://dx.doi.org/10.1016/j.jconrel.2009.12.030
64. Webster M, Miao J, Lynch B, Green DS, Jones-Sawyer R, Linhardt RJ, Mendenhall J (2012) Tunable thermo-responsive poly(N-vinylcaprolactam) cellulose nanofibers: synthesis, characterization, and fabrication. Macromol Mater Eng:n/a-n/a. doi:10.1002/mame.201200081
65. Chen M, Dong M, Havelund R, Regina VR, Meyer RL, Besenbacher F, Kingshott P (2010) Thermo-responsive core-sheath electrospun nanofibers from poly (N-isopropylacrylamide)/polycaprolactone blends. Chem Mater 22:4214–4221. doi:10.1021/cm100753r
66. DiBenedetto F, Mele E, Camposeo A, Athanassiou A, Cingolani R, Pisignano D (2008) Photoswitchable organic nanofibers. Adv Mater 20:314–318. doi:10.1002/adma.200700980
67. De Sousa FB, Guerreiro JDT, Ma M, Anderson DG, Drum CL, Sinisterra RD, Langer R (2010) Photo-response behavior of electrospun nanofibers based on spiropyran-cyclodextrin modified polymer. J Mater Chem 20:9910–9917
68. Chen M, Besenbacher F (2011) Light-driven wettability changes on a photoresponsive electrospun mat. ACS Nano 5:1549–1555. doi:10.1021/nn103577g
69. Chae SK, Park H, Yoon J, Lee CH, Ahn DJ, Kim JM (2007) Polydiacetylene supramolecules in electrospun microfibers: fabrication, micropatterning, and sensor applications. Adv Mater 19:521–524. doi:10.1002/adma.200602012
70. Aguilar MR, Elvira C, Gallardo BS, Vazquez B, Roman JS (2007) Smart polymers and their applications as biomaterials. In: Ashammakhi N, Reis RL, Chiellini E (eds) Topics in tissue engineering. vol 3. pp 1–27
71. Gestos A, Whitten PG, Spinks GM, Wallace GG (2010) Crosslinking neat ultrathin films and nanofibres of pH-responsive poly(acrylic acid) by UV radiation. Soft Matter 6:1045–1052
72. Wang L, Topham PD, Mykhaylyk OO, Howse JR, Bras W, Jones RAL, Ryan AJ (2007) Electrospinning pH-responsive block copolymer nanofibers. Adv Mater 19:3544–3548. doi:10.1002/adma.200700107
73. Filipcsei G, Fehér J, Zrínyi M (2000) Electric field sensitive neutral polymer gels. J Mol Struct 554:109–117. doi:http://dx.doi.org/10.1016/S0022-2860(00)00564-0
74. Li L, Hsieh YL (2005) Ultra-fine polyelectrolyte hydrogel fibres from poly(acrylic acid)/poly(vinyl alcohol). Nanotechnology 16:2852. doi:10.1088/0957-4484/16/12/020
75. Son YH, Lee JK, Soong Y, Martello D, Chyu M (2010) Enhanced magnetic response of fluids using self-assembled petal-like iron oxide particles. Appl Phys Lett 96:121903–121905. doi:10.1063/1.3371713
76. Lin TC, Lin FH, Lin JC (2012) In vitro feasibility study of the use of a magnetic electrospun chitosan nanofiber composite for hyperthermia treatment of tumor cells. Acta Biomater 8:2704–2711. doi:http://dx.doi.org/10.1016/j.actbio.2012.03.045
77. Huang C, Soenen SJ, Rejman J, Trekker J, Chengxun L, Lagae L, Ceelen W, Wilhelm C, Demeester J, De Smedt SC (2012) Magnetic electrospun fibers for cancer therapy. Adv Funct Mater 22:2479–2486. doi:10.1002/adfm.201102171
78. Wang M, Singh H, Hatton TA, Rutledge GC (2004) Field-responsive superparamagnetic composite nanofibers by electrospinning. Polymer 45:5505–5514. doi:http://dx.doi.org/10.1016/j.polymer.2004.06.013

79. Kriha O, Becker M, Lehmann M, Kriha D, Krieglstein J, Yosef M, Schlecht S, Wehrspohn RB, Wendorff JH, Greiner A (2007) Connection of hippocampal neurons by magnetically controlled movement of short electrospun polymer fibers—a route to magnetic micromanipulators. Adv Mater 19:2483–2485. doi:10.1002/adma.200601937
80. Heo YJ, Shibata H, Okitsu T, Kawanishi T, Takeuchi S (2011) Long-term in vivo glucose monitoring using fluorescent hydrogel fibers. Proc Natl Acad Sci. doi:10.1073/pnas.1104954108
81. Shibata H, Heo YJ, Okitsu T, Matsunaga Y, Kawanishi T, Takeuchi S (2010) Injectable hydrogel microbeads for fluorescence-based in vivo continuous glucose monitoring. Proc Natl Acad Sci. doi:10.1073/pnas.1006911107
82. Wang L, Li C, Ryan AJ, Armes SP (2006) Synthesis and peptide-induced degradation of biocompatible fibers based on highly branched poly(2-hydroxyethyl methacrylate). Adv Mater 18:1566–1570. doi:10.1002/adma.200600314
83. Law B, Weissleder R, Tung C-H (2007) Protease-sensitive fluorescent nanofibers. Bioconjugate Chem 18:1701–1704. doi:10.1021/bc070054z
84. Qi Q, Zhang T, Wang L (2008) Improved and excellent humidity sensitivities based on KCl-doped TiO[sub 2] electrospun nanofibers. Appl Phys Lett 93:023103–023105
85. Li Z, Zhang H, Zheng W, Wang W, Huang H, Wang C, MacDiarmid AG, Wei Y (2008) Highly sensitive and stable humidity nanosensors based on LiCl doped TiO2 electrospun nanofibers. J Am Chem Soc 130:5036–5037. doi:10.1021/ja800176s
86. Wang X, Ding B, Yu J, Wang M, Pan F (2010) A highly sensitive humidity sensor based on a nanofibrous membrane coated quartz crystal microbalance. Nanotechnology 21:055502. doi:10.1088/0957-4484/21/5/055502
87. Wang X, Ding B, Yu J, Wang M (2011) Highly sensitive humidity sensors based on electrospinning/netting a polyamide 6 nano-fiber/net modified by polyethyleneimine. J Mater Chem 21:16231–16238
88. Yang D-J, Kamienchick I, Youn DY, Rothschild A, Kim I-D (2010) Ultrasensitive and highly selective gas sensors based on electrospun SnO2 nanofibers modified by Pd loading. Adv Funct Mater 20:4258–4264. doi:10.1002/adfm.201001251
89. Shin J, Choi S-J, Lee I, Youn D-Y, Park CO, Lee J-H, Tuller HL, Kim I-D (2012) Thin-wall assembled SnO2 fibers functionalized by catalytic Pt nanoparticles and their superior exhaled-breath-sensing properties for the diagnosis of diabetes. Adv Funct Mater:n/a-n/a. doi :10.1002/adfm.201202729
90. Heo YJ, Takeuchi S (2013) Towards smart tattoos: implantable biosensors for continuous glucose monitoring. Adv Healthcare Mater 2:43–56. doi:10.1002/adhm.201200167
91. Zhang Y, Yarin AL (2009) Stimuli-responsive copolymers of n-isopropyl acrylamide with enhanced longevity in water for micro- and nanofluidics, drug delivery and non-woven applications. J Mater Chem 19:4732–4739
92. Cui W, Qi M, Li X, Huang S, Zhou S, Weng J (2008) Electrospun fibers of acid-labile biodegradable polymers with acetal groups as potential drug carriers. Int J Pharm 361:47–55. doi:http://dx.doi.org/10.1016/j.ijpharm.2008.05.005
93. Yun J, Im JS, Lee Y-S, Kim H-I (2011) Electro-responsive transdermal drug delivery behavior of PVA/PAA/MWCNT nanofibers. Eur Polym J 47:1893–1902. doi:http://dx.doi.org/10.1016/j.eurpolymj.2011.07.024
94. Fu G-D, Xu L-Q, Yao F, Li G-L, Kang E-T (2009) Smart nanofibers with a photoresponsive surface for controlled release. Acs Appl Mater Inter 1:2424–2427. doi:10.1021/am900526u
95. Kim Y-J, Ebara M, Aoyagi T (2013) A smart hyperthermia nanofiber with switchable drug release for improved skin cancer therapy. Adv Funct Mater 23:5753–5761. doi:10.1002/adfm.201300746
96. Yoshida H, Klinkhammer K, Matsusaki M, Möller M, Klee D, Akashi M (2009) Disulfide-crosslinked electrospun poly(γ-glutamic acid) nonwovens as reduction-responsive scaffolds. Macromol Biosci 9:568–574. doi:10.1002/mabi.200800334

97. Zou W, Huang Y, Luo J, Liu J, Zhao C (2010) Poly (methyl methacrylate–acrylic acid–vinyl pyrrolidone) terpolymer modified polyethersulfone hollow fiber membrane with pH sensitivity and protein antifouling property. J Membr Sci 358:76–84. doi:http://dx.doi.org/10.1016/j.memsci.2010.04.028
98. Cheng C, Ma L, Wu D, Ren J, Zhao W, Xue J, Sun S, Zhao C (2011) Remarkable pH-sensitivity and anti-fouling property of terpolymer blended polyethersulfone hollow fiber membranes. J Membr Sci 378:369–381. doi:http://dx.doi.org/10.1016/j.memsci.2011.05.028

# Chapter 6
# Smart Bioconjugates

## 6.1 Introduction

This chapter focuses on the synthesis, characterization, and applications of bioconjugates of smart polymers and bioactive molecules such as drugs, peptides, enzymes, antibodies, viruses and cells. Bioconjugations with synthetic polymers have been a versatile way to add new value, advanced features and unique properties to inert biomolecules. Polymer-protein conjugates, for example, have been extensively investigated over the past 35 years. In 1970s, Ringsdorf [1] proposed a general scheme of designing a drug delivery system using a synthetic polymer backbone as a carrier for low-molecular weight drugs. The proposed system contains solubilizing groups or targeting moieties that render water solubility and targeting properties on the carrier. In 1980s, Hiroshi Maeda laid the foundations for Ringsdorf's visionary model by showing efficient accumulation of polymer-antitumor protein conjugates within tumors, so-call EPR (enhanced permeability and retention) effect [2]. Covalent attachment of polymer chains to bioactive molecules also offers the possibility of exerting control over their biological activity. This principle is now being widely exploited in pharmaceutical development, as covalent attachment of polyethylene glycol (PEG) to therapeutic proteins, called "PEGylation", has been shown to improve the safety and efficiency without losing their biological functions [3]. Many PEGylated pharmaceuticals are currently on the market. This technology can be also used as a means to improve the in vivo pharmacokinetics of the viral vectors [4, 5] or to silence the antigenic response of red blood cells (RBCs) toward the development of universal blood transfusion [6–8].

Although polymer-conjugation studies are already well advanced, controlling the specific functions of these molecules in biological systems under changing conditions is difficult. In this context, smart polymer-protein conjugates have been also investigated over the past 30 years. The conjugation of smart polymer to single molecule can generate a nano-scale switch (Fig. 6.1). The early publications on smart-polymer conjugates were appeared in 1970s, where proteins were conjugated to carboxylated polymers that phase-separated either at low pH or by

M. Ebara et al., *Smart Biomaterials*, NIMS Monographs,
DOI: 10.1007/978-4-431-54400-5_6,

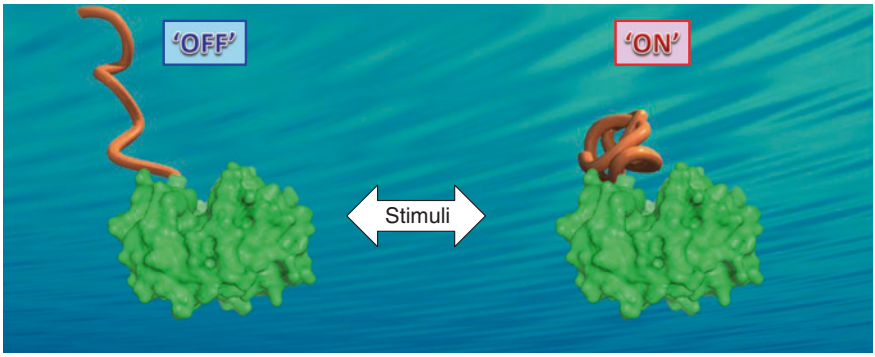


**Fig. 6.1** Schematic illustration of a smart-polymer-conjugated enzyme. The smart polymer serves as a molecular antenna and actuator to reversibly turn the enzyme activity on and off in response to external stimuli

the addition of calcium ions [9, 10]. Until today, pioneering work in this area has been carried out by Hoffman and co-workers [11, 12]. They first demonstrated the selective separation of certain proteins out of blood serum using "monomer conjugation plus copolymerization" method. They conjugated vinyl groups to a protein and then copolymerized the monomer-derivatized protein with hydroxyethyl methacrylate (HEMA), causing it to phase separation because HEMA polymer was not water soluble while HEMA monomer was water soluble. In 1980s, Hoffman and co-workers [13, 14] have further developed the thermally-induced phase separation immunoassay (TIPSIA) using temperature-responsive polymers, such as poly(N-isopropylacrylamide) (PNIPAAm). PNIPAAm undergoes a sharp coil-globule transition in water at 32 °C (lower critical solution temperature: LCST), being hydrophilic below this temperature and hydrophobic above it. The PNIPAAm-monoclonal antibody conjugates thus enabled the partition and separation of target antigen in aqueous environment on the basis of solubility. Since then, many researchers have conjugated smart polymers to proteins for a great variety of applications in affinity separations [15, 16], enzyme bioprocesses [17–19], drug delivery [20–23], diagnostics and biosensors [24, 25], cell culture processes including tissue engineering [26–28], and DNA motors [29, 30]. Biomolecules that can be conjugated with smart polymers include not only proteins but also peptides [31, 32], polysaccharides [33–35], and DNA [25, 36], and lipids [37, 38] etc. Smart polymers may be conjugated randomly or site-specifically to biomolecules to produce a new hybrid type of molecules that can synergistically combine the individual properties of the two components to yield a large family of polymer-biomolecule systems that can respond to biological as well as physical and chemical stimuli. The activity of the overall conjugate can be regulated by altering the response stimulus, and how and where it is attached. There are many different chemical reactions that can be used to derivatize polymer-reactive groups for subsequent conjugation to biomolecules. Polymers with pendant reactive groups can be synthesized using random copolymerization techniques with functional

comonomers. One of the most attractive advantages of random copolymers is that they can be designed to react with more than one protein or at multiple sites. Polymer with only one reactive end group can be also synthesized using chain transfer polymerization techniques with chain transfer agents. Usually, the lysine amino groups are the easiest and preferred reactive sites for conjugation of polymers to proteins, but other possible sites include -COOH groups of aspartic or glutamic acid, -OH groups of serine or tyrosine and, especially, -SH groups of cysteine residues. Because the conjugations usually are designed to occur randomly at lysine sites, the polymer may react with and conjugate to several different lysine sites on the same protein surface. If the amino acid sequence of a protein is known, on the other hand, site-specific mutagenesis of the protein may be used to substitute one amino acid at a specific site with another. For example, a cysteine residue can be introduced by such techniques to yield a mutant protein with an exposed thiol group. Then, polymers with terminal or pendant maleimide, vinyl, or vinyl sulfone groups can be conjugated to the protein. Stayton et al. [39] were the first to demonstrate the versatility of site-specific conjugation by conjugating PNIPAAm far away from and close to the active site of streptavidin. In another approach, non-natural amino acids may be inserted into a protein structure by genetic engineering of the protein expression process within cells [40]. Although coupling polymers to reactive sites on proteins allows the synthesis of conjugates from a library of preformed polymers (commonly called the "grafting-to" approach), it is also possible to derivatize the thiol group with a polymerization initiator group via a disulfide linkage, and then polymerize the smart polymer directly from that particular site. This "grafting-from" approach is particularly well suited to the preparation of conjugates with high molecular weight homopolymers or block copolymers. This approach also offers the ease purification because unreacted monomer is readily removed from the final polymer-protein conjugate.

In the following sections of this chapter, we review different types of smart polymer-biomolecule conjugates that have been developed in the last few decades. In Sect. 6.2, we describe the classifications of smart bioconjugates on the basis of conjugation routes and types of biomolecule that may be conjugated to a smart polymer. The characterization methods are discussed in Sect. 6.3. In Sect. 6.4, certain applications of the smart bioconjugates are discussed. The chapter ends with an overview of some of the future trends in applications in biotechnology and biomedicine.

## 6.2 Classification on the Basis of Conjugation Routes

Nowadays, a variety of bioconjugation techniques are known for both in vitro and in vivo studies. In general, conjugation of biomolecules can be broadly separated into two categories: (1) covalent and (2) noncovalent conjugations. The covalent conjugation is divided into three sub-categories: (a) random conjugation

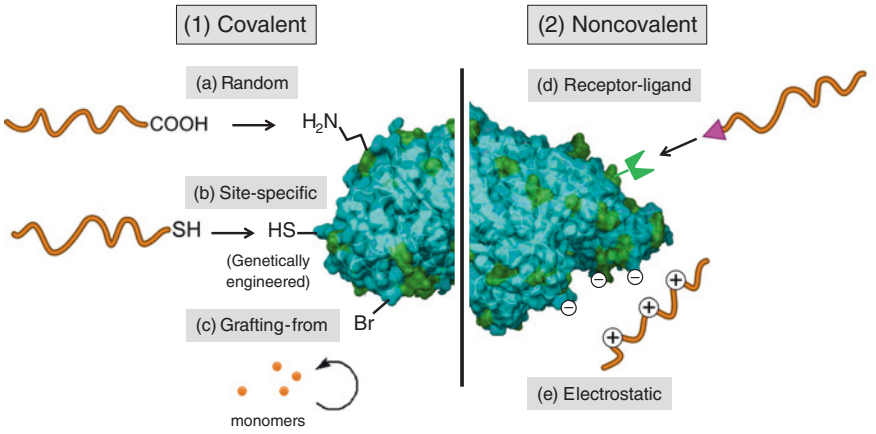


**Fig. 6.2** Schematic illustration of polymer-protein conjugation methods by (*1*) covalent and (*2*) noncovalent modification. The covalent conjugation is divided into three subcategories: **a** random conjugation, **b** site-specific conjugation, and **c** grafting-from protein-reactive initiators. The noncovalent conjugation is divided into two subcategories: **d** receptor-ligand and **e** electrostatic conjugation

(b) site-specific conjugation, and (c) grafting from approach using protein-reactive initiators. The noncovalent conjugation is divided into two subcategories: (d) receptor-ligand and (e) electrostatic conjugations (see Fig. 6.2).

### *6.2.1 Random Conjugation*

The random conjugation has been achieved through pendant groups along the polymer backbone or one end of a polymer (Fig. 6.2a). Common types of random conjugation are amine coupling of lysine amino acid residues through amine-reactive succinimidyl esters, sulfhydryl coupling of cysteine residues with either other sulfhydryl groups or in a Michael addition via a sulfhydryl-reactive maleimide. The use of *N*-hydroxyl-succinimidyl ester (NHS) is one of the most common methods for condensation reaction between a carboxylic acid and an amino group of membrane proteins. Other possible sites include -COOH groups of aspartic or glutamic acid, -OH groups of serine or tyrosine, and -SH groups of cysteine residues. For example, free-radical polymerization of NIPAAm initiated by 2,2'-azobisisobutyronitrile (AIBN) with β-mercaptoethanol as the chain-transfer agent resulted in the α-hydroxyl-functionalized PNIPAAm. The α-hydroxyl group was then converted to the vinyl sulfone through coupling with divinyl sulfone in the presence of a base. Maleimides react selectively with the thiols of cysteine residues in the pH range of 6.5–7.5 via Michael addition. Multiple attachments are especially likely to occur if a polymer chain has multiple pendant amino-reactive

groups and the protein has multiple lysine sites. Conjugations via end groups, especially where there is only one reactive end group, usually yield conjugates that are the most clearly defined in structure and composition. Chen et al. [41] have compared the enzyme activity of α-amylase covalently immobilized with NIPAAm by single-point attachment and multiple-point attachment. α-Amylase immobilized to the polymer with a single functional end group had a higher activity than that immobilized to the polymer with multiple functional groups, and the specific activity can be higher than that of the free enzyme. However, the enzyme immobilized to the latter polymer is more thermally stable and the recovery is better than with the former one. Matsukata et al. [42] have also compared the enzyme activity of trypsin covalently immobilized with NIPAAm by single-point attachment and multiple- point attachment. The single-point attachment was achieved by conjugating a semitelechelic copolymer of NIPAAm with *N,N*-dimethylacrylamide (DMAAm) with a single carboxyl end group to trypsin. The multiple-point attachment was achieved by conjugating a copolymer of NIPAAm with DMAAm and acrylic acid (AAc) to trypsin. The trypsin conjugated to the polymer with multiple points showed higher stability than that immobilized to the polymer with a single point. Polymers with only one reactive end group may be synthesized using traditional chain transfer polymerization techniques with mercaptyl amines, carboxylic acids, or alcohols as chain transfer agents.

PNIPAAm with one carboxyl group at the end of the chain has been conjugated to β-D-glucosidase [43] and trypsin [44]. The carboxyl groups were activated using *N,N'*-dicyclohexylcarbodiimide (DCC) and *N*-hydroxysuccinimide (NHS). More than 95 % of the conjugate can be recovered by thermally induced precipitation. Takei et al. have polymerized a carboxyl-terminated PNIPAAm by polymerization with 3-mercaptopropionic acid, and it was used for conjugation to IgG via a coupling reaction of an activated ester with a protein amino group. The IgG-PNPIPAm conjugates reduced the original specific antigen binding activity by approximately 60 % [16]. More recently, "living" free radical polymerization methods, such as reversible addition-fragmentation chain transfer (RAFT) polymerization [45] and atom transfer radical polymerization (ATRP) [46], have been used to yield polymers with controlled MWs, narrow MW distributions, and one reactive end group. Amine-reactive polymers have been synthesized with NHS- and acetal-functionalized initiators for ATPR in order to target lysine side chains in proteins. The NHS-functionalized initiator was synthesized in one step by coupling NHS with 2-bromopropionic acid to form the 2-bromopropionate NHS ATRP initiator [47]. Acetal-functionalized initiators are employed because the resulting polymer can be hydrolyzed, exposing aldehyde groups for reaction with amines via reductive amination [48]. This functionalized initiator for ATRP was synthesized by reaction of 2-chloro-1,1-dimethoxyethane, followed by esterification with 2-bromoisobutyryl bromide. One special feature of these controlled, living free radical polymerizations is that block copolymers may also be synthesized where one or both of the blocks are smart polymers. In the latter case, the two blocks can have different responses to different stimuli [35, 49].

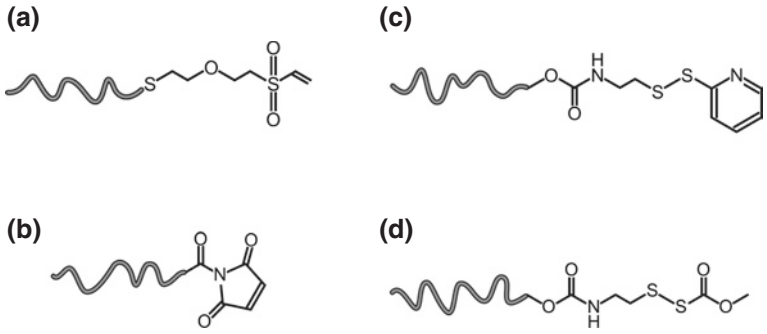


**Fig. 6.3** Thiol-reactive end-groups. **a** Vinyl sulfone end-group, **b** maleimide end-group, **c** a,w-pyridyl disulfide end-group, and **d** methoxy carbonyl end-group

In the case of random conjugation, however, problems in controlling the conjugation chemistry frequently arise because the number and location of lysine residues vary greatly in native proteins and because the location of reactive groups on proteins is random. Thus, the stoichiometry of the protein-polymer conjugate and the attachment sites of the polymer to the protein cannot be precisely controlled, although they are factors that might have important implications for protein stability and function. These limitations can be circumvented by the appropriate design of polymer-protein conjugates.

### *6.2.2 Site-Specific Conjugation*

Although random conjugation strategies offer facile procedures, the conjugated products are heterogeneously linked at different sites with distinct activity, binding efficacy, or in vivo pharmacokinetics. Therefore, site-specific conjugation strategies have been developed (Fig. 6.2b). If the amino acid sequence of a protein is known, site-specific mutagenesis ("genetic engineering" of the protein) may be used to substitute one amino acid at a specific site with another. For example, a cysteine residue can be introduced by such techniques to yield a mutant protein with an exposed thiol group. Then, polymers with terminal or pendant maleimide, vinyl, or vinyl sulfone groups can be conjugated to the protein (Fig. 6.3). These groups react preferentially with thiol groups rather than with lysine amino groups [39, 50]. Furthermore, pendant or terminal thiol or disulfide groups on smart polymers may be used to form disulfide linkages of the polymer to the protein [51]. Such site-specific conjugation of smart polymers to proteins can be carried out either near or far away from the active site. In the former case, the protein activity can be directly affected. Thus, by stimulating the polymer first to collapse and then to rehydrate, the collapsed smart polymer coil can first "block" (turn "off"") the protein active site, and then "unblock"' (turn back "on") the active site [52].

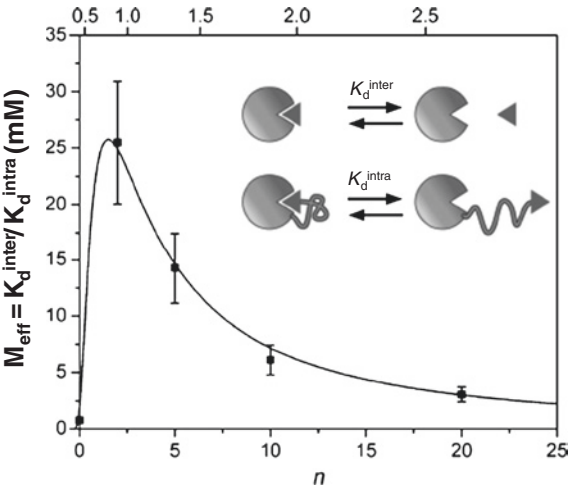


**Fig. 6.4** Effective molarity ($M_{\text{eff}}$) with linker length ($n$; related to the root-mean-square distance between the ends of the linker) for an intramolecular protein-ligand binding event [53]

However, it is expected that both the location of the conjugation site and the volume (or MW) of the smart polymer coil, either before or after collapse, can control protein activity. Krishnamurthy et al. [53] have reported dissociation constants and "effective molarities" ($M_{eff}$) for the intramolecular binding of a ligand covalently attached to the surface of a protein by oligo(ethylene glycol) (oEG) linkers of different lengths ($n = 0$, 2, 5, 10, and 20) and compared these experimental values with theoretical estimates from polymer theory. They found a strong influence on enzyme inhibition of both the conjugation site and the MW of a PEG-inhibitor molecule conjugated at various sites on an enzyme (see Fig. 6.4). The value of $M_{eff}$ is lowest when the linker is too short ($n = 0$) to allow the ligand to bind noncovalently at the active site of the protein without strain. On the other hand, the value of $M_{eff}$ is highest when the linker has the optimal length ($n = 2$) to allow such binding to occur, and decreases monotonically as the length increases past this optimal value. These experimental results are not compatible with a model in which the single bonds of the linker are quantitatively compatible with a model that treats the linker as a random-coil polymer.

Chilkoti et al. [54] were the first to demonstrate the versatility of site-specific conjugation by conjugating PNIPAAm far away from the active site of cytochrome-$b_5$. A genetically engineered mutant of cytochrome-$b_5$, incorporating a unique cysteine residue, was conjugated to maleimide end-functionalized PNIPAAm. Since the native cytochrome-$b_5$ does not contain any cysteine residues, this substitution provided a unique attachment point for the polymer. The resultant polymer-protein conjugate displayed LCST behavior and could be reversibly precipitated from solution by varying the temperature. This approach has proved to be very versatile, and a large number of polymer-biopolymer conjugates incorporating biological components as diverse as antibodies, protein A, streptavidin, proteases, and hydrolases have now been prepared. The biological functions or activities of these conjugate systems were all similar to their native counterparts, but were switched on

or off as a result of thermally induced polymer phase transitions. Both temperature and photochemically switchable enzymes, which display varying and opposite activities depending on temperature or UV/Vis illumination, have also been demonstrated [19, 55]. Pyridyl disulfide- and maleimide-functionalized initiators for ATRP have also been synthesized to enable conjugation to the free cysteines of proteins. Unlike targeting amines, this approach allows for the formation of well-defined conjugates. The pyridyl disulfide-functionalized 2-bromoisobutyrate initiator for ATRP was synthesized in two steps by the reaction of 2,2'-dithiopyridine with 3-mercapto-1-propanol to form pyridyl disulfide propanol [56]. Subsequent esterification yielded the ATRP initiator. An advantage of this approach is that no post polymerization modification of the chains was necessary prior to conjugate formation and that the conjugate formation was reversible. The maleimide initiator for ATRP was synthesized in three steps beginning with a Diels–Alder reaction between maleic anhydride and furan to form 3,6-epoxy-1,2,3,6-tetrahydrophthalic anhydride [57]. Subsequent reaction with ethanolamine formed the protected maleimide alcohol, which was then esterified with 2-bromoisobutyryl bromide to afford the initiator.

Another approach for a site-specific conjugation is to take advantage of the presence of an N-terminal serine or threonine, which can be converted by very mild periodate oxidation to a glyoxylyl derivative [58], and to functionalize the polymer with a complementary reactive function, the aminooxy group. An analogous method was shown to be straightforward for incorporating synthetic peptides into a protein backbone by introducing a hydrazide function at the C-terminus of one fragment or peptide to be recoupled [59] and a glyoxylyl group at the N-terminus of the other. In the same way, the aminooxy function will specifically react with the generated aldehyde group at the N-terminus of the polypeptide to form an oxime bond, which is more stable than the hydrazone bond. This approach has already been exploited for the site-specific labeling of IL-8 at the N-terminus with an aminooxy-functionalized fluorescent probe [60]. A convenient method for the construction of site-specifically modified polymer-protein conjugates by generating a reactive carbonyl group in place of the terminal amino group has also been reported [61]. If the protein has N-terminal serine or threonine, this can be achieved by very mild periodate oxidation and generates a glyoxylyl group. A method less restricted by the nature of the N-terminal residue, but which requires somewhat harsher conditions, is metal-catalyzed transamination, which gives a keto group. The N-terminal-introduced reactive carbonyl group specifically reacts, under mild acidic conditions, with an aminooxy-functionalized polymer to form a stable oxime bond.

### *6.2.3 Grafting from Protein-Reactive Initiators*

Generating polymers directly from proteins at defined initiation sites provides the opportunity to evade all post polymerization modification strategies and protein-polymer coupling reactions (Fig. 6.2c). An additional advantage of polymerizing

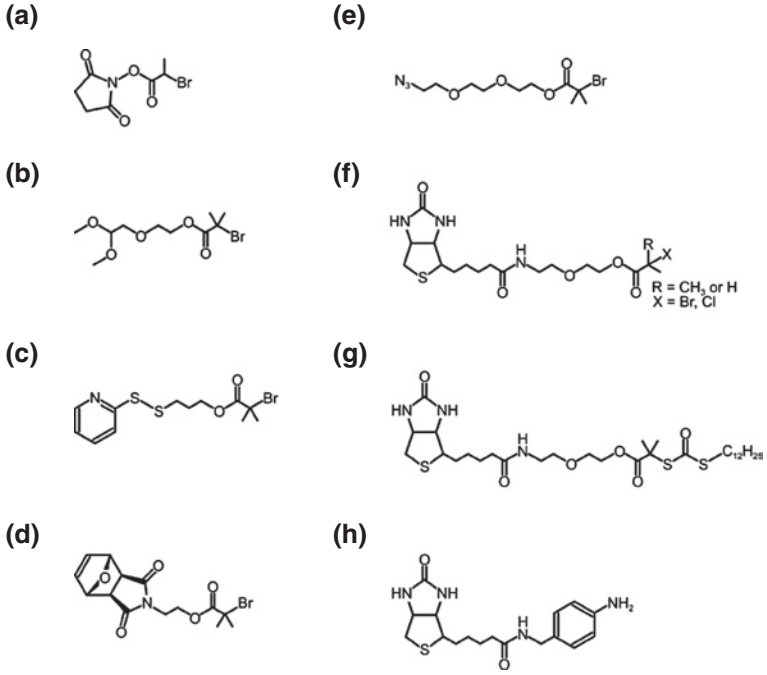


**Fig. 6.5** Protein-reactive initiators. **a** NHS, **b** acetal, **c** pyridyl disulfide, **d** protected maleimide, **e** azide, and **f** biotinylated initiators for ATRP. **g** Biotinylated RAFT chain transfer agent. **h** Biotinylated-initiator for cyanoxyl-mediated polymerization

directly from proteins is that the purification of the final bioconjugate from an unreacted monomer or catalyst is simplified. Also, the precise number and placement of polymer chains is predetermined, thereby facilitating the synthesis and characterization of well-defined conjugates. RAFT and ATRP have been proven most effective for the synthesis of polymer-protein conjugates by the grafting-from approach. ATRP is well suited for the preparation of bioconjugates by a grafting-from approach (Fig. 6.5). Early reports described the preparation of "protein-reactive initiators" of bovine serum albumin (BSA) [62] and chymotrypsin [46].

ATRP is well suited for the preparation of bioconjugates by a grafting-from approach owing to its applicability to a wide range of monomers commonly polymerized in aqueous environments, such as (meth)acrylates and (meth)acrylamides. Heredia et al. [62] have developed a technique to produce well-defined conjugates via ATPR directly from a protein. Free cysteines, Cys-34 of bovine serum albumin (BSA) and Cys-131 of T4 lysozyme V131C, were modified with initiators for ATRP either through a reversible disulfide linkage or irreversible bond by reaction with pyridyl disulfide- and maleimide-functionalized initiators, respectively (Fig. 6.5c and d). Polymerization of NIPAAm from the protein macroinitiators resulted in thermosensitive BSA-PNIPAAm

and lysozyme-PNIPAAm in greater than 65 % yield. Bontempo and Maynard have also conducted polymerization directly from an SA macroinitiator [63]. The protein initiator was formed by coupling a biotinylated ATRP initiator with SA in phosphate-buffered saline (PBS)-methanol to obtain an SA macroinitiator (Fig. 6.5f). Polymerization of NIPAAm in water at ambient temperature with copper bromide and 2,2'-bipyridine (bipy) formed the SA-PNIPAAm conjugates. Polymerization was conducted in the presence of 2-bromoisobutyrate-functionalized Wang resin as the sacrificial initiator in order to increase the concentration of initiation sites. Le Droumaguet and Velonia [64] reported on the facile and high-yielding ATRP-mediated preparation of a giant amphiphile of BSA-polystyrene. In this work, a maleimide-capped ATRP initiator was synthesized and coupled to C34 of BSA under a mild condition. Depp et al. [65] have reported a comparison of the in vitro serum stability and enzyme activity retention for PEGylated chymotrypsin along with biocompatible chymotrypsin conjugates prepared by polymerizing from chymotrypsin covalently modified with an ATRP initiator. The chymotrypsin-initiated ATRP conjugates had higher catalytic activity than PEGylated chymotrypsin. These exciting results suggest that polymerizing from proteins is promising for the development of long-lasting biocompatible pharmaceuticals. Magnusson et al. [66] have also demonstrated improved pharmacokinetic properties upon polymerization from recombinant human growth hormone (rhGH) via ATRP. Gao et al. [67] have reported PEG conjugates via site-specific polymerization from the N-terminus of myoglobin and the C-terminus of green fluorescent protein (GFP) [68].

Despite the success of ATRP for the synthesis of polymer-protein conjugates, the reliance on transition metal catalysts has often been cited as a potential concern. In this respect, RAFT becomes a highly useful method for the synthesis of polymer conjugates. Polymer conjugates have been prepared by polymerization from protein modified with suitable RAFT chain transfer agents. The RAFT agent (Z-C(=S)S-R) is immobilized to the biological substrate via its R-group such that the thiocarbonylthio moiety is distal to the protein and readily accessible for chain transfer with propagating chains in solution, a key step of the RAFT mechanisms responsible for molecular weight control. Moreover, this "R-group approach" leads to the relatively labile thiocarbonylthio group residing on the free end of the immobilized polymer such that it is not responsible for the conjugation linkage. Therefore, the conjugates prepared in this way may demonstrate increased stability and the potential for transformation into thiol groups for subsequent surface immobilization, labeling, or chain extension. For example, a RAFT agent containing an activated ester was conjugated to amines on lysozyme, and NIPAAm was polymerized by grafting directly from the modified protein in aqueous buffer [69]. Retention of the active thiocarbonylthio moieties on the ω end of the conjugated chains allowed chain extension via polymerization of *N,N*-dimethylacrylamide (DMAAm) to yield lysozyme-PNIPAAm-b-PDMAAm block copolymer conjugates. De et al. [70] have prepared PNIPAAm-BSA conjugates by RAFT polymerization from a macro-RAFT agent prepared by modifying the BSA at its single reduced cysteine residue. This was accomplished in aqueous media. Hong and

Pan [71] synthesized PNIPAAm-b-poly(N-(2-hydroxylpropyl)methacrylamide) (PHPMA) via one-step RAFT polymerization using biotinylated trithiocarbonate as the RAFT agent (Fig. 6.5h). An alternative approach for the formation of well-defined polymer-protein conjugates involves immobilization of the RAFT agent to the protein via its Z-group. While not strictly a grafting-from process, this highly efficient "transfer-to" method was the first reported to lead to polymer-protein conjugates directly during RAFT polymerization [72]. A benefit of this approach is that having the polymer linked to the protein via its Z-group ensures that only dormant "living" chains are conjugated, because all termination products remain in solution. Additionally, to allow separate characterization of the polymer or for in vivo applications in which triggered chain cleavage is beneficial, having the polymer and protein linked via the relatively labile thiocarbonylthio group can be advantageous.

In another approach, nonnatural amino acids may be inserted into a protein structure by genetic engineering of the protein expression process within cells, combined with appropriate cell culture conditions [40, 73–76]. Figure 6.6 shows a variety of nonnatural amino acids bearing different reactive groups. Recently, the synthesis of a nonnatural amino acid bearing an ATRP initiating group, 4-(2'-bromoisobutyramido) phenylalanine, and its genetic expression into the GFP have been reported [77, 78]. This was accomplished using an engineered *M. jannaschii* tyrosyl tRNA/aminoacyl-tRNA-synthetase pair vector in *E. coli*. By using genetic engineering, the specific placement of the initiating amino acid was selected to be expressed at the 134 position of GFP, thereby protecting the protein's active sites and structurally weak regions. Furthermore, genetic engineering allows precise control over the number of chains attached (i.e., the number of initiation sites) to the protein, overcoming a primary drawback of traditional protein-polymer conjugates. Thus, genetically engineered proteins have unique capabilities to solve some of the traditional limitations of smart conjugates.

### *6.2.4 Receptor-Ligand Conjugation*

An alternate route to prepare well-defined protein reactive polymers involves using polymers containing ligand end-groups (Fig. 6.2d). The near-covalent bond between SA and biotin has generated much interest in the synthesis of polymers with biotin end-groups for applications in biotechnology owing to the high-affinity interaction with $K_a \approx 10^{15}$ $M^{-1}$. The naturally occurring carboxylic acid of biotin presents an easy handle for modification. Biotinylated smart polymers have been synthesized for conjugation to both SAs. Kulkarni et al. [79] synthesized a biotinylated PNIPAAm via RAFT polymerization of NIPAAm. Hydrolysis of the dithioester end-group in a methanol-aqueous sodium hydroxide solution resulted in a thiol-terminated PNIPAAm. Subsequent coupling with a maleimide-functionalized biotin formed the biotinylated PNIPAAm. Aggregation of mesoscale SA-PNIPAAm particles prepared from these conjugates was investigated for potential use in microfluidic devices

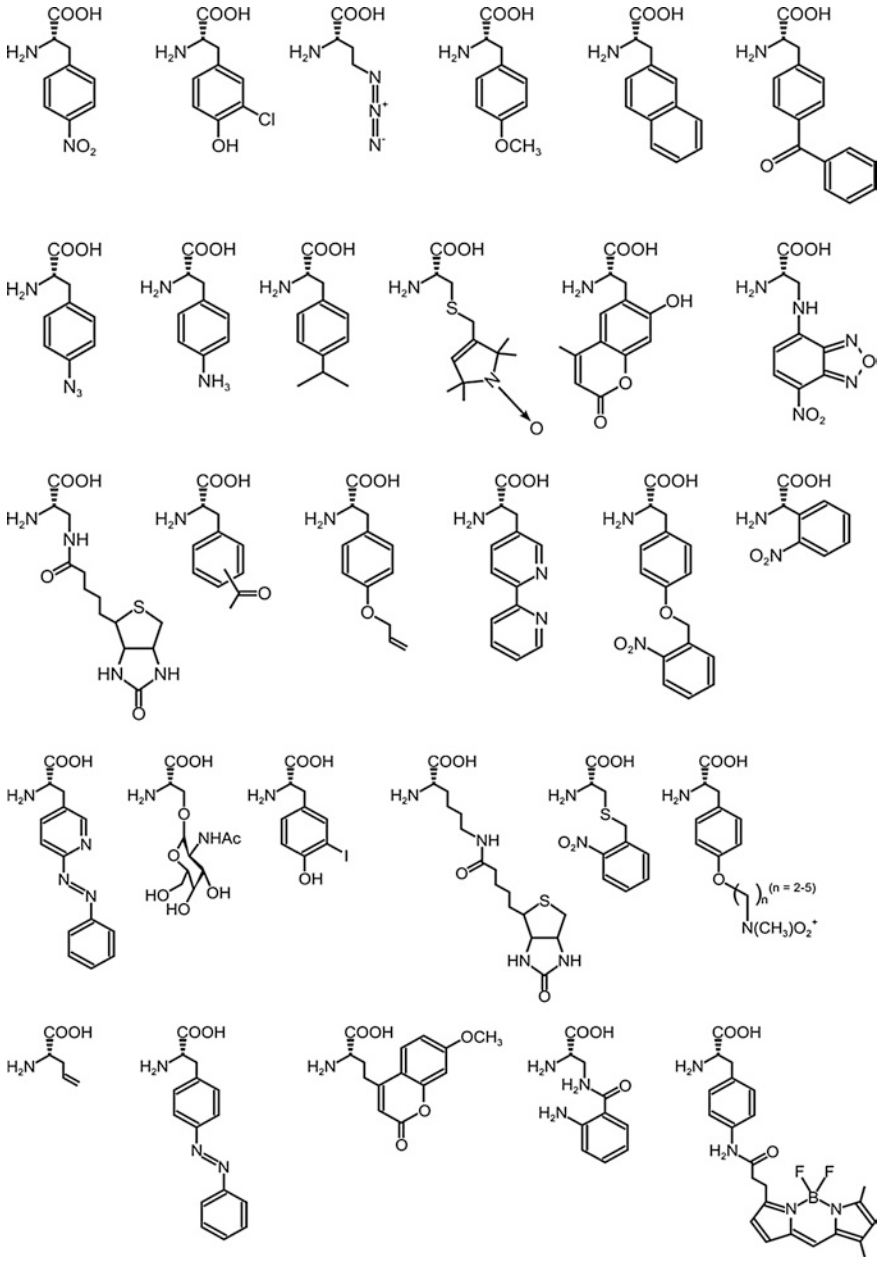

**Fig. 6.6** Structures of non-natural amino acids carrying a variety of specialty side groups

for the capture and release of biomolecules [80]. Giant amphiphiles comprised of an SA-polystyrene conjugate were synthesized through the use of a biotinylated

polystyrene [81]. The biotin functionality was introduced via coupling of an amine-functionalized biotin derivative with a carboxylic acid-terminated polystyrene. Cofactor reconstitution of horseradish peroxidase (HRP) was also demonstrated to prepare amphiphilic, bioactive protein-polymer conjugates [82]. A cofactor-terminated polymer was synthesized via amidation between a carboxylic-acid-terminated polystyrene and a monoprotected diamine. Subsequent deprotection to form the free amine, coupling with one carboxylic acid group of protoporphyrin IX, and addition of ferrous chloride tetrahydrate resulted in a polystyrene cofactor. HRP was reconstituted with the polymeric cofactor, resulting in vesicular aggregates that displayed enzymatic activity. This approach has great potential for producing controlled nanostructures of bioactive enzymes and proteins for biotechnology applications. Sun and colleagues [83, 84] have employed a biotinylated initiator for cyanoxyl-mediated free-radical polymerization of glycomonomers. The arylamine initiator was synthesized in two steps after coupling an NHS-activated biotin with *p*-nitrobenzylamine and reducing the nitro group with hydrogen/palladium. The formation of the diazonium salt followed by the addition of sodium cyanate and glycomonomer generated the biotinylated polymer. SA-glycopolymer conjugates were readily achieved by the interaction of the two species. The biotinylated ATRP initiators were also synthesized by activating the carboxyl group of biotin with *N,N'*-disuccinimidyl carbonate, followed by the addition of 2-(2-aminoethoxy)ethanol. Esterification of the resulting alcohol with 2-chloropropionic acid or 2-bromoisobutyric acid formed the biotin ATRP initiators. Biotinylated PNIPAAm was synthesized from these initiators [85].

### *6.2.5 Smart Conjugations with Multiple Proteins*

The majority of protein-polymer conjugates contain one protein and one to several polymer chains. Recently, homo- and heterotelechelic bioreactive polymers have been synthesized. The incorporation of the same protein onto each end of a polymer generates a triblock material with a wide range of possible applications. The polymer should provide the same benefits as described above, and in addition, exhibit higher binding affinities than mono-functionalized conjugates with improved pharmacokinetics over dimers synthesized using small molecules.

ATRP telechelic polymers have been prepared by employing bis-functional initiators, with subsequent transformation of the halogen chain ends (Fig. 6.7a). Kopping et al. [86] reported the synthesis of aminooxy-end functionalized polystyrene using ATRP followed by ATR coupling. A 1-bromoethyl ATRP initiator with an NHS group was used to polymerize styrene by copper-mediated ATRP with a high initiator efficiency. Polymerization kinetics showed that polymers were produced with the targeted molecular weights and low PDIs. Subsequent ATR coupling and deprotection with hydrazine yielded the telechelic aminooxy end-functionalized polymers. End-group reactivity was demonstrated using 4-bromobenzaldehyde as a model to confirm efficient and complete oxime bond

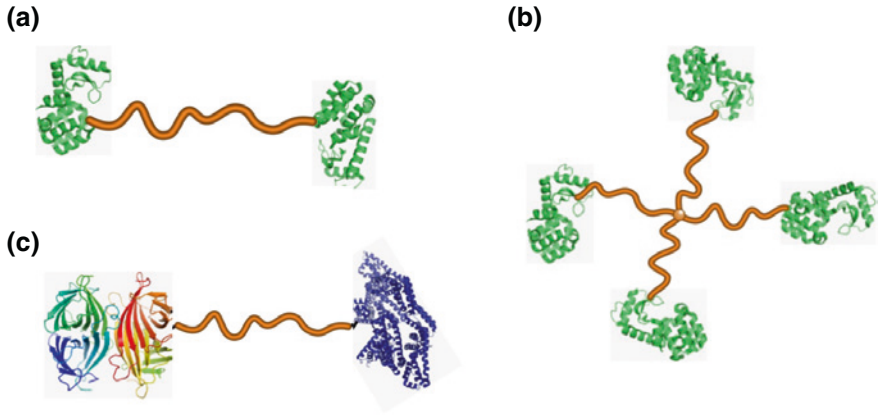


**Fig. 6.7** Design of telechelic-bioreactive polymers. **a** Homodimeric [86–88], **b** multimeric [89], and **c** heterodimeric protein-polymer conjugates [90–92]

formation. In a similar manner, cysteine reactive telechelic polystyrene was also synthesized [87]. In this example, a dimethylfulvene-protected maleimide-functionalized ATRP initiator was used to polymerize styrene. The authors have also reported the straightforward synthesis of homodimeric protein polymer conjugates by RAFT polymerization that exploits the inherent reactivity of trithiocarbonate end-groups [88]. A telechelic maleimide-end-functionalized PNIPAAm was synthesized by RAFT polymerization. Subsequent radical addition of the protected maleimide azo-initiator to the chain ends and retro-Diels Alder afforded the telechelic maleimide-end-functionalized PNIPAAm. Conjugation to a V131C mutant T4 lysozyme with only one reactive cysteine gave the protein dimer. Four-armed PNIPAAm was also synthesized by RAFT polymerization in the presence of a tetrafunctionalized trithiocarbonate chain transfer agent (CTA) (Fig. 6.7b) [89]. Maleimide functional groups were introduced at the chain ends by heating the polymers in the presence of a furan-protected azo-initiator. This allowed for site-specific conjugation of V131C T4 lysozyme to the polymers to generate multimeric protein-polymer conjugates. This simple strategy provides ready access to star protein-polymer conjugates for application in the fields of drug discovery, drug delivery, and nanotechnology.

Heterodimeric conjugates offer other interesting possibilities. A variety of strategies have been extended toward the synthesis of heterodimeric protein-polymer conjugates (Fig. 6.7c). An α-azide, ω-pyridyl disulfide CTA was used to produce well-defined PNIPAAm [90]. The azide was utilized for a Huisgen cycloaddition with an alkyne-functionalized biotin, allowing for conjugation to SA. The pyridyl disulfide was used for the reversible conjugation of glutathione or BSA. Heredia et al. [91] have demonstrated the ability to synthesize heterodimeric protein-polymer conjugates via radical coupling with a furan-protected azo-initiator to biotinylated

PNIPAAm synthesized by RAFT. NIPAAm was polymerized in the presence of a biotinylated CTA and biotinylated CTA with a disulfide between biotin and the site of polymer growth [92]. BSA was then conjugated to the maleimide end-group of both polymers. The ability to tether two biomolecules would allow for surface immobilization or attachment of various tags, fluorophores, peptides, antibodies, and other proteins to be linked to the biomolecule-polymer conjugate of interest.

### *6.2.6 Electrostatic Conjugation*

Electrostatic interactions also represent an interesting class of noncovalent conjugations useful for stabilizing proteins via multiple-point attachment (Fig. 6.2e). Although the resulting conjugates are less well-defined than their analogs prepared by single-point attachment, the multi-point attachment of enzymes to polymers has been widely studied and is considered to be the most general approach to stabilize these proteins against different denaturing conditions [93]. Indeed, multi-point attachment has increased the thermal stability and enzymatic activity of various enzymes. It has also been reported that ionic interactions between the polymer/enzyme played a role in the pH-dependent activity profiles of the conjugate [94]. Several groups have explored the interactions of cationic polymers and DNA [95]. Both electrostatic and hydrophobic interactions contribute to the formation of complexes between cationic polymer/DNA. Because many cationic polymers can condense DNA spontaneously, a series of chemically different cationic polymers are currently being investigated for gene delivery applications. The cationic polymer/DNA binding has also been utilized in a microarray format for the sensitive detection of DNA without the need for target labeling. Electrostatic conjugation has also been employed for the surface coating of cells or viruses represented by a layer-by-layer (LbL) technique of anionic and cationic polymers. The versatility of this technique allows for the construction of a thin polymer layer on the surface. In addition, the surface property can be controlled by the outermost layer of the polymer [96]. When the LbL method is applied on the erythrocyte surface, a camouflage shell can prevent antibody recognition [7, 8]. The multilayered film consisting of a protective shell and a camouflage shell was successfully created on RBCs through the LBL technique by Mansouri et al. [8]. A drawback of this technique is cytotoxicity when polycations are used as the first layer, which directly interacts with the cell surface. In addition to mammalian cells, electrostatic conjugation of surface proteins has evolved into a powerful tool for engineering the surfaces of viruses, bacteria, and yeast cells, for example. The viral surface can potentially be modified to provide a better means of preparation, purification, concentration, detection, tracking, imaging, and targeting for diagnostics, vaccine development, and drug/gene therapy. We have successfully created a nanoscale layer of hyaluronic acid (HA) on inactivated Hemagglutinating Virus of Japan Envelope (HVJ-E) via an LbL assembly technique for CD-44 targeted delivery [97].

### *6.2.7 Elastin-Like Polypeptides*

Recombinant artificial elastin-like polypeptides (ELPs), which are composed of Val-Pro-Gly-Xaa-Gly amino acid repeat units (Xaa is a 'guest residue' except proline), were reported to replace synthetic smart polymers as smart bioconjugates. Interestingly, ELPs are water soluble below their transition temperature, but they precipitate owing to their aggregation caused by hydrophobic interactions above the transition temperature. The phase transition temperature can be precisely controlled by varying the chain length and peptide sequence. Various ELP versions responsive to pH, light, and other stimuli, such as an electrochemical potential or analyte concentration, can be found in the literature. Rodríguez-Cabello et al. [98] have developed the ELPs that presented modulated pH and T sensitivities covering the most interesting range of biomedical applications. ELPs have also been modified with photoresponsive molecules such as azobenzenes and spiropyranes. A series of experiments have been performed by Urry [99] for the study of designed ELPs for more than a decade. The genetically engineered protein-based polymers can provide many advantages. First, they will, in principle, be able to show the same simple or complex properties present in natural proteins. In this sense, this method offers an opportunity to exploit the huge functional resources that have been hoarded and refined to the extreme by biology during the long process of natural selection. Second, we can design and produce materials exhibiting desired functions of particular technological interest because we can construct a coding gene. Third, they are characterized as being strictly monodisperse and can range from a few hundred daltons to more than 200 kDa. Fourth, the number of different combinations attainable by combining the 20 natural amino acids is practically infinite. In a simple calculation, the number of possible different combinations to obtain a small protein consisting of 100 amino acids is as high as $1.3 \times 10^{130}$. The smart response of ELPs has already found applications in different fields. For example, Chilkoti and colleagues have designed temperature- and pH-responsive ELPs for targeted drug delivery [23]. They have obtained responsive ELPs that conjugate to drugs and enable thermally targeted drug delivery to solid tumors with their transition temperature between body temperature and the temperature in a locally heated region [100]. In another example, Kostal et al. [101] have designed tunable ELPs for heavy metal removal. The presence of the histidine clusters enabled $Cd_2C$ to bind strongly to the biopolymers. Recovery of biopolymer-$Cd_2C$ complexes was easily achieved by triggering aggregation upon increasing the temperature above the transition temperature.

## 6.3 Characterization Methods

A variety of techniques for characterizing bioconjugates have been reported in the literature. The most commonly used methods include microscopy, spectroscopy, scattering, mass spectroscopy, and thermal technique. Some of the most recently used methods for conjugate characterization are described in the following subsections.

### 6.3.1 Determination of Molecular Sizes

Owing to an important influence of polymer architecture on the grafting process, the determination of the molecular weight is necessary. Gel permeation chromatography (GPC) is an established method of determining the molecular mass of polymers. The detectors used are either refractive index (RI) or ultraviolet (UV) detectors. Compared with other methods of analysis, such as osmometry and static light scattering, it has the advantage that it determines not merely average values but the complete distribution of molecular weights. In GPC, molecules are separated according to their hydrodynamic volume. Their molecular weights (MWs) and molecular weight distributions can be determined from the measured retention volume (RV) using a calibration curve (log MW against RV), which must be set up with the aid of a number of standards of known molecular weight. However, as the relationship between molecular weight and size depends on the type of polymer, the calibration curve depends on the polymer used, with the result that true molecular masses can only be obtained if the calibration standards and the sample are of the same type. In all other instances, the results are only relative. Large deviations from the true molecular weight occur in branched samples in particular, because the molecular density in such a case is substantially higher than in linear chains.

To overcome this limitation and meet the growing demand for the characterization of increasingly complex polymers, detectors sensitive to molecular weight, such as light scattering, can be used in GPC. The signal of light-scattering detectors is directly proportional to the molecular weights of the polymers. The concentration and refractive index increment (dn/dc) must be known to determine the molecular mass. The advantage of light scattering in GPC is that the molecular weight can be directly determined without a calibration curve, provided that the signal-to-noise ratio is adequate for this. When it comes to determining the structure, on the other hand, viscosity detectors are more suitable, because they measure structural differences directly and can be used over a substantially wider range of molecular weights. Therefore, triple detection combines these detection capabilities into a single system to give true molecular weight distributions as well as size distributions and further structural information, such as the degree of polymer branching.

Mass spectrometry (MS) also deals with accurate mass measurement by producing charged molecular species in vacuum and their separation by magnetic and electric fields on the basis of the mass-to-charge ratio. Because MS requires the ability to deconvolute molecular fragments, it is more appropriate for low-molecular-weight derivatized proteins and conjugates. The development of matrix-assisted laser desorption/ionization time-of-flight mass spectrometry (MALDI-TOF-MS) allows the ionization of fragile macromolecules such as proteins of $10^5$ molecular weight without promoting decomposition. Therefore, MALDI-TOF-MS is an attractive approach for the determination of the accurate molecular weight of intact proteins [88, 102]. Tao et al. used MALDI-TOF-MS to determine the architecture of multimeric lysozyme/PNIPAAm conjugates. They prepared polymer samples by mixing

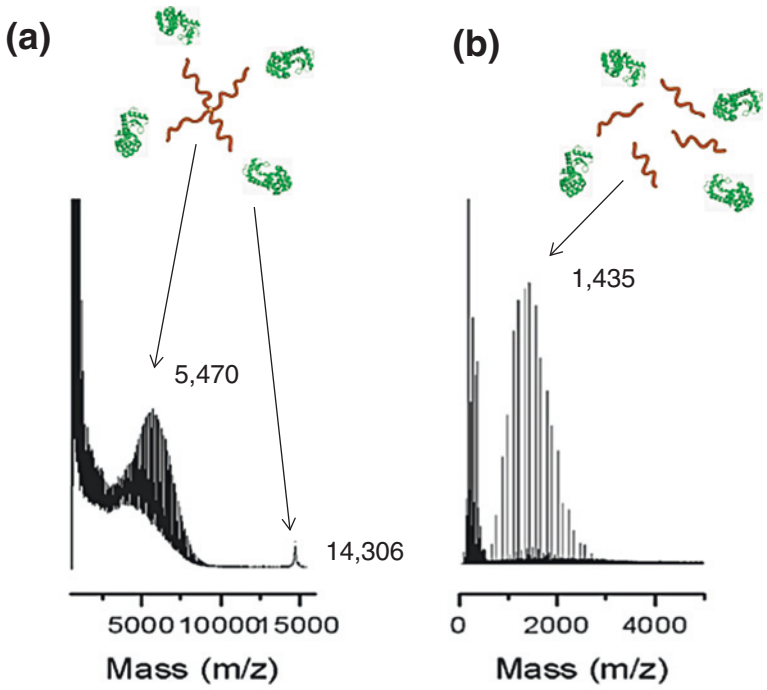


**Fig. 6.8** MALDI-TOF spectra of four-armed PNIPAAm before **a** and after **b** aminolysis with butylamine [89]

trans-2-[3-(4-tert-butylphenyl)-2-methyl-2-propenylidene] malononitrile (DTCB) matrix, potassium trifluoroacetate, and polymer in a ratio of 5:1:5 v/v/v [89]. The MALDI-TOF spectra gives an MW of 5470 Da for four-armed PNIPAAm, which was close to the theoretical value (6,000 Da) (Fig. 6.8a). Aminolysis with butylamine was utilized to cleave the arms from the core to confirm that the polymer contained four arms of similar molecular weight. The mass of the cleaved arms was 1,435 Da (theoretical value, 1,351 Da) (Fig. 6.8b). This result suggested that the desired four-armed star had been synthesized. The choice of the matrix depends on the type of analyte to be analysed.

### *6.3.2 Determination of Conjugation*

A number of methods have demonstrated wide utility in the characterization of polymer/bioconjugates. Gel electrophoresis (GE) and GPC can be used to compare conjugate molecular weight to native protein and provide a semiquantitative measure of conjugate polydispersity. In GE, the presence of more than one conjugate band for a given conjugation protocol indicates a polydisperse conjugate

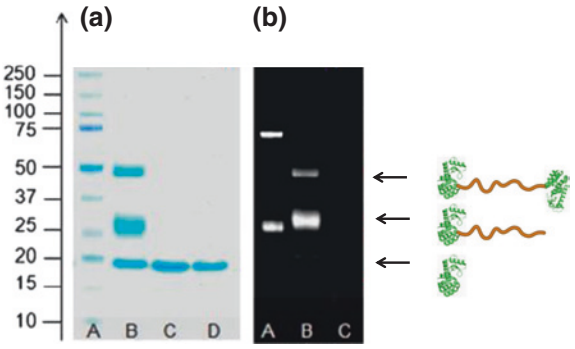


**Fig. 6.9** SDS-PAGE analysis of the homodimeric lysozyme-PNIPAAm conjugates **a** stained with Coomassie blue and **b** visualized with UV light (lane A: control; lane B: conjugates; lanes C and D: lysozyme only) [88, 89]

population. The free (unconjugated) polymer usually results in a blurry band. Therefore, an ion exchange column or thermal precipitation may be needed to remove the conjugates from the free polymer. When protein is reacted with polymer to form 1:1 protein:polymer conjugates, several distinct bands are usually visualized. Each band corresponds to an integer multiple of polymer, indicating that there is a significant population of conjugates with more than one polymer per protein. This can be rationalized using the polymer micelle results. Tao and coworkers have performed sodium dodecyl sulfate polyacrylamide gel electrophoresis (SDS-PAGE) analysis to determine the resulting structure of homodimeric lysozyme/PNIPAAm conjugates [88]. After Coomassie staining, the gel revealed two new spots with higher molecular weight than that of unmodified lysozyme. These new spots were attributed to the monomer and dimer protein/polymer conjugate adducts (Fig. 6.9). They have also performed SDS-PAGE analysis to determine the structure of heterotelechelic SA-BSA/PNPAAm conjugates [91]. Blue fluorescent SA was used to enable visualization by UV light and Coomassie Blue staining. SDS-PAGE of the SA-BSA heterodimer was observed first under UV light and then with Coomassie Blue stain. Using both visualization techniques, it was clarified that the SA was present in the conjugate and that the SA-BSA heterodimer was formed.

When biotinylated PNIPAAm is conjugated to SA, 2-(4'-hydroxyazobenzene) benzoic acid (HABA) assay can be used to characterize the binding stoichiometry of PNIPAAm to SA. In the HABA assay, displacement of HABA from SA by biotinylated polymer results in a loss of absorbance by HABA at 500 nm. This change in absorbance can be compared with a standard curve for the measurement of the average protein:polymer ratio. For molecular weights lower than 20 kDa, no more than four polymers may be added to a single SA. When the polymer molecular weight is above 20 kDa, only one polymer may be added to a given SA face, resulting in a maximum of two polymers per protein. By mixing SA:30 kDa PNIPAAm in a 1:1.5 mol ratio, conjugates with an average of 1:1 polymer:protein were created. These conjugates should provide one open face for subsequent biotin binding and are useful for further conjugation reactions.

### 6.3.3 Structural Analysis

Circular dichroic (CD) spectroscopy has also been applied to examine the changes in the tertiary structure of the enzyme before and after conjugation. CD has proved to be extremely useful in understanding the various structural elements in proteins, and structural transitions from order to disorder can be well documented by CD. Yan et al. [103] measured the CD spectra of the native trypsin and the conjugated trypsin with poly(3-dimethyl(methacryloyloxyethyl) ammonium propane sulfonate) (PDMAPS). The native trypsin has 8.6 % α-helix and 32.3 % β-sheet, while the conjugated trypsin has 7.17 % α-helix and 24.8 % β-sheet. The conjugation with PDMAPS had a weak effect on the content of the α-helix but a slightly stronger effect on the content of the β-sheet, leading to a reduction from 30.3 to 24.8 %. Sharma et al. [104] conjugated α-chymotrypsin with Eudragit S-100. The CD showed that there are definite changes in the secondary structure upon immobilization. The small α-helical content is totally gone and there is a decrease in the content of the β-sheet/β-turn structure. The randomness in the structure increased by about 17 %.

### 6.3.4 Determination of Transition-Point

The phase separation behavior of smart bioconjugate aqueous solutions has been investigated in the literature by a wide variety of experimental techniques, including IR spectroscopy, viscometry, light scattering, $^{1}$H NMR spectroscopy, fluorescence, calorimetry, Raman spectroscopy, and FTIR spectroscopy. These experimental techniques can provide different information during phase separation of smart polymers. The simplest method of detecting a point of phase separation in aqueous polymer solutions is the cloud-point method. It is based on a visual observation of the macroscopic phase separation at a specific temperature, pH, or salt concentration. The strong increase in the scattering intensity results from the grown concentration fluctuations near the critical point when the size of those fluctuations exceeds the wavelength of the scattered light. Usually, a standard UV-Vis spectrophotometer is used to determine the cloud point. One of the major advantages of this method is rapid and easy measurement. However, the cloud-point method only measures the relative changes in scattering intensity in the course of nearing the transition point. In addition, the solution may remain transparent, and it may be difficult to determine the phase transition point based on visual observation or even with the use of a UV-Vis apparatus.

Thermal techniques can aid in determining the thermal stability of the biomolecules. Differential scanning calorimetry (DSC) is used to study various material transitions including melting, crystallization, glass transition, and decomposition. DSC is an inexpensive and rapid method of measuring heat capacities of condensed phases. From these measurements, enthalpy changes for phase transitions can easily be determined. DSC has been applied to a wide variety of problems,

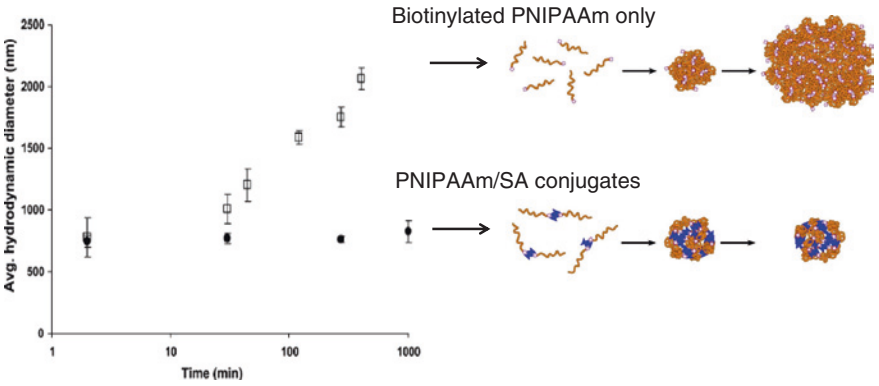


**Fig. 6.10** DLS analysis of the particle formation kinetics of mesoscale PNIPAAm/SA conjugates above the LCST. The particles formed by the PNIPAAm/SA conjugates are stable in size for over 16 h. In contrast, aggregates of biotinylated PNIPAAm aggregated over time into larger particles [79]

from coal combustion to protein denaturation. Subsequent analysis can indicate the state of the bioconjugate, including the stability of the biomolecules, and structural information on both the polymer and biomolecule.

The light scattering (LS) technique is the most precise method of observing the process of phase separation not only in the polymer solutions, but also in binary mixtures of organic solvents. Static light scattering (SLS) allows one to follow the growing fluctuations of concentration by recording the scattering intensity at the scattering angles suitable for the hydrodynamic regime. DLS allows one to detect changes in the hydrodynamic size and shape of macromolecules and their aggregation following their precipitation in the course of transition. Kulkarni et al. [79] observed reversible particle formation and dissolution kinetics of mesoscale PNIPAAm/streptavidin conjugates by DLS. The scattering intensity in counts per second (CPS) was used as an index of nanoparticle formation, since sizing measurements cannot be performed within short time intervals. The transition from soluble conjugates to particles was found to be rapid (within 20 s) and to occur in a narrow temperature range at the critical point. The time lapse of ca. 100 s was observed after the temperature of the solution increased because there was an induction period with early nucleation events. After reversal of the temperature stimulus, the scattering intensity decreased by more than 90 % within 2 min. The particle formation and dissolution kinetics of smart bioconjugates also depend on the concentration. The particle size increases with the concentration of the bioconjugate. Interestingly, the particles were stable once formed (>16 h) and further dilution at the elevated temperatures did not significantly affect the size of the particles. Particle sizes were comparable for the 25.9, 14.9, and 4.8 kDa conjugates, with no significant change in size with a change in molecular weight (Fig. 6.10). The particle sizes also depend on the molecular weight of the PNIPAm used for conjugation. Conjugates of higher molecular weight polymers form more uniform particles.

The heating rate is also important for particle formation of smart bioconjugates. Smaller particles were formed at higher heating rates, and nanoparticles of fixed sizes could be formed by varying the heating rate. For example, the size of the 14.9 kDa PNIPAAm-streptavidin conjugate could be tightly controlled to 675 nm at a concentration of 1 μM by choosing a heating rate of 0.12 °C/s. The particles had a wider distribution when formed at lower heating rates. On the other hand, the final temperature did not affect the particle size significantly. These results indicate that the particle size is largely governed by the kinetics of aggregation at defined concentrations and polymer molecular weights.

### *6.3.5 Determination of Catalytic or Binding Activity Assay*

One of the most important characterizations for polymer/protein conjugates to exploit is the effect of polymer conjugation on the protein activity. Heterogeneity in the structure is generally reflected in the biological properties of the conjugate and often results in decreased protein activity. Enzyme activities are determined by measuring the amount of product that is formed when an enzyme acts upon a specific substrate. The speed at which the enzyme acts upon a substrate and converts it to a product is affected by several factors, including the specific substrate that is used in the reagent, the concentration of the substrate, the pH of the reagent containing the substrate, and the presence or absence of certain compounds in the reagent that modulate the rate at which an enzyme can work. Heredia et al. [62] compared the lytic ability of the PNIPAAm/lysozyme with respect to the lyophilized substrate *Micrococcus lysodeikticus*. Lysozyme, lysozyme initiators, and isolated lysozyme conjugates were prepared with equal protein concentrations, and then the enzyme solution was mixed with *M. lysodeikticus* solution. Upon cell wall lysis, the solution became less turbid, and this decrease in absorbance was monitored at 450 nm. Activity was expressed in activity units (AU). One AU is defined as a change in absorbance of 0.001 per min. The lytic activity assay was also performed on the lysozyme conjugates using fluorescein-labeled *M. lysodeikticus*. When protein/polymer conjugates were prepared by polymerization from the initiator-modified proteins, the enzymatic activity was fully retained. Therefore, creating well-defined conjugates is important, and site-specific modification of the protein is a better approach for preparing such biomolecules.

Site-specific modification of proteins is also important for directed immobilization onto surfaces and ensures that biorecognition sites are accessible. For smart polymer switches, placement of the polymer chain near the protein or enzyme active site is critical for reversible activity control. Shimoboji et al. [19, 55] have successfully demonstrated thermally or photoinduced switching of enzyme activity on the basis of the site-directed conjugation of end-reactive smart polymers to a unique cysteine residue positioned near the enzyme active site. The polymer was conjugated to the endoglucanase 12 A (EG 12A) site-directed mutant N55C, directly adjacent to the cellulose binding cleft, and to the S25C mutant, where the

conjugation site is more distant. The N55C conjugate displayed a greater activity shutoff efficiency in the collapsed polymer state than the S25C conjugate. Increasing the polymer molecular weight was also shown to increase the shutoff efficiency of the switch. Related to these effects of conjugation site and polymer size, the switching efficiency was found to be strongly dependent on substrate size. With a small substrate, *o*-nitrophenyl-β-D-cellobioside (ONPC), there was minimal blocking of enzyme activity when the polymer was in the expanded state. With a large substrate, hydroxyethyl cellulose (HEC), there was a large reduction of enzyme activity in the polymer expanded state, even with relatively small polymer chains, and a further reduction when the polymer was collapsed. Similar general trends for the interactive effects of conjugation site, polymer size, and substrate size were observed for immobilized conjugates. To elucidate the mechanism of the stimuli-response switches, the kinetic parameters $K_m$ and $k_{cat}$ were determined by Lineweaver-Burk analysis assuming Michaelis-Menten conditions. Kinetic studies demonstrated that the switching activity was due to the blocking of substrate association by the collapsed polymers. These investigations provided mechanistic insight that can be utilized to design molecular switches for a variety of stimuli-responsive polymer-protein conjugates. When polymers are conjugated to an antibody, a competition assay and an ELISA can be used to characterize the binding activity through the measurement of analyte depletion.

### *6.3.6 Cytotoxicity Assay*

Since many of the polymer bioconjugates are intended for use as biomedical and/or therapeutic polymers, in vitro cytotoxicity assays are essential for determining the responses of cells to bioconjugates. Cell viability, cell proliferation and many important live-cell functions, including apoptosis, cell adhesion, chemotaxis, multidrug resistance, endocytosis, secretion, and signal transduction, can be stimulated or monitored with various chemical and biological reagents. Many of these processes lead to changes in intracellular radicals, free-ion concentrations, or membrane potential that can be followed with appropriately responsive fluorescent indicators. Proliferation assays are primarily designed to monitor the growth rate of a cell population or to detect daughter cells in a growing population. Fluorometric assays of cell viability and cytotoxicity are easy to perform with the use of a fluorescence microscope, fluorometer, fluorescence microplate reader, or flow cytometer, and they offer many advantages over traditional colorimetric and radioactivity-based assays. The LIVE/DEAD Viability/Cytotoxicity kit provides an exceptionally easy fluorescence-based method for determining the viability of adherent or nonadherent cells and for assaying cytotoxicity. The kit comprises two probes: calcein AM and ethidium homodimer-1. Calcein AM is a fluorogenic esterase substrate that is hydrolyzed to a green-fluorescent product; thus, green fluorescence is an indicator of cells that have esterase activity as well as an intact membrane to retain the esterase products. Ethidium homodimer-1 is a

high-affinity, red-fluorescent nucleic acid stain that is only able to pass through the compromised membranes of dead cells.

Reagents for counting cells and quantitating cell proliferation are also valuable research and diagnostic tools. Most cell proliferation assays estimate the number of cells either by incorporating 5-bromo-2-deoxyuridine (BrdU) into cells during proliferation or by measuring the total nucleic acid or protein content of lysed cells. BrDU is a synthetic nucleoside that is an analogue of thymidine. BrDU is commonly used in the detection of proliferating cells in living tissues. BrDU can be incorporated into the newly synthesized DNA of replicating cells (during the S phase of the cell cycle), substituting for thymidine during DNA replication.

The MTT calorimetric assay determines the ability of viable cells to convert a soluble tetrazolium salt [3–(4,5-dimethylthiazol-2-yl)-2,5-diphenyltetrazolium bromide] (MTT) into an insoluble formazan precipitate. Tetrazolium salts accept electrons from oxidized substrates or appropriate enzymes, such as NADH and NADPH. In particular, MTT is reduced at the ubiquinone and cytochrome b and c sites of the mitochondrial electron transport system and is the result of succinate dehydrogenase activity. This reaction converts the yellow salts to blue-colored formazan crystals that can be dissolved in an organic solvent whose concentration can be spectrophotometrically determined. Owing to the many advantages of the assay, it is considered today a significant advance over traditional techniques. In fact, it is rapid, versatile, quantitative, and highly reproducible with a low intratest variation between data points. Moreover, the test can also be used for floating cells, such as those of leukemia and small cell lung carcinoma, and always allows sufficient time for cell replication, drug-induced cell death, and loss of enzymatic activity, which generates the formazan product from the MTT substrate.

## 6.4 Applications of Smart Bioconjugates

There have been several successful applications in medicine and biotechnology for such smart polymer biomolecule systems, and as such, they represent an important extension of polymeric biomaterials. The smart polymers can provide switchable-solubilization/precipitation for biomolecules such as enzymes, liposomes, and plasmid vectors, when these polymers are conjugated to specific sites within these biomolecules. Some of the most successfully demonstrated applications are described in the following subsections.

### *6.4.1 Bioseparations and Immunoassays*

Smart conjugate systems have been used for many years in bioseparations and immunoassays. Hoffman and coworkers were the first to demonstrate a phase separation immunoassay [11–13]. The thermally induced precipitation of a PNIPAAm-protein

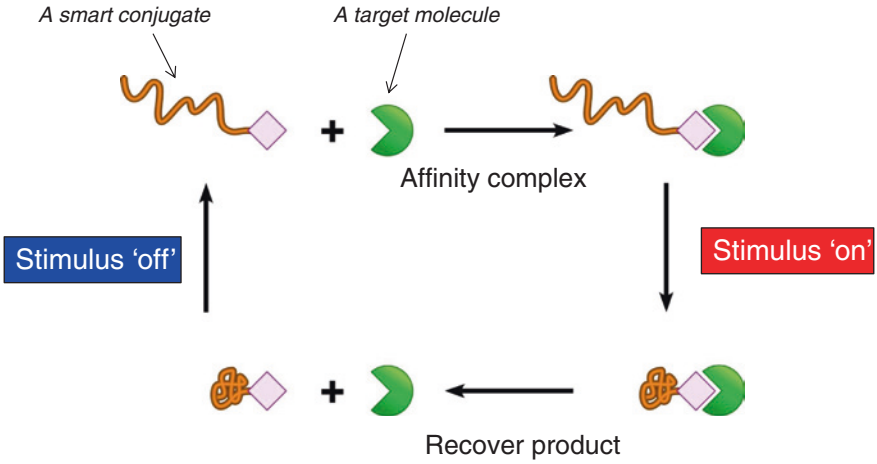


**Fig. 6.11** Schematic illustration of the thermally induced phase separation of a smart polymer and a ligand or a receptor, such as enzymes, antibodies, cell membrane receptors, and many others. This general process should be useful for removing any specific molecule from a complex mixture for the purpose of recovery and possible recycling of that molecule

bioconjugate from a complex solution can simultaneously and selectively remove only the protein that is conjugated to the PNIPAAm from the solution (Fig. 6.11). They have used this phenomenon for the separation of an enzyme from its reaction solution, to enable both recovery of the product from the supernatant and recycling of the enzyme. If the conjugated protein forms a complex with another biomolecule, for example, by affinity recognition, then the complex will also be selectively precipitated from solution. This phenomenon can be used to selectively remove IgG from solution as a PNIPAAm-protein A/IgG complex, in a fashion similar to affinity chromatography, but in this case, it is carried out by reversible phase separation from a solution, instead of flowing through and eluting from a packed column. This thermally induced affinity precipitation process may be extended to stimuli-induced phase separation of a biotinylated target molecule that is complexed to avidin or streptavidin. In this case, a biotinylated target molecule is first complexed with an excess of avidin or streptavidin molecules in solution, such that at least one of the four (on average) biotin binding sites remains free. Then, an end-linked biotin smart polymer conjugate is permitted to bind to the free site on the avidin or streptavidin molecules. Following this, the bioconjugate/affinity complex can be phase-separated by raising the temperature above the LCST of the smart polymer, which selectively removes the biotinylated target molecule from solution. Hoffman and coworkers have extended the affinity phase separation concept to the selective isolation and assay of an analyte from a complex mixture such as a serum sample. This is done by conjugating a first antibody to the polymer, complexing the analyte by affinity to the first antibody, and then introducing a second, labeled antibody, which then binds to the analyte by affinity to a similar or different site (epitope) on the analyte. This yields a temperature-sensitive

polymer conjugated to an immune complex sandwich, which can then be selectively removed by thermally induced precipitation. This is an especially important separation step, because an excess of the labeled, second antibody is usually added to the sample. Washing and dissolution in cold buffer permit easy assay of the analyte. This immunoassay resembles an enzyme-linked immunosorbent assay (ELISA) carried out in solution. This concept has been extended to the assay of two different analytes in the same test sample. If NIPAAm is copolymerized with a more hydrophilic or a more hydrophobic comonomer, then copolymers with higher or lower LCSTs can be obtained, respectively. If one of each of these two different LCST copolymers is conjugated to a different antibody, then two different analytes may be assayed in the same serum sample by sequentially raising the temperature of the system to sequentially phase-separate the two different polymer-conjugated immune complex sandwiches. One could also carry out such a dual affinity separation or dual immunoassay using combinations of two different pH-sensitive smart polymers, or one temperature- and one pH-sensitive smart polymer. Another approach to controlling biological reactions using smart polymers is to prepare recombinant proteins with built-in polymer binding sites close to ligand or cell binding sites. This technique has been used to control ligand and cell binding activity, based on a variety of triggers including temperature and light. The time and costs involved in purifying proteins might be reduced significantly by using these smart polymer systems.

Concanavalin A (ConA)- or wheat germ lectin (WGL)-conjugated PNIPAAm have also been used in the purification of various polysaccharides or polysaccharide-containing compounds such as glucan [105]. The thermally reversible soluble-insoluble PNIPAAm-dextran derivative conjugate has been synthesized by conjugating amino-terminated PNIPAAm to a dextran derivative via ethyl-3-(3-dimethylaminopropyl)-carbodiimide (EDC), and the conjugate was used as a tool to purify polyclonal antibodies in serum samples from rabbits subcutaneously immunized with the derivatized dextran [106]. Chang et al. reported an effective and rapid method of purifying glutathione S-transferase (GST) using glutathione (GSH)-modified PNIPAAm and mild thermal conditions. They employed a chain transfer agent modified with pyridyl disulfide in the RAFT polymerization of NIPAAm [107]. Conjugation of GSH to the pyridyl disulfide-PNIPAAm reached 95 % within 30 min, as determined by UV-Vis monitoring of the release of pyridine-2-thione. GST was successfully thermoprecipitated upon heating the GSH-PNIPAAm above the LCST. Owing to its simplicity and high efficiency, this method holds great potential for large-scale purification of GST-tagged proteins. A thermally induced phase separation system has also been used for the specific separation of animal cells [28]. Monoclonal antibodies were modified with itaconic anhydride and copolymerized with NIPAAm, and ligand-conjugated carriers were added to the PEG 800-dextran T500 aqueous two-phase systems. CD34-positive human acute myeloid leukemia cells were specifically separated from human T lymphoma cells by applying anti-CD34 conjugated with PNIPAAm in the aqueous two-phase system.

Extensive efforts by Mattiasson and colleagues [108–110] have also been made to establish effective metal-chelate affinity precipitation using smart polymers. In metal

chelating affinity precipitation, metal ligands such as imidazole are covalently coupled to the reversible soluble–insoluble smart polymers. The copolymers carrying metal-chelating ligands are charged with metal ions and the target protein binds the metal-loaded polymer in solution via the interaction between the histidine on the protein and the metal ion. Many proteins both containing natural metal ion binding residues and recombinant proteins containing His-tag residues have been purified using metal chelate affinity precipitation. Therefore, His-tagged proteins or cells or bioparticles can be purified through the precipitation of a target molecule–metal-loaded polymer complex from the mixture. The precipitated complex is solubilized by reversing the precipitation conditions, and the target molecule is dissociated from the precipitated polymer by using imidazole or EDTA as an eluting agent. The biomolecule is recovered from the copolymer by precipitating the latter at elevated temperature in the presence of NaCl. In a recent study, purification of extracellularly expressed six histidine-tagged single-chain Fv-antibody fragments ($His_6$-scFv fragments) from a recombinant *Escherichia coli* cell culture broth was performed. The precipitation efficiency was lower with Ni(II)-poly(VI-NIPAAm) than with Cu(II)-poly(VI-NIPAAm), but the selectivity was better in the former case. The bound His6-scFv fragments were recovered almost completely (>95 %) by elution with 50 mM EDTA buffer, pH 8.0 [111].

Besides protein purification, the metal-ion charged copolymer of poly(VI-NIPAAm) can also be applied to the separation of single-stranded nucleic acids, such as RNA from double-stranded linear and plasmid DNA, by affinity precipitation [112]. The separation method utilizes the interaction of metal ions to the aromatic nitrogens in exposed purines in single-stranded nucleic acids [113].

### *6.4.2 Molecular Switching*

Since an important aspect of many technologies that utilize biomolecular components is the control of their recognition properties, there is considerable interest in developing molecular switches that control recognition processes with mild signals. Smart polymers have been utilized to control protein activity as molecular switches. The ability to reversibly control protein and enzyme activities using external stimuli could provide new opportunities for the development of molecular diagnostics, bioprocesses, affinity separations, lab assays, BioMEMS, bioelectronics, and biosensor technologies. Chilkoti et al. have been demonstrating a new approach to molecular switches, in which site-specific conjugation of smart polymers is utilized. The site-specific conjugation is designed to assure minimal loss in the activity of the protein after conjugation with the smart polymer. They first reported the site-specific attachment of maleimide-terminated PN1PAAm to a genetically engineered mutant of cytochrome $b_5$, incorporating a unique cysteine residue by site-directed mutagenesis techniques [54]. This conjugation technique permits the site-specific and stoichiometric conjugation of the polymer with the protein. A genetically engineered SA mutant, which has only one cysteine residue, was also conjugated site specifically via sulfhydryl groups with a PNIPAAm that

has pendant sulfhydryl-reactive vinyl sulfone groups [39]. Cys was substituted for Asn at position 49, which is near the outer edge of the biotin-binding pocket. Normal binding of biotin to the modified SA occurred below the LCST, whereas above the LCST, the polymer collapsed and blocked binding. Site-directed mutagenesis techniques were also used to replace the native glutamate at position 116 with cysteine [114]. Since the conjugation site is near the tryptophan 120 residue, which forms a van der Waals contact with biotin, which is important in generating the large binding free energy, the temperature-induced conformational change of the polymer at position 116 may lead to structural changes in the region of tryptophan 120, which are responsible for the reversible binding between biotin and the conjugated SA. The conjugate repeatedly bound and released biotin as temperature was cycled through the LCST. With the incorporation of pH-sensitive units such as acrylic acid (AAc) in a random copolymer with NIPAAm, a copolymer becomes completely soluble at 37 °C and pH 7.4 and insoluble at 37 °C and pH 4.0. This copolymer has been conjugated to a specific cysteine thiol site inserted by genetic engineering near the recognition site of SA [115]. The biotin binding at 37 °C is significantly reduced at pH 4.0, compared with pH 7.4. This is most likely due to the more compact copolymer coil at pH 4.0 and 37 °C compared with that at pH 7.4 and 37 °C. The bound biotin was able to be released by changing the conditions to pH 4.0.

To investigate the detailed mechanism of the smart polymer activity switches, the roles of the conjugation site and the free polymer were determined using a new end-reactive polymer, *N,N*-dimethyl acrylamide-*co*-4-phenylazophenylacrylate (DMAA). The use of this polymer and a control SA mutant has allowed an accurate determination of the conjugation ratio. The site selectivity of the switch was first investigated with the S139C SA mutant that contains a unique cysteine at the C-terminus. The purified S139C conjugate, where the DMAA is distant from the binding site, did not display switching activity. The previously characterized E116C streptavidin mutant displayed switching activity when the DMAA was conjugated at this cysteine near the biotin binding site [116]. Because the release of biotin was shown to proceed with the same kinetics as the biotin off-rate for wild-type streptavidin, the mechanism for release was shown to be the blocking of biotin reassociation by the collapsed DMAA. The reversible temperature-induced collapse of DMAA has also been used as a molecular switch to control the catalytic activity of endoglucanase 12A (EG 12A) (Fig. 6.12) [117]. The polymer was conjugated to the EG 12A site-directed mutant N55C, directly adjacent to the cellulose binding cleft, and to the S25C mutant, where the conjugation site is more distant. The N55C conjugate displayed a larger activity shutoff efficiency in the collapsed polymer state than the S25C conjugate. Increasing the polymer molecular weight was also shown to increase the shutoff efficiency of the switch. Related to these effects of conjugation site and polymer size, the switching efficiency was found to be strongly dependent on substrate size. With a small substrate, there was minimal blocking of enzyme activity when the polymer was in the expanded state. With a large substrate, on the other hand, there was a large reduction in enzyme activity in the polymer expanded state, even with relatively small polymer chains,

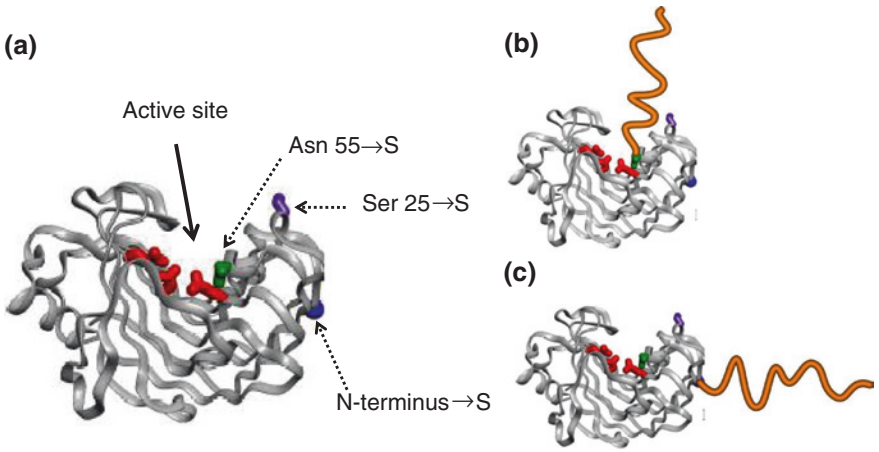


**Fig. 6.12** (**a**) Schematic model of site-directed mutant endoglucanase 12A (EG 12A). The *red residues* represent the catalytic glutamic acid side chains at the active site of EG 12A, the *green residue* is the Asn 55 position, the *purple residue* is the Ser 25 position, and the N-terminus is represented as the *blue circle*. The polymer is conjugated to the EG 12A site-directed mutant N55C, directly adjacent to the active site (**b**), and to the S25C mutant, where the conjugation site is more distant (**c**). The N55C conjugate displays a larger activity shutoff efficiency in the collapsed polymer state than the S25C conjugate [117]

and a further reduction when the polymer was collapsed. Similar general trends for the interactive effects of the conjugation site, polymer size, and substrate size were observed for immobilized conjugates.

Temperature-responsive poly(*N,N*-diethylacrylamide) (PDEAAm) was attached to the SA approximately 20 Å from the binding site for biotinylated proteins. Below the LCST, the polymer is in its extended state and acts as a 'shield' to block the binding of large biotinylated proteins. Above the LCST, it collapses and exposes the binding site, thereby allowing binding. The degree of shielding depends on both the size of the biotinylated protein and the size of PDEAAm (Fig. 6.13) [50]. The biotinylated IgG (MW 150 kD), for example, was unable to bind to the SA conjugate whether the polymer was above or below its LCST, whereas the biotinylated Protein G (MW 6.2 kD) was able to bind whether the polymer was hydrated or collapsed. An intermediate-size biotinylated bovine serum albumin (BSA) (MW 67 kD) exhibited increased binding as the temperature was raised through the LCST. These results suggest that smart polymer shields could be tailored to achieve a wide range of size-dependent ligand discrimination for use in affinity separations, biosensors, and diagnostics technologies.

Light-regulated molecular switches that reversibly control biomolecular function could also provide new opportunities for controlling activity in diagnostics, affinity separations, bioprocessing, therapeutics, and bioelectronics applications. Hohsaka et al. [118] have prepared a monoclonal antibody against a non-natural amino acid carrying an azobenzene group, L-*p*-(phenylazo)phenylalanine.

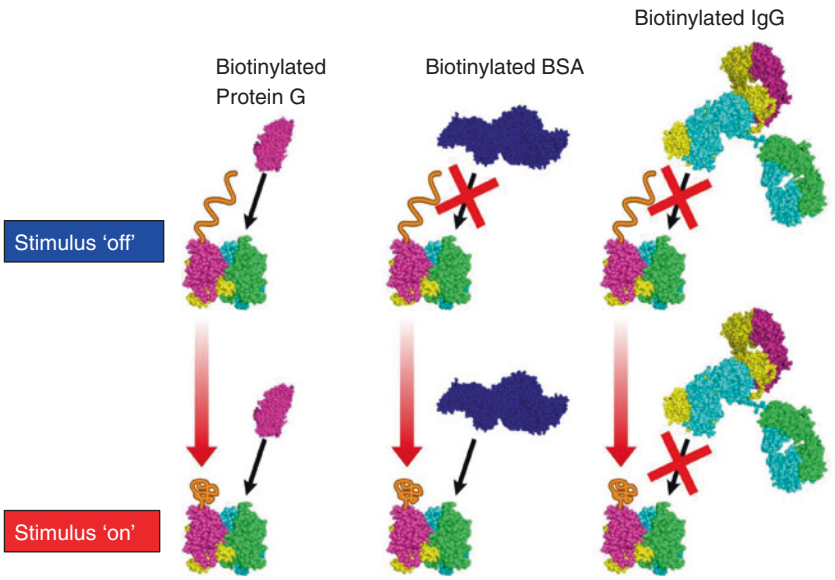


**Fig. 6.13** Size-dependent control of the binding of biotinylated proteins to SA using a polymer shield. The biotinylated IgG is unable to bind to the SA conjugate whether the polymer was above or below its LCST, whereas the biotinylated Protein G is able to bind whether the polymer was hydrated or collapsed. An intermediate-size biotinylated BSA exhibited increased binding as the temperature was raised through the LCST [50]

The antibody binds an azobenzene group when it is in the *trans* form, but releases it when the latter is photoisomerized to the *cis* form. Ueda et al. have replaced $Trp^3$ of phospholipase $A_2$(PLA2) by non-natural aromatic amino acids, 3-(2-naphthyl)-L-alanine (Nap), 3-(9-anthryl)-DL-alanine (Ant), and p-phenylazo-L-phenylalanine (AzoF). UV irradiation during the hydrolysis reduced the activities of Nap-AMPA and Ant-AMPA. However, AzoF-AMPA with a *cis*(Z) configuration of the AzoF unit showed, upon UV irradiation, hydrolytic activity. The change in enzymatic activity induced by UV irradiation is ascribed to a conformational change in the mutant proteins. Shimoboji et al. [55] have successfully shown that the photoinduced changes in the size and hydration of a smart polymer chain coil can be used to regulate substrate access and enzyme activity when conjugated to the enzyme at a specific point just outside the active site (Fig. 6.14). In order to enable photocontrol of enzyme activity, two different copolymers that exhibit combined temperature sensitivity and photosensitivity were prepared by copolymerizing *N,N*-dimethyl acrylamide (DMA) with two different light-sensitive comonomers, 4-phenylazophenyl acrylate (AZAA) and *N*-4-phenylazophenyl acrylamide (AZAAm). Under the isothermal conditions at their photoresponsive temperatures, the AZAAm copolymer precipitated under UV light irradiation (350 nm), whereas the AZAA copolymer dissolved under the same UV light irradiation. The copolymers were conjugated to the E116C SA mutant via thiol coupling. One of these

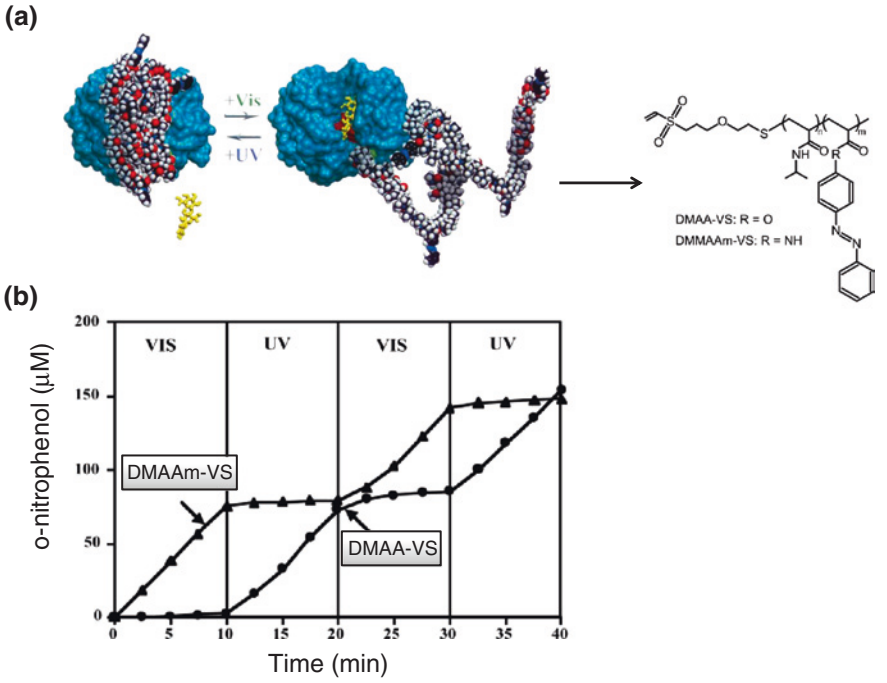


**Fig. 6.14** **a** Schematic model of the photoresponsive enzyme switch. **b** Sequential photoswitching of the activity of the DMAA-VS and DMAAm-VS conjugates [55]

copolymer-E116C SA conjugates exhibited blocking of free biotin and triggered the release of bound biotin under VIS irradiation; the other demonstrated the same phenomena under UV irradiation [19]. These opposite photoresponsive biotin-blocking or biotin-releasing responses corresponded to the original photoinduced phase transition properties of the copolymers. The photoresponsive switch was not observed when a 4-phenylazoaleinanil monomer was conjugated directly to the protein.

Smart polymer conjugation techniques have also been utilized for the control of gene expression. Murata et al. [119] have prepared a smart antisense reagent comprised of phosphodiester-linked oligodeoxynucleotides (ODNs) and PNIPAAm, and evaluated the antisense activity and nuclease stability of the conjugate. The antisense ODN-PNIPAAm conjugate demonstrated a thermoresponsive regulation of the hybridization between the conjugate and the target RNAs [36]. In this strategy, antisense ODN can be used without chemical modification at the phosphodiester linkage of the ODN, which means that the conjugate may retain its binding affinity for the target RNA. These characteristics of the conjugate are promising for its use as an antisense ODN carrier in gene therapy. Pennadam et al. [29] have successfully designed protein-polymer nanomachines to control the EcoR124I motor function (Fig. 6.15). PNIPAAm with reactive end-groups was attached

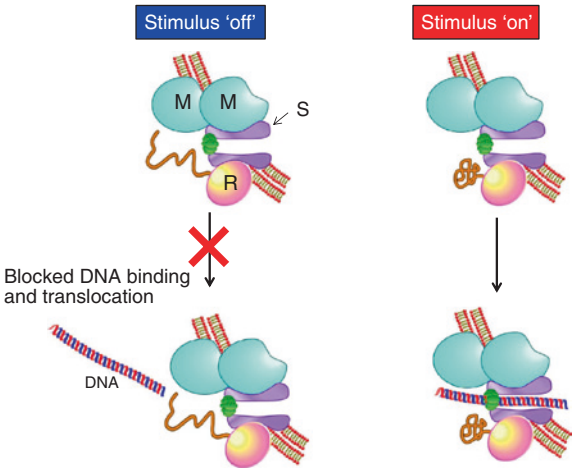


**Fig. 6.15** Schematic illustration of the switchable control of molecular motor function by a temperature-responsive polymer switch. M, R, and S denote the specific motor subunit. Chain extension of the polymer below LCST provides a steric shield blocking the active site. Chain collapse (above LCST) enables access to the active site and restoration of enzyme function [29]

to the motor subunit of EcoR124I via coupling of a maleimide-tipped linker. The protein-polymer conjugates were stable to extensive purification and, when combined with the M2S complex, the activity of this conjugate motor system was similar to that of its native counterpart, but can be switched on or off as a result of thermally induced polymer phase transitions [30]. Thus, the conjugation of the responsive polymer to the molecular motor generates a nanoscale switchable device, which can translocate DNA under one set of conditions.

### *6.4.3 Drug/Gene Delivery*

There are many peptide-, protein-, antibody-, and DNA-based therapeutics under development in the biotechnology and pharmaceutical industries. Intracellular delivery, for example, represents a promising approach for the treatment of a wide variety of diseases. DNA delivery systems based on attenuated viruses have shown the greatest successes to date, but numerous concerns over the safety of these vectors have led to the development of nonviral vectors for use in gene therapy. The efficacy achieved with these nonviral vectors, however, is significantly lower than that achieved with viral vectors. The low transfection efficiencies are due to the multiple biological barriers encountered during delivery from extracellular locations into the cell nucleus. A number of biological organisms have evolved surface proteins to solve similar trafficking problems, and a variety of viral-based, fusogenic peptides have been studied as pH-dependent membrane-disruptive components in gene delivery systems to enhance transport from the endosome to the cytoplasm. Lackey et al. [120] have investigated whether synthetic polymers could provide an alternative approach to pH-dependent membrane destabilization in drug delivery systems. They focused on pH-responsive polymers containing

hydrophobic moieties inspired by the amino acid side chains of leucine and isoleucine, for example, and demonstrated that poly(propyl acrylic acid) (PPAAc) displays interesting improvements in the pH dependence of red blood cell hemolysis. PPAAc is not hemolytic at pH 7.4 and reaches maximum hemolysis at approximately pH 6.0 and below. This pH-sensitive, membrane-disruptive PPAAc can be used to enhance the release of drugs from the acidic endosomal compartment to the cytoplasm. Jones et al. [121] compared the hemolytic ability of three poly(2-alkylacrylic acid)s, PPAAc, poly(2-ethylacrylic acid) (PEAAc), and poly(2-methylacrylic acid) (PMAAc). PMAAc showed little hemolytic activity at all pHs tested, reaching a maximum of about 2 % at pH 5.0. By contrast, both PEAAc and PPAAc showed significant levels of haemolysis. As the pH decreased, the hemolytic activity of PEAAc increased, reaching a peak at pH 5.4. In contrast, the haemolytic activity of PPAAc increased with pH to a maximum at pH 5.8–6.2. Kyriakides et al. [122] have found that one PPAAc significantly enhances in vitro transfections of lipoplex formulations in cell culture, and does so in the presence of as much as 50 % serum. They have also extended the cell culture studies to an in vivo murine excisional wound healing model. A pilot study with a green fluorescent protein (GFP)-encoding plasmid indicated that injection of formulations containing PPAAc into healing wounds resulted in increased GFP expression. Subsequently, by administering sense and antisense DNA for the angiogenesis inhibitor thrombospondin-2 (TSP2), they were able to alter the wound healing response in TSP2-null and wild-type mice, respectively. These results suggest that PPAAc can provide significant improvements in the in vivo efficacy of drugs such as DNA-controlled medications.

Cell membrane ligands may also be conjugated to the polymer molecule when it has two reactive end groups or multiple reactive pendant groups, for targeting a conjugated protein drug to a specific cell. Antibody-targeting ligands have been linked to a pH-sensitive smart polymer by biotinylating both the antibody and the smart polymer and using SA to link the two together [22]. A biotinylated monoclonal antibody to a CD-3 lymphoma cell receptor and a biotinylated pH-sensitive, lipid-membrane-disruptive smart polymer, PPAAc, were linked together by SA. The PPAAc phase separates sharply as the pH in the endosome drops, and in so doing, PPAAc disrupts the endosomal vesicle membrane. Thus, when the antibody-SA-PPAA conjugate was endocytosed after binding to the CD-3 receptor in Jurkat lymphoma cells, the conjugate was observed to escape from the endosome to the cytosol. This is a desirable event for a protein drug since, otherwise, it would be trafficked to the lysosome where lysosomal enzymes would degrade it. Berguig et al. [123] used the antibody-SA-polymer conjugate to study the intracellular trafficking dynamics of an anti-CD22-internalizing HD39 monoclonal antibody (mAb) with PPAAc (Fig. 6.16). The PPAAc conjugate was shown to alter the intracellular trafficking kinetics strongly relative to HD39/SA alone or HD39/SA conjugates with a control polymer, PMAAc. Subcellular trafficking studies revealed that after 6 h, only 11 % of the HD39/SA–PPAAc conjugates had been trafficked to acidic lysosomal compartments with values at or below pH 5.6. In contrast, the average intracellular pH of HD39/SA alone dropped from

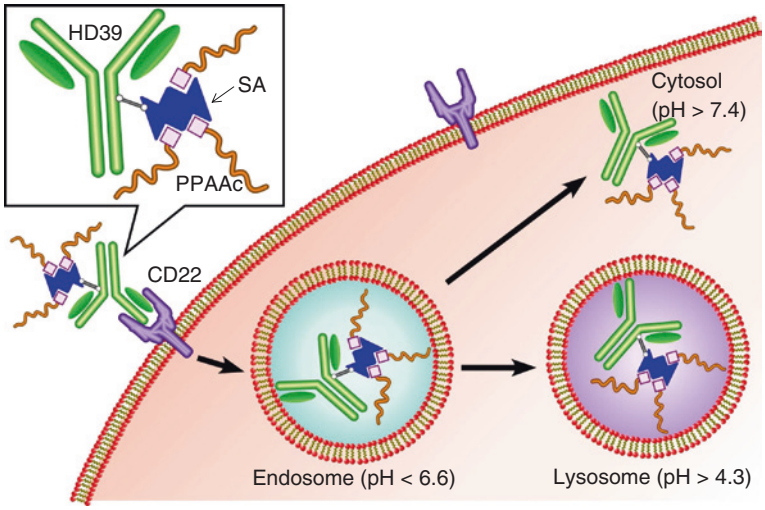


**Fig. 6.16** Intracellular trafficking of the HD39/SA-PPAAc conjugate. Ligation of the anti-CD22 monoclonal antibody (HD39) to CD22 leads to receptor-mediated endocytosis. A portion of the conjugate is trafficked from endosomes to lysosomes while a second fraction is released into the cytosol via endosomal escape mediated by PPAAc [123]

6.7 ± 0.2 at 1 h to 5.6 ± 0.5 after 3 h and 4.7 ± 0.6 after 6 h. Conjugation of the control polymer PMAA to HD39/SA showed an average pH drop similar to that of HD39/SA. Subcellular fractionation studies with tritium-labeled HD39/SA demonstrated that after 6 h, 89 % of HD39/SA was associated with endosomes and lysosomes, while 45 % of HD39/SA–PPAAc was translocated to the cytosol. These results demonstrate the endosomal-releasing properties of PPAAc with antibody-polymer conjugates and detail their intracellular trafficking dynamics and subcellular compartmental distributions over time. Dubé et al. [124] have demonstrated that folate-targeting conjugates can facilitate tumor cell uptake of the conjugates. They designed a family of NIPAAm copolymers carrying a small number of octadecyl groups and folic acid residues grafted along the chain via a short ethylenedioxy chain. The folate conjugates were obtained by amidation of an aminated precursor copolymer. Cytotoxicity assays confirmed that the folate-NIPAAm conjugates bind specifically to KB cells overexpressing the folate receptor. The cellular uptake of the copolymer was found to be temperature dependent. Benoit et al. [125] also reported a facile approach to provide folate-receptor-specific delivery of polymer therapeutics by employing a de novo synthesized folate-functionalized CTA. Folate functionalization provided specific polymer therapeutic-folate receptor interactions and elicited gene knockdown through the delivery of siRNA. Many polymer therapeutics can be functionalized by this strategy, and this approach is highly versatile for functionalizing RAFT polymers.

The PPAAc-based membrane-disruptive system has also been used for antigen delivery systems. While many infectious diseases are controlled by vaccine

strategies, important limitations continue to motivate the development of better antigen delivery systems. Flanary et al. [126] developed a pH-sensitive polymeric carrier based on PPAAc to address the need for more potent CD8 cytotoxic T-cell (CTL) responses. Ovalbumin, as the protein antigen, was conjugated to poly(propylacrylic acid-*co*-pyridyldisulfide acrylate) (PPAA-PDSA) by disulfide exchange to form reversible conjugates that could be reduced by the glutathione redox system in the cytosol of antigen-presenting cells. The PPAA-PDSA ovalbumin conjugates displayed the pH-sensitive membrane disruptive properties of the parent polymer as determined by their hemolysis activities. The polymer-ovalbumin conjugates exhibited strong 22-fold increases in the MHC-1 presentation and ovalbumin-specific CTL activation compared with free ovalbumin. No CTL activation was observed with control conjugates of ovalbumin and PMAAc. This system was further evaluated to test whether improved cytosolic delivery of a protein antigen could enhance CD8+ cytotoxic lymphocyte generation and prophylactic tumor vaccine responses. PPAA was directly conjugated to the ovalbumin antigen via reducible disulfide linkages and was also tested in a particulate formulation after condensation with cationic poly(dimethylaminoethyl methacrylate) (PDMAEMA) [127]. In an EG.7-OVA mouse tumor protection model, PPAA-containing carriers robustly inhibited tumor growth and led to an approximately 3.5-fold increase in the longevity of tumor-free survival relative to controls. Mechanistically, this response was attributed to the 8-fold increase in the production of ovalbumin-specific CD8+ T-lymphocytes and an 11-fold increase in the production of anti-ovalbumin IgG. This is one of the first demonstrated examples of in vivo immunotherapeutic efficacy using soluble protein-polymer conjugates. This system shows promise for protein vaccine strategies against cancer and viruses and is also applicable to any technique requiring improved delivery of a protein cargo to the cytoplasm of a cell. Albarran et al. [128] showed that PPAAc can strongly enhance target cell killing through the intracellular delivery of a functional proapoptotic peptide. The Bak BH3 peptide induces apoptosis via antagonization of suppressor targets such as Bcl-2 and Bcl-xL. A genetically engineered streptavidin that contains an N-terminal TAT peptide sequence was used to optimize the pinocytotic cell uptake of biotinylated BH3 peptide and end-biotinylated PPAAc. Approximately 30 % of cells treated with TAT-SA:BH3 complexes revealed morphologically distinct nuclear condensation, a hallmark of apoptosis. Together with the PPAA, the TAT-SA adaptor complex could prove useful as a carrier of peptide/protein cargo to cultured cells. Fujimoto et al. [32] reported a novel drug delivery system for apoptosis induction by a smart polymer vehicle possessing temperature responsivity and bioaffinity. The cell-adhesive RGDS peptide was conjugated with the NIPAAm copolymer as a ligand model for bioaffinity. Dolichyl phosphate (dol-p), which is an apoptotic inducer, was added to the copolymer at around the precipitation temperature for incorporation. Aggregates incorporating dol-p were added to a human promonocytic leukemia U937 cell suspension at 37 °C. When the temperature was lowered to 25 °C, cells underwent apoptosis in the presence of $Ca^{2+}$ because copolymer vehicles were concentrated on the cell surface through the binding of RGDS and integrin, and lipid inducers were released by the disruption of

vehicles in response to temperature. This system would also be expected to provide a therapeutic application for targeting a drug to the cell and triggering its release in the body by cooling.

In addition to the pH-responsive system, reduction-oxidation-sensitive polymers have also been utilized for intracellular delivery, because the reduction-oxidation state of intracellular compartments changes: the endosome is rendered reductive, whereas the lysosomal compartment is substantially oxidative, compared with the mildly oxidative extracellular environment. Oxidation-sensitive smart polymers can be engineered by designing block copolymers containing a hydrophobic polypropylene sulphide (PPS). On exposure to oxidative conditions, the block is converted to hydrophilic polypropylene sulphoxide and, ultimately, to the more hydrophilic polypropylene sulphone [129]. On the other hand, earlier in the processes of endolysosomal processing, endocytosed compounds encounter a reductive environment. Smart bioconjugates with a reducible disulphide connection have been shown to destabilize, releasing the pendant drugs or DNA. El-Sayed et al. [130] reported membrane-destabilizing and glutathione-reactive polymers. ODN was ionically complexed to cationic peptides grafted onto the polymer backbone via disulfide linkages to the pyridyl disulfide acrylate (PDSA) units. This unique design allowed for the release of the disulfide-conjugated cationic peptides with the complexed ODN into the cytoplasm by the reducing action of the glutathione enzyme, which is commonly present in the cytoplasm. Manickam and Oupicky [131] synthesized high-molecular-weight polypeptides containing disulfide bonds in the backbone by oxidative copolymerization of a histidine-rich peptide (HRP) and a nuclear localization sequence (NLS) peptide. Cytotoxicity and transfection activity of DNA polyplexes were evaluated in vitro. In comparison with control polyethylenimine (PEI), only minimum toxic effects were observed on the metabolic activity and membrane integrity of human endothelial cells.

Furgeson et al. [23] have developed a smart doxorubicin-polypeptide conjugate for thermally targeted delivery to solid tumors. A temperature-responsive, genetically engineered ELP was conjugated to doxorubicin (Dox) molecules through pH-sensitive, maleimide-activated, hydrazone linkers. The highest release of the ELP–Dox conjugate by cleavage of the hydrazone bond at pH 4 was nearly 80 % over 72 h and was exhibited by the conjugate with the shortest linker. The endocytotic uptake of a thermally responsive ELP was also observed to be significantly enhanced by the thermally triggered phase transition of the polypeptide in cell culture for three different tumor cell lines [132]. ELPs conjugated to drugs also enable thermally targeted drug delivery to solid tumors if their transition temperatures are between body temperature and the temperature in a locally heated region. In vivo studies of ELP delivery to human tumors (SKOV-3 ovarian carcinoma and D-54MG glioma) implanted in nude mice demonstrated that hyperthermic targeting of the thermally responsive ELP for 1 h provides a twofold increase in tumor localization compared with the same polypeptide without hyperthermia. By exploiting the phase-transition-induced aggregation of these polypeptides, this method provides a new way of thermally targeting polymer-drug conjugates to solid tumors [100].

### 6.4.4 Diagnostic Technologies

The ability to sequentially control biomolecular recognition and activity could open new opportunities or improve existing applications in the diagnostic fields. Since the smart polymers serve as both antennae and actuators, to sense signals and respond to them, leading to the control of biorecognition events, smart conjugates with protein and DNA have also drawn considerable attention in the diagnostic fields. Their characteristic 'on-off' responses to small changes in pH, temperature, and/or UV-visible light permits rapid and precise control of molecular events. Agasti et al. [133] for example, developed a photocleavable DNA barcode-antibody conjugate for rapid, quantitative, and multiplexed detection of protein expression in single live cells (Fig. 6.17). Irradiation of the labeled cells with light (∼365 nm) cleaves the linker between the antibodies and the barcodes, causing the barcodes to be released into the solution for easy isolation. Barcode amplification by polymerase chain reaction (PCR) and subsequent gel electrophoresis analysis of the amplified barcodes allows simultaneous detection and quantification of multiple protein analytes from single cells. Maeda and coworker [25, 134–136] have developed a single-nucleotide polymorphism (SNP)-responsive diagnostic using DNA-PNIPAAm conjugates. The graft copolymer consisting of PNIPAAm and single-stranded DNA (ssDNA) forms nanoparticles above physiological temperature. Non-crosslinking aggregation of the DNA-PNIPAAm nanoparticles is induced by the hybridization of the surface DNA with the full-match complementary DNA (Fig. 6.18). This aggregation mechanism was applicable for the target 24mer DNA corresponding to k-ras (oncogene) codons 10–17, as well as for SNP sites of CYP2C9. Each nanoparticle was aggregated by the hybridization with its full-match complementary DNA fragment, but not with one-base mismatch. These results demonstrated that the non-crosslinking aggregation of DNA-PNIPAAm nanoparticles is useful for analyzing various SNPs.

The switchability of smart polymer conjugates also opens the door to potential uses in microfluidic formats where the differential diffusive and physical properties might be exploited for separation, analyte concentration, and signal generation. Microfluidic platforms have shown promise for conducting diagnostic measurements in both clinical and point-of-care settings [137, 138]. While great strides have been made, the potential of this technology has not yet been fully realized and several challenges remain. One important outstanding need is the handling of dilute antigens and biomarkers, particularly their purification and enrichment from complex biological fluids. Several chromatographic strategies have been demonstrated to address analyte purification and enrichment issues in microfluidic systems. Affinity moieties have been conjugated directly to microchannel walls, attached to particles and packed into microchannels and immobilized within porous monolithic slabs. These techniques suffer from several shortcomings, including complex packing and modification steps, high flow resistance and limitations in scaling-up and manufacturability. These strategies also usually allow the separation of only a single analyte and cannot be modified once introduced. Kulkarni et al. [49, 79] have developed a series of PNIPAAm-protein conjugates that separate and enrich analytes

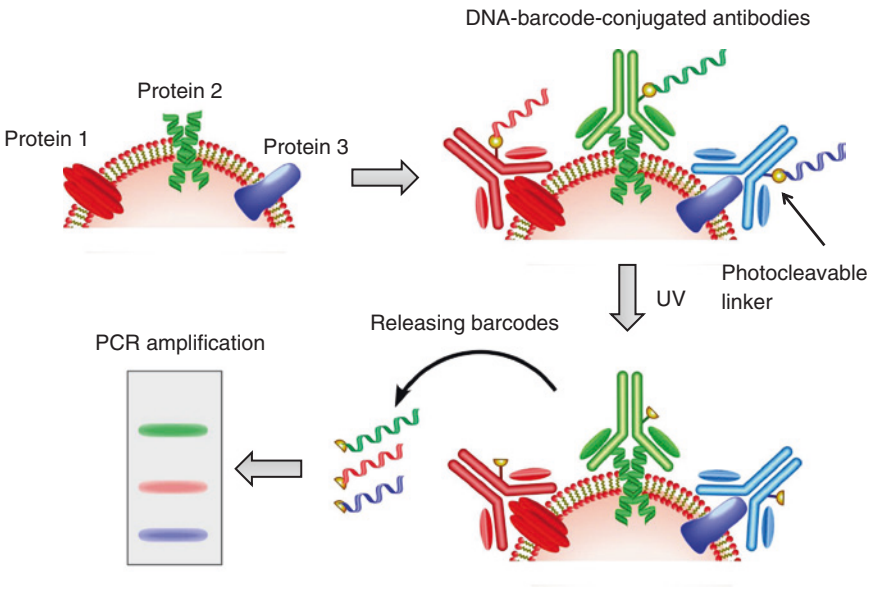


**Fig. 6.17** Schematic illustration of the light-mediated cellular barcoding strategy. Protein targets are labeled with DNA-barcode-conjugated antibodies and then photocleaved to release the DNA barcodes. Amplified barcodes are analyzed using gel electrophoresis for multiplexed detection of protein biomarkers from single cells [133]

from solution and enable detection. Because smart conjugates bind analytes in solution prior to separation, conjugate-analyte binding avoids steric and mass transport limitations associated with surface-based techniques [139, 140]. A reversible microchannel surface capture system has been further developed for bioanalytical samples [141–143]. The capture/release efficiency and enrichment of PNIPAAm-antibody conjugates in PNIPAAm-grafted PDMS microchannels have been investigated using a helical flow, circular microreactor. The conjugate's immobilization and release were limited by mass transport to and from the functionalized PNIPAAm surface. Transport and adsorption efficiencies were dependent on the aggregate size of the PNIPAAm–streptavidin conjugate above the LCST as well as on whether the conjugates were heated in the presence of the stimuli-responsive surface or pre-aggregated and then flowed across the surface. Mixing and recirculation substantially increase the conjugate release rate and sharpness once the temperature has dropped below the phase transition temperature. The concentration of protein-polymer conjugates could be achieved by a continuous conjugate flow into the heated recirculator, allowing nearly linear enrichment of the conjugate reagent from larger volumes. This capability was shown with anti-p24 HIV monoclonal antibody reagents that were enriched over fivefold by using this protocol. pH-responsive surface traps have also been constructed in the channel wall by the same methods. Magnetic nanoparticles have also been developed for diagnostic target isolation because smaller particles display better association and binding

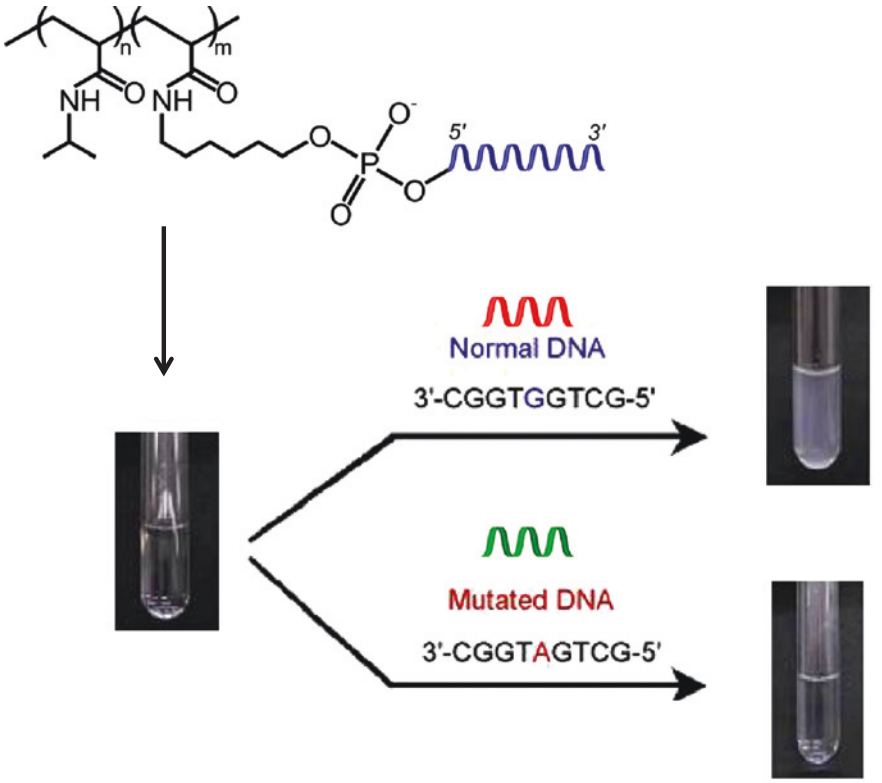


**Fig. 6.18** Sequence-specific affinity precipitation of oligonucleotide using PNIPAAm-oligonucleotide conjugate [25, 134–136]

properties to the target analytes [144, 145]. A reversible surface capture system for smart bioconjugates has also been demonstrated on porous membrane filters for the detection of the malaria antigen *Plasmodium falciparum* histidine-rich protein 2 (PfHRP2) (Fig. 6.19) [24]. The carboxyl end-groups of semi-telechelic PNIPAAm synthesized by RAFT polymerization were modified with tetrafluorophenol to yield amine-reactive ester groups for conjugation to amine groups of anti-streptavidin and anti-PfHRP2 antibodies. Stimuli-responsive membranes were constructed from 1.2-μm-pore-size, hydroxylated, nylon-6,6 filters. The surface hydroxyl groups on the filters were conjugated to a 2-ethylsulfanylthiocarbonylsulfanyl-2-methyl propionic acid (EMP) RAFT chain transfer agent, and the surface-grafted PNIPAAm was obtained by subsequent polymerization. The PNIPAAm grafted membranes showed greater than 80 % anti-streptavidin capture efficiency. The PfHRP2 antigen could be processed and detected at clinically relevant concentrations of this malaria biomarker. These studies provide insight into the mechanism of smart polymer–protein conjugate capture and release in grafted channels and show the potential of this purification and enrichment module for processing diagnostic samples.

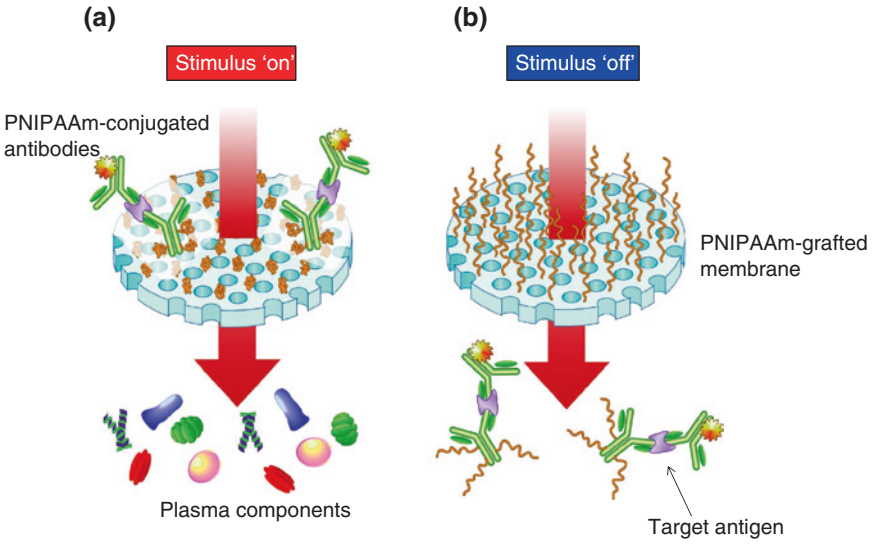


**Fig. 6.19** Smart fluidic system for purifying and concentrating diagnostic biomarkers using temperature-responsive antibody conjugates and membranes. PNIPAAm-conjugated antibodies are captured at the membrane above the LCST, while unconjugated plasma components flow through (**a**). When the membrane region is cooled, the conjugates are released back into the flow stream (**b**) [24]

## 6.5 Conclusions and Future Trends

Smart bioconjugate-based technologies are becoming the premier tool for a wide range of applications in the areas of medicine and biotechnology. Conjugating proteins, peptides, DNA, and cells with smart polymers has been a versatile way to add new value, advanced features and unique properties to inert polymers. For example, creating nanoscale antennae and actuators to sense signals and respond to them significantly improves biological properties as well as introduces new unique properties, leading to the control of biorecognition events. This chapter mainly addresses the developments of smart bioconjugates specifically applied in bioseparation, molecular switching, diagnosis, sensors, and drug/gene delivery. An ongoing challenge is to synthesize well-defined conjugates. Traditionally, the reactive polymers were prepared by the modification of preformed chains. However, with the advent of new controlled/'living' polymerization techniques that are tolerant to a wide range of functional groups, the use of protein-reactive initiators to form well-defined polymers is now possible. This strategy is less time-consuming and results in polymers amenable to coupling to proteins without any further modification. Native chemical ligation, tRNA engineering methods, and other advances in protein engineering also allow for the synthesis of proteins containing non-natural amino acids. So far, the incorporation of functional groups that react

orthogonally to natural amino acids has been underexploited in the preparation of polymer bioconjugates. The combination of controlled radical polymerization with non-natural protein engineering could result in unprecedented control over polymer conjugation, resulting in precise bioconjugates for a variety of applications. Therefore, novel strategies for the design of smart bioconjugates including proteins, DNA, mammalian cells, bacteria, yeast cells, and viruses will facilitate the creation of a new class of biomaterials in the future.

## References


1. Ringsdorf H (1975) Structure and properties of pharmacologically active polymers. J Polym Sci: Polym Symp 51:135–153. doi:10.1002/polc.5070510111
2. Matsumura Y, Maeda H (1986) A new concept for macromolecular therapeutics in cancer chemotherapy: mechanism of tumoritropic accumulation of proteins and the antitumor agent smancs. Cancer Res 46:6387–6392
3. Abuchowski A, McCoy JR, Palczuk NC, van Es T, Davis FF (1977) Effect of covalent attachment of polyethylene glycol on immunogenicity and circulating life of bovine liver catalase. J Biol Chem 252:3582–3586
4. Mok H, Palmer DJ, Ng P, Barry MA (2005) Evaluation of polyethylene glycol modification of first-generation and helper-dependent adenoviral vectors to reduce innate immune responses. Mol Ther 11:66–79
5. O'Riordan CR, Song A (2008) PEGylated adenovirus for targeted gene therapy. In: Doux J (ed) Gene therapy protocols, vol 434. Methods in molecular biology™. Humana Press, pp 133–160. doi:10.1007/978-1-60327-248-3_9
6. Scott MD, Murad KL, Koumpouras F, Talbot M, Eaton JW (1997) Chemical camouflage of antigenic determinants: Stealth erythrocytes. In: Proceedings of the national academy of sciences, vol 94. U.S.A., pp 7566–7571
7. Hashemi-Najafabadi S, Vasheghani-Farahani E, Shojaosadati SA, Rasaee MJ, Armstrong JK, Moin M, Pourpak Z (2006) A method to optimize PEG-coating of red blood cells. Bioconjug Chem 17:1288–1293. doi:10.1021/bc060057w
8. Mansouri S, Merhi Y, Winnik FM, Tabrizian M (2011) Investigation of layer-by-layer assembly of polyelectrolytes on fully functional human red blood cells in suspension for attenuated immune response. Biomacromolecules 12:585–592. doi:10.1021/bm101200c
9. Charles M, Coughlin RW, Hasselberger FX (1974) Soluble–insoluble enzyme catalysts. Biotechnol Bioeng 16:1553–1556. doi:10.1002/bit.260161113
10. Van Leemputten E, Horisberger M (1976) Soluble–insoluble complex of trypsin immobilized on acrolein–acrylic acid copolymer. Biotechnol Bioeng 18:587–590. doi:10.1002/bit.260180410
11. Shoemaker SG, Hoffman AS, Priest JH (1987) Synthesis and properties of vinyl monomer/enzyme conjugates. Appl Biochem Biotechnol 15:11–24. doi:10.1007/bf02798503
12. Auditore-Hargreaves K, Houghton RL, Monji N, Priest JH, Hoffman AS, Nowinski RC (1987) Phase-separation immunoassays. Clin Chem 33:1509–1516
13. Hoffman AS (1987) Applications of thermally reversible polymers and hydrogels in therapeutics and diagnostics. J Controlled Release 6:297–305. http://dx.doi.org/10.1016/0168-3659(87)90083-6
14. Monji N, Hoffman A (1987) A novel immunoassay system and bioseparation process based on thermal phase separating polymers. Appl Biochem Biotechnol 14:107–120. doi:10.1007/bf02798429
15. Luong JHT, Nguyen A-L (1990) Affinity partitioning of bioproducts. Nat Biotech 8:306–307

16. Takei YG, Aoki T, Sanui K, Ogata N, Sakurai Y, Okano T, Matsukata M, Kikuchi A (1994) Temperature-responsive bioconjugates. 3. Antibody-poly(N-isopropylacrylamide) conjugates for temperature-modulated precipitations and affinity bioseparations. Bioconjug Chem 5:577–582. doi:10.1021/bc00030a013
17. Fujimura M, Mori T, Tosa T (1987) Preparation and properties of soluble–insoluble immobilized proteases. Biotechnol Bioeng 29:747–752. doi:10.1002/bit.260290612
18. Ito Y, Kotoura M, Chung DJ, Imanishi Y (1993) Trypsin modification by vinyl polymers with variable solubilities in response to external signals. Bioconjug Chem 4:358–361. doi:10.1021/bc00023a009
19. Shimoboji T, Ding ZL, Stayton PS, Hoffman AS (2002) Photoswitching of ligand association with a photoresponsive polymer-protein conjugate. Bioconjug Chem 13:915–919. doi:10.1021/bc010057q
20. Dainiak MB, Izumrudov VA, Muronetz VI, Galaev IY, Mattiasson B (1998) Conjugates of monoclonal antibodies with polyelectrolyte complexes—an attempt to make an artificial chaperone. Biochim Biophys Acta 1381:279–285. http://dx.doi.org/10.1016/S0304-4165(98)00035-X
21. Muronetz VI, Kazakov SV, Dainiak MB, Izumrudov VA, Galaev IY, Mattiasson B (2000) Interaction of antibodies and antigens conjugated with synthetic polyanions: on the way of creating an artificial chaperone. Biochim Biophys Acta 1475:141–150. http://dx.doi.org/10.1016/S0304-4165(00)00060-X
22. Lackey CA, Press OW, Hoffman AS, Stayton PS (2002) A biomimetic pH-responsive polymer directs endosomal release and intracellular delivery of an endocytosed antibody complex. Bioconjug Chem 13:996–1001. doi:10.1021/bc010053l
23. Furgeson DY, Dreher MR, Chilkoti A (2006) Structural optimization of a "smart" doxorubicin–polypeptide conjugate for thermally targeted delivery to solid tumors. J Controlled Release 110:362–369. http://dx.doi.org/10.1016/j.jconrel.2005.10.006
24. Golden AL, Battrell CF, Pennell S, Hoffman AS, J. Lai J, Stayton PS (2010) Simple fluidic system for purifying and concentrating diagnostic biomarkers using stimuli-responsive antibody conjugates and membranes. Bioconjug Chem 21:1820–1826. doi:10.1021/bc100169y
25. Mori T, Maeda M (2003) Temperature-Responsive formation of colloidal nanoparticles from poly(N-isopropylacrylamide) grafted with single-stranded DNA. Langmuir 20:313–319. doi:10.1021/la0356194
26. Ebara M, Uto K, Idota N, Hoffman JM, Aoyagi T (2012) Shape-memory surface with dynamically tunable nano-geometry activated by body heat. Adv Mater 24:273–278. doi:10.1002/adma.201102181
27. Kim Y-J, Ebara M, Aoyagi T (2012) A smart nanofiber web that captures and releases cells. Angew Chem Int Ed 51:10537–10541. doi:10.1002/anie.201204139
28. Kumar A, Kamihira M, Galaev IY, Mattiasson B, Iijima S (2001) Type-specific separation of animal cells in aqueous two-phase systems using antibody conjugates with temperature-sensitive polymers. Biotechnol Bioeng 75:570–580. doi:10.1002/bit.10080
29. Pennadam S, Firman K, Alexander C, Gorecki D (2004) Protein-polymer nano-machines. Towards synthetic control of biological processes. J Nanobiotechnol 2:8
30. Pennadam SS, Lavigne MD, Dutta CF, Firman K, Mernagh D, Górecki DC, Alexander C (2004) Control of a multisubunit DNA Motor by a thermoresponsive Polymer Switch. J Am Chem Soc 126:13208–13209. doi:10.1021/ja045275j
31. Stoica F, Alexander C, Tirelli N, Miller AF, Saiani A (2008) Selective synthesis of double temperature-sensitive polymer-peptide conjugates. Chem Commun 37:4433–4435
32. Fujimoto K, Iwasaki C, Arai C, Kuwako M, Yasugi E (2000) Control of cell death by the smart polymeric vehicle. Biomacromolecules 1:515–518. doi:10.1021/bm000082j
33. Vázquez-Dorbatt V, Tolstyka ZP, Maynard HD (2009) Synthesis of aminooxy end-functionalized PNIPAAm by RAFT polymerization for protein and polysaccharide conjugation. Macromolecules 42:7650–7656. doi:10.1021/ma9013803
34. Lima A, Song W, Blanco-Fernandez B, Alvarez-Lorenzo C, Mano J (2011) Synthesis of temperature-responsive dextran-MA/PNIPAAm particles for controlled drug delivery using superhydrophobic surfaces. Pharm Res 28:1294–1305. doi:10.1007/s11095-011-0380-2

35. Kotsuchibashi Y, Ebara M, Idota N, Narain R, Aoyagi T (2012) A 'smart' approach towards the formation of multifunctional nano-assemblies by simple mixing of block copolymers having a common temperature sensitive segment. Polym Chem-Uk 3:1150–1157
36. Murata M, Kaku W, Anada T, Sato Y, Kano T, Maeda M, Katayama Y (2003) Novel DNA/polymer conjugate for intelligent antisense reagent with improved nuclease resistance. Bioorg Med Chem Lett 13:3967–3970. http://dx.doi.org/10.1016/j.bmcl.2003.08.062
37. Ta T, Convertine AJ, Reyes CR, Stayton PS, Porter TM (2010) Thermosensitive liposomes modified with poly(N-isopropylacrylamide-co-propylacrylic acid) copolymers for triggered release of doxorubicin. Biomacromolecules 11:1915–1920. doi:10.1021/bm1004993
38. Kono K, Nakai R, Morimoto K, Takagishi T (1999) Thermosensitive polymer-modified liposomes that release contents around physiological temperature. Biochim Biophys Acta 1416:239–250. http://dx.doi.org/10.1016/S0005-2736(98)00226-0
39. Stayton PS, Shimoboji T, Long C, Chilkoti A, Ghen G, Harris JM, Hoffman AS (1995) Control of protein-ligand recognition using a stimuli-responsive polymer. Nature 378:472–474
40. Kiick KL, Tirrell DA (2000) Protein engineering by in vivo incorporation of non-natural amino acids: control of incorporation of methionine analogues by methionyl-trna synthetase. Tetrahedron 56:9487-9493. http://dx.doi.org/10.1016/S0040-4020(00)00833-4
41. Chen J-P, Chu D-H, Sun Y-M (1997) Immobilization of α-amylase to temperature-responsive polymers by single or multiple point attachments. J Chem Technol Biotechnol 69:421–428. doi:10.1002/(sici)1097-4660(199708)69:4<421:aid-jctb730>3.0.co;2-3
42. Matsukata M, Aoki T, Sanui K, Ogata N, Kikuchi A, Sakurai Y, Okano T (1996) Effect of molecular architecture of poly(N-isopropylacrylamide)–trypsin conjugates on their solution and enzymatic properties. Bioconjug Chem 7:96–101. doi:10.1021/bc950082u
43. Chen G, Hoffman AS (1993) Preparation and properties of thermoreversible, phase-separating enzyme-oligo (N-isopropylacrylamide) conjugates. Bioconjug Chem 4:509–514. doi:10.1021/bc00024a013
44. Plourde R, Phillips AT, Wu CH, Hays RM, Chowdhury JR, Chowdhury NR, Wu GY (1996) A hepatocyte-targeted conjugate capable of delivering biologically active colchicine in vitro. Bioconjug Chem 7:131–137. doi:10.1021/bc950083m
45. Chiefari J, Chong YK, Ercole F, Kristina J, Jeffery J, Le TPT, Mayadunne RTA, Meijs GF, Moad CL, Moad G, Rizzardo E, Thang SH (1998) Living free-radical polymerization by reversible addition—fragmentation chain transfer: the RAFT process. Macromolecules 31:5559–5562. doi:10.1021/ma9804951
46. Lele BS, Murata H, Matyjaszewski K, Russell AJ (2005) Synthesis of uniform protein-polymer conjugates. Biomacromolecules 6:3380–3387. doi:10.1021/bm050428w
47. Lecolley F, Tao L, Mantovani G, Durkin I, Lautru S, Haddleton DM (2004) A new approach to bioconjugates for proteins and peptides ("pegylation") utilising living radical polymerisation. Chem Commun 0:2026–2027
48. Tao L, Mantovani G, Lecolley F, Haddleton DM (2004) α-Aldehyde terminally functional methacrylic polymers from living radical polymerization: application in protein conjugation "pegylation". J Am Chem Soc 126:13220–13221. doi:10.1021/ja0456454
49. Kulkarni S, Schilli C, Grin B, Müller AHE, Hoffman AS, Stayton PS (2006) Controlling the aggregation of conjugates of streptavidin with smart block copolymers prepared via the RAFT copolymerization technique. Biomacromolecules 7:2736–2741. doi:10.1021/bm060186f
50. Ding Z, Fong RB, Long CJ, Stayton PS, Hoffman AS (2001) Size-dependent control of the binding of biotinylated proteins to streptavidin using a polymer shield. Nature 411:59–62
51. Bulmus V, Woodward M, Lin L, Murthy N, Stayton P, Hoffman A (2003) A new pH-responsive and glutathione-reactive, endosomal membrane-disruptive polymeric carrier for intracellular delivery of biomolecular drugs. J Controlled Release 93:105–120. http://dx.doi.org/10.1016/j.jconrel.2003.06.001
52. Stayton PS, Hoffman AS, El-Sayed M, Kulkarni S, Shimoboji T, Murthy N, Bulmus V, Lackey C (2005) Intelligent biohybrid materials for therapeutic and imaging agent delivery. Proc IEEE 93:726–736. doi:10.1109/jproc.2005.844619

53. Krishnamurthy VM, Semetey V, Bracher PJ, Shen N, Whitesides GM (2007) Dependence of effective molarity on linker length for an intramolecular protein–ligand system. J Am Chem Soc 129:1312–1320. doi:10.1021/ja066780e
54. Chilkoti A, Chen G, Stayton PS, Hoffman AS (1994) Site-specific conjugation of a temperature-sensitive polymer to a genetically engineered protein. Bioconjug Chem 5:504–507. doi:10.1021/bc00030a004
55. Shimoboji T, Larenas E, Fowler T, Kulkarni S, Hoffman AS, Stayton PS (2002) Photoresponsive polymer–enzyme switches. Proc Natl Acad Sci 99:16592–16596. doi:10.1073/pnas.262427799
56. Bontempo D, Heredia KL, Fish BA, Maynard HD (2004) Cysteine-reactive polymers synthesized by atom transfer radical polymerization for conjugation to proteins. J Am Chem Soc 126:15372–15373. doi:10.1021/ja045063m
57. Mantovani G, Lecolley F, Tao L, Haddleton DM, Clerx J, Cornelissen JJLM, Velonia K (2005) Design and synthesis of N-maleimido-functionalized hydrophilic polymers via copper-mediated living radical polymerization: a suitable alternative to PEGylation chemistry. J Am Chem Soc 127:2966–2973. doi:10.1021/ja0430999
58. Geoghegan KF, Stroh JG (1992) Site-directed conjugation of nonpeptide groups to peptides and proteins via periodate oxidation of a 2-amino alcohol. Application to modification at N-terminal serine. Bioconjug Chem 3:138–146. doi:10.1021/bc00014a008
59. Gaertner HF, Offord RE, Cotton R, Timms D, Camble R, Rose K (1994) Chemo-enzymic backbone engineering of proteins. Site-specific incorporation of synthetic peptides that mimic the 64-74 disulfide loop of granulocyte colony-stimulating factor. J Biol Chem 269:7224–7230
60. Alouani S, Gaertner HF, Mermod J-J, Power CA, Bacon KB, Wells TNC, Proudfoot AEI (1995) A fluorescent interleukin-8 receptor probe produced by targetted labelling at the amino terminus. Eur J Biochem 227:328–334. doi:10.1111/j.1432-1033.1995.tb20393.x
61. Gaertner HF, Offord RE (1996) Site-specific attachment of functionalized poly (ethylene glycol) to the amino terminus of proteins. Bioconjug Chem 7:38–44. doi:10.1021/bc950074d
62. Heredia KL, Bontempo D, Ly T, Byers JT, Halstenberg S, Maynard HD (2005) In situ preparation of protein—"smart" polymer conjugates with retention of bioactivity. J Am Chem Soc 127:16955–16960. doi:10.1021/ja054482w
63. Bontempo D, Maynard HD (2005) Streptavidin as a macroinitiator for polymerization. In Situ protein-polymer conjugate formation. J Am Chem Soc 127:6508–6509. doi:10.1021/ja042230+
64. Le Droumaguet B, Velonia K (2008) In Situ ATRP-mediated hierarchical formation of giant amphiphile bionanoreactors. Angew Chem Int Ed 47:6263–6266. doi:10.1002/anie.200801007
65. Depp V, Alikhani A, Grammer V, Lele BS (2009) Native protein-initiated ATRP: a viable and potentially superior alternative to PEGylation for stabilizing biologics. Acta Biomater 5:560–569. http://dx.doi.org/10.1016/j.actbio.2008.08.010
66. Magnusson JP, Bersani S, Salmaso S, Alexander C, Caliceti P (2010) In situ growth of side-chain PEG polymers from functionalized human growth hormone—a new technique for preparation of enhanced protein-polymer conjugates. Bioconjugate Chem 21:671–678. doi:10.1021/bc900468v
67. Gao W, Liu W, Mackay JA, Zalutsky MR, Toone EJ, Chilkoti A (2009) In situ growth of a stoichiometric PEG-like conjugate at a protein's N-terminus with significantly improved pharmacokinetics. Proc Natl Acad Sci 106:15231–15236. doi:10.1073/pnas.0904378106
68. Gao W, Liu W, Christensen T, Zalutsky MR, Chilkoti A (2010) In situ growth of a PEG-like polymer from the C terminus of an intein fusion protein improves pharmacokinetics and tumor accumulation. Proc Natl Acad Sci. doi:10.1073/pnas.1006044107
69. Li H, Li M, Yu X, Bapat AP, Sumerlin BS (2011) Block copolymer conjugates prepared by sequentially grafting from proteins via RAFT. Polym Chem Uk 2:1531–1535
70. De P, Li M, Gondi SR, Sumerlin BS (2008) Temperature-regulated activity of responsive polymer-protein conjugates prepared by grafting-from via RAFT polymerization. J Am Chem Soc 130:11288–11289. doi:10.1021/ja804495v

71. Hong C-Y, Pan C-Y (2006) Direct synthesis of biotinylated stimuli-responsive polymer and diblock copolymer by RAFT polymerization using biotinylated trithiocarbonate as RAFT agent. Macromolecules 39:3517–3524. doi:10.1021/ma052593+
72. Liu J, Bulmus V, Herlambang DL, Barner-Kowollik C, Stenzel MH, Davis TP (2007) In situ formation of protein-polymer conjugates through reversible addition fragmentation chain transfer polymerization. Angew Chem Int Ed 46:3099–3103. doi:10.1002/anie.200604922
73. Hohsaka T, Sisido M (2002) Incorporation of non-natural amino acids into proteins. Curr Opin Chem Biol 6:809–815. http://dx.doi.org/10.1016/S1367-5931(02)00376-9
74. Katti KS, Ambre AH, Peterka N, Katti DR (2010) Use of unnatural amino acids for design of novel organomodified clays as components of nanocomposite biomaterials. Philoso Trans R Soc A 368:1963–1980. doi:10.1098/rsta.2010.0008
75. Dieterich DC, Link AJ, Graumann J, Tirrell DA, Schuman EM (2006) Selective identification of newly synthesized proteins in mammalian cells using bioorthogonal noncanonical amino acid tagging (BONCAT). Proc Natl Acad Sci 103:9482–9487. doi:10.1073/pnas.0601637103
76. Kolb HC, Finn MG, Sharpless KB (2001) Click chemistry: diverse chemical function from a few good reactions. Angew Chem Int Ed 40:2004–2021. doi:10.1002/1521-3773(20010601)40:11<2004:aid-anie2004>3.0.co;2-5
77. Peeler JC, Woodman BF, Averick S, Miyake-Stoner SJ, Stokes AL, Hess KR, Matyjaszewski K, Mehl RA (2010) Genetically encoded initiator for polymer growth from proteins. J Am Chem Soc 132:13575–13577. doi:10.1021/ja104493d
78. Averick SE, Magenau AJD, Simakova A, Woodman BF, Seong A, Mehl RA, Matyjaszewski K (2011) Covalently incorporated protein-nanogels using AGET ATRP in an inverse miniemulsion. Polym Chem-Uk 2:1476–1478
79. Kulkarni S, Schilli C, Müller AHE, Hoffman AS, Stayton PS (2004) Reversible mesoscale smart polymer-protein particles of controlled sizes. Bioconjugate Chem 15:747–753. doi:10.1021/bc034215k
80. Hoffman JM, Ebara M, Lai JJ, Hoffman AS, Folch A, Stayton PS (2010) A helical flow, circular microreactor for separating and enriching “smart” polymer-antibody capture reagents. Lab Chip 10:3130–3138
81. Hannink JM, Cornelissen JJLM, Farrera JA, Foubert P, De Schryver FC, Sommerdijk NAJM, Nolte RJM (2001) Protein-polymer hybrid amphiphiles. Angew Chem Int Ed 40:4732–4734. doi:10.1002/1521-3773(20011217)40:24<4732:aid-anie4732>3.0.co;2-p
82. Boerakker MJ, Hannink JM, Bomans PHH, Frederik PM, Nolte RJM, Meijer EM, Sommerdijk NAJM (2002) Giant amphiphiles by cofactor reconstitution. Angew Chem Int Ed 41:4239–4241. doi:10.1002/1521-3773(20021115)41:22<4239:aid-anie4239>3.0.co;2-e
83. Sun X-L, Faucher KM, Houston M, Grande D, Chaikof EL (2002) Design and synthesis of biotin chain-terminated glycopolymers for surface glycoengineering. J Am Chem Soc 124:7258–7259. doi:10.1021/ja025788v
84. Hou S, Sun X-L, Dong C-M, Chaikof EL (2004) Facile synthesis of chain-end functionalized glycopolymers for site-specific bioconjugation. Bioconjug Chem 15:954–959. doi:10.1021/bc0499275
85. Bontempo D, Li RC, Ly T, Brubaker CE, Maynard HD (2005) One-step synthesis of low polydispersity, biotinylated poly(N-isopropylacrylamide) by ATRP. Chem Commun 0:4702–4704
86. Kopping JT, Tolstyka ZP, Maynard HD (2007) Telechelic aminooxy polystyrene synthesized by ATRP and ATR coupling. Macromolecules 40:8593–8599. doi:10.1021/ma071606b
87. Tolstyka ZP, Kopping JT, Maynard HD (2007) Straightforward synthesis of cysteine-reactive telechelic polystyrene. Macromolecules 41:599–606. doi:10.1021/ma702161q
88. Tao L, Kaddis CS, Ogorzalek Loo RR, Grover GN, Loo JA, Maynard HD (2009) Synthetic approach to homodimeric protein–polymer conjugates. Chem Commun 0:2148–2150
89. Tao L, Kaddis CS, Loo RRO, Grover GN, Loo JA, Maynard HD (2009) Synthesis of maleimide-end-functionalized star polymers and multimeric protein-polymer conjugates. Macromolecules 42:8028–8033. doi:10.1021/ma901540p

90. Boyer C, Liu J, Bulmus V, Davis TP, Barner-Kowollik C, Stenzel MH (2008) Direct synthesis of well-defined heterotelechelic polymers for bioconjugations. Macromolecules 41:5641–5650. doi:10.1021/ma800289u
91. Heredia KL, Grover GN, Tao L, Maynard HD (2009) Synthesis of heterotelechelic polymers for conjugation of two different proteins. Macromolecules 42:2360–2367. doi:10.1021/ma8022712
92. Heredia KL, Tao L, Grover GN, Maynard HD (2010) Heterotelechelic polymers for capture and release of protein-polymer conjugates. Polym Chem-Uk 1:168–170
93. Yoshimoto T, Takahashi K, Ajima A, Matsushima A, Saito Y, Tamaura Y, Inada Y (1985) Activation and stabilization of asparaginase by anti-asparaginase IgG and its Fab. FEBS Lett 183:170–172. http://dx.doi.org/10.1016/0014-5793(85)80978-9
94. Zhang Y-Q, Tao M-L, Shen W-D, Mao J-P, Chen Y-h (2006) Synthesis of silk sericin peptides–L-asparaginase bioconjugates and their characterization. J Chem Technol Biotechnol 81:136–145. doi:10.1002/jctb.1370
95. Xia F, Zuo X, Yang R, Xiao Y, Kang D, Vallée-Bélisle A, Gong X, Heeger AJ, Plaxco KW (2010) On the binding of cationic, water-soluble conjugated polymers to DNA: electrostatic and hydrophobic interactions. J Am Chem Soc 132:1252–1254. doi:10.1021/ja908890q
96. Decher G (1997) Fuzzy nanoassemblies: toward layered polymeric multicomposites. Science 277:1232–1237. doi:10.1126/science.277.5330.1232
97. Okada T, Uto K, Sasai M, Lee CM, Ebara M, Aoyagi T (2013) Nano-decoration of Hemagglutinating Virus of Japan Envelope (HVJ-E) using Layer-by-Layer Assembly Technique. Langmuir 29:7384–7392. doi:10.1021/la304572s
98. Carlos Rodríguez-Cabello J, Reguera J, Girotti A, Alonso M, Testera AM (2005) Developing functionality in elastin-like polymers by increasing their molecular complexity: the power of the genetic engineering approach. Prog Polym Sci 30:1119–1145. http://dx.doi.org/10.1016/j.progpolymsci.2005.07.004
99. Urry DW (2004) The change in Gibbs free energy for hydrophobic association: derivation and evaluation by means of inverse temperature transitions. Chem Phys Lett 399:177–183. http://dx.doi.org/10.1016/j.cplett.2004.09.137
100. Meyer DE, Kong GA, Dewhirst MW, Zalutsky MR, Chilkoti A (2001) Targeting a genetically engineered elastin-like polypeptide to solid tumors by local hyperthermia. Cancer Res 61:1548–1554
101. Kostal J, Mulchandani A, Chen W (2001) Tunable biopolymers for heavy metal removal. Macromolecules 34:2257–2261. doi:10.1021/ma001973m
102. Wan X, Zhang G, Ge Z, Narain R, Liu S (2011) Construction of polymer-protein bioconjugates with varying chain topologies: polymer molecular weight and steric hindrance effects. Chem Asian J 6:2835-2845. doi:10.1002/asia.201100489
103. Yan M, Ge J, Dong W, Liu Z, Ouyang P (2006) Preparation and characterization of a temperature-sensitive sulfobetaine polymer–trypsin conjugate. Biochem Eng J 30:48–54. http://dx.doi.org/10.1016/j.bej.2006.02.001
104. Sharma S, Kaur P, Jain A, Rajeswari MR, Gupta MN (2003) A smart bioconjugate of chymotrypsin. Biomacromolecules 4:330–336. doi:10.1021/bm0256799
105. Pan LC, Chien CC (2003) A novel application of thermo-responsive polymer to affinity precipitation of polysaccharide. J Biochem Bioph Methods 55:87–94. http://dx.doi.org/10.1016/S0165-022X(02)00180-X
106. Anastase-Ravion S, Ding Z, Pellé A, Hoffman AS, Letourneur D (2001) New antibody purification procedure using a thermally responsive poly(N-isopropylacrylamide)–dextran derivative conjugate. J Chromatogr B: Biomed Sci Appl 761:247–254. http://dx.doi.org/10.1016/S0378-4347(01)00336-X
107. Chang C-W, Nguyen TH, Maynard HD (2010) Thermoprecipitation of glutathione S-transferase by glutathione–poly(N-isopropylacrylamide) Prepared by RAFT Polymerization. Macromol Rapid Commun 31:1691–1695. doi:10.1002/marc.201000333
108. Mattiasson B, Kumar A, Galaev IY (1998) Affinity precipitation of proteins: design criteria for an efficient polymer. J Mol Recognit 11:211–216. doi:10.1002/(sici)1099-1352(199812)11:1/6<211:aid-jmr425>3.0.co;2-y

109. Galaev IY, Mattiasson B (1993) Affinity thermoprecipitation: contribution of the efficiency of ligand–protein interaction and access of the ligand. Biotechnol Bioeng 41:1101–1106. doi:10.1002/bit.260411113
110. Kumar A, Srivastava A, Galaev IY, Mattiasson B (2007) Smart polymers: physical forms and bioengineering applications. Prog Polym Sci 32:1205–1237. http://dx.doi.org/10.1016/j.progpolymsci.2007.05.003
111. Kumar A, Wahlund P-O, Kepka C, Galaev IY, Mattiasson B (2003) Purification of histidine-tagged single-chain Fv-antibody fragments by metal chelate affinity precipitation using thermoresponsive copolymers. Biotechnol Bioeng 84:494–503. doi:10.1002/bit.10810
112. Balan S, Murphy J, Galaev I, Kumar A, Fox G, Mattiasson B, Willson R (2003) Metal chelate affinity precipitation of RNA and purification of plasmid DNA. Biotechnol Lett 25:1111–1116. doi:10.1023/a:1024148316322
113. Murphy JC, Jewell DL, White KI, Fox GE, Willson RC (2003) Nucleic Acid Separations Utilizing Immobilized Metal Affinity Chromatography. Biotechnol Progr 19:982–986. doi:10.1021/bp025563o
114. Ding Z, Long CJ, Hayashi Y, Bulmus EV, Hoffman AS, Stayton PS (1999) Temperature control of biotin binding and release with a streptavidin-poly(N-isopropylacrylamide) site-specific conjugate. Bioconjug Chem 10:395–400. doi:10.1021/bc980108s
115. Bulmus V, Ding Z, Long CJ, Stayton PS, Hoffman AS (1999) Site-specific polymer–streptavidin bioconjugate for ph-controlled binding and triggered release of biotin. Bioconjug Chem 11:78–83. doi:10.1021/bc9901043
116. Shimoboji T, Ding Z, Stayton PS, Hoffman AS (2001) Mechanistic investigation of smart polymer-protein conjugates. Bioconjug Chem 12:314–319. doi:10.1021/bc000107b
117. Shimoboji T, Larenas E, Fowler T, Hoffman AS, Stayton PS (2003) Temperature-induced switching of enzyme activity with smart polymer–enzyme conjugates. Bioconjug Chem 14:517–525. doi:10.1021/bc025615v
118. Hohsaka T, Kawashima K, Sisido M (1994) Photoswitching of NAD+-mediated enzyme reaction through photoreversible antigen-antibody reaction. J Am Chem Soc 116:413–414. doi:10.1021/ja00080a064
119. Murata M, Kaku W, Anada T, Soh N, Katayama Y, Maeda M (2003) Thermoresponsive DNA/polymer conjugate for intelligent antisense strategy. Chem Lett 32:266–267
120. Lackey CA, Murthy N, Press OW, Tirrell DA, Hoffman AS, Stayton PS (1999) Hemolytic activity of pH-responsive polymer-streptavidin bioconjugates. Bioconjugate Chem 10:401–405. doi:10.1021/bc980109k
121. Jones RA, Cheung CY, Black FE, Zia JK, Stayton PS, Hoffman AS, Wilson MR (2003) Poly(2-alkylacrylic acid) polymers deliver molecules to the cytosol by pH-sensitive disruption of endosomal vesicles. Biochem J 372:65–75. doi:10.1042/bj20021945
122. Kyriakides TR, Cheung CY, Murthy N, Bornstein P, Stayton PS, Hoffman AS (2002) pH-Sensitive polymers that enhance intracellular drug delivery in vivo. J Controlled Release 78:295–303. http://dx.doi.org/10.1016/S0168-3659(01)00504-1
123. Berguig GY, Convertine AJ, Shi J, Palanca-Wessels MC, Duvall CL, Pun SH, Press OW, Stayton PS (2012) Intracellular delivery and trafficking dynamics of a lymphoma-targeting antibody-polymer conjugate. Mol Pharm 9:3506–3514. doi:10.1021/mp300338s
124. Dubé D, Francis M, Leroux J-C, Winnik FM (2002) Preparation and Tumor Cell Uptake of Poly(N-isopropylacrylamide) Folate Conjugates. Bioconjugate Chem 13:685–692. doi:10.1021/bc010084g
125. Benoit DSW, Srinivasan S, Shubin AD, Stayton PS (2011) Synthesis of Folate-Functionalized RAFT Polymers for Targeted siRNA Delivery. Biomacromolecules 12:2708–2714. doi:10.1021/bm200485b
126. Flanary S, Hoffman AS, Stayton PS (2009) Antigen delivery with poly(Propylacrylic acid) conjugation enhances MHC-1 presentation and t-cell activation. Bioconjug Chem 20:241–248. doi:10.1021/bc800317a
127. Foster S, Duvall CL, Crownover EF, Hoffman AS, Stayton PS (2010) Intracellular delivery of a protein antigen with an endosomal-releasing polymer enhances cd8 t-cell production and prophylactic vaccine efficacy. Bioconjug Chem 21:2205–2212. doi:10.1021/bc100204m

128. Albarran B, Hoffman AS, Stayton PS (2011) Efficient intracellular delivery of a pro-apoptotic peptide with a pH-responsive carrier. React Funct Polym 71:261–265. http://dx.doi.org/10.1016/j.reactfunctpolym.2010.09.008
129. Napoli A, Valentini M, Tirelli N, Muller M, Hubbell JA (2004) Oxidation-responsive polymeric vesicles. Nat Mater 3:183–189. http://www.nature.com/nmat/journal/v3/n3/suppinfo/nmat1081_S1.html
130. El-Sayed MEH, Hoffman AS, Stayton PS (2005) Rational design of composition and activity correlations for pH-sensitive and glutathione-reactive polymer therapeutics. J Controlled Release 101:47–58. http://dx.doi.org/10.1016/j.jconrel.2004.08.032
131. Manickam DS, Oupický D (2006) Multiblock reducible copolypeptides containing histidine-rich and nuclear localization sequences for gene delivery. Bioconjug Chem 17:1395–1403. doi:10.1021/bc060104k
132. Raucher D, Chilkoti A (2001) Enhanced Uptake of a Thermally Responsive Polypeptide by Tumor Cells in Response to Its Hyperthermia-mediated Phase Transition. Cancer Res 61:7163–7170
133. Agasti SS, Liong M, Peterson VM, Lee H, Weissleder R (2012) Photocleavable DNA barcode-antibody conjugates allow sensitive and multiplexed protein analysis in single cells. J Am Chem Soc 134:18499–18502. doi:10.1021/ja307689w
134. Maeda M (2006) Sequence-specific aggregation behavior of DNA-carrying colloidal nanoparticles prepared from poly(N-isopropylacrylamide)-graft-oligodeoxyribonucleotide. Polym J 38:1099–1104
135. Mori T, Maeda M (2001) Formation of DNA-carrying colloidal particle from poly(*N*-isopropylacrylamide)-*graft*-DNA copolymer and its assembly through hybridization. Polym J 33:830
136. Mori T, Maeda M (2002) Stability change of DNA-carrying colloidal particle induced by hybridization with target DNA. Polym J 34:624
137. Marie Dupuy A, Lehmann S, Paul Cristol J (2005) Protein biochip systems for the clinical laboratory. Clin Chem Lab Med 43:1291–1302. doi:10.1515/cclm.2005.223
138. Toner M, Irimia D (2005) Blood-on-a-Chip. Annu Rev Biomed Eng 7:77–103. doi:10.1146/annurev.bioeng.7.011205.135108
139. Malmstadt N, Hoffman AS, Stayton PS (2004) "Smart" mobile affinity matrix for microfluidic immunoassays. Lab Chip 4:412–415
140. Malmstadt N, Yager P, Hoffman AS, Stayton PS (2003) A smart microfluidic affinity chromatography matrix composed of poly(N-isopropylacrylamide)-coated beads. Anal Chem 75:2943–2949. doi:10.1021/ac034274r
141. Ebara M, Hoffman JM, Hoffman AS, Stayton PS (2006) Switchable surface traps for injectable bead-based chromatography in PDMS microfluidic channels. Lab Chip 6:843–848
142. Ebara M, Hoffman JM, Stayton PS, Hoffman AS (2007) Surface modification of microfluidic channels by UV-mediated graft polymerization of non-fouling and 'smart' polymers. Radiat Phys Chem 76:1409–1413. http://dx.doi.org/10.1016/j.radphyschem.2007.02.072
143. Ebara M, Hoffman AS, Stayton PS, Lai JJ (2013) A photo-induced nanoparticle separation in microchannels via pH-sensitive surface traps. Langmuir 29:5388–5393. doi:10.1021/la400347r
144. Lai JJ, Hoffman JM, Ebara M, Hoffman AS, Estournès C, Wattiaux A, Stayton PS (2007) Dual magnetic-/temperature-responsive nanoparticles for microfluidic separations and assays. Langmuir 23:7385–7391. doi:10.1021/la062527g
145. Lai JJ, Nelson KE, Nash MA, Hoffman AS, Yager P, Stayton PS (2009) Dynamic bioprocessing and microfluidic transport control with smart magnetic nanoparticles in laminar-flow devices. Lab Chip 9:1997–2002

# Chapter 7
# Shape-Memory Materials

## 7.1 Introduction

In this chapter, we focus on the synthesis, characterization, and applications of shape-memory materials, especially in a polymer system (Fig. 7.1). Shape-memory materials are a class of smart and intelligent materials that have the ability to "memorize" a given shape as permanent or temporary, and then "recover" to an original (permanent) shape when triggered by external stimuli. Shape-memory materials have attracted much attention from basic and fundamental (academic) research to industrial and practical applications. Many academic and industrial researchers are interested in shape-memory materials because of their ability to remember two or more shapes under different conditions.

The most noteworthy and extensively researched shape-memory materials are "shape-memory alloys (SMAs)". Ölander first discovered and reported in 1932 a novel metallic transformation of gold-cadmium (AuCd) alloys, which was considered as pseudoelasticity and triggered unusual macroscopic deformation [1]. Greninger and Mooradian also discovered in 1938 a similar transformation of copper-zinc (CuZn) alloys, which was the formation and disappearance of a martensite phase by changing the temperature [2]. Although both findings were directly connected with the macroscopic deformation of metallic alloys triggered by temperature, which is the shape-memory effect, it is well accepted that Chang and Read were the first to observe the shape-memory transformation of AuCd alloys in 1951 [3]. The shape-memory effect seems like an innovative finding; however, it was only a subject in the field of academic research because it was believed that this effect was not a general phenomenon and likely expressed in a limited number of materials at that time. In 1963, Buehler et al. described the shape-memory effect in equiatomic nickel-titanium (NiTi) alloy, which is well known as nitinol [4]. Since then, the shape-memory alloy has grown into a major field of research in both academia and industry, and significant research efforts started in the early 1970s. On the other hand, the history of "shape-memory polymers" (SMPs) is also old and goes back to the 1940s.

M. Ebara et al., *Smart Biomaterials*, NIMS Monographs,
DOI: 10.1007/978-4-431-54400-5_7,

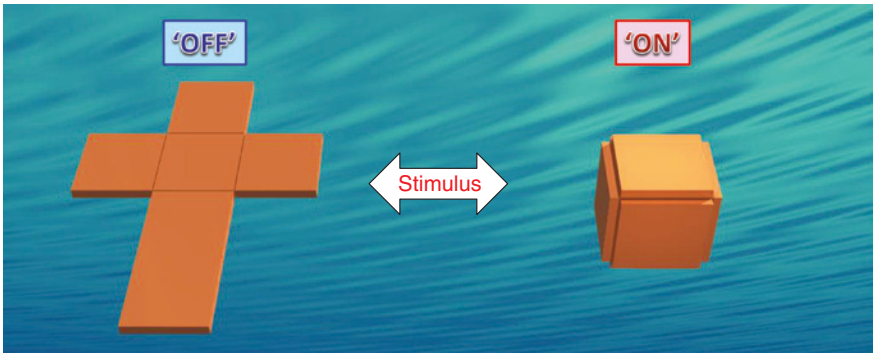


**Fig. 7.1** Schematic illustrations of thermally induced shape-memory effect in SMPs

The first mention of SMPs is in a United States patent applied by Vernon and Vernon in 1941 [5, 6]. They demonstrated that their developed dental restoration materials, which are thermoplastic synthetic resins made of methacrylic acid ester, have an "elastic memory" property, that is, the materials could change shape upon pressure application and then reassume their original shape upon heating. Despite this early discovery, interest in and the importance of SMPs did not permeate until the 1960s, when covalently cross-linked polyethylene found its way into heat-shrinkable tubing and films [7–10]. Here, the permanent shape is also fixed by covalent cross-links, and the switching process is controlled by adjusting the melting temperature of the polyethylene crystallites. Many efforts to design and develop SMPs started in the late 1980s. The term SMPs became well known with the discovery of poly(norbornene), which was developed by CDF-Chimie (a French company) and commercialized by Nippon Zeon (a Japanese company) using the brand name Norsorex in the 1980s. Other types of SMPs, such as TP-301 based on poly(trans-isoprene) and Asmer based on poly(styrene-butadiene), were subsequently developed by two other Japanese companies (Kurare Corporation and Asahi Kasei Corporation, respectively.) [11, 12]. This age was considered as the first golden age of SMP research, and Japan was the leader in shape-memory materials research as shown by the fact that most of the publications were by Japanese researchers and companies until the early 1990s. In particular, the segmental polyurethane-based SMPs were developed by Mitsubishi Heavy Industries (a Japanese company) in the early 1990s, which further accelerated the development of SMPs because of the flexibility of urethane-based chemistry, which narrowed the limitations such as the thermal and mechanical properties for individual applications [13–18]. The earlier works on shape-memory polymers were mainly in industrial fields and the main focus was designing and searching for these new materials for various industrial applications. In addition, the discovery of the "shape memory" of gels and biodegradable polymers from the 1990s to the early 2000s [19–25] has been in progress since then.

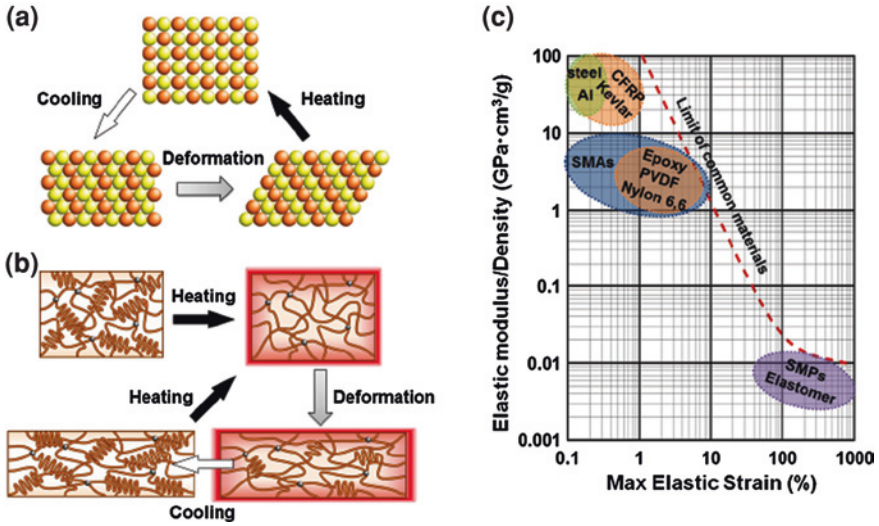


**Fig. 7.2** Schematic representation of the mechanism of shape-memory effects for **a** shape-memory alloys (SMAs) based on a martensitic transformation and **b** shape-memory polymers (SMPs) based on a crystal-amorphous transition in a semicrystalline-based polymer network. **c** Comparison of mechanical properties among SMAs, SMPs and other conventional materials [27]

As shown in Fig. 7.2, the mechanisms of the shape-memory effect in SMAs and SMPs are intrinsically different. Metallic materials are generally deformed when external force is applied. Although these materials generate a plastic deformation that is maintained in a normal metallic system, SMAs can return to their original (memorized) shape when they are heated. The origin of the shape-memory effect of SMAs is the solid-phase transition without the diffusion of molecules between the austenite phase at higher temperature and the martensite phase at lower temperature. Because the temperature of the martensite transformation in SMAs is lower than those of conventional metallic materials and within room temperature, SMAs can be easily deformed into a desired shape. In addition, this phase transformation from austenite to martensite is fully reversible, as shown in Fig. 7.2a. Therefore, SMAs can exhibit the two-way-type shape-memory effect after a proper thermal process. The SMAs do remember both the external shape in the parent phase and that in the martensite phase. On the other hand, the shape-memory effect in SMPs relies on the phase transformation of switching domains or segments such as glass-rubber and crystal-amorphous transitions. SMPs can remember only the original (permanent) shape, although the temporary (deformed) shape can be memorized by applying external force and the proper thermal process, as shown in Fig. 7.2b. Details of the mechanism of the shape-memory effect in SMPs will be discussed in "Sect. 7.4.1".

With extensive investigation and rapid development in this field, the polymeric shape-memory materials become more valuable and prominent for broad applications. As found in Fig. 7.2c, SMPs possess several advantages compared

with the SMA system [26, 27]: (1) large deformation ability: they can deform under strain up to more than a few hundred percent for most materials, but those of SMAs are less than 10 %; (2) low cost: although this strongly depends on the components of materials, the cost of SMPs is approximately twenty times lower than that of SMAs; (3) low density: whereas the density of SMAs is 6–8 g $cm^{-3}$, most polymers have a density of approximately 1 g $cm^{-3}$, which is light weight; (4) environmentally friendly processing: the processing conditions of SMAs generally require both high temperature and high pressure; (5) potential biocompatibility and biodegradability: some of the SMAs are biocompatible but not biodegradable, although SMPs can program these properties into the materials. These advantages are especially significant for biomedical applications. More importantly, compared with SMAs, the thermal and mechanical properties of SMPs can be easily manipulated by designing and processing the materials, and this will open the way for broader applications of SMPs because their ranges of properties are apparently wider than those of SMAs. However, SMPs and SMAs basically have distinct applications because of their intrinsic differences in mechanical, viscoelastic, thermal, optical, and conductive properties. Therefore, combining SMPs and SMAs is also an important way to cooperatively and/or synergistically enhance their properties.

Since there are many types of smart material, which have the ability to change their shape when triggered by external stimuli, how to choose and use the word "shape memory" is often confusing and requires a clear definition of what "shape-memory" ability is, especially in polymer-based materials (SMPs). Behl and Lendlein, who are authorities in the field of shape memory of polymer systems, have propounded two general categories of such smart materials, namely, "shape-memory materials" and "shape-changing materials" [28, 29]. In brief, shape-memory materials are based on two important processes: the "programming or fixing" process to memorize the designed shapes by deformation, and the "recovery" process to remember and return to the original shape. More importantly, the materials once recovered to their original shape can be programmed again to the same or other shapes. On the other hand, the change in shape is reversible, and the material can remain in a certain temporary shape only when the sample is exposed to a stimulus. The sample can return to its original shape after removing the stimulus. These processes of deformation and recovery by switching "on" and "off" of the stimulus in shape-changing materials are always the same even in subsequent cycles. Although these two types of material are basically realized by different mechanisms and should be distinguished clearly, they offer macroscopic mechanical action by applying external stimulus, and so are also broadly called actively moving materials. In this review, we focused on "shape-memory" materials in a polymer system, although composites with other types of material, according to the definition by Behl and Lendlein, are also discussed. Some shape-memory effects different from those of conventional SMPs are also discussed later. In this review, we also adopt a somewhat distinct perspective, including a classification based on network architectures. We also discuss the synthesis and characterization of SMPs, and finally,

we provide an overview of recent applications. Although many multifunctional SMPs driven by various external stimuli have been reported (discussed in Sect. 7.2.5), the main focus in this review is thermoresponsive SMPs because other stimuli except heat are also consequently converted into heat energy in these systems.

## 7.2 Classification on the Basis of Polymer Network Architecture

Often complex requirements for properties, such as mechanical and thermal properties, and functions, in addition to shape-memory materials, need to be fulfilled to meet the application-derived specific demand. The shape-memory effect is not related to a specific material property of single polymers; it rather results from a combination of the polymer structure and the polymer morphology together with the applied processing and programming technology. Therefore, the control of molecular structure and architecture is particularly important for the functions of shape-memory materials. The mechanism of the thermally driven shape-memory effect in SMPs is based on the formation of a molecular switching domain, which changes the structural properties in response to a temperature change. In addition, the shape-memory effect of SMPs will be expressed if the structure of SMPs can be stabilized and maintained against the temperature change or deformation. These can be achieved by introducing cross-linking into the materials to enhance the structural integrity, and selecting the polymer chains that act as a molecular switch in a network for particular applications. From these perspectives, the shape-memory material in a polymer system can be broadly classified into two types of network architecture: (1) a physically cross-linked network (type I) and (2) a covalently cross-linked network (type II). In addition, these can also be specifically separated by type of switching temperature ($T_{switch}$), that is, glass transition temperature ($T_g$) (types I and II with $T_g$) and melting temperature ($T_m$) (types I and II with $T_m$). On the other hand, multiple-network systems (type III) including their blends, interpenetrating network (IPN) structures and the hybridization with SMPs and other materials such as nanoparticles, fluorescent dyes and conductive materials are called shape-memory composites (SMCs) and often used to endow multifunctionality to SMPs, although these can be classified on the basis of cross-linking methods and types of $T_{switch}$. We basically divided the SMPs into these three types (types I–III) on the basis of their molecular structures. This classification, in other words, categorized their differences in fixing mechanism and origin of permanent shapes, which is also the "states" of their architectures. In this review, we outlined the development in the fields of SMPs, and especially focused on the recent progress of SMP systems with discussion based on the above three categories as shown in Fig. 7.3.

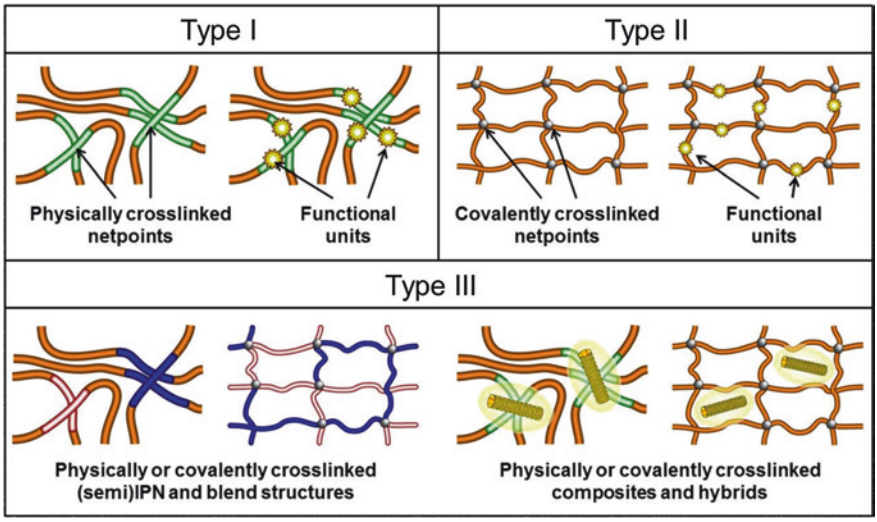


**Fig. 7.3** Classification on the basis of types of polymer network architecture: physically cross-linked (*Type I*) and covalently cross-linked SMPs (*Type II*) with single or multipolymer component, and physically or chemically cross-linked shape-memory multinetwork and composites as multifunctional materials (*Type III*) [89]

### 7.2.1 *Physically Cross-Linked Glassy Networks (Type I $T_{switch} = T_g$)*

One of the major types of SMPs is a physically cross-linked glassy polymer (type I) with glass transition temperature ($T_g$), which is the temperature of reversible transition in amorphous materials or in amorphous regions within semicrystalline materials from a hard glassy state to a rubbery molten state. Although the physical cross-linking generally results in less structurally stable networks than the chemical cross-linking, this type of network can be designed by introducing another phase as physical network points separated from the switching phase that determines the $T_{switch}$ in a system. The phase provides the mechanical strength of the network structure in shape-memory materials at $T < T_{switch}$ as well as acts as the fixation domain that determines the permanent (original) shape of materials. We can easily design this class of SMPs by simultaneously introducing both the hard segments, which determine the highest thermal transition ($T_{high}$ or $T_{perm}$ that is the temperature stabilizing the permanent shape by acting as physical netpoints), and the soft segments, which determine the switching temperature ($T_{switch}$) in materials. In type I SMP networks, the shape of materials is maintained at $T < T_{perm}$; however, it is more viscous and fluid at $T > T_{perm}$. Therefore, $T_{high}$ and $T_{perm}$ dictate the stable temperature range of SMPs designed by physical cross-linking. From this consideration of molecular properties, a block copolymer system is the most prominent building block of type I SMPs, and this class of SMPs (type I)

is constructed using conventional thermoplastics technology. The materials are also divided into two categories according to the type of the hard segment, that is, either the $T_{perm}$ is a $T_g$ or a $T_m$ in a two-way shape-memory system. This type of SMP that has a glassy amorphous domain or a highly crystalline domain in materials may serve as physical cross-linking points affording the mechanical strength above $T_g$ of switching domains required for the shape memory to be developed, basically in the form of phase-segregated block copolymers. In the case of SMPs driven by $T_g$, one observes a relatively broad transition in most cases over a broad temperature range, and it is important for this type of SMP that the $T_g$ is within a narrow temperature range, and a prerequisite is $T_g$ that is set above the usual operating temperature of this material. When the temperature surpasses $T_{perm}$ ($T_g$ or $T_m$ derived from the component of hard segments) of these physically cross-linked domains, materials will flow and become molten, but can still be processed and transformed into other shapes as described above. Another continuous domain with a lower $T_g$ ($T_{switch}$) behaves as a softened rubbery state at $T_{switch} < T < T_{perm}$ and can be fixed as a secondary shape by cooling to $T < T_{switch}$. Therefore, $T_g$ in phase-separated block copolymers can be used as a switching temperature to drive the shape-memory effect. In this paragraph, we mentioned that the shape-memory effect in polymer systems can be triggered using glass transition phenomena.

Thermoplastic polyurethane (PU) elastomers are typical SMPs that can now be produced on an industrial scale by prepolymer methods (discussed in detail in "Sect. 7.3.2"). In the 1980s, a Japanese company (Mitsubishi Heavy Industries, MHI) marketed a shape-memory polymer driven by $T_g$. Hayashi and co-workers fabricated shape-memory linear PU that exhibits a $T_g$ in the range between −30 and 30 °C [30, 31], and these PU systems were described in a patent in 1992 [32]. Currently, $T_g$ of MHI's PUs is freely adjustable in the range between −40 and 120 °C by controlling the type of material component, molecular weight and composition [33]. This on-demand regulation of $T_g$ in a broad range is one of the most prominent features of SMP systems. These PU elastomers were basically composed of hard-segment phases, which are synthesized using isocyanate/alcohol compounds, and the switching-segment phases are polymer blocks such as polyesters and polyethers. Generally, PU systems are multiblock copolymers consisting of alternating oligomeric sequences of hard and switching (soft) segments. Hard segments form physical cross-linking points by means of van der Waals, dipole-dipole interaction, hydrogen bonding, or crystallization, with such cross-linking being capable of withstanding moderately high temperatures without being destroyed, especially at $T < T_{perm}$. In the case of the material system with perfect phase separation, the $T_g$ can be used as the $T_{switch}$ that originated from the switching-segment block. However, materials show mixed $T_g$ values compared with those of hard and switching segments in a system with less phase separation, that is, the solubility is different between the components. In this case, $T_{switch}$ can typically be found for short switching-segment blocks because the increase in length of the switching segment generally results in the increase in $T_g$. This mixed $T_g$ would clearly be observed between the $T_g$ values of the hard and switching segments in a pure system [34, 35]. Lin and Chen reported

on the PU systems with hard segments composed of methylene diphenyl diisocyanate (MDI) and 1,4-butanediol and a polyether switching segment composed of poly(tetramethylene oxide) (PTMO), also called poly(tetrahydrofuran) (PTHF) with low molecular weights. By changing the contents of the hard and switching (soft) segments of PUs, the morphology of the phase-separated structure, which depends on the content of the hard segment, also changed [34]. In fact, the PUs with a greater amount of MDI and 1,4-butanediol, that is, in the case of large hard-segment contents, showed higher $T_g$, and a lower modulus ratio of the PUs was obtained. In addition, they also reported that the $T_g$ of the switching-segment phase was affected by the molecular weight of PTMO (component of switching segments) [35]. Since the differences in structures of the hard and switching (soft) segments in the PU system strongly affected their shape-memory behavior, these results suggest that the precise control of molecular architectures such as the molecular weight and phase-separation structures is particularly important for the fabrication of better shape-memory materials. Besides the PU system combined with PTMO, other polymers such as poly(ethylene adipate) [15], poly(propylene oxide), and poly(butylene adipate) [30, 32] have been utilized as building blocks of the switching-segment-forming phase in PU systems.

On the other hand, poly(norbornene) (PN) is also classified under this type I SMPs. As described in "Sect. 7.1" (Introduction), PN was developed by the French company CDF-Chimie and was commercialized in Japan by Nippon Zeon Company in the 1980s under the brand name "Norsorex". Norsorex is synthesized by a ring-opening metathesis polymerization of norbornene monomer, which was made from ethylene and cyclopentadiene, in the presence of a catalyst, tungsten-carbene complex. Norsorex is a linear and amorphous PN, which has an ultrahigh molecular weight (Mw $= 3 \times 10^6$) [12, 36, 37]. PNs have $T_g$ of 35 °C, and they have been used as synthetic rubber because of their low hardness but high strength, low resilience and large vibration absorption ability. Different from the network system constructed using PU, physically cross-linked network points in Norsorex were formed by entanglements of the ultrahigh-molecular-weight PN chains. The thermal and shape-memory properties can also be controlled by manipulating the molecular architecture, which is the content of the trans-linked norbornene in the PN system, that is, stereoisomerism of the polymer. Despite these desirable characteristics, PN exhibits relatively poor resistance to creep in the retracted state at $T > T_g$, which limits the application of the PN system especially at high temperature. Jeon et al. addressed this problem using PN reinforced with polyhedral oligomeric silsesquioxane (POSS) macromer [38]. This POSS macromer has a spherical inorganic silica core surrounded by seven inert alkyl groups and one reactive group. Because the POSS macromer is a well-defined cluster whose diameter is approximately 15 Å and its properties such as its solubility can be freely adjusted by modifying the functional group on POSS, the introduction of POSS macromers into the polymer backbone by polymerization with norbornene and a single reactive site on the POSS macromer leads to changes in thermal property ($T_g$ and $T_{perm}$) and mechanical reinforcement, in addition to oxidation resistance and flammability based on the molecular structural features

[39–43]. The microstructural ordering of POSS macromers in the matrix (physically cross-linked networks) has been found to depend on the types of modified corner's functional group present on the POSS macromer. More importantly, the POSS microstructures in the matrix clearly affected their thermal, mechanical and shape-memory properties. Clearly, better shape-memory properties in PN reinforced with functionalized POSS can be observed relative to that in the pure PN (Norsorex) system.

These two miscible blend systems in type I SMPs have been extensively studied by Mathers and co-workers, for example, poly(vinyl acetate) (PVAc)/poly(lactic acid) (PLA) and PVAc or poly(methylmethacrylate) (PMMA)/poly(vinyldiene fluoride) (PVDF) [44, 45]. These two systems are both molten and miscible independent of blend ratios, PVAc and PMMA being totally amorphous in the system. In contrast, both PLA and PVDF show semicrystalline features, and have a degree of crystallinity of about 50 % individually. The degree of crystallinity of the blends can be varied from 0 to 50 % according to the blend ratio of PLA and PVDF. In this system, the crystal regions serve as physical cross-linking points, and also, the crystallinity controlled the rubbery modulus. In fact, the $T_g$ of the amorphous phase works as a $T_{switch}$ and can be tailored between the $T_g$ values of PLLA and PVDF depending on the blended ratios. These results also indicate the importance of molecular design in SMPs.

### 7.2.2 *Physically Cross-Linked (Semi)Crystalline Networks (Type I $T_{switch} = T_m$)*

If we selected and introduced some crystallizable block polymers as the component of the switching (soft)-domain-forming phase to prepare the physically cross-linked networks, their melting temperature ($T_m$), where the polymer changes state from solid to molten liquid, will act as shape-memory switching temperature, and the secondary temporary shapes can thus be fixed by crystallizing this phase. In the same way as described above (Sect. 7.2.1, type I $T_{switch} = T_g$), this type of SMP has a glassy amorphous domain or a highly crystalline domain serving as physical cross-linking points affording the mechanical strength above $T_m$, instead of $T_g$. Basically, the enthalpy change of the phase transition from a solid to molten liquid is much larger than that of the glass-rubber transition. Therefore, the use of the melting property is favorable for creating more sensitive temperature-responsive SMPs. As a major example of this type of SMP, block copolymers were synthesized from styrene and 1,4-butadiene. In the 1990s, styrene-butadiene-based SMPs were developed and commercialized by Asahi Kasei Corporation under the trade name Asmer [12]. Asmer is the block or graft copolymer of poly(styrene-*block*(*graft*)-butadiene) and physically cross-linked (thermoplastic) shape-memory resins, in which the $T_m$ was adjusted to 60 °C by controlling the contents of transform poly(1,4-butadiene) (PBD) as the switching-segment-forming phase. Similar to the PN (or PN reinforced with POSS) described above, the stereoisomerism of

the polymer is also one of the factors that determine the shape-memory property. Owing to the immiscibility between the poly(styrene) (PS) and PBD block, the copolymer phase separates and PS blocks form discontinuous, amorphous microdomain structures. The $T_m$ of the PBD crystallites represents the $T_{switch}$ for the thermally induced shape-memory actuation, that is, it works as the switching (soft) domain in the physically cross-linked SMP network. Moreover, PS exhibits a softening temperature of approximately 100 °C and acts as a hard-segment forming phase in Asmer. This high $T_g$ that originated from the PS blocks in the copolymer inhibits the slipping of PBD chains under stretching condition. Importantly, regulation of the mechanical property affects not only the range of elastic strain but also the shape recovery because of the entropy relaxation in SMPs that originated from the amorphous regions of the PBD phase. In addition, Sakurai and coworkers also further studied the details of these block copolymers [46, 47]. For the block copolymer with the higher content of high-molecular-weight PBD, the formation of two different crystal phases in PBD blocks has been found. As a result of the formation of the two crystal phases, a reversible solid-state transformation is possible between these two crystal phases. However, the existence of the two different crystal phases does not allow the exact tuning of $T_{switch}$, although the $T_m$ usually provides a sharp transition. Interestingly, a higher recovery rate was observed even for the sample that was subjected to more than five times larger strain than the original length and then fixed. The strange and unique shape-memory effect is explained by the formation of an oriented crystal phase, which forms a fibril-like morphology with high regularity over large distances, upon application of high elongations of up to 600 %, and the formed single fibrils are linked through amorphous PBD chains that are anchored together with several crystallites at the same time. Not only the diblock copolymer but also the triblock copolymers of poly(styrene-butadiene-styrene) (P(St-BD-St) as those of a similar system have been reported [48]. In the case of P(St-BD-St), the triblock copolymer is prone to segregate strongly with a minor component (only 10–30 vol%) of PS blocks. In a similar fashion to the diblock copolymer system, the PS domain at each end part of the triblock copolymer serves as a hard segment and poly(butadiene) (PBD) parts serve as a switching (soft) segment. Because the hard-segment content is low, a major component is the switching segment in this system. Therefore, a sharp transition behavior in shape-memory activation will be expected in this type of SMP.

A further example of this type of SMP is the linear, phase-separated block copolymers made of poly(ethylene terephthalate) (PET) and poly(ethylene oxide) (PEO) [49–52]. In this PET-PEO block copolymer, PET and PEO form the hard and switching (soft) segments, respectively. In PET-PEO block copolymers, $T_{perm}$ that originated from $T_m$ of the hard segment-forming PET blocks is 260 °C. The $T_m$ and degree of crystallization of PEO can be varied between 40 and 60 °C depending on both the molecular weight of PEO and PET content in the copolymer, and the crystal phases formed by PEO determine the $T_{switch}$ in the SMP network. A similar structural transformation of crystallites upon stretching and elongating the sample in the P(St-BD) copolymer was also observed in the PET-PEO block copolymer system. Triblock copolymers made from PTHF

and poly(2-methyl-2-oxazoline) (PMO) are also classified into type I with $T_{switch} = T_m$. These triblock copolymers (P(MO-THF-MO)) were successfully synthesized by cationic ring-opening polymerization, and the copolymer has a central PTHF block and terminal PMO blocks [53]. The PMO blocks exhibit $T_g$ at approximately 80 °C, and these blocks serve as hard segments. The PTHF blocks are semicrystalline and exhibit $T_m$ between 20 and 40 °C; this $T_m$ can be used as $T_{switch}$ for a thermally driven shape-memory effect. Because these triblock copolymers exhibit a clear microphase separation, both $T_g$ that originated from PMO and $T_m$ that originated from PTHF have almost the same values compared with those of homopolymers. At the same time, the elastic properties of PTHF parts in the triblock copolymer are different from those of the PTHF homopolymer, that is, the softening that occurred at above $T_m$ is incomplete in copolymerized PTHF because of a network formation by physically cross-linked PMO blocks.

On the other hand, PUs with a semicrystalline polymer as the switching (soft) segments can be classified into type I with $T_{switch} = T_m$. As described in "Sect. 7.2.1", conventional PUs are considered as multiblock copolymers consisting of random sequences of oligomeric hard and switching (soft) segments. Poly($\varepsilon$-caprolactone) (PCL) is often used as the switching segment forming polymer networks. PCLs with more than one hydroxyl group at the end group, such as PCL-diol, are generally used to incorporate the PCL as switching (soft) segments into the PU network. Polyesterurethanes (PEUs) are PUs with a hard segment synthesized from methylenebis(4-phenylisocyanate) (MDI) and 1,4-butanediol and with a switching segment of PCL [54–56]. The crystallizable PCL forms the thermally reversible switching segments caused by crystal-amorphous transition, and the temporary shape can be fixed by crystallizing these segments. The $T_{switch}$ for shape-memory activation in PEUs can be easily changed by adjusting the molecular weight and fraction of PCL, that is, the amount of the switching segment in the system. The advantages of polyurethane systems including not only PEUs but also polyetherurethane, which is the often used PEO that contains ether bonds in the polymer main chain as the switching-segment-forming phase. Those are simplicity and ease of modulating their $T_{switch}$, stiffness at room temperature, and their compositions, opening the possibility of being biocompatible and biodegradable.

We defined type I SMPs as the network structure stabilized by physical cross-linking. The methods of physical cross-linking are not only the entanglement of polymer chains with higher molecular weight and molecular interaction of a hard-segment forming phase as discussed above, but also the incorporation of ionic and mesogenic components into the hard-segment phase in SMP networks, which have been reported [57, 58]. Both ionic and mesogenic components incorporated in the hard segment can influence the mechanical and shape-memory properties. This is why the degree of phase separation as a result of the introduction of additional intermolecular interactions is enhanced. These functional components can stably form the domain structures, and will further enhance the degree of physical cross-linking in the system, and result in mechanical and related shape-memory properties. In fact, networks with ionic components introduced showed elasticity similar to that of a covalently cross-linked network [59,

60]. In addition, owing to the easy processing and manufacturing of this type of SMP, which is usually called thermoplastic technology, various fabrication processes such as electrospinning and foam technology can be used to design the other types of fabric such as shape-memory fibers and foams; thus, these will be used for various applications.

### 7.2.3 Covalently Cross-Linked Glassy Networks (Type II $T_{switch} = T_g$)

One of the major types of SMP is a cross-linked glassy polymer with glass transition temperature ($T_g$). In this book, we defined the covalently cross-linked networks as type II SMPs. This class of materials (type II) has attractive characteristics that include an excellent degree of shape recovery afforded by rubbery elasticity owing to the nature of the permanent (or near permanent) cross-linking, tunable work capacity during recovery owing to a rubbery modulus that can be adjusted through the extent of covalent cross-linking, and an absence of molecular slippage between chains seen in physically cross-linked SMP networks owing to strong chemical cross-linking of covalent nature. However, in contrast to the physically cross-linked SMPs (type I), in this type of SMP (type II), it is difficult to reshape the materials once the shape is formed by cross-linking because the permanent (original) shape is covalently fixed. In contrast to the term "thermoplastic" in the case of type I, they are often also called thermoset (thermosetting plastic). A typical material of this type (type II), cross-linked poly(vinyl chloride) (PVC), can be prepared by thermal dehydrochlorination and subsequent cross-linking of PVC in HCl atmosphere [61]. It is well known that many factors such as molecular weight of polymers, reaction temperature and reaction time affect the properties of the material created by the dehydrochlorination of PVC. It is widely accepted that the dehydrochlorination of PVC occurs through the zip (zipper) mechanism. The first step (initiation) is the formation of an olefin site. Because of the activation in allyl groups, the double bond present in the polymer chain activated the monomeric unit in its vicinity (the zipper propagation) [62, 63]. Skákalová et al. studied the cross-linking reaction of PVC with a molecular weight of ca. 50,000, and revealed that the dehydrochlorination reaction in a short time effectively worked to obtain the stable cross-linked structures by changing the degree of dehydrochlorination [61]. However, an increasing level of degradation of the polymer chains takes place, which is accompanied by a loss in the thermal and mechanical stabilities of the resultant cross-linked PVC in the samples with a higher degree of dehydrochlorination. This feature also affected their shape-memory properties, that is, although the very weakly dehydrochlorinated sample shows almost no recovery, the samples with a higher degree of dehydrochlorination exhibit a better shape-memory property. These results suggest that the cross-linking method is also one of the factors that determine the properties of SMPs.

On the other hand, other SMPs classified into type II ($T_{switch} = T_g$) are those based on renewable natural sources. Li and co-workers extensively studied this type of SMP for the system comprising copolymerization and chemical cross-linking of renewable natural oils with acrylate monomers to obtain copolymer networks. They mainly focused on the SMP networks made of soybean oil as biological oil and various alkenes by cationic copolymerization [64–68]. Soybean oil is one of the cheapest and most abundant annually renewable resources. Although the original double bonds of carbon (C=C bonds) of the soybean oil side chains typically remain unreacted during the free radical copolymerization, they have successfully prepared a series of random copolymers synthesized by the cationic copolymerization of regular soybean oil, low-saturation soybean oil, or conjugated low-saturation soybean oil with various alkene comonomers. The SMP networks based on the soybean oils and alkene comonomer show tunable glass transition and mechanical properties by changing the monomer ratio. These SMP networks exhibit excellent shape fixing and shape recovery properties at sufficiently higher temperature than $T_g$. Because of the broad nature of glass transition behaviors and the coexistence of rigid glassy and soft elastic segments, incomplete shape recovery is also observed in this system. The idea of utilizing abundant renewable resources is important and prominent for overcoming the energy problem that besets the world.

The copolymer networks with the shape-memory property can also be designed using a combination of a star-shaped reactive polymer and diisocyanate. Isocyanate chemistry is not only useful for the preparation of physically cross-linked shape-memory networks as described above, but can also be utilized for the design of covalently cross-linked shape-memory networks. In this case, the cross-linking reaction requires a polymer with multiple reactive groups and compounds with more than two isocyanate groups to obtain the stable network structures. Lendlein et al. have developed $T_g$-based chemically crosslinked SMP networks that were prepared from the star-shaped hydroxyl-telechelic poly(*rac*-lactide-co-glycolide) (PLGA) and aliphatic diisocyanates [69]. The advantage of this system is the ease of manipulation of structural variation, which allows for the regulation of $T_g$ in the range between 48 and 66 °C. The resultant copolymer networks exhibit good shape-memory properties (high shape-fixing ratio ~98 %, high shape-recovery ratio 98 %: more details of these characterizations (calculation) will be discussed in "Sect. 7.4.2"). In addition, these SMP networks are biodegradable and show relatively fast degradation compared with a single PCL network, which have used slightly different components to form the SMP networks, as reported by the same group [25]. Since the completely amorphous polymer networks with thermally induced shape-memory effects described in the literature up to this time were not originally developed for biomedical applications and are nonbiodegradable, this report is important for first designing amorphous, biodegradable, shape-memory networks. Similar network structures have also been prepared by the conetwork formation of PLGA-dimethacrylate and two different alkyl acrylate comonomers. In the case of PLGA-dimethacrylate alone, the formed networks tend to

be brittle below $T_g$ (55 °C) and difficult to handle in the course of the network synthesis and extraction without destroying the samples. To overcome this problem, Lendlein et al. studied the incorporation of a second amorphous phase with a low $T_g$ into the PLGA network, which keeps the material elastic, which is a potential strategy to effectively improve the mechanical properties of the networks with PLGA-based segments [70]. This utilization of comonomers in network formation is often used to design stable and robust covalently cross-linked SMP networks.

### 7.2.4 Covalently Cross-Linked (Semi)Crystalline Networks (Type II $T_{switch} = T_m$)

Aside from the glass transition as a critical temperature, the melting transition of semicrystalline networks can also be employed to trigger shape recovery, typically giving a sharper recovery event similarly to a physically cross-linked network driven by $T_m$. Here, the secondary shapes are fixed by crystallization instead of being fixed by vitrification seen in the system of $T_{switch} = T_g$. Similarly to the first class, the permanent shapes are established by chemical cross-linking and cannot be reshaped after processing. Compared with glassy materials, this class of materials is generally more compliant below the critical temperature, with a stiffness that is sensitive to the degree of crystallinity, and thus indirectly to the extent of cross-linking because the cross-linking usually tends to inhibit the crystallization of polymer chains. Shape recovery speeds are also faster for this first-order transition with an often sharper transition zone owing to the higher enthalpy of transition than $T_g$. This class of materials includes bulk polymers, such as semicrystalline rubbers and liquid-crystal elastomers (LCEs), and hydrogels with phase-separated crystalline microdomains.

Semicrystalline rubbers have been favored as shape-memory materials as a result of their superelastic rheological characteristics, fast shape recovery, and flexible modulus at the fixed stage. One classic material of this family of SMPs is chemically cross-linked trans-polyisoprene (TIP) [71], which is a semicrystalline polymer with a $T_m$ of 67 °C and a degree of crystallinity of approximately 40 %, giving a stiffness of about 100 MPa at room temperature. TIP was chemically cross-linked by peroxides, the enzyme for catalyzing the oxidation-reduction reaction, at 145 °C for 30 min to form a three-dimensional network, thus establishing the permanent (primary) shape and creating the superelastic property required for shape recovery above its $T_m$. Thermal instability inhibits the final application of this material owing to the high density of unsaturated double bonds, which are the cause of the high toxicity. On the other hand, Mather's group has successfully developed a chemically cross-linked, semicrystalline trans-polyoctenamer (polycyclooctene, PCO) with a trans content of 80 %, a $T_g$ of 270 °C, a $T_m$ of 58 °C, and a much better thermal stability, for shape-memory applications [72]. When cooling a strained sample to sufficiently below

$T_m$, crystalline domains begin to form and ultimately percolate the sample, at that point establishing strain fixing. When heated above $T_m$, in fact, they were heated to 80 °C, the crystals melt to an amorphous phase, which is a molten phase with high mobility, leaving the chemical crosslinks to reestablish the primary shape. This cross-linked PCO has elasticity similar to that of rubber at temperatures above $T_m$ and thus can be deformed easily by applying an external force to obtain a new secondary shape. The secondary shape can be fixed by crystallization during the subsequent cooling process to a temperature sufficiently below the $T_m$. The cross-linked SMP network will maintain this temporary shape as long as the crystals are not destroyed at the temperature below the $T_m$. Therefore, the SMP with temporary shape is extremely stable below $T_{switch}$. On the other hand, the fixed deformation as the temporary shape can return to the primary original shape immediately when the samples are heated above their $T_{switch}$ ($T_m$ in this system), where the fixing phase disappears. The stiffness at room temperature, transition temperatures ($T_{switch}$), and rubbery modulus can be tuned independently by blending with rubbery or solid components, manipulating the tacticity of PCO and controlling the cross-linking degree, that is, by designing the network structures [73]. Similarly, polyethylene (PE) has been modified to endow the shape memory ability by radiation cross-linking. It has been well known as heat-shrinkable tubes used for many applications, although the $T_m$ is inconveniently high ($110 < T_m < 150$ °C) [74, 75].

Using an analogous concept, Lendlein et al. have developed shape-memory biodegradable polymers by synthesizing and copolymerizing a narrowly dispersed, oligomeric PCL dimethacrylate with n-butyl acrylate under UV radiation to yield a multiblock structure [25]. The PCL segments form a crystalline structure as switching segments to fix the secondary shape at low temperature, leaving the $T_m$ of the PCL segments to control the shape recovery temperature. Meanwhile, the amorphous n-butyl acrylate main chains, together with the PCL dimethacrylate as a cross-linker, form a network that gives rise to the permanent shape and provides the excellent shape recovery by a softening effect with its low $T_g$ (−55 °C). The advantage of this class of material lies with the very sharp melting transition, owing to the uniformity of the crystals generated by PCL segments with almost identical molecular length. In other words, the uniformity of the crystals is strongly affected by the homogeneity of the PCL structure at the molecular scale. A sharp transition should ensure a sharp and fast shape recovery. However, this SMP characteristically returns to its primary shape in 20 s on a hot plate at 70 °C, which is too slow, even though the heating temperature is sufficiently high. A plausible reason for such a slow recovery is that the sample may not have been uniformly and effectively heated. An additional contribution of their system is the application of a photocuring method to quickly fabricate shape-memory polymers directly to their permanent shapes. Another advantage of the photocuring method is its applicability to a more complex three-dimensional (3D) shape and configuration. Recently, other synthetic methods based on radiation cross-linking have also been proposed to construct biodegradable PCL networks exhibiting excellent shape-memory properties [76–79].

### 7.2.5 Shape-Memory Multiple Networks and Composites (Type III)

Driven by potential applications, such as intelligent implants, devices or textiles, the question arises whether the shape-memory effect of polymers can be combined with different functions that are not directly linked to the shape-memory effect. Examples of such functionality combinations are electrical conductivity and shape-memory effect, change of color and shape-memory effect, or degradability and shape-memory effect [24, 80, 81]. Multifunctionality is the targeted combination of material functions that are not linked with each other [82]. The development of such multifunctional materials is a highly interesting challenge in basic research. Several approaches have been explored for creating multifunctionality, involving one-component polymer systems as well as multimaterial systems, e.g., combining two polymers or a polymer and inorganic (nano)particles. One example of a single macromolecule, in which several functionalities have been integrated into the polymer structure, is polymer networks, in which an additional functionality (e.g., hydrolytical degradability) was obtained by inserting easily hydrolysable bonds [25, 83, 84]. That is, the information of objective function can be directly input into the structure of the designed polymers by synthetic (molecular design) approaches. Multifunctional one-component polymer systems were realized as multiblock copolymers, in which the additional functionality has been incorporated in one or both segments [24, 85]. In multimaterial systems, the additional functionality, e.g., electrical conductivity, results from the integration of an additional material (e.g., carbon nanotubes) in a polymer network or multiblock copolymer [86–88].

As shown in Fig. 7.4, the various external stimuli, such as not only heat [26, 89] but also light (photo) [81, 90–94], moisture (water) [95–98], magnetic field [99–104], radio frequency [105] and infrared (IR) light [106–108], can be utilized as the trigger to activate the shape-memory effects. In 2005, Lendlein et al. first demonstrated the light-induced shape-memory polymers [90]. They introduced the cinnamic acid or cinnamylidene acetic acid groups as photoresponsive molecular switches, which are known to undergo efficient photoreversible [2 + 2] cycloaddition when the sample is exposed to an alternating wavelength ($\lambda > 260$ nm, $\lambda < 260$ nm in this experiment) to achieve the photoresponsive shape-memory effects. For this light-induced SMP, shape-memory properties such as the strain fixing ratio are much lower than those of thermally induced SMPs. However, the unique characteristics of light-induced SMPs enable the remote activation of shape memory, and many applications that are difficult to achieve with the thermoresponsive SMPs will be developed in the near future. Their group has also developed the magnetoresponse SMP [99]. The magnetically induced shape-memory effect was achieved using the composites from the physically cross-linked polymer multinetwork (type I), which is formed by PCL as the switching (soft) segment and poly(*p*-dioxanone) as the hard segment, and magnetic nanoparticles, which consisted of an iron(III) oxide core in a silica matrix. In this system, the

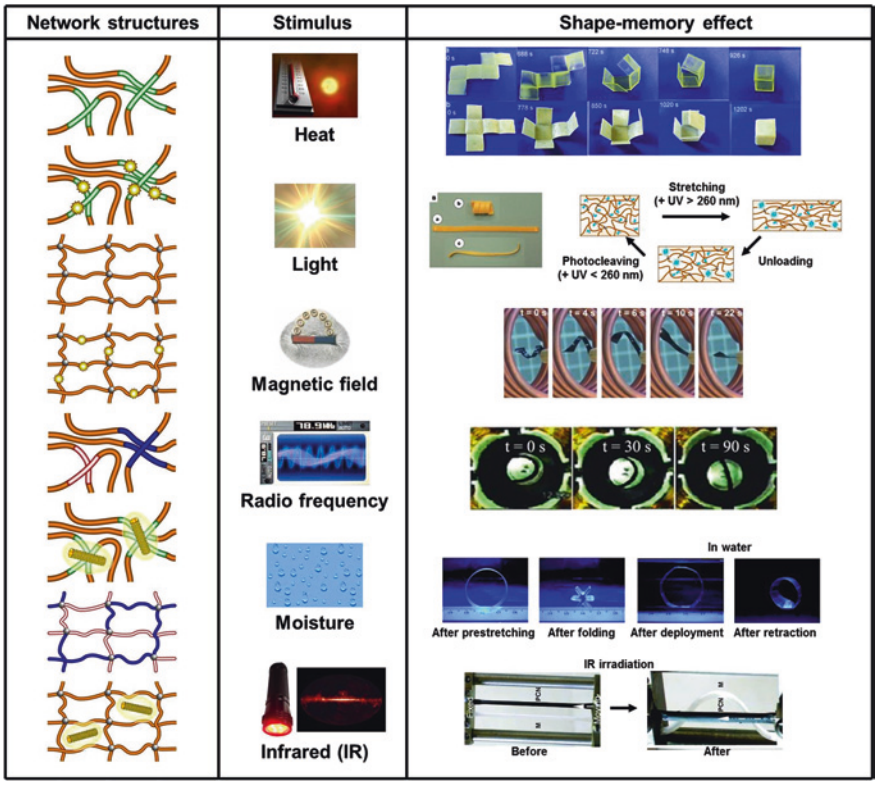


**Fig. 7.4** Various external stimulus-induced SMPs. By introducing the switching function into the molecular structure or their network, activation other than heating can be integrated into the SMPs

power of the magnetic field is converted to thermal energy, that is, induction heating of magnetic nanoparticles. On the other hand, Hazelton et al. developed the radio-frequency-induced SMP using a composite of covalently cross-linked epoxy network (type II SMP) and magneto-electroelastic particles [105]. They demonstrated that radio-frequency energy coupling is strongly dependent on the applied radio frequency and the level of filled magneto-electroelastic particles, and the radio-frequency energy can be used to actuate the shape-memory effect without interfering with the performance of the SMP. By a similar approach using nanocarbon particles, an infrared light-active SMP was also developed by Leng et al. [106]. Because of the high storage modulus and high infrared absorption capability of the nanocarbon particles, the better shape-memory effect of these composites was reported. From these results, the multiple-network formation such as that of IPN, a blended structure, and a composite with other functional materials should be a very efficient method of obtaining the SMP with multifunctional properties; hence, we classified this class of SMP as type III SMPs.

## 7.3 Synthetic Methods

### *7.3.1 Synthesis of SMPs as Building Blocks*

We already discussed the classification of SMPs according to the nature of their formed network points that are either physically cross-linked (type I) or covalently cross-linked (type II) SMPs. In addition, these SMPs were subdivided based on their switching type into either $T_g$-type SMPs with an amorphous phase or $T_m$-type SMPs with a crystalline phase as described earlier. The shape-memory properties are closely related to the molecular architectures because the thermal and mechanical properties strongly depend on the molecular structure of SMPs. Therefore, the design and synthesis of SMPs as building blocks and their network structures are critical for regulating the shape-memory properties on demand for any application. Generally, conventional polymerization methods including step polymerization and addition polymerization can be used for both the synthesis of polymer building blocks and network formation. From the viewpoint of the synthesis of polymer building blocks, polymeric materials are synthesized from small molecules called monomers with more than two reactive sites on the monomer. There are essentially two types of polymerization reaction. In the condensation reaction (sometimes called step-growth polymerization), two reactants with degrees of polymerization, m and n, combine to form their respective polymers. The characteristics of this type of polymerization are (1) stoichiometric concerns, (2) relatively slow reactions, (3) successive condensation reactions or "coupling", (4) gradual increase in molecular weight, (5) release of small molecules such as $H_2O$ and HCl, and (6) repeat unit often not the same as the monomer structure. For example, polymers such as polyesters, polyamides, polyethers and polysiloxanes are synthesized by condensation polymerization where polymer chains are formed through the reaction between carboxylic acid and alcohol, carboxylic acid and amine, dehydration of diols, and condensation of SiOH (silanol). Condensation polymerization of this type is called polycondensation polymerization because the polymerization proceeds successively to form the polymer chains. Although the condensation polymerization is accompanied by the elimination of small molecules during the reaction, there is the same condensation polymerization that proceeds without liberating small molecules. This type of condensation polymerization is called polyaddition polymerization, and it can be applied to the network formation of SMPs such as polyurethanes and polyureas (discussed in detail in Sect. 7.3.2). On the other hand, addition polymerization, which is also called chain-growth polymerization, was also used to synthesize the network-forming SMP components. Among them, the addition polymerization, which can be initiated by free radicals, is free radical polymerization that is often used to synthesize the SMP component and for the network formation of SMPs. In this polymerization, one monomer is added at a time to the growing chain. Free radical polymerization can be applied to many vinyl monomers such as ethylene, propylene, styrene, vinyl chloride and vinyl acetate to obtain the homopolymers and

copolymers. In addition, ionic polymerization is also considered as a similar type of addition polymerization. In ionic polymerization, the active center is the ionic charge instead of the free radical. Therefore, ionic polymerization is more monomer specific than initiation by free radicals. Only monomers that can sufficiently stabilize positive or negative charges will undergo ionic polymerization, which is called cationic or anionic polymerization, respectively, depending on the charge of the species. For example, it is well known that rubbers made of isobutylene and isoprene were synthesized by cationic copolymerization in the presence of a Lewis acid initiator ($AlCl_3$), and the polymerization of styrene in liquid ammonia is one of the first examples of anionic polymerization. Recently, living polymerization has also been spotlighted to construct the SMP components with a precise molecular structure. Living polymerization is a form of addition polymerization where the capability of a growing polymer chain to terminate its own growth has been removed [109]. This can be accomplished in various ways. Chain termination and chain transfer reactions, which are the main causes of the nonuniformity of conventional polymerization, are absent, and the rate of chain initiation is also much higher than the rate of chain propagation. The result is that the polymer chains grow at a more constant rate than seen in traditional chain polymerization, and their lengths remain very similar, which means that they have a very low polydispersity index. Living polymerization is now a popular method for synthesizing not only homopolymers but also block copolymers because the polymer can be synthesized in stages, each stage containing a different monomer. Additional advantages are predetermined molar mass and control over end groups that are well-defined molecular structures.

Designing SMPs includes selecting suitable network points, which determine the permanent shape, and net chains, which act as switching segments. Furthermore, appropriate synthetic strategies have to be developed as described above for the synthesis of SMP components. The risk of possible toxic effects of polymers can already be minimized by selecting monomers whose homo- or copolymers have been proven to be biocompatible, and this is a very important issue for biomedical applications. Appropriate switching segments for degradable SMPs can be found by considering the thermal properties of well-established degradable implant materials. The respective macrodiols, which can be used for the synthesis of shape-memory polymers, can be produced by means of "ring-opening polymerization" of lactones and cyclic diesters [110]. Ring-opening polymerization is classified into chain-growth polymerization, in which the terminal end of a polymer acts as a reactive center of polymerization, where further cyclic monomers join to form a larger polymer chain through ionic propagation. The treatment of some cyclic compounds with catalysts brings about cleavage of the ring followed by polymerization to yield high-molecular-weight polymers. When the reactive center of the propagating chain is a carbocation, the polymerization is called cationic ring-opening polymerization; on the other hand, if the active center is a carbanion, the reaction is an anionic ring-opening polymerization, which is the case of polypropylene oxide synthesis. A different type of ring-opening polymerization, based on olefin metathesis, uses catalysts rather than

cationic or anionic propagation. Ring opening polymerization can apply to the synthesis of both homopolymers and copolymers. Since 1994, our group has been studying the synthesis of SMPs, especially focused on the aliphatic polyester with biocompatibility and biodegradability. The first aim of the study is to investigate the application of a crystalline polymer network to a thermoresponsive biomaterial [111]. To achieve this purpose, crosslinkable aliphatic polyesters containing a PCL segment were prepared from tetrafunctional star-shaped macromonomers. The tetra-branched PCL-based copolymers were synthesized by ring-opening polymerization of CL and L-lactide (LLA) initiated with pentaerythritol, which is a tetra-alcoholic compound. The obtained materials, which consisted of CL homopolymer and LLA/CL block copolymer, exhibited a phase transition temperature derived from the melting of the PCL segment. The transition temperatures ($T_m$) of developed polymers can be successively controlled by molecular design such as by manipulation of the ratio of CL to LLA in copolymers and chain length (molecular weight). We have also succeeded in regulating the transition temperature of SMPs by copolymerization of CL and D,L-lactide (DLLA) [112–114]. The regulation of $T_m$ of polymers as building blocks is extremely important to form the SMP network because these $T_m$ values also affect the transition behavior of resulting cross-linked materials as described below (Sect. 7.3.3).

### *7.3.2 Prepolymer Method (Type I Network)*

All the linear polyurethane systems presented in this section are synthesized by the prepolymer method. Thermoplastic polyurethane (PU) elastomers are produced on an industrial scale by this technique. In this process, isocyanate-terminated prepolymers are obtained by the reaction of difunctional, hydroxy-terminated oligoesters and oligoethers with an excess of a low-molecular-weight diisocyanate (Fig. 7.5a). Low-molecular- weight diols and diamines are added as so-called chain extenders to further couple these prepolymers. Linear, phase-segregated PU or polyurethane urea (PUU) block copolymers are obtained in this way (Fig. 7.5a). Each polymer chain contains segments of high polarity composed of urethane and urea bonds that are linked through chain-extender molecules with hydroxyl and amine groups. As a result of their high intermolecular interaction, they form the so-called hard segments. Strictly speaking, they form the hard-segment phase that is embedded in an amorphous elastic matrix. This amorphous matrix, with its low $T_g$ lying far below the normal operating temperature, forms the so-called switching (soft) segment. In the case of PUs with shape-memory effects, this segment serves as a switching segment. For this purpose, it is modified in such a way that the thermal transition is located in a temperature range relevant for the respective application. Hard-segment “clusters” with dimensions under micrometer scales are formed by the phase-separation process that occurs. These clusters have high $T_g$ or $T_m$ values and act as multifunctional physical network points determined as $T_{high}$ and $T_{perm}$ in the SMP network. These are also called plastic domains because

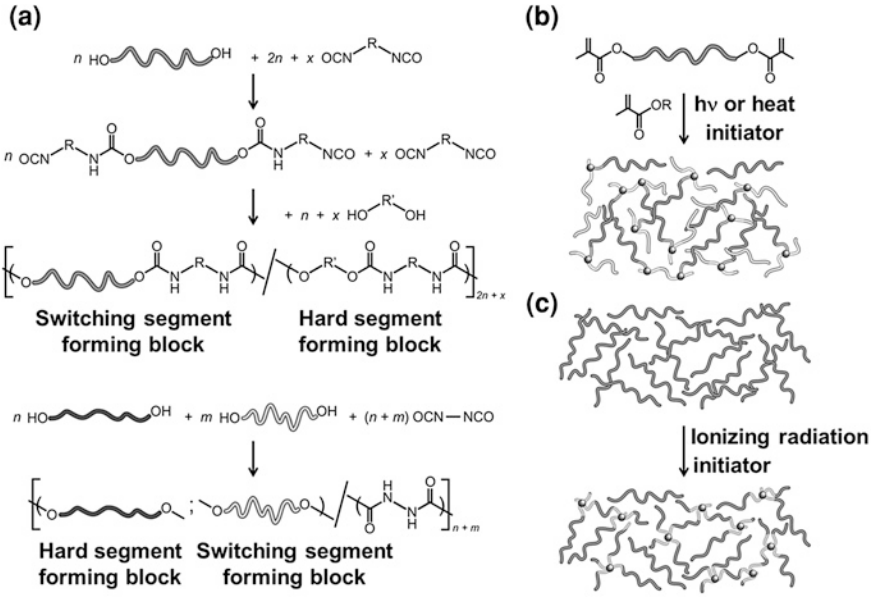


**Fig. 7.5** **a** Prepolymer method for the synthesis of physically cross-linked shape-memory polyurethanes (SMPUs) (*top*) and multiblock copolymer network (*bottom*). Synthesis strategies for chemically cross-linked SMP network by **b** polymerization method and **c** direct cross-linking method of linear polymers [110]

they play the role of reinforcing the filler in the matrix. Their capability to deflect mechanical energy by deformation prevents the growth of microcracks. They also impart breaking strength and impact strength to the SMP network [115–118]. Ji and co-workers have reported that the PUs were prepared with PCL as the component of switching (soft) segments and 4,4′-diphenylmethane diisocyanate as the chain extender and 1,4-butanediol as the component of hard segments by the prepolymer method [119]. They also demonstrated the nonaromatic shape-memory PUUs, which were synthesized with isophorone diisocyanate as the nonaromatic chain extender and aliphatic or cycloaliphatic diamines as the component of hard segments by the prepolymer method [120]. Then, they compared the developed shape-memory PUs and PUUs, and revealed that the recovery stress of shape memory in shape-memory PUUs was much higher than that of shape-memory PUs and that can be successfully controlled by adjusting the content of the hard segment [120]. On the other hand, Chen et al. prepared the shape-memory PU made of poly(hexylene adipate) (PHA), 4,4′-diphenylmethane diisocyanate and 1,4-butanediol as a chain extender by this prepolymer method, and they successfully synthesized the shape-memory PU with different switching (soft) segment lengths and hard segment contents by a two-step reaction containing the prepolymer method [121]. Their related study showed that the shape-memory property of PHA-based shape-memory PU was much better than that of PCL-based shape-memory PU. Korley et al. also reported the shape-memory PU prepared by the

prepolymer method [122]. They designed the series of PUs with higher molecular weight containing the PEO and the triblock copolymer made of PEO and poly(propylene oxide) (PPO) as the switching (soft) segment forming component. They found that the PEO-based PU exhibits improved storage modulus and toughness of the segmented PUs below the $T_m$ of the switching (soft) segment. They suggested that these different mechanical behaviors of PEO-based and triblock-copolymer-based shape-memory PUs originated from the crystalline switching (soft) segment that serves as an additional load-bearing component in the system during deformation. As found in these studies, the prepolymer method is a simple and versatile method of preparing the shape-memory PU and their derivatives such as PUUs by only selecting the building blocks to form the SMP network. Moreover, not only the components of hard and switching (soft) segments but also their phase-separated (segregated) structure, which is an important factor for the shape-memory property, can be easily manipulated by altering the preparation process. Therefore, many researchers have adopted this method in the design of SMP networks, and work toward practical application in various fields using the prepolymer method.

### *7.3.3 Polymerization Method and Direct Cross-Linking of Linear SMPs (Type II Network)*

There are two strategies for the synthesis of covalently cross-linked polymer networks. Firstly, the polymer network can be synthesized by polymerization, polycondensation, or polyaddition of difunctional monomers and macromonomers by the addition of trifunctional or higher functional crosslinkers. Figure 7.5b shows the synthesis of covalently bonded networks by treating methacrylate monomers with an oligomeric dimethacrylate as a macromolecular crosslinker. The chemical, thermal, and mechanical properties of the network can be adjusted by choosing the monomers, their functionality, and the crosslinker content. Practically all polymerization methods can be used to synthesize SMPs, including addition [120], condensation [49, 123], free-radical [124] and photochemical polymerization [25, 111], acyclic diene metathesis polymerization [125], and even ring-opening polymerization [126]. Although, for example, the shape-memory PUs and ethylene oxide–ethylene terephthalate segmented copolymers are generally synthesized via condensation polymerization [49], the SMP network formation by polymerization can be achieved by the reaction between the functionalized polymers. That is, in Fig. 7.5b, the SMP networks were covalently generated by the radical polymerization of end groups of macromolecular crosslinker (macromonomer). As one of the polymerization methods to obtain the SMP network, Yakacki et al. have developed direct network formation. In this procedure, they fabricated the network with poly(ethylene glycol)-dimethacrylate (PEGDMA) as macromonomer and methyl methacrylate (MMA) as additional monomer. The PEGDMA-MMA networks were prepared by photoradical polymerization in the presence of photoinitiators.

By combining the macromonomer and additional monomer, $T_m$ and mechanical properties such as elastic modulus of cross-linked SMPs could be independently and successfully controlled. Similar (copolymer or AB-type polymer) networks have been fabricated by several researchers [25, 72, 127–129]. In the case of a linear polymer with monofunctionality, the stable covalent network cannot be formed by this process because it only increases their molecular weight similarly to the chain extender as described in "Sect. 7.3.2" and the cross-linker may be required to form the three-dimensional network structures. However, an additional comonomer, that is, MMA in the study of Yakacki et al. [127] is not necessary to form the stable SMP network. If the networks composed of only macromonomer, namely, without the addition of comonomer, can be designed, the networks with a well-defined structure based on the property of the macromonomer will be obtained. This is the reason for our developed multibranched PCL-based copolymer as described in "Sect. 7.3.1". In fact, we have developed the covalent network formation of PCL-based SMP (type II) by the polymerization method. In this process, the cross-linked polyester membranes were prepared by radical polymerization of the macromonomers with visible light irradiation in the presence of an initiator and sensitizer without any comonomer [111]. The obtained cross-linked materials are extremely stable not only in aqueous environment but also in a good solvent for developed (co)polymers. Not only copolymerization with other materials but also the precise design of the branched numbers and chain length in the homo-PCL system can adjust to the transition temperature of cross-linked (type II) SMPs on demand in the range between 30 and 45 °C without adding any comonomers [130], and these temperature ranges are ideal for biomedical applications. Because the $T_m$ of the conventional PCL homopolymer is approximately 60 °C and it is too high to apply as a thermoresponsive material in biological applications even though PCL has excellent biocompatibility and biodegradability, this cross-linked homo-PCL system with $T_m$ at approximately the biological temperature range is very interesting. In addition, although the copolymerization with other monomers is sometimes caused by the broadening of the transition behavior, our developed cross-linked homo-PCL showed the sharp phase transition from the crystal to the amorphous phase within a narrow temperature range, that is, it could successfully achieve a smart drug delivery device with a sharp "on-off" controllability.

The second strategy to obtain polymer networks is the subsequent cross-linking of linear or branched polymers (Fig. 7.5c). Cross-linked PE is generally prepared through a radiation reaction. In all the methods aimed at subsequent cross-linking of linear polymers, the structure of the obtained network is strongly dependent on the reaction conditions and reaction (curing) times, especially the cross-linking density. The cross-linking of linear polymers can take place by a radical mechanism involving ionizing radiation or by the elimination of low-molecular-weight compounds to generate unsaturated carbon bonds. These have the capability to form chemical and covalent cross-linking. Zhu et al. have demonstrated the preparation of cross-linked PCL (type II SMP) by $\gamma$-radiation [131], and revealed that both the molecular weight of polymers and radiation dose affect the cross-linking density of resultant materials. The addition of radical initiators to linear polymers

also makes it possible to convert polymer chains into radicals that are able to recombine intermolecularly. Ware et al. have developed the covalently cross-linked (type II) SMP composed of poly(methyl acrylate) (PMA) and poly(ethylene glicol)-diacrylate (PEGDA) [132]. In their method, the PEGDA was used as the sensitizer of radiation crosslinking. The blended PMA and PEGDA were exposed to ionizing radiation to obtain the cross-linked SMP. By introducing the sensitizer, the minimum dose for gelation was decreased, and the rubbery modulus was increased after crosslinking. Interestingly, they also showed that the length of the sensitizer, that is, the molecular weight of PEGDA, also affects the cross-linking state and mechanical properties. Although the structure obtained by radiation cross-linking is somewhat unclear, the capability of wide polymer types is one of the attractive features.

### *7.3.4 Synthesis Techniques of SMP Composites (Solution/ Melt Mixing and In Situ or Interactive Polymerization)*

Significant progress has been made in recent decades in designing, synthesizing, characterizing, and applying SMP nanocomposites by adding various types of nanofiller to obtain SMPs with multifunctionality (type III). Consequently, in thermally induced SMPs, the shape-memory effect can be triggered by the direct application of heat and also by Joule (electrical) heating and inductive (magnetic or electromagnetic) heating as described earlier. In this section, we overview the synthesis and designs that especially focus on PU-based SMP composites because their techniques are basically similar regardless of SMP type.

In general, there are two types of preparation method to obtain the SMP composites. First, in the solution mixing method, particles and polymers are mixed in a suitable solvent, followed by the precipitation or evaporation of the solvent. Therefore, the composites of polymers and other materials can be easily obtained. The advantages of using this method include the following: (1) nanometric materials are obtained first; (2) the effects of reaction conditions on the formation of inorganic structures (a serious problem via traditional methods) can be avoided; and (3) the fixed inorganic structure benefits the characterization of the final composites [133]. These mean that pre-prepared materials, which possess well-defined structural features by a general synthetic approach, can be directly adopted. Although there is an in situ approach that the components are synthesized directly in the SMP matrix, it often causes the inhomogeneous material formation owing to the nonuniformity of the reaction. Moreover, direct mixing usually does not provide uniform solutions because of the aggregations of nanoparticles (NPs) or nanotubes (NTs). Agitation with ultrasonication, magnetic, and shear mixing methods can be used to enhance dispersion. However, NPs and NTs are not well dispersed so much in the SMP matrix using simple solvent mixing methods [134]. A high-power ultrasonication process using equipment such as a homogenizer is more effective than other processes in forming a good dispersion

of NPs or NTs. Ultrasonic irradiation has been extensively used in dispersing, emulsifying, crushing, and activating the particles [135]. For example, by taking advantage of the multiple effects of ultrasound, the aggregates and entanglements of carbon nanotubes (CNTs) can be effectively broken down, obtaining good dispersion. Cho and co-workers have successfully prepared polyurethane-multiwall carbon nanotube (MWCNT) composites with better dispersion of CNTs up to 20 wt% in polyurethane, although the higher content of CNTs causes them to aggregate even though high-power ultrasonication is applied [135, 136]. Other polymer composites, including PU-CNTs [137, 138], PS-CNTs [139], epoxy-CNTs [140, 141], poly(vinyl alcohol)-CNTs [142], and PE-CNTs [143], have been fabricated by the solution mixing method with improved CNT dispersivity. However, recent advances in the surface modification technology of NPs and NTs will be advantageous for the preparation of SMP nanocomposites. By modifying the surfaces of NPs and NTs, they can more easily disperse in proper aqueous and organic solutions than nonmodified NPs and NTs. Therefore, the higher dispersivity of NPs and NTs will result in a more homogeneous incorporation into the SMP matrix. In addition, the NPs and NTs with high dispersivity may not require the high-power ultrasonication to obtain the good dispersion of NPs and NTs. In solution mixing, the sol-gel process is convenient and versatile for preparing nanocomposites under ambient conditions and it allows in situ entrapment of inorganic NPs or organic, organometallic, and biological molecules within microporous networks of sol-gel-derived matrices [144, 145]. In general, the sol-gel process involves the transition of a system from a liquid sol (mostly colloidal) into a solid gel phase. Sol-gel materials have controllable surface areas of NPs and average particle or pore sizes. They can be miniaturized to micro- or nanosizes and allow control of conductivity by choosing the appropriate metal or metal oxide [146].

On the other hand, many polymers are insoluble in liquids, especially in aqueous solution, and melt mixing may be one option. Melt mixing is a common and simple method that is particularly useful for thermoplastic polymers, that is, physically cross-linked SMP (type I) with $T_m$. It involves the melting of polymers to form a viscous molten liquid; then, additives are included for shear mixing, followed by molding, templating or extrusion to form samples [147]. Special care should be taken as thermal processing may be detrimental to components of composites such as CNTs or cause polymer degradation because the high-temperature processing often alters the material functions and properties [148, 149]. This approach, however, is simple and compatible with current industrial production. The large shear forces can be applied to entangle aggregates such as filler components or prevent their formation. In fact, Zhang et al. have prepared nylon-6-MWCNT composites containing 1 wt% MWCNT via a melt mixing method using a twin-screw mixer [150]. The disadvantage was that the dispersion of inorganic nanocomponents in the polymer matrix was poor compared with the dispersion achieved by solution mixing, along with other potential problems such as changes in surface properties of nanocomponents during melting and high viscosities of composites at higher loading of nanocomponents such as CNTs.

In situ or interactive polymerization is crucial for preparing composites with polymers that cannot be processed by solution or melt mixing, e.g., insoluble and thermally unstable polymers. Therefore, in situ polymerization can be applied for most nanocomposites. Modification may involve noncovalent or covalent bonding between CNT and polymer. Noncovalent CNT modification applies physical adsorption or wrapping of polymer molecules to the surface of the CNTs through van der Waals and π–π interactions [151, 152]. Sahoo and co-workers have reported that the graphitic sidewalls of CNTs provide possibilities for π-stacking interactions with conjugated polymers and organic polymers containing heteroatoms with free electron pairs [153, 154]. The advantage is that noncovalent functionalization does not destroy the conjugated system of CNT sidewalls and therefore does not affect the final structural properties of the nanocomposites. In the case of conductive polymers, the polymers may be attached to CNT surfaces by in situ polymerization to improve processability and also electrical, magnetic, and optical properties [153–156]. For example, MWCNTs are first dispersed in PCL-diol, followed by adding MDI to the mixture, which is combined with MWCNTs, and the conventional prepolymer method. A butanediol chain extender is added to this prepolymer, and finally, a PU-MWCNT composite is simply synthesized. However, Xia and Song have suggested that single-wall carbon nanotubes (SWCNTs) are not dispersed well by this method instead of MWCNTs [157, 158]. Therefore, they synthesized PU-SWCNT nanocomposites using polyurethane-grafted SWCNTs. This improved the dispersion of SWCNTs through the grafting in the polyurethane matrix and strengthened the interfacial interaction between PU and SWCNT [158]. In addition, Guo and co-workers have reported that the introduction of iron oxide, alumina, and barium titanate NPs-PU nanocomposites based on surface-initiated polymerization may improve the structural integrity of a nanocomposite through better chemical bonding between NPs and the polymer matrix with a uniform particle distribution [159, 160]. Jung et al. also reported that the synthesis of PU-MWCNT nanocomposites is a two-step process [161]. In the first step, a prepolymer was prepared from a reaction of MDI and PCL at 80 °C for 90 min. In the second stage, carboxylated MWCNTs were added to the prepolymer at 110 °C, and then reacted for 150 min to obtain the final cross-linked polyurethane-MWCNT nanocomposites.

In brief, incorporating a functional group is an effective way of reducing the surface energies of nanofillers and improving the compatibility of the organic and inorganic interfaces [162]. End grafting of polymers onto a solid surface is an important technique in many areas of science and technology, e.g., colloidal stabilization, adhesion, lubrication, tribology, and rheology. Recently, new techniques including anionic polymerization, cationic polymerization and atom transfer radical polymerization have been proposed and successfully applied to surface-initiated graft polymerization to synthesize nanocomposites. Generally, the two main strategies for the covalent grafting of polymers to NPs are “grafting to” and “grafting from” (described in detail in “Chap. 4”). The method of “grafting to” CNT defect sites indicates that polymers with reactive end groups can react with the

functional groups on NT surfaces. An advantage of the "grafting to" method is that preformed commercial polymers of controlled molecular weights may be used. The main limitation is that the initial binding of polymer chains hinders the diffusion of additional macromolecules to the CNT surfaces, leading to a low grafting density [162]. Also, only polymers containing reactive functional groups can be used. On the other hand, the "grafting from" technique involves the polymerization of monomers from surface-derived initiators on the MWCNTs or SWCNTs. These initiators are covalently attached via various functionalization reactions developed from small molecules including acid defect group chemistry and sidewall functionalization of CNTs [163]. The advantage of "grafting from" is that the polymer growth is not limited by steric hindrance, allowing efficient grafting of high-molecular-weight polymers. However, this method requires strict control of the amounts of initiator and substrate along with accurate control of conditions required for the polymerization reaction [164]. As described above, using other nanocomponents, such as magnetic and electromagnetic components and gold instead of CNTs, also enables the design of a multifunctional SMP that can be actuated by various external stimuli and will be fabricated according to a similar approach described in this section.

## 7.4 Characterization Methods

### *7.4.1 Mechanism of Thermally Induced SMPs*

A change in shape caused by a change in temperature is called a thermally induced shape-memory effect as described above. Although many stimuli were adopted to induce the shape-memory effect as described above, the main focus of this review article is on thermally driven shape-memory polymers because most systems are based on this type of phenomenon. Polymers that are chemically or physically cross-linked have elastic to large strain above $T_{switch}$, for example, $T_g$ and $T_m$ in amorphous and crystal materials with bulk thermal property. The associated modulus of elasticity is determined by the entropy of the polymer configuration that occurs with the deformation of the constituent polymer chain and is therefore called "entropy elasticity", which is often observed in rubber materials. For $T > T_{switch}$, polymer networks exhibit "superelasticity" based on the glass-rubber and crystal-amorphous transitions in polymers against temperature change. In this process, polymer chain segments between crosslinking points can freely deform and randomly twist via rotation in backbone bonds, maintaining a maximum entropy and minimum internal energy as macroscopic deformation occurs. The probability of a conformation, a strongly coiled conformation, which is the state for an amorphous linear polymer chain, can be described using the following equation:

$$S = K_B \ln \Omega, \tag{7.1}$$

where $S$, $K_B$ and $\Omega$ are entropy, Boltzmann's constant, and number of configurations, respectively. In addition, the resulting elastic shear modulus, $G$, can also be described using Eq. 7.2 according to the classical principle of rubber elastic theory:

$$G = \nu K_B T = \rho RT/M_c, \tag{7.2}$$

where $\nu$ is the number density of network chains, $\rho$ is the mass density, $R$ is the gas constant, and $M_c$ is the molecular weight between crosslinking points. This equation means that $G$ is proportional to both crosslinking density and temperature. A rubber usually has an elastic modulus of several MPa ($10^6$ N m$^{-2}$), a state that is very flexible and allows easier deformation under external force compared with that of shape-memory alloys (several hundred MPa). On the other hand, an ideal elastomer system will not change the inner energy when it is stretched. For this reason, the Helmholtz equation for the free energy, $U$, is reduced according to the following well-known equation:

$$U = -T\Delta S, \tag{7.3}$$

In the polymer network with a low degree of crosslinking, network points are sufficiently far away from each other; therefore, the change in free energy for the stretching of a standard volume can be described using the following equation [165]:

$$U = \frac{1}{2}NkT(\lambda_x^2 + \lambda_y^2 + \lambda_z^2 - 3), \tag{7.4}$$

where $\lambda_x$, $\lambda_y$, and $\lambda_z$ represent the elongation ratios in three dimensions. Also, $\lambda_{x,y,z}$ can also be converted to $(l/l_0)_{x,y,z}$ where $l$ represents the length of the segments between the network points in the stretching state, and $l_0$ is the unloaded state. Therefore, the shape-memory effect in a polymer is predominantly an entropic phenomenon. The changes in temperature and macroscopic shape in a typical dual-shape-memory cycle are described in Fig. 7.6. In its permanent macroscopic shape, the molecular chains of an SMP adopt conformations with the highest entropy, that is, the chains are thermodynamically stable. Upon heating above $T_{switch}$, the chain mobility is significantly activated. When an external deformation load is applied, the chain conformations are changed, leading to a lower entropy state and macroscopic shape change. When the SMP is cooled below $T_{switch}$, this lower entropy state (or the temporary shape) is kinetically trapped owing to the freezing of the molecular chain segments, resulting in the macroscopic shape fixation. Upon reheating above $T_{switch}$ under a stress-free condition, the molecular mobility is reactivated, which allows the chains to return to their highest entropy state, and therefore, recovered to the permanent shape. Here, the exact nature of chain conformation change during deformation has not been a major focus in the literature. One would, however, anticipate that this would strongly depend on the molecular structure of the SMP and may have to be considered on a case-by-case basis.

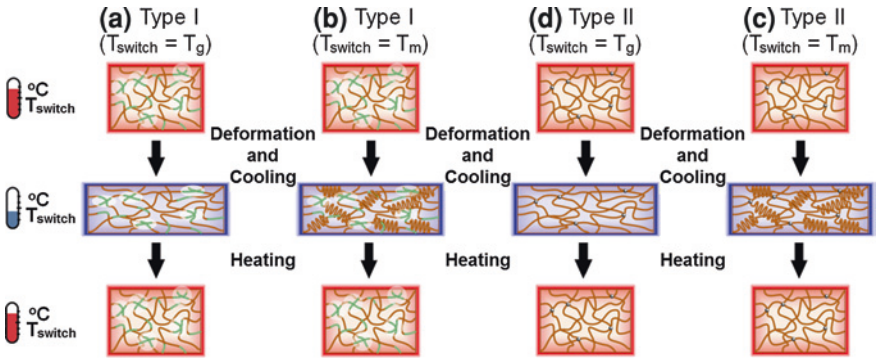


**Fig. 7.6** Molecular mechanisms of conventional thermally induced shape-memory effect in SMPs. Thermally induced shape memory effect of physically cross-linked **a** glassy and **b** (semi) crystalline networks and covalently cross-linked **c** glassy and **d** (semi)crystalline networks

For a polymer to display a dual shape-memory effect, it has to meet two structural requirements: (1) a reversible thermal transition for temporary shape fixing and recovery, and (2) a crosslinking network that sets the permanent shape. The first requirement allows the suppression and activation of the molecular mobility for entropy trapping and releasing in shape fixing and recovery, respectively. Polymers are in general intrinsically viscoelastic materials with at least one thermal reversible phase transition (glass transition or melting transition), with a few exceptions for which the polymer may decompose before it reaches the thermal transition temperature, that is, the thermal transition is practically nonexistent. From this viewpoint, most polymers meet the first requirement. On the other hand, the network that sets the permanent shape can be chemically and physically cross-linked. Without the crosslinking, the deformation force imposed onto a polymer above its thermal transition would lead to long-range chain slippage that is reflected as macroscopic material flow. Under such a condition, the polymer does change its macroscopic shape, yet with little or no change in polymer chain conformation (i.e., entropy). The entropic energy, which is the driving force for the shape recovery, is thus absent. As a consequence, the polymer would not possess the shape-memory effect. By prohibiting the long-range chain slippage, the crosslinking network ensures that the macroscopic shape change arises from entropy, which is recoverable. Complete prohibition of the long-range chain slippage is thus necessary for ideal shape recovery performance, as is often the case for the chemically cross-linked SMP system. By comparison, incomplete suppression of the long-range chain slippage would lead to compromised shape-memory behaviors. From these results, not only the shape-memory property but also thermal, mechanical (viscoelastic), and structural characterizations of SMPs are extremely important for designing and developing the SMP system from both basic and application viewpoints.

### 7.4.2 Thermal/Mechanical Properties

"Switching (transition) temperature" ($T_{switch}$) is the temperature at approximately which a material changes from one state to another. $T_{switch}$ could be either melting temperature ($T_m$) or glass transition temperature ($T_g$). In addition, "memory (shape fixing) temperature" ($T_{memory}$) is the temperature for fixing the temporary shape. $T_{memory}$ could be either glass transition temperature ($T_g$) or crystallization temperature ($T_c$). Although the relationship $T_{switch} > T_{memory}$ is a common interpretation in typical SMPs, strictly speaking, $T_{switch}$ and $T_{memory}$ to drive the shape-memory activation and fix the temporary shape are basically not different. Both glass-rubber ($T_g$) and crystal-amorphous ($T_m$ and $T_c$) transitions of materials are accompanied by a drastic change in mechanical properties. Therefore, understanding the thermal and mechanical properties or thermomechanical properties is essential. Here, we review some techniques for characterizing the thermal and mechanical properties.

Differential scanning calorimetry (DSC) is a technique based on monitoring the heat flux (power) to the sample over time or at various temperatures in a specified atmosphere. Practically, it is the difference in heat flux between a pan containing the sample and an empty pan as a reference. DSC can measure the material information (properties) as follows: (1) transition temperature: glass-rubber and crystal-amorphous transitions and (2) enthalpy change in the transition (Fig. 7.7a). $T_g$ is the temperature beyond which a polymer turns from a hard, glasslike state to a rubberlike state as described above. This effect is accompanied by a "stepwise" decrease and could be observed as the shift of the baseline of the DSC endotherm curve. For ease of comparison of conventional polymers, a single $T_g$ value taken from the midpoint of this broader transition is often used in the literature. However, since the width of the glass transition has a profound impact on the shape-memory performance of SMPs, it will be more appropriate to report the width of the transition along with the midpoint $T_g$ value, or to report the onset glass transition temperature ($T_{g\_onset}$) and the ending glass transition temperature ($T_{g\_end}$) along with the midpoint $T_g$ value. The melting temperature ($T_m$) is the temperature at which a material changes from solid (crystal) to molten liquid (amorphous), and is also characterized by DSC. Generally, it is well known that (semi)crystalline polymers generally melt over a wide temperature range because of the imperfections in the crystallites and nonuniformity in their size. From this reason, the smaller or less perfectly formed crystallites will melt at lower temperature. The endothermic fusion effect as measured by DSC is in many cases indicated by the temperature of the maximum heat flow (the $T_m$) and by the total heat involved in the fusion process (the $\Delta H_m$), as shown in Fig. 7.7a. Therefore, $T_m$ and enthalpy change of melting ($\Delta H_m$) in SMPs can be estimated from the peak top and area of a large endothermic peak attributed to the melting process of the polymer, respectively. If we know the melting enthalpy of a perfect polymer crystal ($\Delta H_{m100\ \%\ crystalline}$), the degree of crystallization ($X_c$) in the

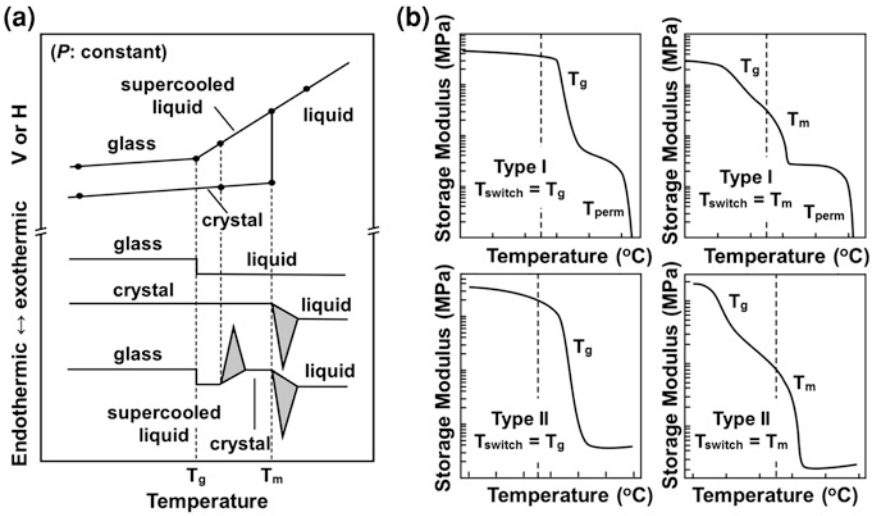


**Fig. 7.7** Thermal/mechanical property characterization of SMPs. **a**-*top* Volume (V) or enthalpy (H) against temperature (T) of a (semi)crystalline material under constant pressure. **a**-*bottom* Typical DSC curve of glassy and (semi)crystalline polymers. **b** Dynamic mechanical behavior of four types of SMP with different shape-memory mechanisms [26]

system can be calculated from the value of the estimated $\Delta H_m$ as in the following equation:

$$X_c(\%) = \Delta H_{m(\text{sample})} / \Delta H_{m100\,\%\,\text{crystalline}} \times 100. \tag{7.5}$$

On the other hand, the peak attributed to the crystallization can also be observed in the DSC curve of a semicrystalline polymer. It should be noted that the crystallization peak ($T_c$) is at a higher temperature than $T_g$ because the temperature above $T_g$ allows more freedom of movement of the polymer chain. The polymer chains have enough energy at the crystallization temperature to rearrange themselves from a random molecular arrangement into a more uniform pattern to form the crystal. This transition from amorphous to crystal was observed as the exothermic process in the DSC curve as shown in Fig. 7.7a. The degree of crystallization of the semicrystalline polymer can also be determined from a peak of exothermic crystallization [166]. These $T_g$, $T_m$ and $T_c$ are important parameters for designing and applying the SMPs for practical applications because those determine the $T_{switch}$ and $T_{memory}$ of the shape-memory effect. Therefore, the precise characterization of phase transition temperature such as $T_g$, $T_m$ and also $T_c$ in SMPs will be required for achieving a defined and accurate performance of SMP.

Although DSC measures the change in heat capacity, that is, the physical quantity related to the enthalpy, thermomechanical analysis (TMA) basically measures the change in coefficient of thermal expansion, which is the quantity based on the sample volume. Because the enthalpy and volume are equal thermodynamic parameters, TMA can also be applied to the measurement of transition

temperature, such as $T_g$, $T_m$ and $T_c$; however, TMA takes a step back compared with the DSC measurement. One of the reasons is that TMA does not characterize the proper change in volume, but characterizes the more macroscopic behaviors of dimension including thickness accompanied by the expansion/shrinking, softening, thermal deformation, fluidic behavior, and heat shrinking ratio of a drawn polymer unlike the DSC measurement. For this reason, TMA is a practical tool for property analysis rather than an analytical instrument.

The tensile test is probably the most extensively used method for the mechanical characterization of materials. In this test, tensile stress is applied to the specimen from its ends until it breaks while continuously recording the applied force and the elongation produced in the sample, thereby determining the stress-strain curve characteristic of each material. Stress ($\sigma$) is defined as the force exerted on the material per area. The ultimate tensile stress that leads to the tensile failure of an SMP, or the ultimate tensile strength, and the lowest stress that produces a permanent deformation in an SMP, or the yield strength, are both utilized in the characterization of SMPs. In addition, strain ($\varepsilon$) is defined as the deformation per unit length due to stress. The strain-to-failure value indicates the maximum strain that an SMP could reach under external stress. Modulus ($E$) is also referred to as Young's modulus or elastic modulus. It is the slope of the linear elastic region of a stress-strain curve obtained from the tensile test. $E$ changes significantly with temperature in thermal-responsive SMPs. The glassy or crystal state modulus of an SMP at a lower $T_g$ or $T_m$ can be several orders of magnitude higher than its rubbery or amorphous state modulus at a higher temperature. The other basic parameters determined in this test are the yield stress and yield strain (if it exists) and tensile strength and elongation. In addition, the shape-memory property can also be characterized by using the physical quantity obtained from the tensile test as discussed in "Sect. 7.4.4".

Alternatively, dynamic mechanical thermal analysis (DMA) can also be applied as the instrument to characterize the SMPs. In DMA, a sinusoidal stress is applied and the strain in the sample is measured, which is the stress-strain relationship similar to that in the tensile test, allowing one to determine the complex modulus including both viscosity and elasticity, that is, the viscoelastic property. The temperature of the sample or the frequency of the stress is often varied, leading to variations in the complex modulus. Because DMA measures the change in elastic modulus during the thermal transition, the thermomechanical property of SMPs can be characterized. In other words, both the transition temperature such as $T_g$, $T_m$ and $T_c$ and complex elastic modulus can be simultaneously estimated as shown in Fig. 7.7b. This complex elastic modulus ($G$) can be simply expressed using the following equation:

$$G = \left(G'^2 + G''^2\right)^{1/2}, \tag{7.6}$$

where $G'$ is the storage modulus and is a measure of the recoverable strain energy, which means the elastic property of the sample. When loading is sufficiently small, this value approximately equals the Young's modulus ($E$). $G''$ is defined as

the loss modulus and is related to the energy dissipation, which represents the viscosity of the sample. The phase angle (tan$\delta$) is also given by

$$\tan\delta = G''/G'. \tag{7.7}$$

This value can be used to judge whether the viscosity or elastic factor is dominant in the system. DMA can be applied to not only the solid but also the viscous liquid sample. Therefore, DMA is most commonly used to identify the location of transition that frequently has a significant effect on the modulus values. This similar thermomechanical investigation can also be performed using a tensile tester, which is described above as the part equipped with a thermochamber.

### *7.4.3 Structural Characterizations*

Not only the thermal and mechanical properties but also the identification of the structure composing the SMP system is important. The structural properties such as the molecular weight, composition, and component in a polymer or its network are characterized respectively using conventional methods, such as nuclear magnetic resonance (NMR), gel permeation chromatography (GPC), Fourier transform infrared (FT-IR) spectroscopy, and Raman spectroscopy. In the case of focusing on the surface of SMPs, X-ray photoelectron spectroscopy (XPS) and atomic force microscopy (AFM) are often used to characterize or directly observe the surface structure. On the other hand, as already discussed in "Sects. 7.2 and 7.3" (classification and synthesis methods, respectively), some SMP systems possess the phase-segregated or phase-separated structure. From this perspective, characterizing the structure of SMPs is also essential to identify the unique properties based on the structural features. One of the methods of characterizing the SMPs is the direct observation of those microstructures by microscopy.

Morphology is defined as the science of structural forms. The term is also used to designate different structural shapes. The morphology of polymer blends, block copolymers, semicrystalline polymers and liquid-crystalline polymers can be directly observed, and the microstructure is in most cases assessed without the need for a sophisticated model. At a lower magnification, coarser structural forms such as spherulites are observed using a polarizing microscope (POM) because the sizes of spherulites often fall in the micrometer range. A POM is equipped with two crossed polarizers. The first polarizer is located in front of the sample and the second, the analyzer, is located behind the objectives. Transmitted light phase contrast converts the refractive index difference in such samples into light and dark image regions. Therefore, POM could be used to study the morphology birefringence that disappears as the crystallites enter into the polymer melt. Changes in birefringence can be observed with a hot-stage microscope by using crossed polarizers. The point of disappearance of the last trace of birefringence can also be used to determine the crystalline melting temperature, that is, $T_m$. For example, Nagahama et al. have characterized the morphology of a phase structure

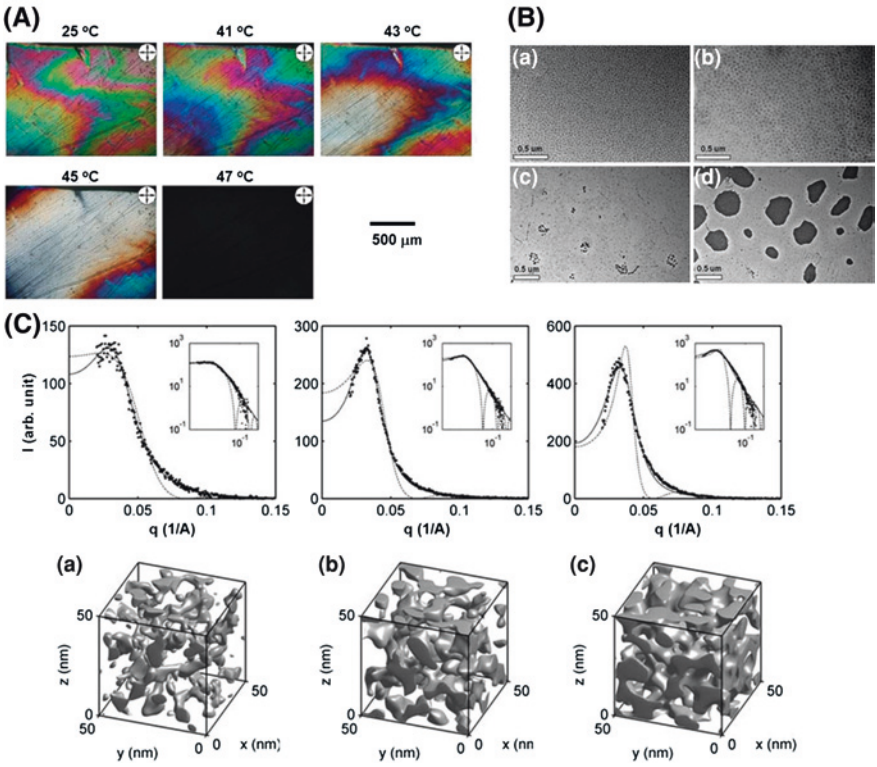


**Fig. 7.8** Structural characterization of SMPs. **A** Polarized optical microscopy (POM) images of cross-linked oligo-PCL-10 at various temperatures [167]. **B** TEM images of phase-segregated structures of SEBS/paraffin composites; **B-a** 100/0 **B-b** 80/20 **B-c** 50/50 and **B-d** 20/80 [170]. **C** Small-angle scattering patterns of samples (HDI/PCL/BDO) 3.5/1.0/2.0 (**C-a**), 6.2/1.0/5.2 (**C-b**), and 12.9/1.0/11.9 (**C-c**) measured at 70 °C, and their best fit with the clipped GRF model (*solid line*) and with the hard-sphere model (*dotted line*); in both cases, the volume fraction f was fixed to the value obtained from NMR. The *insets* show the same data on logarithmic scales. The *bottom row* shows realizations of the GRF model based on the fitted parameters [176]

in a branched oligo-CL (bOCL) and a cross-linked one (XbOCL) by POM [167]. The morphologies of their phase structures are significantly different depending on the chain length and the presence or absence of crosslinking. A unique morphology, which is the well-defined continuous birefringent domain of macroscopic size in all areas of the film, was observed in XbOCL with 10 CL units. More interestingly, this material showed cooperative and macroscopic transitions, with the birefringent domains persisting despite the increased temperature even though the temperature was in the range of the melting process estimated from DSC measurement, as shown in Fig. 7.8A. Other researchers also reported the POM observation of crystalline texture and morphological change against temperature in semicrystalline PU [168] and also a glassy thermoset system [169].

Transmission electron microscopy (TEM) is a technique analogous to optical microscopy, but uses an electron beam and electrostatic or electromagnetic lenses rather than a light beam and glass lenses, respectively. TEM can be useful for determining the morphology of a block copolymer or a blend system in SMPs, if there is sufficient contrast between the phases in the sample provided. Song et al. proposed a new strategy that utilizes the microphase separation of a block copolymer comprising styrene-*b*-(ethylene-*co*-butylene)-*b*-styrene (SEBS) and phase transition of small molecules, paraffins, for designing SMPs [170]. Because paraffins are midblock-selective molecules for SEBS, they did preferentially enter and swell EB blocks supporting paraffins as an excellent switch phase for the shape-memory effect. In this system, microstructures of SEBS/paraffin blends were clearly observed by TEM, as shown in Fig. 7.8B. In these TEM images, the dark characteristics correspond to styrene-rich microdomains, which were preferentially stained with electron-dense $RuO_4$, and it was found that those microstructures were strongly dependent on the amount of paraffin. In addition, TEM can also be useful for verifying the distribution and uniformity of organic/inorganic materials such as CNTs and magnetic nanoparticles especially in SMCs. Similarly to TEM, an image of the surface of a polymer can be produced by scanning electron microscopy (SEM). In this technique, a fine electron beam (5–10 nm in diameter) is scanned across the sample surface in synchrony with a beam from a cathode-ray tube. The scattered electrons produce an image with a depth of field that is usually 300–600 times greater than that of an optical microscope, and also enables a 3D image to be obtained. Most SEM have a magnification range from several tens to several million times. As most polymers are not good conductors, they sometimes need to be coated with a thin layer of a conduction material such as gold. The unique and regular patterns on the surface of SMPs as described in "Sect. 7.5.4", the shape-memory elastomeric composites with 3D fiber structure [171, 172] and the SMC system such as SMP with embedded micron-sized Ni powder chains [173] have been characterized by SEM.

Diffraction occurs when a wave encounters a series of regularly spaced obstacles that are capable of scattering the wave and have spacing that is comparable in magnitude to the wavelength of the radiation. X-rays have high energy and wavelength on the order of the atomic spacing for solids. When a beam of X-rays encounters a solid, a portion of the beam is scattered in all directions by the electrons associated with each atom that lies within the path of the beam. X-ray diffraction can be measured by using a diffractometer. Monochromatic X-ray radiation is produced by bombarding a metal target with a beam of high-voltage electrons. The intensities of the diffracted beams are detected by a counter mounted on a movable carriage. Its angular position is measured in terms of $2\theta$. As the counter moves at a constant angular velocity, a recorder plots the diffracted beam intensity as a function of $2\theta$ (the diffraction angle). Wide-angle X-ray diffraction (WAXD), which is also called wide-angle X-ray scattering (WAXS), is useful for obtaining information about semicrystalline polymers with a range of inter-atomic distances from 0.1 to 5 nm. The size of crystals can be determined from measurements of the relative intensities of the diffraction peaks in the crystalline region.

The crystallinity of a polymer and the distance between the parallel planes in the crystallites could also be calculated from WAXD. To evaluate the relative change in an amorphous region, one approach is to connect the lowest points between the diffraction peaks with a smooth curve such that the observed intensity is separated into crystalline and amorphous phases. Below the smooth curve is the amorphous component. The crystallinity $X_c$ is also given by the following equation:

$$X_c = \frac{\int s^2 I_c(s) ds}{\int s^2 I(s) ds}, \tag{7.8}$$

where s = 2sin$\theta/\lambda$, $I_c$(s) is the intensity of the crystal component, and $I$(s) is the intensity of the total component. The distance between the parallel planes in the crystallites $d$ could be calculated as

$$d = n\lambda/2 \sin\theta, \tag{7.9}$$

where $\theta$ is the incident angle, $\lambda$ is the wavelength of the radiation, and $n$ is an integer indicating the order of diffraction. This equation is well known as Bragg's equation. Thus, each element emits its own characteristic X-ray line spectrum, that is, it has the same d spacing value. This data could be used to identify the crystal structure of a polymer. In fact, our group has characterized the cross-linked CL-DLLA copolymer and PCL homopolymer system against temperature, and showed that the change in the crystallinity depended on their structure, and the disappearance of the crystal structure above $T_m$ was observed from the diffraction peaks of XRD (WAXD) [111, 130]. Small-angle X-ray scattering (SAXS) is also the same as WAXS (or WAXD) based on the X-ray scattering (diffraction). Small-angle scattering is a phenomenon whereby the elastic scattering of X-rays with sub-nanometer wavelength by a sample that has inhomogeneities in the nanometer range is recorded at very low angles of typically 0.1–10°. This angular range enables information about the shape and size of polymers, characteristic distances of ordered materials, pore sizes, and other data to be obtained. SAXS is also useful for characterizing the structure of SMPs as described below.

In multiblock copolymers, these crosslinks result from a phase segregation or separation of hard segments and switching segments, and these structures can be directly or indirectly observed by electron microscopy and X-ray diffraction as described above. Ping et al. discussed the influence of the hard segment type on the phase structure and shape-memory properties of PCL (semicrystalline polymer)-based shape-memory PUs [174]. In their work, for a sample with 30 % hard segment, they suggested that the microphase separation gave rise to the morphology of interconnected hard-segment domains from the results of rheological measurement. This fact was experimentally confirmed by Ji et al. on the basis of thermal characterization and SAXS, and revealed the better shape-memory properties of samples in which the hard-segment domains are disconnected [119]. However, these data analyses either lacked a detailed morphological interpretation, or relied on the assumption of a lamellar morphology. As shown by these studies, not only the characterization of the morphological structures but also their

deformation and shape-memory properties in SMPs have been proposed by structural analysis [175]. Recently, D'Hollander et al. have approached the modeling of the morphology and mechanical behavior of shape-memory PUs based on the technical combination of solid-state NMR and synchrotron SAXS/WAXD [176]. In this study, the SAXS data could be easily and properly interpreted using the data provided by solid-state NMR. Importantly, this report is the first complete description of the shape-memory PU phase morphology as a function of the hard-segment content, relying on advanced morphological models and SAXS data interpretation procedures, as shown in Fig. 7.8C. Temperature- and strain-dependent synchrotron WAXD was also used to corroborate the suggested micromechanical models. Because the morphological model (Fig. 7.8C) proposed by D'Hollander et al. enables the material's mechanical and shape-memory behaviors during repeated cycles to be explained, the importance of the structural characterization of SMPs is strongly suggested.

### *7.4.4 Determination of Shape-Memory Ability*

In essence, the shape-memory property is a combination of thermal and mechanical properties as described in this section. The extent to which a deformation can be fixed as a temporary shape and the recoverability of the permanent shape are the most important properties determined for quantifying the performance of SMPs on the macroscopic level. These properties depend on parameters of the procedure of shape-memory creation, such as thermal conditions, kinetics, and type of mechanical deformation. The standard procedure for the investigation of shape-memory performance is based on the characterization of the stress-strain-temperature ($\sigma$-$\varepsilon$-$T$) relationship [31, 177]. Derived from this basic procedure, the most common quantification of the shape-memory performance is presently described as the percentage of strain fixing (strain fixation ratio $R$f) and extent of strain recovery (strain recovery ratio $R$r) determined in cyclic thermomechanical tensile tests [110]. The measurements are generally performed by using a tensile tester equipped with a thermochamber.

This test includes a programing module, which is the creation of temporary shape, and a recovery module, which is the recovery of the permanent shape. Although the programming module can be performed under stress- or strain-controlled conditions, the recovery module can be carried out under stress-free conditions or under constant strain. By these combinations of programming module and recovery module, different and much information can be obtained by cyclic thermomechanical tests. In addition, it is well known that different test protocols, such as cold drawing ($T < T_{\text{switch}}$) or a heating-stretching-cooling ($T > T_{\text{switch}} \rightarrow T < T_{\text{memory}}$) process, whereby cooling can be performed under stress or strain control, influence the obtained information [84]. A strain-controlled thermomechanical test allows the changes in strain to be recorded. On the other hand, in a stress-controlled thermomechanical test, it allows the stress on the

sample to be measured under defined thermal conditions, as shown in Fig. 7.9A. A typical test protocol is as follows: (*Step* 1) The sample is heated to a temperature above the $T_{switch}$ and is stretched to the maximum strain $\varepsilon_m$. In the case of physically cross-linked SMPs, it is important not to exceed the highest thermal transition $T_{perm}$, which would cause the polymer sample to melt and lose its shape. (*Step* 2) The sample is cooled below the $T_{memory}$ under constant strain $\varepsilon_m$ to $T_{low}$, thus fixing the temporary shape. (*Step* 3) The applied stress of the sample returns to zero, that is, unloading occurs, by retracting the clamps of the tensile tester at $T_{low}$. (*Step* 4) The sample is heated from $T_{low}$ to $T > T_{switch}$, which allows the recovery from temporary shape to original shape. (*Step* 5) After the permanent shape is recovered, the next cycle then begins again.

If retracting the clamps of the tensile tester to the original distance of 0 % strain causes the sample to bend between *step* 3 and *step* 4, the result of such a measurement is usually presented in a stress ($\sigma$)-strain ($\varepsilon$) curve. This is the reason why this test protocol is called a "two-dimensional (2D) measurement". Figure 7.9B represents this schematic curve. Different effects can result in changes in the curve, particularly when the stretched sample is cooled (region 2 in Fig. 7.9B). Among others, the following effects play a role in these changes: differences in the expansion coefficient of the stretched sample at temperatures above and below $T_{switch}$ as a result of entropy elasticity, as well as volume changes arising from crystallization in the case of $T_{memory}$ being a $T_c$ in semicrystalline SMPs. In addition to the elastic modulus $E$ above the $T_{switch}$, which can be determined from the initial slope in the measurement region 1 in Fig. 7.9B, the elastic modulus of the stretched sample at $T_{low}$ can also be determined from the slope of the curve in region 3 in Fig. 7.9B. The important quantities to be determined for describing the shape-memory performance of the material are the strain fixing ratio and the strain recovery ratio.

The shape fixing ratio ($R_f$) can be determined to quantify the effect of programming. $R_f$ describes the ability to fix the mechanical deformation, which has been applied during the programming process, i.e., $R_f$ is equal to the amplitude ratio of the fixed deformation to the total deformation ($\varepsilon_m$ in Fig. 7.9B, C), according to the following equations.

Strain-controlled test:

$$R_f(N) = \frac{\varepsilon_u(N)}{\varepsilon_m} \tag{7.10}$$

Stress-controlled test:

$$R_f(N) = \frac{\varepsilon_u(N)}{\varepsilon_l(N)} \tag{7.11}$$

In a strain-controlled programming protocol, $R_f$ is given by the ratio of the strain in the stress-free state after the withdrawal of the tensile stress in the $N$th cycle $\varepsilon_u(N)$ to the maximum strain $\varepsilon_m$. In the case of a stress-controlled programming protocol, $R_f$ is given by the ratio of the tensile strain after unloading, $\varepsilon_u(N)$, to the maximum strain at $\sigma = \sigma_m$ after cooling to $T_{low}$, $\varepsilon_l(N)$ [69].

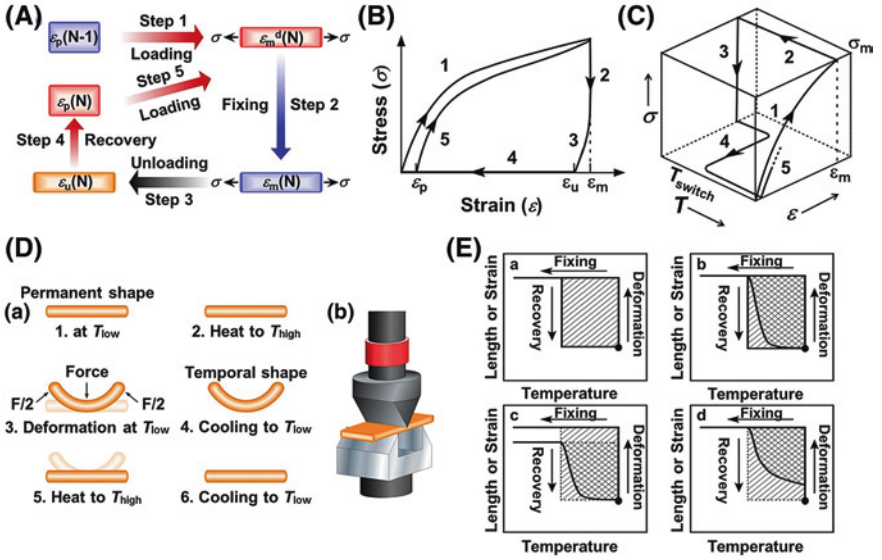


**Fig. 7.9** Shape-memory performance characterizations. **A** Programming steps in a stress-controlled cyclic thermomechanical test of SMP. Representative **B** two-dimensional (2D) and **C** three-dimensional (3D) plots for presenting cyclic thermomechanical test [110]. **D** Scheme of a three-point flexural test. **D-a** Scheme of the shape-memory effect (SME) in polymers as defined by four critical temperatures. $T_g$ is a material property. $T_{low}$ is always less than $T_g$, whereas $T_{high}$ may be above or below $T_g$, depending on the desired recovery response. **D-b** Schematic of the three-point flexure thermomechanical test setup [179]. **e** Classifications of shape-memory polymers by their shape fixing and shape-recovery abilities. **E-a** Ideal shape-memory material; **E-b** shape-memory material with excellent shape fixing and shape recovery; **E-c** shape-memory material with excellent shape recovery but poor shape fixing; **E-d** shape-memory material with attractive shape fixing but poor shape recovery. The fill factor is defined as $f_{sm} = A_{cross\text{-}hatch}/A_{ideal}$ [26]

The shape recovery ratio ($R_r$) quantifies how well the permanent shape has been memorized, which is a measure of how far a strain that was applied in the course of the programming is recovered as a result of the shape-memory effect. $R_r$ can be described using the following equations.

Strain-controlled test:

$$R_r(N) = \frac{\varepsilon_m - \varepsilon_p(N)}{\varepsilon_m - \varepsilon_p(N-1)} \tag{7.12}$$

Stress-controlled test:

$$R_r(N) = \frac{\varepsilon_l(N) - \varepsilon_p(N)}{\varepsilon_l(N) - \varepsilon_p(N-1)} \tag{7.13}$$

In a strain-controlled protocol, the strain that occurs during the programming step in the $N$th cycle $\varepsilon_m - \varepsilon_p(N-1)$ is related to the change in strain that occurs during the

present process of shape-memory effect $\varepsilon_m - \varepsilon_p(N)$. The strain of the samples in two successively passed cycles in the stress-free state before application of yield stress is represented by $\varepsilon_p(N-1)$ and $\varepsilon_p(N)$. In the case of a stress-controlled programming and stress-free recovery after cooling to $T_{low}$ of the $N$th cycle $\varepsilon_l(N)$, the shape recovery ratio $R_r$ quantifies the ability of the material to memorize its permanent shape. For this purpose, the change in strain that occurs during the programming step in the $N$th cycle $\varepsilon_l(N) - \varepsilon_p(N)$ is compared with the change in strain, which occurs as a result of the shape-memory effect $\varepsilon_l(N) - \varepsilon_p(N-1)$.

An important variable, which is $T_{switch}$, cannot be determined by a 2D measurement in a thermomechanical test. In this respect, the three-dimensional (3D) test record is interesting, and is shown schematically in Fig. 7.9C. In contrast to the 2D measurement, the sample is cooled in a controlled way at a strain of $\varepsilon_m$ and a constant tensile stress $\sigma_m$. The change in strain in this region is influenced by the temperature dependence of the coefficient of thermal expansion of the stretched polymer and volume effects based on the thermal transition as described above. Having reached $T_{low}$, the strain is driven back until a stress-free state is reached. The sample is then heated to $T_{perm}$ in a controlled way. In the course of this experiment, the tensile stress is kept constant at 0 MPa, which means that the clamps follow the movement of the test piece. The mechanical movement occurring in the course of the shape-memory effect is recorded as a function of temperature. Both the temperature interval as well as $T_{switch}$ in which the shape-memory effect takes place can be determined from the interpretation of the $\varepsilon$-$T$ plane of the $\varepsilon$-$T$-$\sigma$ diagram. Generally, the first few cycles can differ from each other in cyclic thermomechanical tests as shown in Fig. 7.9B, C. However, the curves become more similar with increasing number of cycles. The process of deformation and recovery of the permanent shape becomes highly reproducible. The changes in the first few cycles are attributed to the history of the sample, thus, processing and storage play an important role. During the first cycles, a reorganization of the polymer on the molecular scale takes place, which involves deformation in a certain direction. Single polymer chains arrange in a more favorable way in regard to the direction of deformation. Covalent bonds may be broken during this process.

Other tests to characterize the shape-memory performance are based on bending the polymer samples. In the course of the bending test, a sample is bent at a given angle $\theta_i$ at a temperature above the switching transition and is kept in this shape. The so-deformed sample is cooled to a temperature $T_{low} < T_{memory}$ and the deforming stress is released. Finally, the sample is heated to the measurement temperature $T_{perm} > T_{trans}$ and the recovery of the permanent shape is recorded. The deformation angle $\theta_f$ varies as a function of time. According to the method of evaluating the shape-memory behavior of the shape-memory alloy [178], Lin and Chen have defined that the recovery bending ratio $R_b$ is calculated from the ratio of the different angles before and after recovery $\theta_f$ and the deformation angle $\theta_i$ in the temporary shape as in the following equation [34, 35]:

$$R_b = \frac{(\theta_i - \theta_f)}{\theta_i}. \tag{7.14}$$

Although this characterization method is a rather simple bending test, there is another more complex system that is a three-point flexural test as shown in Fig. 7.9D. Three-point flexural tests provide values for the modulus of elasticity in bending, flexural stress, flexural stain, and the flexural stress-strain response of the tested material [179, 180]. Therefore, this test can be used to determine the strain recovery and stress recovery ratios. As shown in Fig. 7.9D, this test is based on the three-point flexure loading, which allows reasonable stress/strain levels in the sample for the temperature range spanning from the glassy to the rubbery state. In fact, the polymers, which are photopolymerized materials synthesized from a *tert*-butyl acrylate monomer with a moderate amount of a diethyleneglycol diacrylate crosslinker, show a sigmoidal free strain recovery response as a function of increasing temperature at a constant heating rate [179]. Free strain recovery was determined to depend on the temperature during predeformation; lower predeformation temperatures ($T < T_g$) decreased the temperature required for free strain recovery. The lower temperature required for recovery may be used to deploy polymers within the body even when they have relatively high $T_g$ values. Constrained stress recovery shows a complex evolution as a function of temperature, and also depends on the temperature during predeformation. Stress recovery after low-temperature predeformation ($T < T_g$) shows a peak in the generated recovery stress, whereas stress recovery after high-temperature predeformation ($T > T_g$) is sigmoidal. The stress recovery peak after low-temperature deformation may be exploited in biomedical applications requiring elevated forces during deployment. The isothermal free strain recovery, as a function of time, was found to increase with increasing temperature or decreasing predeformation temperature. Therefore, Gall et al. have concluded that the isothermal recovery results provide a guideline for the fraction of strain recovery expected for a given temperature, relative to $T_g$ [179]. Although a drawback is that the stress and strain are nonuniform and therefore more difficult to analyze, other advantages are that many applications that involve bending and large displacements can be achieved in flexure at much more modest strain levels.

The heat-induced shrinking ability of polymers is an important factor mainly in the field of encapsulation, and is being utilized in various applications. Because this ability has a strong correlation with their elastic (shape) memory, this is also one of the important values for shape-memory performance [181–183]. This shrinkage determination of heat-shrinkable materials is based on the following process: The test samples stretched at room temperature are kept under a constant stress and heated above $T_{switch}$. For example, in the case of polyethylene crosslinked by ionizing rays, which is one of the major heat-shrinkable materials, the material is heated above the $T_m$ of the polyethylene crystallites. The heat shrinkage ($S_h$) is then given by the ratio as shown in the following equation:

$$S_h(\%) = \frac{l_{strech} - l_{shrink}}{l_{strech} - l_0} \times 100 = \frac{l_{strech} - l_{shrink}}{l_{strech}(1 - \lambda^{-1})}, \tag{7.15}$$

where $l_{strech}$ is the length of the sample after stretching, $l_{shrink}$ is the length of the sample after shrinking, $l_0$ is the original length of the sample, and $\lambda = l_{strech}/l_{shrink}$.

Moreover, instead of the original length of the sample $l_0$, the stretching ratio λ, the ratio of the length of the stretched sample $l_{\text{strech}}$ to $l_0$, is used. The shrinkage process depends on the temperature $T_{\text{high}}$. Therefore, the shrinkage $l_{\text{shrink}}$ $(t)$ is often determined as a function of time for a given shrinkage temperature $T_{\text{high}}$.

Although many researchers have tried to quantify the shape fixing and recovery of their systems, most of the quantifications are limited to the percentage of shape fixing and extent of shape recovery, although some have endeavored to assess the speed of shape recovery. However, no standard method has been published on the overall performance of shape-memory polymers for comparison of one system with the next. Mather's group has newly proposed a shape-memory cycle analysis method to characterize and compare the shape-fixing and shape-recovery abilities in a standard way [26]. A schematic shape-memory cycle is shown in Fig. 7.9E, which is a projection from a three-dimensional, length–temperature–force plot of Fig. 7.9C. Beginning at the point denoted with a closed circle, a sample is first loaded from a small preload to a certain stress at a constant stress rate and a temperature of $T_{\text{swtich}}$ +20 °C. This is indicated by the deformation process in Fig. 7.9E. The sample is then subjected to this stress for a period of time until equilibrium to reveal any creep. The stretched sample is then cooled to $T_{\text{switch}}$ −20 °C at a constant cooling rate (fixing process in graph) under the stress. Following equilibration, the stress is then released, and length shrinkage (if any) is observed. The sample is finally heated to $T_{\text{switch}}$ +20 °C at a constant heating rate (they recommend 2 °C $\text{min}^{-1}$), and the prescribed stress (usually negligible compared with the maximum stress) and shape-recovery profile upon heating are recorded (recovery process in graph). Besides conventional visual comparison of the shape fixing and shape recovery extents by inspection, they define shape fixing with reference to Fig. 7.9E as

$$R_{\text{f}}(\%) = (L_{\text{u}} - \text{L}_{\text{i}})/(L_{\text{t}} - L_{\text{i}}) \times 100 \tag{7.16}$$

and shape recovery ratio as

$$R_{\text{r}}(\%) = (L_{\text{u}} - \text{L}_{\text{f}})/(L_{\text{t}} - L_{\text{i}}) \times 100, \tag{7.17}$$

where $L_{\text{i}}$ is the initial length, $L_{\text{t}}$ is the temporary length, $L_{\text{u}}$ is the unloaded length, and $L_{\text{f}}$ is the final recovered length. Besides defining the extent of fixing and recovery, each being its own figure-of-merit, they also define a more inclusive figure-of-merit, termed "shape-memory fill-factor ($f_{\text{m}}$)", allowing classification of shape-memory materials into five types, according to performance, as shown in Fig. 7.9E. The five classes of shape-memory materials are (E-a) ideal shape-memory material (E-b) shape-memory material with excellent shape fixing and shape recovery but finite sharpness (E-c) shape-memory material with excellent shape recovery but poor shape fixing (E-d) shape-memory material with attractive shape fixing but poor shape recovery, and (E-other) shape-memory material with both poor shape fixing and shape recovery (figure not shown). Mather's group define fill factor, $f_{\text{m}}$, as the ratio of the cross-hatched $L$–$T$ (or strain-$T$) areas to the hatched $L$–$T$ area as in the following equation:

$$f_{\text{m}} = \text{Area}_{(\text{cross-hatch})}/\text{Area}_{(\text{ideal})}, \tag{7.18}$$

where the ideal system (E-a) case is as an overall figure-of-merit for shape-memory materials. An ideal shape-memory polymer, with the same workability as the work input, thus has a $f_m$ of 1.0, while an extremely poorly fixed sample, such as a rubber band without any shape-fixing ability and, hence, no shape recovery occurring later has a $f_m$ of 0. They also define that a realistic "good" shape-memory polymer demonstrates a fill factor of about 0.5. Several points bear mentioning at this stage. First, measurements of $f_m$ are sensitive to the selection of temperature limits and care should be taken to ensure consistency. Second, a higher fill factor is not necessarily a better solution for a particular application of SMPs. For example, if a slow, prolonged recovery event is needed, then the response shown schematically in Fig. 7.9E-b would be better than that shown in Fig. 7.9E-a, that is, a lower $f_m$ would be better.

Thus far, we have discussed the characterization of shape-memory performance in two-way-type SMPs. In 2006, Bellin et al. discovered that two distinct thermal transitions in a cross-linked network can be independently utilized to fix and recover two temporary shapes, all in one shape-memory cycle [184]. This is called the triple-shape-memory effect, indicative of a total of three shapes involved (including the permanent shape). The triple-shape-memory effect represents more or less an extension of the traditional dual-shape-memory effect, which relies on one thermal transition for one temporary shape. In retrospect, the timing of the discovery is thus somewhat surprising given the long history of SMP. The significance of the triple-shape-memory effect, however, cannot be overemphasized since it has the potential to drastically impact the technological development. Xie and co-workers have proposed the triple-shape-memory effect and the quantitative triple-shape cycle, as illustrated in Fig. 7.10a for a cross-linked polymer with two distinctive $T_g$s (38 and 75 °C) [185, 186]. Relative to the dual-shape cycle that has one shape-fixing step and one shape-recovery step as discussed above, a triple-shape cycle comprises two shape-fixing steps and two shape-recovery steps. In the two-step shape-fixing process in the photographs shown in Fig. 7.10a, the permanent shape "A" was first heated to $T_{high}$ (90 °C, above both $T_g$s) and deformed by imposing a first stress. Cooling under this stress to $T_{mid}$ (56 °C, between the two $T_g$s) and releasing the stress fixed the temporary shape "B", corresponding to $\varepsilon_B$. In the second fixing step, shape "B" was further deformed by imposing a second stress that is different from the first stress. This stress is maintained while the sample is cooled to $T_{low}$ (20 °C, below both $T_g$s). Removal of the second stress after cooling led to temporary shape "C" ($\varepsilon_c$). Here, the vitrification of the high-$T_g$ component at $T_{mid}$ and the low-$T_g$ component at $T_{low}$ was responsible for fixing "B" and "C", respectively. Shape recovery, on the other hand, is conducted under a stress-free condition. Heating of shape "C" to $T_{mid}$ yields the recovered shape "B" ($\varepsilon_{Brec}$). Further heating of the recovered shape "B" to $T_{high}$ leads to the recovered shape "A" ($\varepsilon_{Arec}$). With X and Y denoting two different shapes, the respective shape fixation ($R_f$) and shape recovery ($R_r$) can be calculated with the following equations using the thermomechanical data from the results of a thermomechanical test, as shown in Fig. 7.10(a):

$$R_f(X \rightarrow Y) = (\varepsilon_y - \varepsilon_x)/(\varepsilon_{y\,load} - \varepsilon_x), \tag{7.19}$$

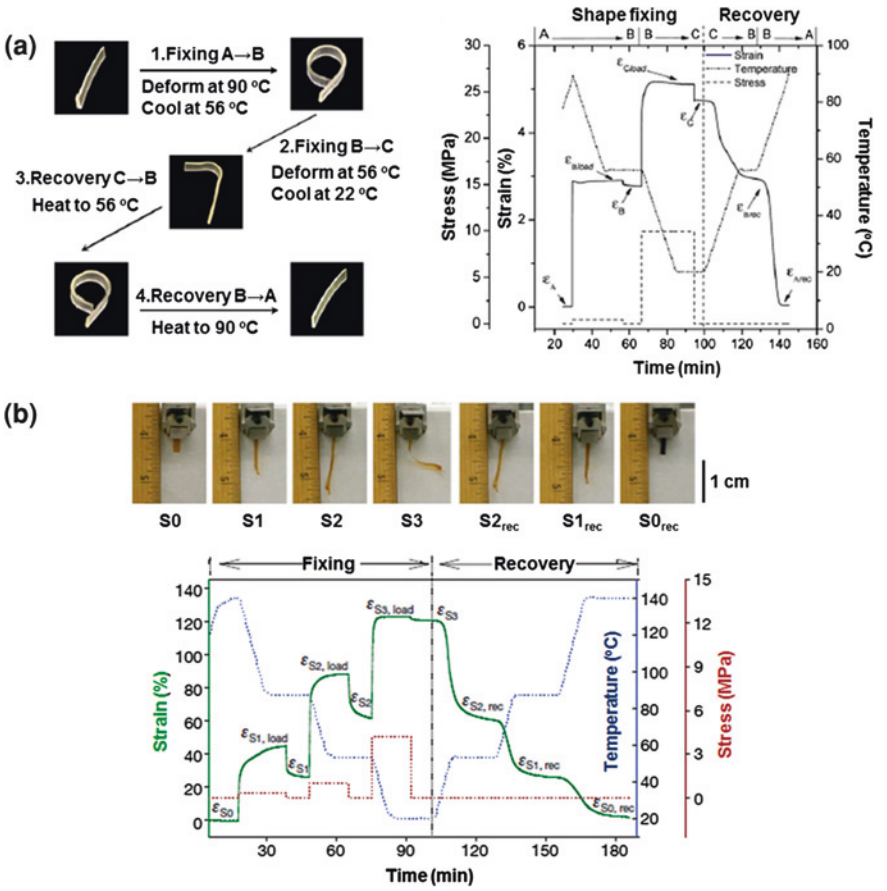


**Fig. 7.10** **a** Photographs of triple-shape memory effect and quantitative thermomechanical test [186]. **b** Photographs and quantitative thermomechanical test of quadruple-shape-memory properties of perfluorosulphonic acid ionomer (PFSA) [187]

$$R_r(Y \rightarrow X) = (\varepsilon_y - \varepsilon_{x\,rec})/(\varepsilon_y - \varepsilon_x), \tag{7.20}$$

where $\varepsilon_{y\,load}$ represents the maximum strain under load, $\varepsilon_y$ and $\varepsilon_x$ are fixed strains after cooling and load removal, and $\varepsilon_{x\,rec}$ is the strain after recovery. In addition, Xie et al. [187] have recently reported that perfluorosulphonic acid ionomer (PFSA), which has only one broad reversible phase transition, exhibited dual-, triple-, and at least quadruple-shape-memory effects, all highly tunable without any change in the material composition as shown in Fig. 7.10b. They also successfully demonstrated the quantification of shape-memory performance in triple- or quadruple-shape-memory effect. These studies mean that, using a combination of temperature and strain control during the shape-fixing step, it is potentially possible to manipulate the transition temperature, which would lead to tunable shape recovery

behavior. Therefore, PFSA is an attractive SMP that has been largely unnoticed until recently, and these concepts suggest strategies for expanding tunable multishape-memory effects to a broad range of polymers, the availability of which could significantly expand the technical potential for shape-memory polymers.

## 7.5 Applications of Shape-Memory Materials

As a novel kind of smart material, SMPs currently cover a broad range of applications especially in medicine and biotechnology. Particularly in 2002, Lendlein and Langer demonstrated the concept of biodegradable thermally responsive SMP sutures [24]. Many researchers are getting into SMPs to introduce biocompatibility and biodegradability to implant materials as well as minimally invasive surgical procedures in biomedical applications, which has led to substantially improved health care. In addition, SMPs also present additional potential in the area of micro-electro-mechanical systems (MEMS), actuators, self-healing, unique adhesion devices and cell culture platforms.

### *7.5.1 Implantable SMP Devices*

The aging population in Japan is not only driving the medical care and pharmaceutical industry but also the medical devices market. Currently, the medical devices market in Japan is worth about 2.3 trillion yen, according to the report "Attractive Sectors Healthcare" by the Japan External Trade Organization (JETRO). It is ranked third, following those of the USA and Germany. According to the Ministry of Health, Labor and Welfare, the market size is expected to reach about 3 trillion yen by 2015. The USA and Germany are the only countries that import more medical equipment than Japan. Conversely, Japan is the eighth largest exporter of medical devices in the world. A rapidly ageing population has burdened the healthcare system in terms of both funding and facilities. As a result, payments made by the government to medical institutions have been slashed. The growing number of patients requiring long-term care and the advent of the elderly health insurance system offers great potential within the market. Japan has the most expensive medical equipment in the world. It should however be kept in mind that some of the reasons for this lie with a distribution system that hikes up retail prices with hidden costs. An awkward regulatory system, a slow approval process and cultural differences have often put off overseas investors, although recent legislation has attempted to address many access difficulties. In this interdisciplinary field, scientists, medical doctors, and engineers are continually looking to new materials to increase device performance and functionality. Biocompatibility has been defined as having an inert biological response as well as the desired and manipulatable response [188]. Polymeric materials have been developed into multiplatform

technologies to offer biomedical materials with multifunctionality [189, 190]. For example, in addition to a structural role, polymeric medical devices offer biodegradability and enable controlled therapeutic drug release [191, 192].

Polymeric medical devices can also be engineered to elicit a shape-memory effect. SMPs are a class of mechanically functional "smart" materials that can recover relatively large strains in response to a stimulus. The activating stimulus can include temperature, pH, humidity, light, electric power, or other means capable of facilitating molecular motion and enabling shape recovery. SMPs have most notably been promoted owing to their potential in minimally invasive surgery, where a compacted device could be passed through a smaller incision and deployed to its full shape once inside the body. For biomedical devices, the heating of the polymer to activate the shape-memory effect has been proposed via body heat [128, 193], optical/laser heating [194, 195], and remote inductive heating [99, 196]. Other SMP biomedical device reviews have primarily summarized proposed devices and material chemistries [197]. The intent of this section is to focus on the importance and benefits of using SMPs for implantable medical devices. Furthermore, the development status of these devices is covered along with fundamental studies aimed at bringing these devices closer to the market.

Stents are expandable scaffolds designed to prevent vasospasms and restenosis of a vessel after balloon angioplasty. Stenosis is defined as the narrowing of a blood vessel often caused by coronary artery disease (atherosclerosis), in which plaque builds within the arterial wall and constricts the flow of blood. Stenting was first performed in 1986 by Sigwart et al. and was designed to eliminate elastic recoil and negative remodeling caused by angioplasty alone [198]. Since this pioneering surgery, stenting has been one of the most revolutionary and rapidly adopted medical interventions of all time [199]. The first study and first clinical trial of an SMP stent may have occurred as a result of an unexpected artifact during a clinical trial of a poly(L-lactide) (PLLA) stent. A study of the Igaki–Tamai stent, which is a balloon-expandable PLLA stent, was published in 2000, in which the authors documented the stent's ability for self-expansion, as shown in Fig. 7.11a [200, 201]. Furthermore, the deployment time was recorded as a function of temperature, with the stent deploying in 0.2, 13, and 1200 s at 70, 50, and 37 °C, respectively. However, because the full processing and packaging conditions of the PLLA stent were not reported, it is difficult to separate out shape recovery from viscoelasticity. More importantly, the authors demonstrated the feasibility and efficacy of a pure polymer stent manufactured from a shape-memory material, which was successfully implanted into 15 patients and monitored over 6 months without major cardiac events. On the other hand, because the use of polymers in stent design led to the breakthrough of Drug Eluent Stents (DESs), researchers have proposed the use of pure polymer stents. The potential advantages of pure polymer stents over bare metal stents include increased biocompatibility, biodegradability, increased drug loading, enhanced compliance matching, reduced cost, ease of fabrication for patient-specific devices, molecular surface engineering, and the use of the shape-memory effect. Wache et al. first reported the development of an SMP stent as a new vehicle for drug delivery in

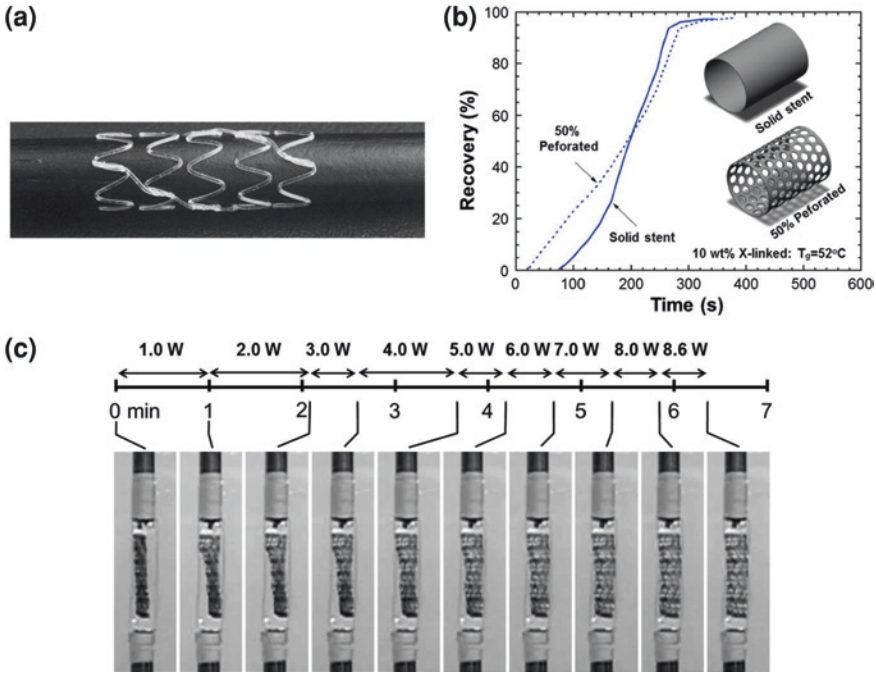


**Fig. 7.11** **a** The Igaki–Tamai stent is a premounted, ballon-expandable PLLA stent that also has self-expansion ability [200]. **b** Recovery property of solid and perforated stents at 37 °C [193]. **c** Photographs of stent deployment. Timeline of SMP stent deployment in the mock artery (zero flow) as the laser power was gradually increased (Laser duration was approximately 6.3 min) [195]

2003 [202]. Prototype stents were manufactured using a thermoplastic PU, which was injection molded, extruded, then tested in vitro. In this study, the activation temperature was set in close proximity to body temperature, although the details on optimizing the shape-memory effect were not reported. On the other hand, Gall et al. reported the fabrication of SMP stents, in which the shape-memory effect of thermoset PMMAs is well characterized [179] and applied to the unconstrained recovery of SMP stents in an in vitro setup [193]. They demonstrated the use of the shape-memory effect in polymers for cardiovascular stent interventions to reduce the catheter size for delivery and offer highly controlled and tailored deployment at body temperature. Actually, covalently cross-linked networks were synthesized via photo-polymerization of *tert*-butyl acrylate and PEGDMA to provide precise control over the thermomechanical response of the system. The free recovery response of the polymer stents at body temperature was also shown as a function of $T_g$, cross-linking density, geometrical perforation, and deformation temperature, all of which can be independently controlled as shown in Fig. 7.11b. Room-temperature storage of the stents was shown to be highly dependent on $T_g$ and crosslink density. In addition, the deformation recovery rate of the stents was shown to increase with respect to decreasing $T_g$ and increasing storage modulus

of recovery ($E'_r$), although the strain storage was adversely affected by the same conditions (decreased $T_g$ and increased $E'_r$). Finally, they concluded that this polymer system exhibits a wide range of shape-memory effect and thermomechanical responses to adapt and meet specific needs of minimally invasive cardiovascular devices. As another approach in SMP stents, Baer and co-workers demonstrated the SMP prototypes that were fabricated from thermoplastic PU for neurovascular stents [203, 204]. In these studies, they proposed the use of SMPs owing to their high degree of compliance for navigating a stent through the tortuous neurovasculature. The forces on the stent during deployment and after implantation were then evaluated and verified experimentally. In addition, they newly developed a thermoplastic polyurethane that was tested in a mock artery and deployed via laser heating, that is, laser-activated stents, as shown in Fig. 7.11c [195]. The stent was incapable of full deployment owing to convective losses under flow conditions. However, a considerable amount of work was put into investigating the amount of heat and power needed to activate the stent via a laser without damaging the surrounding vasculature. Other new proposals and the feasibility of SMPs for stenting have been studied by many groups. Aside from the obvious strict biocompatibility and hemocompatibility requirements needed for regulatory approval, future work still needs to be performed on the long-term efficacy of SMP stents. Of course, future studies on SMP stents should include not only fatigue (stability) test but also in vivo experiments performed on animal models.

Each year, over 130,000 Japanese people die from a stroke and it is a disease that is one of the main causes of death according to the statistical data from Ministry of health, Labour and Welfare in Japan. Most ischemic strokes are caused by thrombotic vascular occlusion, which is the formation of a blood clot, in the arterial network supplying the brain [205]. Interruption of blood flow in these vessels deprives the brain of oxygen, often resulting in permanent disability. Traditionally, treatment has been limited to the administration of a recombinant tissue plasminogen activator such as t-PA, a thrombolytic (clot-dissolving) drug that is infused over a 1 h period into the systemic circulation. Clinical protocol requires that treatment may only be initiated within 3 hours of the onset of symptoms [206–210]. Other mechanical thrombectomy methods, including photoacoustic thrombolysis [211, 212], capture of the clot using a snare device [213] or a nitinol wire, which is an SMA, basket [214], and a saline jet device to fragment and aspirate the clot [215], are under investigation. In addition to expanding the patient population eligible for treatment, these and other nonpharmacological means of vessel reperfusion may offer a faster, safer alternative to thrombolytic drug therapy after ischemic stroke. From these perspectives, Maitland and coworkers demonstrated clot-removal devices based on SMPs in 2002 [216, 217]. Maitland's group is the leader in developing SMPs for clot removal devices. Their studies first demonstrated useful information about the polymer structure, which is a PU-based material, conditions for device actuation, and an estimation of the recovery forces the device is capable of delivering during the transition between its straight and coiled shape, because the designed SMP device was manufactured as a wire. In addition, they also clearly demonstrated that the

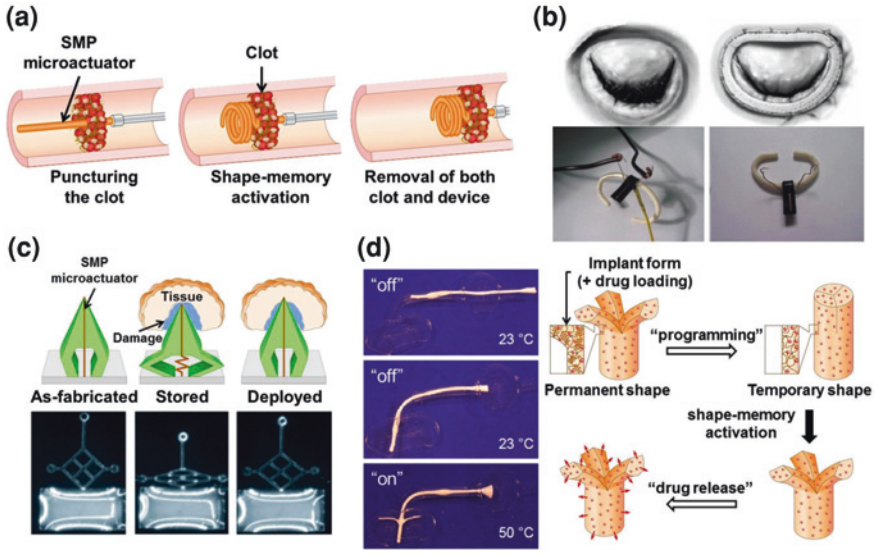


**Fig. 7.12** **a** A proposed thrombectomy device based on the laser-activated SMP coupled to an optical fiber [218]. **b** Diagram of how an annuloplasty ring acts to correct mitral insufficiency and recovery of the initial geometry of an annuloplasty ring prototype through the shape-memory effect by heating [221, 222]. **c** Schematic representation of the SMP neuronal probe actuator. The probe is fabricated with an enclosed conductor (*vertical line*) and deformed into a "crouched" conformation. The heat from the body then causes slow actuation of the SMP probe back to its original conformation and moves the probe tip beyond the zone of tissue damage created by implantation [224]. **d** A potential application of the SMP for the development of a ureter stent and DES [231, 234]

designed microactuator coil can hold a clot, and the designed devices can also be successfully actuated by a laser [217]. As a follow-up study, Small et al. in the same research group have also developed an intravascular device using PU-based SMPs to mechanically retrieve the thrombus and restored blood flow following an ischemic stroke [218]. Their unique PU-based material can maintain a stable secondary shape and, upon controlled heating, returned to its primary shape. In their device, the primary shape is a tapered corkscrew and the secondary shape is a straight rod, as shown in Fig. 7.12a. They proposed to deliver the SMP microactuator in its secondary straight rod form through a catheter distal to the vascular occlusion. The microactuator, which was mounted on the end of an optical fiber, was then transformed into its primary corkscrew shape by laser heating. Once deployed, the microactuator was retracted and the captured thrombus was removed from the body to restore blood flow. In this paper, the fabrication techniques and the optical, photothermal, and thermomechanical properties of the device are also discussed. In addition, the problems prior to in vivo study, including the incorporation of (1) a torqueable sheath around the optical fiber to allow the surgeon to maneuver the device through the tortuous paths of the neurovasculature (2) radiopacity for visualization under fluoroscopic guidance, and (3) a means of securing

the captured clot after retraction for withdrawal from the body were demonstrated. Also, the diameter of the SMP corkscrew may have to be scaled down slightly for human use, depending on the clot location. Notwithstanding the lack of these design elements in the initial prototype, the laser-activated SMP thrombectomy device should be improved for treating ischemic stroke without the need for systemic infusion of thrombolytic drugs and future in vivo study.

Mitral valve insufficiency occurs when the mitral valve does not close properly, resulting in the regurgitation of blood from the left ventricle to the left atrium (flow reversal). Valve repair (e.g., ring annuloplasty), as opposed to replacement, is the preferred method of treatment [219, 220]. The current ring annuloplasty procedure consists of implanting a prosthetic ring to immediately reduce the orifice diameter and improve contact between the valve leaflets. In recent years, a large amount of interest has been shown in the development of annuloplasty techniques by a percutaneous path (which would not require open surgery or connection to an extracorporeal circulation pump), some of the paths being based on the anatomical proximity between the coronary sinus and the mitral valve ring. There are already various devices being developed that are inserted by the venous path (jugular or femoral) and are placed in the coronary sinus, and which, after the application of traction, retraction or heat, reduce their perimeter, achieving a reduction in the mitral ring and the degree of insufficiency, as shown in the top image of Fig. 7.12b. Lantada and co-workers have proposed a resistively heated SMP ring to enhance the annuloplasty procedure for remotely controlled postoperative diameter reduction as shown in the bottom image of Fig. 7.12b [221]. First, they demonstrated the procedure for designing, manufacturing, and programming the "shape-memory" effect and in vitro trials for an active annuloplasty ring for the treatment of mitral valve insufficiency, developed by using PU-based SMPs. The thermally responsive SMP ring would be implanted in a temporary shape corresponding to the shape of the patient's malfunctioning mitral valve, reducing the acute impact of the procedure on the heart. The SMP ring diameter would be reduced gradually postoperatively by applying a current to the embedded resistive elements while monitoring the valve operation. They have also recently demonstrated a personalized development of an annuloplasty ring based on the combined use of information from medical imaging, from computer-aided design and manufacturing technology (CAD-CAM) design programs and prototype manufacture using rapid prototyping technologies [222]. In this paper, the authors firstly explain the problem of mitral insufficiency and how its treatment using annuloplasty rings could benefit from the use of personalized designs.

Neuroprosthetics, which is also called neural prosthetics, is a discipline related to neuroscience and biomedical engineering concerned with developing neural prostheses. Neural prostheses are a series of devices that can substitute a motor, sensory or cognitive modality that might have been damaged as a result of an injury or a disease. In this system, neuronal probes used to monitor and stimulate brain activity are susceptible to failure owing to the issue of damage induced during the initial insertion procedure [223]. To reduce the extent of damage, Sharp et al. designed a prototype neuronal probe using a body-temperature-activated SMP microactuator

for slow insertion into the brain tissue, as shown in Fig. 7.12c [224]. Generally, the widespread application of neuronal probes for chronic recording of brain activity and functional stimulation has been slow to develop partially owing to the long-term biocompatibility problems with existing metallic and ceramic probes and the tissue damage caused during probe insertion. Stiff probes are easily inserted into soft brain tissue but cause astrocytic scars that become insulating sheaths between electrodes and neurons. To overcome and address these problems, they explore the feasibility of a new approach to the composition and implantation of chronic electrode arrays. They demonstrated that softer polymer-based probes can be inserted into the olfactory bulb of a mouse and that slow insertion of the probes reduces astrocytic scarring. They further presented the development of a micromachined SMP probe, which provided a vehicle to self-deploy an electrode at suitably low rates and which could provide sufficient force to penetrate the brain, as shown in Fig. 7.12c. They could also successfully tailor the deployment rate and composition of SMP probes by polymer chemistry and actuator design. Results in mice showed that slow insertion (1 mm per 40 min) reduced the amount of tissue damage. Therefore, they concluded that it is feasible to fabricate shape-memory polymer-based electrodes that would slowly self-implant compliant conductors into the brain, and both decrease initial trauma resulting from implantation and enhance long-term biocompatibility for long-term neuronal measurement and stimulation.

The choice of a suitable material and processes in order to allow the addition of desired functions is crucial and will only be effective when the underlying fundamental principles can be attributed to different structural elements at the molecular level. Multifunctional polymers that combine two functions such as shape-memory effect and biodegradability [24] or biodegradability and drug release [225] have been realized. However, a material that combines the three functions, namely, shape-memory capability, controlled drug release, and biodegradability, has not yet been demonstrated. As described in this section, this would allow us to combine the shape-memory effect for enabling minimally invasive implantation of bulky devices [226], biodegradability to avoid a second surgery for implant removal [227], and controlled drug release for treating infections [228], reducing inflammatory responses [229], or, later, supporting regeneration processes [230]. A drug-loaded, degradable stent [231] and an anchorable drug release system that stimulates the matrix [232] have been demonstrated by Lendlein's group and Sheares' group, respectively. Although to achieve multifunctionality, a material is usually integrated and combined with several components into a system, Lendlein and co-workers successfully combined the multifunctionality into one polymeric material [231]. This simple and versatile idea opened a new way to design highly functional SMP materials. In addition, they demonstrated a first example of the potential application of such SMPs as ureteral stents, as shown in Fig. 7.12d [231]. The designed SMP can be anchored in the body, release both hydrophilic and hydrophobic drugs, such as Ethacridine lactate and Enoxacin, and subsequently degrade, thus avoiding painful removal. They also showed the potential of drug-loaded SMPs as injectable or implantable self-anchoring implant rods, which could enable spatial fixation for a local drug release, as shown in Fig. 7.12d [233, 234].

The advent of biodegradable SMPs spurred the investigation of their use as a vehicle for tissue engineering. In theory, tissue can be grown on collapsible SMP scaffolds in vitro and potentially delivered into the body using minimally invasive techniques such as with a catheter and implanted to initiate repair or reconstruction of tissue organs. The previously reported implantable embolic devices and stents represent potential endovascular tissue engineering applications, as both types of device result in the eventual in-growth of cells around the SMP structure as part of the healing process. Other biodegradable SMP scaffolds could be applied to pharyngeal mucosa reconstruction, bone regeneration, and organ repair. Despite this feasibility of SMPs for tissue engineering, some demonstrations exist that relate to in vitro studies using cells in contact with SMPs [112, 113, 129, 235–237]; there is a little report that describes the impact of the shape-memory effect on adhered cells [238], as discussed later (Sect. 7.5.4).

Additionally, not only the stent applications but also other devices such as for orthopedics [128], orthodontics [239], and blood dialysis [240] have already been reported. Future research in this field will, in cooperation with clinicians, have to reveal further fields of applications and eventually first conduct animal studies. To do so, SMPs will have to be specifically designed for a certain application, for example, by establishing in vitro the desired $T_{switch}$, mechanical features, drug loading levels, release rates, and degradation properties. Synergistic or independent effects of several stimuli are potential areas of research. Then, the next preclinical stages will have to be passed in order to provide the desired devices for animal studies.

### *7.5.2 MEMS and Actuators*

Micro-electro-mechanical and nano-electro-mechanical systems (MEMS and NEMS) are devices integrating electrical and mechanical functionalities on the micro- and nanoscale, respectively. MEMS and NEMS typically integrate transistor-like nano(micro)electronics with mechanical actuators, pumps, or motors, and may thereby form physical, biological, and chemical sensors. The name derives from typical device dimensions in the micro- and nanometer range, leading to low mass, high mechanical resonance frequencies, potentially large quantum mechanical effects such as zero point motion, and a high surface-to-volume ratio useful for surface-based applications, especially in NEMS. In recent years, it has been reported that the shape-memory effect in SMPs is not only a macroscopic phenomenon, but also occurs even on the several tens of nanometer scale in bulk SMPs [241]. As such, SMPs have great potential for micron- and even submicron-scale actuation for MEMS and NEMS applications, micro/nanopatterning [242, 243], and biomedical devices [197, 244]. Micron-sized thermo/moisture-responsive PU SMP/Ni powder chains were fabricated and their shape recovery was investigated as an indirect way to demonstrate the SME in micron/submicron-sized SMPs. Vertical protrusive SMP/Ni chains were fabricated by applying a

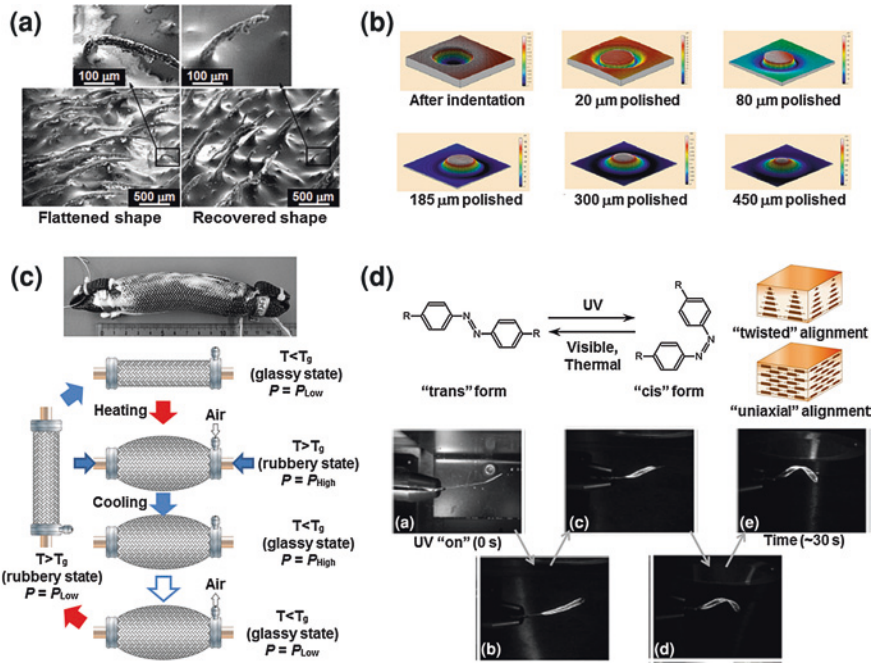


**Fig. 7.13** **a** SEM images of vertical protrusive SMP/Ni chains (2 vol% Ni) and their shape-memory effect [27]. **b** Photographs of forming a microprotrusion bump atop the SMP using laser polishing [245]. **c** Schematic representation of McKibben artificial muscle that uses SMP (*PH* high pressure, *PL* low pressure) and photograph of prototype of developed actuator with SMP [251]. **d** Concept of azobenzene-driven SMP actuation. The azobenzene-based network undergoes an E–Z isomerization between rodlike and bent states upon exposure to UV radiation. Response of aligned azobenzene-based films to UV/visible illumination and UV-induced coiling of a film in the twisted configuration [253]

vertical magnetic field during curing of the SMP/Ni mixture. Figure 7.13a shows the morphology of the array of flattened chains atop the 2 vol% Ni sample and the morphology after subsequent heating for shape recovery [27, 241]. The magnified view of a small chain reveals that in the flattened shape, the initially vertical chain was bent at approximately 90°. However, after heating, the bending angle was largely recovered, which reveals the shape recovery phenomenon in the chain and indirectly demonstrates the SME in micron/submicron-sized SMP. The shape-memory effect in an array of such chains (like a microbrush) may provide a simple mechanism and convenient approach to achieve reversible surface morphology for a significant change in many surface-related properties such as friction and wetting ability. Other microsized protrusion arrays can be realized by laser heating [245]. During the fabrication, a precompressed SMP is heated by a local laser beam. The working principle of forming a protrusive bump atop the SMP by laser heating was demonstrated. First, a polished SMP sample is precompressed. A laser beam (or simple heating) is then shone atop its surface, and the protrusive SMP arrays

are produced, as shown in Fig. 7.13b. Liu et al. demonstrated a generic approach for producing unique protrusive features with different shapes and sizes using styrene copolymer SMP. Their method in combination with micro/nanoindentation and surface polishing can be used to fabricate a more complex surface structure by a simple process [243]. In fact, Fig. 7.13b shows that the surface microstructure can be regulated by adjusting the depth of surface polishing, although the precompressed strain is the same. They also demonstrated that this method can apply to nanoscale or more unique structures such as cylinder, crown, and butterfly shape. SMP-based MEMS systems have also been proposed by several researchers for the rapid and accurate blind placement and release of medical devices in the body [246–250]. Also, micropumps for drug delivery have been designed from SMAs for fine control potential owing to the relatively low stiffness of SMPs. This issue has triggered efforts to develop composite SMPs that can provide the biocompatibility of polymers as well as the stiffness/conductivity of metal alloys. However, applying the SMPs to MEMS and NEMS systems is still challenging; thus, further examination will be required for potential applications.

Actuation entails the use of an actuator to move or control a mechanism or system as a type of motor. It is driven by a source of external energy, such as heating, electric current, radiation or air pressure. SMPs as smart materials can sense the specific external stimulus to automatically recover to their permanent shape from a programmed temporary shape. Therefore, they have already been provided with the capacity to release their entropic energy and move a system upon triggering. Thus, actuation uses the recovery force from the thermomechanical SME cycle of a polymer as a motor. Diversified triggering patterns for actuation that use heating, electricity and alternating magnetic fields for the design of actuators have been developed. In some specific actuator structures, the shape fixation of SMPs provides the advantages of fixing a rigid shape or stiffening a particular functional shape without the need for continuous control. In this case, the actuation arises from the other driving part of the actuator structure, and SMPs impart the controllable supporting force to achieve the designed function. Takashima et al. have developed a McKibben artificial muscle that can be fixed into a rigid shape without the need for continuous control [251]. The McKibben-type pneumatic actuator usually has a simple structure consisting of an internal bladder (e.g., rubber tube) wrapped in a braided mesh shell with flexible yet nonextensible threads (e.g., nylon or fiberglass mesh). The actuator has a fitting attached at one end through which the internal bladder is pressurized. When a positive air pressure (with respect to atmospheric pressure) is introduced to the bladder, it expands. The braided mesh shell is radially deformed and, resembling the Chinese finger puzzle and a pantograph, the mesh changes configuration in a scissorlike action owing to the nonextensibility of the threads. This action resolves the radial expansion forces into axial contraction forces. The result is a shortening of the whole actuator if it is unloaded or the generation of a significant axial force if a mechanical load is attached. The SMP-based McKibben artificial muscle was made by coating SMPs onto the braided mesh shell of a commercial McKibben artificial muscle as shown in Fig. 7.13c [251]. When heated above the $T_g$ of the SMP, it can be used as

a conventional McKibben muscle. When the actuator reaches the desired length, cooling to below the $T_{memory}$ ($T_g$) can 'freeze' the structure into a rigid, actuated state without any air supply or control system. In this way, the SMP enhances the versatility of this type of artificial muscle. Likewise, in a nitinol-core/SMP-shell thermally activated endovascular thrombectomy device, the SMP reaches its $T_g$ and undergoes a reduction in its elastic modulus, allowing the microactuator to transform from a straight form for endovascular delivery to a preprogrammed corkscrew form for clot retrieval. In this case, an electric current in the nitinol provides the electroresistive (Joule) heat. When the current is turned off, the nitinol and SMP cool below $T_g$, and the polymer returns to its glassy rigid state, ensuring enhanced stiffness to the corkscrew shape for clot removal [252]. In addition, triple (two-way) shape-memory effects have also been applied to the actuator applications. These systems are good candidates to achieve bending actuation. For example, the liquid crystal elastomer (LCE) systems developed by Harris' group with a densely cross-linked and twisted configuration of azobenzene units demonstrated a high room-temperature elastic modulus, on the order of 1 GPa as shown in Fig. 7.13d [253]. Because mechanical energy is related to the elastic modulus, the systems are expected to provide great work output as light-driven actuator materials. Consequently, LCEs with azobenzene units are intriguing smart actuator devices for the conversion of light energy into mechanical energy [254, 255].

As the development of lab-on-a-chip technology increases in a wide range of applications, the choice of materials as well as appropriate fabrication techniques is of particular importance for a specific application. This is mostly due to the high surface-to-volume ratio that exists within such small structures. A number of materials, including silicon [256, 257], quartz [258, 259], glass [260, 261], metal [262, 263], and polymers [264–267] have been used to date to fabricate microfluidic devices. Generally, careful consideration of physical and chemical properties of the component materials is essential. In addition, it becomes increasingly apparent that on-demand switchable materials that can respond to external stimuli or their environment to produce dynamic and reversible change in critical properties have enabled progress in a growing number of diverse applications including bio/chemical analysis, chemical synthesis, cell manipulation, biomedical monitoring, and point-of-care clinical diagnostics. From these perspectives, 'smart' microfluidic systems have been extensively studied using stimuli-responsive materials because they can receive device-generated signals and act as switches by themselves. Beebe and co-workers, for example, used a pH-responsive hydrogel-based valve that opened or closed depending upon the pH of the flowing solution [268]. A bistrip valve and an arrowhead-shaped valve have also been reported to allow flow in only one direction [269, 270]. The triggered control of interfacial properties provided by immobilized stimuli-responsive polymers at the solid-water interface has also been developed for designing smart microfluidic systems [271, 272]. Several research groups have explored the use of microcapillaries coated with a temperature-responsive poly(*N*-isopropylacrylamide) (PNIPAAm) layer for creating an 'on-off' valve for the liquid flow. Nanometer-sized surface-grafted PNIPAAm layers within microcapillaries stopped the flow below LCST because

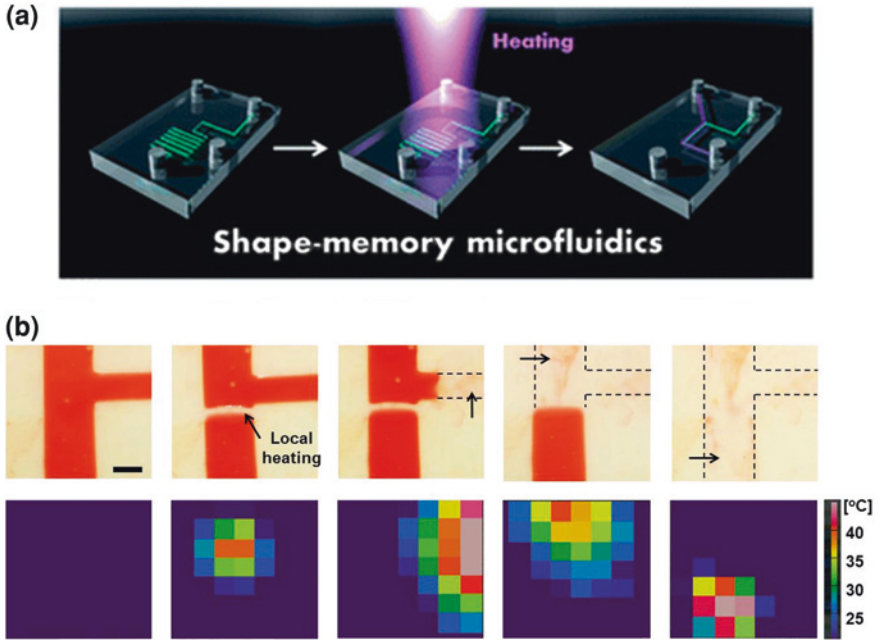


**Fig. 7.14** **a** Schematic illustration of proposed shape-memory microchips. **b** On-demand channel closing by local heating without valve. Water was filled in the channel and heat was locally applied to the channel (bar 1000 μm). (*bottom*) Infrared thermal images of the PCL channel shown in (**b**) [279]

hydration of PIPAAm-grafted chains at the capillary interfaces increased the microviscosity of the hydration layers at the wall interfaces without physically occluding the capillary lumen, significantly influencing the flow frictional resistance [273, 274]. This system produced complete and reversible 'on–off' flow valving in microchannels under relevant hydrostatic pressures useful for microfluidics approaches. The 'on–off' switchable surface trap systems have also been developed to separate and enrich target analytes with simple control of the external stimuli such as friction heat, light and magnet for point-of-care diagnostics in the low-infrastructured sites [275–278]. According to these backgrounds, we have recently reported on-demand switchable microchip materials that display potent rewritable and shape-memory properties, which are shown to contribute to fluidic control as pumps and valves, as shown in Fig. 7.14a [279]. Semicrystalline PCL was chemically cross-linked to show shape-memory effect over its $T_m$ because the cross-linking points set the permanent shape and the crystalline domains serve as a thermally reversible mobile phase. The $T_m$ was adjusted to near biologically relevant temperatures by cross-linking two- and four-branched PCL macromonomers with different ratios. The $T_m$ decreased proportionally with increasing four-branched PCL because an increase in density imposes restrictions on chain mobility and reduces the crystallization [130]. The sample with 50/50 wt% mixing ratio of two- and four-branched PCLs exhibits a $T_m$ of approximately 33 °C.

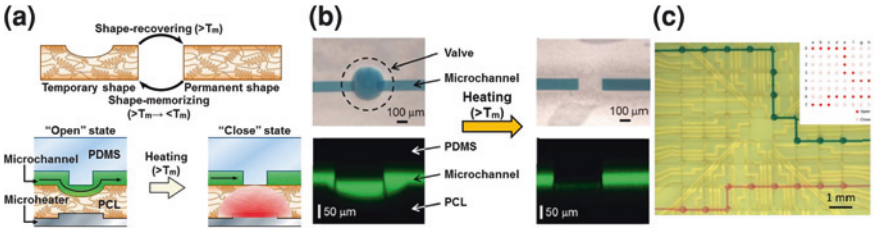


**Fig. 7.15** **a** Schematic of SMP and proposed SMP microvalve (N/O valve). **b** Optical and fluorescence microscopy images of an SMP microvalve. **c** Optical photograph of programmed microchannel networks and schematic of programmed valve opening and closing ($8 \times 8 = 64$ valves). Selected valves were closed, and the designed blue and red fluid lines were successfully observed [280]

Permanent surface patterns were first generated by cross-linking the macromonomers in a mold, and temporary surface patterns were then embossed onto the permanent patterns. From the cross-sectional profiles, almost 100 % recovery of the permanent pattern was successfully achieved after shape-memory transition. The effects of dynamic geometric changes of the shape-memory channels on the microfluidic flow were also investigated, and shape-memory channel closing was achieved by the application of heat, as shown in Fig. 7.14b. The proposed system can be potentially applied as a new class of microfluidic control techniques that enable portable microfluidics-based diagnostic tools for biomedical applications and environmental monitoring allowing on-site analysis.

Moreover, Ichiki's group in collaboration with our group has also developed a novel SMP microvalve suitable for integration into micro-total analysis systems (micro-TAS) devices [280, 281]. This microvalve is compatible with electronics and is considered to be applicable to low-cost disposable chips. The microvalve has a simple design and is constructed with two adjacent microchannels and a polymeric sheet microvalve with a thin-film heater, but can provide either normally open (N/O) or normally closed (N/C) microvalve functions. We also demonstrated a field-programmable microvalve array (FPVA) with $8 \times 8 = 64$ microvalves, which enables the custom design of microfluidic devices by analogy with a field-programmable gate array (FPGA) in LSI technology. Although extensive research has been conducted on microvalve technologies [282, 283], the development of a simple and robust microvalve remains a challenge. To overcome this issue, we developed a microvalve that is actuated by the shape recovery of an SMP. Compared with well-known metallic SMAs, SMPs show large deformability and changes in the elastic modulus at their response temperature, which are highly advantageous for the simple design and reliable actuation of microvalves. Figure 7.15a shows the proposed SMP microvalve. PCL was used as the SMP. PCL can memorize the shape of microstructures at the sub-micrometer level and reverts to its original shape near 50 °C. Microvalve actuation was inspected by vertical imaging, as shown in Fig. 7.15b. They also applied this system to more complex device systems in which the N/O and N/C microvalves are arranged in

tandem. An N/O microvalve has a concave shape as its temporary shape and a flat shape as its permanent shape, and vice versa for an N/C microvalve. Tandemly arranged microvalves can actuate in sequence from a closed state to an open state and finally to a closed state. This sequence is one of the most frequently used sequences for performing the batch processing of liquid samples on a chip. Finally, they fabricated an FPVA, as shown in Fig. 7.15c. This FPVA is analogous to an FPGA, which is a programmable integrated circuit that interconnects several logic modules. In contrast, the FPVA has a microchannel network that interconnects microfluidic components such as chambers, mixers and sensors. Microvalves are arranged at each crossing point of the microchannel network. Selective microvalve actuation enables the on-demand formation of an arbitrary microfluidic network. In summary, we developed a novel SMP microvalve that can operate as either N/O or N/C microvalves and fabricated an FPVA with $8 \times 8 = 64$ microvalves to demonstrate the suitability for integration into a microfluidic network. The simple microvalve design and applicability of low-cost fabrication technology such as plastic molding and circuit printing are advantageous for use in disposable chips. Also, the electronically controllable feature is expected to be useful for realizing full-scale micro-TAS devices.

### *7.5.3 Bulk and Surface Shape Memory for Dynamic Regulation of Cel l Functions*

Traditional synthetic substrates and matrices for cell culture have proven to be of only limited utility in efforts to understand and control cell behavior, in large part because they fail to capture the multifarious biochemical, mechanical, geometric and dynamic characteristics of in vivo environments. However, recent advances in materials chemistry and engineering have begun to provide researchers with a toolbox to mimic the complex characteristics of natural extracellular matrices (ECMs), providing new pathways to explore cell–matrix interactions and direct cell fate under physiologically realistic conditions.Even though shape-memory materials are well known as one of the actively moving materials, as discussed in "Sect. 7.5.1", there is still limited knowledge on the dynamic regulation and manipulation of cell behavior using SMPs. However, from recent studies, SMP-based cell culture substrates have the potential to dynamically regulate the cellular function and fate. In this review, we describe recent developments in shape-memory materials as dynamic cell culture substrates. In particular, we focused on the mechanostructural stimuli such as topology and elasticity as the cues against adhered cells on the substrate to manipulate and regulate cellular functions and fate. These results should provide further understanding of how cells respond to spatiotemporal variations in an extracellular environment.

Regarding the design of dynamic cell culture substrates and matrices whose properties can be engineered to vary over time in well-defined and controlled ways, most studies rely on stimulus-responsive materials. In those studies, the

term stimulus is broadly defined as any perturbation, externally applied or induced by the cultured cells themselves, capable of inducing well-defined variations in the cell–material interaction. As described in other chapters, there are many smart materials, including those that respond to light and electric and magnetic fields, introduction of biomolecules, changes in temperature, pH or ionic strength, and mechanical work applied on the substrate [284]. However, most dynamic materials that respond to external stimuli change their physicochemical properties such as hydrophilicity/hydrophobicity (surface energy) and the state of charge at the surface scale.

Researchers have reported the use of thermally responsive SMPs as an extracellular matrix for growing various tissues in vitro. Rickert et al. reported cell seeding on a biodegradable thermoplastic SMP based on PCL [285]. To investigate the possibility of reconstructing the mucosa of the upper aerodigestive tract, rat pharyngeal cells were seeded on smooth and porous surfaces of the SMP with encouraging results, and excellent biocompatibility and biofunctionality were demonstrated for a series of developed multifunctional biodegradable, polymeric biomaterials both in vitro and in vivo. Novel, multifunctional polymeric biomaterials offer a highly specific adjustment to the physiological, anatomical and surgical requirements and can thereby facilitate new therapeutic options in head and neck surgery. However, the shape-memory effect on cell culture has not been well studied. Neuss et al. were the first to demonstrate the shape-memory effect on adhered cells [238]. They characterized the behaviors of L929 mouse fibroblasts, human mesenchymal stem cells, human mesothelial cells, and rat mesothelial cells on a PCL-based SMP network. They synthesized the PCL networks by radical polymerization of PCL-dimethacrylate (Mn ~15,000 g/mol), and showed a $T_m$ of 52 °C. The developed polymer was cytocompatible for all tested cell types, supporting cell viability and proliferation. The differentiation capacity of mesenchymal stem cells was also supported by the SMP. In fact, they determined the shape-memory effect on adhered L929 cells upon activation by a 10 s heating incubation at 54 °C. As shown in Fig. 7.16a, this short 54 °C incubation on glass slides (control sample) without a shape-memory effect did not affect the L929 cells, and all cells were viable and the cell monolayer remained confluent. After the activation of the shape-memory effect, the cell monolayer was disconnected, the cell number was reduced and some cells underwent apoptosis, resulting in blebbing cells, as observed in the photographs (Fig. 7.16a). Importantly, no necrotic cells were observed in this system. They explained that, owing to varying shear forces at different points on the surface of the polymer, unaffected confluent cell monolayers as well as subconfluent regions and regions with apoptotic cells were observed, possibly the polymer region with the highest shear force during shape-memory activation. Nevertheless, no necrotic cells were detectable; thus, they concluded that no inflammation caused by adherent cells would occur after transplantation of the cell-seeded PCL network. Since the 100 % strain-fixed sample was used as a temporal pattern in this system, the use of a lower-strain-fixed sample may be required to reduce the number of apoptotic cells because it should minimize the shear forces generated upon shape-memory activation. Moreover, the transition

temperature in this system is too high, and it is difficult to directly apply this system in vivo. However, these first findings will open a new way to establish the foundation for the future success of SMPs in the field of biomaterials.

Although Neuss et al.'s approach relied on the bulk shape-memory effect, the cells are likely adhered on the surface (or interface) of the material. In bulk shape memory, the macroscopic motion of SMP will result in the large dimensional change; in turn, the surface shape memory will inhibit or minimize this effect on the adhered cells. The first to investigate the surface shape-memory effect was Nelson et al. [286]. By using AFM probe tips, they successfully formed the surface nanoscale indents with depth from 3 to 16 nm and lateral dimensions of approximately 200–300 nm onto a cross-linked thermoset epoxy-based SMP surface. Despite the expected heterogeneity of the cross-linked network structures, which originated from the molecular cross-linking, the indents can fully recover upon sufficient heating at the molecular level. The erasable nature of the nanoscale deformation (nanoindents or nanoimprints), when combined with a massively parallel operation of scanning probes, makes it attractive for use as rewritable high-density data storage media [287]. On a more general basis, the surface shape-memory effect could become an increasingly attractive option for soft lithography (e.g., microcontact printing and microfluidics), given the erasable and reprogrammable nature of the nanoscale deformation [288, 289]. Another notable use of the surface shape-memory effect lies in the creation of localized surface-wrinkle-based structural colors [290]. In general, surface wrinkling occurs when a rigid thin film supported on a soft substrate is compressed laterally beyond a critical strain. Typically, surface wrinkling is created uniformly on a rubber substrate. The use of an SMP as the wrinkle substrate presents a unique opportunity to create localized wrinkle structures. The process of forming localized wrinkles is as follows: Localized indents are first created on an SMP surface, followed by the deposition of a metallic thin film. Heat-triggered recovery of the indent induced a lateral compressive strain at the edge of the indent, resulting in localized wrinkle formation. The wavelength of the resulting surface wrinkles falls within the vicinity of the visible wavelength. As such, the wrinkled surface showed angle-dependent structural colors. Reflecting the flexible and controllable nature of the wrinkling process, the method can be utilized to capture any macroscopic object when the object itself is used as the indenter. These surface patterns based on localized wrinkle formation can be applied as the cell culture substrate because anisotropic geometries are critical for eliciting cell alignment to dictate tissue microarchitectures and biological functions. In addition, surface metallic coating will sometimes complicate the observation of cells and biological characterization. From this perspective, Wang et al. have recently presented a novel simple, solvent-free, and reproducible method via uniaxial stretching for incorporating anisotropic topographies on biodegradable films with ambitions to realize stem cell alignment control, as shown in Fig. 7.16b [291]. Although this system does not require the metal coating, uniaxial stretching of PCL (Mw = 80,000 g/mol) films resulted in a three-dimensional micro-ridge/groove topography (inter-ridge distance: ~6 μm; ridge length: ~90 μm; ridge

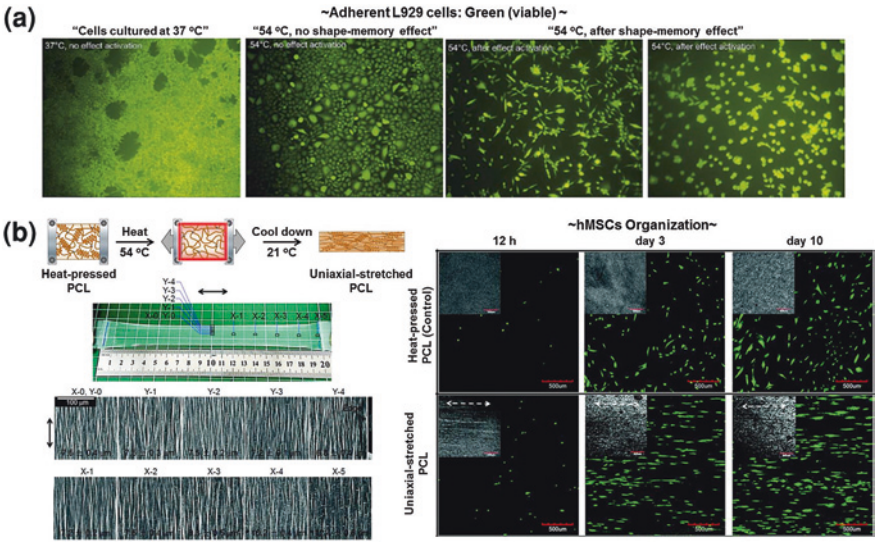


**Fig. 7.16** **a** Influence of shape-memory activation on adherent cells on PCLDMA network. The shape-memory effect was activated by 10 s heat incubation at 54 °C [238]. **b** Schematic of fabrication and anisotropic topography of uniaxial-stretched PCL and field-emission scanning electron microscopy (FESEM) images of uniaxial-stretched PCL at representative regions (*left*). CLSM images of hMSCs on flat and uniaxial-stretched PCL (*right*) [291]

depth: 200–900 nm) with uniform distribution and controllable orientation in the direction of the stretch on the whole film surface. When the stretch temperature and draw ratio were increased, the inter-ridge distance was reduced and the ridge length increased. Through modification by hydrolysis, increased surface hydrophilicity was also achieved, while maintaining the morphology of PCL ridge/grooves. Upon seeding human mesenchymal stem cells (hMSCs) on uniaxial-stretched PCL films, aligned hMSC organization was obtained. Compared with unstretched films, hMSCs on uniaxial-stretched PCL had a larger increase in cellular alignment (>85 %) and elongation, without any indication of cytotoxicity or reduction in cellular proliferation. This aligned hMSC organization was homogenous and stably maintained with controlled orientation along the ridges on the whole uniaxial-stretched PCL surface for over 2 weeks. Moreover, the hMSCs had a higher level of myogenic gene expression on the uniaxial-stretched PCL than on the unstretched films. Therefore, their data suggested that uniaxial stretching, which is a surface feature, has potential in patterning film topography with anisotropic structures. The uniaxial-stretched PCL in conjunction with hMSCs could be used as "basic units" to create tissue constructs with microscale control of cellular alignment and elongation for tissue engineering applications. However, this study also did not examine the impact of shape-memory activation on adhered cells, and the shape-memory effect was utilized in the fabrication of uniaxial-stretched PCL maybe because of the high $T_m$ of PCL.

At the same time, Lam et al. first demonstrated the application of the dynamic topography to cultured cells using reversible poly(dimethylsiloxane) (PDMS) surfaces, although this system does not include SMP [292]. In this system, reversible wavy microfeatures were fabricated by subjecting the PDMS surfaces to plasma oxidation and subsequently applying compressive stress to induce surface buckling. Myoblast cells that initially adhered with random orientations onto the flat substrate then aligned parallel to the direction of waves, and regained their random orientation upon relaxation of the substrate features. Their results strongly suggest that dynamic topographical change affects the adhered cell function, and the surface shape-memory effect can surely be applied to dynamic cell culture substrates.

The first example of the surface shape-memory effect applied to a dynamic cell culture substrate was shown by Davis et al. [293]. To enable surface-shape memory during cell culture, they prepared a glassy SMP from Norland Optical Adhesive 63 (NOA-63) because the recovery temperature can be tuned by manipulating the cross-linking condition in this system [169]. To reveal the feasibility of the surface shape-memory effect during cell culture, they embossed an initially flat NOA-63-based SMP substrate to produce a temporary topography of parallel microscale grooves. After plating the cells on the substrate, they triggered shape-memory activation using a change in temperature tailored to be compatible with mammalian cells such as mouse embryonic fibroblasts, thereby causing a topographic transformation back to the original flat surface. They found that the programmed erasure of substrate topography caused a decrease in cell alignment as evidenced by an increase in angular dispersion with corresponding remodeling of the actin cytoskeleton. Cell viability remained higher than 95 % before and after topography change and temperature increase.

PCL is a common choice in surface SMP because it is biocompatible and has a $T_{switch}$ that can be adjusted close to body temperature by introducing branching in the polymer backbone. We have already demonstrated this ability to modulate the $T_m$ of PCL materials by controlling the nanoarchitectures of cross-linked PCL, such as branched arm numbers and molecular weight [111–114, 130]. To obtain the PCL-based substrates desired for cell culture, shape-memory PCL substrates were prepared by cross-linking tetra-branched PCL with acrylate end groups in the presence of linear PCL telechelic diacrylates [294, 295]. The $T_m$ of cross-linked PCLs proportionally decreased with decreasing tetra-branched PCL content while the relatively high melting enthalpy at approximately the $T_m$ ($\Delta H_m$) was maintained. In particular, the sample with 50/50 wt% mixing ratio of tetra-/di-branched PCL had a $T_m$ of approximately 33 °C. Surprisingly, the transition occurred over a few °C and was associated with a large elastic modulus decrease from approximately 43 to 1 MPa. The bulk shape-memory properties for these samples were investigated by cyclic thermomechanical tests. For the cross-linked PCLs, $R_f$ and $R_r$ were approximately 99 and 90 %, respectively. Thus, by precisely tailoring the nanoarchitectures of semicrystalline PCL, the shape-memory switching temperatures could be successfully adjusted near body temperature while maintaining a sharp mechanical transition over a narrow temperature range. To program temporary surface patterns, the substrates were compressed in a thermochamber. A compressive stress of 0.1 MPa was

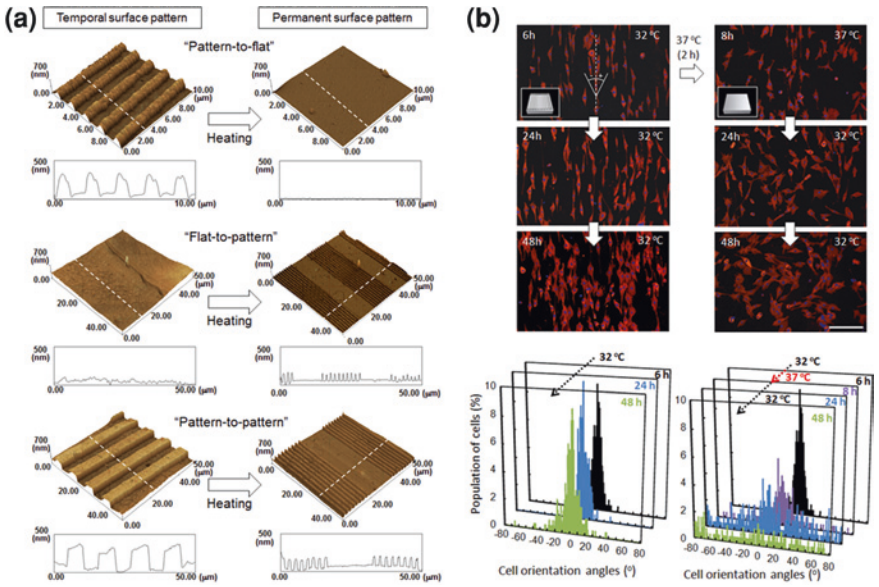


**Fig. 7.17** **a** Topographic surface images of PCL films (4*b*10/2*b*20 = 50/50 wt%) observed by AFM before and after shape-memory transition by a 37 °C heating. Three different surface shape-memory transitions are demonstrated. **b** Fluorescence microscopy images of NIH 3T3 fibroblasts seeded on the PCL films with the temporary grooved surface (bar 200 μm). Dynamic regulation of NIH 3T3 fibroblast orientation was demonstrated by surface shape-memory activation [294, 295]

applied to the samples at 37 °C and held for 5 min. The embossing stress was then released at 4 °C after cooling for 10 min. Figure 7.17a shows topographic surface images observed by AFM. When a flat PCL substrate was embossed with a grooved pattern by application of pressure at 37 °C and subsequent cooling, the substrate was deformed and fixed into the grooved topography of the master (grooves with a width of 1 μm and a height of 300 nm are spaced 2 μm apart). The temporary surface pattern was quickly erased by heating, and the permanent shape, a flat surface in this case, was completely recovered, as shown in Fig. 7.17a. To investigate the role of dynamic and reversible surface nanopatterns on cell behavior, specifically cell alignment on the PCL substrates before and after a topographic transition, NIH 3T3 fibroblasts were seeded on a fibronectin-coated PCL substrate with a temporary grooved topography (Fig. 7.17b, and cultured at 32 °C for 6 h. Cells aligned parallel to the grooves, as seen in Fig. 7.17b (bottom). Cells migrated and grew horizontally to the surface grooves with cultivation time. Upon transition from the grooved topography to a flat surface, cell alignment was lost and random cell migration and growth ensued. The cell angle dispersion (defined as the angle between the pattern and cell orientation) increased with time even though the incubation temperature was returned to 32 °C after 2 h of incubation at 37 °C. Cells seeded on flat films grew randomly regardless of incubation temperature. The distribution of cell-orientation

angles correlated well with the topographic features of the underlying substrates before transition. On the other hand, angular histograms clearly show the time-dependent dispersion of cell angles after shape-memory transition to a flat shape. Thus, the shape-memory surfaces based on cross-linked PCL demonstrated the important role of surface nanotopology in time-dependent cell migration and alignment. A similar study that used PCL as the SMP was reported by Le et al. [296]. They also successfully demonstrated that the hMSC morphology switched from highly aligned to stellate shaped in response to a surface transformation between a 3 to 5 μm channel array and a planar surface, although the temperature range to transform from a temporary to a permanent surface pattern in Ashby's group ($T_{below}$: 28 °C, $T_{above}$: 37 °C; 9 °C) is broader than that of our system ($T_{below}$: 32 °C, $T_{above}$: 37 °C; 5 °C). Because these systems relied on the temperature change during cell culture to induce the topographical change using the surface shape-memory effect, the sharp transition, which means that materials can act at a narrow temperature range, is an extremely important factor in these systems. The versatility and biologically friendly nature of these PCL-based shape-memory surfaces could potentially enable the realization of novel and diverse applications, especially in biomaterial development and basic cell biology.

### *7.5.4 Novel Methods of Fabrication of SMPs*

As already discussed, SMPs have very unique elastic and structural features in response to external stimuli, such as heating, light, and electric and magnetic fields. The principles of shape-memory materials are simple, even for systems with multifunctionality; thus, SMPs could have broad applications, although the optimization of shape-memory properties tailored for any specific application is surely required as described above. Therefore, how to apply these features to systems is a great challenge, and we must consider and discover such materials for future SMP systems. In this section, we introduce examples based on such unique ideas as well as new concepts.

Self-healing materials are a class of smart materials that have the structurally incorporated ability to repair damage caused by mechanical usage over time. The inspiration comes from biological systems, which have the ability to heal after being wounded. For a material to be defined as self-healing, it is necessary that the healing occurs without human intervention. Cracks that form in the bulk of a polymeric material caused by thermal, mechanical, chemical, and/or UV radiation stimulation are hard to detect and thus repair [297]. This damage has become a problem as the material's mechanical properties are severely compromised. The major self-healing systems involve the incorporation of microencapsulated healing agents where a propagated crack will rupture the capsule allowing the agent to fill in the damaged site by capillary action and bond the crack surface via in situ polymerization [298]. Currently, there are many self-healing approaches and mechanisms including molecular interdiffusion, photo-induced healing, recombination

of chain ends, and reversible bond formation [297]. Cheng and co-workers have demonstrated a method of producing "self-healing surfaces" based on the use of shape-memory materials [299]. Although the examples described are restricted to the SMA system (Ni-Ti alloys), they showed the complete recovery of a dented or scratched surface by heating (up to 150 °C) and then cooling the materials. However, these approaches are successful in healing damage at a small (micro-length) scale. Moreover, the self-healing systems described above all rely solely on a rebonding reaction, but do not necessarily require crack closure before healing To address this need, the utilization of the shape-memory effect has been explored. White and co-workers have reported the sensational approach of integrating both shape-memory effect and self-healing in a single material system [300]. In this system, a small number of pretensioned SMA wires were placed perpendicular to the crack surfaces of a tapered dual-cantilever beam specimen made of a diethylene-triamine-cured epoxy resin with Grubb's catalyst embedded in the resin matrix for later healing. "Self-healing" was conducted by manually injecting reactive monomers to the crack and activating the recovery (contraction) of SMA wires by passing through an electrical current, which led to a significant crack closure (reduction of crack surface separation) and improved healing. They have also demonstrated that a similar strategy was later adopted in a microcapsule-based system to achieve autonomous self-healing [301]. Although proven to be effective in obtaining better healing under controlled laboratory conditions, this SMA-based approach presents several drawbacks for practical applications: (1) difficulty in determining repair direction and (2) cost and processing complexity. The utilization of SMPs has the potential as the solution approach to overcome the drawbacks of the SMA system to achieve crack closure in a self-healing system. In 2009, Mather and co-workers first demonstrated fully polymeric systems exhibiting both shape-memory and self-healing ability [302]. They reported on miscible blends comprised of linear-PCL and chemically cross-linked PCL networks. The blends demonstrate unique shape-memory-assisted self-healing (SMASH), which is the material's ability to close local microscopic cracks and heal those cracks by bonding the crack surfaces. This SMASH material can achieve reversible plasticity shape memory (RPSM), which they defined as the recovery of both the temporal elastic and plastic regions of deformation [303]. Thermomechanical analysis revealed that the cross-linked PCL with a large plastic deformation is fully recoverable upon heating. Therefore, this shape memory assists in closing any cracks formed during deformation and damage while linear PCL chains make the crack surfaces adhesive by diffusion to the free surface and ultimately across the area of damage during the same heating step as used for the shape-memory effect, as shown in Fig. 7.18(a). In addition, they investigated the controlled damage and SMASH of blends with varying compositions by tensile testing the essential work function of fracture film specimens, and revealed that the healing component, the linear PCL, had a high $M_w$ ($M_w$ ~65 k g/mol) to enable re-entanglement after diffusion across the interface, whereas the shape-memory component, the cross-linked PCL, was prepared from PCL telechelic diacrylates and a tetrathiol crosslinker, yielding excellent shape memory by Michael addition reaction. They revealed the excellent self-healing of films by the

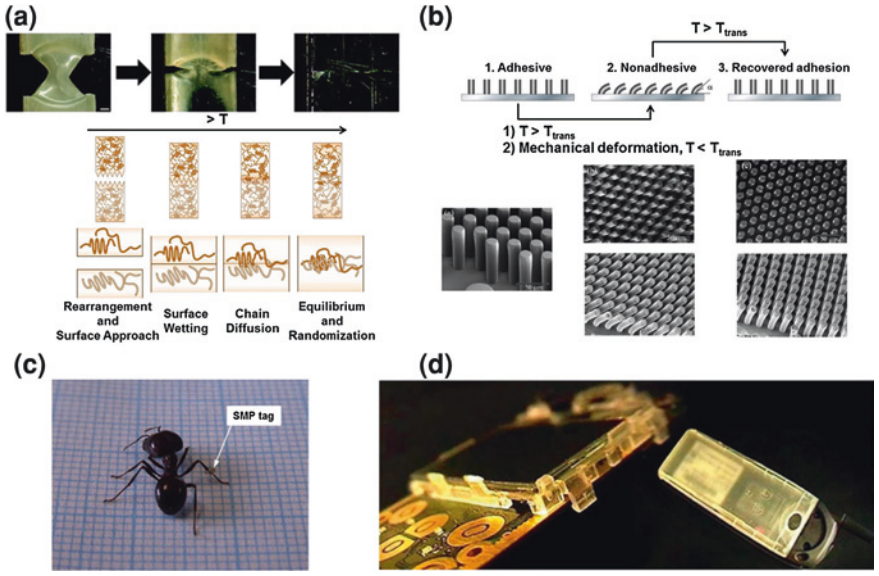


**Fig. 7.18** **a** Shape-memory-assisted self-healing system. Snapshots of crack closure and crack rebonding (stereo micrographs scale bar: 500 μm) and schematic of five stages of healing process [303]. **b** SMP-pillar-based "on-off" switchable dry adhesive as the low-strain applications of SMP [313]. **c** Example of SMP microtag as the active assembly [244] and **d** a Nokia phone as the active disassembly [317]

SMASH mechanism, with nearly complete healing for linear PCL contents exceeding 25 wt%. It is important to note that the RPSM-based self-healing mechanism heals only nonpermanent damage such as surface scratches. If, during a scratching situation, permanent damage such as cracking occurs, heating would only reduce the crack width but the cracks would not heal. Such a limitation is somewhat inherent to SMPs. Deformation related to a scratch corresponds to a more condensed packing of molecular chains, that is, entropy change, whereas cracking means macroscopic material separation. Healing macroscopic material separation would require material flow such as the linear PCL in Mather's system as demonstrated in Fig. 7.18a, which is contrary to the molecular origin of the polymer shape-memory effect. As one alternative approach, Xiao et al. have demonstrated the improvement of the cracking resistance of SMPs. In fact, they have overcome this problem by adding a trace amount of nanolayered graphene into the SMP matrix, which is the SMP composite system [304]. They showed that the composites displayed significant property enhancement over unfilled SMPs, including scratch resistance and thermal healing capability under stress-free conditions. Recently, Kohlmeyer et al. have also demonstrated the combination of remote, local, and chemical programming of the multishape-memory effects, which offers unparalleled shape and function control in carbon nanotube-Nafion composites [305]. They suggested that the strategy not only allows the high-fidelity encoding and extraction of designed

material shapes at different length scales (macro, micro, and nano) but also enables the reversible tunability of material functions, such as the ability of shape memory, mechanical properties, surface hydrophobicity, and material resealability, in a single nanocomposite. It is important to note that these approaches using shape-memory effects can be separated from the primary origin of self-healing as they do not directly repair structural defects. The focus of these technologies on nonstructural repairs makes comparison with traditional self-healing polymers difficult. However, these properties represent novel developments opening avenues to alternative applications of self-healing polymeric systems.

It is commonly believed that SMP has a big advantage over SMA in that the former can be tailored to exhibit very large maximum recoverable strains (as large as 1000 %) compared with that of SMAs. As pointed out previously by Xie [185], although some SMP applications may indeed require large recoverable strains, that an SMP has to have a large recoverable strain to be useful is a misconception. Many real-world applications of shape-memory materials involve geometric changes; although drastic, they are actually associated with small strains. Despite their low recoverable strains, SMAs have found more success in commercial applications than SMPs owing to their fast actuation and high recovery stress. The more important advantage of SMPs thus lies in their processability, that is, they can be easily processed into complex bulk devices, not necessarily in the recoverable strain. One typical example that does not require the large strain is the application of SMP to an adhesion system. Xie's group and Mather's group independently demonstrated the reversible dry adhesion system using SMPs [306, 307]. In Xie's approach, the adhesive comprises two layers: a rigid SMP backing layer and a sticky elastomer layer, that is, the two thermoset epoxy layers. Both layers are cross-linked thermoset SMPs, that is, a cross-linking system, thus making the system a dry adhesive. Their as-fabricated original bilayer adhesive forms a slight curvature because of the thermal mismatch between the two layers. Owing to this curvature, the adhesive does not form an intimate contact when placed on a flat countersubstrate; thus, the adhesion is low. Owing to the SMP backing layer, the bilayer adhesive can be deformed to achieve conformal contact with the substrate, leading to adhesion as high as 200 N $cm^{-2}$ [306]. Upon heating, the shape recovery of the SMP layer creates a peeling force that detaches the adhesive. In the bonding and debonding processes, only a very small strain change occurred instead of a large recoverable strain; excellent shape fixing and large recovery stress are important in this instance.

On the other hand, in Mather's system, they developed a unique self-adhesive material that maintains a high degree of rigidity at the adhesive state while processing the ability to easily debond upon heating, that is, the material is both a rigid and reversible adhesive [307]. Their material is initially a miscible blend of PCL and diglycidyl ether of bisphenol A/diaminodiphenylsulfone epoxy, processed to a unique morphology via polymerization-induced phase separation. The fully cured material features a biphasic, "bricks-and-mortar" morphology in which epoxy formed highly interconnected spheres (brick region) that interpenetrate with a continuous PCL matrix (mortar region). When heated above $T_m$ of PCL,

the epoxy bricks remain rigid owing to the high epoxy $T_g$ while PCL liquefies to become a melt adhesive. Moreover, the PCL molten liquid undergoes microscopic dilatational flow to the sample surfaces owing to its high volumetric expansion in excess of epoxy bricks expansion, a phenomenon they termed differential expansive bleeding (DEB). Remarkably, the samples remain rigid at this state, and their surfaces become covered by a thin layer of PCL able to wet, and subsequently bond through cooling to a variety of substrates. They actually observed high bonding strengths (100–1000 N $cm^{-2}$), which they attribute to a combination of good wetting and subsequent formation of a thin layer of semicrystalline PCL with high cohesive strength upon cooling. This adhesive layer can be melted again by heating ($T > T_m$) to easily debond, and a subsequent rebonding capacity was demonstrated, indicating repeated availability of the PCL melt adhesive to the surface by the DEB mechanism. It is also well known that the ability of geckos and insects to adhere reversibly to almost any surface relies on the surface topography of their attachment pads [308, 309]. As found in nature, these are covered with fine structures (setae) with characteristic dimensions and geometries. Many attempts to fabricate artificial biomimetic structures have been reported [310, 311]. An important difference between animal adhesive setae and the micro- and nanofabricated adhesives is the fact that setae are oblique and their tips point in a particular direction [312]. This tilted arrangement is responsible for the "on-off" nature of the adhesion process and seems to be crucial for avoiding self-sticking and allowing detachment during animal locomotion. This switchability in adhesion as found in nature can be achieved using SMPs. Reddy et al. first demonstrated the switchable structured dry adhesives (gecko-like adhesives) [313]. As shown in Fig. 7.18b, this system contains SMP micropillars perpendicular to the surface, and the pillars can be deformed and fixed into a tilted shape by using the shape-memory effect. Despite the small strain related to such a deformation, the adhesion exhibited by the original surface (~3 N $cm^{-2}$) was transitioned to a nondetectable level for the tilled pillar surface. In addition, they have also demonstrated the repeated switching function between the adhesive and nonadhesive states. Xie and co-workers also reported thin-film terminated microfibrillar adhesives made of adhesive polymers and SMPs that are both cross-linked epoxy-based polymers as reversible dry adhesives with thermally controllable adhesion [314]. Structurally different adhesives were fabricated by coating a continuous thin layer of an elastomeric adhesive polymer onto either a flat or a fibrillar shape-memory polymer surface. Experimental results showed that pull-off forces of the adhesives can be up to four times different depending on thermal conditions. These differences originate from the temperature dependence of either the intrinsic adhesion properties of the adhesive polymer or the stiffness of the subsurface shape-memory polymer. Therefore, the shape-memory ability of cross-linked elastomer (Type II SMPs) has been taken advantage of to fabricate a switchable adhesive surface.

"Tailor-made" means specially made for a particular purpose, and this term is now often used in medical and diagnostics fields. For example, a screw is a commonly used component for assembly. Conventionally, screws of different sizes are required for holes of respectively different sizes. Although tailor-made is an

important concept, sometimes it is not better than “ready-to-wear” or “one-for-all” because the coverage in the tailor-made system is extremely limited. SMP-based materials can be used as a one-for-all solution for a range of different objectives in a single and same material system. Huang and co-workers demonstrated that one SMP screw can fit holes of different sizes with/without tread and even a screw driver is not needed for tightening [315]. They also expanded this idea to an SMP coupling system that provides a good solution to tightly hold two tubes in a range of different diameters together. They defined these processes as “active assembly”, and demonstrated a microtag fixed to the leg of an ant, as shown in Fig. 7.18c [244]. The advantages of the SMP tag are: (1) owing to a high recoverable strain normally on the order of 100 %, the SMP tag can be pre-expanded into a very large diameter. As such, it is easy to mount it onto the leg of an ant. (2) The required heating temperature to trigger the SME, which is a polyurethane shape-memory foam, can be tailored in a broad range. (3) The recovery stress upon heating can be controlled to avoid overcompression to the leg. (4) After cooling back to room temperature, the SMP tag becomes hard and perfectly matched to the leg. Meanwhile, SMPs have also been proposed as a possible cost-effective approach for the active disassembly of obsolete electrical devices, such as cellular phones, for effective recycling in a cost-effective manner and reusing to protect our environment. Chiodo et al. first demonstrated this concept of the disassembly of consumer electronic products using SMPs in the design of embedded releasable fasteners [316]. Chiodo et al. set up a company called “Active Disassembly Research” (ADR), which carries out its own research as well as working on behalf of other companies to develop and patent methods. In fact, ADR Ltd. and Nokia have created a prototype of a cell phone with active disassembly ability that dissembles itself in two seconds as shown in Fig. 7.18d [317]. The idea of this system is to disassemble a mobile phone by a heat-activated mechanism without any contact. By using a centralized heat source like laser heating, an SMA actuator is activated, and the mobile phone covers are opened. The battery, display, printed wiring board and mechanical parts are separated and can then be recycled by material-specific recycling processes. The required temperature for the disassembly is 60-150 °C. Today, most cell phones and other small electronics are shredded instead of taken apart for recycling, because the disassembly time is too expensive for the amount of material reclaimed. Because the materials design including not only during use but also after use will provide further additional values to the present system, these concepts should be actively introduced into future material design.

The structural changes of a polymer, such as glass-rubber and crystal-amorphous transitions, induced by applying external stimuli, are usually transformed into a macroscopic large motion (moving) in most SMP systems as described in this chapter. On the other hand, a metal alloy can exhibit a shape-memory effect if it has two phases that can interconvert reversibly. These shape-memory effects were expressed without requiring additional materials and atoms to diffuse through the structure. Although the moisture (water)-responsive SMP was developed by many researchers [318, 319], the water molecules (bound water)

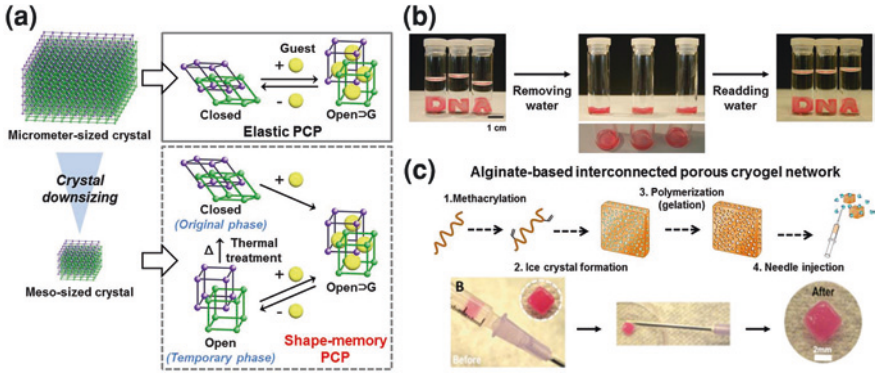


**Fig. 7.19** **a** Schematic illustration of a shape-memory effect in crystalline porous coordination polymers (PCPs) through crystal downsizing [320]. **b** Liquid- and solidlike properties of the DNA hydrogel as a metamaterial. Designed D-, N- and A-shaped hydrogel and series of photographs showing the process of DNA hydrogel returning to its original shape after reintroducing water at 25 °C within the first 3 s (t = 0–3 s) [323]. **c** Overview of the preparation process of alginate-based interconnected porous cryogel and photographs showing placement of a cryogel in a 1-mL syringe (before injection) and gel recovery (after injection) via a conventional 16-gauge needle [324]

are directly induced by the structural change of SMPs, that is, the bound water molecules only weaken the hydrogen bonding and thus reduce $T_g$ to trigger the shape recovery. Recently, Sakata et al. have reported a molecular-scale shape-memory effect (MSME) in crystalline porous coordination polymers (PCPs) [320] (Fig. 7.19a). It is generally well known that the flexible PCPs cooperatively reconfigure their framework structures in response to the incorporation of molecules into the nanopores. This adsorption process triggers the deformation of the pore shape; however, the pore recovers its original shape after the removal of the adsorption stress (that is, the desorption of the guest molecules), which leads to the so-called framework elasticity property [321]. Flexible PCPs developed by Sakata et al. change their structure in response to molecular incorporation but recover their original configuration after the guests, which are DMF, ethanol, or methanol in this study, have been removed. They demonstrated that the crystal downsizing of twofold interpenetrated frameworks of $[Cu_2(dicarboxylate)_2(amine)]_n$ regulates the structural flexibility and induces a shape-memory effect in the coordination frameworks. In addition to the two structures that contribute to the sorption process (that is, a nonporous closed phase and a guest-included open phase), they were able to successfully isolate an unusual, metastable open dried phase by downsizing the crystals to the mesoscale, and the closed phase was recovered by thermal treatment. Crystal downsizing suppressed the structural mobility and stabilized the open dried phase. The successful isolation of two interconvertible empty phases, the closed phase and the open dried phase, provided switchable sorption properties with or without gate-opening behavior. Interestingly, they also demonstrated the expression of MSME for $CO_2$.

These results suggest that the induction of an MSME for both liquid- and gas-phase molecules could be exploited as smart materials that respond to microscopic environmental changes.

It is known that polymer gels with thermally induced shape-memory effect can be obtained from biologically based macromolecules such as deoxyribonucleic acid (DNA). This gel is swollen in dimethylsulfoxide (DMSO) and is therefore called an "organogel" [322]. Such gel was prepared by cross-linking DNA and trimethylhexadecylammonium bromide with isophorone diisocyanate. The gel can be deformed above 65 °C and retains a new temporary shape when cooled to room temperature under a fixed load and subsequent unloading. When the temperature is increased above 65 °C, the gel recovers its original shape. The temporary shape is fixed at low temperature owing to an expulsion of solvent leading to a stacking of the DNA/lipid strands, while the polar urethane crosslinks fix the permanent shape. Apart from this DNA gel system, Lee et al. have recently demonstrated the strange shape-memory behavior of a DNA gel [323]. As shown in Fig. 7.19b, they show that DNA metamaterials with unusual mechanical properties can be prepared using DNA as a building block. Their DNA metamaterials were prepared using the polymerase enzyme to elongate the DNA chains and weave them noncovalently into a hydrogel. The gel is made from water and DNA molecules, and has a very low elastic modulus (~10 Pa). The material is so soft that it completely collapses under its own weight in the absence of water and can conform to the shape of a container. Moreover, upon the addition of water, and after complete deformation, this hydrogel can be made to return to its original shape. Although these unusual properties of this material are more closely related to SMPs, the significant difference between the DNA gel developed by Luo's group and SMPs is that the temporary shapes of the gel are not fixed. More specifically, instead of solid shape-to-solid shape transitions in SMPs as described in this book, the gel provides an arbitrary liquid shape (that of the container or an 'amoeba' shape if unconfined)-to-solid shape transition. In this regard, it is better termed "shape-remembering" ability rather than the shape-memory effect, in our opinion. However, the liquidlike shape multiplicity of the material should give the material an advantage in transporting through narrow channels like a T-1000 in the movie Terminator 2.

On the other hand, injectable biomaterials are also increasingly being explored to minimize risks and complications associated with surgical implantation. Similarly to the concepts of shape-memory effect in soft materials with the described DNA gel, Bencherif et al. have recently developed a delivery strategy via conventional needle–syringe injection of large preformed macroporous scaffolds with well-defined properties [324]. Their developed injectable 3D scaffolds, in the form of elastic spongelike matrices, were prepared by environmentally friendly cryotropic gelation of a naturally sourced polymer, which is methacrylated alginate, as shown in Fig. 7.19c. The process of cryogelation takes place via the following steps: phase separation with ice crystal formation, cross-linking, and polymerization followed by thawing of ice crystals (porogens) to form an interconnected porous cryogel network. Interestingly, fabricated cryogels with shape-memory properties may be molded to a variety of shapes and sizes, and may be optionally loaded with

therapeutic agents or cells. These scaffolds have the capability to withstand reversible deformations at over 90 % strain level, and a rapid volumetric recovery allows the structurally defined scaffolds to be injected through a small-bore needle with nearly complete geometric restoration once delivered. These gels demonstrated long-term release of biomolecules in vivo. Furthermore, cryogels impregnated with bioluminescent reporter cells provided enhanced survival, higher local retention, and extended engraftment of transplanted cells at the injection site compared with a standard injection technique. Although the meaning of "shape memory" between this book and Mooney's report may also be somewhat different, there is no doubt that the injectable scaffolds with shape-memory ability show great promise for various biomedical applications, including cell therapies. In addition, these meta- or soft materials have potential for real-world application, especially in biomedical fields such as tissue engineering and cell therapy.

## 7.6 Conclusions and Future Trends

Although it may be debatable whether the shape-memory effect is an intrinsic polymer property, its molecular origin clearly suggests that polymer shape-memory effects should not be regarded as "magic" properties reserved to a small number of specially designed polymers. Not only the design of materials but also the design of the programming conditions, on the other hand, relies on the fundamental physics of polymers. With the above analogy, the relative importance of polymer chemistry and physics becomes obvious.

We have discussed the great potential of SMPs for diverse applications in different arenas. A number of application ideas, prototypes and initial commercial trials have been proposed and implemented, but many conflicting issues remain to be resolved. Normally, specific application situations pose special requirements on the overall properties of SMPs. For example, for biomedical applications, challenges exist with the incorporation of the shape-memory effect to fulfill the multidimensional requirements of the modulus, triggering/fixing conditions, degree and rate of fixing/recovery, level of recovery force, biocompatibility, rate of biodegradability and drug-eluting and drug-releasing kinetics. The other key issue may lie in the control of the shape-memory effect inside the human body, where the material must interact with flexible mechanical constraints, such as tissue surroundings and daily motion, biological metabolism and complicated chemical environments, such as acids, salts and alkali. For textile applications, difficulties lie in meeting the stringent requirements for all aspects of appearance, such as color, dimensional stability, comfort and tactile properties, washability, strength, flexibility, stretchability and shape memory, as well as compatibility with many other chemical, mechanical and thermal processing requirements and low-cost production. For engineering applications, the low recovery stress of SMPs and the fact that the materials become too soft above the switch temperature of the SMP composites remain major concerns that are well known but still present difficult problems.

Although the shape recovery stress can be improved to a certain degree by compounding or blending with other materials, under most circumstances, this method causes problems with low shape recovery ratios and low deformable strains.

Finally, we have made significant progress in enabling SMP technologies, such as materials, processes, and techniques; however, these application successes remain limited. Innovating the integration of all or major functions in practice is worth our concerted effort. As for the distinctive weak points, such as low recovery stress, we must look for new technologies to produce more powerful materials. While we cannot be unreasonable in our expectations for the near future, the existing problems can be overcome by finding more innovative applications that exploit the existing features and capacity of SMPs. This goal requires tremendous creativity and sharp vision as well as investment.

Finally, as the history of SMPs has clearly indicated, the future prospect of SMP would hinge heavily on how best to take advantage of such not so uncommon properties in innovative ways. On the positive front, the application potential for SMPs appears almost unlimited as manifested in the highly diverse application concepts that have appeared in both peer-reviewed journals and patent literature as discussed in this chapter. This is, however, in sharp contrast to the very few real- world applications such as low-value-added toys, and the SMA system is now more valuable and useful in the real world than SMP. The real key thus lies in the discovery of high-value-added applications for which SMPs are enablers or, at minimum, highly attractive alternatives. Whereas biomedical applications of SMPs represent a major focus for SMP research today, stringent requirements and a lengthy regulatory approval process present obstacles for commercial implementations. Although there are many research studies of SMPs for biomedical applications as described in this chapter, under this scenario, whether or not any "silver bullets" beyond biomedical applications may emerge is also an important issue. Finally, however, we ardently hope that, with further study, SMPs will be applied to the field of biomedicine in the near future.

## References

1. Ölander A (1932) An electrochemical investigation of solid cadmium-gold alloys. J Am Chem Soc 54:3819–3833. doi:10.1021/ja01349a004
2. Greninger AB, Mooradian VG (1938) Papers—strain transformation in metastable beta copper-zinc and beta copper-tin alloys (with discussion). Trans AIME 128:337–368
3. Chang LC, Read TA (1951) Plastic deformation and diffusionless phase changes in metals—the gold-cadmium beta-phase. T Am I Min Met Eng 191:47–52
4. Buehler WJ, Wiley RC, Gilfrich JV (1963) Effect of low-temperature phase changes on mechanical properties of alloys near composition TiNi. J Appl Phys 34:1475 (1473 pages). doi:10.1063/1.1729603
5. Vernon LB, Vernon HM (1941) Process of manufacturing articles of thermoplastic synthetic resins. US Patent 2234993
6. Vernon LB, Vernon HM (1941) Article formed of thermoplastic synthetic resins and process manufacturing the same. US Patent 2234993

7. Charlesby A (1960) Atomic radiation and polymers. vol 1, International series of monographs on radiation effects in materials. Pergamon Press, Oxford
8. Ota S (1981) Current status of irradiated heat-shrinkable tubing in Japan. Radiat Phys Chem 18:81–87. doi:10.1016/0146-5724(81)90066-2
9. Chen W, Xing K, Sun L (1983) The heat shrinking mechanism of polyethylene film. Radiat Phys Chem 22:593–601. doi:10.1016/0146-5724(83)90068-7
10. Machi S (1996) New trends of radiation processing applications. Radiat Phys Chem 47:333–336. doi:10.1016/0969-806x(95)00125-H
11. Nakayama K (1990) Properties and application of shape memory. Polymer. Nippon Gomu Kyokaishi 63:529–534
12. Nakayama K (1991) Properties and applications of shape-memory polymers. Int Polym Sci Technol 18:T43–T48
13. Hayashi S, Kondo S, Kapadia P, Ushioda E (1995) Room-temperature-functional shape-memory polymers. Plast Eng 51:29–31
14. Ito K, Abe K, Li HL, Ujihira Y, Ishikawa N, Hayashi S (1996) Variation of free volume size and content of shape memory polymer polyurethane upon temperature studied by positron annihilation lifetime techniques and infrared spectroscopy. J Radioan Nucl Ch Ar 211:53–60. doi:10.1007/Bf02036255
15. Takahashi T, Hayashi N, Hayashi S (1996) Structure and properties of shape-memory polyurethane block copolymers. J Appl Polym Sci 60:1061–1069. doi:10.1002/(Sici)1097-4628(19960516)60:7<1061:Aid-App18>3.0.Co;2-3
16. Tobushi H, Hara H, Yamada E, Hayashi S (1996) Thermomechanical properties in a thin film of shape memory polymer of polyurethane series. Smart Mater Struct 5:483–491. doi:10.1088/0964-1726/5/4/012
17. Tobushi H, Hashimoto T, Hayashi S, Yamada E (1997) Thermomechanical constitutive modeling in shape memory polymer of polyurethane series. J Intel Mat Syst Str 8:711–718. doi:10.1177/1045389X9700800808
18. Tobushi H, Okumura K, Endo M, Hayashi S (2001) Thermomechanical properties of polyurethane-shape memory polymer foam. J Intel Mat Syst Str 12:283–287. doi:10.1106/Fnsx-Ap9v-Qp1r-Nmwv
19. Hirai T, Maruyama H, Suzuki T, Hayashi S (1992) Effect of chemical cross-linking under elongation on shape restoring of poly(vinyl alcohol) hydrogel. J Appl Polym Sci 46:1449–1451. doi:10.1002/app.1992.070460815
20. Hirai T, Maruyama H, Suzuki T, Hayashi S (1992) Shape memorizing properties of a hydrogel of poly(vinyl alcohol). J Appl Polym Sci 45:1849–1855. doi:10.1002/app.1992.070451019
21. He XW, Oishi Y, Takahara A, Kajiyama T (1996) Higher order structure and thermo-responsive properties of polymeric gel with crystalline side chains. Polym J 28:452–457. doi:10.1295/polymj.28.452
22. Matsuda A, Sato J, Yasunaga H, Osada Y (1994) Order-disorder transition of a hydrogel containing an n-alkyl acrylate. Macromolecules 27:7695–7698. doi:10.1021/ma00104a027
23. Osada Y, Matsuda A (1995) Shape-memory in hydrogels. Nature 376:219. doi:10.1038/376219a0
24. Lendlein A, Langer R (2002) Biodegradable, elastic shape-memory polymers for potential biomedical applications. Science 296:1673–1676. doi:10.1126/science.1066102
25. Lendlein A, Schmidt AM, Langer R (2001) AB-polymer networks based on oligo($\varepsilon$-caprolactone) segments showing shape-memory properties. Proc Natl Acad Sci 98:842–847. doi:10.1073/pnas.98.3.842
26. Liu C, Qin H, Mather PT (2007) Review of progress in shape-memory polymers. J Mater Chem 17:1543–1558. doi:10.1039/B615954k
27. Leng JS, Lan X, Liu YJ, Du SY (2011) Shape-memory polymers and their composites: stimulus methods and applications. Prog Mater Sci 56:1077–1135. doi:10.1016/j.pmatsci.2011.03.001
28. Behl M, Lendlein A (2007) Actively moving polymers. Soft Matter 3:58. doi:10.1039/b610611k
29. Lendlein A (2010) Progress in actively moving polymers. J Mater Chem 20:3332–3334. doi:10.1039/c004361n

30. Shirai Y, Hayashi S, Kaisha MJK (1988) Development of polymeric shape memory material. Mitsubishi Heavy Industries
31. Tobushi H, Hayashi S, Kojima S (1992) Mechanical-properties of shape memory polymer of polyurethane series—(basic characteristics of stress-strain-temperature relationship). Jsme Int J I-Solid M 35:296–302
32. Kobayashi K, Hayashi S (1992) Woven fabric made of shape memory polymer. US Patent 5128197
33. Hayashi S, Tasaka Y, Hayashi N, Akita Y (2004) Development of smart polymer materials and its various applications. Mitsubishi Heavy Industries, Ltd. Technical Review 41:1–3
34. Lin JR, Chen LW (1998) Study on shape-memory behavior of polyether-based polyurethanes. I. Influence of the hard-segment content. J Appl Polym Sci 69:1563–1574. doi:10.1002/(Sici)1097-4628(19980822)69:8<1563:Aid-App11>3.0.Co;2-W
35. Lin JR, Chen LW (1998) Study on shape-memory behavior of polyether-based polyurethanes. II. Influence of soft-segment molecular weight. J Appl Polym Sci 69:1575–1586. doi:10.1002/(Sici)1097-4628(19980822)69:8<1575:Aid-App12>3.0.Co;2-U
36. Sakurai K, Takahashi T (1989) Strain-Induced Crystallization in Polynorbornene. J Appl Polym Sci 38:1191–1194. doi:10.1002/app.1989.070380616
37. Sakurai K, Kashiwagi T, Takahashi T (1993) Crystal-structure of polynorbornene. J Appl Polym Sci 47:937–940. doi:10.1002/app.1993.070470521
38. Jeon HG, Mather PT, Haddad TS (2000) Shape memory and nanostructure in poly(norbornyl-POSS) copolymers. Polym Int 49:453–457. doi:10.1002/(Sici)1097-0126(200005)49: 5<453:Aid-Pi332>3.3.Co;2-8
39. Haddad TS, Lichtenhan JD (1996) Hybrid organic−inorganic thermoplastics: styryl-based polyhedral oligomeric silsesquioxane polymers. Macromolecules 29:7302–7304. doi:10.1021/ma960609d
40. Lee A, Lichtenhan JD (1998) Viscoelastic responses of polyhedral oligosilsesquioxane reinforced epoxy systems. Macromolecules 31:4970–4974. doi:10.1021/ma9800764
41. Mather PT, Jeon HG, Romo-Uribe A, Haddad TS, Lichtenhan JD (1999) Mechanical relaxation and microstructure of poly(norbornyl-POSS) copolymers. Macromolecules 32:1194–1203. doi:10.1021/Ma981210n
42. Haddad TS, Mather PT, Jeon HG, Romo-Uribe A, Lichtenhan JD (1998) Thermoplastics modified with nanoscale inorganic macromers. Abstr Pap Am Chem S 216:U322–U322
43. Romo-Uribe A, Mather PT, Haddad TS, Lichtenhan JD (1998) Viscoelastic and morphological behavior of hybrid styryl-based polyhedral oligomeric silsesquioxane (POSS) copolymers. J Polym Sci Pol Phys 36:1857–1872. doi:10.1002/(Sici)1099-0488(199808)36:11<1857:Aid-Polb7>3.3.Co;2-7
44. Campo CJ, Mather PT (2005) PVDF: PMMA shape memory blends: effect of short carbon fiber addition. Abstr Pap Am Chem S 230:U3760–U3761
45. Liu C, Mather PT (2003) Thermomechanical characterization of blends of poly(vinyl acetate) with semicrystalline polymers for shape memory applications. In: Proceedings of the annual technical conference—society of plastics engineers, ANTEC 2003, vol 2, pp 1962–1966
46. Sakurai K, Shirakawa Y, Kashiwagi T, Takahashi T (1994) Crystal transformation of styrene-butadiene block copolymer. Polymer 35:4238–4239. doi:10.1016/0032-3861(94)90602-5
47. Sakurai K, Tanaka H, Ogawa N, Takahashi T (1997) Shape-memorizable styrene-butadiene block copolymer 1. Thermal and mechanical behaviors and structural change with deformation. J Macromol Sci, Phys 36:703–716. doi:10.1080/00222349708212397
48. Ikematsu T, Kishimoto Y, Karaushi M (1990) Block copolymer. Bumpers with good shape memory. Japan Patent 02022355
49. Luo XL, Zhang XY, Wang MT, Ma DH, Xu M, Li FK (1997) Thermally stimulated shape-memory behavior of ethylene oxide ethylene terephthalate segmented copolymer. J Appl Polym Sci 64:2433–2440. doi:10.1002/(Sici)1097-4628(19970620)64:12<2433:Aid-App17>3.0.Co;2-1
50. Wang MT, Luo XL, Zhang XY, Ma DZ (1997) Shape memory properties in poly(ethylene oxide)-poly(ethylene terephthalate) copolymers. Polym Advan Technol 8:136–139. doi:10.1002/(Sici)1099-1581(199703)8:3<136:Aid-Pat621>3.0.Co;2-I

51. Wang M, Zhang L (1999) Recovery as a measure of oriented crystalline structure in poly(ether ester)s based on poly(ethylene oxide) and poly(ethylene terephthalate) used as shape memory polymers. J Polym Sci, Part B: Polym Phys 37:101–112. doi:10.1002/(sici)1099-0488(19990115)37:2<101:aid-polb1>3.0.co;2-x
52. Wang MT, Luo XL, Ma DZ (1998) Dynamic mechanical behavior in the ethylene terephthalate ethylene oxide copolymer with long soft segment as a shape memory material. Eur Polym J 34:1–5. doi:10.1016/S0014-3057(97)00082-7
53. VanCaeter P, Goethals EJ, Gancheva V, Velichkova R (1997) Synthesis and bulk properties of poly(tetrahydrofuran)-poly(2-methyl-2-oxazoline) ABA triblock copolymers. Polym Bull 39:589–596. doi:10.1007/s002890050190
54. Kim BK, Lee SY, Xu M (1996) Polyurethanes having shape memory effects. Polymer 37:5781–5793. doi:10.1016/S0032-3861(96)00442-9
55. Li FK, Zhang X, Hou JN, Xu M, Lu XL, Ma DZ, Kim BK (1997) Studies on thermally stimulated shape memory effect of segmented polyurethanes. J Appl Polym Sci 64:1511–1516. doi:10.1002/(Sici)1097-4628(19970523)64:8<1511:Aid-App8>3.0.Co;2-K
56. Li FK, Hou JN, Zhu W, Zhang X, Xu M, Luo XL, Ma DZ, Kim BK (1996) Crystallinity and morphology of segmented polyurethanes with different soft-segment length. J Appl Polym Sci 62:631–638. doi:10.1002/(Sici)1097-4628(19961024)62:4<631:Aid-App6>3.0.Co;2-U
57. Kim BK, Lee SY, Lee JS, Baek SH, Choi YJ, Lee JO, Xu M (1998) Polyurethane ionomers having shape memory effects. Polymer 39:2803–2808. doi:10.1016/S0032-3861(97)00616-2
58. Jeong HM, Lee JB, Lee SY, Kim BK (2000) Shape memory polyurethane containing mesogenic moiety. J Mater Sci 35:279–283. doi:10.1023/A:1004728814128
59. Weiss RA, Fitzgerald JJ, Kim D (1991) Viscoelastic behavior of plasticized sulfonated polystyrene ionomers. Macromolecules 24:1064–1070. doi:10.1021/Ma00005a014
60. Weiss RA, Fitzgerald JJ, Kim D (1991) Viscoelastic behavior of lightly sulfonated polystyrene ionomers. Macromolecules 24:1071–1076. doi:10.1021/Ma00005a015
61. Skákalová V, Lukeš V, Breza M (1997) Shape memory effect of dehydrochlorinated crosslinked poly(vinyl chloride). Macromol Chem Phys 198:3161–3172. doi:10.1002/macp.1997.021981014
62. Palma G, Carenza M (1970) Degradation of poly(vinyl chloride). I. Kinetics of thermal and radiation-induced dehydrochlorination reactions at low temperatures. J Appl Polym Sci 14:1737–1754. doi:10.1002/app.1970.070140708
63. Simon P (1994) Polymer degradation by elimination of small molecules. Angew Makromol Chem 216:187–203. doi:10.1002/apmc.1994.052160113
64. Li FK, Larock RC (2000) New soybean oil-styrene-divinylbenzene thermosetting copolymers. II. Dynamic mechanical properties. J Polym Sci Pol Phys 38:2721–2738. doi:10.1002/1099-0488(20001101)38:21<2721:Aid-Polb30>3.0.Co;2-D
65. Li F, Hanson MV, Larock RC (2001) Soybean oil-divinylbenzene thermosetting polymers: synthesis, structure, properties and their relationships. Polymer 42:1567–1579. doi:10.1016/S0032-3861(00)00546-2
66. Li FK, Larock RC (2002) New soybean oil-styrene-divinylbenzene thermosetting copolymers—IV. Good damping properties. Polym Advan Technol 13:436–449. doi:10.1002/Pat.206
67. Li FK, Larock RC (2002) New soybean oil-styrene-divinylbenzene thermosetting copolymers. V. shape memory effect. J Appl Polym Sci 84:1533–1543. doi:10.1002/App.10493
68. Li FK, Larock RC (2003) New soybean oil-styrene-divinylbenzene thermosetting copolymers. VI. Time-temperature-transformation cure diagram and the effect of curing conditions on the thermoset properties. Polym Int 52:126–132. doi:10.1002/Pi.1060
69. Alteheld A, Feng YK, Kelch S, Lendlein A (2005) Biodegradable, amorphous copolyesterurethane networks having shape-memory properties. Angew Chem Int Edit 44:1188–1192. doi:10.1002/anie.200461360
70. Kelch S, Choi NY, Wang Z, Lendlein A (2008) Amorphous, elastic AB copolymer networks from acrylates and poly[(l-lactide)-ran-glycolide]dimethacrylates. Adv Eng Mater 10:494–502. doi:10.1002/adem.200700339

71. Irie M (1998) Shape memory polymers. Shape memory materials. Cambridge University Press, Cambridge
72. Liu CD, Chun SB, Mather PT, Zheng L, Haley EH, Coughlin EB (2002) Chemically cross-linked polycyclooctene: synthesis, characterization, and shape memory behavior. Macromolecules 35:9868–9874. doi:10.1021/Ma021141j
73. Mather PT, Liu C, Coughlin EB, Chun SB (2004) Crosslinked polycyclooctene. US Patent US20040122184 A1
74. Arditti SJ, Avedikian SZ, Bernstein BS (1971) Articles with polymeric memory. US Patent 3563973
75. Hosemann R, Lobodaca J, Cackovic H (1972) Affine deformation of linear polyethylene. Z Naturforsch Pt A A 27:478
76. Lendlein A, Schmidt AM, Schroeter M, Langer R (2005) Shape-memory polymer networks from oligo(epsilon-caprolactone)dimethacrylates. J Polym Sci Pol Chem 43:1369–1381. doi :10.1002/Pola.20598
77. Zhu GM, Xu QY, Liang GZ, Zhou HF (2005) Shape-memory behaviors of sensitizing radiation-crosslinked polycaprolactone with polyfunctional poly(ester acrylate). J Appl Polym Sci 95:634–639. doi:10.1002/app.20989
78. Nagata M, Kitazima I (2006) Photocurable biodegradable poly(epsilon-caprolactone)/poly(ethylene glycol) multiblock copolymers showing shape-memory properties. Colloid Polym Sci 284:380–386. doi:10.1007/s00396-005-1393-3
79. Zhu G, Xu S, Wang J, Zhang L (2006) Shape memory behaviour of radiation-crosslinked PCL/PMVS blends. Radiat Phys Chem 75:443–448. doi:10.1016/j.radphyschem.2005.10.004
80. Kunzelman J, Chung T, Mather PT, Weder C (2008) Shape memory polymers with built-in threshold temperature sensors. J Mater Chem 18:1082–1086. doi:10.1039/B718445J
81. Koerner H, Price G, Pearce NA, Alexander M, Vaia RA (2004) Remotely actuated polymer nanocomposites—stress-recovery of carbon-nanotube-filled thermoplastic elastomers. Nat Mater 3:115–120. doi:10.1038/nmat1059
82. Lendlein A, Kelch S (2005) Degradable, multifunctional polymeric biomaterials with shape-memory. Mater Sci Forum 492–493:219–223. doi:10.4028/www.scientific.net/MSF.492-493.219
83. Kelch S, Steuer S, Schmidt AM, Lendlein A (2007) Shape-memory polymer networks from oligo[(ε-hydroxycaproate)-co-glycolate]dimethacrylates and butyl acrylate with adjustable hydrolytic degradation rate. Biomacromolecules 8:1018–1027. doi:10.1021/bm0610370
84. Choi NY, Lendlein A (2007) Degradable shape-memory polymer networks from oligo[(L-lactide)-ran-glycolide]dimethacrylates. Soft Matter 3:901–909. doi:10.1039/B702515g
85. Behl M, Ridder U, Feng Y, Kelch S, Lendlein A (2009) Shape-memory capability of binary multiblock copolymer blends with hard and switching domains provided by different components. Soft Matter 5:676–684. doi:10.1039/B810583A
86. Lv H, Leng J, Du S (2008) Electro-induced shape-memory polymer nanocomposite containing conductive particles and short fibers. Behavior Mech Multifunct Compos Mater 6929:69291L–69298L. doi:10.1117/12.775736
87. Leng J, Lv H, Liu Y, Du S (2007) Electroactivate shape-memory polymer filled with nanocarbon particles and short carbon fibers. Appl Phys Lett 91:144105 (144103 pages). doi:10.1063/1.2790497
88. Liu Y, Lv H, Lan X, Leng J, Du S (2009) Review of electro-active shape-memory polymer composite. Compos Sci Technol 69:2064–2068. doi:10.1016/j.compscitech.2008.08.016
89. Behl M, Razzaq MY, Lendlein A (2010) Multifunctional shape-memory polymers. Adv Mater 22:3388–3410. doi:10.1002/adma.200904447
90. Lendlein A, Jiang HY, Junger O, Langer R (2005) Light-induced shape-memory polymers. Nature 434:879–882. doi:10.1038/Nature03496
91. Jiang HY, Kelch S, Lendlein A (2006) Polymers move in response to light. Adv Mater 18:1471–1475. doi:10.1002/adma.200502266
92. Li MH, Keller P, Li B, Wang XG, Brunet M (2003) Light-driven side-on nematic elastomer actuators. Adv Mater 15:569–572. doi:10.1002/adma.200304552

93. Scott TF, Draughon RB, Bowman CN (2006) Actuation in crosslinked polymers via photoinduced stress relaxation. Adv Mater 18:2128–2132. doi:10.1002/adma.200600379
94. Scott TF, Schneider AD, Cook WD, Bowman CN (2005) Photoinduced plasticity in crosslinked polymers. Science 308:1615–1617. doi:10.1126/science.1110505
95. Huang WM, Yang B, An L, Li C, Chan YS (2005) Water-driven programmable polyurethane shape memory polymer: Demonstration and mechanism. Appl Phys Lett 86:114105 (114103 pages). doi:10.1063/1.1880448
96. Wang CC, Huang WM, Ding Z, Zhao Y, Purnawali H (2012) Cooling-/water-responsive shape memory hybrids. Compos Sci Technol 72:1178–1182. doi:10.1016/j.compscitech.2012.03.027
97. Fan K, Huang WM, Wang CC, Ding Z, Zhao Y, Purnawali H, Liew KC, Zheng LX (2011) Water-responsive shape memory hybrid: design concept and demonstration. Express Polym Lett 5:409–416. doi:10.3144/expresspolymlett.2011.40
98. Jung YC, So HH, Cho JW (2006) Water-responsive shape memory polyurethane block copolymer modified with polyhedral oligomeric silsesquioxane. J Macromol Sci B 45:453–461. doi:10.1080/00222340600767513
99. Mohr R, Kratz K, Weigel T, Lucka-Gabor M, Moneke M, Lendlein A (2006) Initiation of shape-memory effect by inductive heating of magnetic nanoparticles in thermoplastic polymers. P Natl Acad Sci USA 103:3540–3545. doi:10.1073/pnas.0600079103
100. Buckley PR, McKinley GH, Wilson TS, Small W, Benett WJ, Bearinger JP, McElfresh MW, Maitland DJ (2006) Inductively heated shape memory polymer for the magnetic actuation of medical devices. IEEE T Bio-Med Eng 53:2075–2083. doi:10.1109/Tbme.2006.877113
101. Yang D, Huang W, He XH, Xie MR (2012) Electromagnetic activation of a shape memory copolymer matrix incorporating ferromagnetic nanoparticles. Polym Int 61:38–42. doi:10.1002/Pi.3188
102. Schmidt AM (2006) Electromagnetic activation of shape memory polymer networks containing magnetic nanoparticles. Macromol Rapid Comm 27:1168–1172. doi:10.1002/marc.200600225
103. He ZW, Satarkar N, Xie T, Cheng YT, Hilt JZ (2011) Remote controlled multishape polymer nanocomposites with selective radiofrequency actuations. Adv Mater 23:3192–3196. doi:10.1002/adma.201100646
104. Kumar UN, Kratz K, Wagermaier W, Behl M, Lendlein A (2010) Non-contact actuation of triple-shape effect in multiphase polymer network nanocomposites in alternating magnetic field. J Mater Chem 20:3404–3415. doi:10.1039/B923000a
105. Hazelton CS, Arzberger SC, Lake MS, Munshi NA (2007) RF actuation of a thermoset shape memory polymer with embedded magnetoelectroelastic particles. J Adv Mater-Covina 39:35–39
106. Leng JS, Wu XL, Liu YJ (2009) Infrared light-active shape memory polymer filled with nanocarbon particles. J Appl Polym Sci 114:2455–2460. doi:10.1002/App.30724
107. Gall K, Mikulas M, Munshi NA, Beavers F, Tupper M (2000) Carbon fiber reinforced shape memory polymer composites. J Intel Mat Syst Str 11:877–886. doi:10.1106/EJGR-EWNM-6CLX-3X2M
108. Liang C, Rogers CA, Malafeew E (1997) Investigation of shape memory polymers and their hybrid composites. J Intel Mat Syst Str 8:380–386. doi:10.1177/1045389x9700800411
109. Moad G, Solomon DH (2006) The chemistry of radical polymerization. Elsevier, Amsterdam
110. Lendlein A, Kelch S (2002) Shape-memory polymers. Angew Chem Int Ed Engl 41:2035–2057. doi:10.1002/1521-3773(20020617)41:12<2034:AID-ANIE2034>3.0.CO;2-M
111. Aoyagi T, Miyata F, Nagase Y (1994) Preparation of cross-linked aliphatic polyester and application to thermoresponsive material. J Control Release 32:87–96. doi:10.1016/0168-3659(94)90228-3
112. Miyasako H, Yamamoto K, Nakao A, Aoyagi T (2007) Preparation of cross-linked poly[(epsilon-caprolactone)-co-lactide] and biocompatibility studies for tissue engineering materials. Macromol Biosci 7:76–83. doi:10.1002/mabi.200600188

113. Miyasako H, Yamamoto K, Aoyagi K (2008) Preparation, characterization and biocompatibility study of the scaffold prototype derived from cross-linked poly [(epsilon-caprolactone)-co-lactide] for tissue engineering materials. Polym J 40:806–812. doi:10.1295/polymj.PJ2008036
114. Muroya T, Yamamoto K, Aoyagi T (2009) Degradation of cross-linked aliphatic polyester composed of poly(epsilon-caprolactone-co-D, L-lactide) depending on the thermal properties. Polym Degrad Stabil 94:285–290. doi:10.1016/j.polymdegradstab.2008.12.014
115. Smith TL (1974) Strength of segmented and triblock elastomers. Abstr Pap Am Chem S:8
116. Smith TL (1976) Factors affecting strength of elastomers. Abstr Pap Am Chem S:37
117. Smith TL (1977) Strength of elastomers—perspective. Polym Eng Sci 17:129–143. doi:10.1002/pen.760170302
118. Smith TL (1978) Strength of elastomers—perspective. Rubber Chem Technol 51:225–252. doi:10.5254/1.3545831
119. Ji FL, Hu JL, Li TC, Wong YW (2007) Morphology and shape memory effect of segmented polyurethanes. Part I: with crystalline reversible phase. Polymer 48:5133–5145. doi:10.1016/j.polymer.2007.06.032
120. Ji FL, Hu JL, Han JP (2011) Shape memory polyurethane-ureas based on isophorone diisocyanate. High Perform Polym 23:177–187. doi:10.1177/0954008311398323
121. Chen SJ, Hu JL, Liu YQ, Liem HM, Zhu Y, Liu YJ (2007) Effect of SSL and HSC on morphology and properties of PHA based SMPU synthesized by bulk polymerization method. J Polym Sci Pol Phys 45:444–454. doi:10.1002/Polb.21046
122. Korley LTJ, Pate BD, Thomas EL, Hammond PT (2006) Effect of the degree of soft and hard segment ordering on the morphology and mechanical behavior of semicrystalline segmented polyurethanes. Polymer 47:3073–3082. doi:10.1016/j.polymer.2006.02.093
123. Luo XL, Zhao MC, Wang MZ, Ding LN, Ma DZ (2000) Thermally stimulated shape memory behavior of (ethylene oxide-butylene terephthalate) segmented copolymer. Chin J Polym Sci 18:357–361
124. Li JH, Viveros JA, Wrue MH, Anthamatten M (2007) Shape-memory effects in polymer networks containing reversibly associating side-groups. Adv Mater 19:2851–2855. doi:10.1002/adma.200602260
125. del Rio E, Lligadas G, Ronda JC, Galia M, Cadiz V, Meier MAR (2011) Shape Memory Polyurethanes from Renewable Polyols Obtained by ATMET Polymerization of Glyceryl Triundec-10-enoate and 10-Undecenol. Macromol Chem Phys 212:1392–1399. doi:10.1002/macp.201100025
126. Yang D, Huang W, Yu JH, Jiang JS, Zhang LY, Xie MR (2010) A novel shape memory polynorbornene functionalized with poly(epsilon-caprolactone) side chain and cyano group through ring-opening metathesis polymerization. Polymer 51:5100–5106. doi:10.1016/j.polymer.2010.09.009
127. Safranski DL, Gall K (2008) Effect of chemical structure and crosslinking density on the thermo-mechanical properties and toughness of (meth)acrylate shape memory polymer networks. Polymer 49:4446–4455. doi:10.1016/j.polymer.2008.07.060
128. Yakacki CM, Shandas R, Safranski D, Ortega AM, Sassaman K, Gall K (2008) Strong, tailored, biocompatible shape-memory polymer networks. Adv Funct Mater 18:2428–2435. doi:10.1002/adfm.200701049
129. Rickert D, Lendlein A, Schmidt AM, Kelch S, Roehlke W, Fuhrmann R, Franke RP (2003) In vitro cytotoxicity testing of AB-polymer networks based on oligo(ε-caprolactone) segments after different sterilization techniques. J Biomed Mater Res B Appl Biomater 67B:722–731. doi:10.1002/jbm.b.10069
130. Uto K, Yamamoto K, Hirase S, Aoyagi T (2006) Temperature-responsive cross-linked poly(epsilon-caprolactone) membrane that functions near body temperature. J Control Release 110:408–413. doi:10.1016/j.jconrel.2005.10.024
131. Zhu G, Liang G, Xu Q, Yu Q (2003) Shape-memory effects of radiation crosslinked poly(epsilon-caprolactone). J Appl Polym Sci 90:1589–1595. doi:10.1002/App.12736

132. Ware T, Voit W, Gall K (2010) Effects of sensitizer length on radiation crosslinked shape-memory polymers. Radiat Phys Chem 79:446–453. doi:10.1016/j.radphyschem.2009.10.006
133. Kirk WP, Wouters KL, Basit NA, MacDonnell FM, Tao M, Clark KP (2003) Electrical and optical effects in molecular nanoscopic-sized building blocks. Physica E 19:126–132. doi:10.1016/S1386-9477(03)00298-4
134. Watts PCP, Hsu WK (2003) Behaviours of embedded carbon nanotubes during film cracking. Nanotechnology 14:L7–L10. doi:10.1088/0957-4484/14/5/101
135. Sahoo NG, Jung YC, Yoo HJ, Cho JW (2006) Effect of functionalized carbon nanotubes on molecular interaction and properties of polyurethane composites. Macromol Chem Phys 207:1773–1780. doi:10.1002/macp.200600266
136. Cho JW, Kim JW, Jung YC, Goo NS (2005) Electroactive shape-memory polyurethane composites incorporating carbon nanotubes. Macromol Rapid Comm 26:412–416. doi:10.1002/marc.200400492
137. Chen W, Tao XM (2005) Self-organizing alignment of carbon nanotubes in thermoplastic polyurethane. Macromol Rapid Comm 26:1763–1767. doi:10.1002/marc.200500531
138. Meng QH, Hu JL (2008) Self-organizing alignment of carbon nanotube in shape memory segmented fiber prepared by in situ polymerization and melt spinning. Compos Part a-Appl S 39:314–321. doi:10.1016/j.compositesa.2007.10.007
139. Kota AK, Cipriano BH, Duesterberg MK, Gershon AL, Powell D, Raghavan SR, Bruck HA (2007) Electrical and rheological percolation in polystyrene/MWCNT nanocomposites. Macromolecules 40:7400–7406. doi:10.1021/Ma0711792
140. Song YS, Youn JR (2005) Influence of dispersion states of carbon nanotubes on physical properties of epoxy nanocomposites. Carbon 43:1378–1385. doi:10.1016/j.carbon.2005.01.007
141. Bal S (2007) Influence of dispersion states of carbon nanotubes on mechanical and electrical properties of epoxy nanocomposites. J Sci Ind Res India 66:752–756
142. Shaffer MSP, Windle AH (1999) Fabrication and characterization of carbon nanotube/poly(vinyl alcohol) composites. Adv Mater 11:937–941. doi:10.1002/(Sici)1521-4095(199908)11:11<937:Aid-Adma937>3.0.Co;2-9
143. Bin YZ, Kitanaka M, Zhu D, Matsuo M (2003) Development of highly oriented polyethylene filled with aligned carbon nanotubes by gelation/crystallization from solutions. Macromolecules 36:6213–6219. doi:10.1021/Ma0301956
144. Gupta R, Chaudhury NK (2007) Entrapment of biomolecules in sol-gel matrix for applications in biosensors: problems and future prospects. Biosens Bioelectron 22:2387–2399. doi:10.1016/j.bios.2006.12.025
145. Wen JY, Wilkes GL (1996) Organic/inorganic hybrid network materials by the sol-gel approach. Chem Mater 8:1667–1681. doi:10.1021/Cm9601143
146. Diaz-Garcia ME, Laino RB (2005) Molecular imprinting in sol-gel materials: recent developments and applications. Microchim Acta 149:19–36. doi:10.1007/s00604-004-0274-7
147. Jin Z, Pramoda KP, Xu G, Goh SH (2001) Dynamic mechanical behavior of melt-processed multi-walled carbon nanotube/poly(methyl methacrylate) composites. Chem Phys Lett 337:43–47. doi:10.1016/S0009-2614(01)00186-5
148. Andrews R, Jacques D, Minot M, Rantell T (2002) Fabrication of carbon multiwall nanotube/polymer composites by shear mixing. Macromol Mater Eng 287:395–403. doi:10.1002/1439-2054(20020601)287:6<395:Aid-Mame395>3.0.Co;2-S
149. Andrews R, Weisenberger MC (2004) Carbon nanotube polymer composites. Curr Opin Solid St M 8:31–37. doi:10.1016/j.cossms.2003.10.006
150. Zhang WD, Shen L, Phang IY, Liu TX (2004) Carbon nanotubes reinforced nylon-6 composite prepared by simple melt-compounding. Macromolecules 37:256–259. doi:10.1021/Ma035594f
151. Cadek M, Coleman JN, Ryan KP, Nicolosi V, Bister G, Fonseca A, Nagy JB, Szostak K, Beguin F, Blau WJ (2004) Reinforcement of polymers with carbon nanotubes: the role of nanotube surface area. Nano Lett 4:353–356. doi:10.1021/Nl035009o

152. Velasco-Santos C, Martinez-Hernandez AL, Fisher FT, Ruoff R, Castano VM (2003) Improvement of thermal and mechanical properties of carbon nanotube composites through chemical functionalization. Chem Mater 15:4470–4475. doi:10.1021/Cm034243c
153. Sahoo NG, Jung YC, Yoo HJ, Cho JW (2007) Influence of carbon nanotubes and polypyrrole on the thermal, mechanical and electroactive shape-memory properties of polyurethane nanocomposites. Compos Sci Technol 67:1920–1929. doi:10.1016/j.compscitech.2006.10.013
154. Sahoo NG, Jung YC, Cho JW (2007) Electroactive shape memory effect of polyurethane composites filled with carbon nanotubes and conducting polymer. Mater Manuf Process 22:419–423. doi:10.1080/10426910701232857
155. Yoo HJ, Jung YC, Sahoo NG, Cho JW (2006) Polyurethane-carbon nanotube nanocomposites prepared by in situ polymerization with electroactive shape memory. J Macromol Sci B 45:441–451. doi:10.1080/00222340600767471
156. An KH, Jeong SY, Hwang HR, Lee YH (2004) Enhanced sensitivity of a gas sensor incorporating single-walled carbon nanotube-polypyrrole nanocomposites. Adv Mater 16:1005. doi:10.1002/adma.200306176
157. Xia HS, Song M (2006) Preparation and characterisation of polyurethane grafted single-walled carbon nanotubes and derived polyurethane nanocomposites. J Mater Chem 16:1843–1851. doi:10.1039/B601152g
158. Xia HS, Song M (2005) Preparation and characterization of polyurethane-carbon nanotube composites. Soft Matter 1:386–394. doi:10.1039/B509038e
159. Guo Z, Lee SE, Kim H, Park S, Hahn HT, Karki AB, Young DP (2009) Fabrication, characterization and microwave properties of polyurethane nanocomposites reinforced with iron oxide and barium titanate nanoparticles. Acta Mater 57:267–277. doi:10.1016/j.actamat.2008.09.024
160. Guo ZH, Pereira T, Choi O, Wang Y, Hahn HT (2006) Surface functionalized alumina nanoparticle filled polymeric nanocomposites with enhanced mechanical properties. J Mater Chem 16:2800–2808. doi:10.1039/B603020c
161. Jung YC, Sahoo NG, Cho JW (2006) Polymeric nanocomposites of polyurethane block copolymers and functionalized multi-walled carbon nanotubes as crosslinkers. Macromol Rapid Comm 27:126–131. doi:10.1002/marc.200500658
162. Cui J, Wang WP, You YZ, Liu CH, Wang PH (2004) Functionalization of multiwalled carbon nanotubes by reversible addition fragmentation chain-transfer polymerization. Polymer 45:8717–8721. doi:10.1016/j.polymer.2004.10.068
163. Xie XL, Mai YW, Zhou XP (2005) Dispersion and alignment of carbon nanotubes in polymer matrix: a review. Mat Sci Eng R 49:89–112. doi:10.1016/j.mser.2005.04.002
164. Rozenberg BA, Tenne R (2008) Polymer-assisted fabrication of nanoparticles and nanocomposites. Prog Polym Sci 33:40–112. doi:10.1016/j.progpolymsci.2007.07.004
165. Flory PJ (1953) Principles of polymer chemistry: Paul J. Cornell University, Flory
166. GdC Vasconcelos, Mazur RL, Botelho EC, Rezende MC, Costa ML (2010) Evaluation of crystallization kinetics of polymer of poly (ether-ketone-ketone) and poly (ether-ether-ketone) by DSC. J Aerosp Technol Manage 2:155–162. doi:10.5028/jatm.2010.02026310
167. Nagahama K, Ueda Y, Ouchi T, Ohya Y (2009) Biodegradable shape-memory polymers exhibiting sharp thermal transitions and controlled drug release. Biomacromolecules 10:1789–1794. doi:10.1021/bm9002078
168. Weng S, Xia Z, Chen J, Gong L (2013) Shape memory properties of polycaprolactone-based polyurethanes prepared by reactive extrusion. J Appl Polym Sci 127:748–759. doi:10.1002/app.37768
169. DiOrio AM, Luo X, Lee KM, Mather PT (2011) A functionally graded shape memory polymer. Soft Matter 7:68–74. doi:10.1039/C0SM00487A
170. Song S, Feng J, Wu P (2011) A new strategy to prepare polymer-based shape memory elastomers. Macromol Rapid Comm 32:1569–1575. doi:10.1002/marc.201100298
171. Luo X, Mather PT (2009) Preparation and characterization of shape memory elastomeric composites. Macromolecules 42:7251–7253. doi:10.1021/ma9015888

172. Luo X, Mather PT (2013) Design strategies for shape memory polymers. Curr Opin Chem Eng 2:103–111. doi:10.1016/j.coche.2012.10.006
173. Leng JS, Lan X, Liu YJ, Du SY, Huang WM, Liu N, Phee SJ, Yuan Q (2008) Electrical conductivity of thermoresponsive shape-memory polymer with embedded micron sized Ni powder chains. Appl Phys Lett 92:014104 (14103 pages). doi:10.1063/1.2829388
174. Ping P, Wang W, Chen X, Jing X (2007) The influence of hard-segments on two-phase structure and shape memory properties of PCL-based segmented polyurethanes. J Polym Sci, Part B: Polym Phys 45:557–570. doi:10.1002/polb.20974
175. Waletzko RS, Korley LTJ, Pate BD, Thomas EL, Hammond PT (2009) Role of increased crystallinity in deformation-induced structure of segmented thermoplastic polyurethane elastomers with PEO and PEO−PPO−PEO soft segments and HDI hard segments. Macromolecules 42:2041–2053. doi:10.1021/ma8022052
176. D'Hollander S, Gommes CJ, Mens R, Adriaensens P, Goderis B, Du Prez F (2010) Modeling the morphology and mechanical behavior of shape memory polyurethanes based on solid-state NMR and synchrotron SAXS/WAXD. J Mater Chem 20:3475. doi:10.1039/b923734h
177. Tobushi H, Okumura K, Hayashi S, Ito N (2001) Thermomechanical constitutive model of shape memory polymer. Mech Mater 33:545–554. doi:10.1016/S0167-6636(01)00075-8
178. Lin HC, Wu SK (1992) Strengthening effect on shape recovery characteristic of the equiatomic TiNi alloy. Scr Metall Mater 26:59–62. doi:10.1016/0956-716x(92)90369-p
179. Gall K, Yakacki CM, Liu Y, Shandas R, Willett N, Anseth KS (2005) Thermomechanics of the shape memory effect in polymers for biomedical applications. J Biomed Mater Res, Part A 73A:339–348. doi:10.1002/jbm.a.30296
180. Liu Y, Gall K, Dunn ML, McCluskey P (2003) Thermomechanical recovery couplings of shape memory polymers in flexure. Smart Mater Struct 12:947–954. doi:10.1088/0964-1726/12/6/012
181. Capaccio G, Ward IM (1982) Shrinkage, shrinkage force and the structure of ultra high modulus polyethylenes. Colloid Polym Sci 260:46–55. doi:10.1007/Bf01447675
182. Chowdhury SR, Mishra JK, Das CK (2000) Shrinkability and microstructural properties of composites based on low-density polyethylene (LDPE) and polyurethane (PU) rubber. J Thermoplast Compos 13:400–416. doi:10.1106/V6pp-X3d2-Rgdk-Ft7p
183. Chowdhury SR, Mishra JK, Das CK (2000) Structure, shrinkability and thermal property correlations of ethylene vinyl acetate (EVA)/carboxylated nitrile rubber (XNBR) polymer blends. Polym Degrad Stabil 70:199–204. doi:10.1016/S0141-3910(00)00107-5
184. Bellin I, Kelch S, Langer R, Lendlein A (2006) Polymeric triple-shape materials. P Natl Acad Sci USA 103:18043–18047. doi:10.1073/pnas.0608586103
185. Xie T (2011) Recent advances in polymer shape memory. Polymer 52:4985–5000. doi:10.1016/j.polymer.2011.08.003
186. Xie T, Xiao X, Cheng Y-T (2009) Revealing triple-shape memory effect by polymer bilayers. Macromol Rapid Comm 30:1823–1827. doi:10.1002/marc.200900409
187. Xie T (2010) Tunable polymer multi-shape memory effect. Nature 464:267–270. doi:10.1038/nature08863
188. Ratner BD, Bryant SJ (2004) Biomaterials: where we have been and where we are going. Annu Rev Biomed Eng 6:41–75. doi:10.1146/annurev.bioeng.6.040803.140027
189. Langer R, Tirrell DA (2004) Designing materials for biology and medicine. Nature 428:487–492. doi:10.1038/nature02388
190. Shmulewitz A, Langer R, Patton J (2006) Convergence in biomedical technology. Nat Biotechnol 24:277–280. doi:10.1038/Nbt0306-277a
191. Karp JM, Langer R (2007) Development and therapeutic applications of advanced biomaterials. Curr Opin Biotech 18:454–459. doi:10.1016/j.copbio.2007.09.008
192. Langer R (1998) Drug delivery and targeting. Nature 392(suppl):5–10
193. Yakacki CM, Shandas R, Lanning C, Rech B, Eckstein A, Gall K (2007) Unconstrained recovery characterization of shape-memory polymer networks for cardiovascular applications. Biomaterials 28:2255–2263. doi:10.1016/j.biomaterials.2007.01.030

194. Small W, Buckley PR, Wilson TS, Loge JM, Maitland KD, Maitland DJ (2008) Fabrication and characterization of cylindrical light diffusers comprised of shape memory polymer. J Biomed Opt 13:024018. doi:10.1117/1.2904952
195. Baer G, Small W, Wilson T, Benett W, Matthews D, Hartman J, Maitland D (2007) Fabrication and in vitro deployment of a laser-activated shape memory polymer vascular stent. Biomed Eng Online 6:43. doi:10.1186/1475-925x-6-43
196. Yakacki CM, Satarkar NS, Gall K, Likos R, Hilt JZ (2009) Shape-memory polymer networks with $Fe_3O_4$ nanoparticles for remote activation. J Appl Polym Sci 112:3166–3176. doi:10.1002/App.29845
197. Sokolowski W, Metcalfe A, Hayashi S, Yahia L, Raymond J (2007) Medical applications of shape memory polymers. Biomed Mater 2:S23–S27. doi:10.1088/1748-6041/2/1/S04
198. Sigwart U, Puel J, Mirkovitch V, Joffre F, Kappenberger L (1987) Intravascular stents to prevent occlusion and restenosis after trans-luminal angioplasty. New Engl J Med 316:701–706. doi:10.1056/Nejm198703193161201
199. O'Brien B, Carroll W (2009) The evolution of cardiovascular stent materials and surfaces in response to clinical drivers: A review. Acta Biomater 5:945–958. doi:10.1016/j.actbio.2008.11.012
200. Tamai H, Igaki K, Kyo E, Kosuga K, Kawashima A, Matsui S, Komori H, Tsuji T, Motohara S, Uehata H (2000) Initial and 6-month results of biodegradable poly-l-lactic acid coronary stents in humans. Circulation 102:399–404. doi:10.1161/01.CIR.102.4.399
201. Tsuji T, Tamai H, Igaki K, Kyo E, Kosuga K, Kawashima A, Matsul S, Hata T, Komori H, Motohara S, Uehata H (2000) Clinical and angiographic follow-up of a new biodegradable coronary stent (Igaki–Tamai stent). J Am Coll Cardiol 35:89a–89a
202. Wache HM, Tartakowska DJ, Hentrich A, Wagner MH (2003) Development of a polymer stent with shape memory effect as a drug delivery system. J Mater Sci-Mater M 14:109–112. doi:10.1023/A:1022007510352
203. Baer GM, Wilson TS, Small W, Hartman J, Benett WJ, Matthews DL, Maitland DJ (2009) Thermomechanical properties, collapse pressure, and expansion of shape memory polymer neurovascular stent prototypes. J Biomed Mater Res B 90B:421–429. doi:10.1002/Jbm.B.31301
204. Baer G, Wilson T, Maitland D, Matthews D (2006) Shape memory polymer neurovascular stents. J Invest Med 54:S162–S162. doi:10.2310/6650.2005.X0004
205. Kessel DO, Patel JV (2005) Current trends in thrombolysis: implications for diagnostic and interventional radiology. Clin Radiol 60:413–424. doi:10.1016/j.crad.2004.11.015
206. delZoppo GJ (1996) Tissue plasminogen activator for acute ischemic stroke. New Engl J Med 334:1406. doi:10.1056/NEJM199605233342114
207. Qureshi N (1996) Tissue plasminogen activator for acute ischemic stroke. New Engl J Med 334:1406. doi:10.1056/NEJM199605233342114
208. Koroshetz WJ (1996) Tissue plasminogen activator for acute ischemic stroke. New Engl J Med 334:1405–1406. doi:10.1056/NEJM199605233342114
209. Marler JR (1996) Tissue plasminogen activator for acute ischemic stroke—reply. New Engl J Med 334:1406. doi:10.1056/NEJM199605233342114
210. Friedman HS (1996) Tissue plasminogen activator for acute ischemic stroke. New Engl J Med 334:1405. doi:10.1056/NEJM199605233342114
211. Zhu W, Yin Q, Zhang R, Xu G, Ma M, Fan X, Fan X, Liu X (2011) Effect of intra-arterial thrombolysis with rt-PA and endovascular mechanical recanalization in posterial circulation acute ischemic stroke. Cerebrovasc Dis 32:9
212. Berlis A, Lutsep H, Barnwell S, Norbash A, Wechsler L, Jungreis CA, Woolfenden A, Redekop G, Hartmann M, Schumacher M (2004) Mechanical thrombolysis in acute ischemic stroke with endovascular photoacoustic recanalization. Stroke 35:1112–1116. doi:10.1161/01.Str.0000124126.17508.D3
213. Kerber CW, Barr JD, Berger RM, Chopko BW (2002) Snare retrieval of intracranial thrombus in patients with acute stroke. J Vasc Interv Radiol 13:1269–1274. doi:10.1016/S1051-0443(07)61978-2

214. Mayer TE, Hamann GF, Brueckmann HJ (2002) Treatment of basilar artery embolism with a mechanical extraction device—necessity of flow reversal. Stroke 33:2232–2235. doi:10.1161/01str0000024527l680c6
215. Bellon RJ, Putman CM, Budzik RF, Pergolizzi RS, Reinking GF, Norbash AM (2001) Rheolytic thrombectomy of the occluded internal carotid artery in the setting of acute ischemic stroke. Am J Neuroradiol 22:526–530
216. Metzger MF, Wilson TS, Schumann D, Matthews DL, Maitland DJ (2002) Mechanical properties of mechanical actuator for treating ischemic stroke. Biomed Microdevices 4:89–96. doi:10.1023/A:1014674912979
217. Maitland DJ, Metzger MF, Schumann D, Lee A, Wilson TS (2002) Photothermal properties of shape memory polymer micro-actuators for treating stroke. Laser Surg Med 30:1–11. doi:10.1002/lsm.10007
218. Small W, Wilson TS, Benett WJ, Loge JM, Maitland DJ (2005) Laser-activated shape memory polymer intravascular thrombectomy device. Opt Express 13:8204–8213. doi:10.1364/Opex.13.008204
219. Enriquez-Sarano M, Schaff HV, Orszulak TA, Bailey KR, Tajik AJ, Frye RL (1995) Congestive heart failure after surgical correction of mitral regurgitation. A long-term study. Circulation 92:2496–2503. doi:10.1161/01.CIR.92.9.2496
220. Enriquez-Sarano M, Schaff HV, Orszulak TA, Tajik AJ, Bailey KR, Frye RL (1995) Valve repair improves the outcome of surgery for mitral regurgitation. A multivariate analysis. Circulation 91:1022–1028. doi:10.1161/01.CIR.91.4.1022
221. Lorenzo V, Díaz-Lantada A, Lafont P, Lorenzo-Yustos H, Fonseca C, Acosta J (2009) Physical ageing of a PU-based shape memory polymer: influence on their applicability to the development of medical devices. Mater Des 30:2431–2434. doi:10.1016/j.matdes.2008.10.023
222. Lantada AD, Del Valle-Fernandez R, Morgado PL, Munoz-Garcia J, Sanz JLM, Munoz-Guijosa JM, Otero JE (2010) Development of personalized annuloplasty rings: combination of CT images and CAD-CAM tools. Ann Biomed Eng 38:280–290. doi:10.1007/s10439-009-9805-z
223. Szarowski DH, Andersen MD, Retterer S, Spence AJ, Isaacson M, Craighead HG, Turner JN, Shain W (2003) Brain responses to micro-machined silicon devices. Brain Res 983:23–35. doi:10.1016/S0006-8993(03)03023-3
224. Sharp AA, Panchawagh HV, Ortega A, Artale R, Richardson-Burns S, Finch DS, Gall K, Mahajan RL, Restrepo D (2006) Toward a self-deploying shape memory polymer neuronal electrode. J Neural Eng 3:L23–L30. doi:10.1088/1741-2560/3/4/l02
225. Xue L, Dai S, Li Z (2012) Synthesis and characterization of elastic star shape-memory polymers as self-expandable drug-eluting stents. J Mater Chem 22:7403. doi:10.1039/c2jm15918j
226. Lendlein A, Kelch S (2005) Shape-memory polymers as stimuli-sensitive implant materials. Clin Hemorheol Micro 32:105–116
227. Brem H, Gabikian P (2001) Biodegradable polymer implants to treat brain tumors. J Control Release 74:63–67. doi:10.1016/S0168-3659(01)00311-X
228. Hetrick EM, Schoenfisch MH (2006) Reducing implant-related infections: active release strategies. Chem Soc Rev 35:780–789. doi:10.1039/B515219b
229. Patil SD, Papadmitrakopoulos F, Burgess DJ (2007) Concurrent delivery of dexamethasone and VEGF for localized inflammation control and angiogenesis. J Control Release 117:68–79. doi:10.1016/j.jconrel.2006.10.013
230. Tabata Y (2003) Tissue regeneration based on growth factor release. Tissue Eng 9:5–15. doi:10.1089/10763270360696941
231. Neffe AT, Hanh BD, Steuer S, Lendlein A (2009) Polymer networks combining controlled drug release, biodegradation, and shape memory capability. Adv Mater 21:3394–3398. doi:10.1002/adma.200802333
232. Olson DA, Gratton SEA, DeSimone JM, Sheares VV (2006) Amorphous linear aliphatic polyesters for the facile preparation of tunable rapidly degrading elastomeric devices and delivery vectors. J Am Chem Soc 128:13625–13633. doi:10.1021/Ja063092m

233. Wischke C, Neffe AT, Lendlein A (2010) Controlled drug release from biodegradable shape-memory polymers. Adv Polym Sci 226:177–205. doi:10.1007/12_2009_29
234. Wischke C, Neffe AT, Steuer S, Lendlein A (2009) Evaluation of a degradable shape-memory polymer network as matrix for controlled drug release. J Control Release 138:243–250. doi:10.1016/j.jconrel.2009.05.027
235. Rickert D, Lendlein A, Kelch S, Franke RP, Moses MA (2005) Cell proliferation and cellular activity of primary cell cultures of the oral cavity after cell seeding on the surface of a degradable, thermoplastic block copolymer. Biomed Tech 50:92–99
236. Farè S, Valtulina V, Petrini P, Alessandrini E, Pietrocola G, Tanzi MC, Speziale P, Visai L (2005) In vitro interaction of human fibroblasts and platelets with a shape-memory polyurethane. J Biomed Mater Res, Part A 73:1–11. doi:10.1002/jbm.a.30193
237. Cabanlit M, Maitland D, Wilson T, Simon S, Wun T, Gershwin ME, Van de Water J (2007) Polyurethane shape-memory polymers demonstrate functional biocompatibility in vitro. Macromol Biosci 7:48–55. doi:10.1002/mabi.200600177
238. Neuss S, Blomenkamp I, Stainforth R, Boltersdorf D, Jansen M, Butz N, Perez-Bouza A, Knuchel R (2009) The use of a shape-memory poly(epsilon-caprolactone)dimethacrylate network as a tissue engineering scaffold. Biomaterials 30:1697–1705. doi:10.1016/j.biomaterials.2008.12.027
239. Nakasima A, Hu JR, Ichinose M, Shimada H (1991) Potential application of shape memory plastic as elastic-material in clinical orthodontics. Eur J Orthodont 13:179–186. doi:10.1093/ejo/13.3.179
240. Ortega JM, Small W, Wilson TS, Benett WJ, Loge JM, Maitland DJ (2007) A shape memory polymer dialysis needle adapter for the reduction of hemodynamic stress within arteriovenous grafts. IEEE T Bio-Med Eng 54:1722–1724. doi:10.1109/Tbme.2007.892927
241. Huang WM, Liu N, Lan X, Lin JQ, Pan JH, Leng JS, Phee SJ, Fan H, Liu YJ, Tong TH (2009) Formation of protrusive micro/nano patterns atop shape memory polymers. Mater Sci Forum 614:243–248. doi:10.4028/www.scientific.net/MSF.614.243
242. Liu N, Xie Q, Huang WM, Phee SJ, Guo NQ (2008) Formation of micro protrusion arrays atop shape memory polymer. J Micromech Microeng 18:027001. doi:10.1088/0960-1317/18/2/027001
243. Liu N, Huang WM, Phee SJ, Tong TH (2008) The formation of micro-protrusions atop a thermo-responsive shape memory polymer. Smart Mater Struct 17:057001. doi:10.1088/0964-1726/17/5/057001
244. Huang WM, Lee CW, Teo HP (2006) Thermomechanical behavior of a polyurethane shape memory polymer foam. J Intel Mat Syst Str 17:753–760. doi:10.1177/1045389x06055768
245. Liu N, Huang WM, Phee SJ, Fan H, Chew KL (2007) A generic approach for producing various protrusive shapes on different size scales using shape-memory polymer. Smart Mater Struct 16:N47–N50. doi:10.1088/0964-1726/16/6/N01
246. Lee AP, Northrup MA, Ahre PE, Dupuy PC (1997) Polymer micromold and fabrication process. US Patent 5,658,515
247. Benett WJ, Krulevitch PA, Lee AP, Northrup MA, Flolta JA (1997) Miniature plastic gripper and fabrication method. US Patent 5,609,608
248. Lee AP, Fitch JP (2000) Micro devices using shape memory polymer patches for mated connections. US Patent 6,086,599
249. Lee AP, Northrup MA, Ciarlo DR, Krulevitch PA, Benett WJ (2000) Release mechanism utilizing shape memory polymer material. US Patent 6,102,933
250. Ferrera DA (2001) Shape memory polymer intravascular delivery system with heat transfer medium. US Patent 6,224,610
251. Takashima K, Rossiter J, Mukai T (2010) McKibben artificial muscle using shape-memory polymer. Sens Actuators, A 164:116–124. doi:10.1016/j.sna.2010.09.010
252. Small W, Wilson TS, Buckley PR, Benett WJ, Loge JA, Hartman J, Maitland DJ (2007) Prototype fabrication and preliminary in vitro testing of a shape memory endovascular thrombectomy device. IEEE T Bio-Med Eng 54:1657–1666. doi:10.1109/Tbme.2007.892921
253. Harris KD, Cuypers R, Scheibe P, van Oosten CL, Bastiaansen CWM, Lub J, Broer DJ (2005) Large amplitude light-induced motion in high elastic modulus polymer actuators. J Mater Chem 15:5043–5048. doi:10.1039/B512655J

254. Ikeda T, Ube T (2011) Photomobile polymer materials: From nano to macro. Mater Today 14:480–487. doi:10.1016/S1369-7021(11)70212-7
255. Yamada M, Kondo M, Miyasato R, Naka Y, Mamiya JI, Kinoshita M, Shishido A, Yu Y, Barrett CJ, Ikeda T (2009) Photomobile polymer materials—various three-dimensional movements. J Mater Chem 19:60–62. doi:10.1039/b815289f
256. Manz A, Miyahara Y, Miura J, Watanabe Y, Miyagi H, Sato K (1990) Design of an open-tubular column liquid chromatograph using silicon chip technology. Sensor Actuat B-Chem 1:249–255. doi:10.1016/0925-4005(90)80210-Q
257. Finnskog D, Ressine A, Laurell T, Marko-Varga G (2004) Integrated protein microchip assay with dual fluorescent- and MALDI read-out. J Proteome Res 3:988–994. doi:10.1021/Pr0499287
258. Bings NH, Wang C, Skinner CD, Colyer CL, Thibault P, Harrison DJ (1999) Microfluidic devices connected to fused-silica capillaries with minimal dead volume. Anal Chem 71:3292–3296. doi:10.1021/ac981419z
259. Grosse A, Grewe M, Fouckhardt H (2001) Deep wet etching of fused silica glass for hollow capillary optical leaky waveguides in microfluidic devices. J Micromech Microeng 11:257–262. doi:10.1088/0960-1317/11/3/315
260. Manz A, Harrison DJ, Verpoorte EMJ, Fettinger JC, Paulus A, Ludi H, Widmer HM (1992) Planar chips technology for miniaturization and integration of separation techniques into monitoring systems—capillary electrophoresis on a chip. J Chromatogr 593:253–258. doi:10.1016/0021-9673(92)80293-4
261. Harrison DJ, Fluri K, Seiler K, Fan ZH, Effenhauser CS, Manz A (1993) Micromachining a miniaturized capillary electrophoresis-based chemical-analysis system on a chip. Science 261:895–897. doi:10.1126/science.261.5123.895
262. Golonka LJ, Roguszczak H, Zawada T, Radojewski J, Grabowska I, Chudy M, Dybko A, Brzozka Z, Stadnik D (2005) LTCC based microfluidic system with optical detection. Sensor Actuat B-Chem 111:396–402. doi:10.1016/j.snb.2005.03.065
263. Natarajan G, Humenik JN (2006) 3D ceramic microfluidic device manufacturing. J Phys: Conf Ser 34:533–539. doi:10.1088/1742-6596/34/1/088
264. Becker H, Locascio LE (2002) Polymer microfluidic devices. Talanta 56:267–287. doi:10.1016/S0039-9140(01)00594-X
265. Quake SR, Scherer A (2000) From micro- to nanofabrication with soft materials. Science 290:1536–1540. doi:10.1126/science.290.5496.1536
266. Duffy DC, McDonald JC, Schueller OJA, Whitesides GM (1998) Rapid prototyping of microfluidic systems in poly(dimethylsiloxane). Anal Chem 70:4974–4984. doi:10.1021/ac980656z
267. Muck A, Wang J, Jacobs M, Chen G, Chatrathi MP, Jurka V, Vyborny Z, Spillman SD, Sridharan G, Schoning MJ (2004) Fabrication of poly(methyl methacrylate) microfluidic chips by atmospheric molding. Anal Chem 76:2290–2297. doi:10.1021/ac035030+
268. Beebe DJ, Moore JS, Bauer JM, Yu Q, Liu RH, Devadoss C, Jo BH (2000) Functional hydrogel structures for autonomous flow control inside microfluidic channels. Nature 404:588–590. doi:10.1038/35007047
269. Eddington DT, Beebe DJ (2004) Flow control with hydrogels. Adv Drug Deliver Rev 56:199–210. doi:10.1016/j.addr.2003.08.013
270. Beebe DJ, Moore JS, Yu Q, Liu RH, Kraft ML, Jo BH, Devadoss C (2000) Microfluidic tectonics: a comprehensive construction platform for microfluidic systems. P Natl Acad Sci USA 97:13488–13493. doi:10.1073/pnas.250273097
271. Yu C, Mutlu S, Selvaganapathy P, Mastrangelo CH, Svec F, Frechett JMJ (2003) Flow control valves for analytical microfluidic chips without mechanical parts based on thermally responsive monolithic polymers. Anal Chem 75:1958–1961. doi:10.1021/Ac026455j
272. Ionov L, Houbenov N, Sidorenko A, Stamm M, Minko S (2006) Smart microfluidic channels. Adv Funct Mater 16:1153–1160. doi:10.1002/adfm.200500562
273. Idota N, Kikuchi A, Kobayashi J, Sakai K, Okano T (2005) Microfluidic valves comprising nanolayered thermoresponsive polymer-grafted capillaries. Adv Mater 17:2723. doi:10.1002/adma.200402068

274. Idota N, Kikuchi A, Kobayashi J, Akiyama Y, Okano T (2006) Thermal modulated interaction of aqueous steroids using polymer-grafted capillaries. Langmuir 22:425–430. doi:10.1021/La051968h
275. Malmstadt N, Yager P, Hoffman AS, Stayton PS (2003) A smart microfluidic affinity chromatography matrix composed of poly(N-isopropylacrylamide)-coated beads. Anal Chem 75:2943–2949. doi:10.1021/Ac034274r
276. Ebara M, Hoffman JM, Hoffman AS, Stayton PS (2006) Switchable surface traps for injectable bead-based chromatography in PDMS microfluidic channels. Lab Chip 6:843–848. doi:10.1039/B515128g
277. Techawanitchai P, Yamamoto K, Ebara M, Aoyagi T (2011) Surface design with self-heating smart polymers for on-off switchable traps. Sci Technol Adv Mat 12:044609 (44607 pages). doi:10.1088/1468-6996/12/4/044609
278. Yager P, Domingo GJ, Gerdes J (2008) Point-of-care diagnostics for global health. Annu Rev Biomed Eng 10:107–144. doi:10.1146/annurev.bioeng.10.061807.160524
279. Ebara M, Uto K, Idota N, Hoffman JM, Aoyagi T (2013) Rewritable and shape-memory soft matter with dynamically tunable microchannel geometry in a biological temperature range. Soft Matter 9:3074–3080. doi:10.1039/C3SM27243E
280. Takehara H, Uto K, Ebara M, Aoyagi T, Ichiki T (2012) Shape-memory polymer microvalves. Proc μTAS 2012:1846–1848
281. Takehara H, Jiang C, Uto K, Ebara M, Aoyagi T, Ichiki T (2013) Novel microfluidic valve technology based on shape memory effect of poly(ε-caprolactone). Appl Phys Express 6:037201. doi:10.7567/apex.6.037201
282. Shoji S, Esashi M (1994) Microflow devices and systems. J Micromech Microeng 4:157–171. doi:10.1088/0960-1317/4/4/001
283. Unger MA, Chou H-P, Thorsen T, Scherer A, Quake SR (2000) Monolithic microfabricated valves and pumps by multilayer soft lithography. Science 288:113–116. doi:10.1126/science.288.5463.113
284. Kim J, Hayward RC (2012) Mimicking dynamic in vivo environments with stimuli-responsive materials for cell culture. Trends Biotechnol 30:426–439. doi:10.1016/j.tibtech.2012.04.003
285. Rickert D, Lendlein A, Peters I, Moses M, Franke R-P (2006) Biocompatibility testing of novel multifunctional polymeric biomaterials for tissue engineering applications in head and neck surgery: an overview. Eur Arch Otorhinolaryngol 263:215–222. doi:10.1007/s00405-005-0950-1
286. Nelson BA, King WP, Gall K (2005) Shape recovery of nanoscale imprints in a thermoset "shape memory" polymer. Appl Phys Lett 86:103108. doi:10.1063/1.1868883
287. Altebaeumer T, Gotsmann B, Pozidis H, Knoll A, Duerig U (2008) Nanoscale shape-memory function in highly cross-linked polymers. Nano Lett 8:4398–4403. doi:10.1021/nl8022737
288. Gall K, Kreiner P, Turner D, Hulse M (2004) Shape-memory polymers for microelectromechanical systems. J Microelectromech Syst 13:472–483. doi:10.1109/jmems.2004.828727
289. Burke KA, Mather PT (2010) Soft shape memory in main-chain liquid crystalline elastomers. J Mater Chem 20:3449–3457. doi:10.1039/B924050K
290. Xie T, Xiao X, Li J, Wang R (2010) Encoding localized strain history through wrinkle based structural colors. Adv Mater 22:4390–4394. doi:10.1002/adma.201002825
291. Wang ZY, Teo EY, Chong MS, Zhang QY, Lim J, Zhang ZY, Hong MH, Thian ES, Chan JK, Teoh SH (2013) Biomimetic three-dimensional anisotropic geometries by uniaxial stretch of poly(ε-caprolactone) films for mesenchymal stem cell proliferation, alignment, and myogenic differentiation. Tissue Eng Part C Methods 19:12 pages. doi:10.1089/ten.TEC.2012.0472
292. Lam MT, Clem WC, Takayama S (2008) Reversible on-demand cell alignment using reconfigurable microtopography. Biomaterials 29:1705–1712. doi:10.1016/j.biomaterials.2007.12.010
293. Davis KA, Burke KA, Mather PT, Henderson JH (2011) Dynamic cell behavior on shape memory polymer substrates. Biomaterials 32:2285–2293. doi:10.1016/j.biomaterials.2010.12.006

294. Ebara M, Uto K, Idota N, Hoffman JM, Aoyagi T (2012) Shape-memory surface with dynamically tunable nano-geometry activated by body heat. Adv Mater 24:273–278. doi:10.1002/adma.201102181
295. Ebara M, Uto K, Idota N, Hoffman JM, Aoyagi T (2013) The taming of the cell; shape-memory nanopatterns direct cell orientation. Int J Nanomedicine. In press
296. Le DM, Kulangara K, Adler AF, Leong KW, Ashby VS (2011) Dynamic topographical control of mesenchymal stem cells by culture on responsive poly(epsilon-caprolactone) surfaces. Adv Mater 23:3278. doi:10.1002/adma.201100821
297. Wu DY, Meure S, Solomon D (2008) Self-healing polymeric materials: a review of recent developments. Prog Polym Sci 33:479–522. doi:10.1016/j.progpolymsci.2008.02.001
298. White SR, Sottos NR, Geubelle PH, Moore JS, Kessler MR, Sriram SR, Brown EN, Viswanathan S (2001) Autonomic healing of polymer composites. Nature 409:794–797. doi:10.1038/35057232
299. Ni WY, Cheng YT, Grummon DS (2006) Wear resistant self-healing tribological surfaces by using hard coatings on NiTi shape memory alloys. Surf Coat Tech 201:1053–1057. doi:10.1016/j.surfcoat.2006.01.067
300. Kirkby EL, Rule JD, Michaud VJ, Sottos NR, White SR, Manson JAE (2008) Embedded shape-memory alloy wires for improved performance of self-healing polymers (vol 18, p 2253, 2008). Adv Funct Mater 18:2470. doi:10.1002/adfm.200701208
301. Kirkby EL, Michaud VJ, Manson JAE, Sottos NR, White SR (2009) Performance of self-healing epoxy with microencapsulated healing agent and shape memory alloy wires. Polymer 50:5533–5538. doi:10.1016/j.polymer.2009.05.014
302. Rodriguez ED, Luo X, Mather PT (2009) Shape memory miscible blends for thermal mending. Behav Mech Multifunct Mater Compos 728912. doi:10.1117/12.816042
303. Rodriguez ED, Luo X, Mather PT (2011) Linear/network poly($\varepsilon$-caprolactone) blends exhibiting shape memory assisted self-healing (SMASH). ACS Appl Mater Interfaces 3:152–161. doi:10.1021/am101012c
304. Xiao X, Xie T, Cheng Y-T (2010) Self-healable graphene polymer composites. J Mater Chem 20:3508–3514. doi:10.1039/C0JM00307G
305. Kohlmeyer RR, Lor M, Chen J (2012) Remote, local, and chemical programming of healable multishape memory polymer nanocomposites. Nano Lett 12:2757–2762. doi:10.1021/nl2044875
306. Xie T, Xiao X (2008) Self-peeling reversible dry adhesive system. Chem Mater 20:2866–2868. doi:10.1021/cm800173c
307. Luo X, Lauber KE, Mather PT (2010) A thermally responsive, rigid, and reversible adhesive. Polymer 51:1169–1175. doi:10.1016/j.polymer.2010.01.006
308. Autumn K, Peattie AM (2002) Mechanisms of adhesion in geckos. Integr Comp Biol 42:1081–1090. doi:10.1093/icb/42.6.1081
309. Arzt E, Gorb S, Spolenak R (2003) From micro to nano contacts in biological attachment devices. Proc Natl Acad Sci 100:10603–10606. doi:10.1073/pnas.1534701100
310. Xia F, Jiang L (2008) Bio-inspired, smart, multiscale interfacial materials. Adv Mater 20:2842–2858. doi:10.1002/adma.200800836
311. Geim AK, Dubonos SV, Grigorieva IV, Novoselov KS, Zhukov AA, Shapoval SY (2003) Microfabricated adhesive mimicking gecko foot-hair. Nat Mater 2:461–463. doi:10.1038/nmat917
312. Federle W (2006) Why are so many adhesive pads hairy? J Exp Biol 209:2611–2621. doi:10.1242/Jeb.02323
313. Reddy S, Arzt E, del Campo A (2007) Bioinspired surfaces with switchable adhesion. Adv Mater 19:3833–3837. doi:10.1002/adma.200700733
314. Kim S, Sitti M, Xie T, Xiao X (2009) Reversible dry micro-fibrillar adhesives with thermally controllable adhesion. Soft Matter 5:3689–3693. doi:10.1039/B909885B
315. Sun L, Huang WM, Ding Z, Zhao Y, Wang CC, Purnawali H, Tang C (2012) Stimulus-responsive shape memory materials: a review. Mater Des 33:577–640. doi:10.1016/j.matdes.2011.04.065
316. Chiodo JD, Harrison DJ, Billett EH (2001) An initial investigation into active disassembly using shape memory polymers. P I Mech Eng B-J Eng 215:733–741. doi:10.1243/0954405011518539

317. Active disassembly research. http://www.activedisassembly.com/
318. Yang B, Huang WM, Li C, Lee CM, Li L (2004) On the effects of moisture in a polyurethane shape memory polymer. Smart Mater Struct 13:191. doi:10.1088/0964-1726/13/1/022
319. Huang WM, Yang B, Zhao Y, Ding Z (2010) Thermo-moisture responsive polyurethane shape-memory polymer and composites: a review. J Mater Chem 20:3367–3381. doi:10.1039/B922943D
320. Sakata Y, Furukawa S, Kondo M, Hirai K, Horike N, Takashima Y, Uehara H, Louvain N, Meilikhov M, Tsuruoka T, Isoda S, Kosaka W, Sakata O, Kitagawa S (2013) Shape-memory nanopores induced in coordination frameworks by crystal downsizing. Science 339:193–196. doi:10.1126/science.1231451
321. Triguero C, Coudert F-X, Boutin A, Fuchs AH, Neimark AV (2011) Mechanism of breathing transitions in metal-organic frameworks. J Phys Chem Lett 2:2033–2037. doi:10.1021/jz2008769
322. Liu WG, Zhang JR, De Yao K (2002) DNA/lipid complex organogel with shape-memory behavior. J Appl Polym Sci 86:259–263. doi:10.1002/app.10919
323. Lee JB, Peng S, Yang D, Roh YH, Funabashi H, Park N, Rice EJ, Chen L, Long R, Wu M, Luo D (2012) A mechanical metamaterial made from a DNA hydrogel. Nat Nano 7:816–820. doi:10.1038/nnano.2012.211
324. Bencherif SA, Sands RW, Bhatta D, Arany P, Verbeke CS, Edwards DA, Mooney DJ (2012) Injectable preformed scaffolds with shape-memory properties. P Natl Acad Sci USA. doi:10.1073/ pnas.1211516109